Technical Report ITL-95-3
June 1995

US Army Corps
of Engineers
Waterways Experiment
Station

Three-Dimensional, Nonlinear, Incremental Structural Analysis of a Culvert Valve Monolith Wall, Olmsted Locks

by Barry D. Fehl, Chris A. Merrill

Prepared for U.S. Army Engineer District, Louisville

Technical Report ITL-95-3
June 1995

Three-Dimensional, Nonlinear, Incremental Structural Analysis of a Culvert Valve Monolith Wall, Olmsted Locks

by Barry D. Fehl, Chris A. Merrill

U.S. Army Corps of Engineers
Waterways Experiment Station
3909 Halls Ferry Road
Vicksburg, MS 39180-6199

Final report

Approved for public release; distribution is unlimited

Prepared for U.S. Army Engineer District, Louisville
Louisville, KY 40201-0059

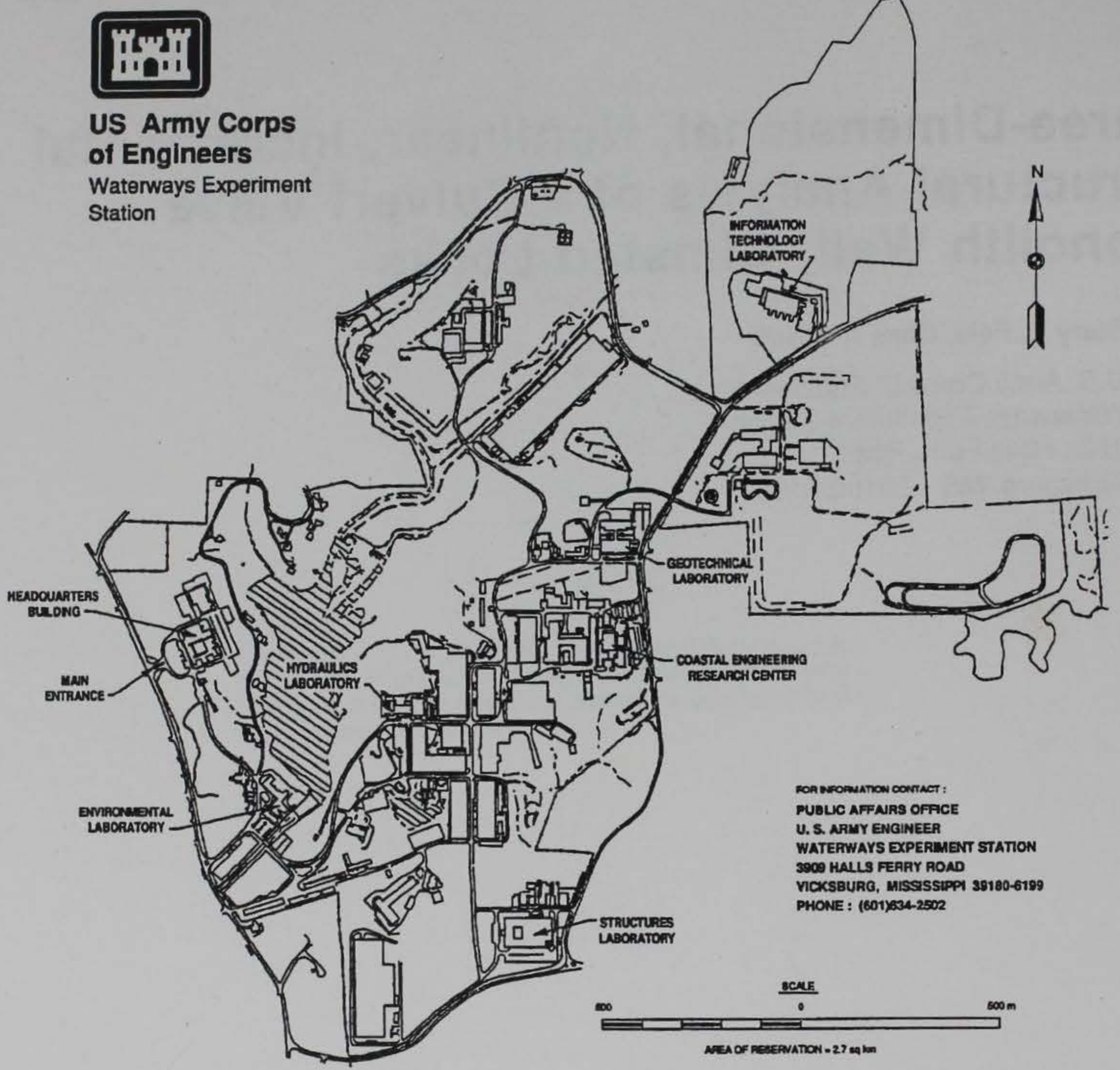

Waterways Experiment Station Cataloging-in-Publication Data

Fehl, Barry D., 1957-

Three-dimensional , nonlinear, incremental structural analysis of a culvert valve monolith wall, Olmsted locks / by Barry D. Fehl, Chris A. Merrill ; prepared for U.S. Army Engineer District, Louisville.

237 p. : ill. ; 28 cm. — (Technical report ; ITL-95-3)

Includes bibliographic references.

1. Locks (Hydraulic engineering) — Ohio River — Models. 2. Structural analysis (Engineering) 3. Locks — Strains and stresses. 4. Thermal stresses — Analysis — Models. I. Merrill, Chris A. II. United States. Army. Corps of Engineers. Louisville District. IV. U.S. Army Engineer Waterways Experiment Station. V. Information Technology Laboratory (U.S. Army Engineer Waterways Experiment Station) VI. Title. VII. Series: Technical report (U.S. Army Engineer Waterways Experiment Station) ; ITL-95-3.

TA7 W34 no.ITL-95-3

Contents

Preface

The work described in this report was conducted for the U.S. Army Engineer District, Louisville, by the Computer-Aided Engineering Division (CAED), Information Technology Laboratory (ITL), U.S. Army Engineer Waterways Experiment Station (WES). The investigation was authorized by Department of Defense Form 448, MIPR No. RMB-92-800, dated 3 Jun 1992.

The investigation was accomplished under the general supervision of Dr. N. Radhakrishnan, Director, ITL, and under the direct supervision of Dr. Reed Mosher, Chief, Structural Mechanics Division, Structures Laboratory, formerly Acting Chief, CAED, and Mr. H. Wayne Jones, Chief, CAED. This report was prepared by Messrs. Barry D. Fehl and Chris A. Merrill, CAED. The authors acknowledge Messrs. Byron McClellan and Jeff Bayers, CEORL-ED-DS, for their support and encouragement during the performance of the work described herein.

The work contained in this report is a portion of the Phase III, Nonlinear Incremental Structural Analysis (NISA) Study of the Olmsted Locks. Analyses of a typical chamber monolith and the lower miter gate monolith were also performed as a part of the Phase III Study. The Phase III Study was a combined effort of Ms. Sharon Garner of the WES Structures Laboratory, Messrs. Chris Merrill and Barry Fehl of ITL and, working under contract to WES, Mr. Randy James and Dr. Robert Dunham of ANATECH Research Corp. The entire Phase III NISA Study was a closely coordinated effort which included review meetings attended by representatives from Headquarters, the Ohio River Division and the Louisville District. The Phase III NISA Study was a part of a larger WES effort on the Olmsted Project with Mr. Glenn Pickering of the WES Hydraulics Laboratory acting as the point of contact.

At the time of publication of this report, Director of WES was Dr. Robert W. Whalin. Commander was COL Bruce K. Howard, EN.

Conversion Factors, Non-SI to SI Units of Measurement

Non-SI to SI units of measurement used in this report can be converted to SI units as follows:

Multiply	By	To Obtain
Btu (International Table) inch per hour, square inch, degree Fahrenheit	20.7688176	watts per meter kelvin
Btu (International Table) per pound (mass), degree Fahrenheit	4,186.8	joules per kiiogram kelvin
Fahrenheit degrees	5/9	celsius degrees or kelvin*
feet	0.3048	meters
inches	2.54	centimeters
kips (force) per inch	175.1268	kilonewtons per meter
pounds (force)	4.448222	newtons
pounds per square inch	6.894757	kilonewtons per meter

*To obtain Celsius (C) temperature readings from Fahrenheit (F) readings, use the following formula: C = (5/9) (F-32). To obtain Kelvin (K) readings, use: K = (5/9) (F-32) + 273.15.

1 Introduction

Background

The Olmsted Locks and Dam project will be located at mile 964.4 of the Ohio River and will consist of two locks (located on the right bank) and a gated dam to control the river during periods of low flow. The two locks are being designed as W-frame type structures and each chamber will be approximately 110 ft wide and 1,200 ft long.[1] The project was authorized for construction by the Water Resources Development Act of 1988. The Olmsted Locks and Dam are being designed by the U.S. Army Engineer District (USAED), Louisville.

Due to the unprecedented nature of the W-frame lock concept, the U.S. Army Engineer Waterways Experiment Station (WES) was requested by the USAED, Louisville, in September 1989 to evaluate the constructability of the lock structure by performing a nonlinear, incremental structural analysis (NISA). A NISA was performed by WES using guidance provided in Engineer Technical Letter (ETL) 1110-2-324, "Special Design Provisions for Massive Concrete Structures," (Headquarters, Department of the Army (HQDOA) 1990). NISA is a design process which uses the finite element (FE) method to model the incremental construction of mass concrete structures as well as models the aging characteristics of concrete. The general purpose code, ABAQUS (Hibbitt, Karlsson and Sorensen 1989) is used to perform a NISA along with software developed by ANATECH Research Corp. (1992) which models the aging of the concrete in the analysis. ABAQUS uses data from the ANATECH developed software through a user subroutine (UMAT). The ANATECH software is discussed in more detail in a report published at WES (Garner and Hammons 1991).

As a result of the request made by the USAED, Louisville, a report was submitted to the district in March 1992 detailing the data used, procedures, and results from the analyses performed. This report has since been published as a WES report entitled "Nonlinear, Incremental

---

[1] A table of factors for converting non-SI units of measurement to SI units is presented on page vi.

Structural Analysis of Olmsted Locks and Dam" (Garner et al. 1992). The report focused on the constructability of a typical chamber monolith including the evaluation of two different placing schemes in Phase I of the study and evaluation of two concrete mixtures using upper and lower bounds for creep and shrinkage in Phase II of the study. The results indicated that a typical chamber monolith was constructable and that possibilities existed for taking measures which would reduce construction costs.

Upon completion of Phases I and II, a meeting was held between Headquarters, U.S. Army Corps of Engineers (HQUSACE), Ohio River Division (ORD), USAED, Louisville, and WES in April 1992. Based on the results obtained from Phases I and II of the NISA study, a determination was made that a Phase III study (Merrill, Fehl, and Garner in preparation) was warranted and that the study should include evaluation of more cost effective construction methods for the typical chamber monolith, an evaluation of the constructability of the lower miter gate monolith, and an evaluation of a culvert valve monolith wall. This report will discuss the parameters and results associated with the evaluation of the culvert valve monolith wall.

Objective

The primary objective in evaluating a wall of a culvert valve monolith is to determine if cracking will occur as a result of the construction process. Cracking at the corners of the culvert valve pits is not uncommon, and therefore, an analysis to determine if this cracking may occur is desirable. Since cracking is very possible, the formation of a crack in the analysis should not necessarily indicate that changes to construction procedures are required. The culvert valve monolith is a reinforced structure and therefore should cracking occur, a secondary objective would be an evaluation of the size of the crack as well as an evaluation of the resulting stresses in the reinforcing. If results for these two parameters proved to be unacceptable, then consideration would need to be given to changing some of the construction conditions.

Another secondary objective which supports the primary objective is to capture the three-dimensional (3-D) behavior of the culvert valve monolith wall. Due to the geometry of a culvert valve monolith wall, two-dimensional (2-D) analyses in the transverse or longitudinal direction would not account for the cracking that would typically be expected for this type of monolith. Therefore, a 3-D analysis must be performed to obtain the behavior which is most likely to create difficulties should they arise.

Scope

The analysis performed in this study was performed using monolith 17. An isometric view of the monolith is shown in Figure 1, and the landwall on the right side of the monolith, looking downstream, was analyzed. As part of the model of the wall of monolith 17, a 24-ft section of the base slab in the chamber was included. While the primary interest in this analysis was the behavior of the wall, it was agreed that a portion of the slab should be modeled to ensure that the boundary conditions used did not effect behavior in the wall. Since evaluation of cracking is a primary objective of this analysis, reinforcing will be included in the model so that if cracking does occur, the benefits of the reinforcement present can be measured. The reinforcing was modeled using a smeared type of reinforcing as opposed to using discrete truss elements and is discussed in further detail in a WES report entitled "Use of Reinforcement in a Nonlinear, Incremental Structural Analysis" (Fehl and Merrill in preparation).

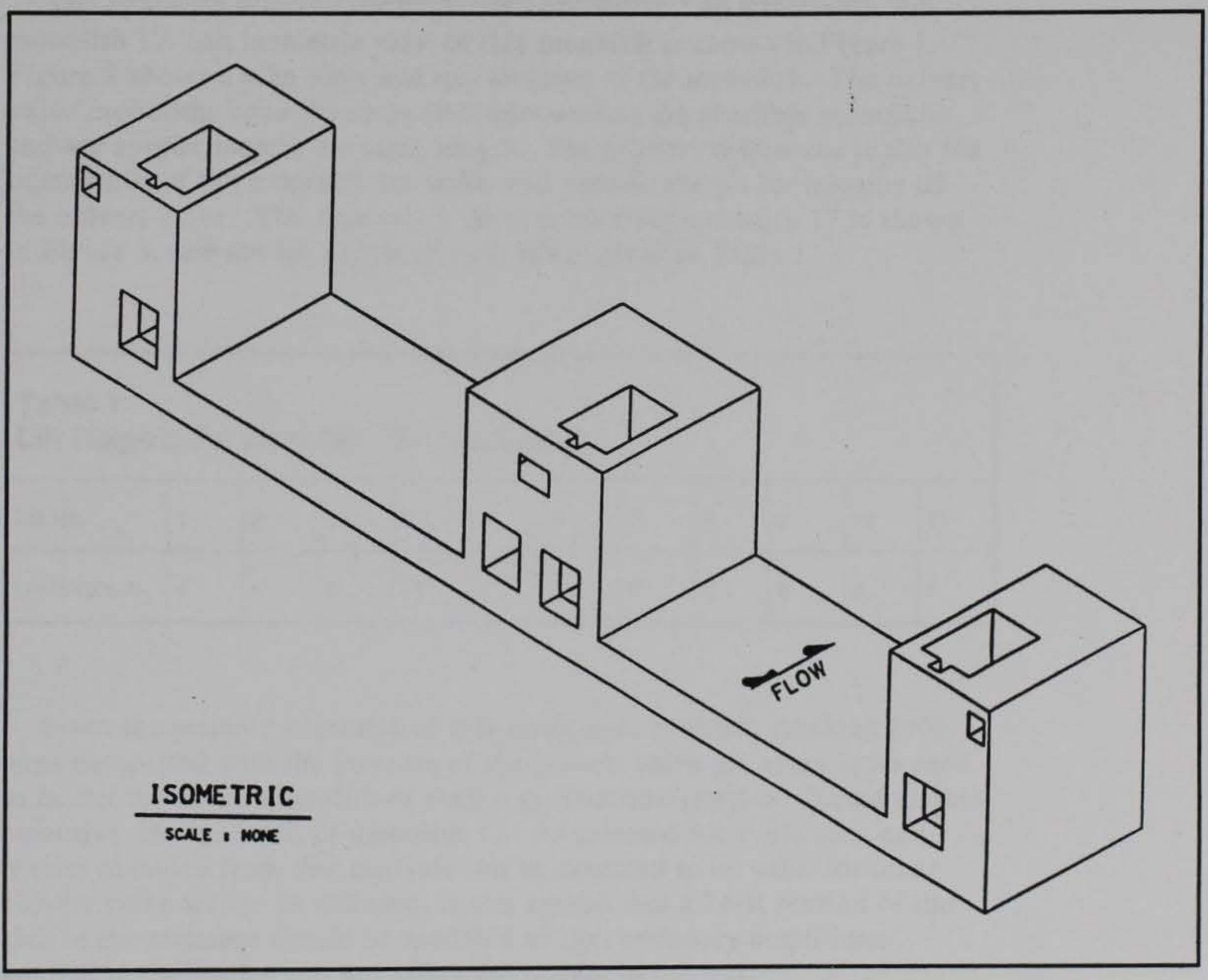

Figure 1. Isometric view of monolith 17

Other Phase III Studies

In addition to the work presented in this report, two other studies were performed during the Phase III portion of the Olmsted study. The first report is on additional 2-D studies performed on a typical chamber monolith and are an extension of the work performed in Phases I and II. The report is titled "Nonlinear, Incremental Structural Analysis of Olmsted Locks: Phase III" (Merrill, Fehl, and Garner in preparation). The report includes discussion of analyses using various start times, different insulation requirements, changes in lift heights, and various placing temperatures, as well as other miscellaneous parametric studies.

A second report is on the analyses performed on the lower miter gate monolith. This study was performed by ANATECH Research Corp., and results are reported in "Nonlinear, Incremental Structural Analysis for Monolith 19 of the Olmsted Locks" (Fehl et al. in preparation). The report discusses the 2-D parametric studies performed on the monolith as well as the results of a 3-D study performed.

2 Modeling Parameters - Analysis 1

Monolith Geometry and Description

The monolith selected for the study of a culvert valve monolith was monolith 17. An isometric view of this monolith is shown in Figure 1. Figure 2 shows a plan view and an elevation of the monolith. The culvert valve monoliths have the same slab thickness as the chamber monoliths and are approximately the same length. The primary difference is that the outer walls of the monolith are wider and contain the pit for housing of the culvert valve. The Analysis 1 lift sequence for monolith 17 is shown in Figure 3, and the lift height of each lift is given in Table 1.

Table 1
Lift Heights for Monolith 17 - Analysis 1

Lift No.	1	2	3	4	5	6	7	8	9	10	11
Lift Height, ft	4	4	4	18	9	9	8	8	8	8	4

Since the primary objective of this study is to evaluate cracking problems associated with the location of the culvert valve pit, there is no need to model the entire monolith or even a symmetrical portion. Based on this objective, the landwall of monolith 17 was selected for evaluation and results obtained from this analysis can be assumed to be valid for other culvert valve walls. In addition, it was agreed that a 24-ft portion of the slab in the chamber should be modeled so that boundary conditions applied to the model will not affect the results in the wall.

The lock monoliths at the Olmsted project are pile founded. The pile foundation is a uniformly spaced layout over the entire width and length of the monolith as shown in Figure 4. The pile will be HP 14 x 117 steel

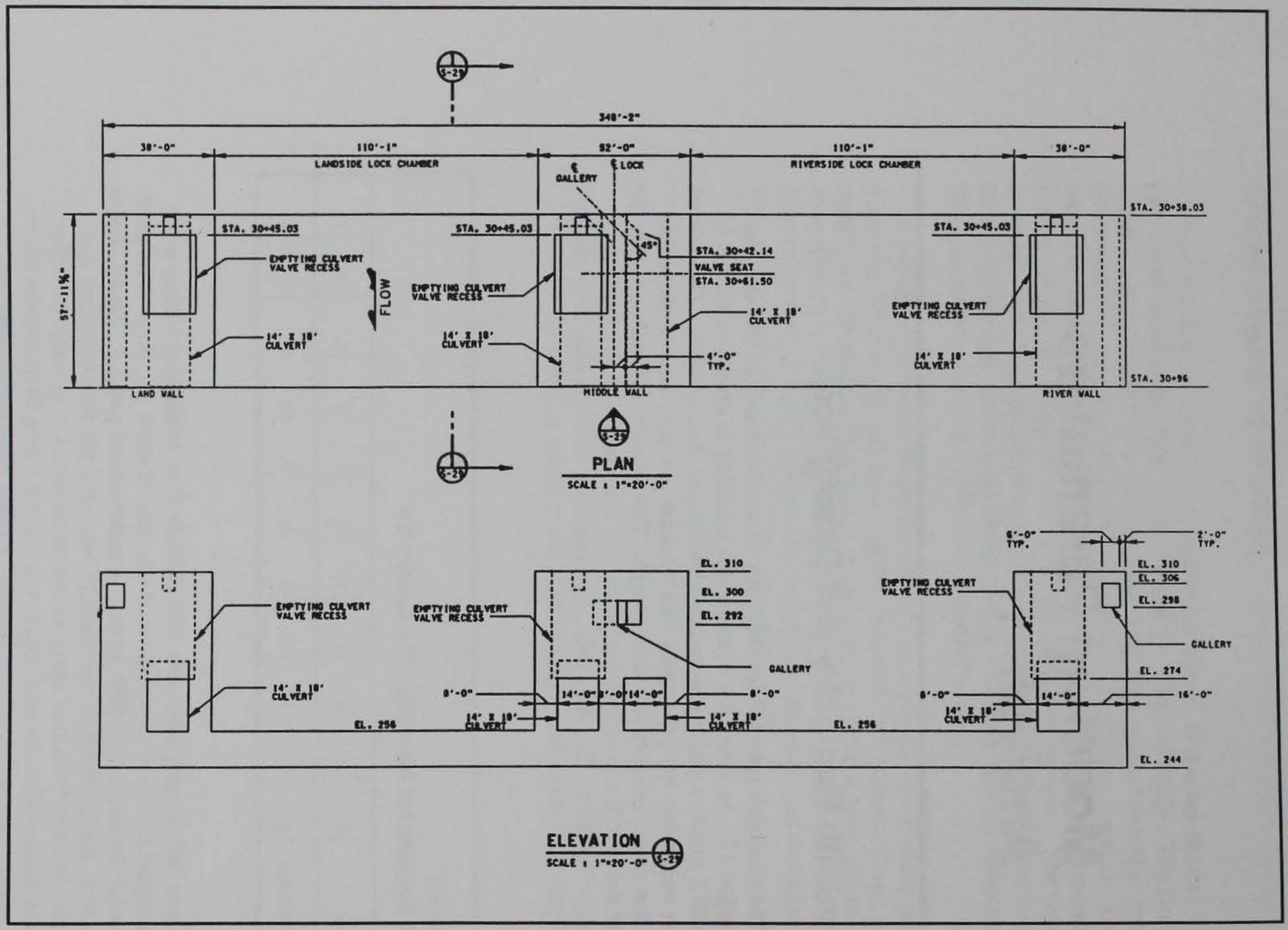

Figure 2. Plan and elevation of monolith 17

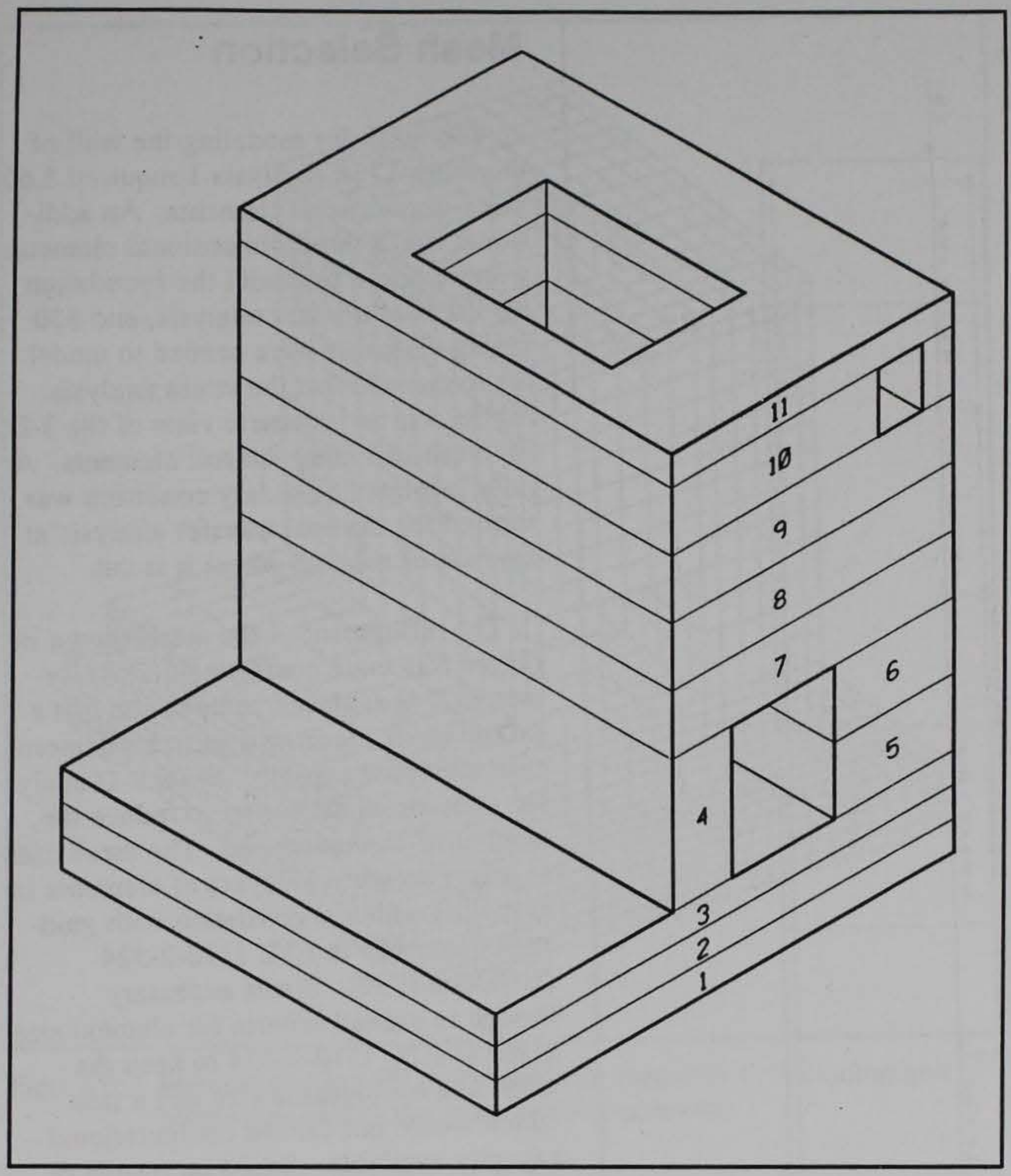

Figure 3. Isometric view of monolith 17 showing sequence of lift placements

piles and will be driven to elevation (el) 190.0.[1] Information regarding pile stiffness is reported in the report on Phases I and II of the Olmsted NISA (Garner et al. 1992).

1 Unless stated otherwise, all elevations (el) cited herein are in feet as referred to in the National Geodetic Vertical Datum of 1929.

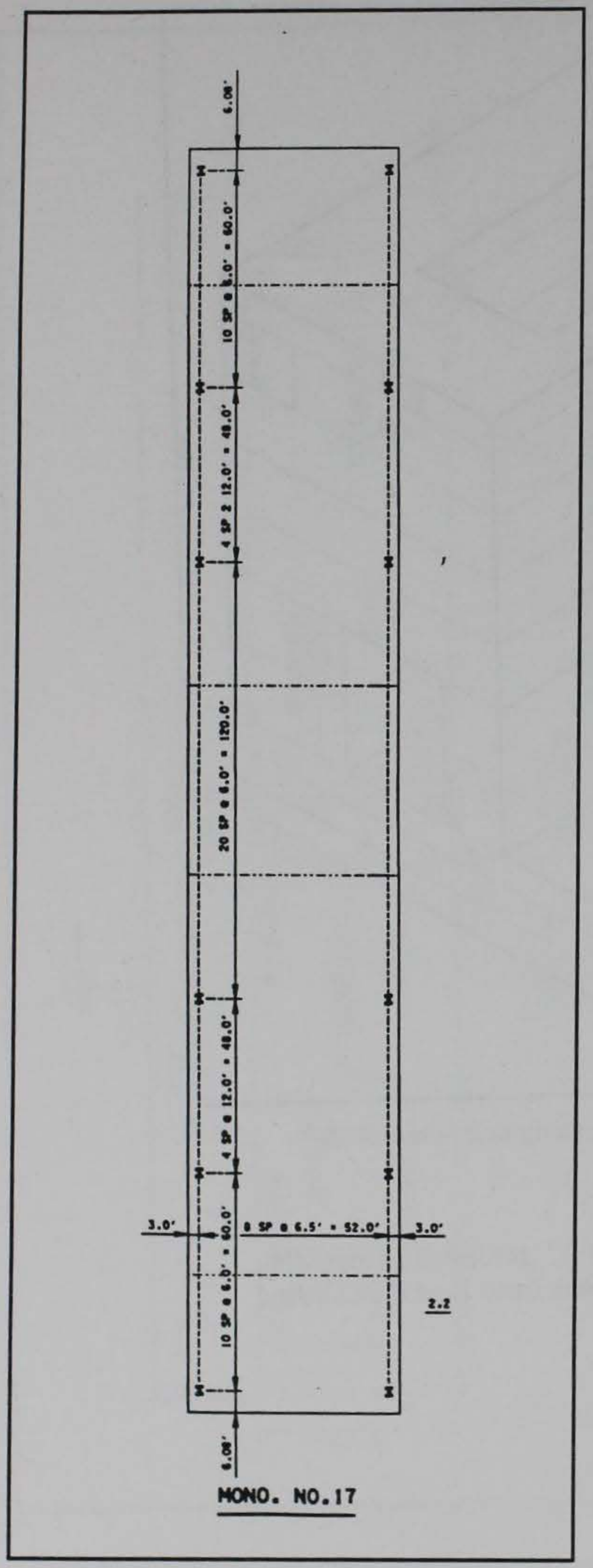

Figure 4. Plan view showing pile spacing for monolith 17

Mesh Selection

The mesh for modeling the wall of monolith 17 in Analysis 1 required 3,600 three-dimensional elements. An additional 2,415 three-dimensional elements were required to model the foundation for the heat transfer analysis, and 830 spring elements were needed to model the foundation for the stress analysis. Figure 5 is an isometric view of the 3-D FE mesh including the soil elements. A fully insulated boundary condition was applied for the heat transfer analysis at the face of the slab where it is cut.

The refinement of the mesh shown in Figure 5 is more coarse than typically seen in 2-D analyses. Due to the fact a 3-D analysis requires significantly more computational capacity than a 2-D analysis, it becomes necessary to reduce the number of elements used. The mesh uses at least two vertical layers of elements in every lift which is consistent with guidance contained in ETL 1110-2-324 (HQDOA 1990). It was necessary though to exceed criteria for element size given in ETL 1110-2-324 to keep the mesh to a manageable size and a size which would not exceed computational capacity available. Based on results of parametric studies performed during the course of the NISA study of the lower miter gate monolith (Fehl et al. in preparation), a decision was made that a time-step of 12 hr could be used in the first 2 days of each lift in the heat transfer analysis without significantly affecting the resulting temperatures. This directly affects the size of element which is allowed by the numerical stability criteria specified in ETL 1110-2-324, since time is a function of how large elements can be and a larger time-step will result in being able to use a larger element. Also, in the same parametric study, it was shown that the numerical stability criteria may be exceeded to some extent and results

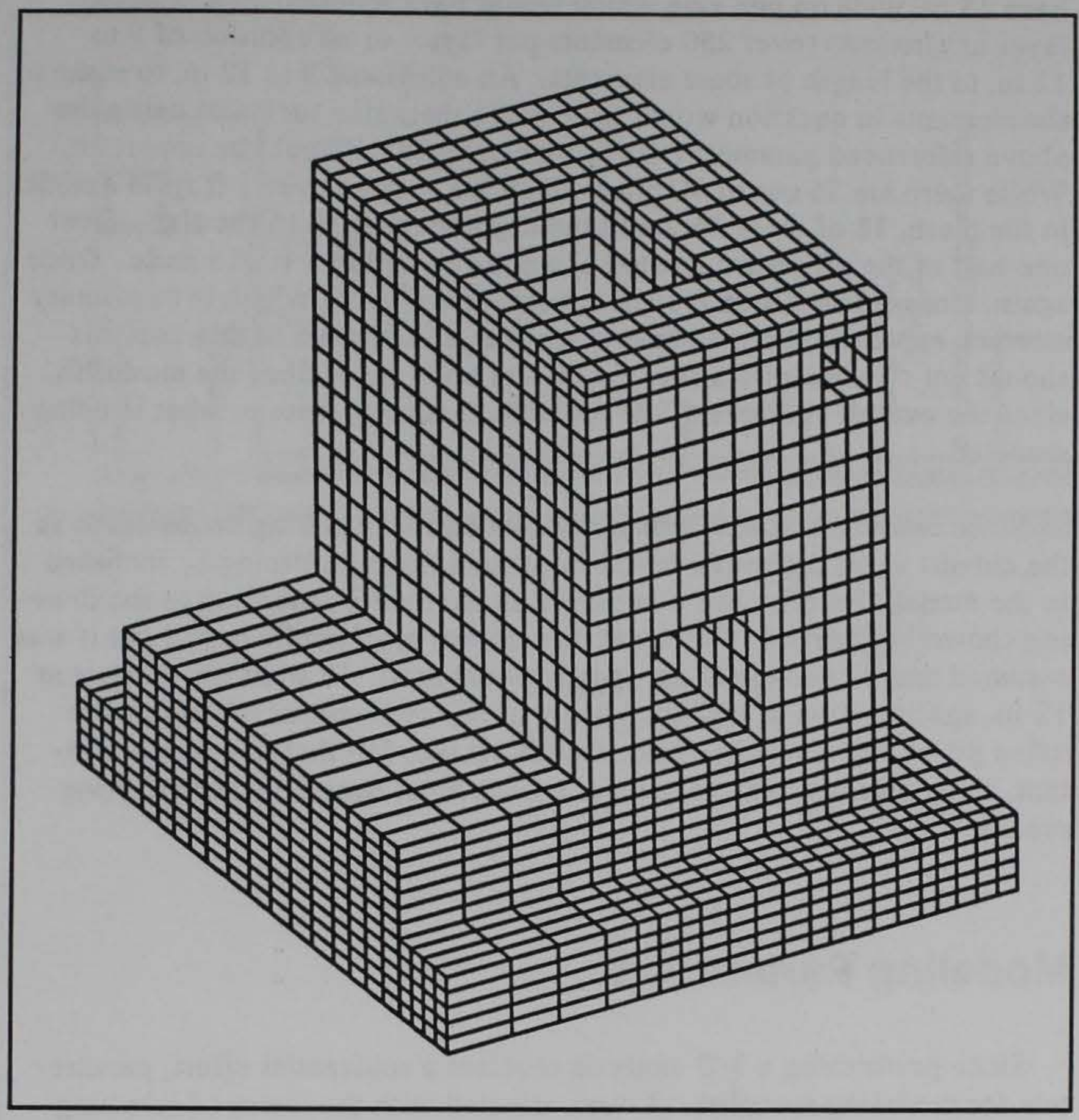

Figure 5. Isometric of the FE mesh used for monolith 17 including soil elements used in the heat transfer analysis

will not change dramatically. Based on the results of these two parametric studies, some elements in the wall exceeded 4 ft in length, but in general were limited to 2-½ to 4 ft in length. In the chamber portion of the slab near the boundary, the criteria is exceeded by a significant amount, but it is in a direction perpendicular to heat flow which has been shown to not largely impact final results (Truman, Petruska, and Ferhi 1992).

Typically the FE mesh is adapted so that a node is located wherever a pile is to be driven so that a spring element may be attached to the node to model the pile. Because the geometry of the structure did not match well with the pile layout, an exception to normal modeling techniques had to be made to keep the mesh relatively uniform and to avoid increasing the number of elements. It was determined that development of the mesh around the geometry of the culvert valve pit was of greater importance than ensuring that nodes were located at each pile location. If the normal modeling procedure had been followed, some elements would have had to

been 15 in. wide on one side which would have required an additional layer of elements (over 250 elements per layer) or an addition of 9 to 12 in. to the length of some elements. An additional 9 to 12 in. to some of the elements in question would have made their size such that using the above referenced parametric study on element size would be uncertain. While there are 36 out of 90 piles which are located over 1 ft from a node in the mesh, 18 of these 36 are in the chamber portion of the slab. Over one-half of the piling are located at a node or within 1 ft of a node. Once again, since it is the area around the culvert valve pit which is of primary interest, approximations such as the piling offsets used in this analysis should not significantly affect the results up in the wall of the monolith, since the overall stiffness of the foundation is very close to what is being modeled.

Since there is a relatively high likelihood that cracking could occur in the culvert valve monolith, it was important that reinforcing be included in the model. Reinforcing was placed in the model according to the drawing shown in Figure 6. For areas that are not specifically called out it was assumed that #9 bars at 12-in. spacing were used. In addition, #9 bars at 12-in. spacing were placed diagonally at the each corner of the culvert valve pit for the entire height of the pit. It was felt that this was important, since diagonal bars at corners are the most beneficial for arresting cracks.

Modeling Parameters

Since performing a 3-D analysis requires a substantial effort, parameters for modeling monolith 17 were selected with the intent of selecting conditions which would produce the worst case while still capturing actual construction procedures. Many parameters selected were based on previous parametric studies performed in 2-D on the typical chamber monolith (Garner et al. 1992 and Merrill, Fehl, and Garner in preparation).

A beginning construction date of September 1 was selected. This start date was chosen so that the monolith would be fully constructed prior to the coldest winter months but would still be maturing to its full strength when the colder winter temperatures began. To achieve this objective, construction of the monolith in 5-day lift intervals was required. The structure was analyzed for 360 days after placement of the initial lift and then the service loads were applied instantaneously. The service loads applied were simply water pressure in the chamber based on upper pool in the chamber at el 300, lower pool on the outside of the monolith at el 285, and an uplift pressure on the base of the structure based on a water el 306. Appropriate pressures were placed in the culvert and valve pit as well. The load also included loads to simulate the bearing pressure applied to culvert valve support system.

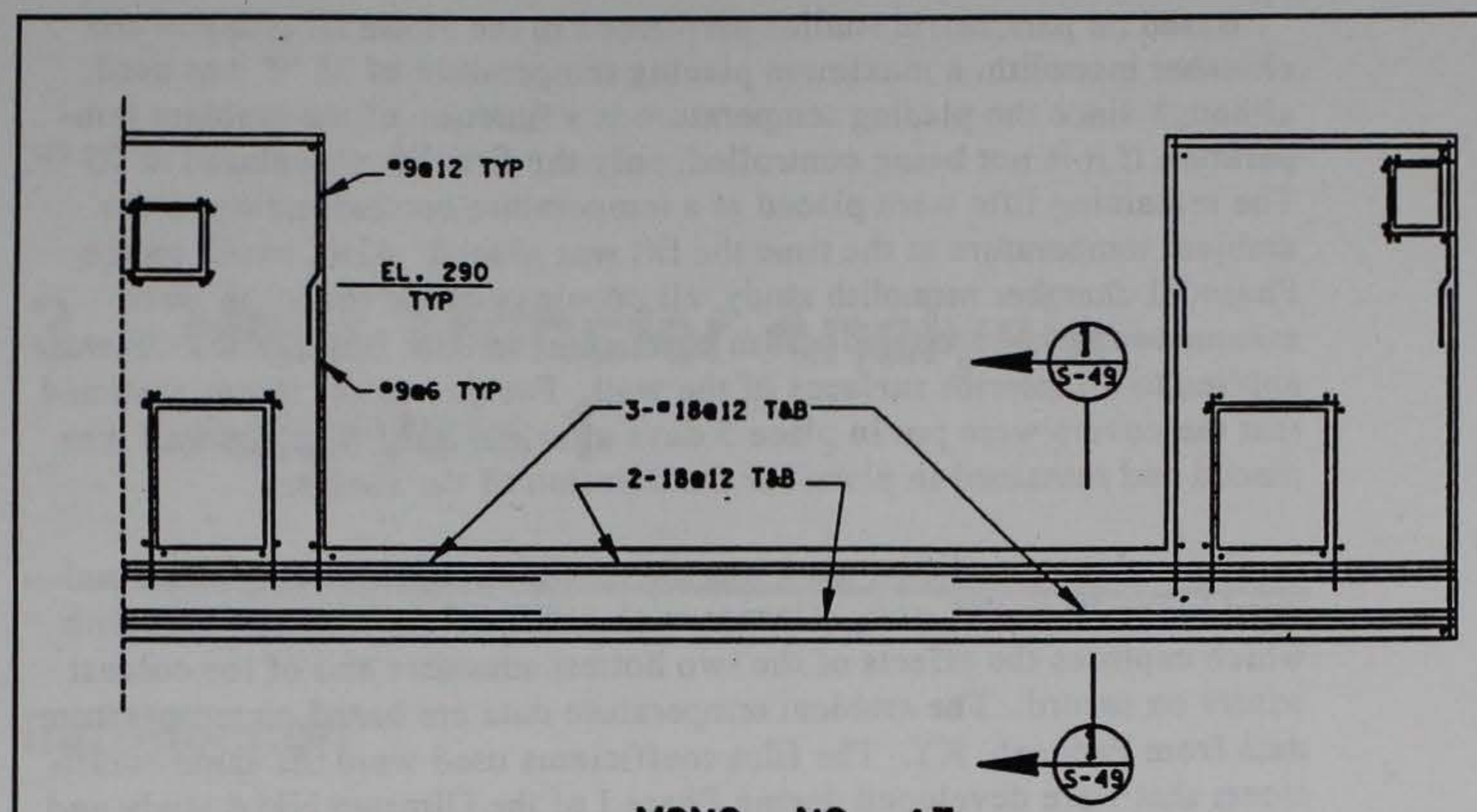

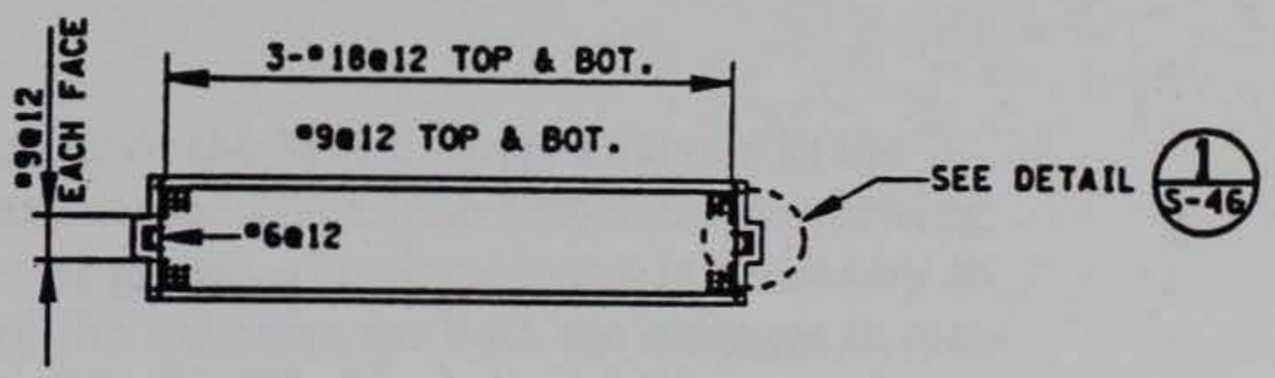

Figure 6. Reinforcing layout for monolith 17

Based on parametric studies performed in the Phase III study of the chamber monolith, a maximum placing temperature of 75 °F was used, although since the placing temperature is a function of the ambient temperature if it is not being controlled, only the first lift was placed at 75 °F. The remaining lifts were placed at a temperature corresponding to the ambient temperature at the time the lift was placed. Also, based on the Phase III chamber monolith study, all openings of the monolith were assumed to be covered and a film coefficient of 0.01 Btu/day-in.^{2}-°F was applied to all interior surfaces of the wall. For this study, it was assumed that the covers were put in place 5 days after the last lift of the wall was placed and remained in place for the duration of the analysis.

The ambient condition used was the extreme ambient condition developed in the Phase III study (Garner et al. 1992) of the chamber monolith which captures the effects of the two hottest summers and of the coldest winter on record. The ambient temperature data are based on temperature data from Paducah, KY. The film coefficients used were the same coefficients that were developed during Phase I of the Olmsted NISA study and can be found in Part III of Volume I of the report on that study (Garner et al. 1992).

Finally, the concrete material was based on mixture 11 as specified in the material's study performed for the Olmsted project (Hammons et al. 1991). The actual properties were altered to agree with load case 5 as discussed in the report on the Phase II studies (Garner et al. 1992) which increases shrinkage by 10 percent and decreases creep by 10 percent.

3 Heat Transfer Analysis - Analysis 1

Introduction

Prior to performing the stress analysis in a NISA, a heat transfer analysis must be performed so that temperatures may be obtained for use in the stress analysis. The heat transfer analysis for monolith 17 assumed a start date of September 1. Most heat transfer analyses for NISA's are begun with a start time some time in the summer months so that the maximum temperature may be obtained. In this case though, it was felt that placing the concrete just before the start of the cold winter months would provide the critical case.

No insulation was required for this analysis since all of the concrete had been placed prior to the required dates for insulation. As mentioned in Chapter 2, all openings to the gallery, culvert, and the culvert valve pit were assumed to be closed 5 days after the placement of lift 11. This condition has a significant effect on both the heat transfer results as well as the stress results.

This chapter will present results of the heat transfer analysis in the form of temperature contours and temperature time-histories. Reviewing results from both of these types of graphical presentations is necessary to fully understand the behavior of the structure for both the changes in temperatures and the changes in the structural behavior once the stress analysis is performed.

Time-History Plots

Time-histories of the temperatures are presented at several locations throughout the monolith in Figures 7 through 19. A key is presented with each figure to show its approximate location. Points presented are distributed along each given line at as even a spacing as allowed by the nodal

locations. Only in Figures 17 through 19 are all points along a given line plotted and at no other sections are any of the surface nodes plotted.

Figure 7 is a plot of a line through the chamber side culvert wall. Node 36122 is the node nearest the chamber. Node 36458 is located near the surface to the culvert and follows the behavior of node 36122 until day 55 when the openings are closed, and then it makes a jump and more closely follows the behavior of node 36146. As was seen in the contour plots, very little difference in temperature exists through the chamber side wall and this is confirmed in Figure 7 by the close proximity of the three lines to each other.

Figure 8 is the landside culvert wall. Again, prior to day 55, the two outside nodes (node 36720 and node 37738) behave similarly, but after closing the openings, node 36720 begins to behave more like an interior node. The addition of the covers to the openings is obvious in the figure when observing the behavior of node 36720 and a change can also be seen in the behavior of node 37030. The main observation is that, throughout the analysis, the temperature remains nearly uniform over half the distance from the culvert wall and that a steep gradient exists at the outside surface of the wall.

Figure 9 displays a different kind of behavior than the first two figures because there are no insulating effects on this section, and the time-histories look like temperature time-histories from other structures where NISA's have been performed. The gradient throughout the slab thickness appears to remain uniform throughout the analysis.

The plots shown in Figures 10 and 11 are almost exactly the same as the plots shown in Figures 7 and 8, because they are taken at the same location in the culvert walls except farther downstream (DS). The difference is minimal because the effects of the downstream surface of the monolith are negligible in sections 4 and 5.

Figure 12 is a plot of nodes through the slab thickness directly below the culvert. If Figure 12 is compared to Figure 9, the plots are identical for the first 55 days, but once the openings are covered the gradient of temperatures is greatly reduced in Figure 12. While the covered openings appear to create a high gradient of temperature in the landside culvert wall, it appears to be very beneficial in reducing the gradient for the slab.

Figures 13 and 14 are lines of nodes through the upstream (US) portion and downstream portion of the monolith, respectively. While the magnitudes are slightly different, the performance at these two locations is similar. Once again, as in the culvert landside wall, after the openings are covered the temperature remains nearly uniform for a significant portion of the section, and then a steep gradient near the exposed surface can be seen.

Sections through the chamber side and landside walls of the culvert valve pit are shown in Figures 15 and 16. The trends and behavior of these two sections are very similar to that seen in the sections through the culvert walls except that the gradients across the sections are not as large since the wall thicknesses are less at these locations.

Finally, three sections through the top of the gallery are shown in Figures 17 through 19. All three sections look very similar although the gradient in Figure 19 is larger than the gradient in the other two figures. This can be attributed to the fact that section 3g is in the thick portion of the downstream end and allows the concrete to retain the warm temperatures longer in the winter and the cool temperatures longer in the summer.

In all of the time-histories it should be noted that somewhere between 150 days and 250 days the gradients across any given section reversed due to the change in the season. Of the sections presented, only section 3 was not affected by the covering of the openings. The significance of this is that the reversed gradient which occurred in section 3 was noticeably less at its peak in the summer when compared with its winter counterpart, but this is not necessarily the case for the sections affected by the covering of the openings. Covering the openings seems to help moderate temperatures in the winter months but may have an adverse affect in the summer by keeping the interior portion of the structure too cool.

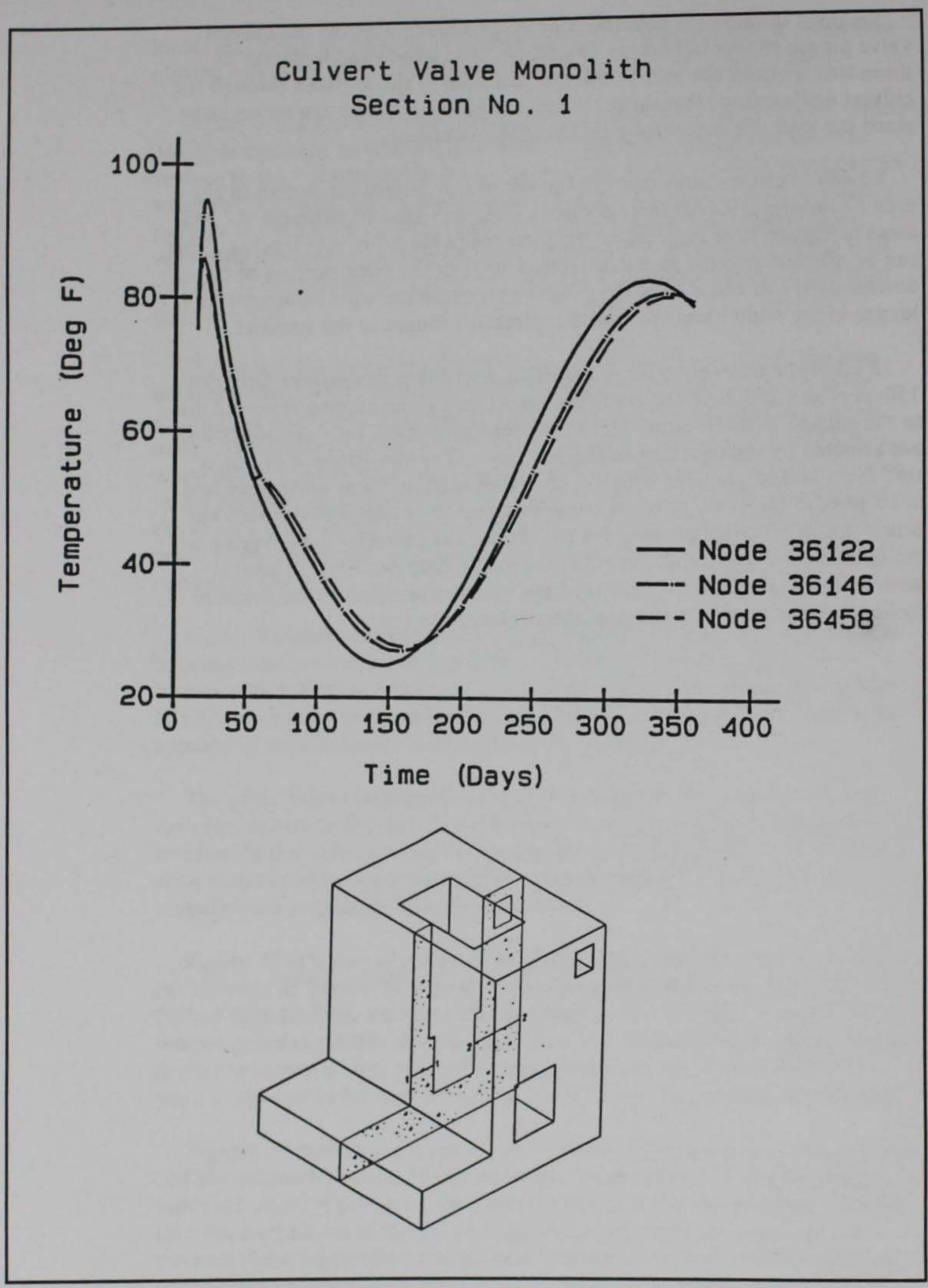

Figure 7. Temperature time-history at section 1

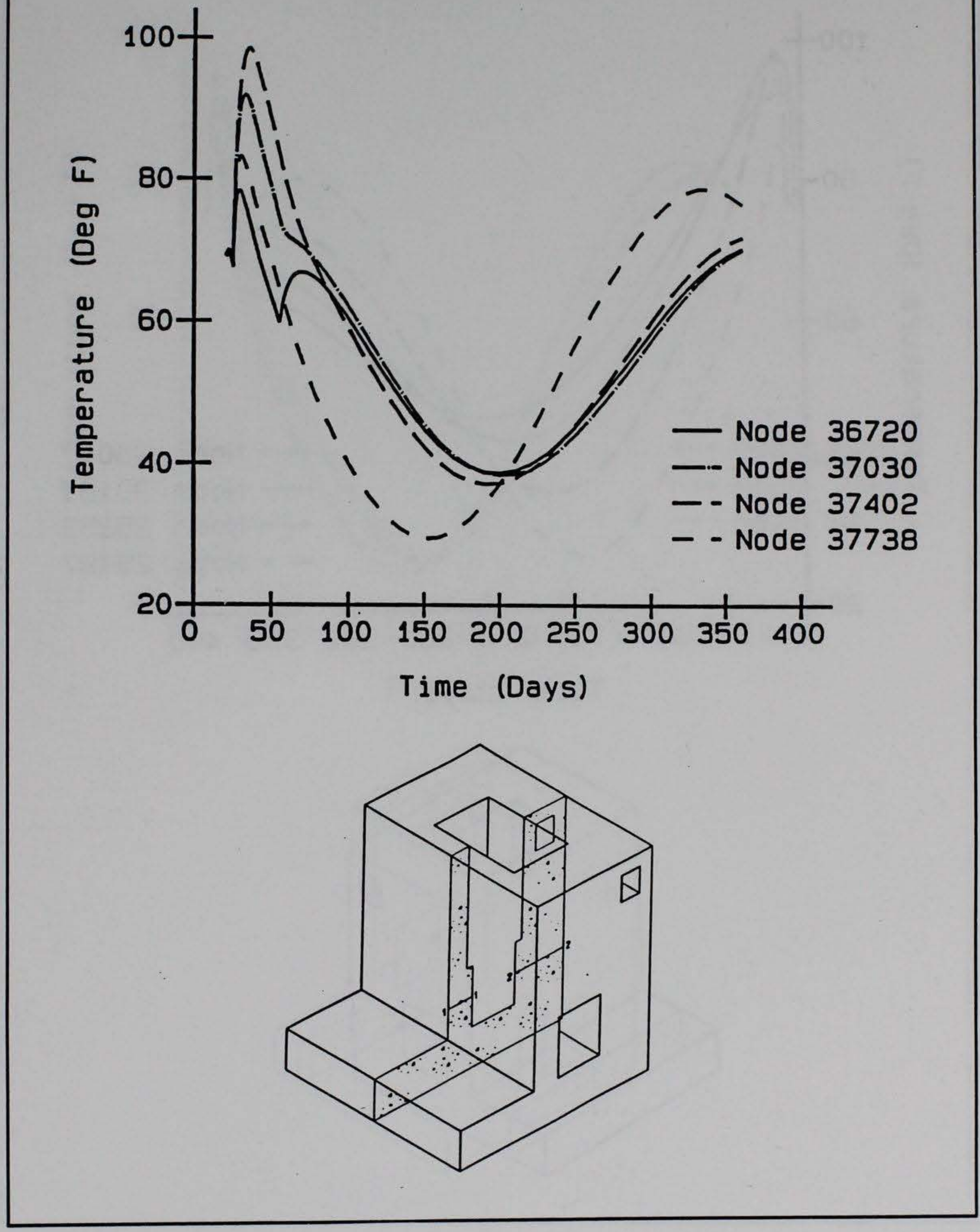

Figure 8. Temperature time-history at section 2

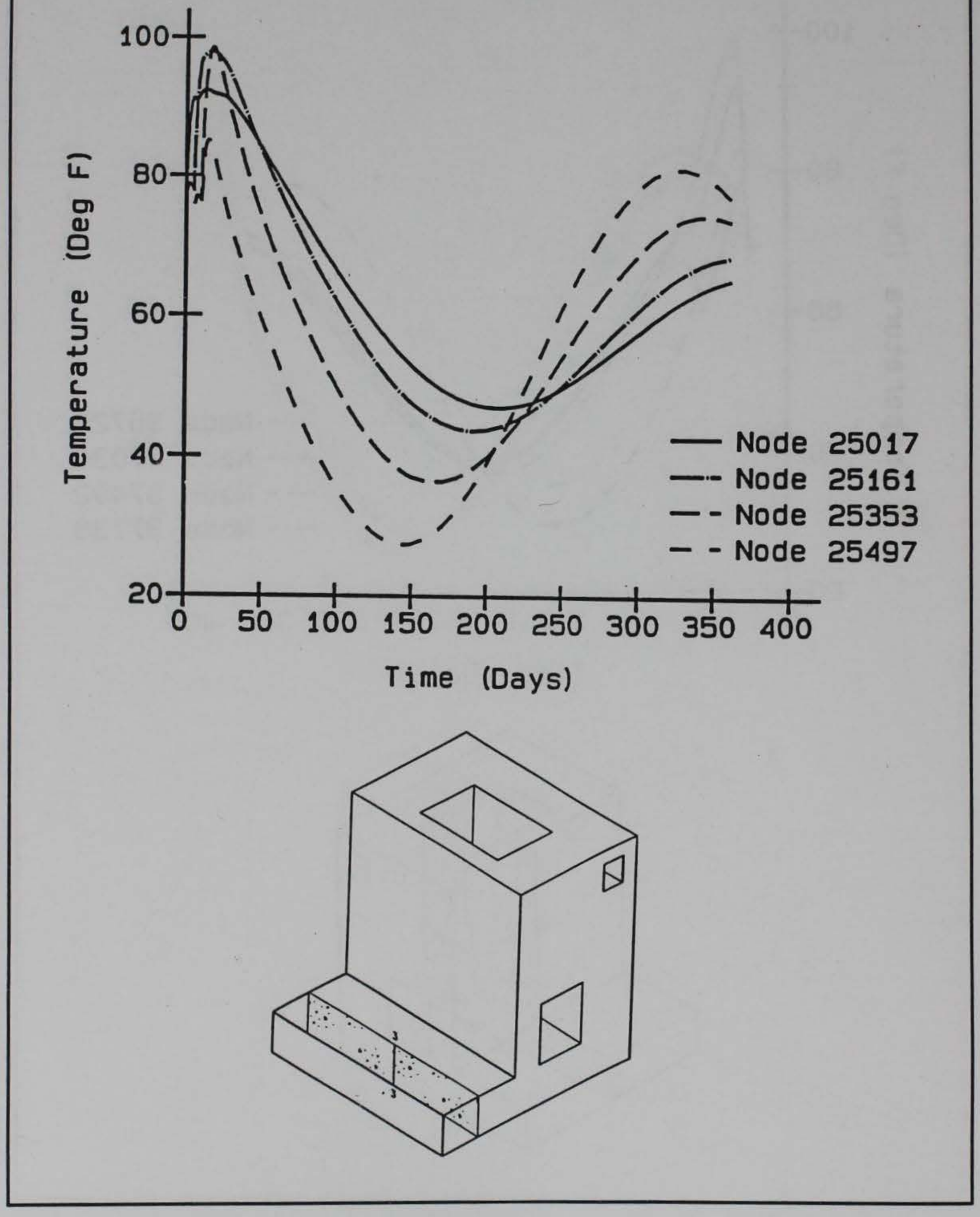

Figure 9. Temperature time-history at section 3

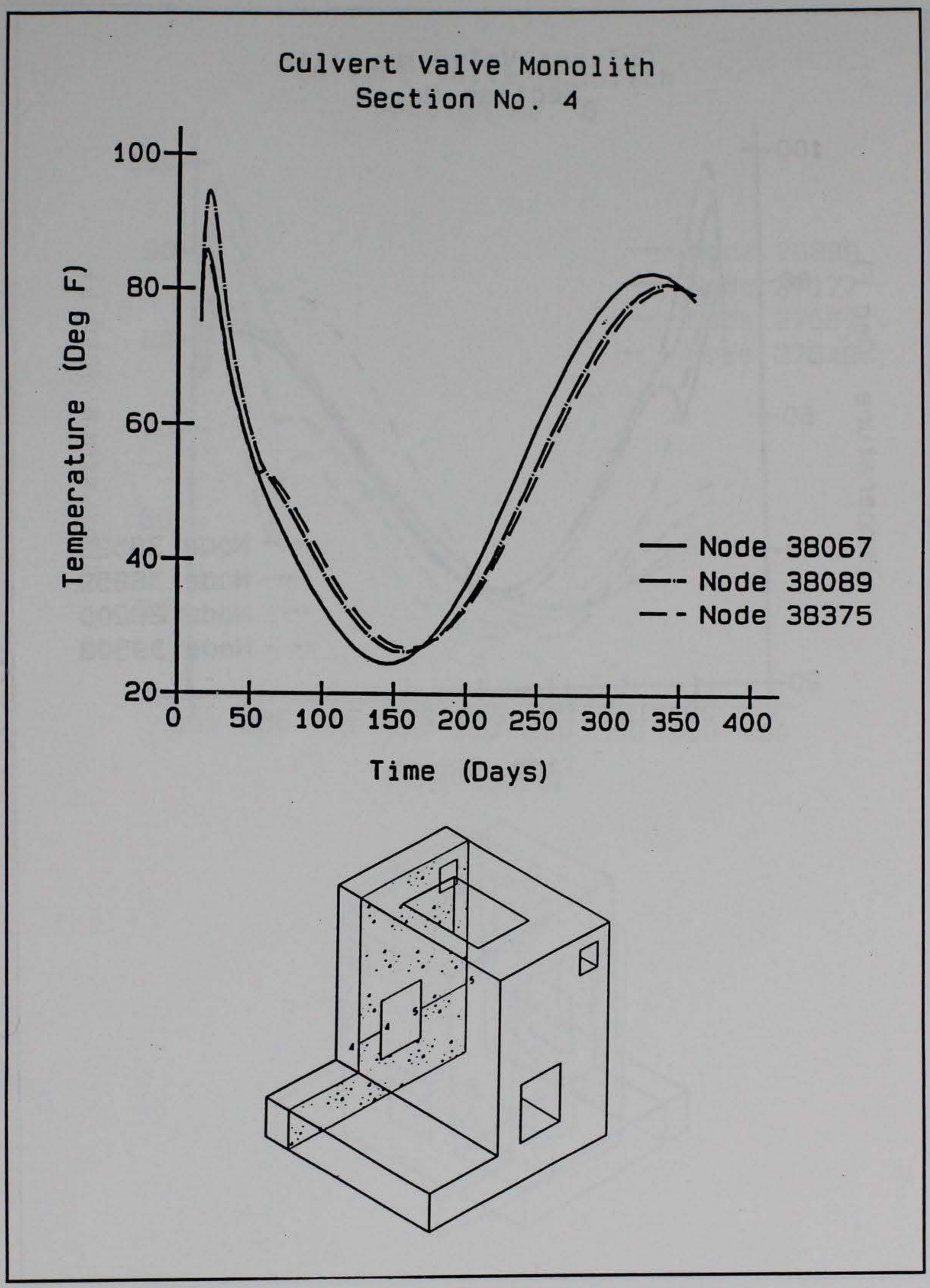

Figure 10. Temperature time-history at **section 4**

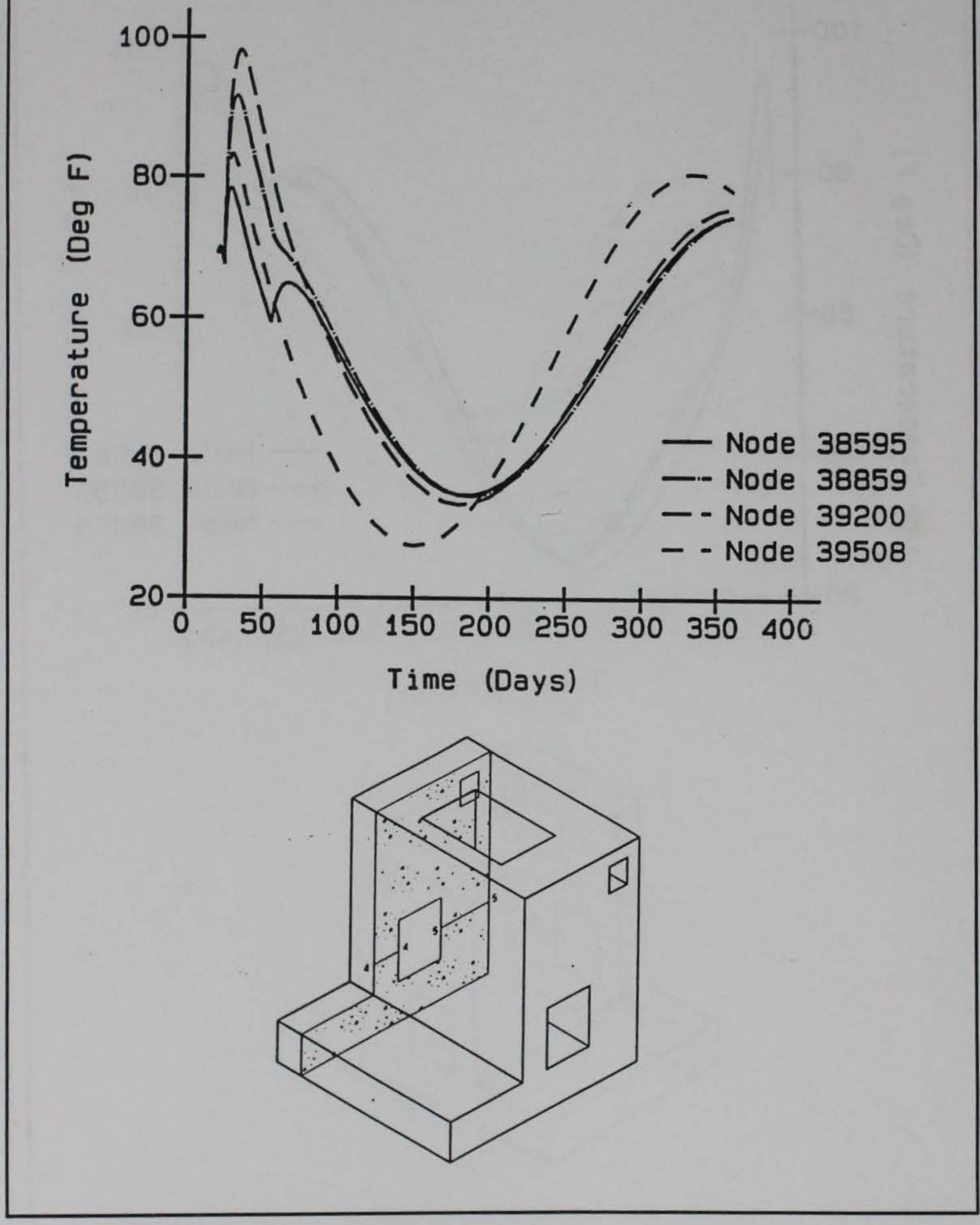

Figure 11. Temperature time-history at section 5

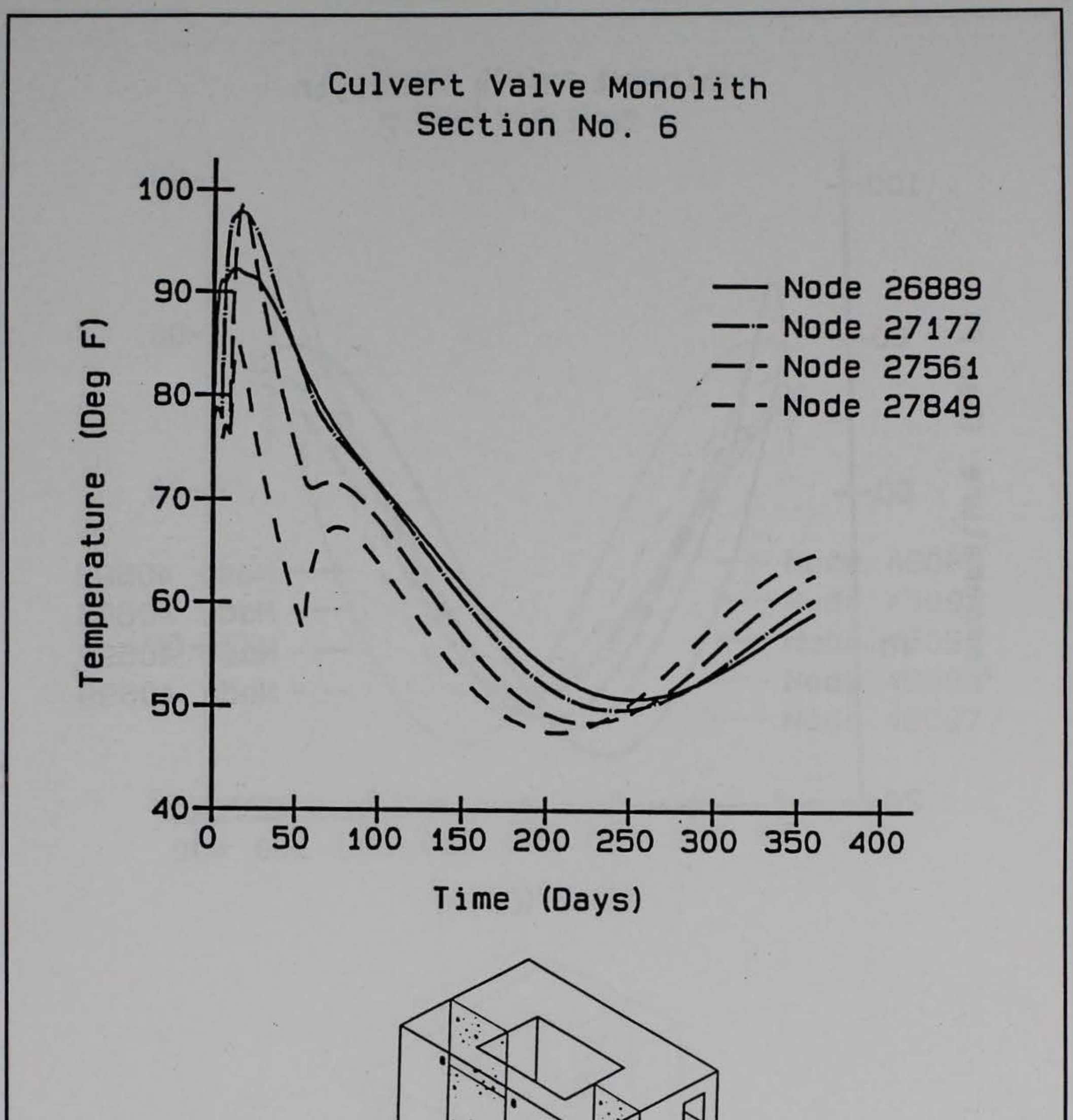

Figure 12. Temperature time-history at section 6

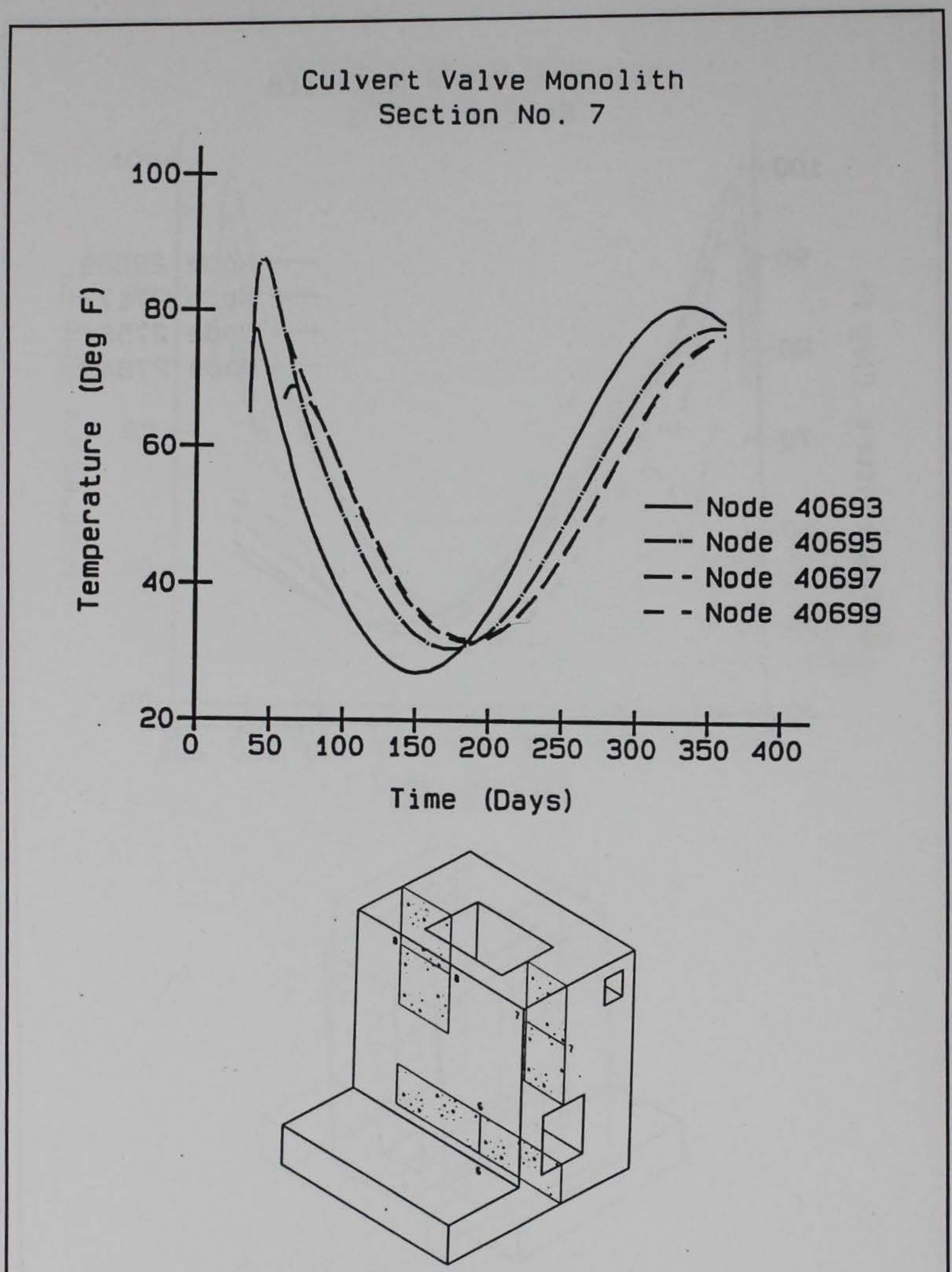

Figure 13. Temperature time-history at section 7

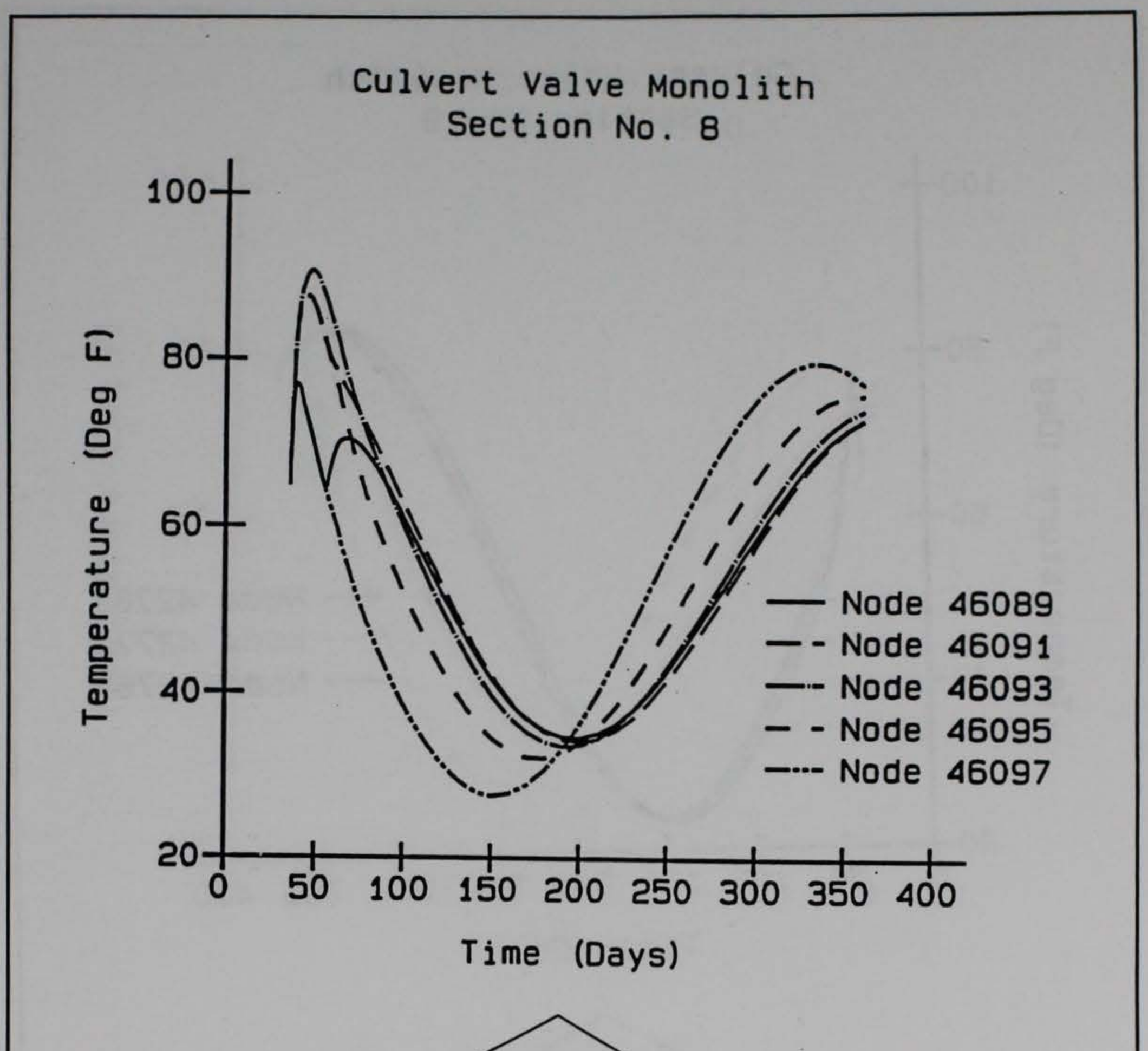

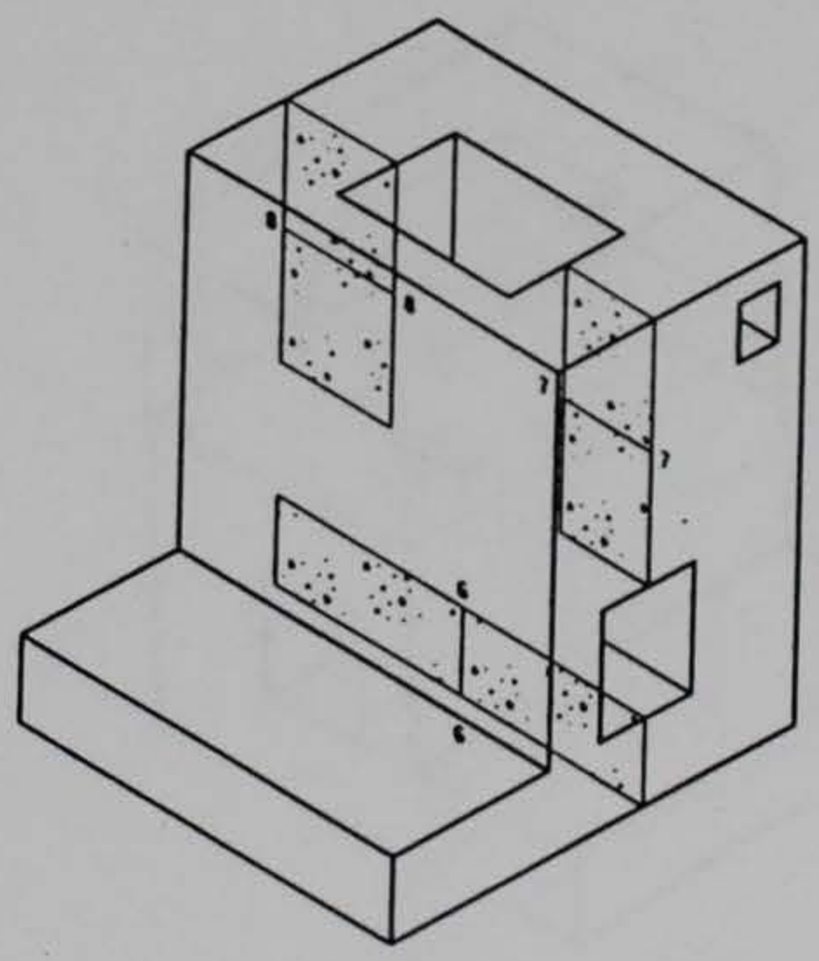

Figure 14. Temperature time-history at section 8

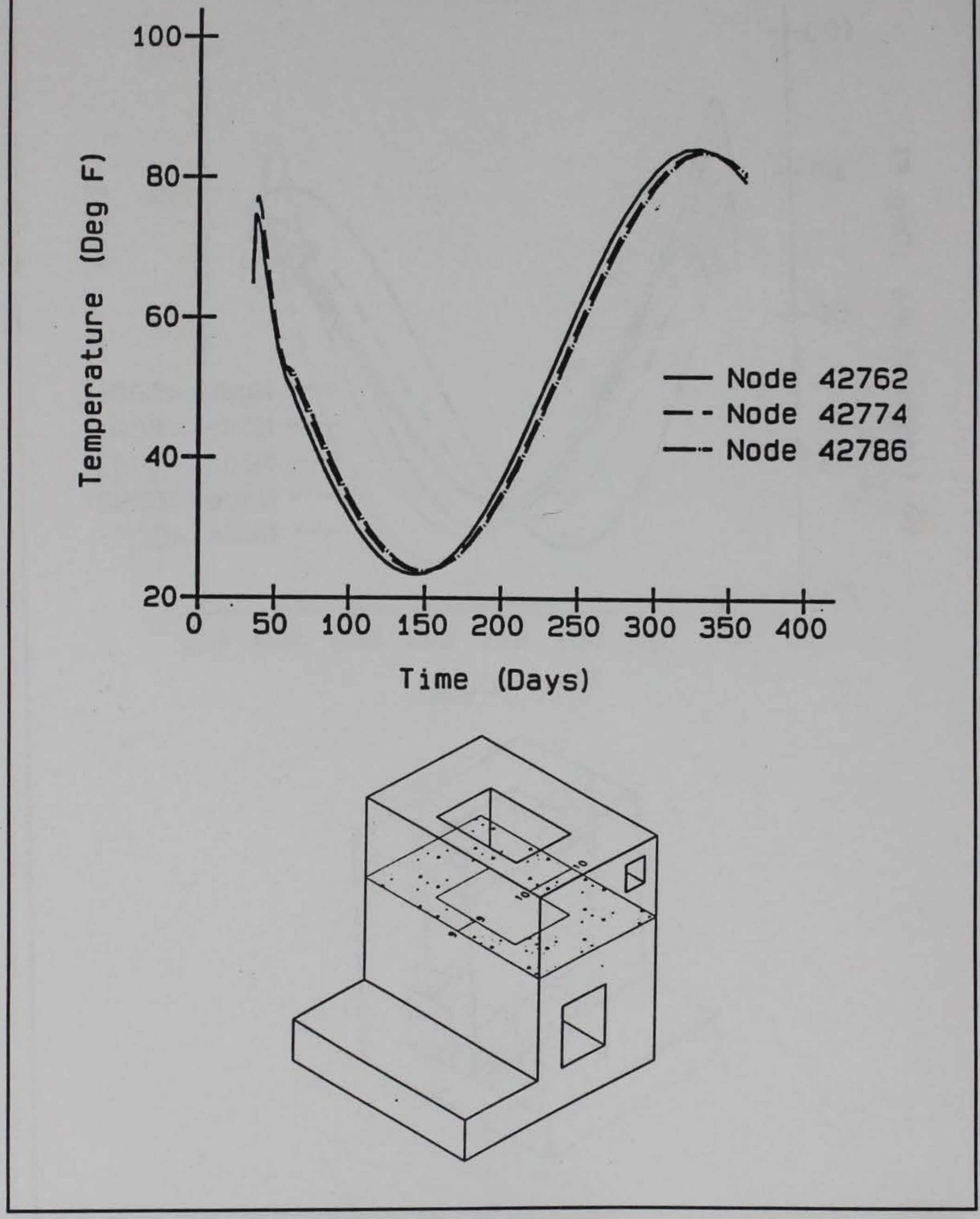

Figure 15. Temperature time-history at section 9

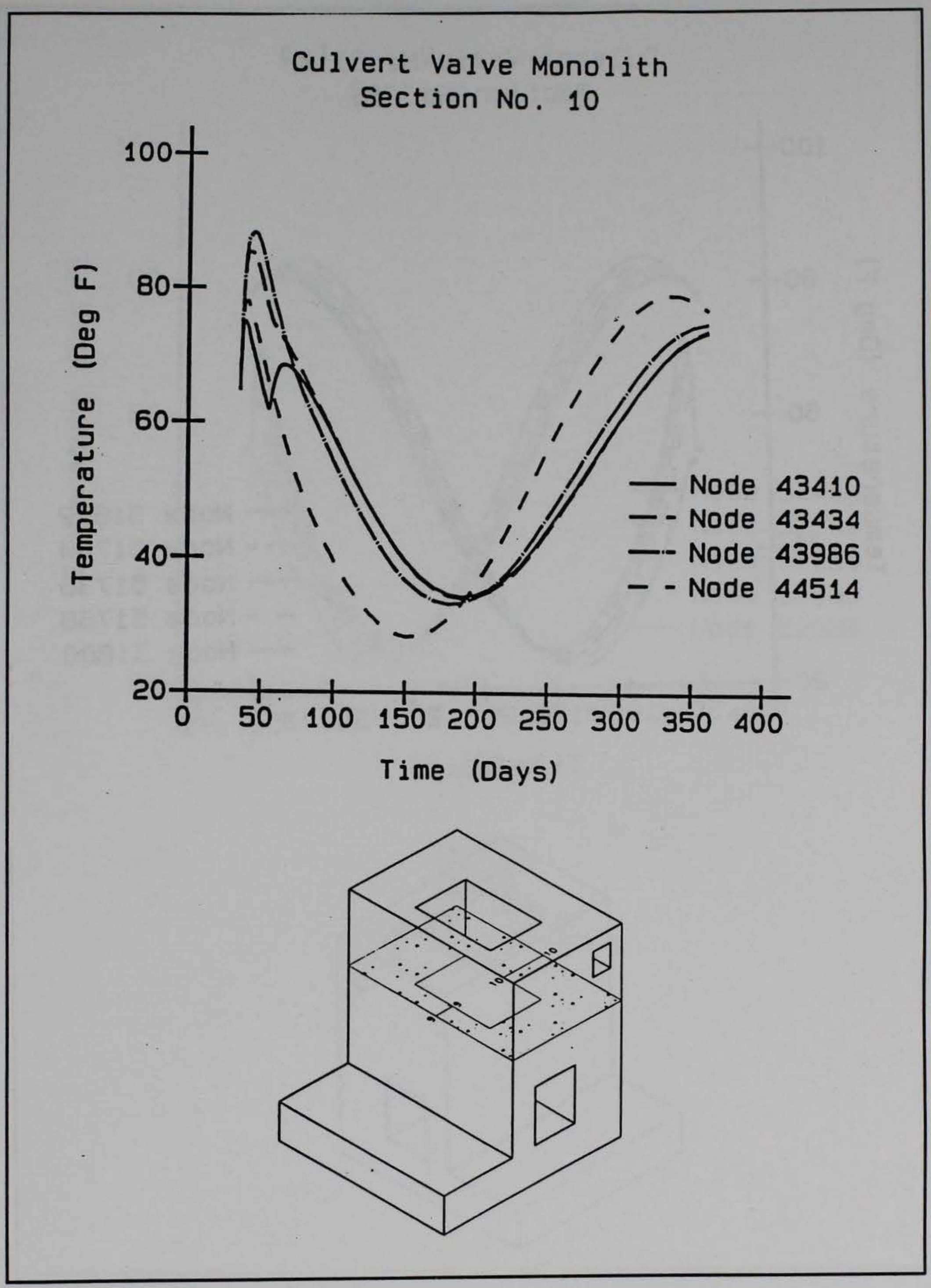

Figure 16. Temperature time-history at section 10

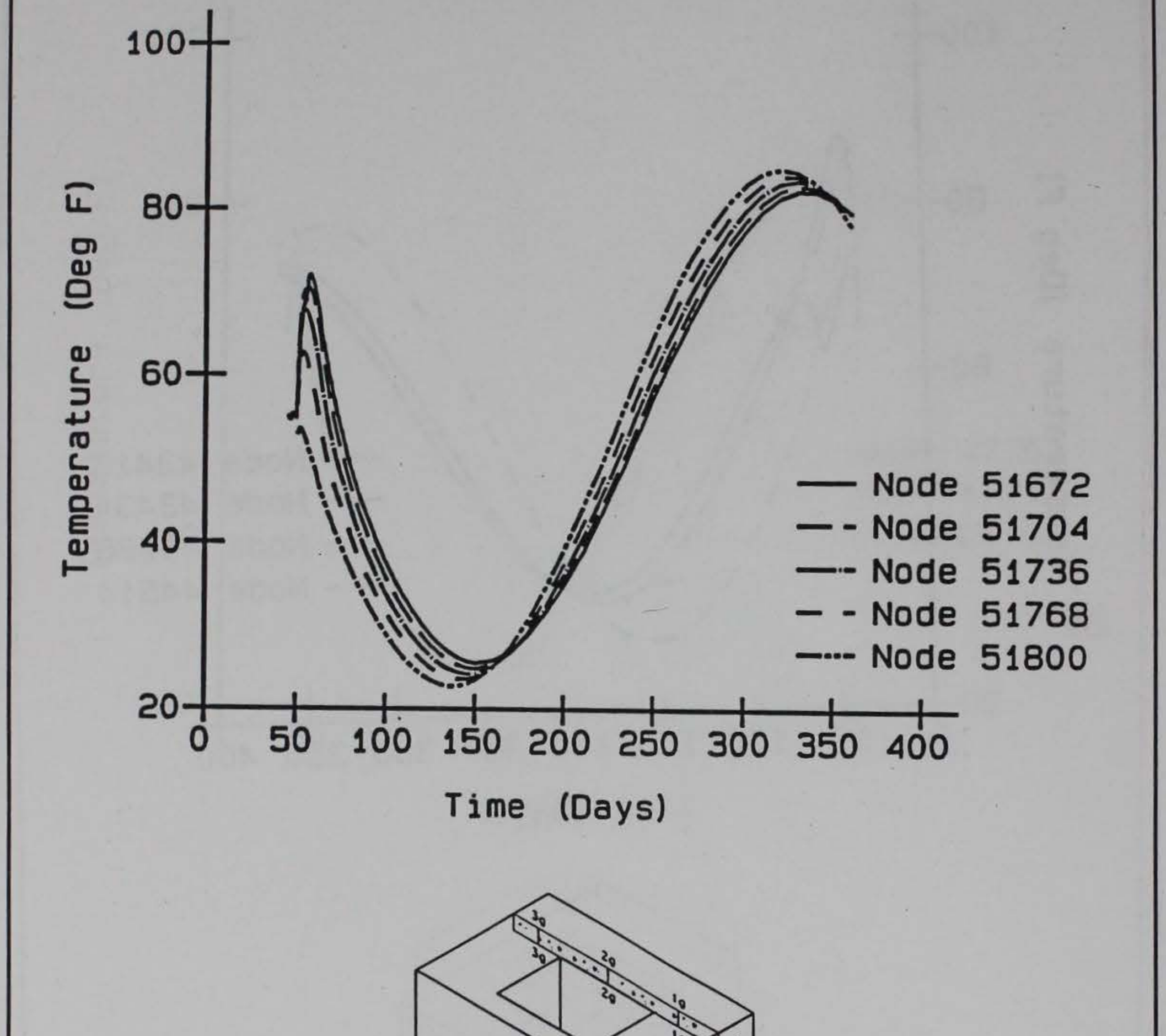

Figure 17. Temperature time-history at section 1g

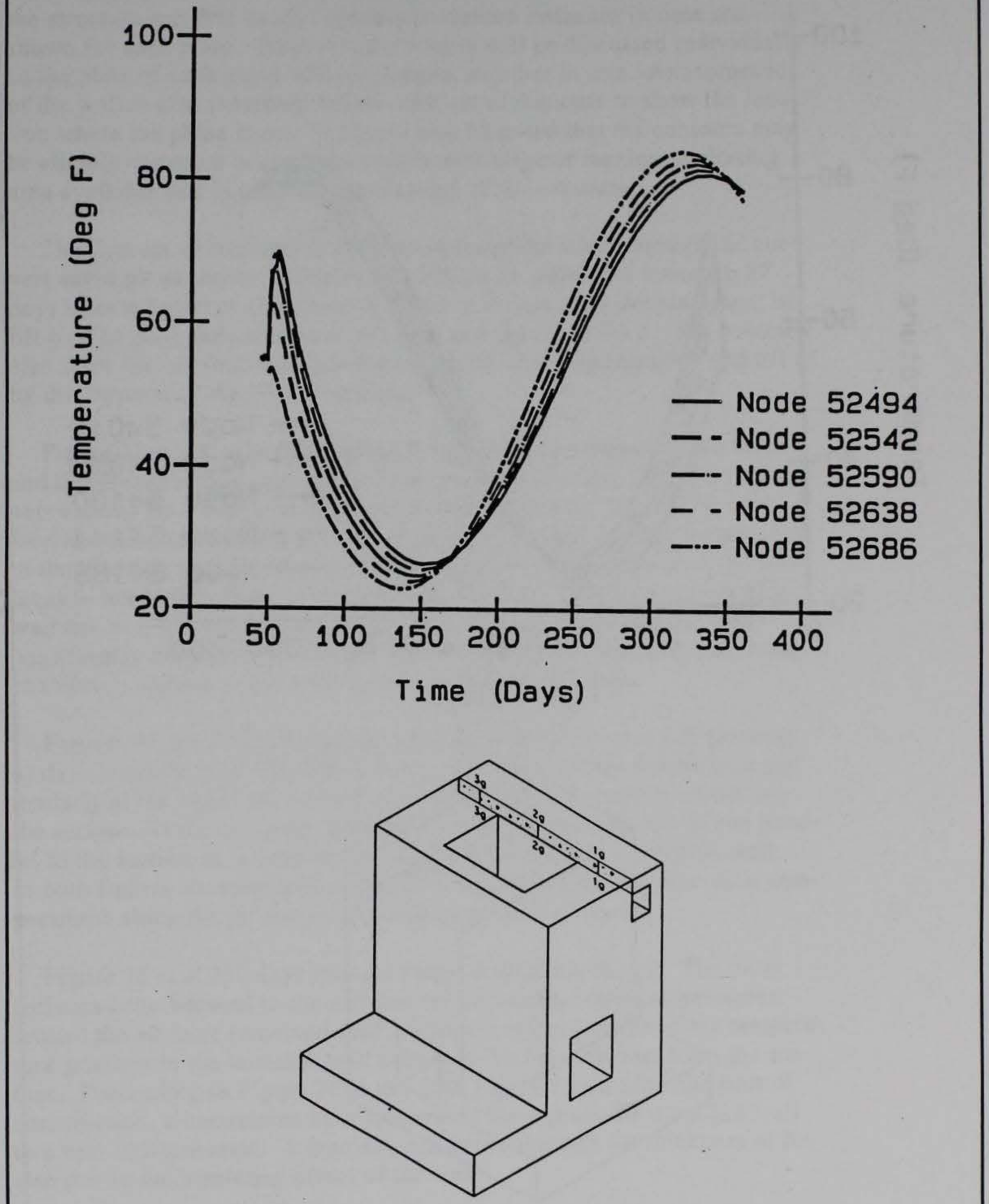

Figure 18. Temperature time-history at section 2g

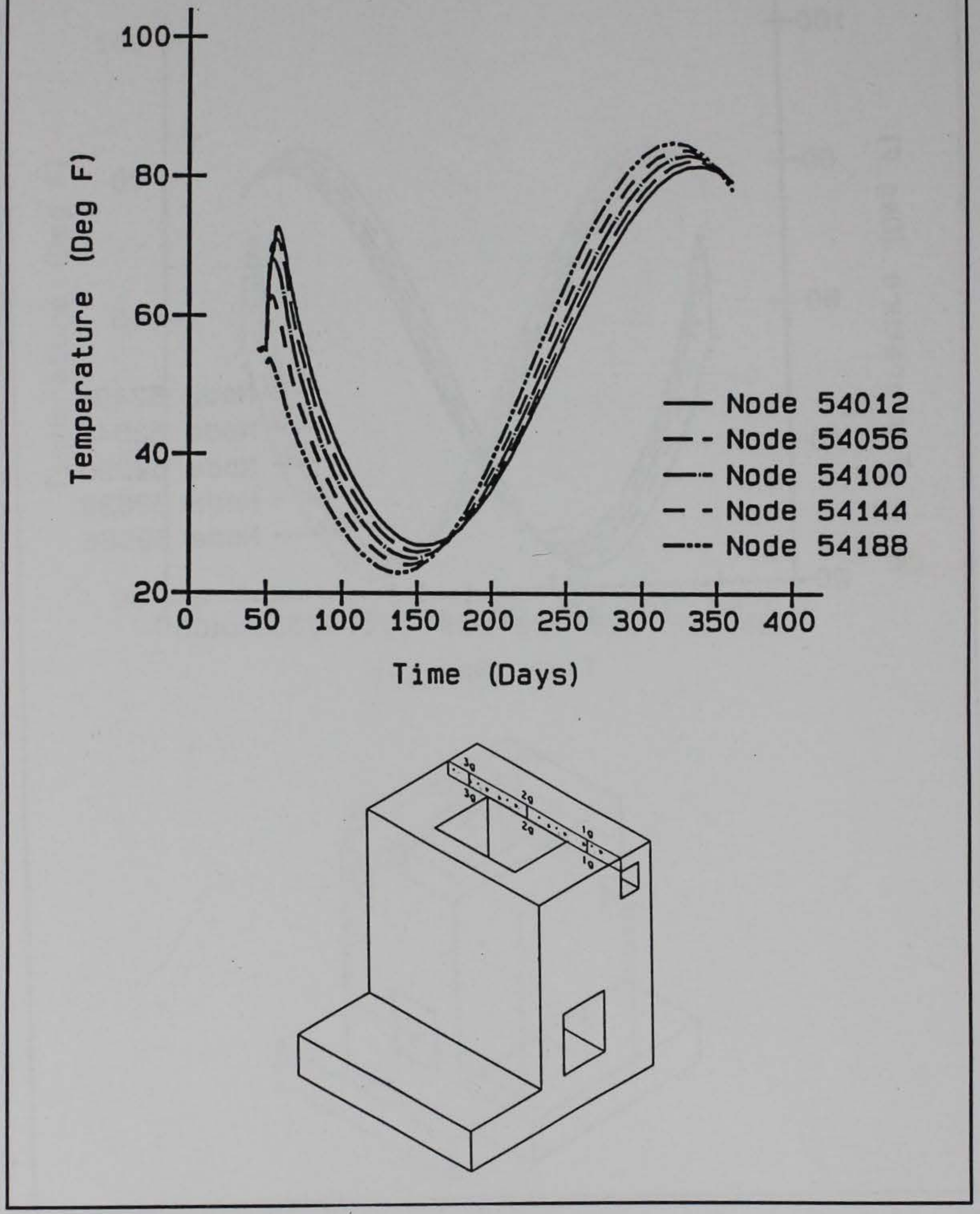

Figure 19. Temperature time-history at section 3g

Temperature Contours

Temperature contours are presented at five different planes cut through the structure and five or six contours at various instances in time are shown for each plane. Each set of contours will be discussed individually so the plots of each plane will be grouped together in sets. An isometric of the wall is also presented before each set of contours to show the location where the plane is cut. It should also be noted that the contours may be slightly distorted in an effort to take advantage of maximum plotting area available and to enhance the viewing of the contours.

The first set of contours is at a transverse plane taken through the culvert valve pit as shown in Figure 20. Figure 21 shows the monolith 27 days after the start of construction which is 2 days after the placement of lift 6. The peak temperature is 101.8 °F and occurs in lift 5. The contours also show the approximate location of the lift line between lift 5 and lift 6 by the location of the 86.5 °F contour.

Figure 22 is a plot of this section 2 days after completion of the wall and therefore the openings in the monolith have not been closed on the culvert and the pit. The peak temperature occurs near the lift 5/lift 6 interface and is approximately 86.6 °F. It should be noted that the temperature in the landside wall (right side of figure) goes from being cool at the surfaces to hot at the center of the wall. At the same time the chamber side wall has nearly a uniform temperature except near the top where concrete has recently been placed. Finally, the gradient across the base slab in the chamber is similar to what has been seen in other NISA's.

Figures 23 and 24 are contours at 90 (November 30) and 125 (January 4) days, respectively. The effects of the closed openings can be seen particularly at the top of the culvert valve pit where the contours curve into the surface. If the openings were not closed, the contours would run parallel to the surface as is seen on the exposed surface of the landside wall. In both figures the temperatures at the surface are near ambient while temperatures along the pit and culvert stay relatively warm.

Figure 25 is at 250 days into the analysis which is May 9. The outer surfaces have warmed to the ambient temperatures, while temperatures around the pit have remained cool. Also, the major portion of the temperature gradient in the landside wall occurs in the first few feet from the surface. Proceeding to Figure 26 at day 360, nearly 1 year after the start of construction, temperatures have moderated throughout the monolith wall to a near uniform state. A gradient still exists through the thickness of the slab due to the insulating effect of the soil.

Figure 27 shows a longitudinal section through the base slab. Figure 28 is a temperature contour at this section 20 days after the start of the construction or 10 days after the placement of lift 3. The maximum temperature was 99.0 °F near the center of the slab, and a gradient exists from

the center to both top and bottom of the slab. Figures 29 through 32 all show nearly constant gradients for at least the middle half of the slab. Although the figures all look very similar, the gradients seen in Figures 29 through 31 are gradients from warm temperatures at the bottom to cool temperatures at the top while Figure 32 is a gradient of cool temperatures at the bottom to hot temperatures at the top. This is of course due to the changing seasons. The maximum gradient in the winter is approximately 37 °F while the gradient at day 250 shown in Figure 32 is only about 17 °F. Finally, at day 360 as shown in Figure 33, the gradient is not as constant as the other figures and the gradient is less than 15 °F. This is primarily due to the fact that the ambient temperatures are beginning to drop and the gradient will again reverse.

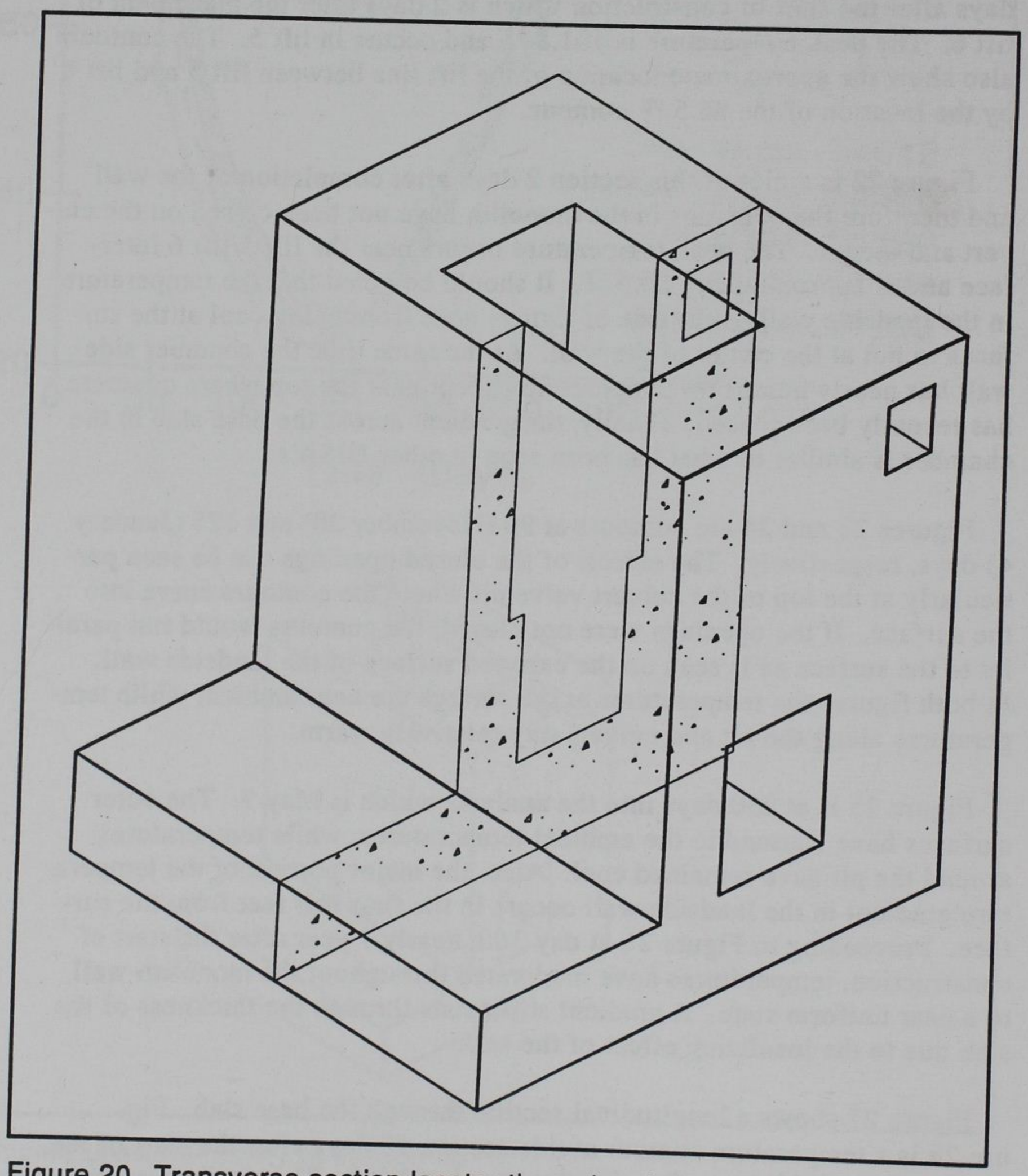

Figure 20. Transverse section locator through culvert valve pit for Figures 21 through 26

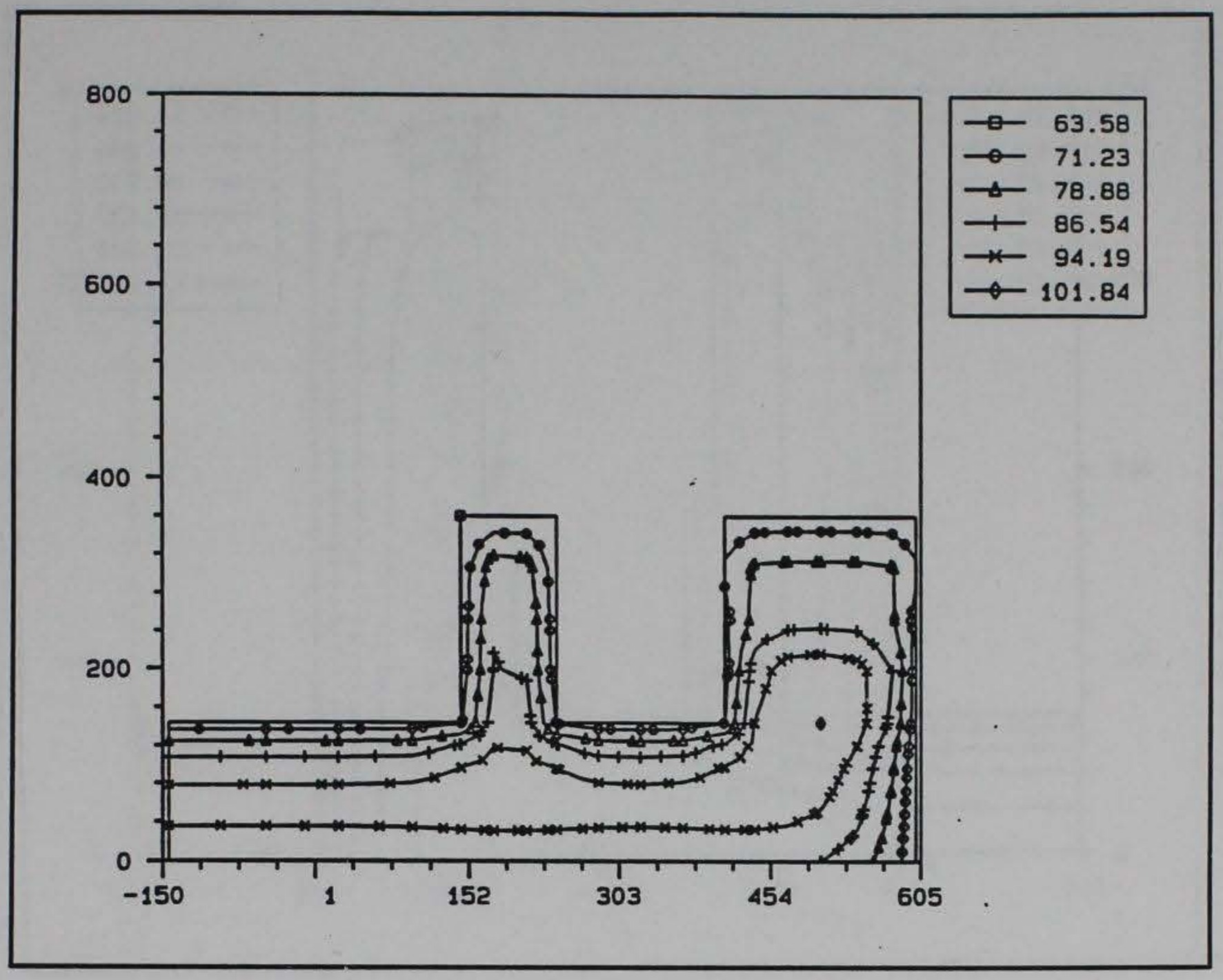

Figure 21. Temperature contour at day 27 at location shown in Figure 20

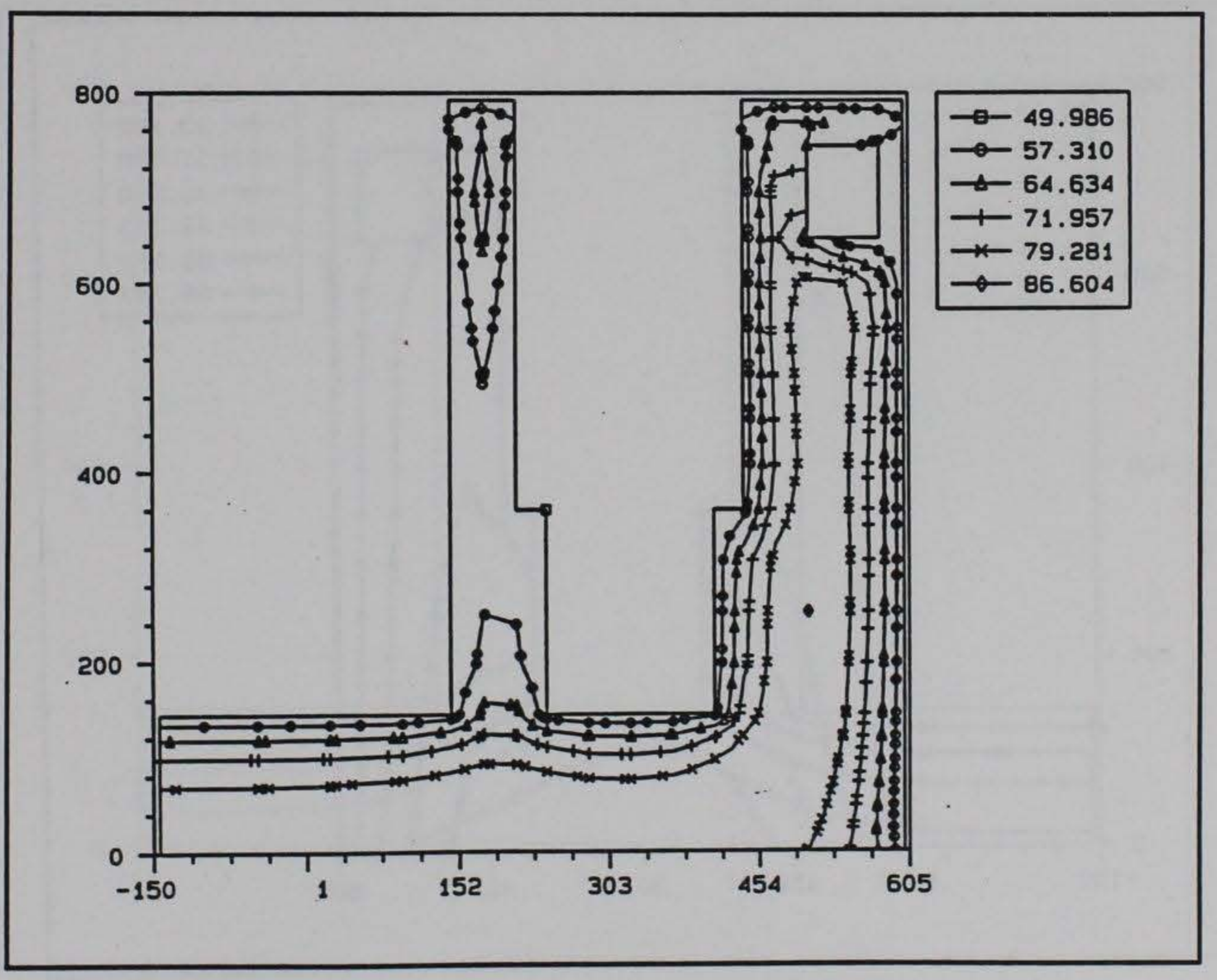

Figure 22. Temperature contour at day 52 at location shown in Figure 20

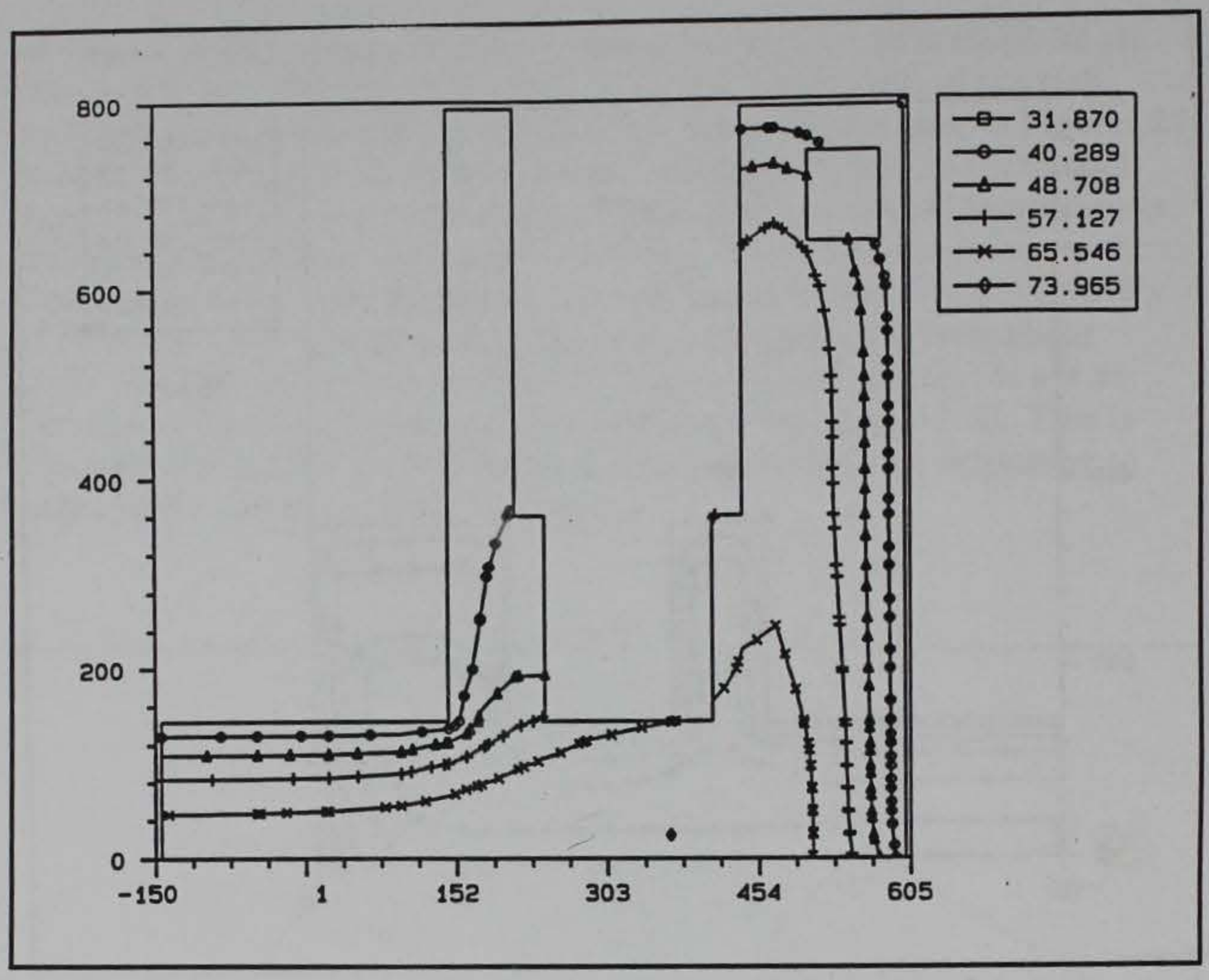

Figure 23. Temperature contour at day 90 at location shown in Figure 20

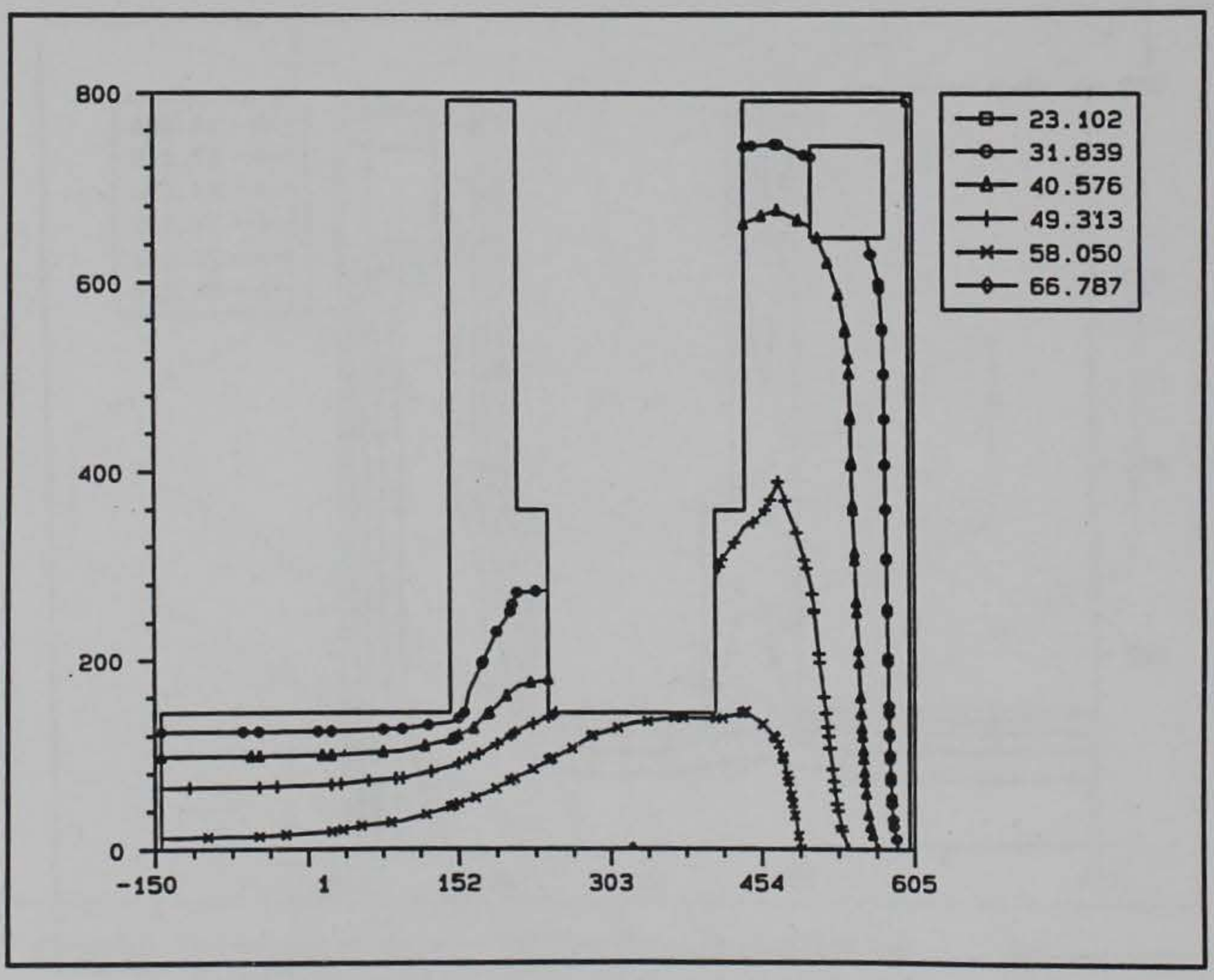

Figure 24. Temperature contour at day 125 at location shown in Figure 20

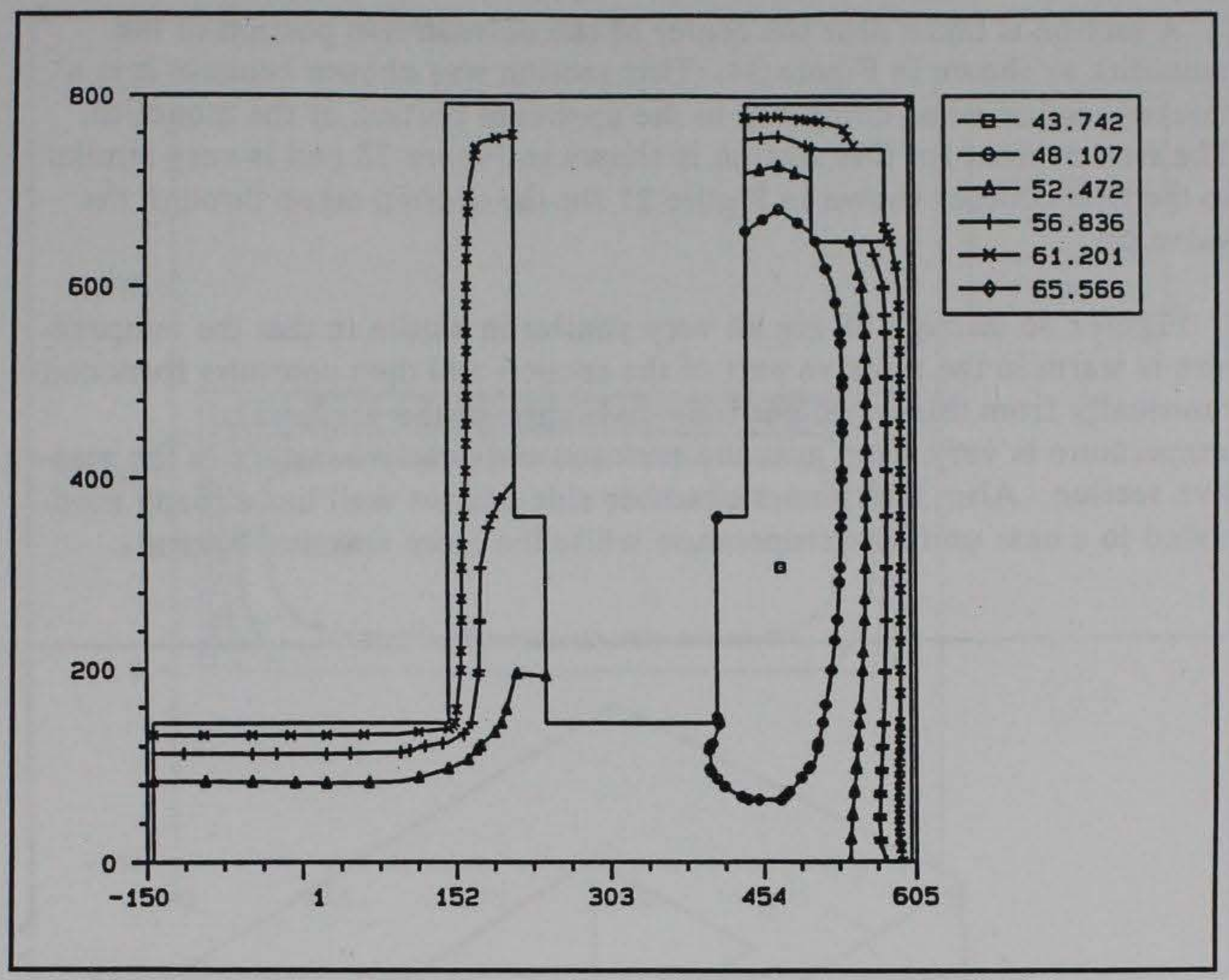

Figure 25. Temperature contour at day 250 at location shown in Figure 20

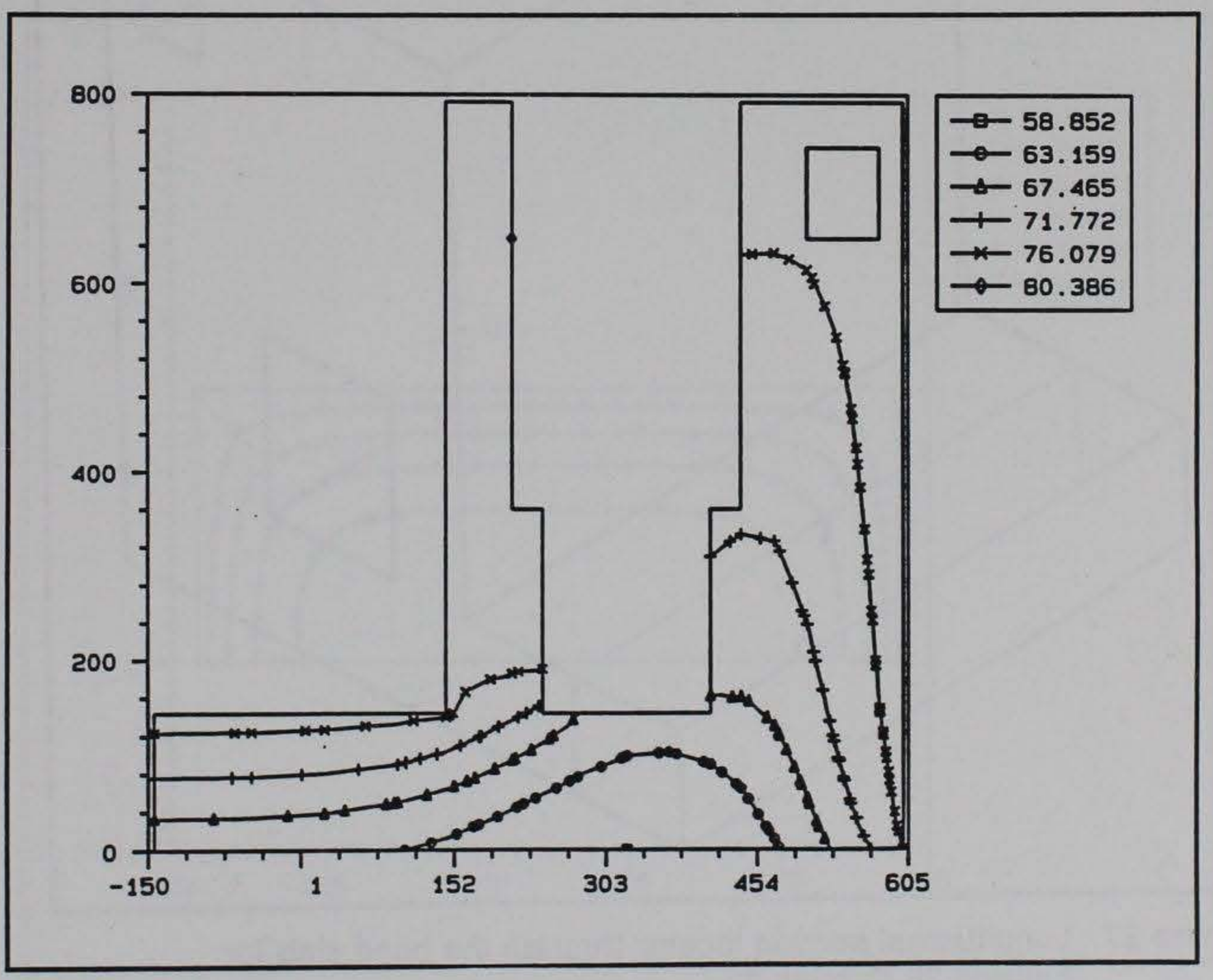

Figure 26. Temperature contour at day 360 at location shown in Figure 20

A section is taken near the center of the downstream portion of the monolith as shown in Figure 34. This section was chosen because it is a thicker section when compared to the upstream portion of the monolith. The first contour for this section is shown in Figure 35 and is very similar to the first contour shown in Figure 21 for the section taken through the valve pit.

Figures 36 through 38 are all very similar in nature in that the temperature is warm in the massive part of the section and then contours form concentrically from this warm portion. In Figure 36 the gradient of temperature is very steep near the surfaces and nearly constant in the massive section. Also, the thinner chamber side culvert wall has already moderated to a near uniform temperature while the more massive landside

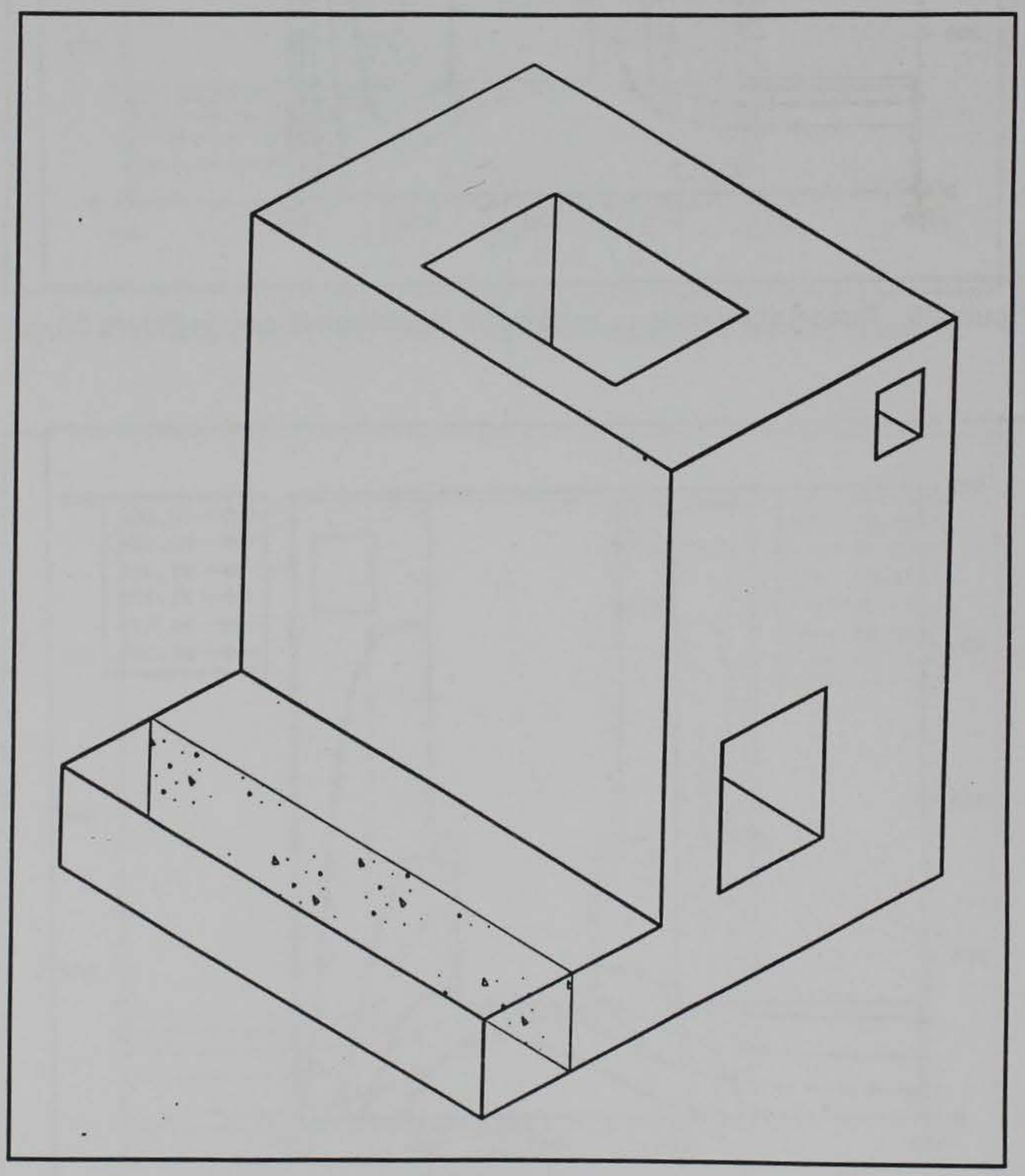

Figure 27. Longitudinal section locator through the base slab for Figures 28 through 33

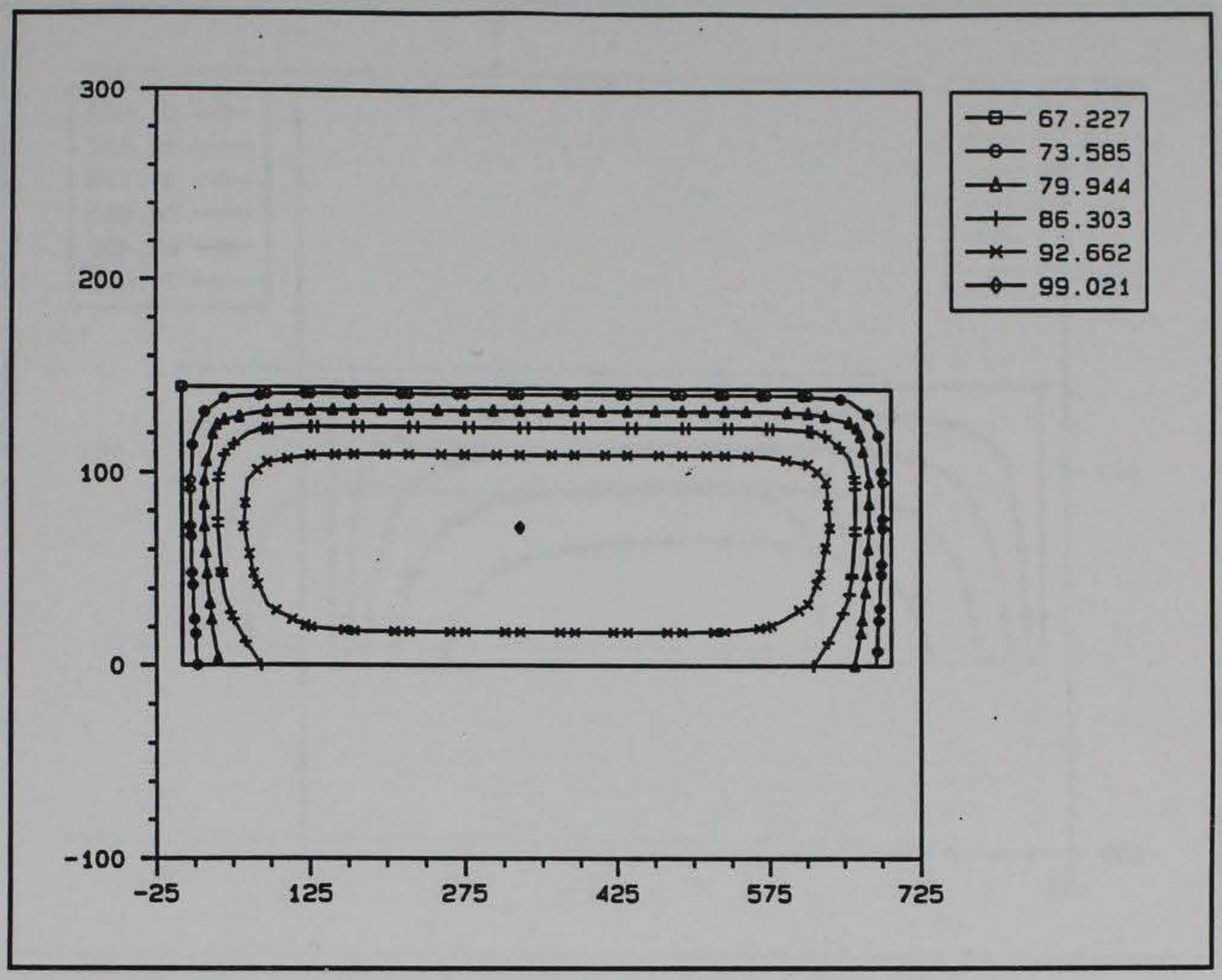

Figure 28. Temperature contour at day 20 at location shown in Figure 27

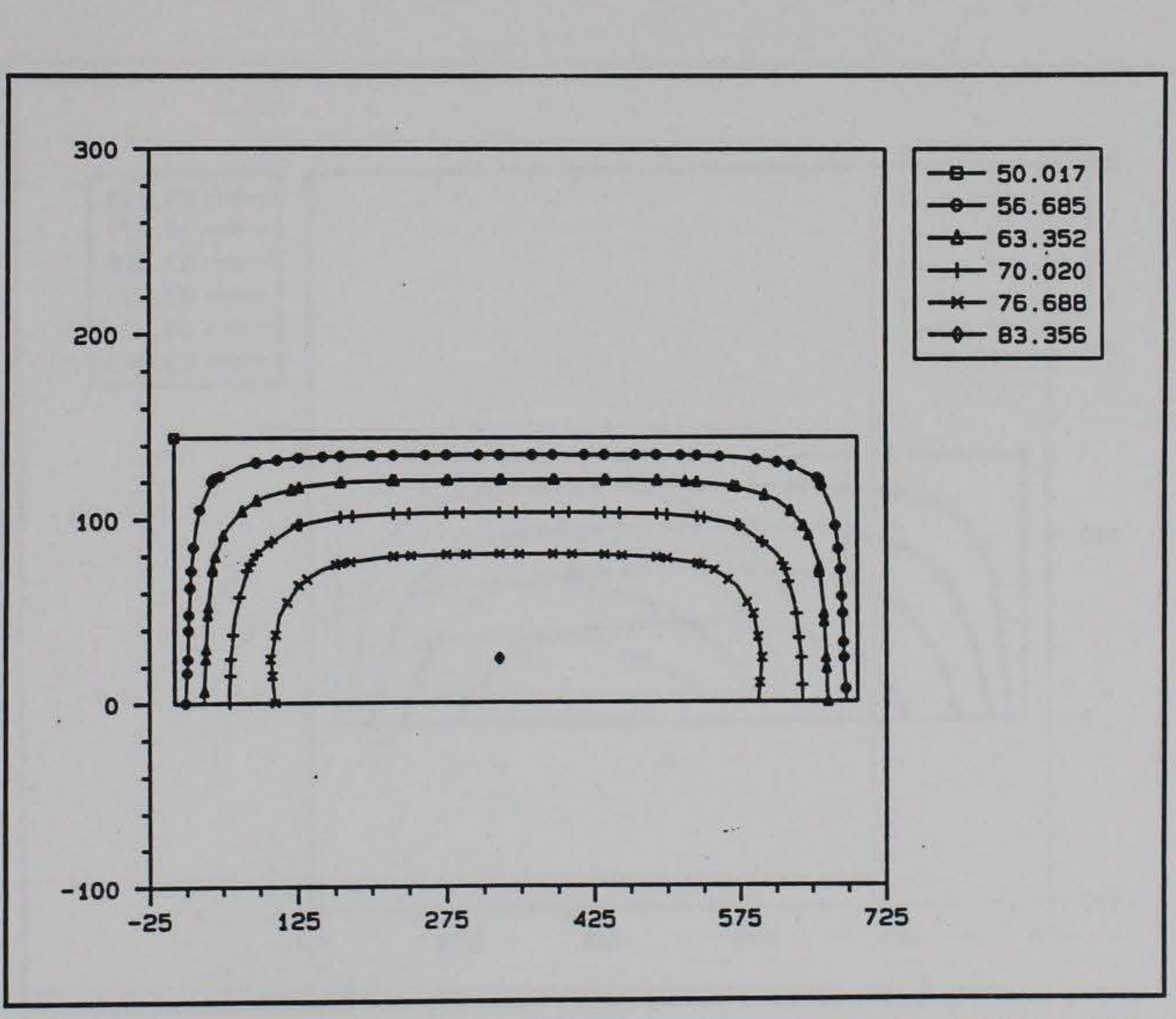

Figure 29. Temperature contour at day 52 at location shown in Figure 27

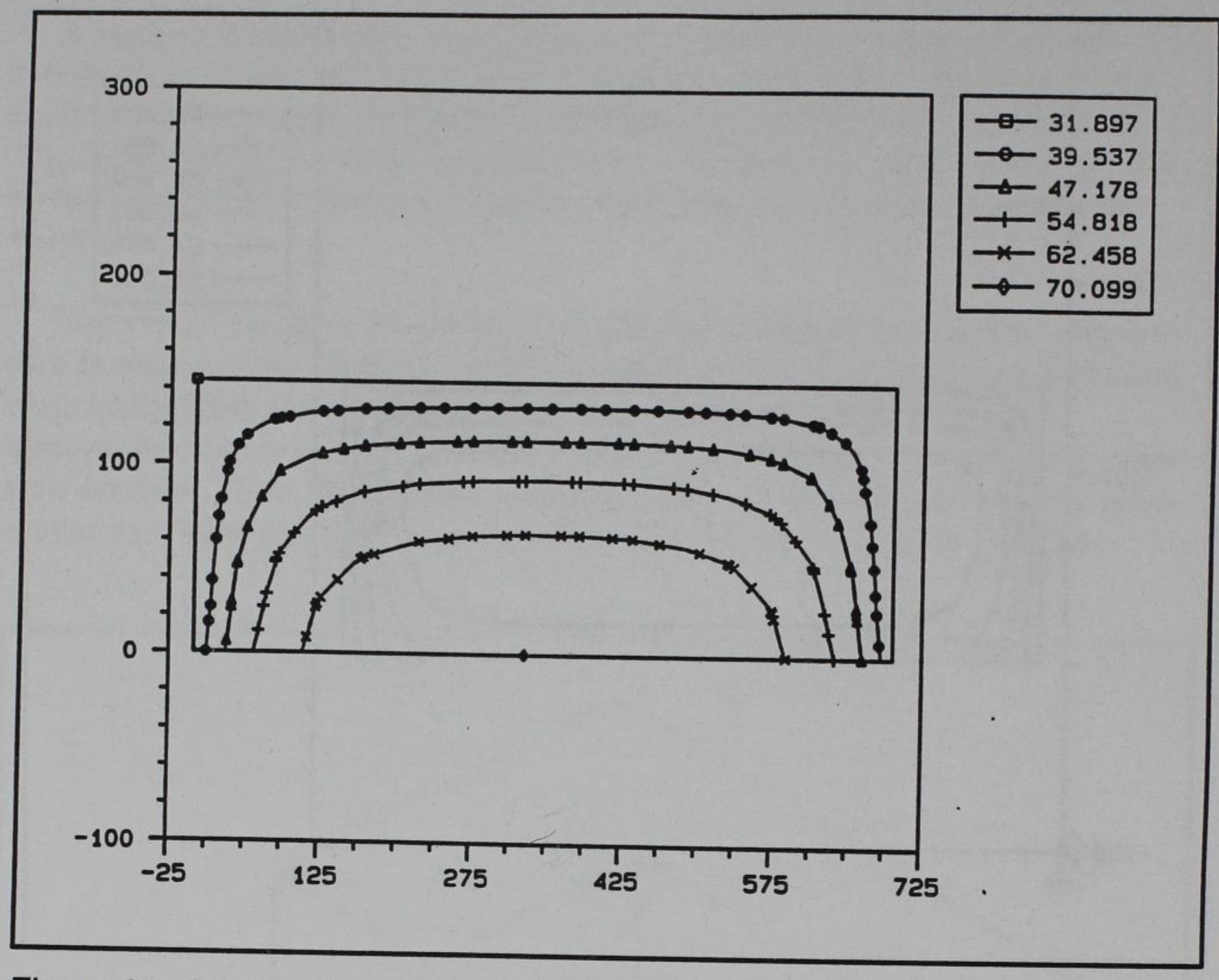

Figure 30. Temperature contour at day 90 at location shown in Figure 27

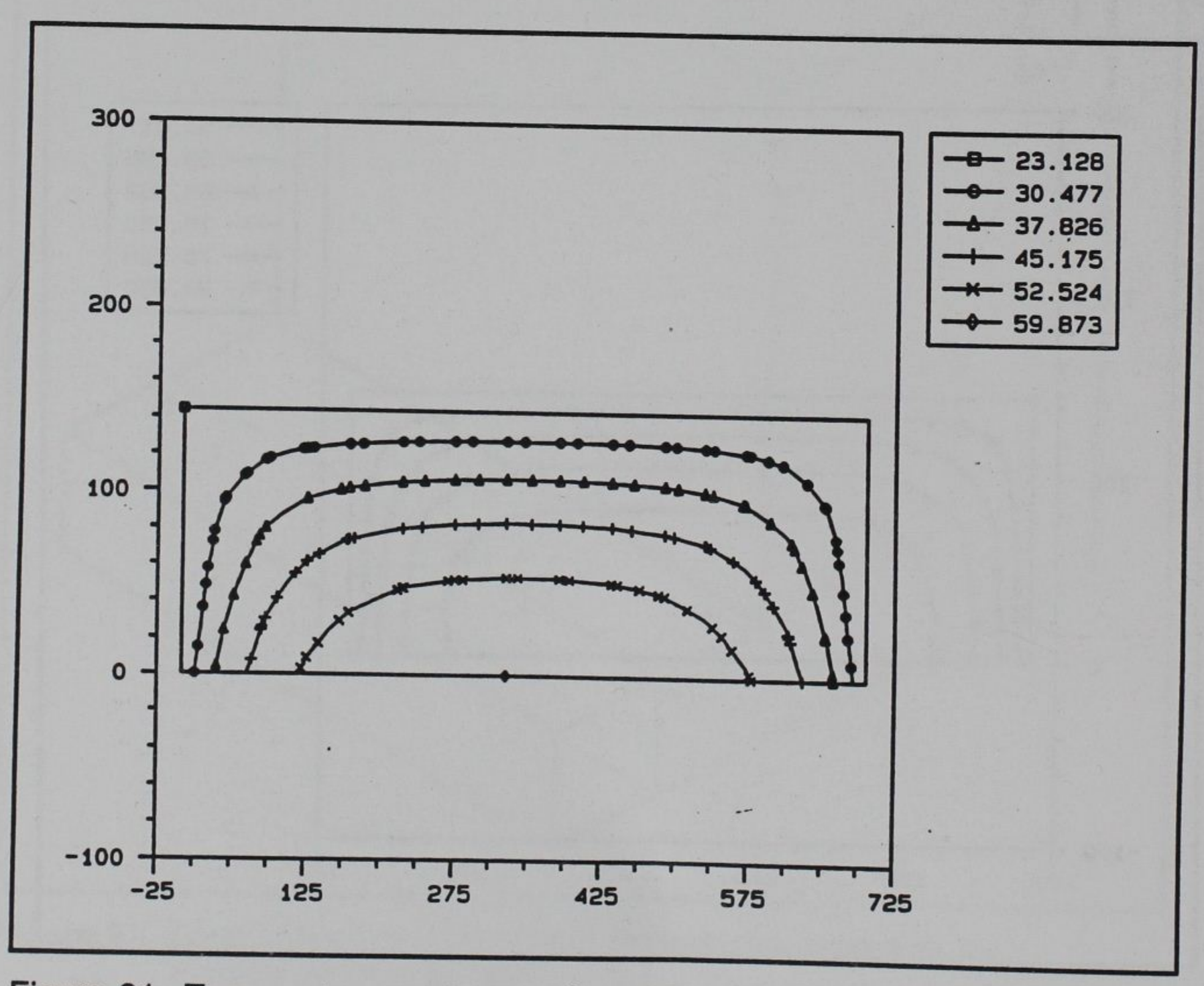

Figure 31. Temperature contour at day 125 at location shown in Figure 27

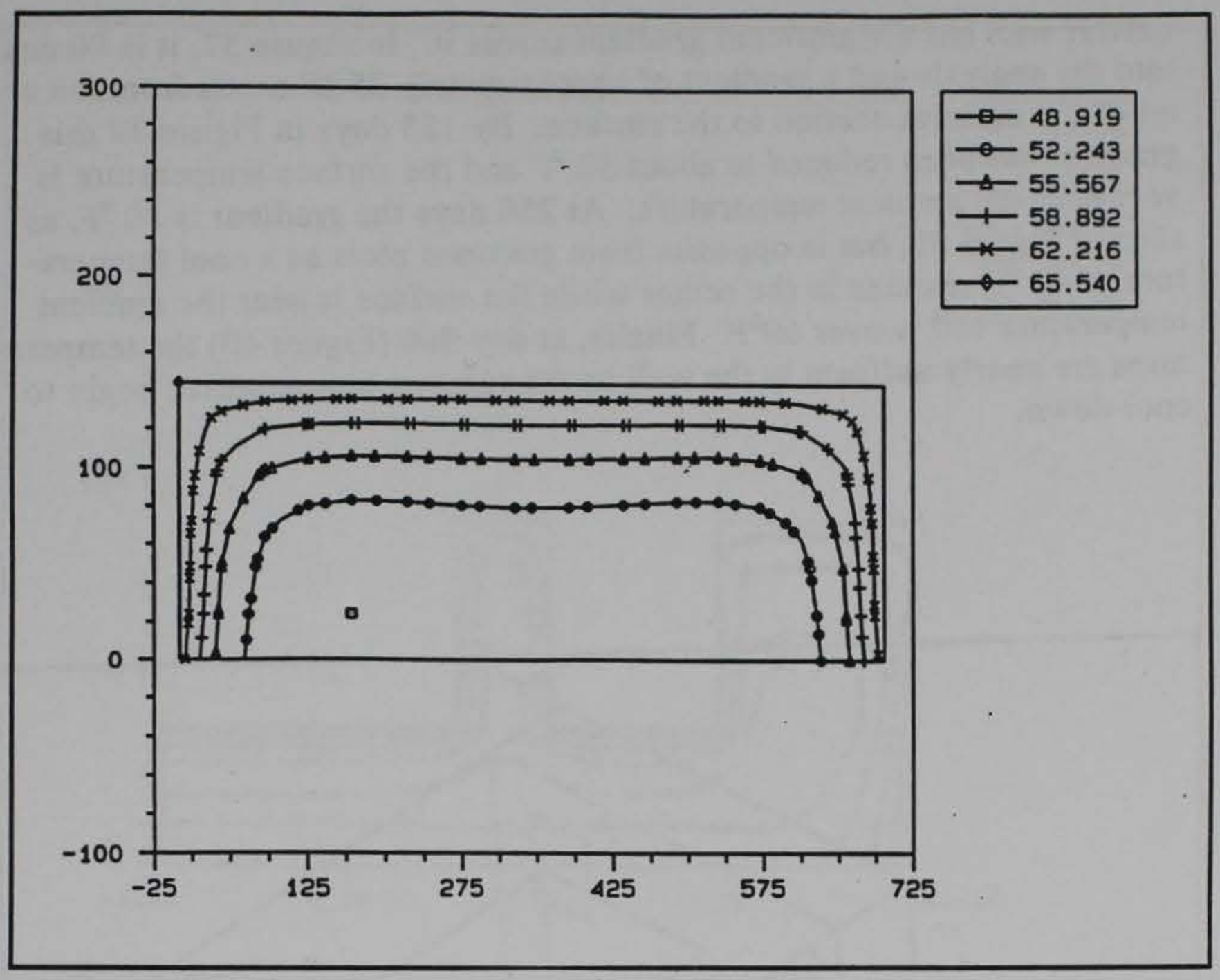

Figure 32. Temperature contour at day 250 at location shown in Figure 27

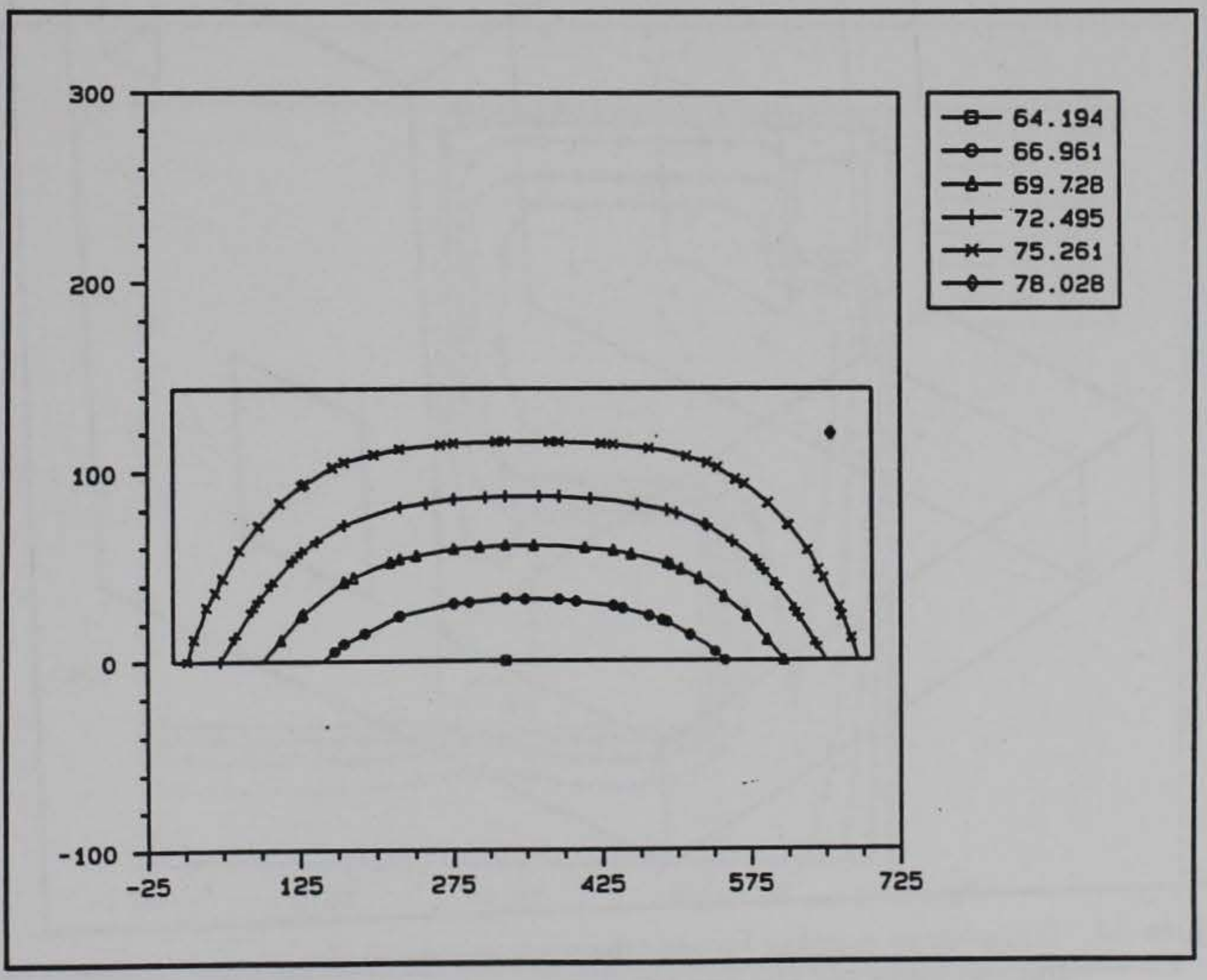

Figure 33. Temperature contour at day 360 at location shown in Figure 27

culvert wall has a significant gradient across it. In Figure 37, it is 90 days into the analysis and a gradient of approximately 35 °F exists from the center of the massive section to the surface. By 125 days in Figure 38 this gradient has been reduced to about 30 °F and the surface temperature is very near the ambient temperature. At 250 days the gradient is 20 °F, as seen in Figure 39, but is opposite from previous plots as a cool temperature of 42 °F remains in the center while the surface is near the ambient temperature and is over 60°F. Finally, at day 360 (Figure 40) the temperatures are nearly uniform in the wall as the summer temperatures begin to cool down.

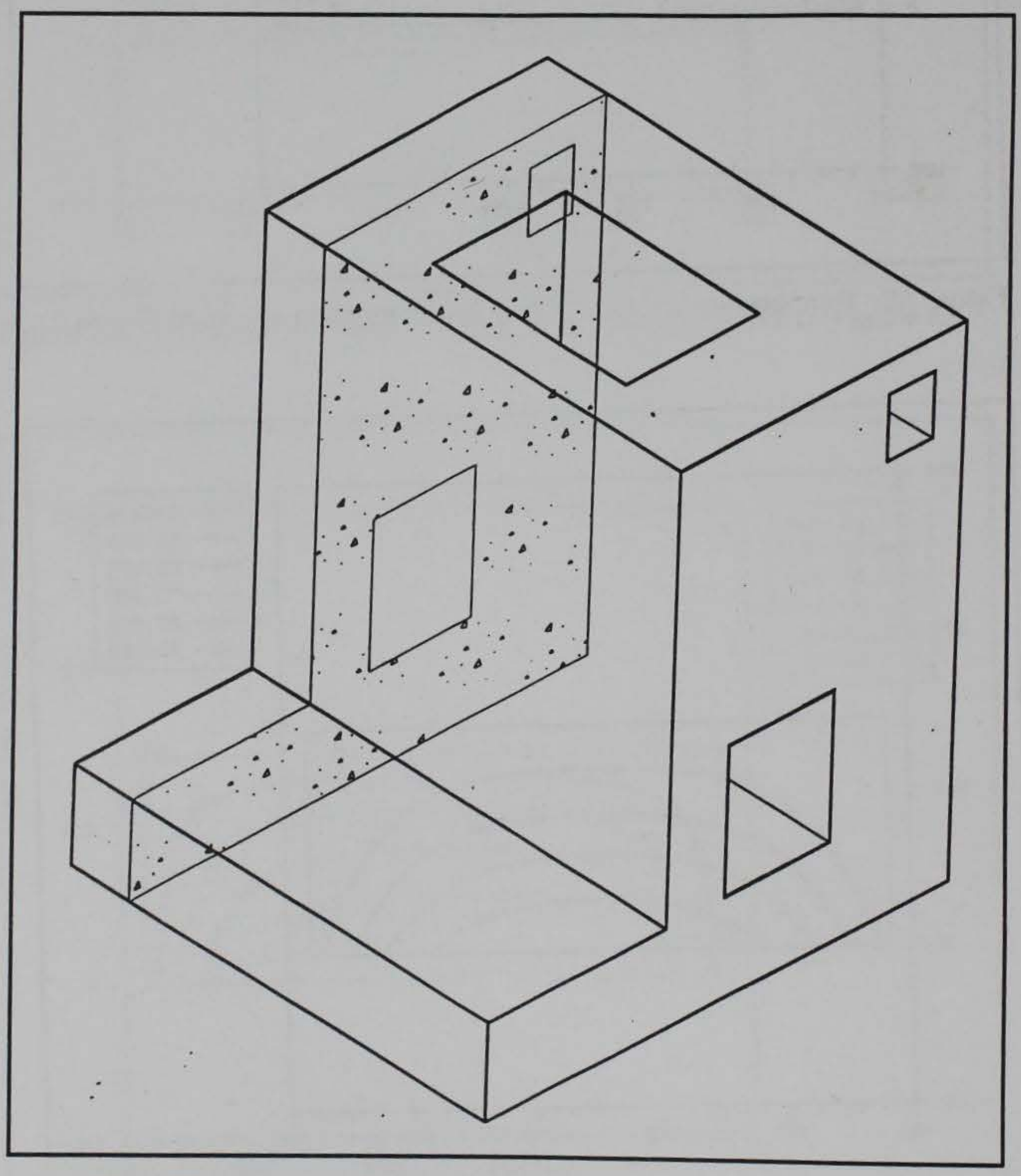

Figure 34. Transverse section locator through the downstream portion of the monolith for Figures 35 through 40

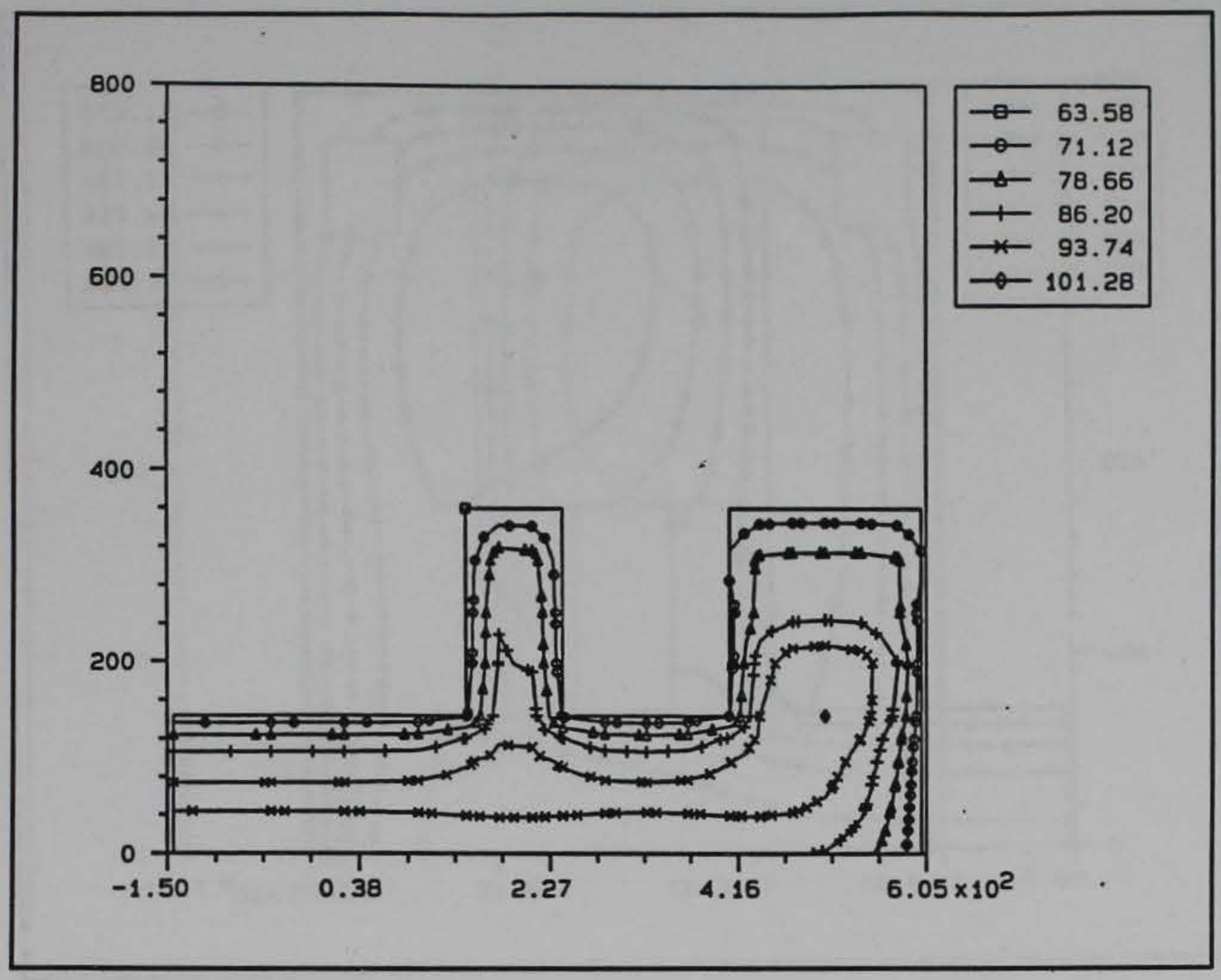

Figure 35. Temperature contour at day 27 at location shown in Figure 34

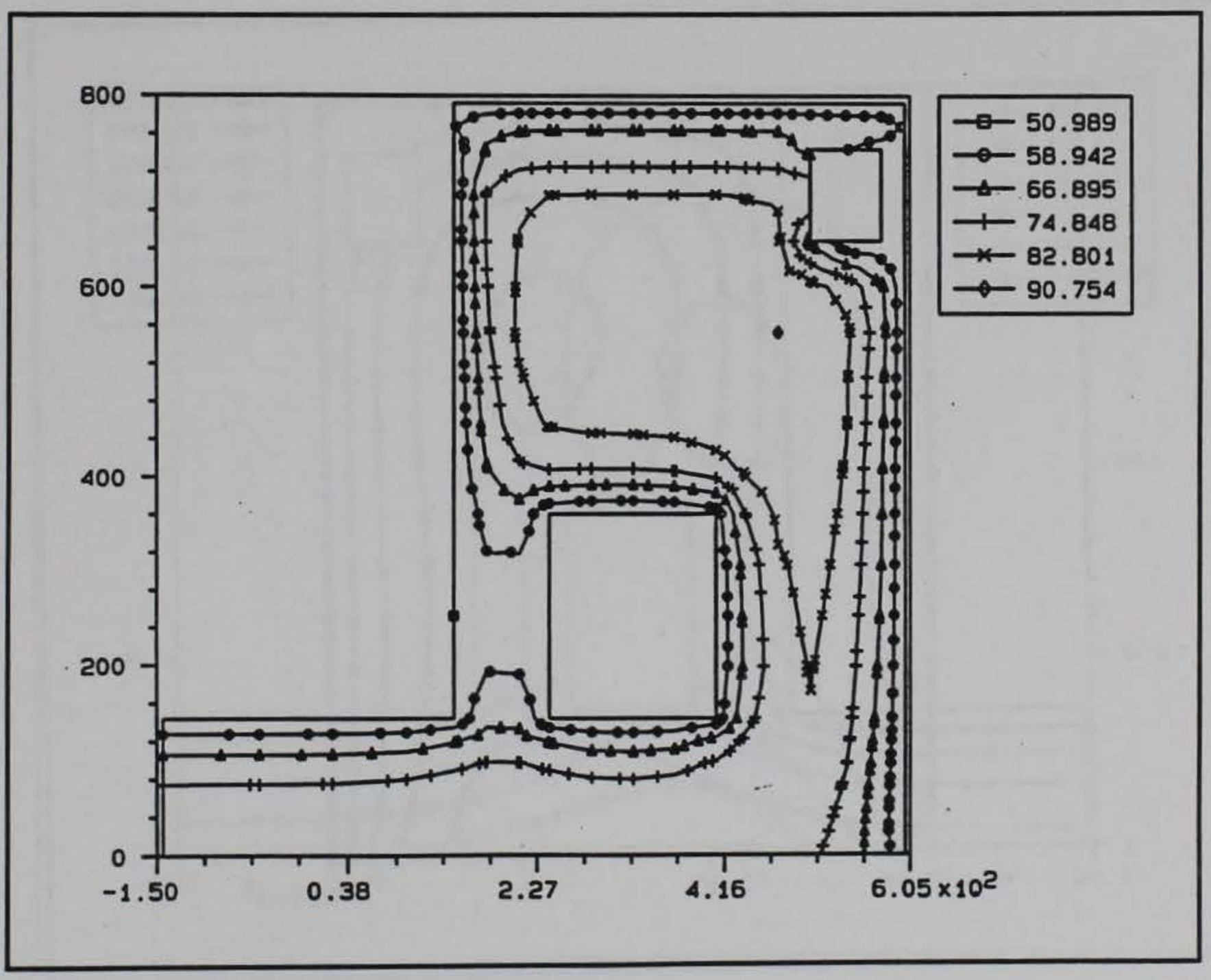

Figure 36. Temperature contour at day 52 at location shown in Figure 34

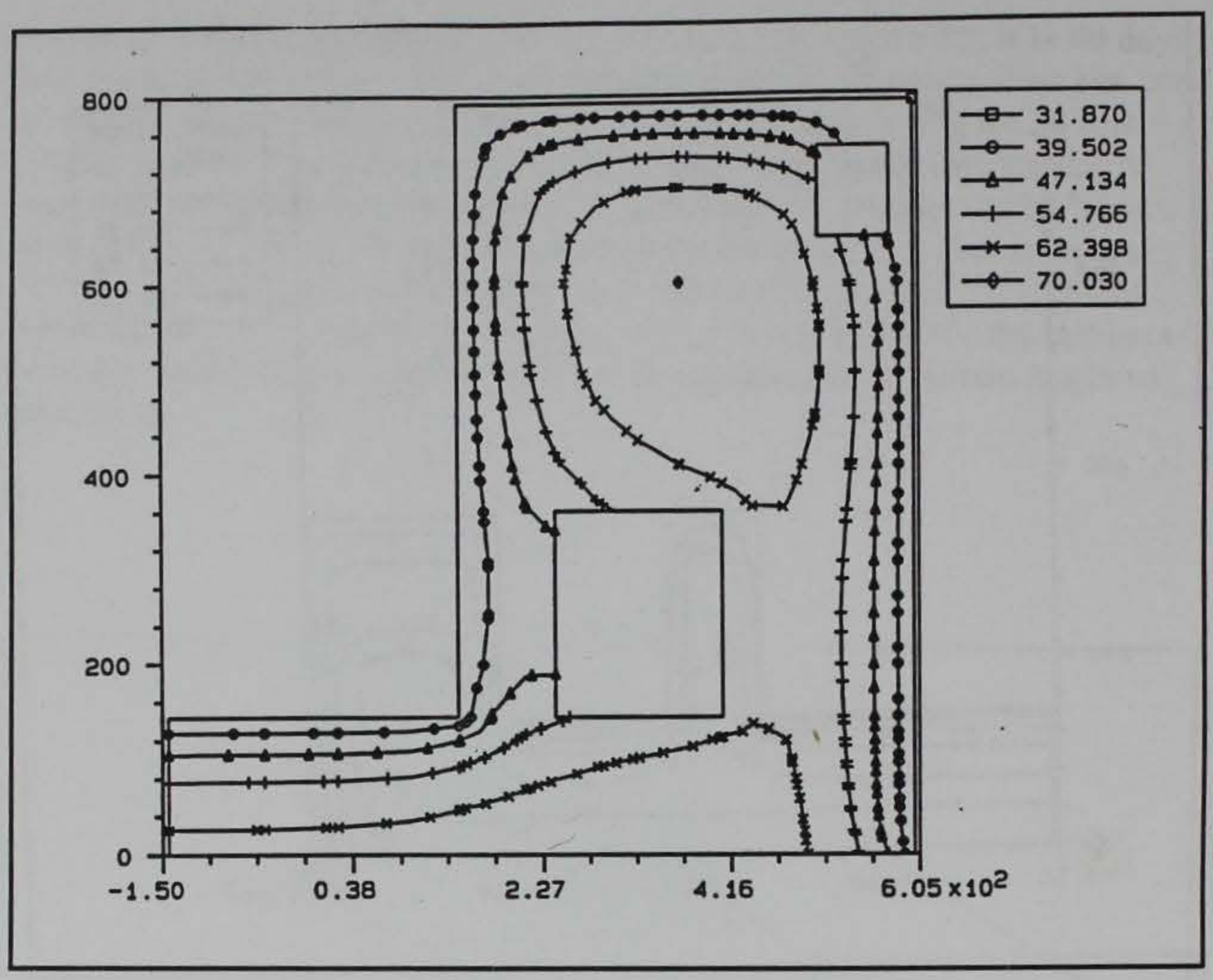

Figure 37. Temperature contour at day 90 at location shown in Figure 34

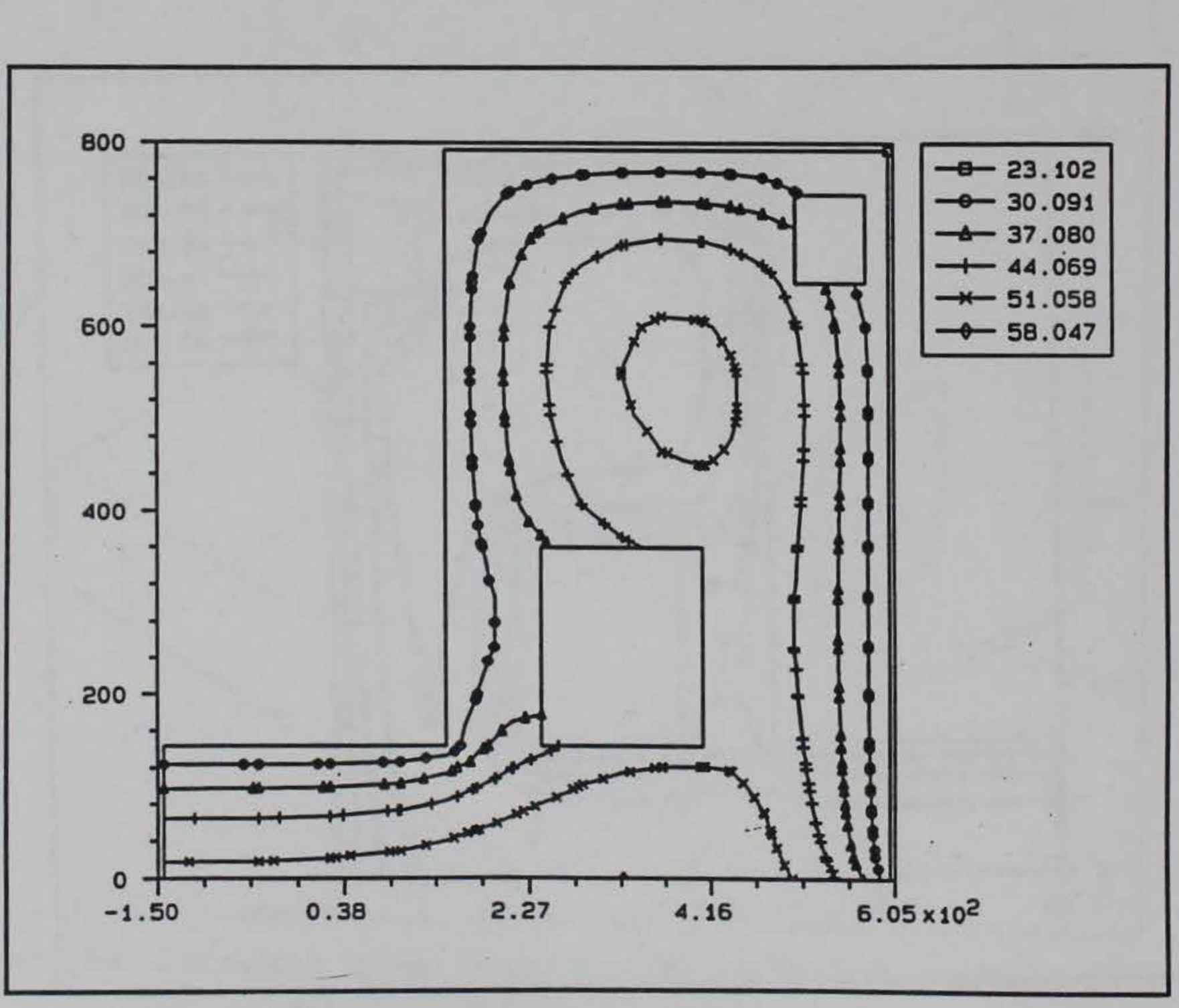

Figure 38. Temperature contour at day 125 at location shown in Figure 34

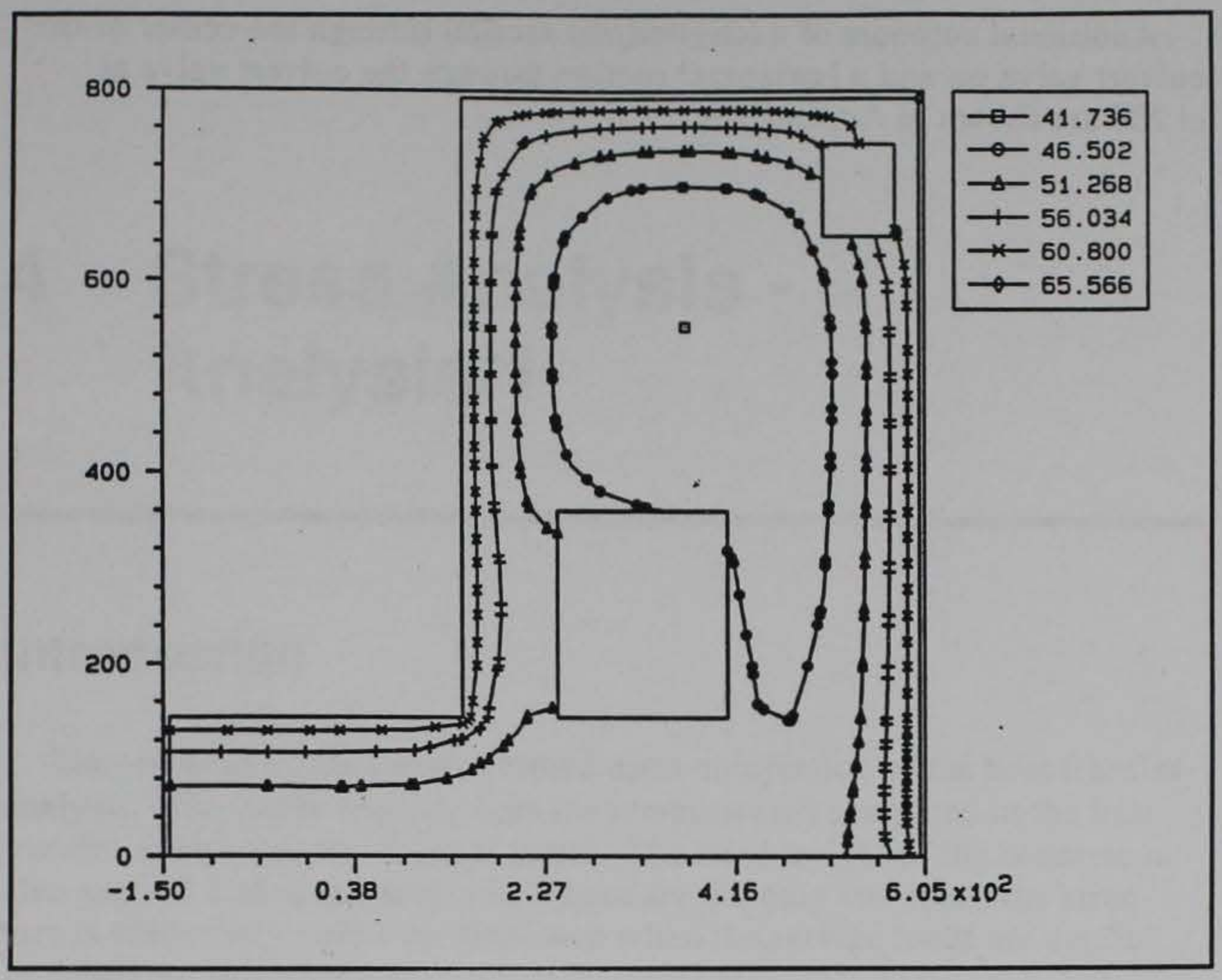

Figure 39. Temperature contour at day 250 at location shown in Figure 34

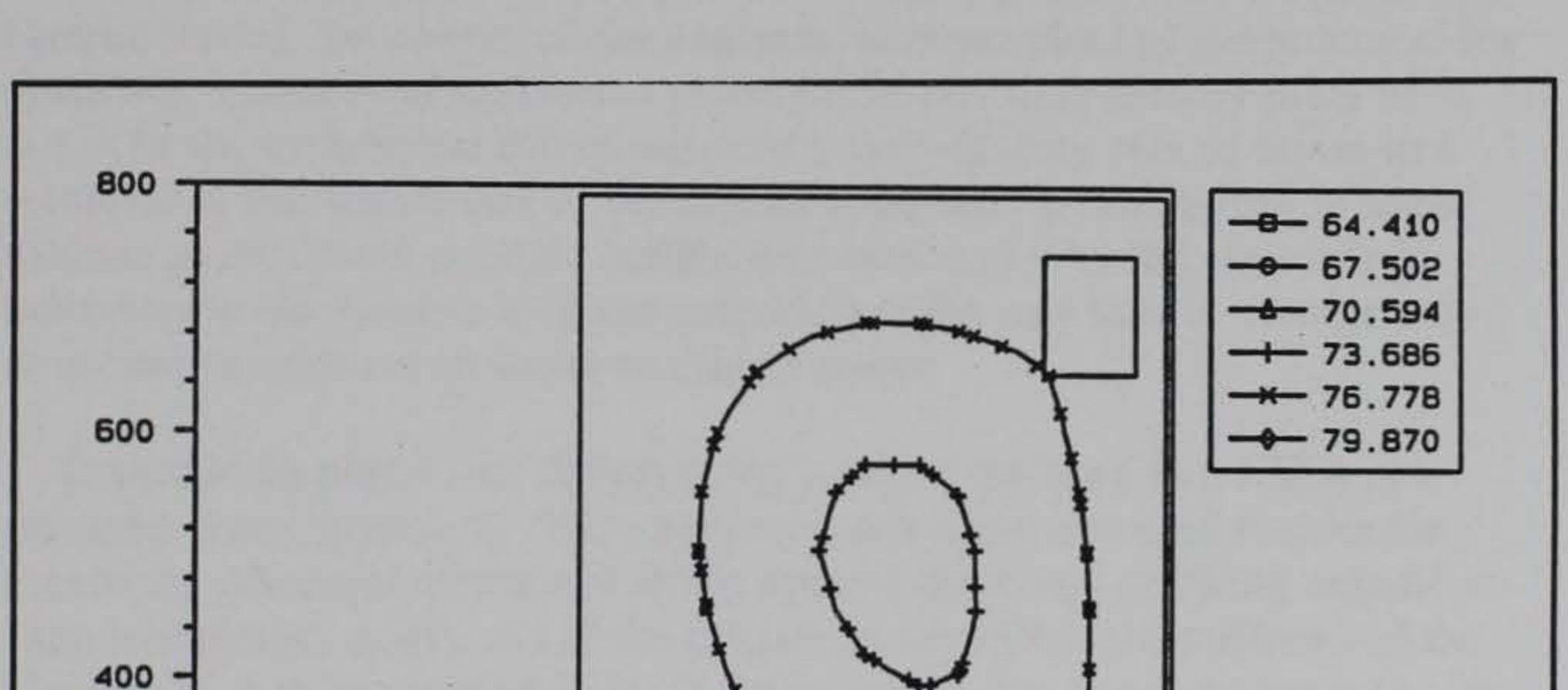

Figure 40. Temperature contour at day 360 at location shown in Figure 34

Additional contours of a longitudinal section through the center of the culvert valve pit and a horizontal section through the culvert valve at el 286 are shown in Appendix A.

4 Stress Analysis - Analysis 1

Introduction

The stress analysis was performed upon completion of the heat transfer analysis. The stress analysis uses the temperatures computed in the heat transfer analysis as the thermal loads. The dead weight of the concrete is also applied during the analysis. These are the only two loads the structure is subjected to until the final step when the service loads are applied as described in Chapter 2.

The results of the stress analysis will include plots of the cracks which formed during the course of the analysis, contour plots of the potential for cracking, contours of maximum principal stress, time-history plots of stress in the orthogonal directions, and a time-history plot of stress in a reinforcing bar where one of the cracks occurred. Examination of these various plots should provide insight into how and why the structure is behaving in the manner it is and provide insight into how to change construction parameters to improve this behavior.

It should be noted that the cracking mechanism used in a NISA is a smeared crack approach. The smeared crack approach used checks the maximum principal stress and strain against the given cracking criteria at each integration point, and if the criteria is exceeded, the stiffness of the element at that integration point is degraded so that it can no longer carry any tensile stress perpendicular to the crack direction. A more detailed discussion on this criteria is contained in the Phase III report of the lower miter gate NISA study (Fehl et al. in preparation).

Crack Location Plots

Figures 41 through 55 present plots of the structure showing where cracks occurred in the structure. Essentially, only one location produced cracking. The chamber side corner of the gallery had a number of

integration points crack indicating a single crack of significant magnitude. While the crack in the gallery is quite extensive, it does not threaten the overall integrity of the structure. Despite this fact, strong consideration should be given to making changes which would alleviate this cracking.

Cracking in the gallery started at day 209 of the analysis and continued through day 289. By the time the cracking stopped, cracks had formed at 111 integration points above the given corner of the gallery and extended almost the entire length of the gallery. Integration points in two different longitudinal strips of elements cracked. The total number of integration points which are located in the planes where the cracking occurred is 240, and therefore, nearly half of the integration points in the plane of the crack are cracked. Table 2 gives the total number of cracked integration points through time.

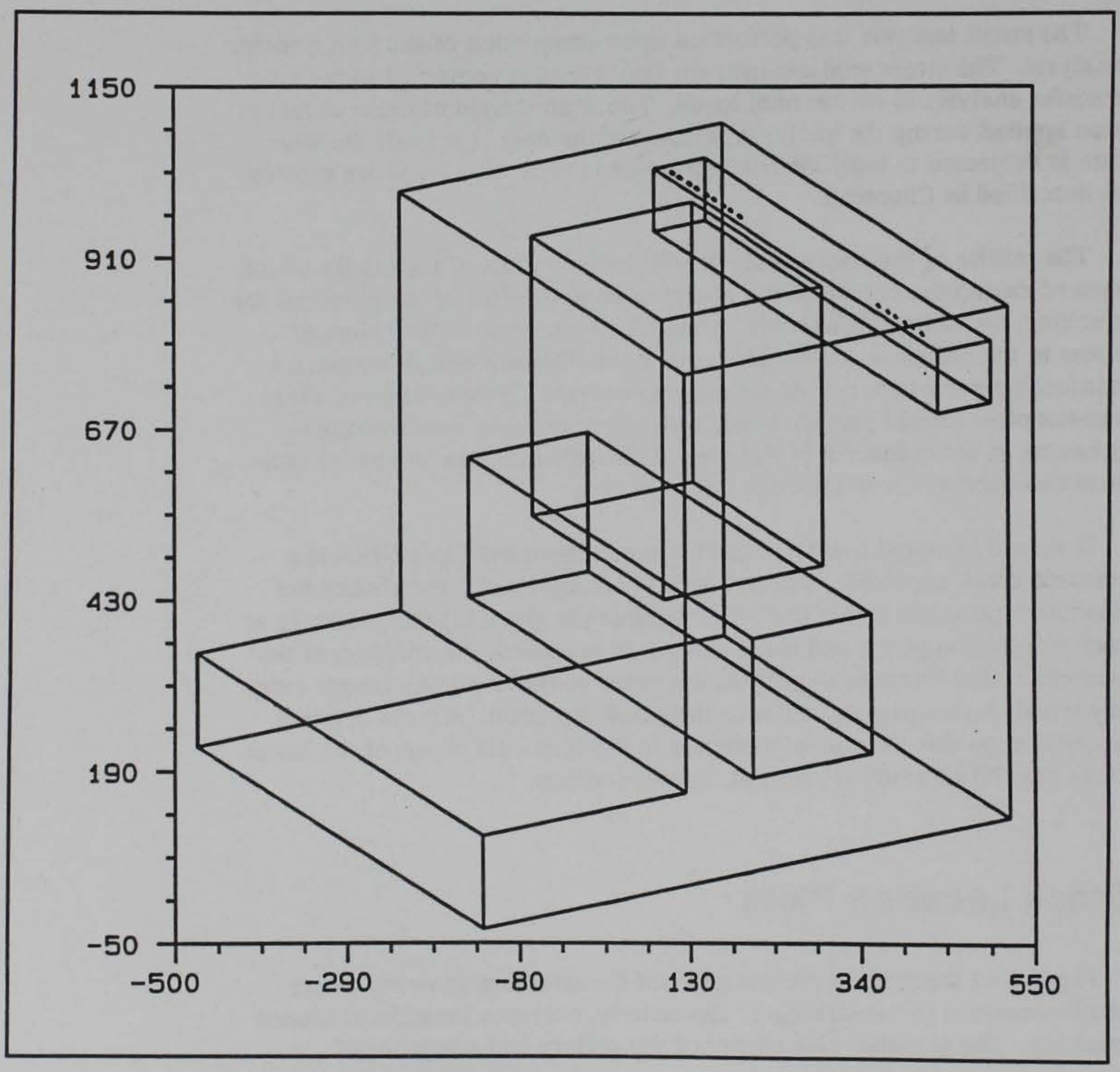

Figure 41. Crack plot, isometric view at day 209

Table 2 Number of cracked integration points above gallery									
Time, days	209	219	229	239	249	259	269	279	289
Number of points cracked	15	24	45	60	77	91	105	109	111

Figure 41 shows an isometric view of the monolith at day 209 when the cracking started. Figures 42, 43, and 44 are a plan view, a front elevation, and a side elevation, respectively. The front elevation in Figure 43 shows that this the crack angles away from the corner of the gallery to some degree. Also, in Figure 44 the crack locations are shown as circles in this view, because the surface of the crack is nearly parallel to this plane.

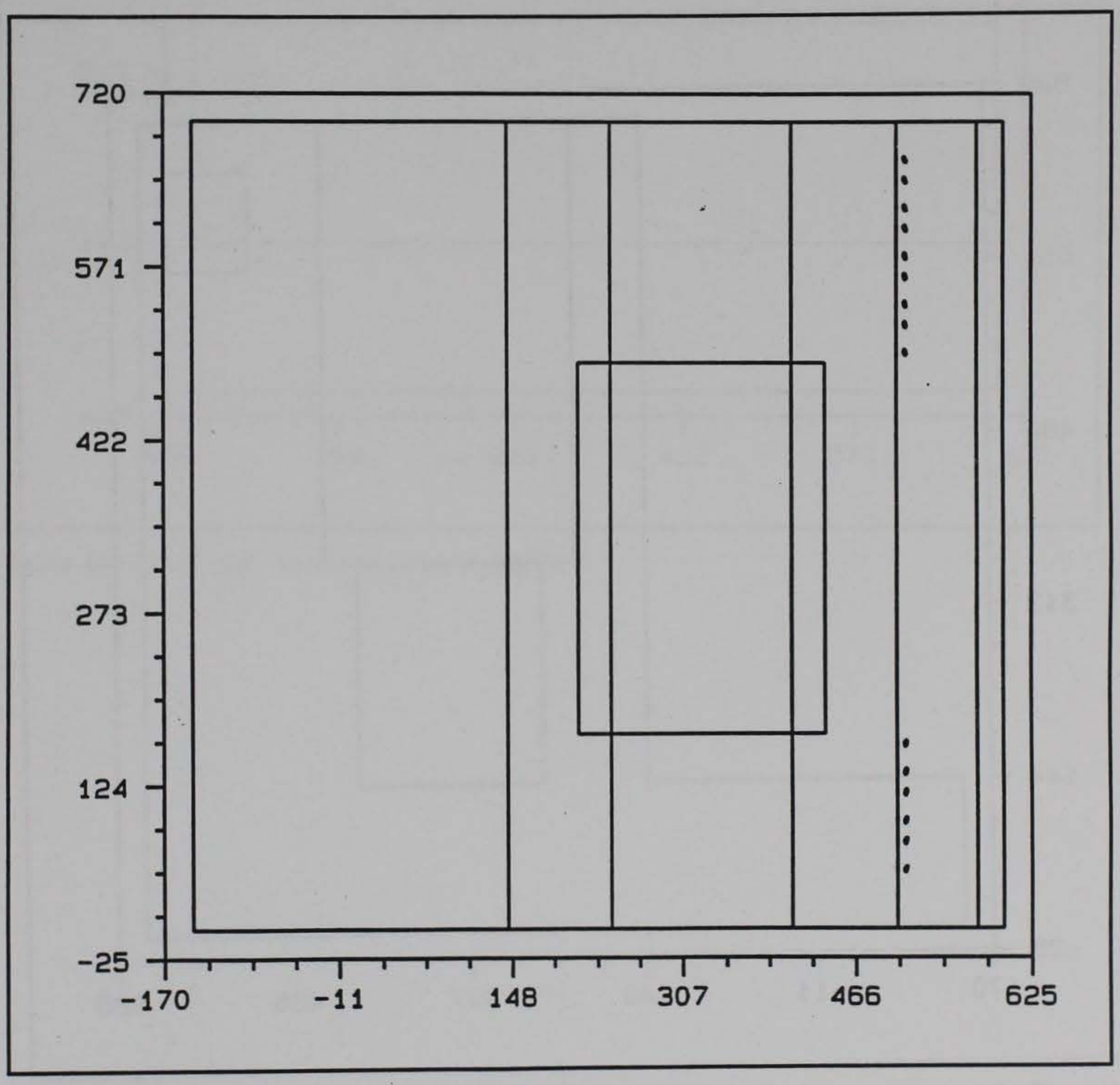

Figure 42. Crack plot, plan view at day 209

Figures 45 through 52 show the progression through time of the crack forming using the isometric view. Paging through the figures, the propagation of the crack is easily identifiable in Figures 45 through 50, but between Figures 50 and 52, the change is not as noticeable. This is due to the fact that by day 269 (Figure 50) most of the cracks have formed, and therefore, the new cracks are hard to identify in Figures 51 and 52. A plan view, a front elevation, and a side elevation are shown in Figures 53, 54, and 55, respectively, to show the final layout of the cracks. Again, the direction of the cracks can be seen in Figure 54, and they angle away from the corner initially and then propagate up.

Discussion of the cause of these cracks will be discussed further in the following sections.

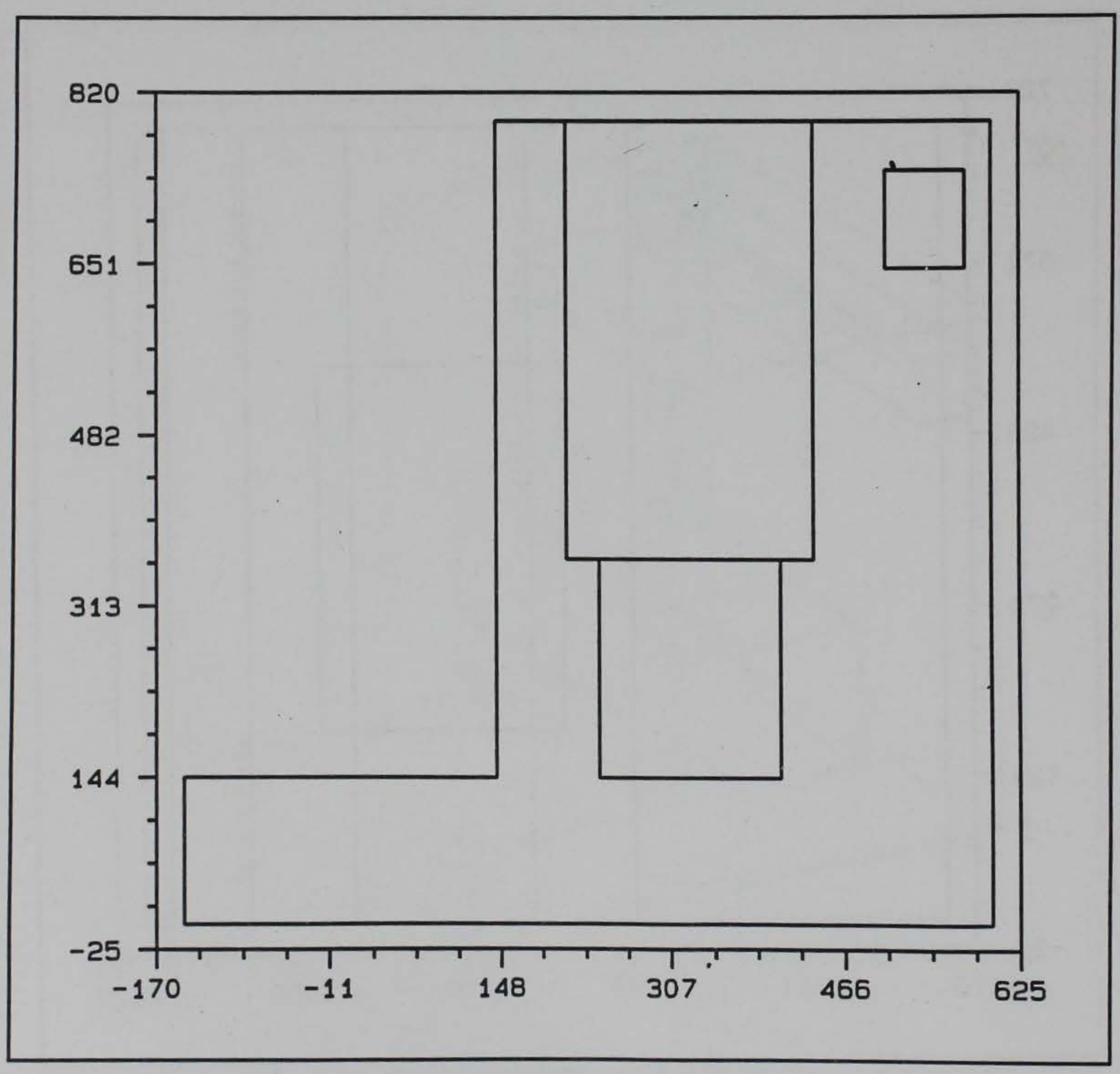

Figure 43. Crack plot, front elevation at day 209

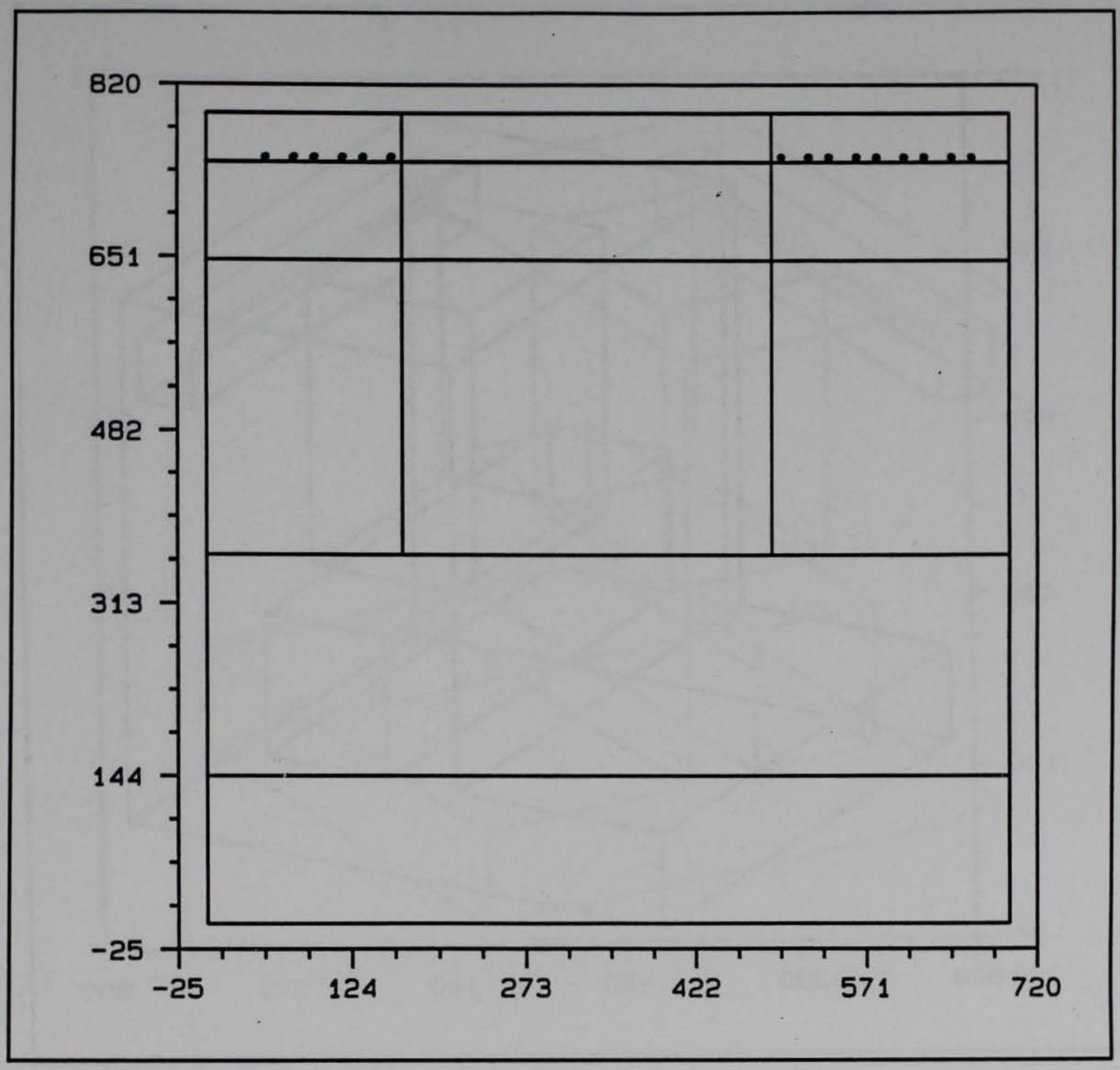

Figure 44. Crack plot, side elevation at day 209

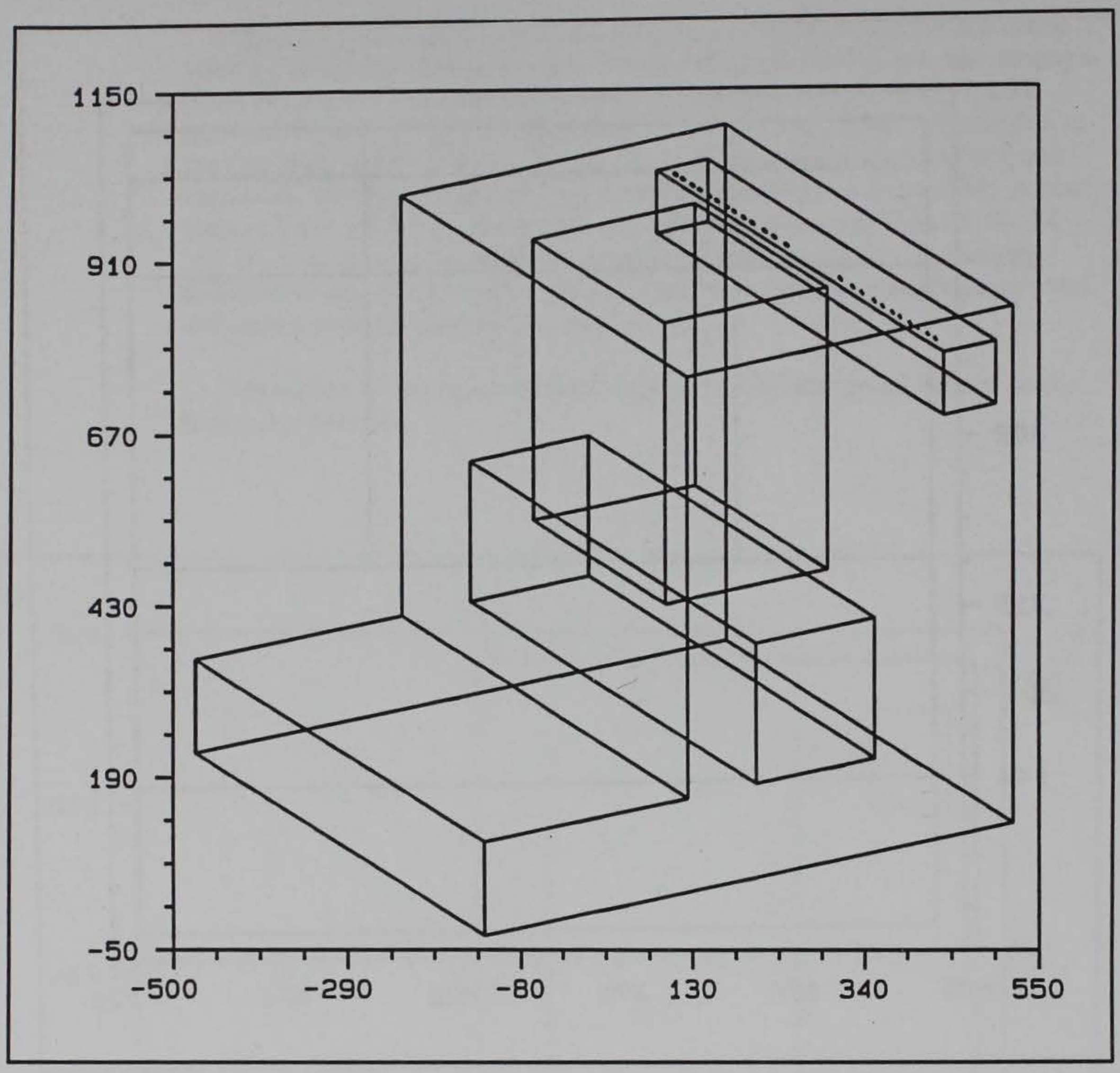

Figure 45. Crack plot, isometric view at day 219

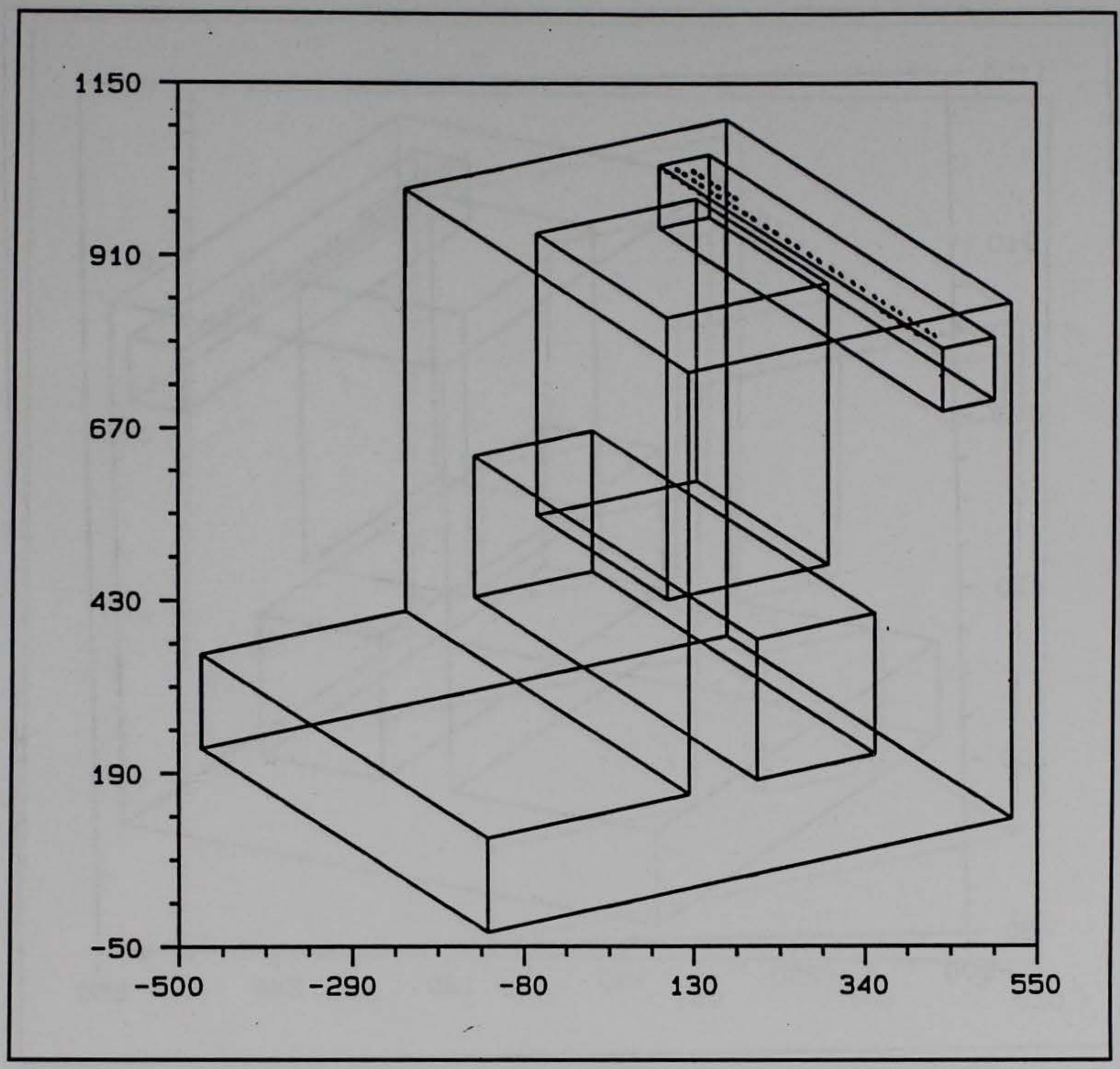

Figure 46. Crack plot, isometric view at day 229

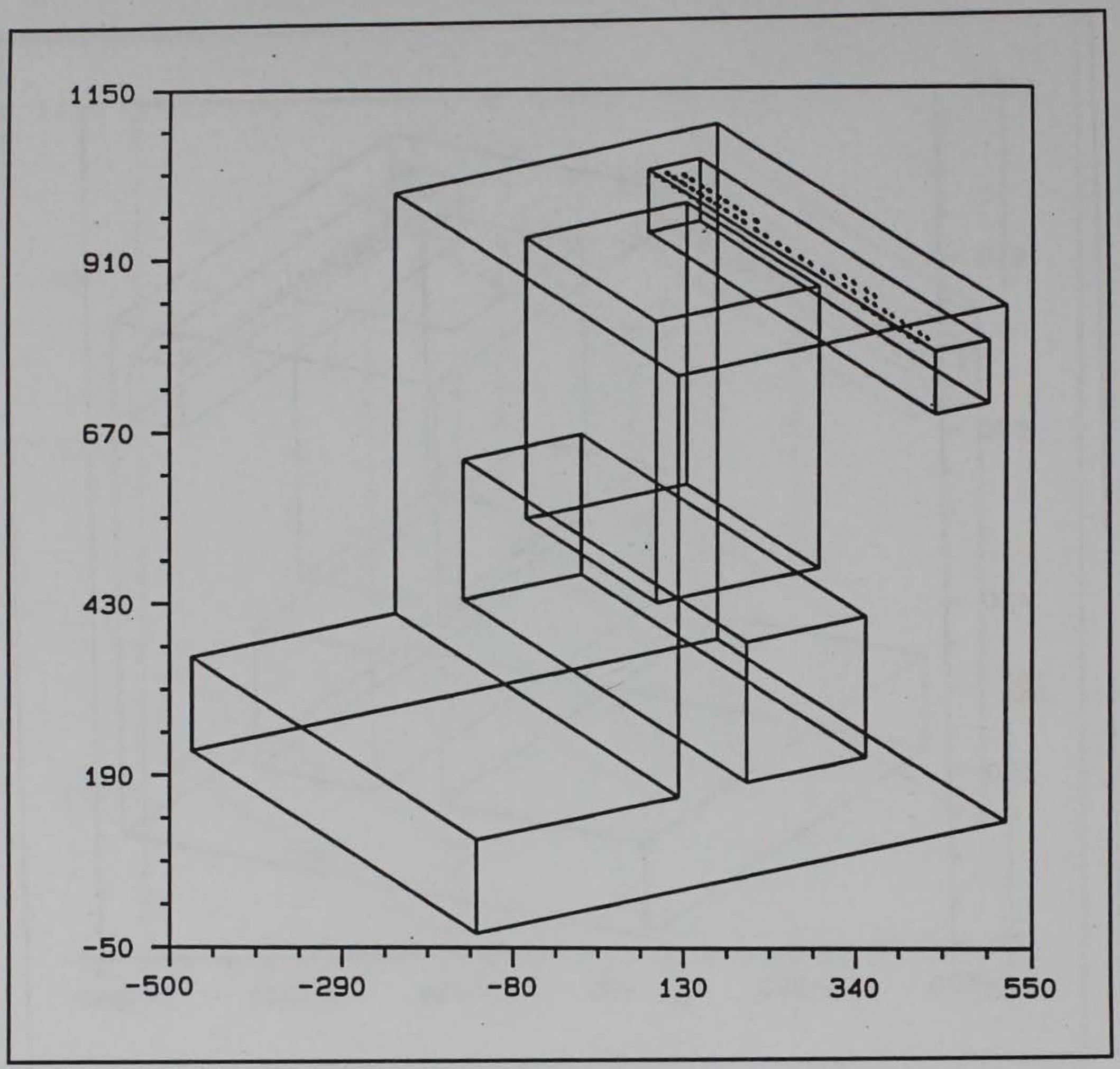

Figure 47. Crack plot, isometric view at day 239

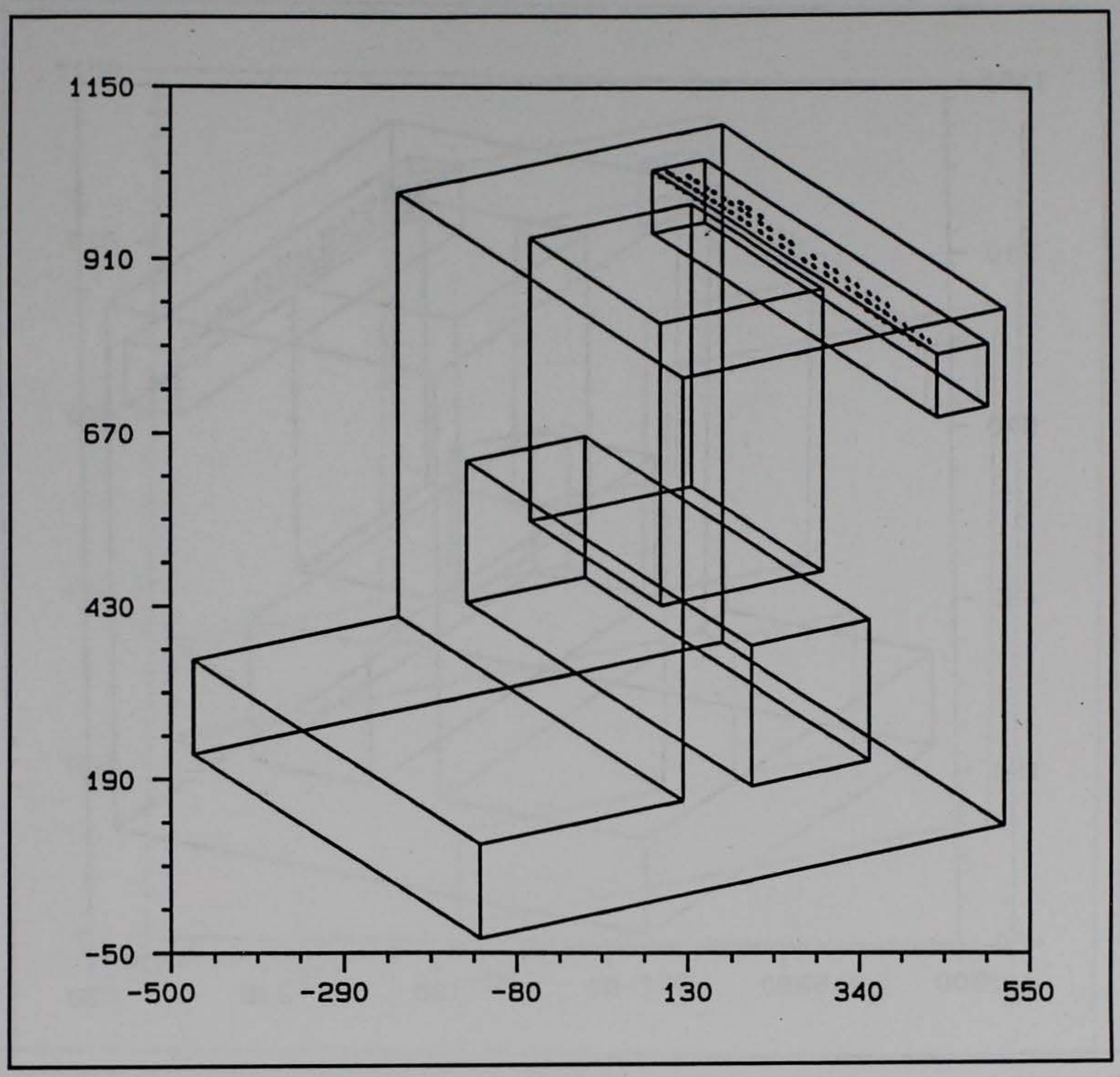

Figure 48. Crack plot, isometric view at day 249

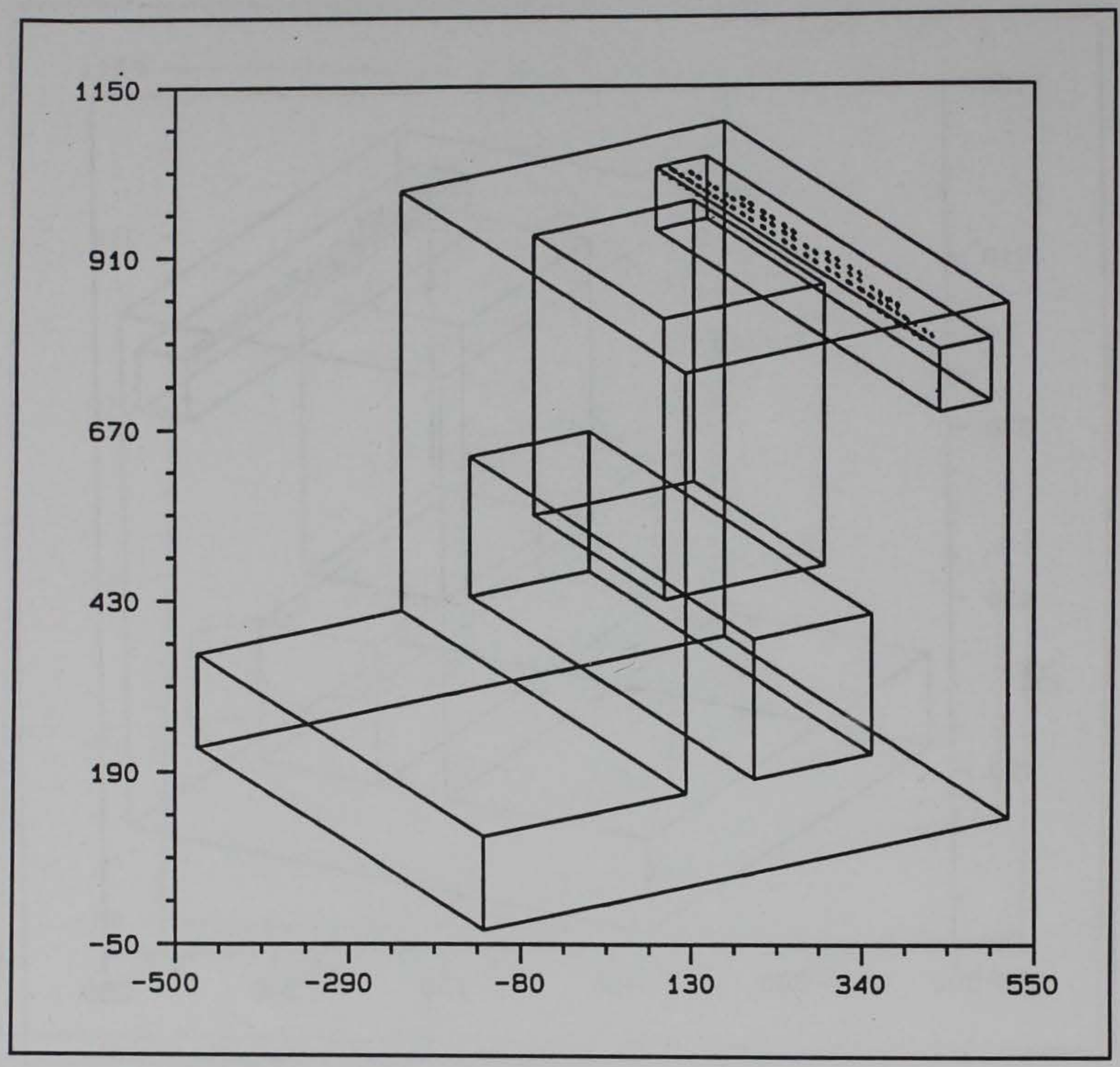

Figure 49. Crack plot, isometric view at day 259

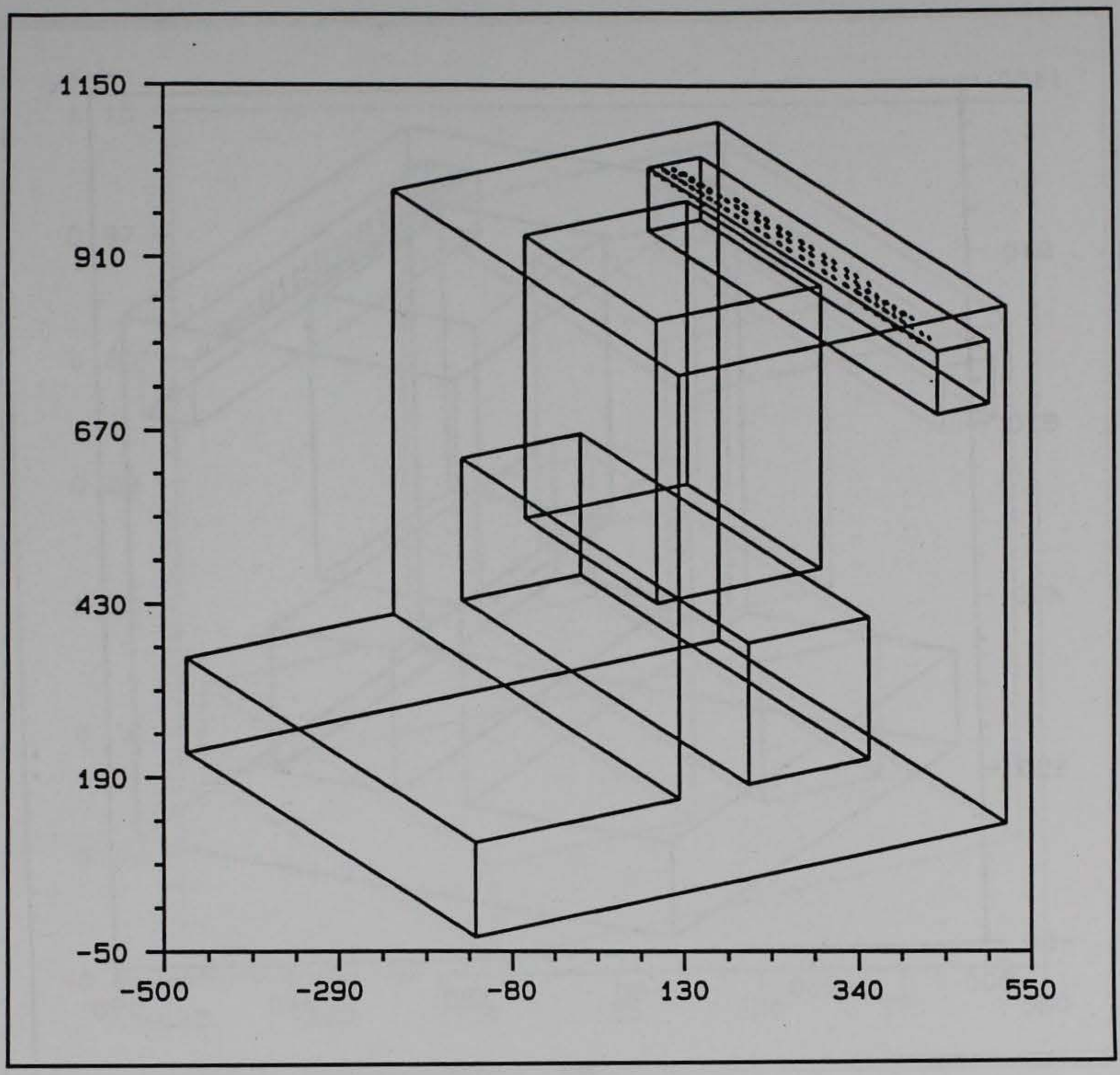

Figure 50. Crack plot, isometric view at day 269

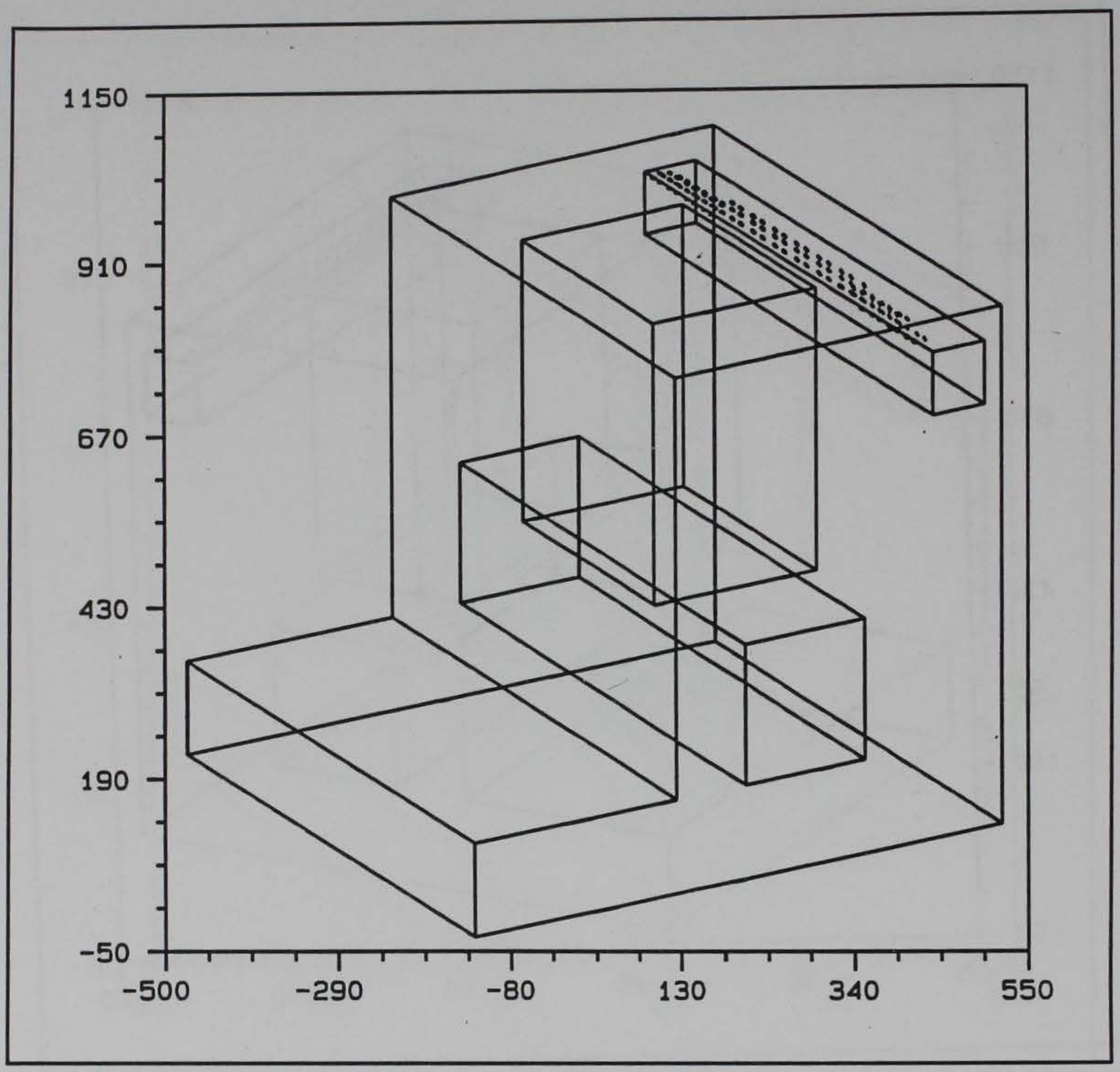

Figure 51. Crack plot, isometric view at day 279

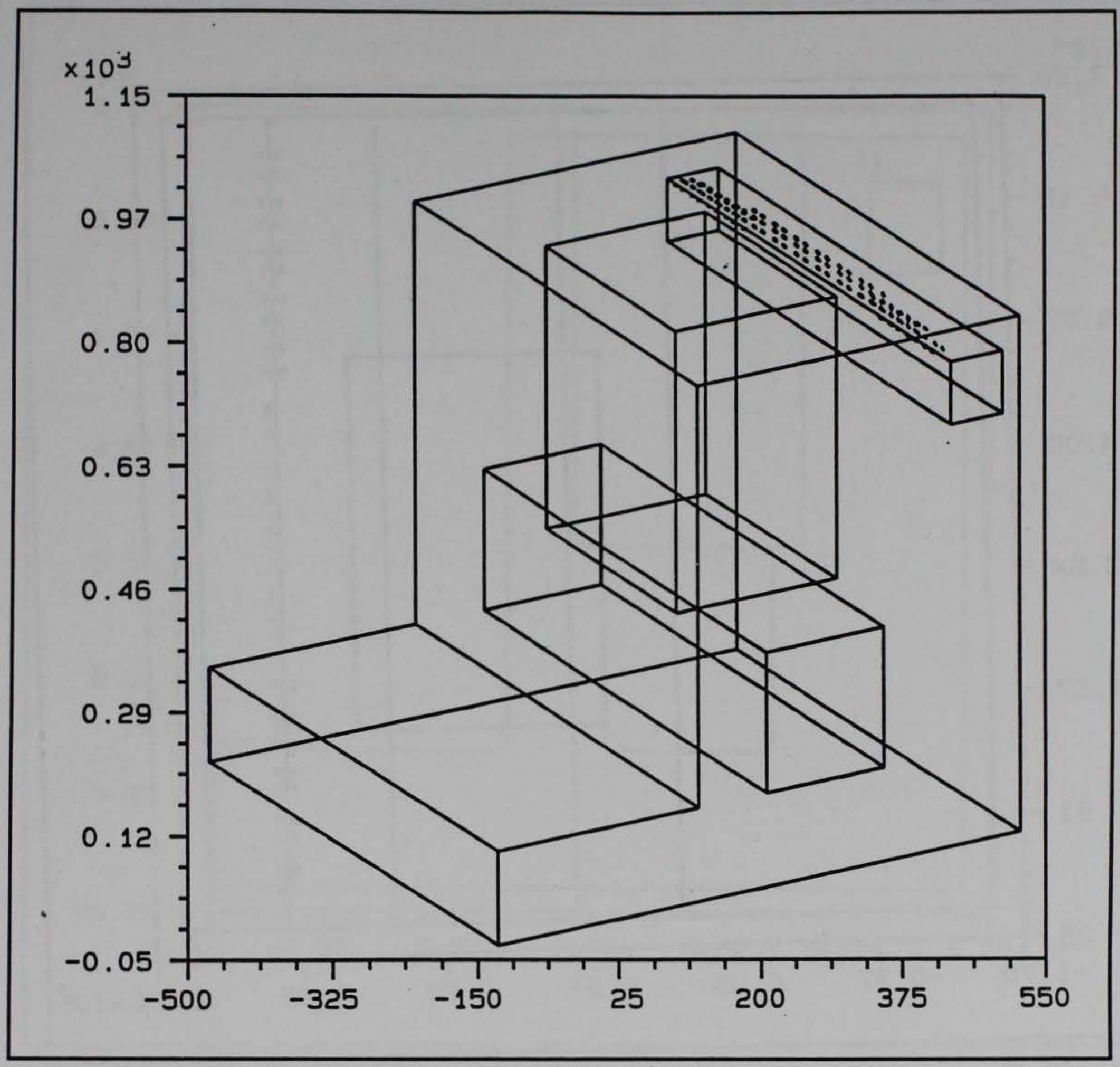

Figure 52. Crack plot, isometric view at day 289

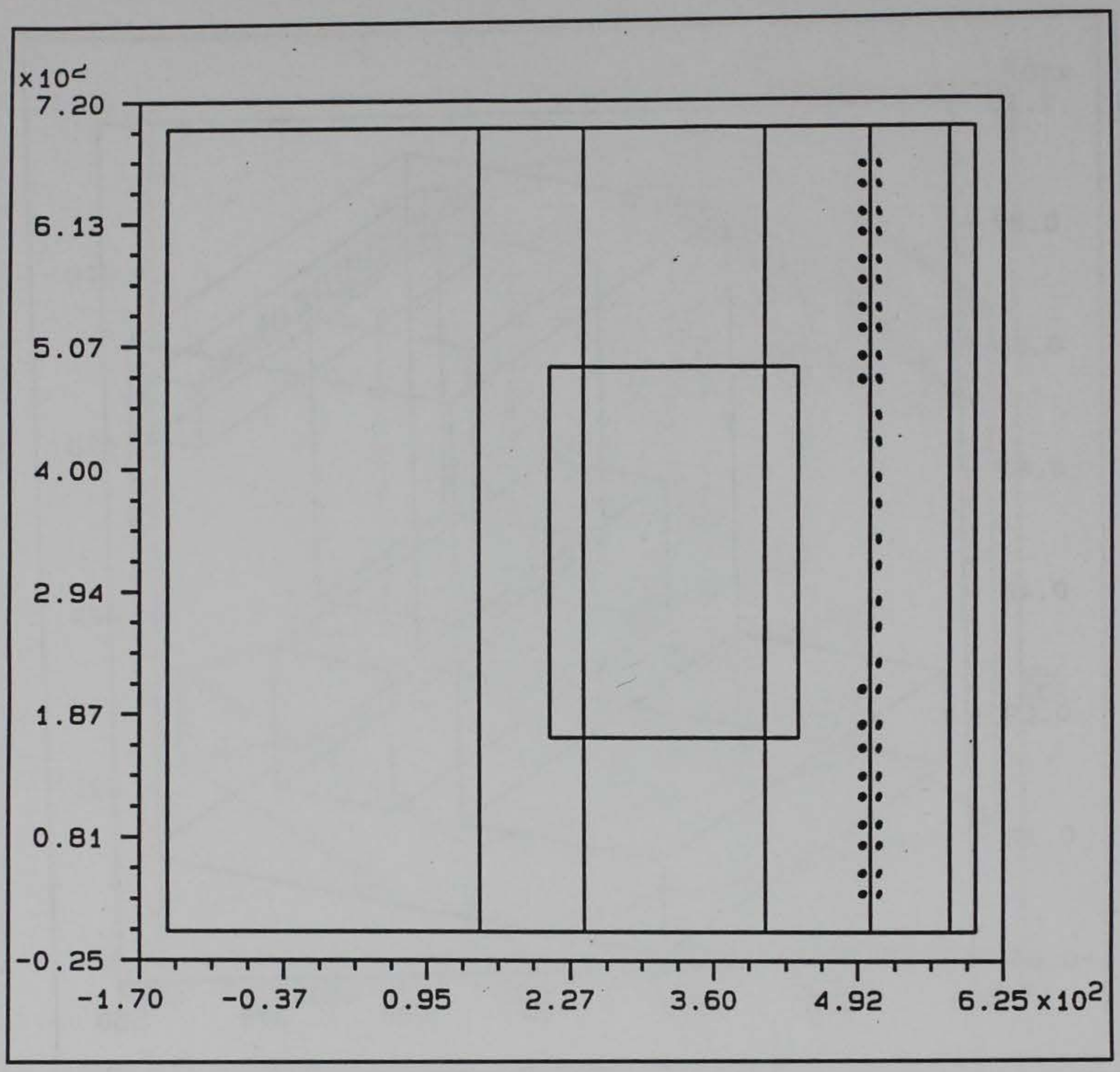

Figure 53. Crack plot, plan view at day 289

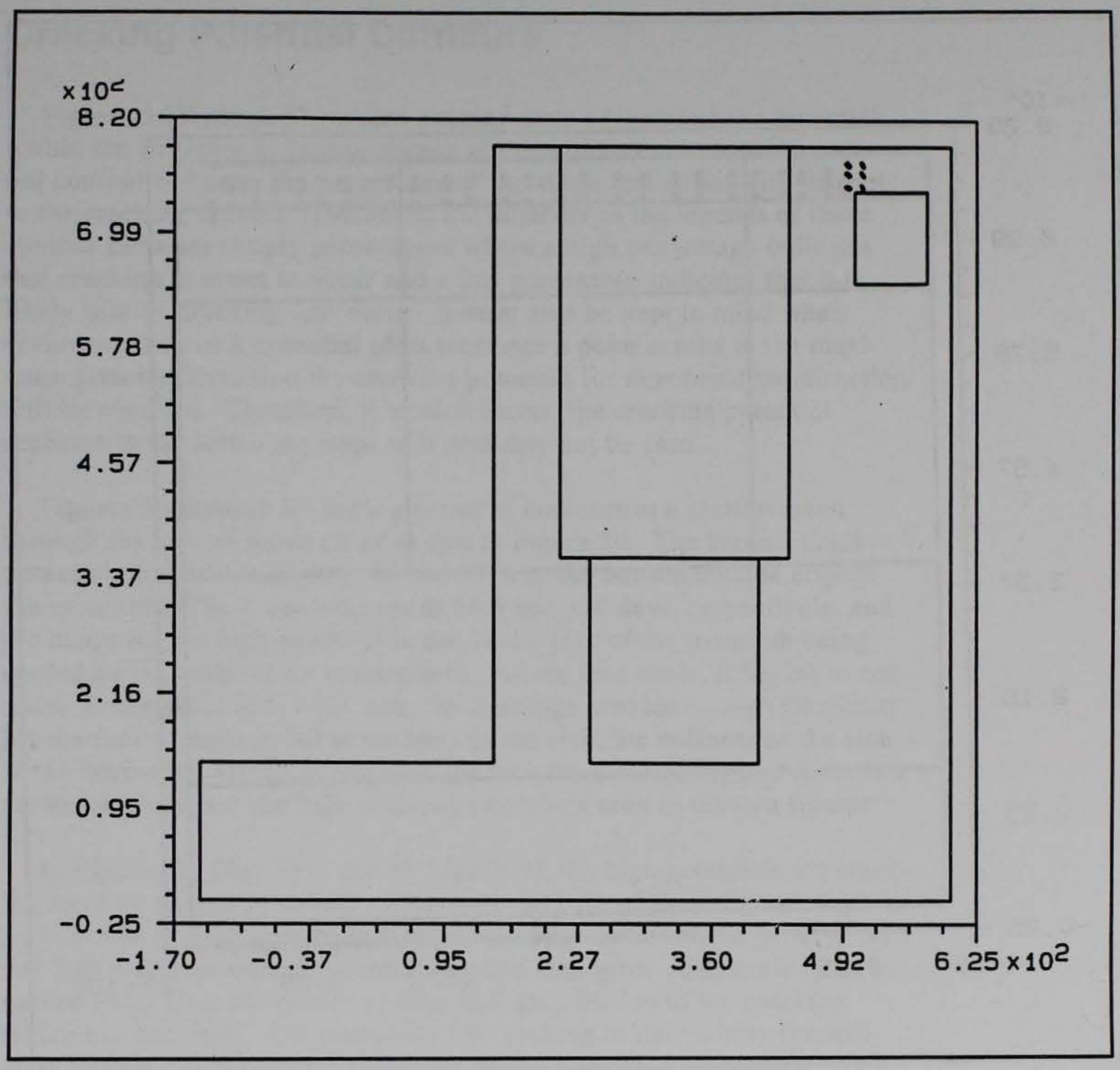

Figure 54. Crack plot, front elevation at day 289

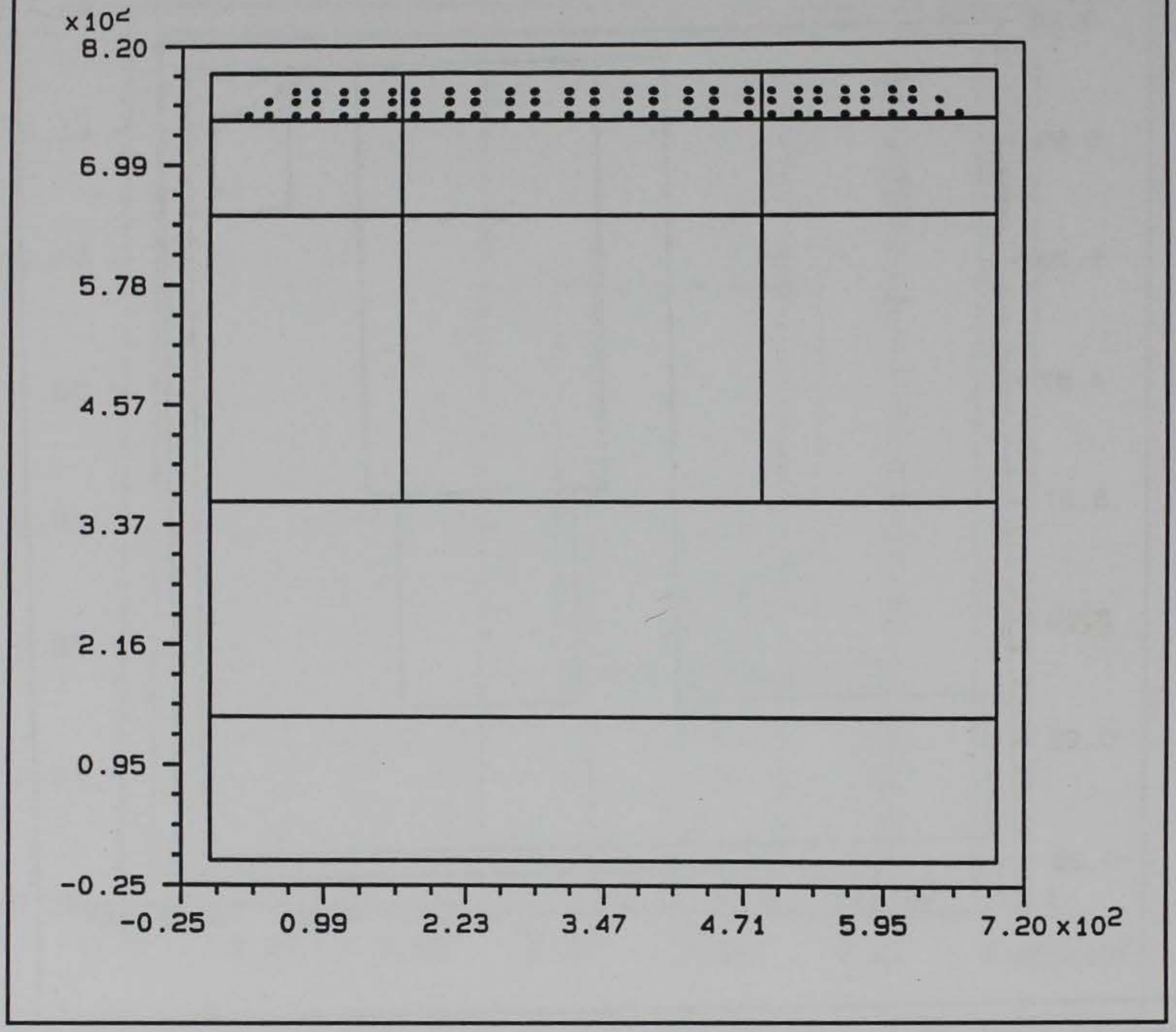

Figure 55. Crack plot, side elevation at day 289

Cracking Potential Contours

Figures 56 through 67 present contour plots of the cracking potential within the structure at various planes of the structure. A cracking potential contour indicates the percentage of the stress and strain with respect to the cracking criteria. Therefore, the numbers in the legends of these contour plots are simply percentages where a high percentage indicates that cracking is about to occur and a low percentage indicates that it is likely that no cracking will occur. It must also be kept in mind when reviewing the crack potential plots that once a point cracks in the maximum principal direction the cracking potential for next principal direction will be reported. Therefore, if a crack forms, the cracking potential reported in the following steps will probably not be zero.

Figures 56 through 61 show a series of contours at a section taken through the culvert valve pit as shown in Figure 20. The highest crack potential observed in Figures 56 and 57 is in the bottom outside edge of the monolith. These contours are at 64.5 and 104 days, respectively, and the cause for the high potential is due to the face of the monolith being cooled by the ambient air temperature. As the face cools, it begins to contract. In the areas above the slab, the openings provide enough flexibility for the face to deflect, but at the base of the slab, the stiffness of the slab in the horizontal direction restrains the face from deflecting and induces a stress which causes the high cracking potentials seen in the two figures.

In Figures 58 (day 179) and 59 (day 209), the high potentials for cracking have all moved to the top of the wall. In both of these figures there is a collection of high potentials around the upper corner of the gallery. By day 269 the collection of potentials around the corner of the gallery have moved away from the corner as seen in Figure 60 due to the cracking which has occurred. The potentials for cracking in the vicinity immediately adjacent to the corner have been reduced in this area because when concrete cracks due to thermal loads, the energy associated with the loading is released. Finally, in Figure 61, the cracking potential at the end of the analysis is presented and, as can be seen the potentials, are relatively low in all areas of the monolith at this particular cross section.

Figures 62 through 66 present crack potentials at a transverse section at the downstream edge of the culvert valve pit. As before, high potentials can be seen in the bottom, outside edge of the wall at 54 days (Figure 62) and 64.5 days (Figure 63). But for this location high potentials begin to form near the top of the wall at day 64.5. The 78-percent maximum crack potential seen in Figure 63 is occurring at the corner of the culvert valve pit. In Figure 64 (day 169), high potentials again form at the top of the wall at the corner of the gallery. In Figure 65 (day 209), potentials are relatively low except around the gallery where they are approaching the threshold of cracking. Then by day 269 (Figure 66), potentials within the lower portions of the wall begin to rise while the potentials at the top of the wall begin to fall.

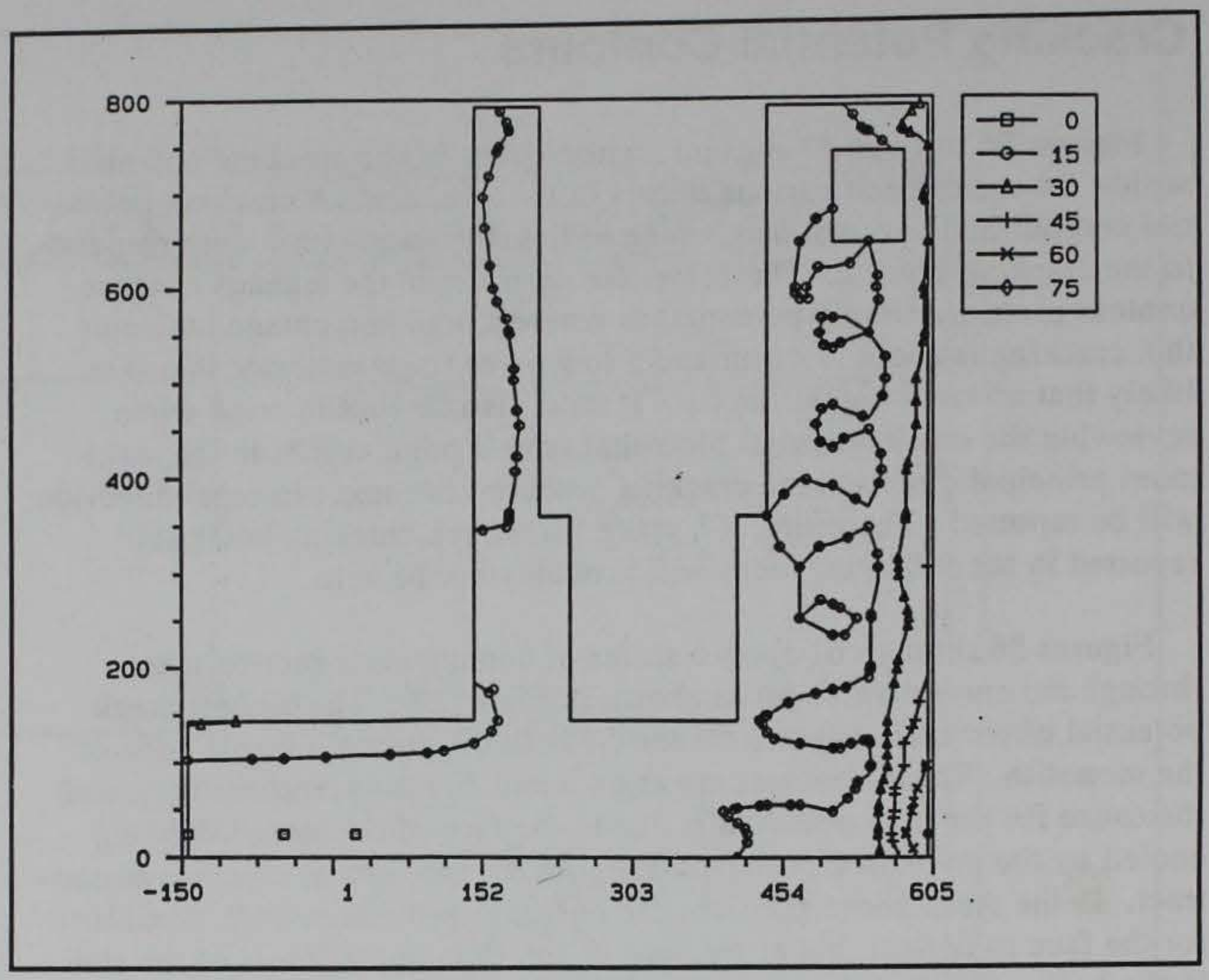

Figure 56. Crack potential contours, transverse section through valve pit at day 64.5

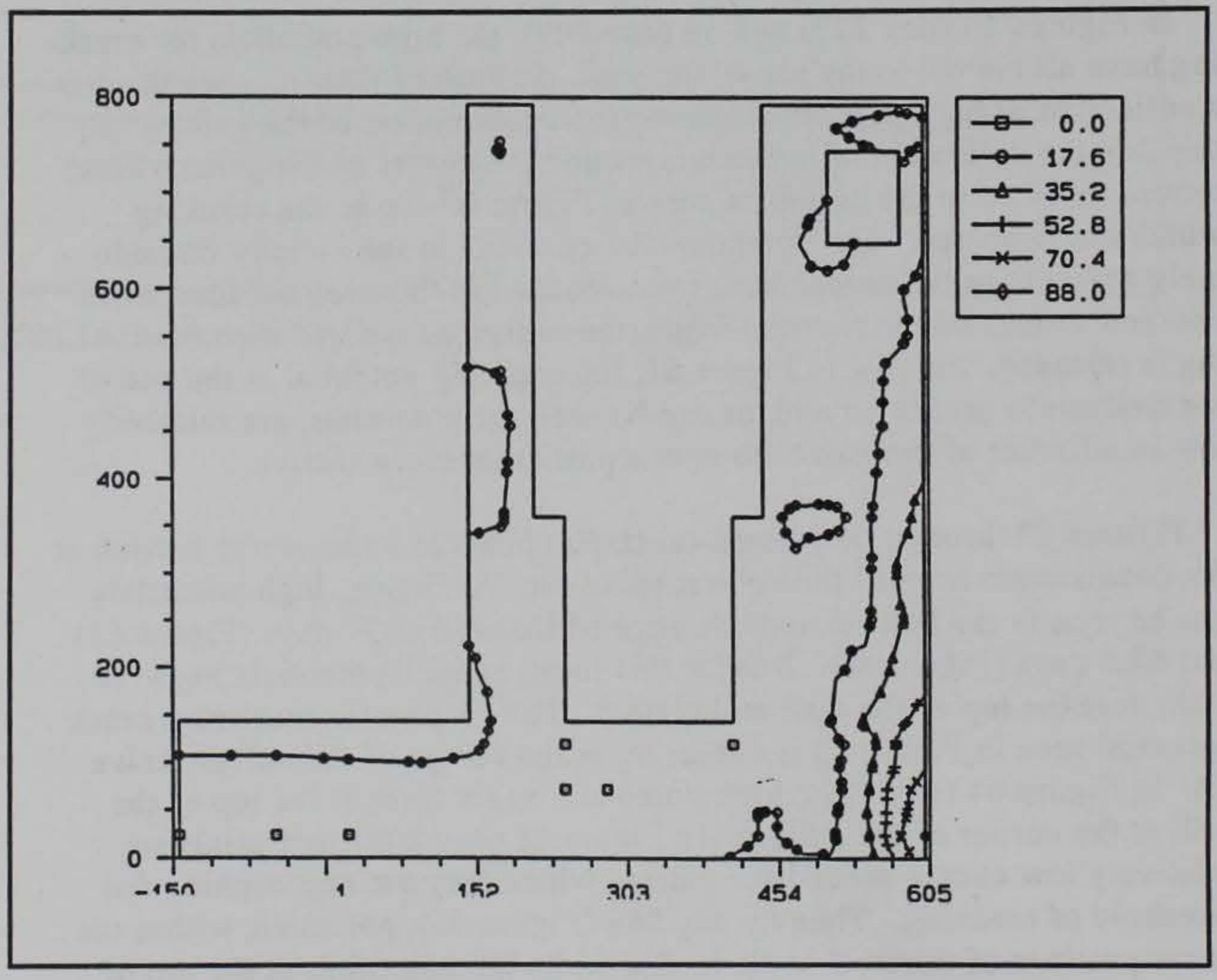

Figure 57. Crack potential contours, transverse section through valve pit at day 104

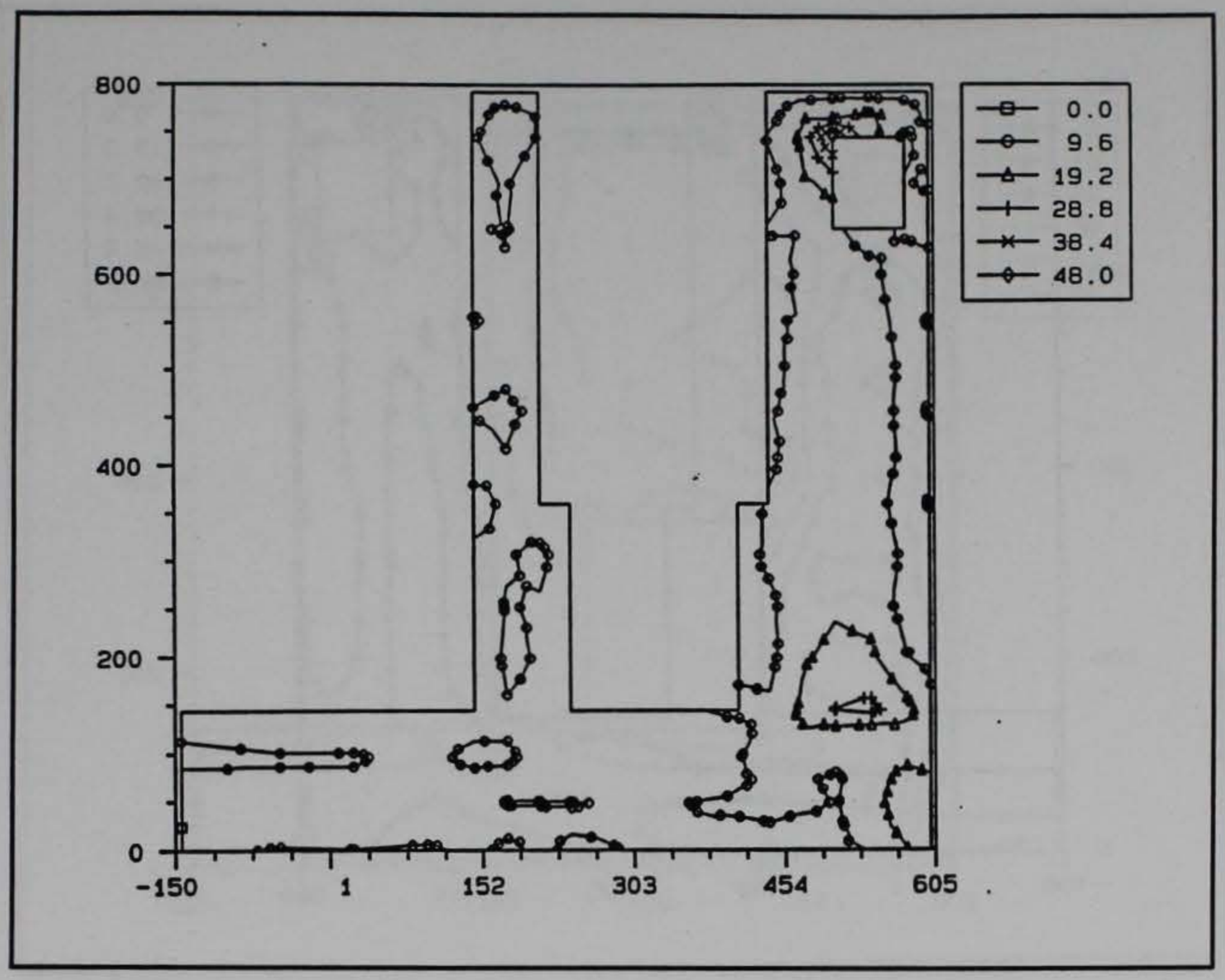

Figure 58. Crack potential contours, transverse section through valve pit at day 179

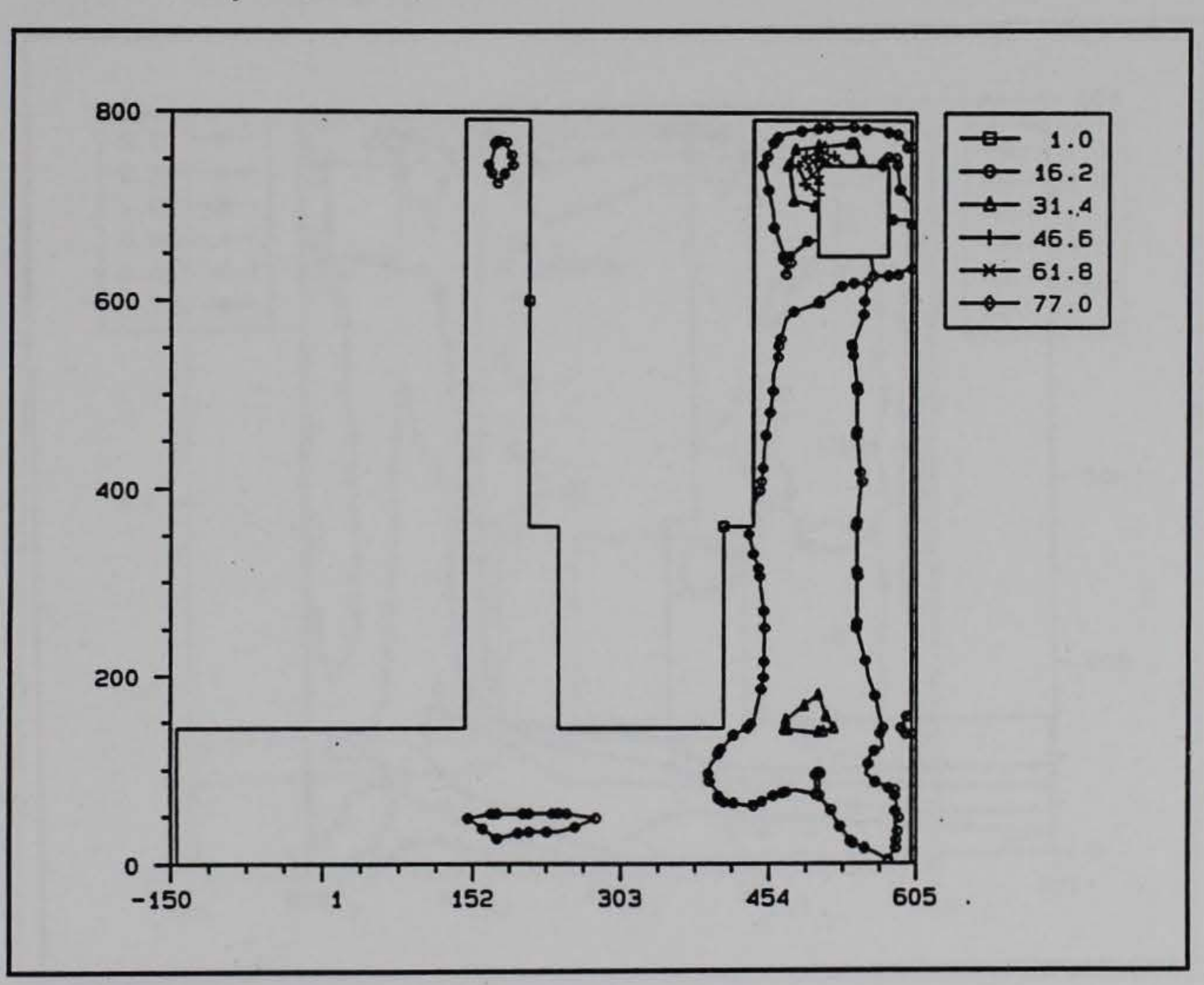

Figure 59. Crack potential contours, transverse section through valve pit at day 209

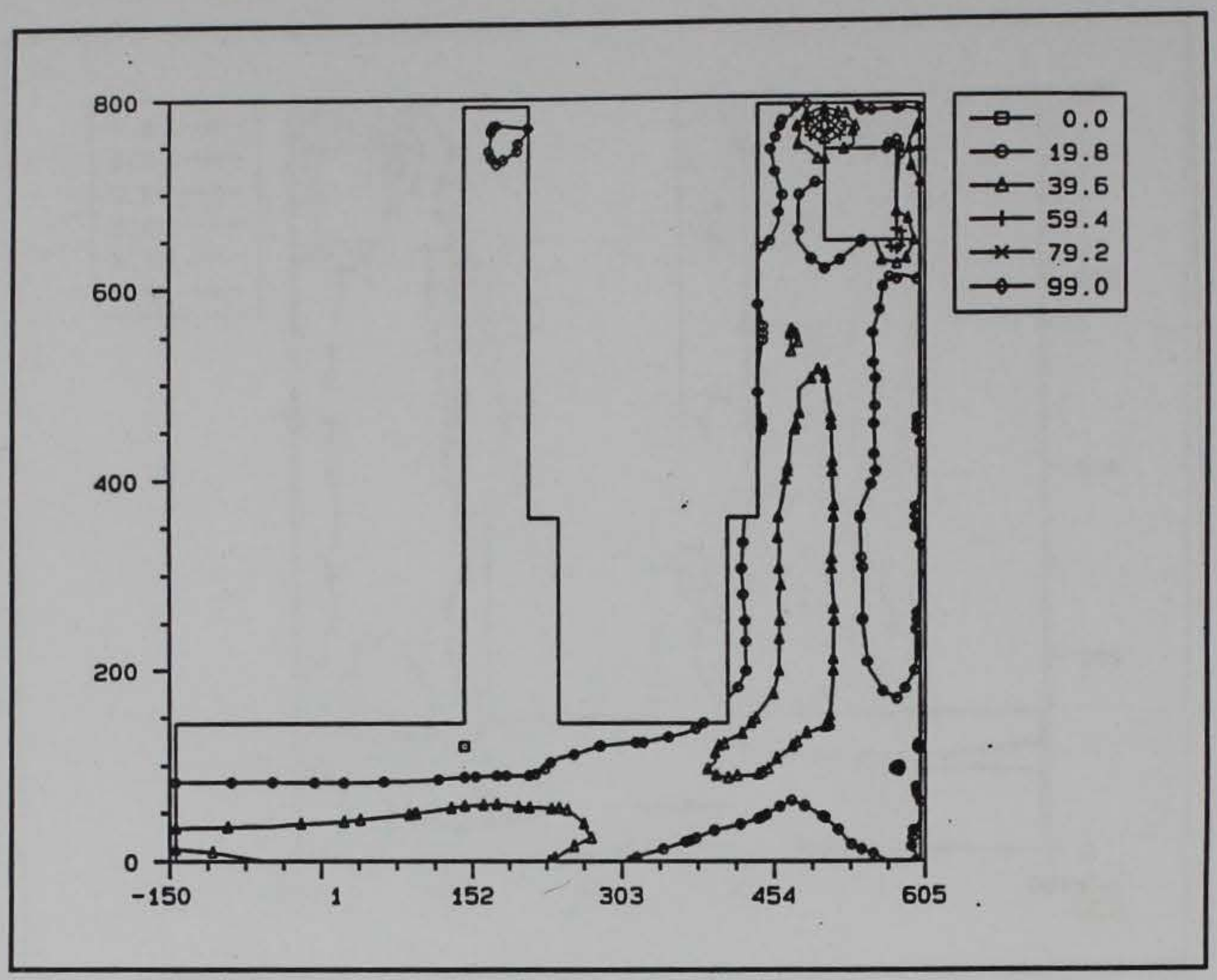

Figure 60. Crack potential contours, transverse section through valve pit at day 269

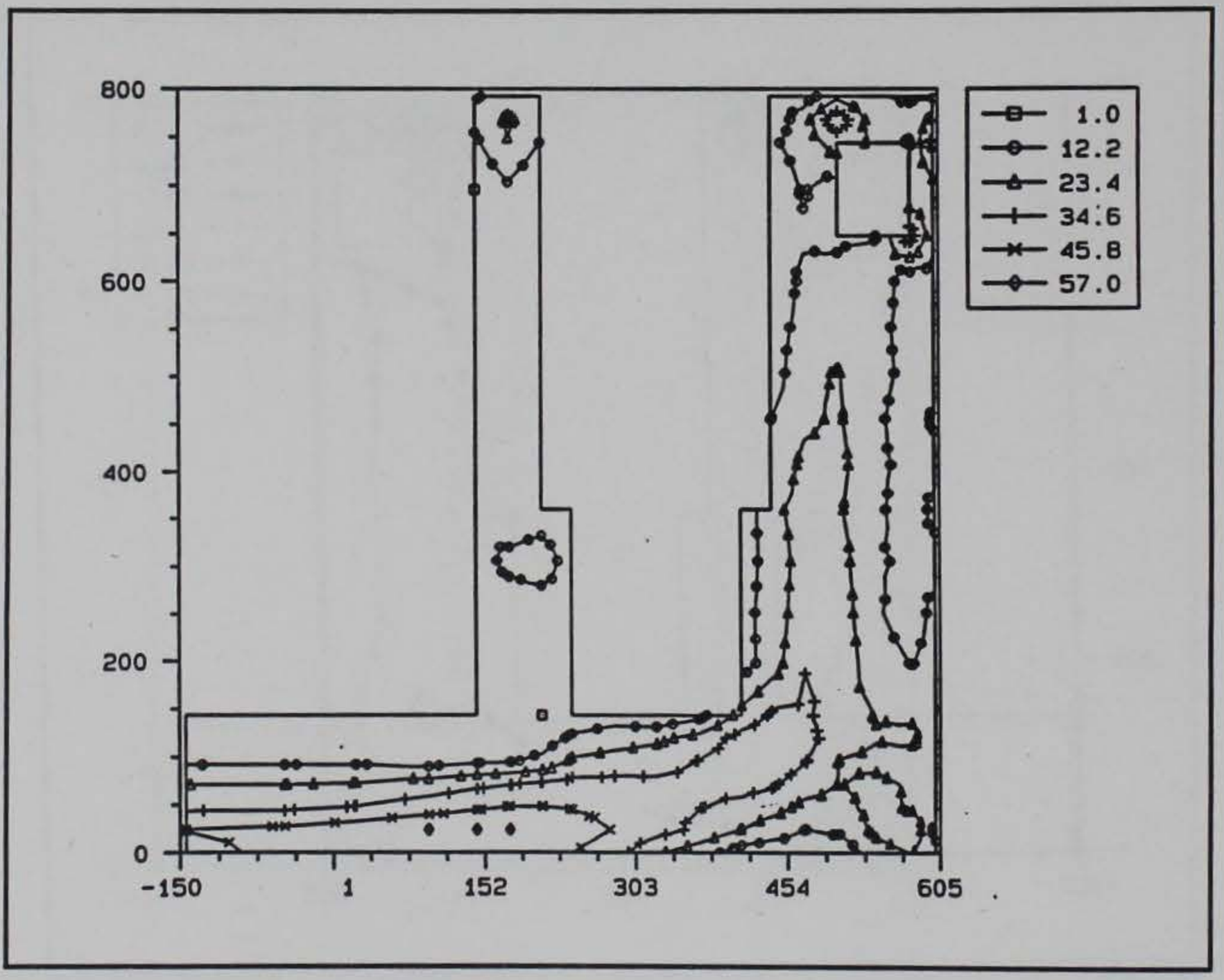

Figure 61. Crack potential contours, transverse section through valve pit at day 359

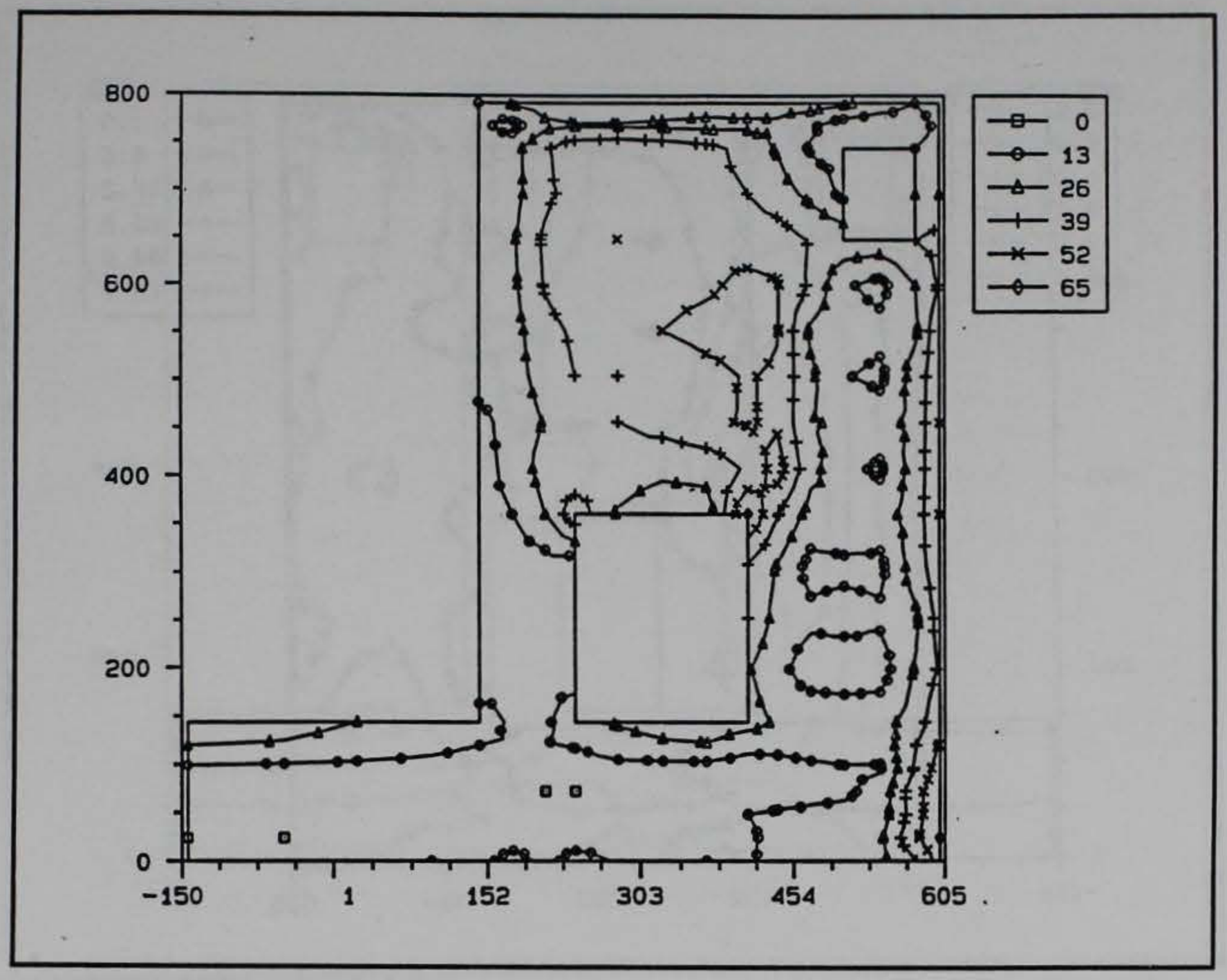

Figure 62. Crack potential contours, transverse section at DS edge of valve pit at day 54

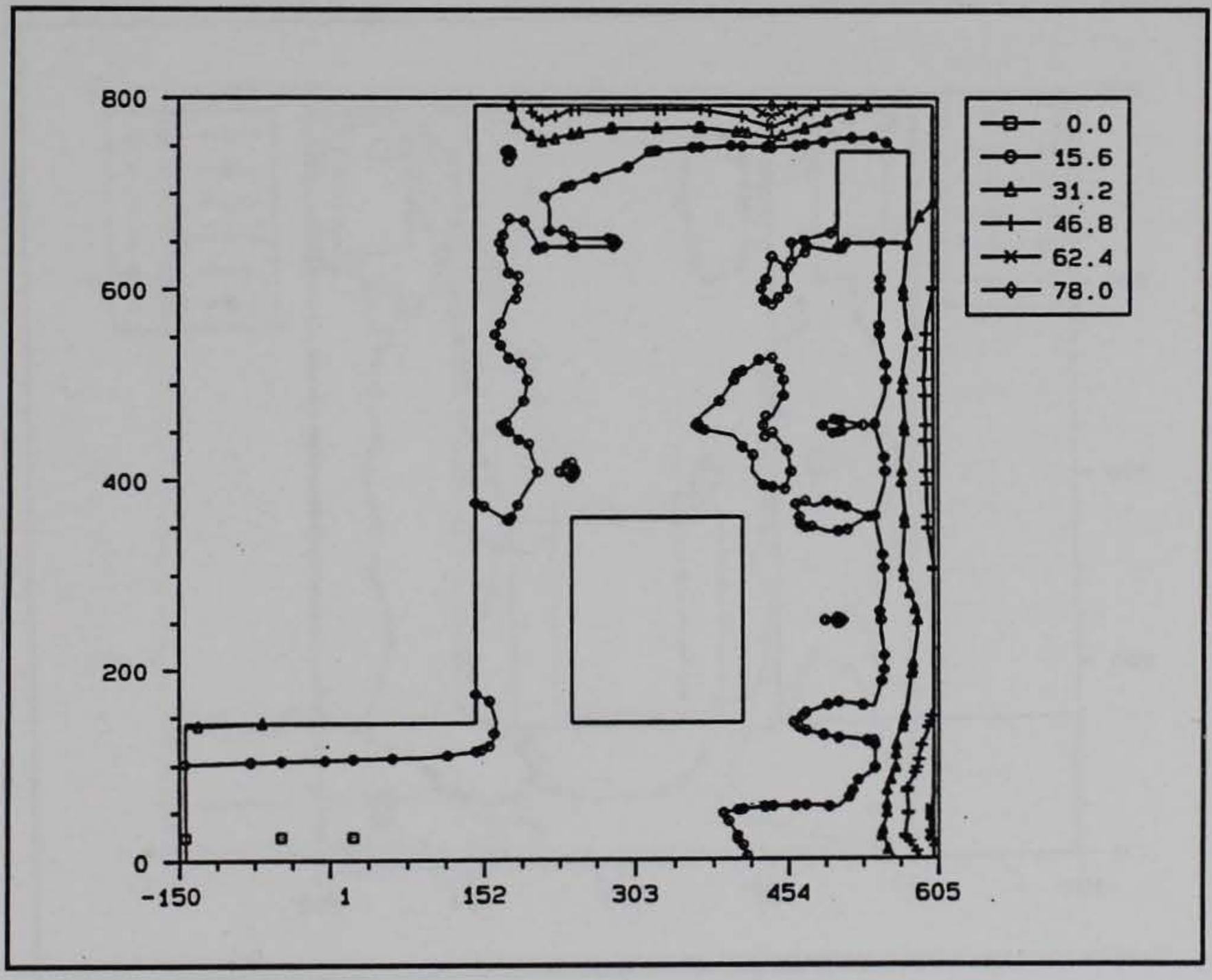

Figure 63. Crack potential contours, transverse section at DS edge of valve pit at day 64.5

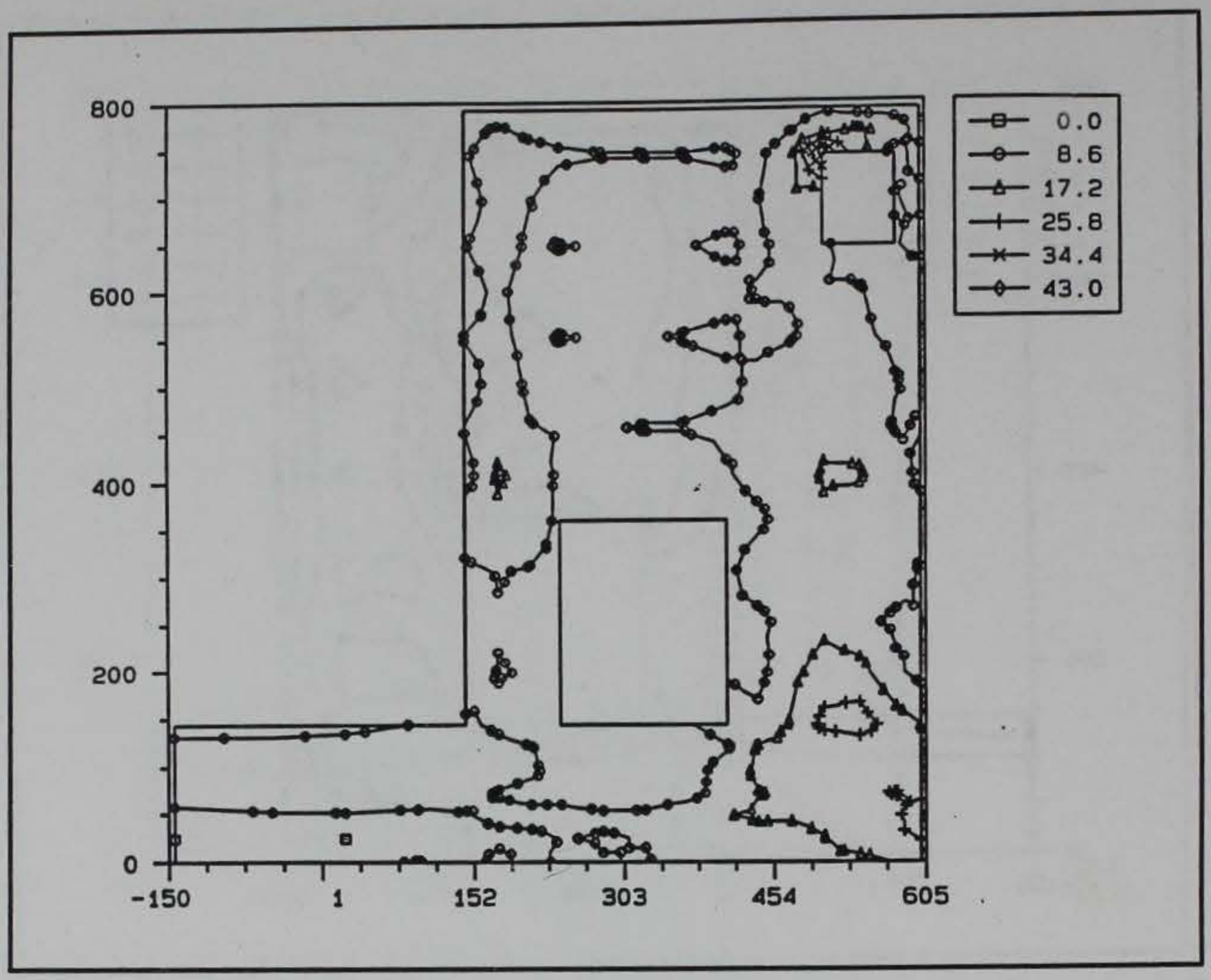

Figure 64. Crack potential contours, transverse section at DS edge of valve pit at day 169

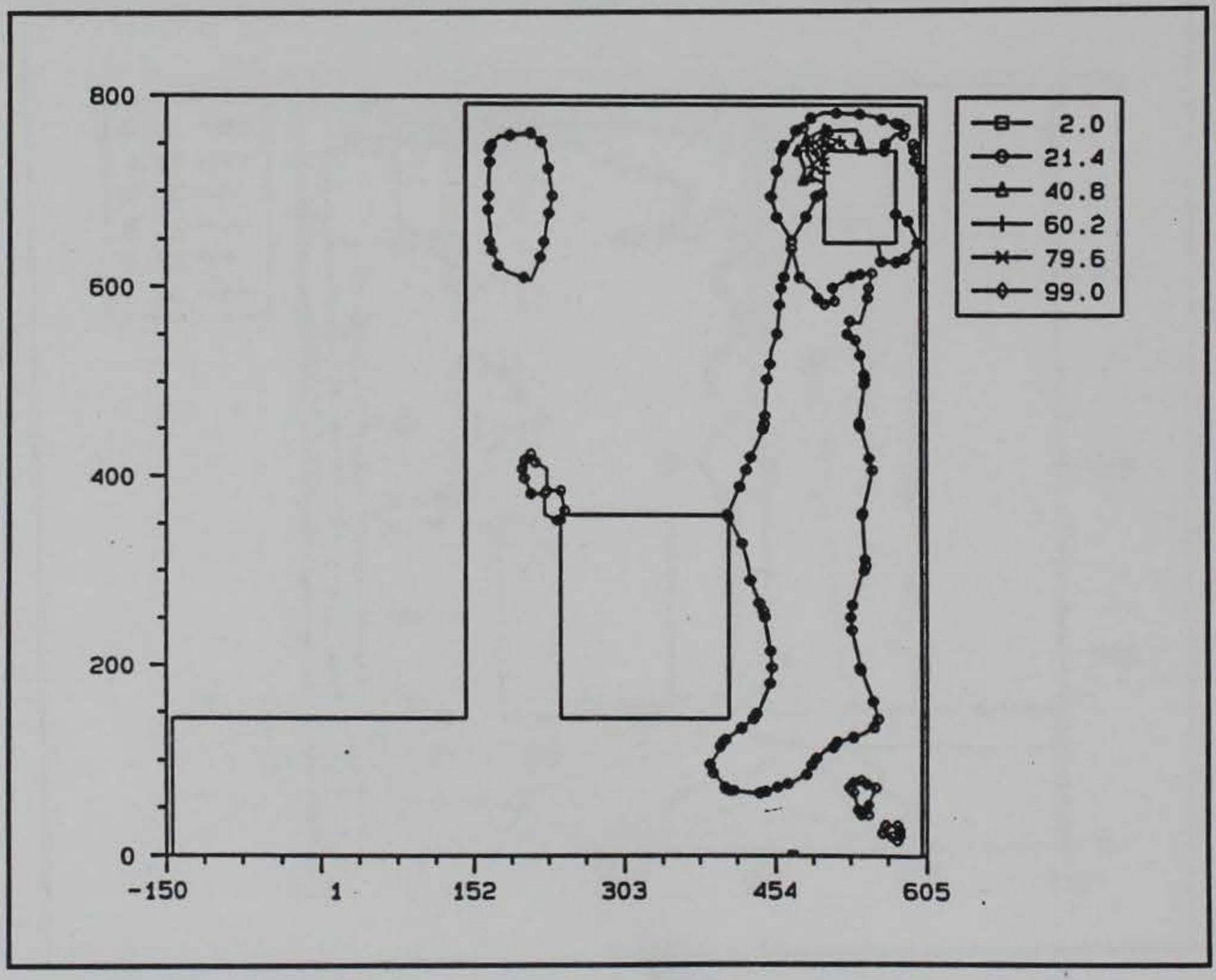

Figure 65. Crack potential contours, transverse section at DS edge of valve pit at day 209

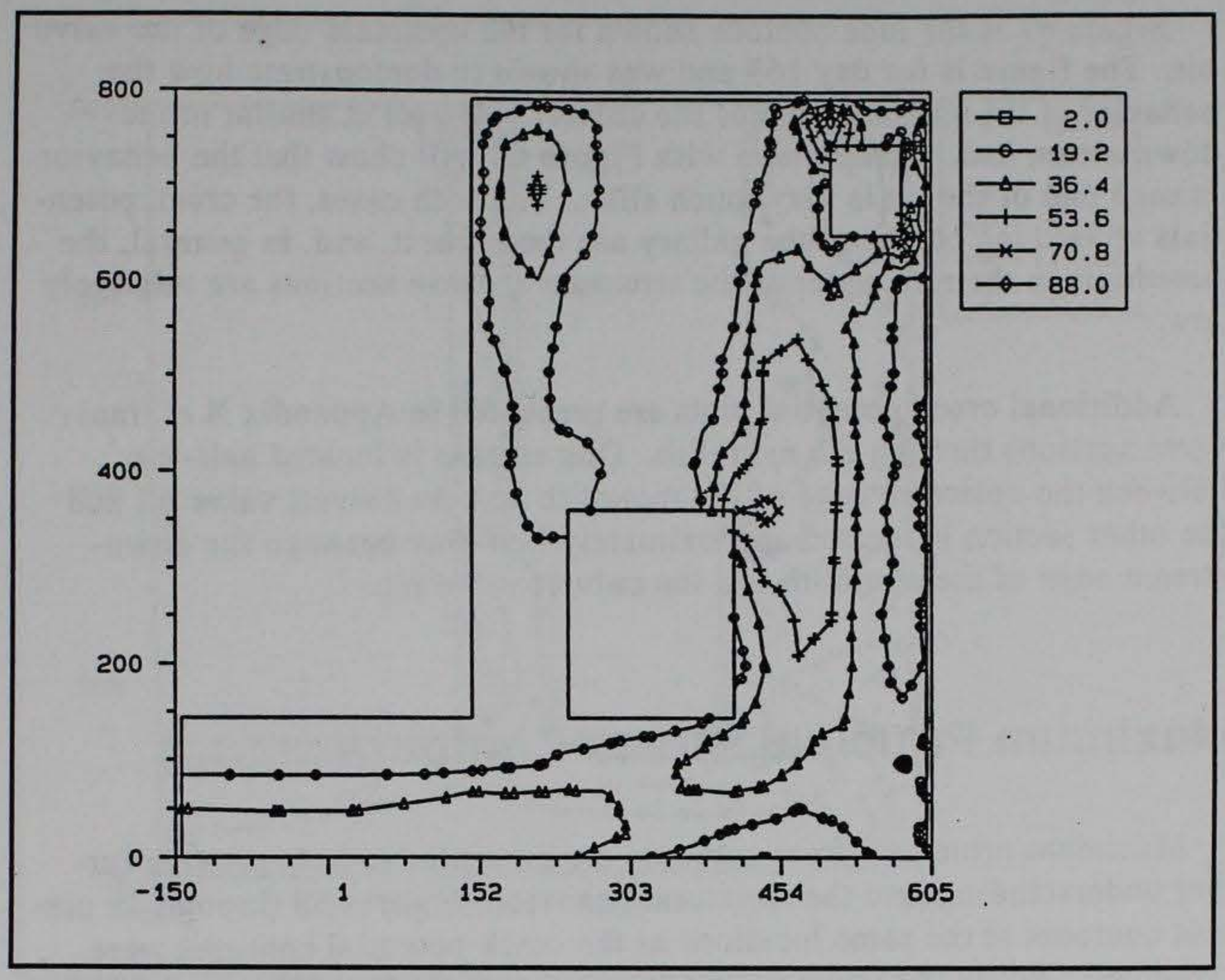

Figure 66. Crack potential contours, transverse section at DS edge of valve pit at day 269

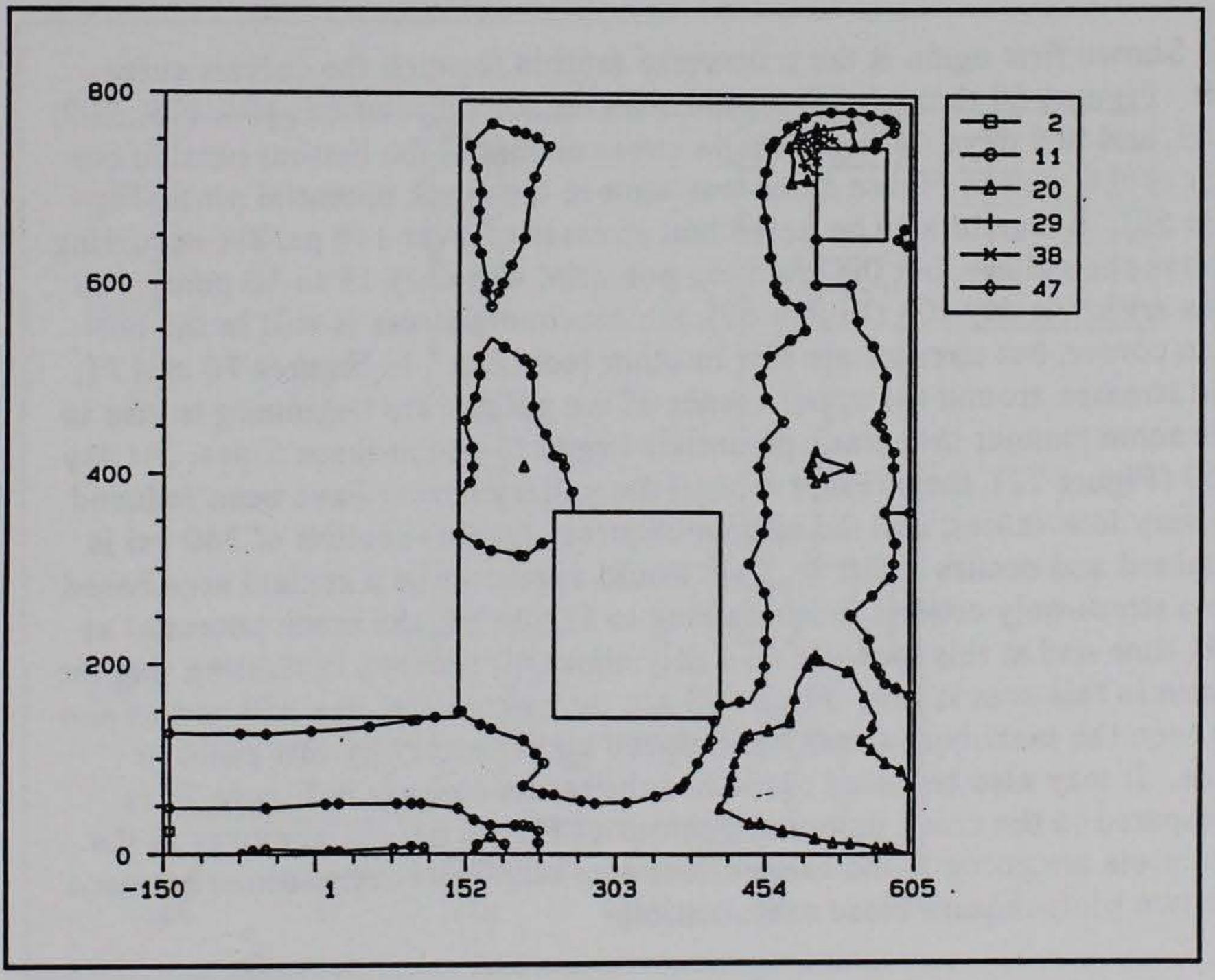

Figure 67. Crack potential contours, transverse section at US edge of valve pit at day 169

Figure 67 is the lone contour shown for the upstream edge of the valve pit. The figure is for day 169 and was shown to demonstrate how the behavior at the upstream end of the culvert valve pit is similar to the downstream end. Comparison with Figure 64 will show that the behavior at each end of the pit is very much alike. For both cases, the crack potentials around the corner of the gallery are the highest, and, in general, the potentials in the remainder of the structure at these sections are relatively low.

Additional crack potential plots are presented in Appendix B at transverse sections through the monolith. One section is located half-way between the upstream edge of the monolith and the culvert valve pit and the other section is located approximately half-way between the downstream edge of the monolith and the culvert valve pit.

Maximum Principal Stress Contours

Maximum principal stress contours are presented to help provide further understanding into the structural behavior. Figures 68 through 79 present contours at the same locations as the crack potential contours were presented. While the stress plots will show correlation to the crack potential plots, it will become obvious that the criteria is more than a stress-based criteria.

Shown first again is the transverse section through the culvert valve pit. Figures 68 through 73 present stresses for times of 65, 104, 179, 209, 269, and 359 days. A high tensile stress occurs in the bottom outside corner of the wall in Figure 68 as was seen in the crack potential plots (Figure 56). It should also be noted that stresses of over 140 psi are occurring above the gallery, but the cracking potential was only 15 to 30 percent in this area. At day 104 (Figure 69), the maximum stress is still in the bottom corner, but stresses are low in other locations. In Figures 70 and 71, the stresses around the upper corner of the gallery are beginning to rise in the same manner that crack potentials began to rise at these times. At day 269 (Figure 72), the stresses around the gallery corner have been reduced to very low values, and the maximum stress for this section of 340 psi is attained and occurs in lift 8. This would appear to be a critical area based on a stress-only criteria, but referring to Figure 59, the crack potential at this time and at this location was only about 40 percent, indicating that the strain in this area is low. Figure 73 are the contours at day 359 and as can be seen the maximum stress has reduced considerably by this point in time. It may also be noted that when the stress contour in Figure 73 is compared to the crack potential contour of Figure 61, the contours in the two plots are going in the same directions, but direct correlations between the two plots require close examination.

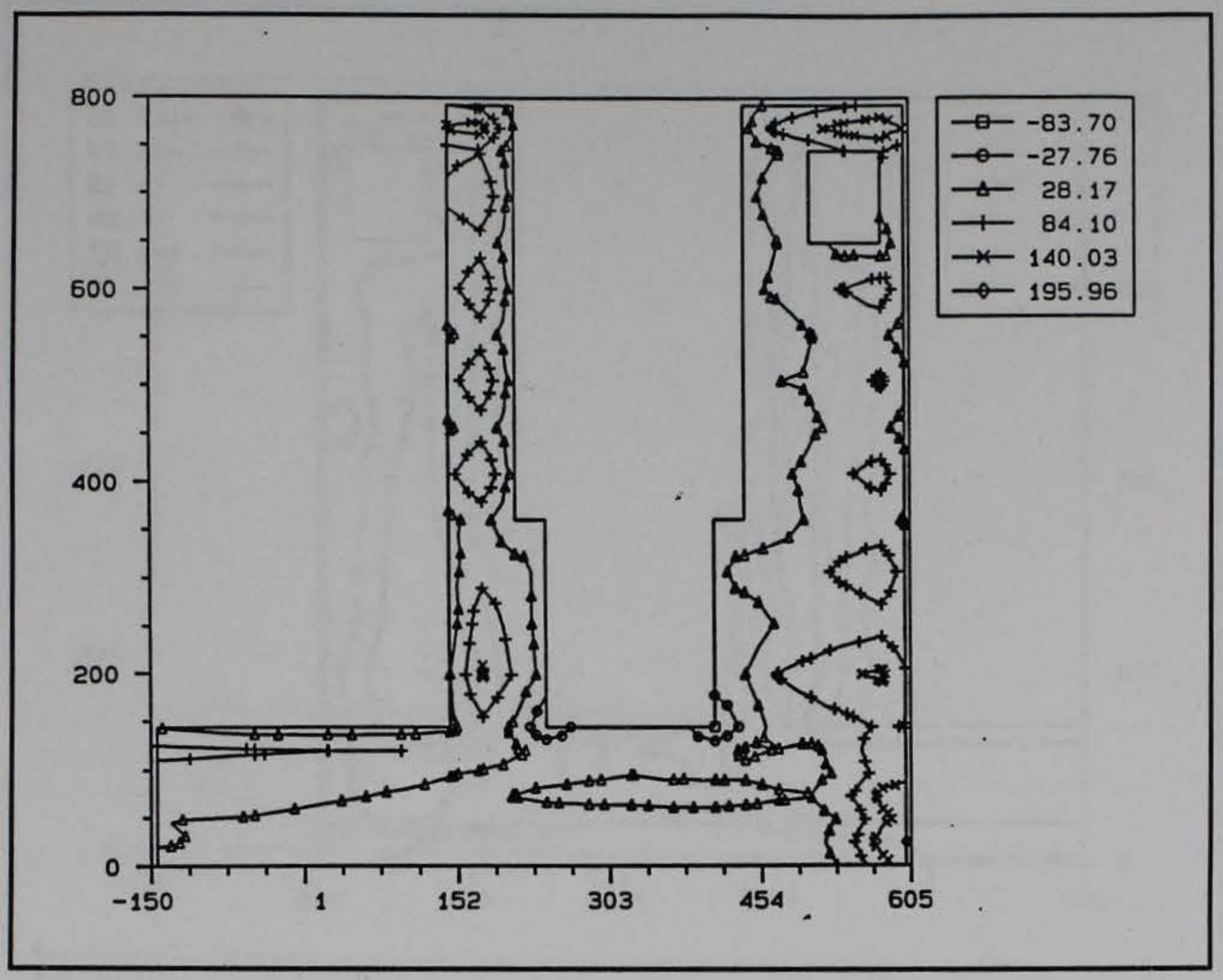

Figure 68. Maximum principal stress, transverse section through valve pit at day 64.5

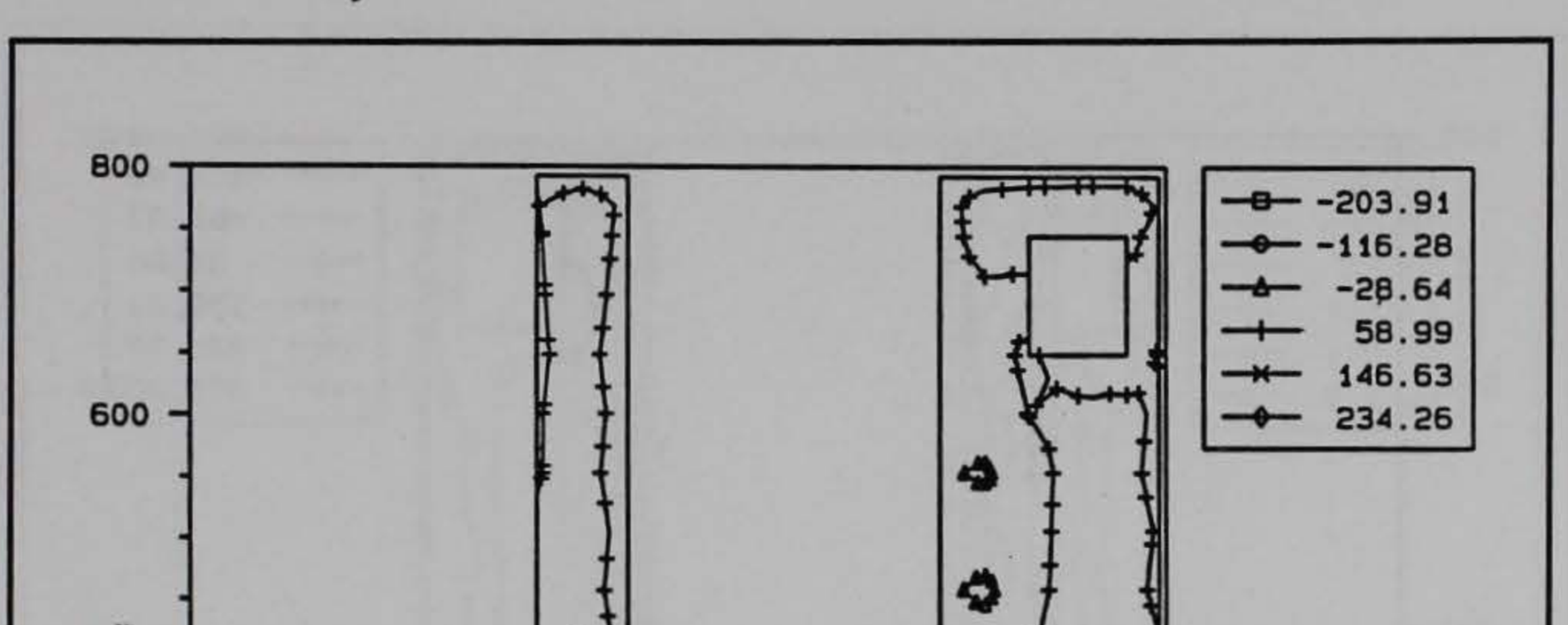

Figure 69. Maximum principal stress, transverse section through valve pit at day 104

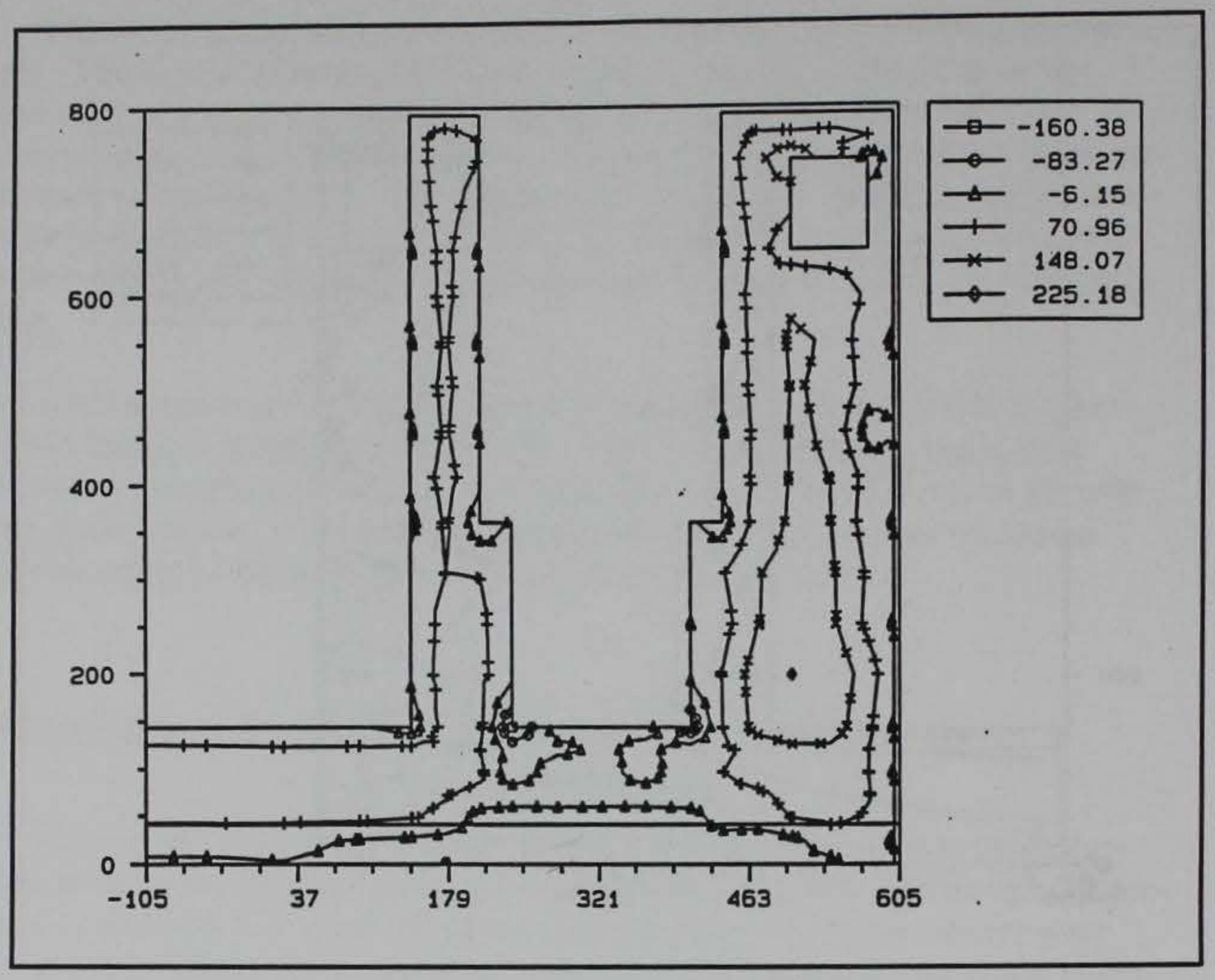

Figure 70. Maximum principal stress, transverse section through valve pit at day 179

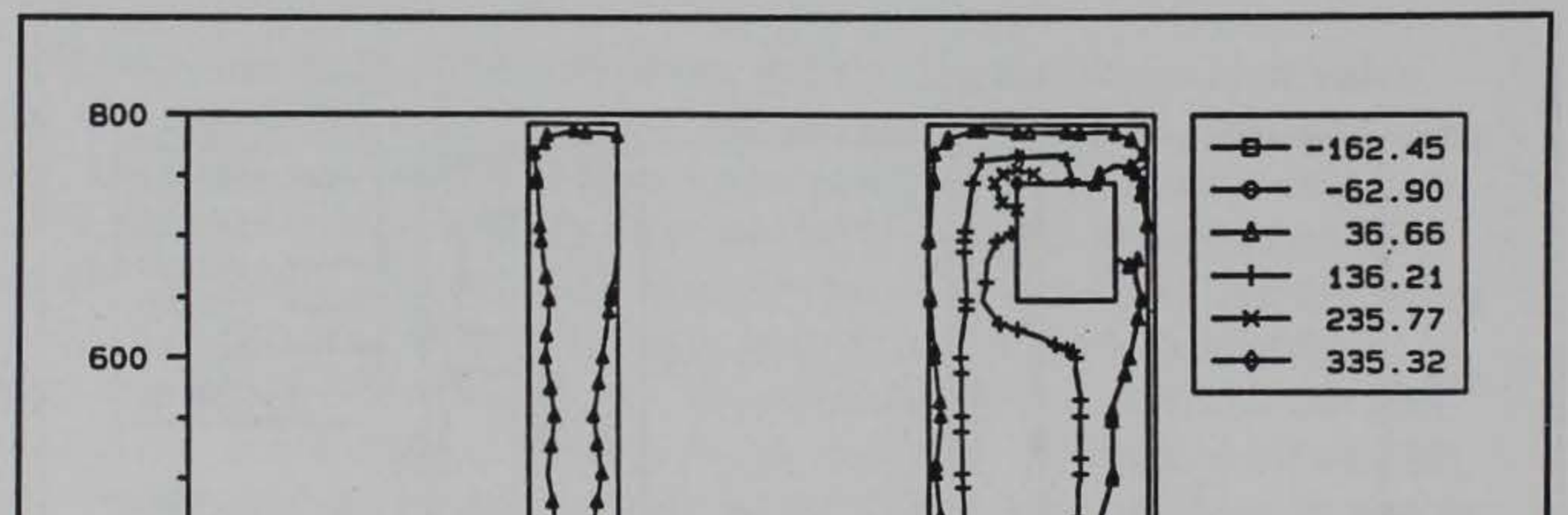

Figure 71. Maximum principal stress, transverse section through valve pit at day 209

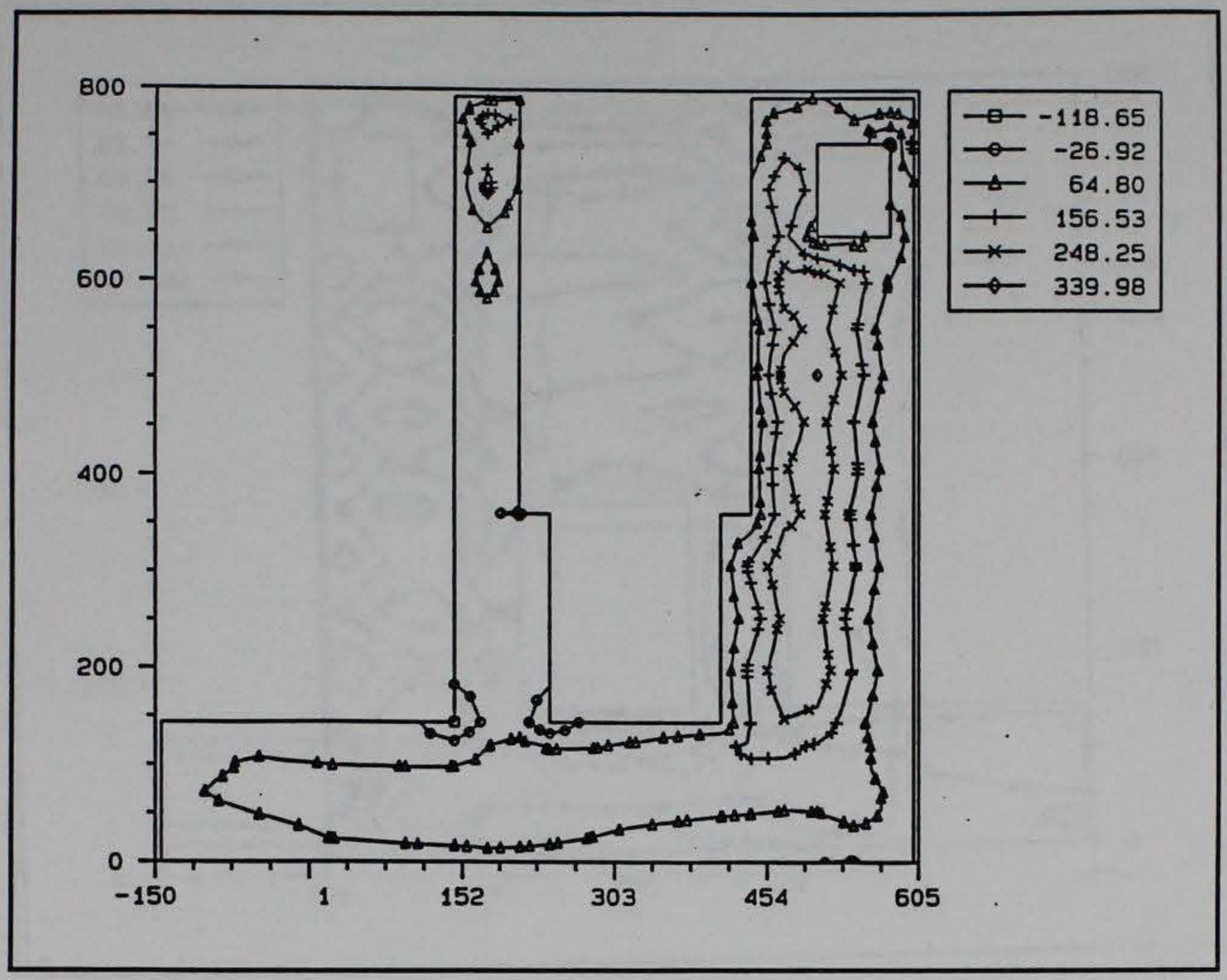

Figure 72. Maximum principal stress, transverse section through valve pit at day 269

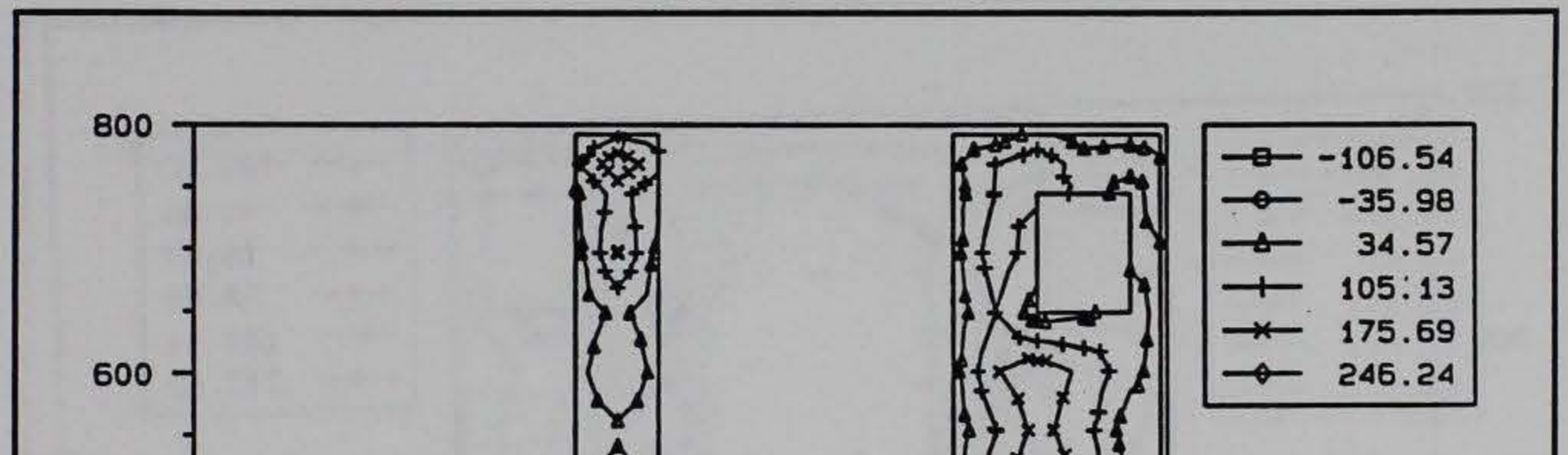

Figure 73. Maximum principal stress, transverse section through valve pit at day 359

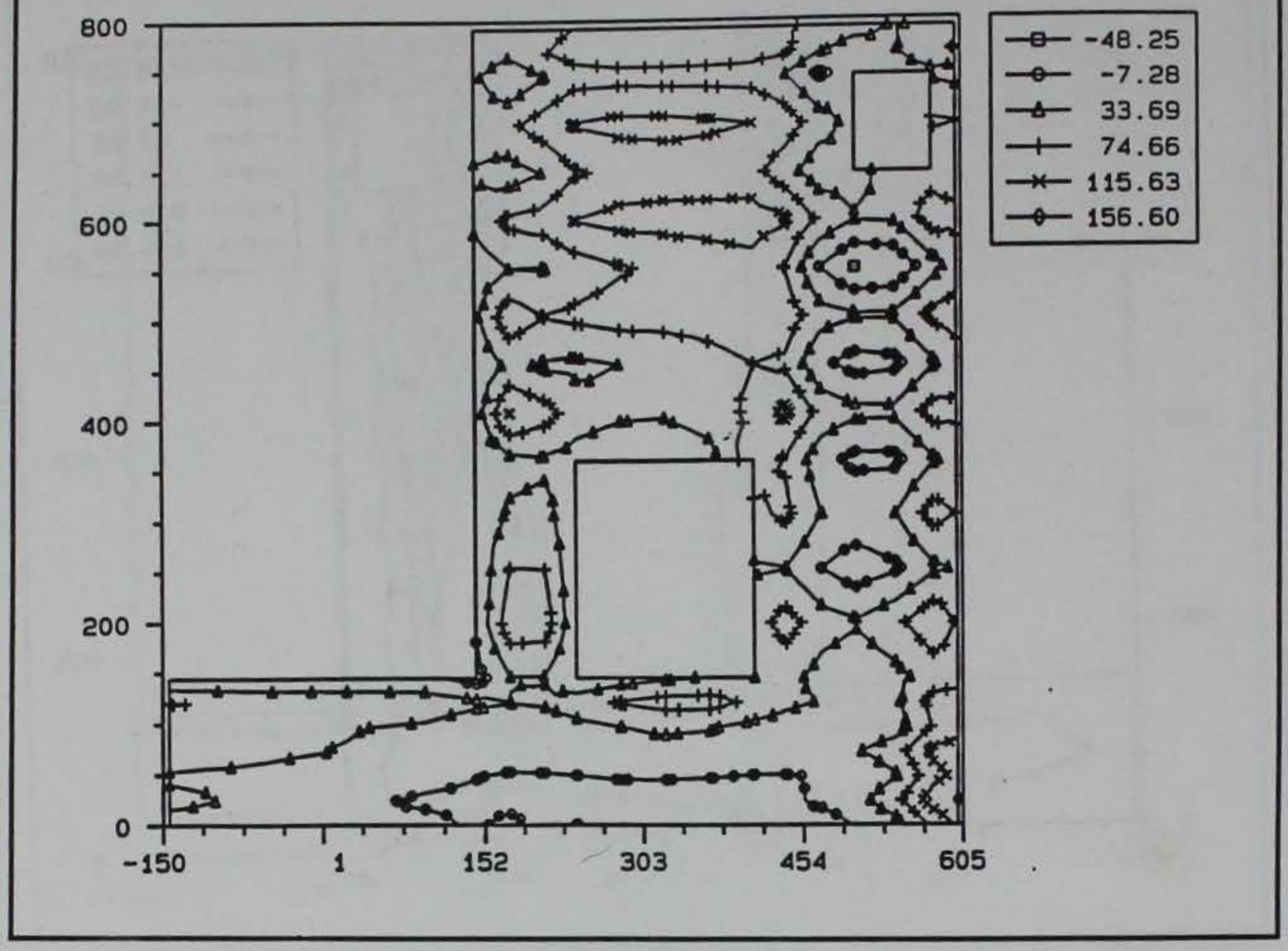

Figure 74. Maximum principal stress, transverse section at DS edge of valve pit at day 54

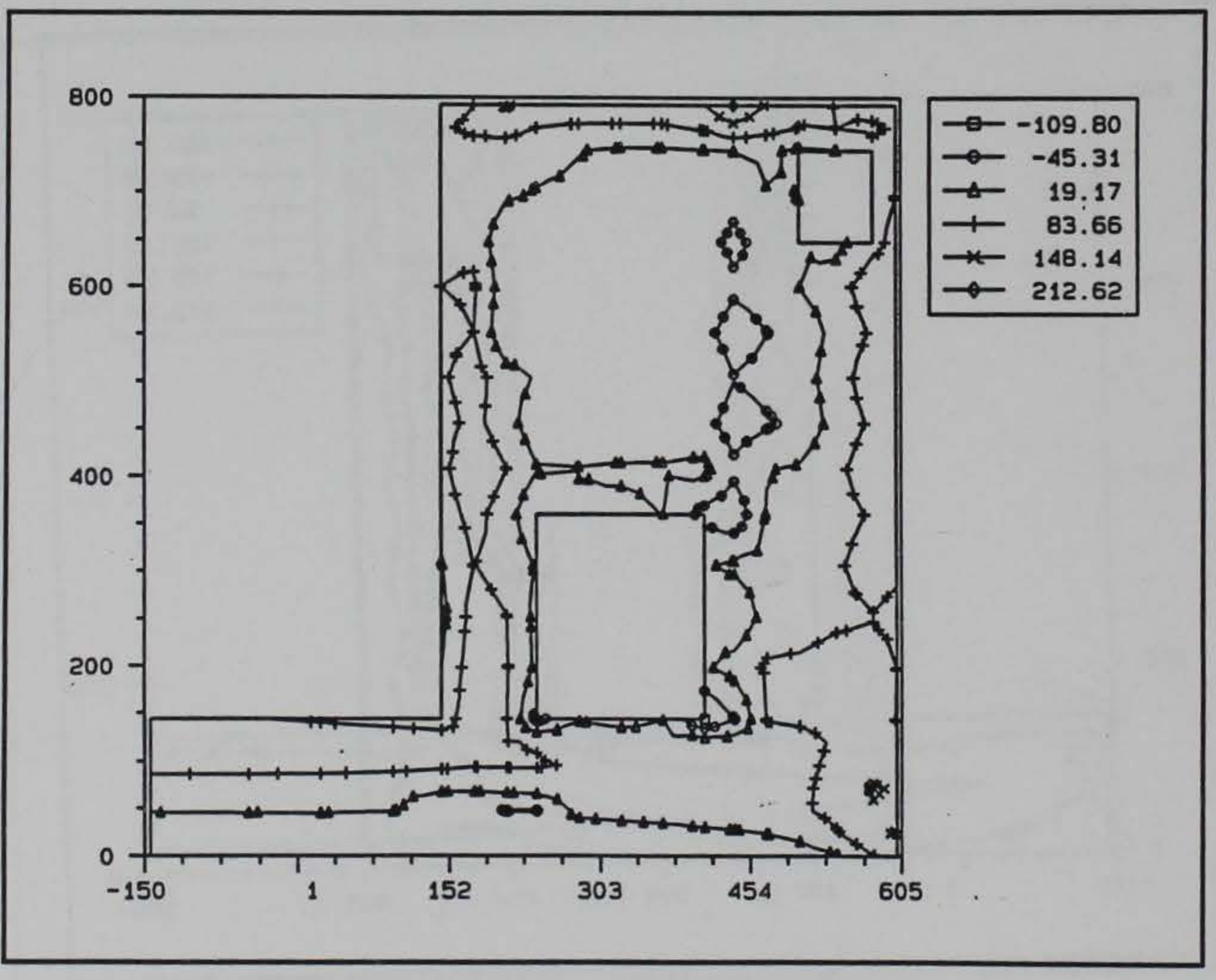

Figure 75. Maximum principal stress, transverse section at DS edge of valve pit at day 65

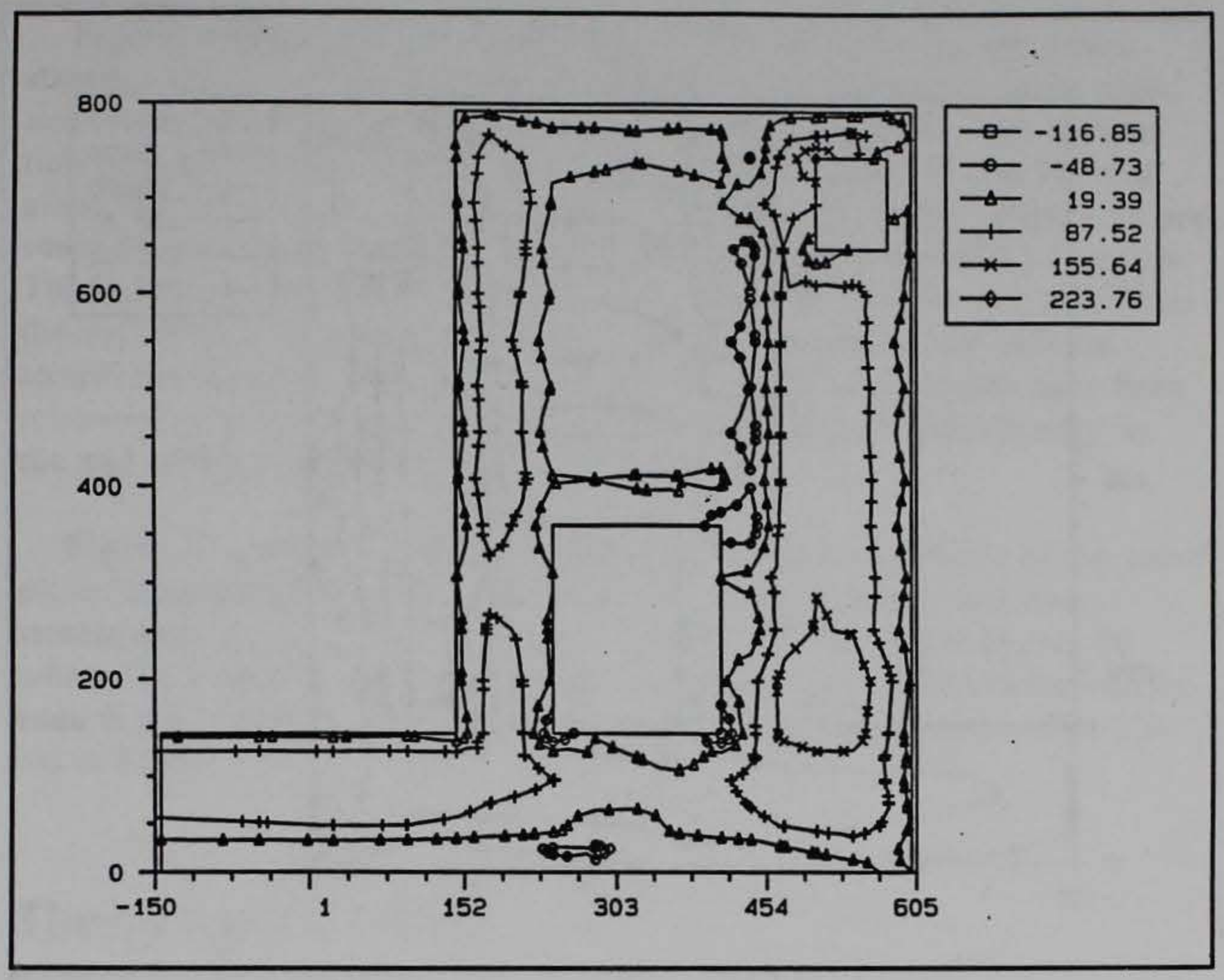

Figure 76. Maximum principal stress, transverse section at DS edge of valve pit at day 169

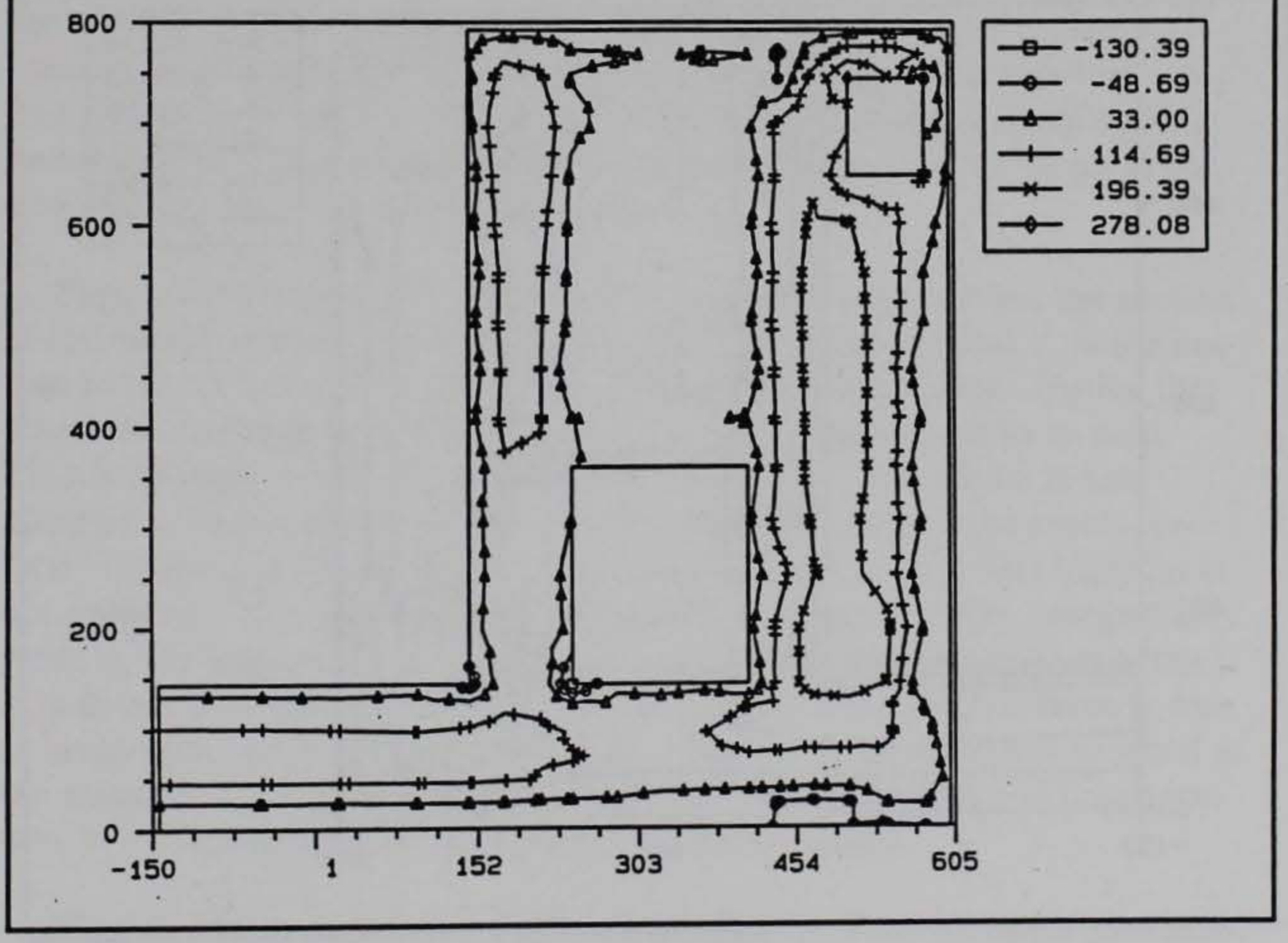

Figure 77. Maximum principal stress, transverse section at DS edge of valve pit at day 209

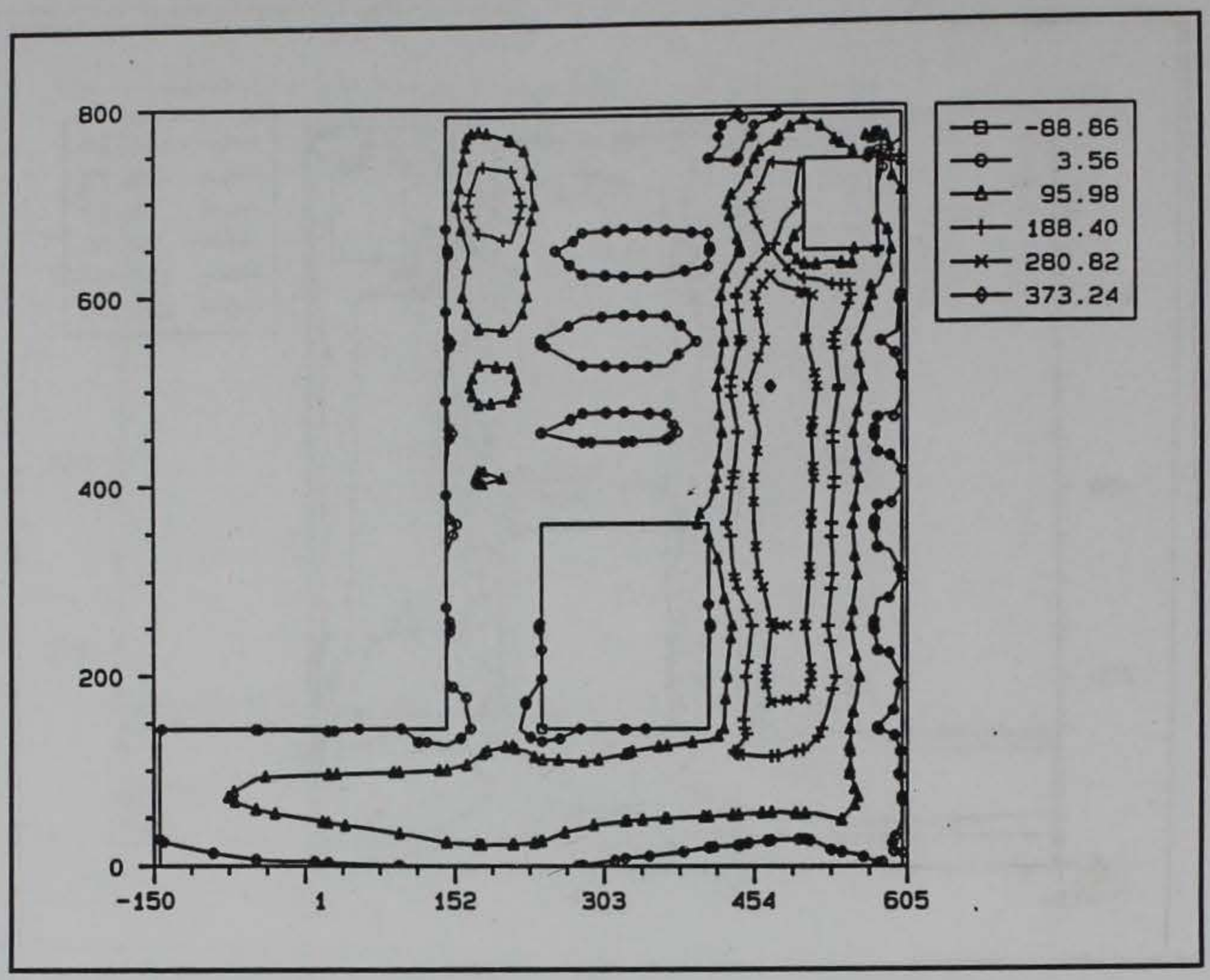

Figure 78. Maximum principal stress, transverse section at DS edge of valve pit at day 269

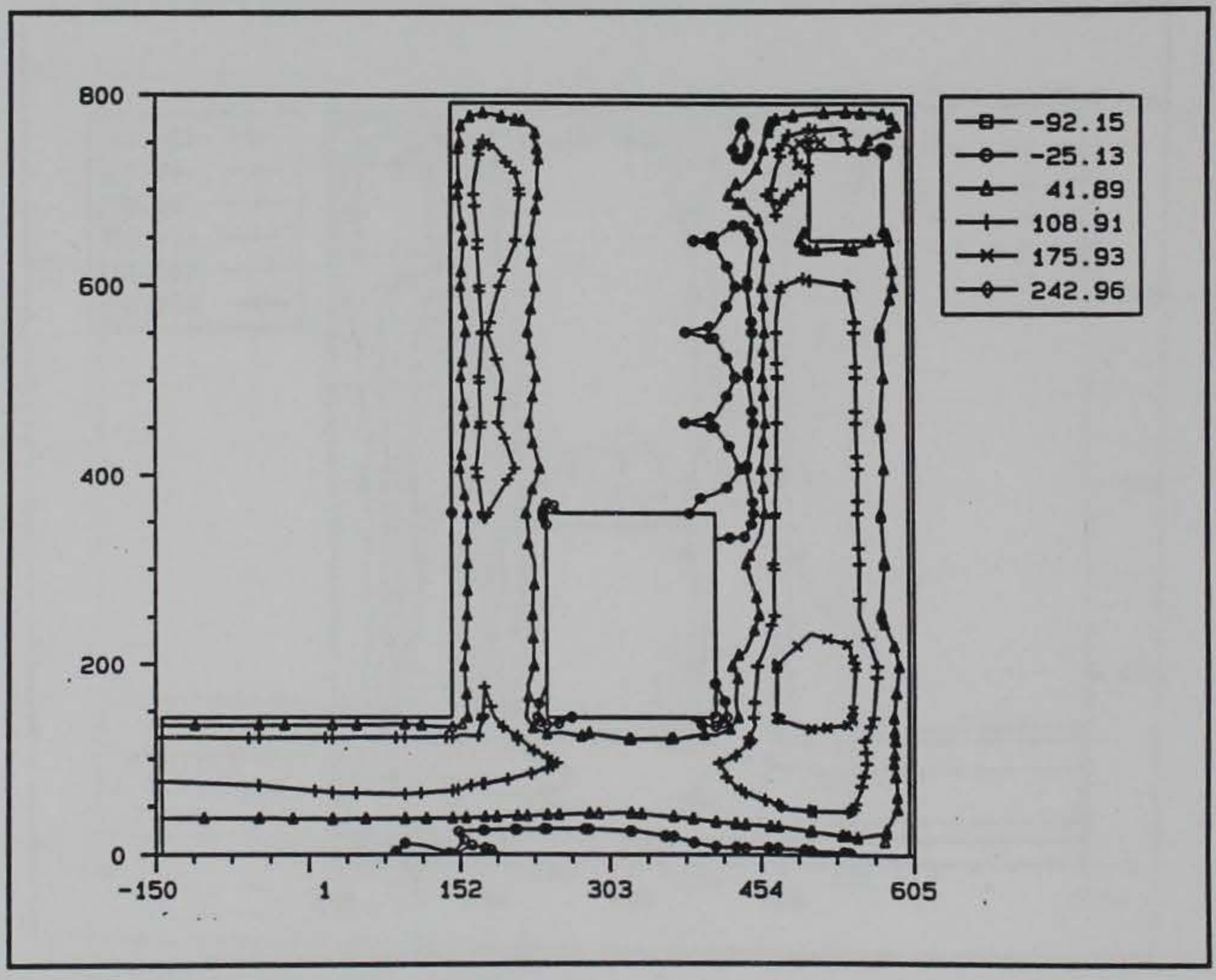

Figure 79. Maximum principal stress, transverse section at US edge of valve pit at day 169

Figures 74 through 78 are plots at a transverse section at the downstream edge of the valve pit. Some similarity exists between these plots and those in Figures 62 through 66 of the crack potentials. Lift interaction effects can be seen in both plots at day 54 (Figures 62 and 74) and areas of high stress correspond with areas of high potential. Figure 78 presents the section at 269 days when the maximum stress of 373 psi occurs. The location of the maximum stress differs significantly in this case from the maximum crack potential shown in Figure 66 at day 269 because strains remain high in the area of the cracking, but the stresses have been relieved by the cracking. Again, stresses have reduced significantly by the end of the analysis as seen in Figure 78.

Figure 79 presents stresses at day 169 at the upstream edge of the valve pit to demonstrate again how the behavior at the upstream and downstream ends are very similar. Figure 79 can be compared to Figure 76 where the shapes of the contours are very much alike. The primary difference is that the maximum stress in Figure 79 is 243 psi compared to 224 psi in Figure 76.

Time-History Plots

Figures 80 through 82 present time-history plots across a section where the cracking occurred and at the corner of the culvert valve pit where cracking often occurs on these types of monoliths. The plots are of stress and are given in two directions for the section at the gallery corner and in the transverse directions at the corner of the valve pit since orthogonal stresses had to be used. One section is taken through elements that are just upstream of the culvert valve pit and adjacent to the gallery's roof, and the other section is taken at the corner of the culvert valve pit at the downstream end and toward the landside.

Figure 80 shows the stresses in the transverse direction for the section at the corner of the gallery. Element 3354, integration point 2, is the bottom point of the section and is one of the points that cracks. Notice that when the cracking begins at day 209, the stress does not drop to zero. This is because when a crack forms, the only direction which is not allowed to carry tension is the direction perpendicular to the crack surface. Looking at Figure 54, it is obvious that the crack at this location is not perpendicular to the transverse direction. Element 3354, integration point 6, has a large jump in tensile stress after the first crack forms, but it also drops in stress when a crack forms at that location. The same is true at integration point 2 of element 3362. Finally, compression is reduced at the remaining uncracked point across the section (element 3362, integration point 6) as the other three points beneath it crack.

Figure 81 presents the vertical stresses for the same elements presented in Figure 80. As was seen in Figure 54, the crack surface at integration point 2 of element 3354 appears to be almost horizontal and, therefore,

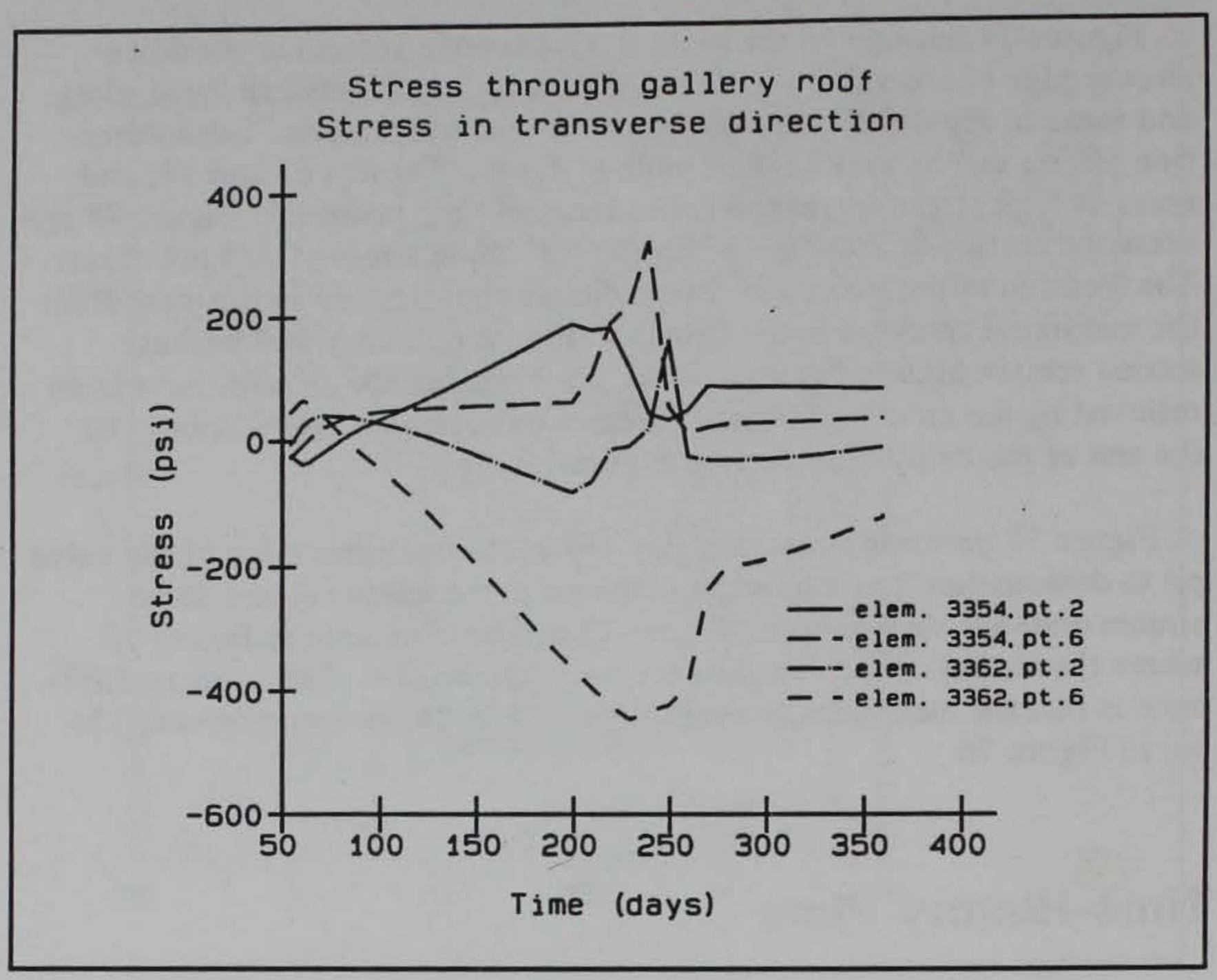

Figure 80. Time-history plot of transverse stress at section adjacent to gallery roof

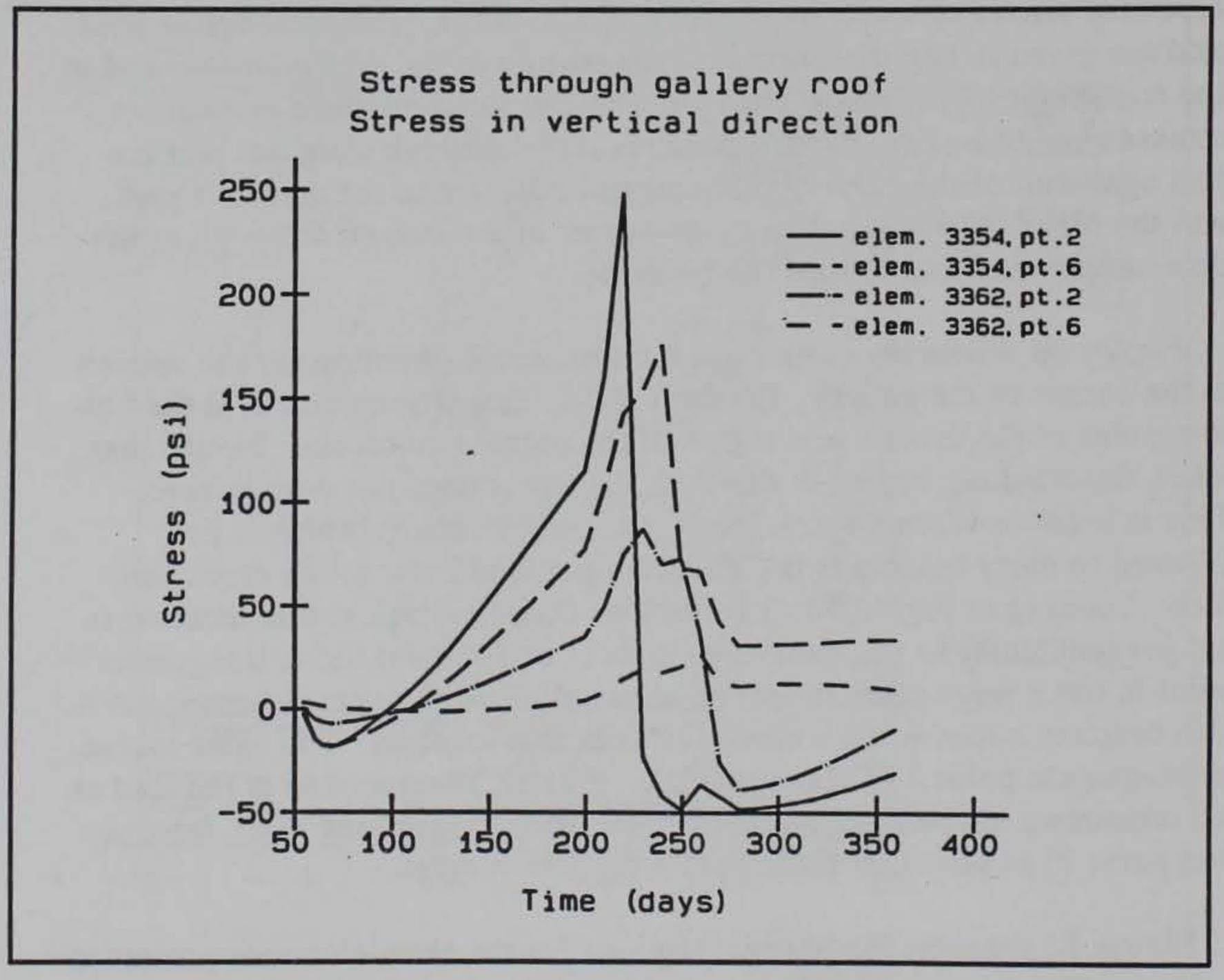

Figure 81. Time-history plot of vertical stress at section adjacent to gallery roof

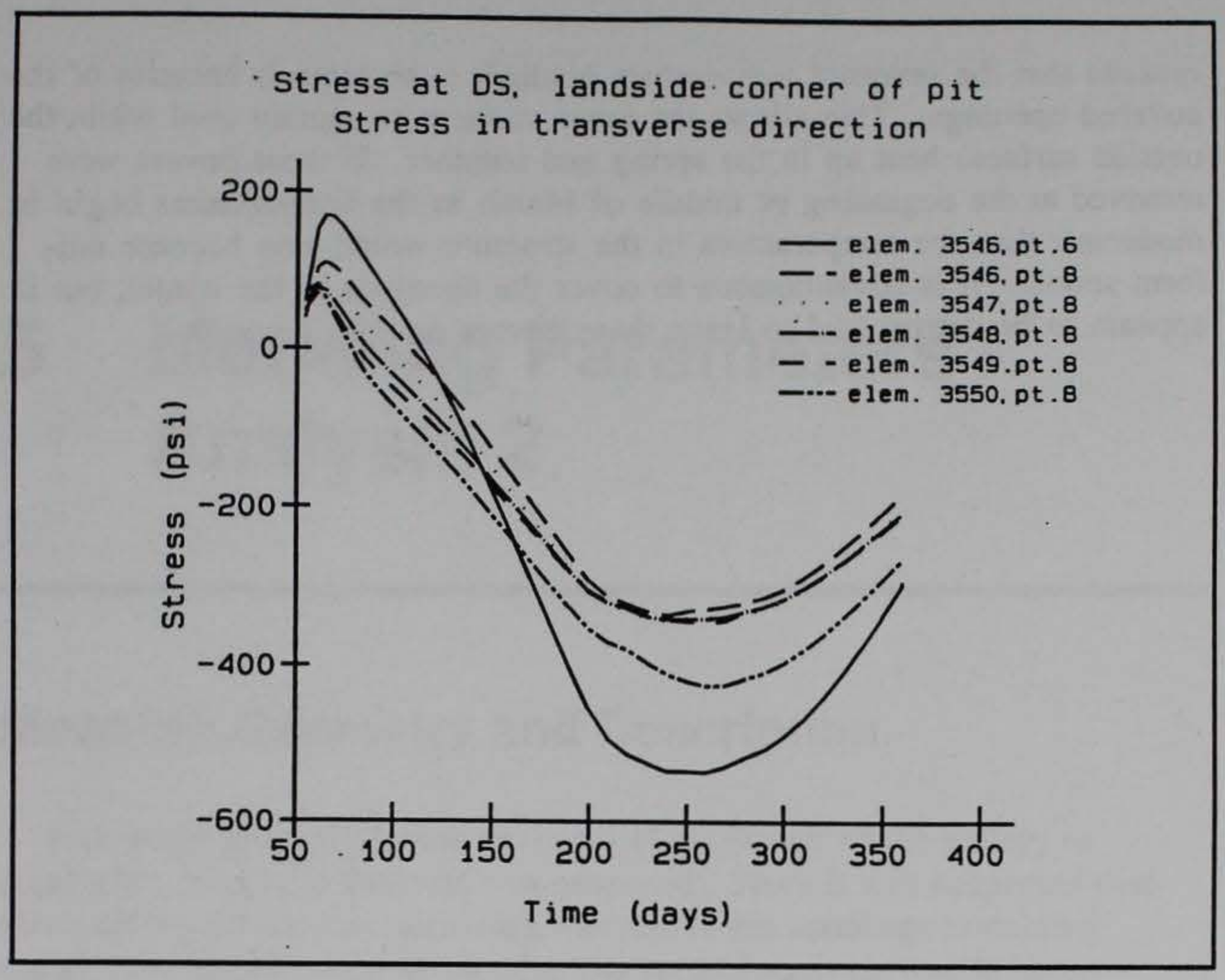

Figure 82. Time-history plot of transverse stress at the downstream, landside corner of the valve pit

there is a very large effect on the vertical stress at this point. For the other two points at which cracks occur, this same behavior is not observed because the cracks are closer to the vertical.

The behavior seen in Figure 82, the transverse stress at the corner of the culvert valve pit, is typical of time-histories seen in the chamber monolith. The stresses seen at this location follow the ambient conditions as did many of the points examined in the analyses of the chamber monoliths (Garner et al. 1992 and Merrill, Garner, and Fehl in preparation). There is some initial tension due to the cold winter temperatures but then the entire section goes into compression during the spring and summer months.

Evaluation of Results

The cracking which occurred at the corner gallery should be evaluated carefully. This crack will not affect the overall performance of the structure, but it could be a maintenance problem some time during the life of the structure. The cracking apparently occurred because of the reversed temperature gradient applied to it as seen in Figures 17 through 19. This reversed temperature gradient created a large stress gradient (Figures 80 and 81) through the roof of the gallery which eventually initiated cracking. One of the

reasons that the reversed temperature gradient is so large is because of the covered openings. This allows the inner surfaces to remain cool while the outside surfaces heat up in the spring and summer. If these covers were removed at the beginning or middle of March as the temperatures begin to moderate, then the temperatures in the structure would also become uniform sooner. It is advantageous to cover the openings in the winter, but it appears to be detrimental to leave these covers on year around.

5 Modeling Parameters - Analysis 2

Monolith Geometry and Description

Due to the cracking which occurred at the corner of the gallery in Analysis 1, a second analysis was proposed. Since it was suspected that the cracking which was occurring was due to the openings remaining closed through the summer months, the second analysis was to be performed with the covers on the openings being removed on March 1. Opening the culverts at this time would prevent the temperature reversal which occurred in Analysis 1.

The geometry for Analysis 2 remained the same except for the arrangement of the lifts. Due to the fact that the corners of the culvert valve pit did not appear to be a critical area as had been expected, a decision was made to increase the lift heights in the portion of the wall above the culvert from 8 to 9 ft. The lift sequence for analysis 2 of monolith 17 is shown in Figure 83 and the heights of the various lifts are shown in Table 3.

Table 3
Lift Heights for Monolith 17 - Analysis 2

Lift No.	1	2	3	4	5	6	7	8	9	10
Lift Height, ft	4	4	4	18	9	9	9	9	9	9

The remaining geometry parameters remain the same as described in Chapter 2 and as shown in Figures 2 and 4.

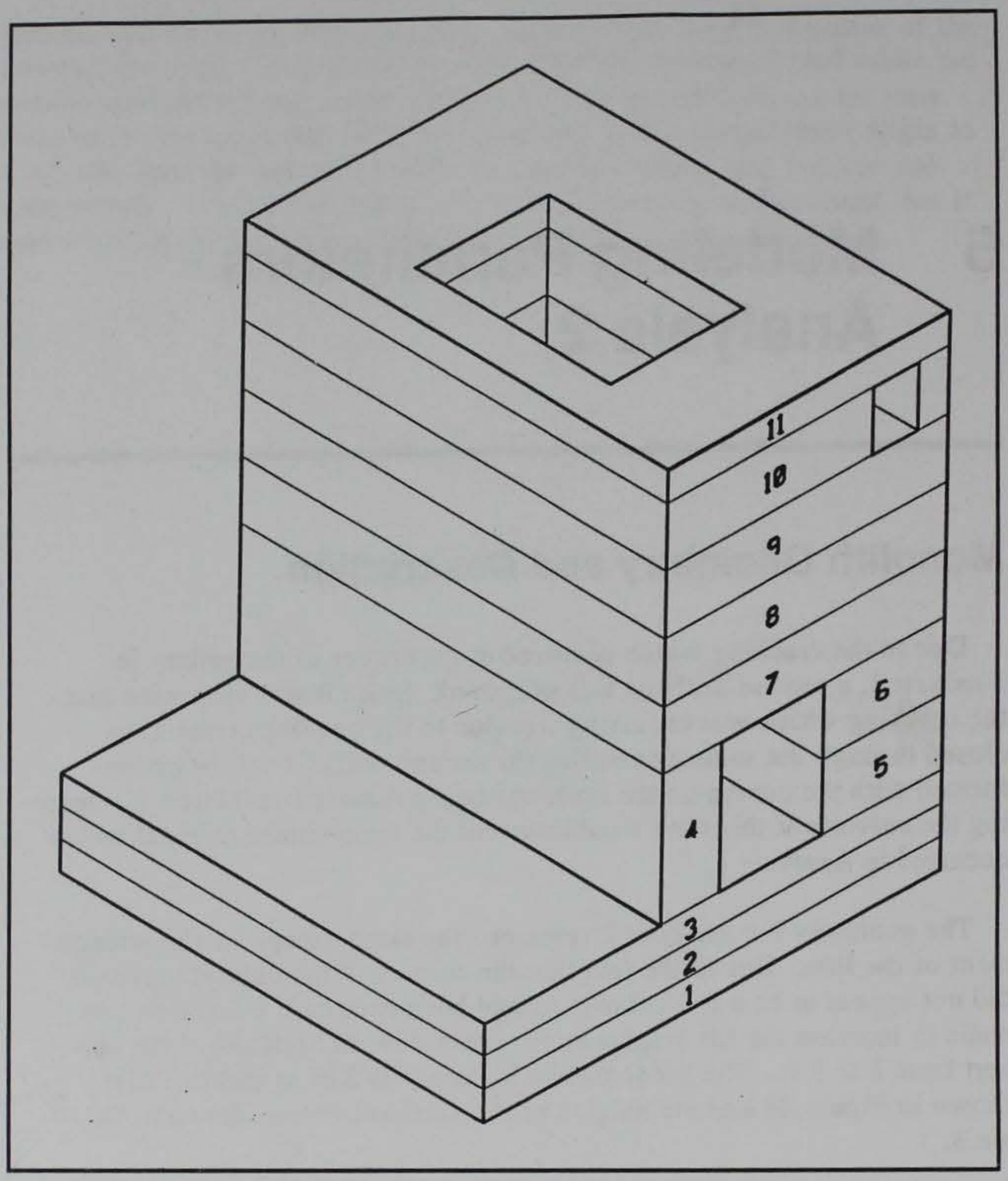

Figure 83. Isometric view of monolith 17 shopwing sequence of lift placements

Mesh Selection

Due to the change in lift heights, a change in the mesh was required for the portion of the monolith above the culvert. This change resulted in a model requiring 4,047 three-D elements which is 447 elements more than were used in Analysis 1 and is shown in Figure 84. Although the Analysis 2 mesh contains more elements than the mesh from Analysis 1, many of the elements exceed the element size limit prescribed in ETL 1110-2-324 (HQDOA 1990). Since none of the elements in Analysis 2 are larger than the elements in Analysis 1, the comments regarding exceeding the element size limitations given in Chapter 2 still apply.

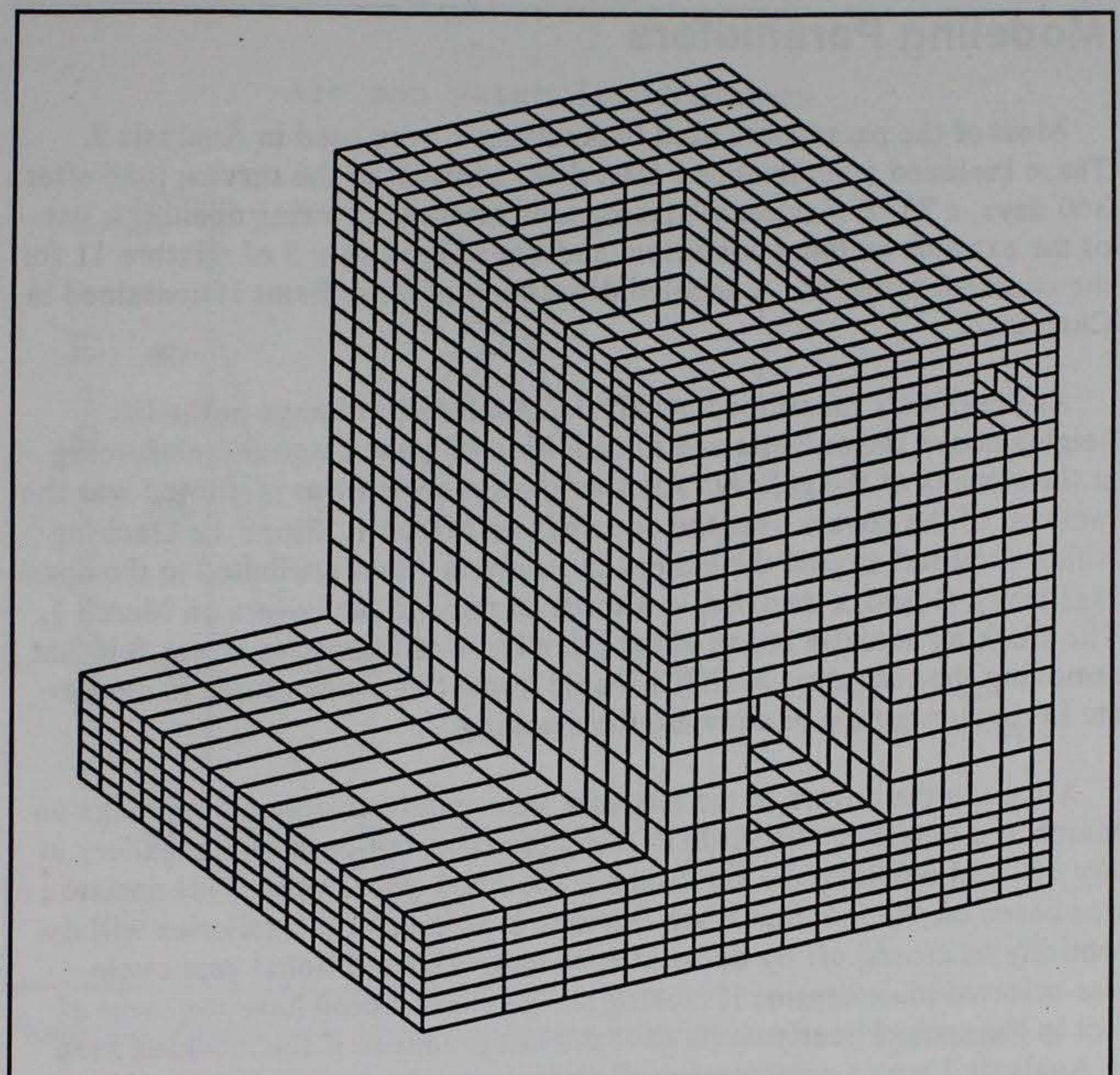

Figure 84. Isometric of the finite element mesh used for monolith 17

The models of the foundation for the heat transfer and stress analysis in Analysis 2 remained the same as were used in Analysis 1. Therefore, comments regarding the modeling of the pile foundation remain the same as presented in Chapter 2. The insulated boundary condition at the location where the slab is cut was also left unchanged.

Reinforcing was included in the Analysis 2 model. The layout as described in Chapter 2 and shown in Figure 6 remained the same except that #9 bars at 12-in. spacing were placed diagonally at the corners of the gallery. These diagonal bars were added due to the cracking at the corner of the gallery which was exhibited in Analysis 1.

Modeling Parameters

Most of the parameters used in Analysis 1 were used in Analysis 2. These included a September 1 start date, addition of the service load after 360 days, a 75 °F maximum placing temperature, covering openings, use of the extreme ambient condition, and use of load case 5 of mixture 11 for the concrete material. A detailed discussion of these items is contained in Chapter 2.

As previously mentioned, Analysis 2 included a change in the lift heights above the culverts and the addition of some diagonal reinforcing at the corners of the gallery. Another change which was instituted was the removal of the covers over the openings on March 1. Since the cracking which occurred around the gallery in Analysis 1 was attributed to the openings being closed, a decision was made to remove the covers on March 1. The cracking actually began about the middle of March, so it was felt that removing the covers on March 1 would allow the temperatures to moderate in time to reduce or alleviate the cracking.

Although the covers in the analysis were removed from all openings on March 1, a decision was made to place the covering back on the gallery at day 360 and continue the analysis for another 1-year cycle. This decision was based on the fact that when the lock is complete, the galleries will essentially be closed off by doors at each end. The additional year cycle was selected to determine if closing the galleries would have the same effect in the second yearly cycle as it did in the first or if the cracking seen in Analysis 1 was a combination of ambient and heat of hydration effect.

In addition to placing covers back on the gallery openings, the service loads were left in place and water was added to the heat transfer analysis for the additional 1-year cycle. To model the water, a film coefficient was applied to the elements which were in contact with water and water temperature cycle was applied as described in the Phase I and II Olmsted report (Garner et al. 1992). The water temperature cycle is essentially the same as the ambient air temperature cycle with a shift of 30 days, and the minimum temperature of the water never drops below 40 °F. A plot of the ambient air temperature and water temperature cycles is shown in Figure 85. The film coefficient was calculated based on boundary layer theory (Ozisik 1985) assuming the water moving at a velocity of 1 mph. The 1-mph velocity was chosen as an average since during filling and emptying the velocity will be much higher, particularly in the culverts, but between lockages the velocity will likely be near zero. The resulting value was 14.5 Btu/(day-in.^{2}-°F). In addition, a reduced value of 0.145 Btu/(day-in.^{2}-°F) was used on the ends of the monolith where water could be expected to seep into.

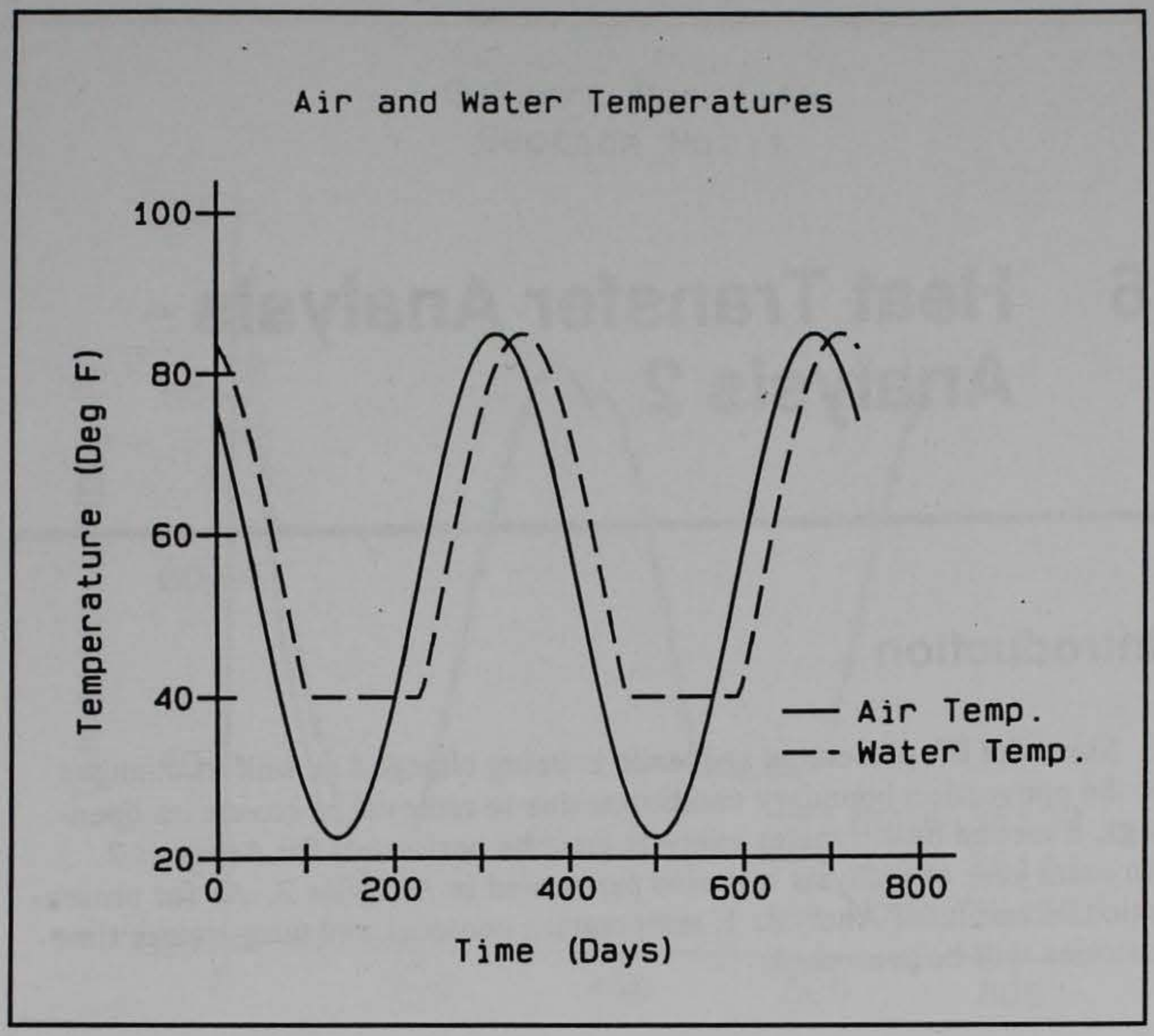

Figure 85. Ambient air and water temperature cycles used in Analysis 2

6 Heat Transfer Analysis - Analysis 2

Introduction

Since the lift placement sequence is being changed as well as changes to the convection boundary conditions due to removal of covers on openings, a second heat transfer analysis must be performed for Analysis 2. An extra year of analysis was also performed in Analysis 2. As for presentation of results of Analysis 1, temperature contours and temperature time-histories will be presented.

Time-History Plots

Figures 86 and 87 are time-histories of a line of nodes taken at mid-height of the culvert walls. Figure 86 illustrates that once the covers are removed at 180 days, the temperatures throughout the wall thickness are very close. Compared to Analysis 1 (Figure 7), the gradient through the wall is reduced significantly in section 1. The gradient is also greatly reduced in section 2 from Analysis 1 to Analysis 2 as can be seen by comparing Figure 8 to Figure 87. Not only is the total gradient reduced but after the covers are removed in Analysis 2, the gradient that is present is distributed evenly throughout the wall thickness. In sections 1 and 2, once the covers are removed the gradient remains small throughout the remainder of the analysis.

Figures 88 and 89 present the results of a line of nodes through the upstream and downstream sections of the monolith, respectively. As in sections 1 and 2, once the covers on the openings are removed at day 180, the gradient through the wall section is greatly reduced. By comparing Figure 88 to Figure 13 and Figure 89 to Figure 14, it is obvious that removing the covers on the openings in Analysis 2 at 180 days reduces the gradient present in Analysis 1. Due to the insulating effect which occurs at the ends when the monolith is assumed to be in service, the gradient

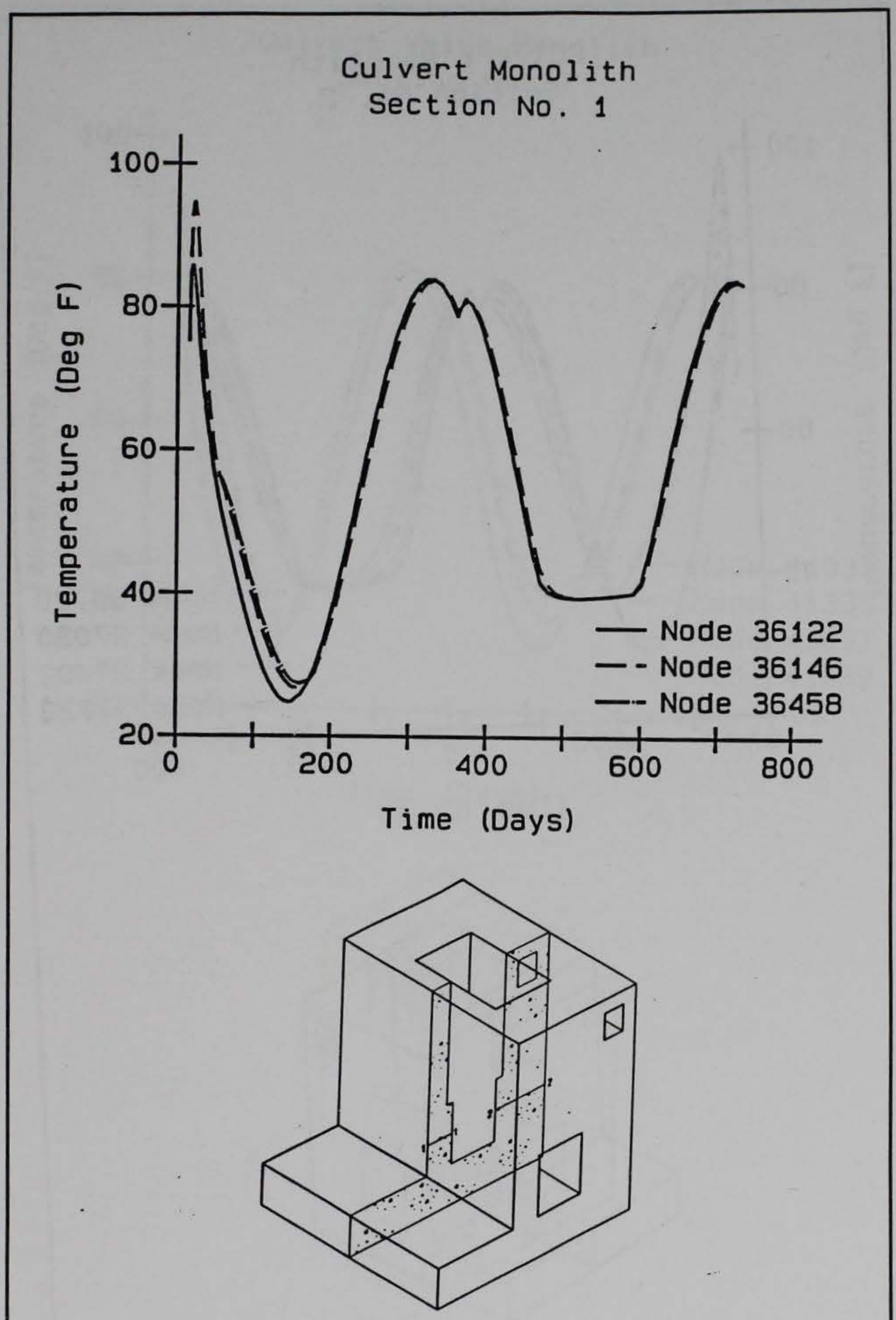

Figure 86. Temperature time-history in section 1

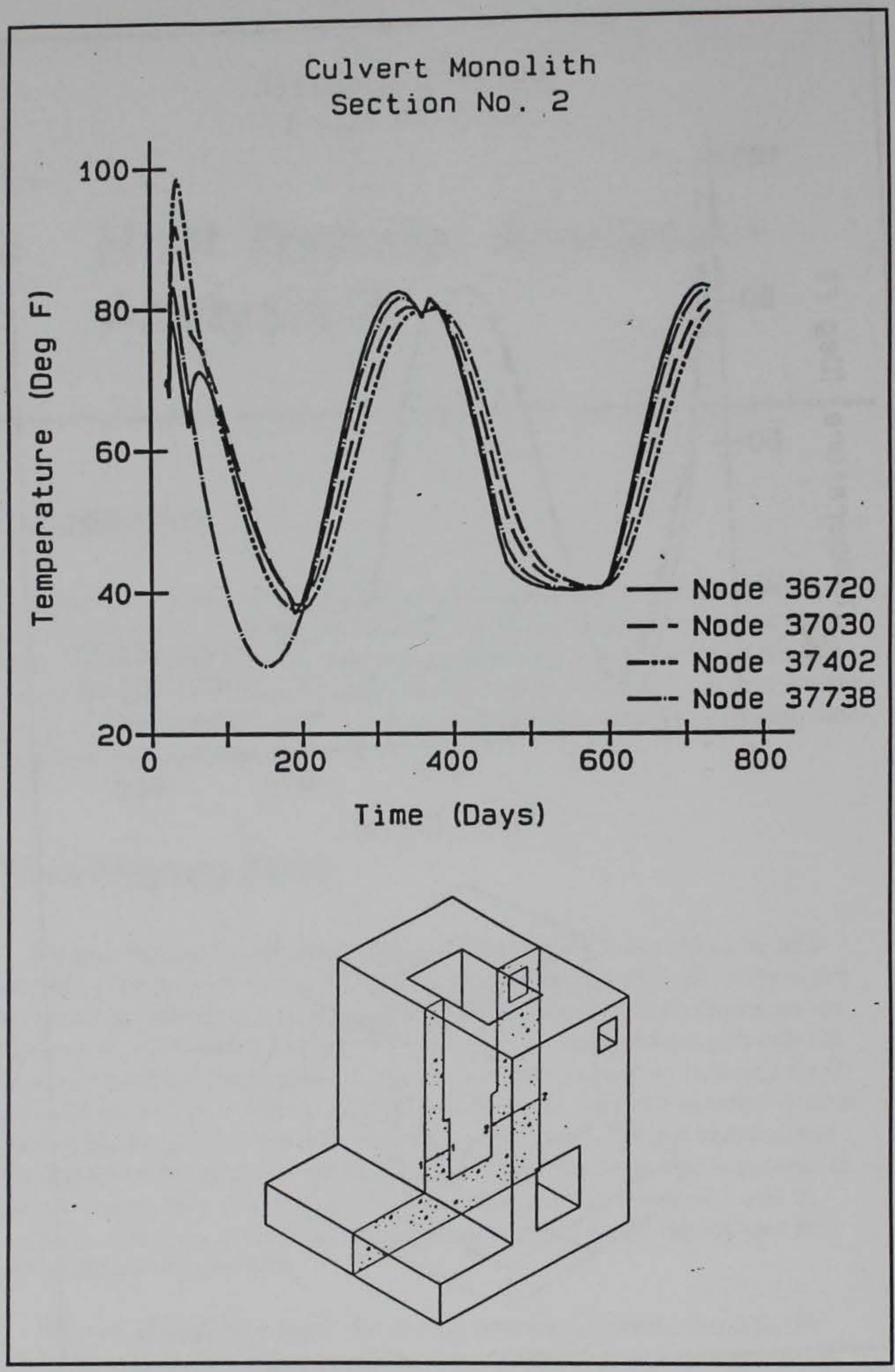

Figure 87. Temperature time-history in section 2

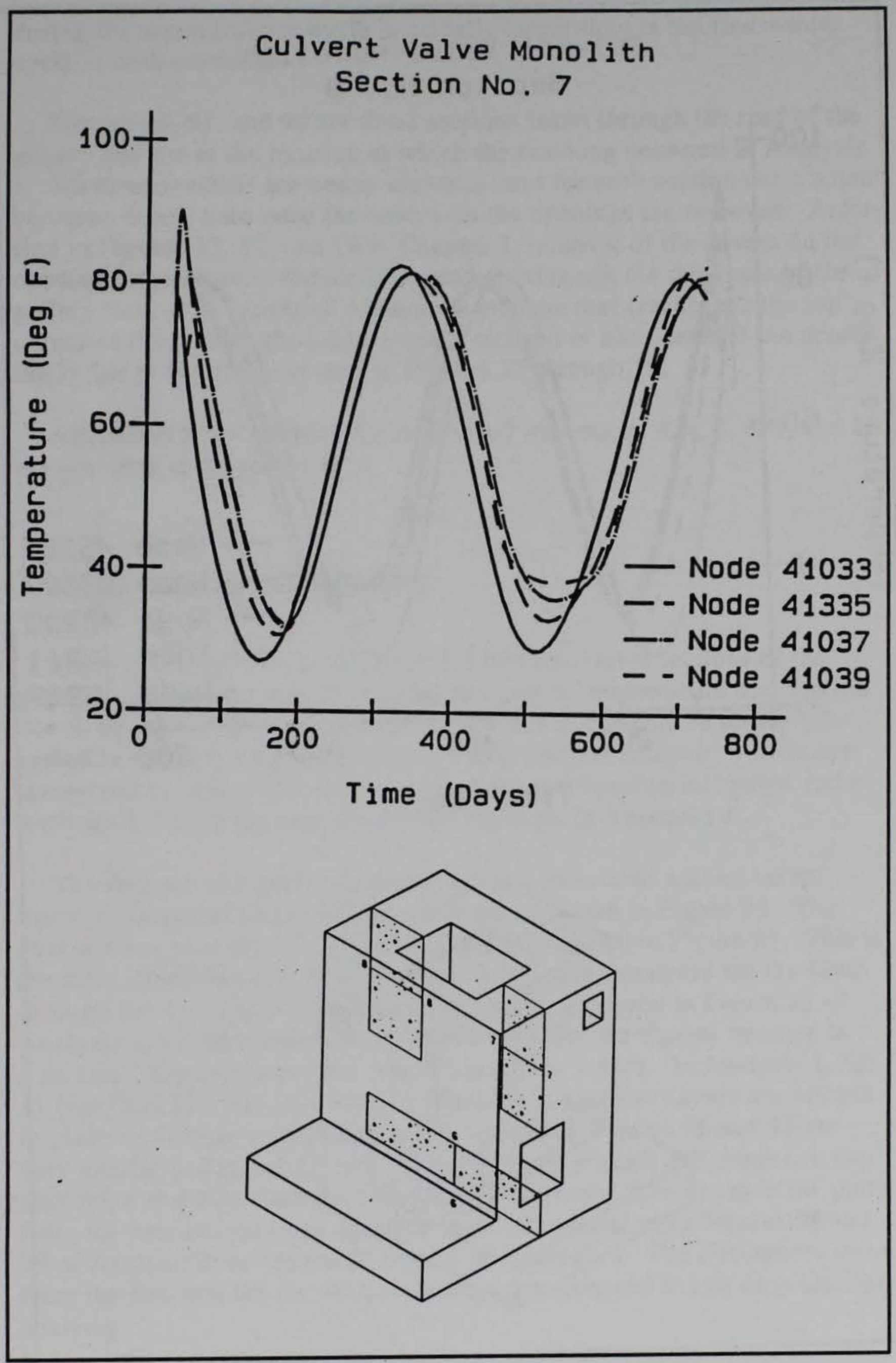

Figure 88. Temperature time-history in section 7

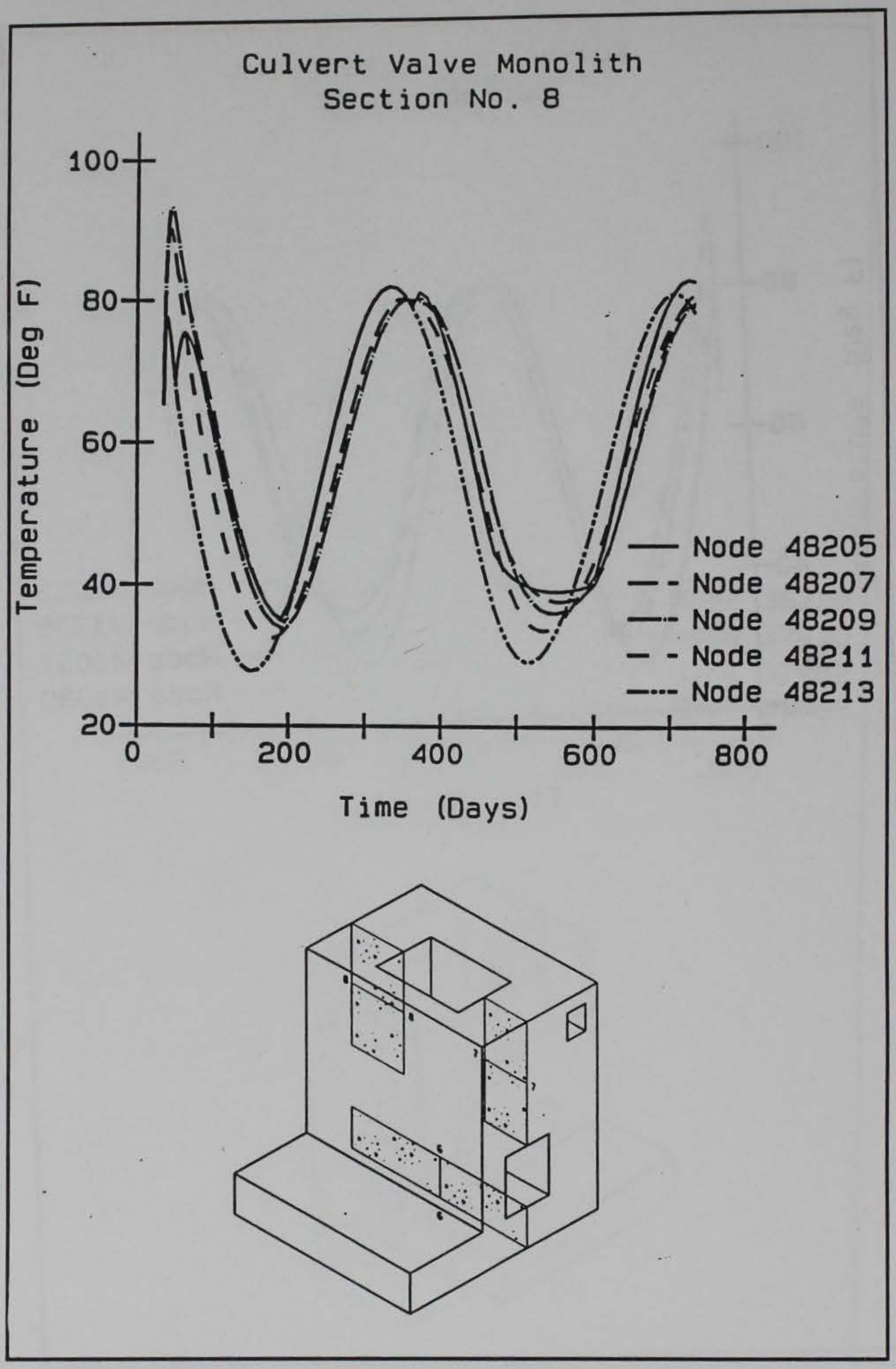

Figure 89. Temperature time-history in section 8

during the second winter cycle is actually larger than in the first winter cycle in both sections.

Figures 90, 91, and 92 are three sections taken through the roof of the gallery and are at the location at which the cracking occurred in Analysis 1. All three sections are nearly identical, and for each section the gradient becomes nearly zero once the covers on the openings are removed. Referring to Figures 17, 18, and 19 in Chapter 3, removal of the covers on the openings significantly reduced the gradient through the thickness of the gallery roof. The results of Analysis 2 indicate that cracking at the top corner of the gallery should be greatly reduced or eliminated if the cracking is due to the gradient seen in Figures 17 through 19.

Additional time-histories for Analysis 2 in sections 3, 4, 5, 6, 9, and 10 are provided in Appendix A.

Temperature Contours

Temperature contours are shown for two transverse sections of the monolith for the purpose of showing the general temperature distribution due to the Analysis 2 temperature results and to compare to results presented in Chapter 3 for the Analysis 1 heat transfer analysis. Additional temperature contour plots are presented for two longitudinal strips and a horizontal section through the culvert valve pit in Appendix A.

The first set of contours is presented at a transverse section taken through the center of the culvert valve pit as shown in Figure 93. The first contour is at day 27 (Figure 94) and is identical to Figure 21. This is the same section at day 27 of Analysis 1, since the analyses are the same through day 30. Figure 95, at day 52, can be compared to Figure 22 of Analysis 1, but differences do exist between the two figures because in Analysis 2 the openings have been covered for 2 days. In Analysis 1, lift 11 (the final lift) has only been in place for 2 days and covers are not put in place until 5 days after the last lift is placed. Figures 96 and 97 are very similar to Figures 23 and 24 with only very small differences in the maximum and minimum temperatures. Noticeable differences in the plots from the two analyses can again be seen when comparing Figures 98 and 99 of Analysis 2 to Figures 25 and 26 of Analysis 1. The differences stem from the fact that the covers on openings are removed at 180 days into the analysis.

Figures 99 through 103 are contours from the second year of Analysis 2. Comparing the plots in these figures to approximately the same times 1 year earlier, the overall temperature gradient throughout the structure has been reduced. In addition, localized gradients at the edges of the monolith appear to be reduced as well. The location of the water elevation can also be identified in each figure by the contours which terminate

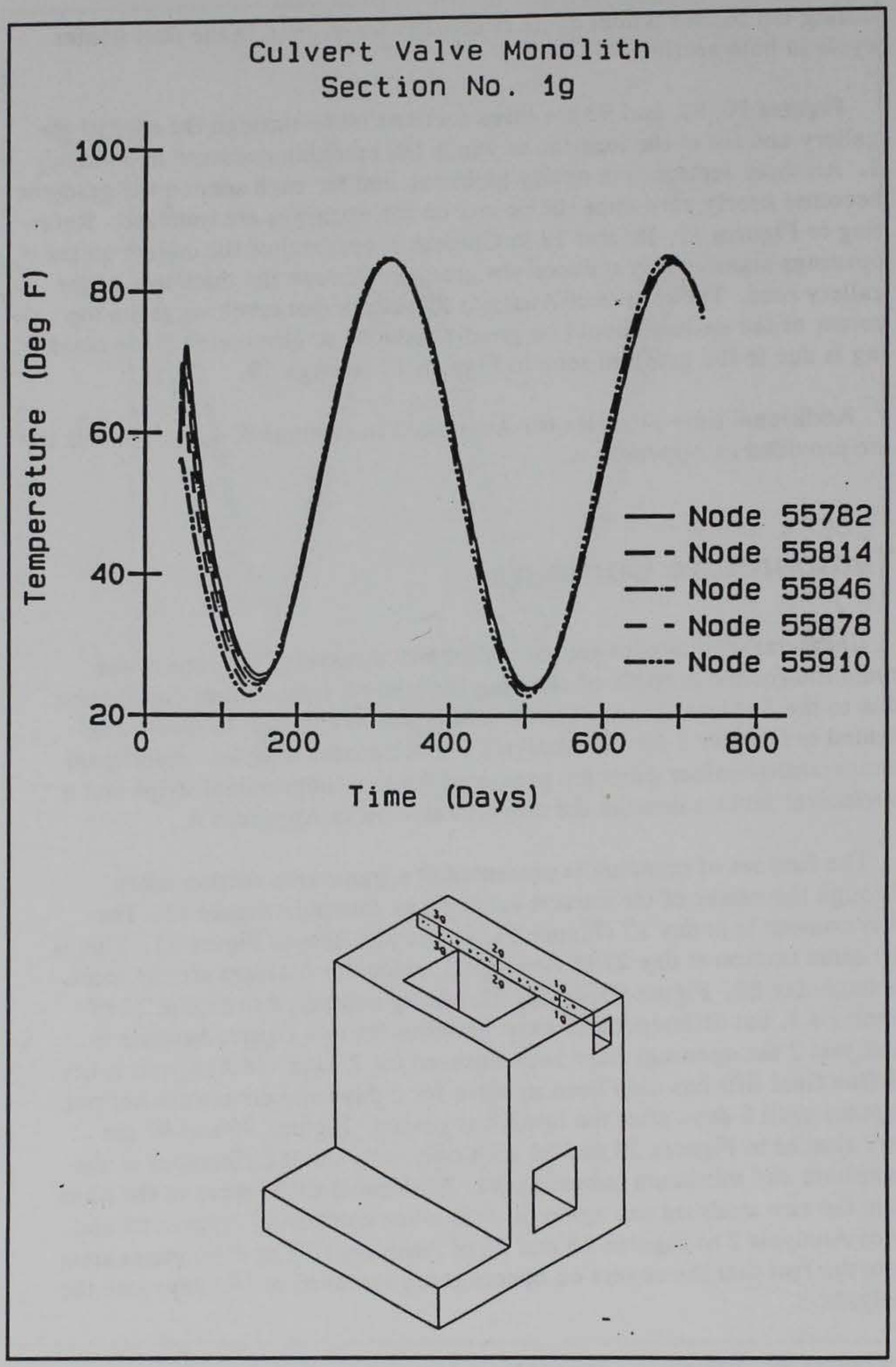

Figure 90. Temperature time-history in section 1g

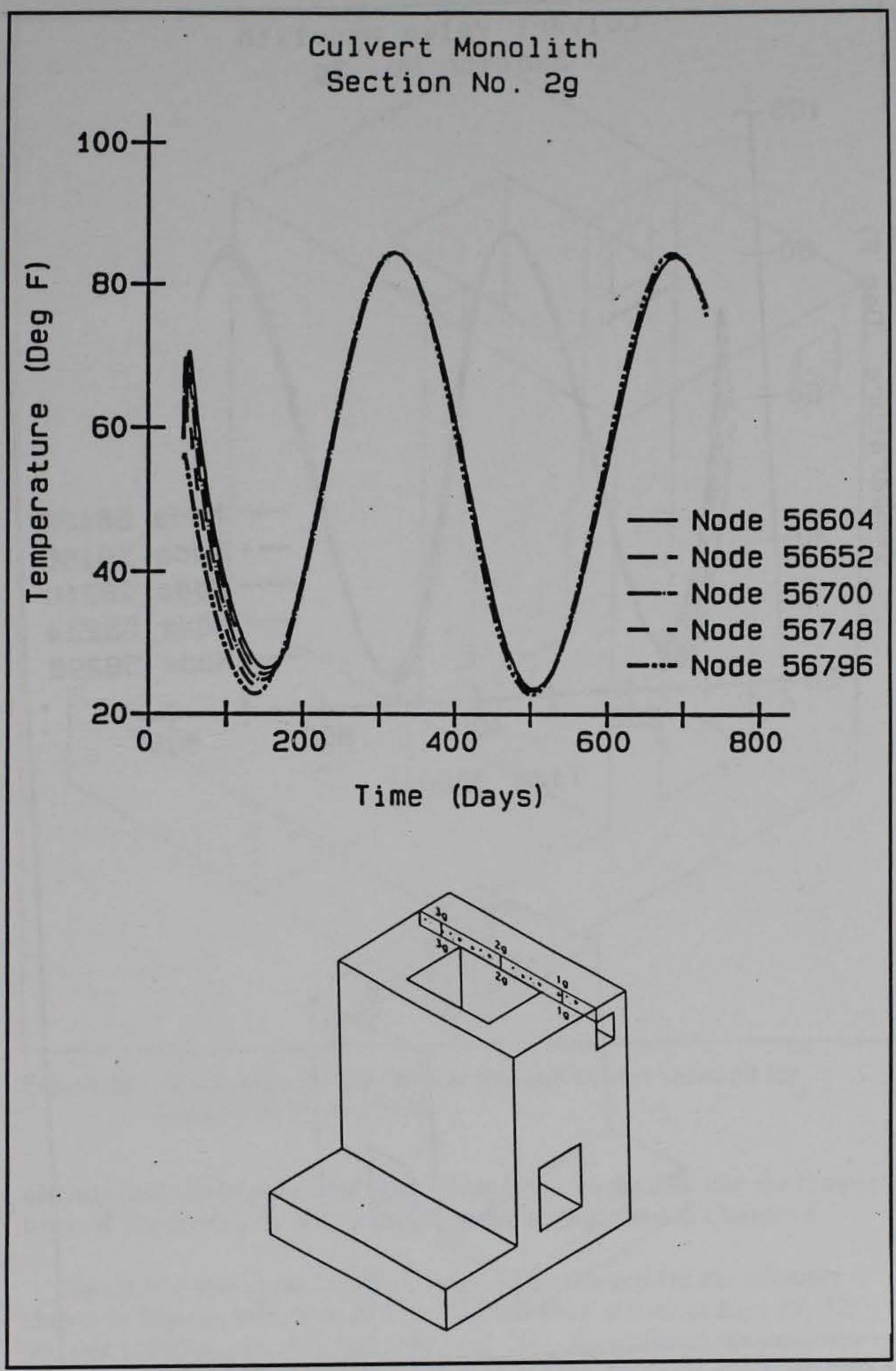

Figure 91. Temperature time-history in section 2g

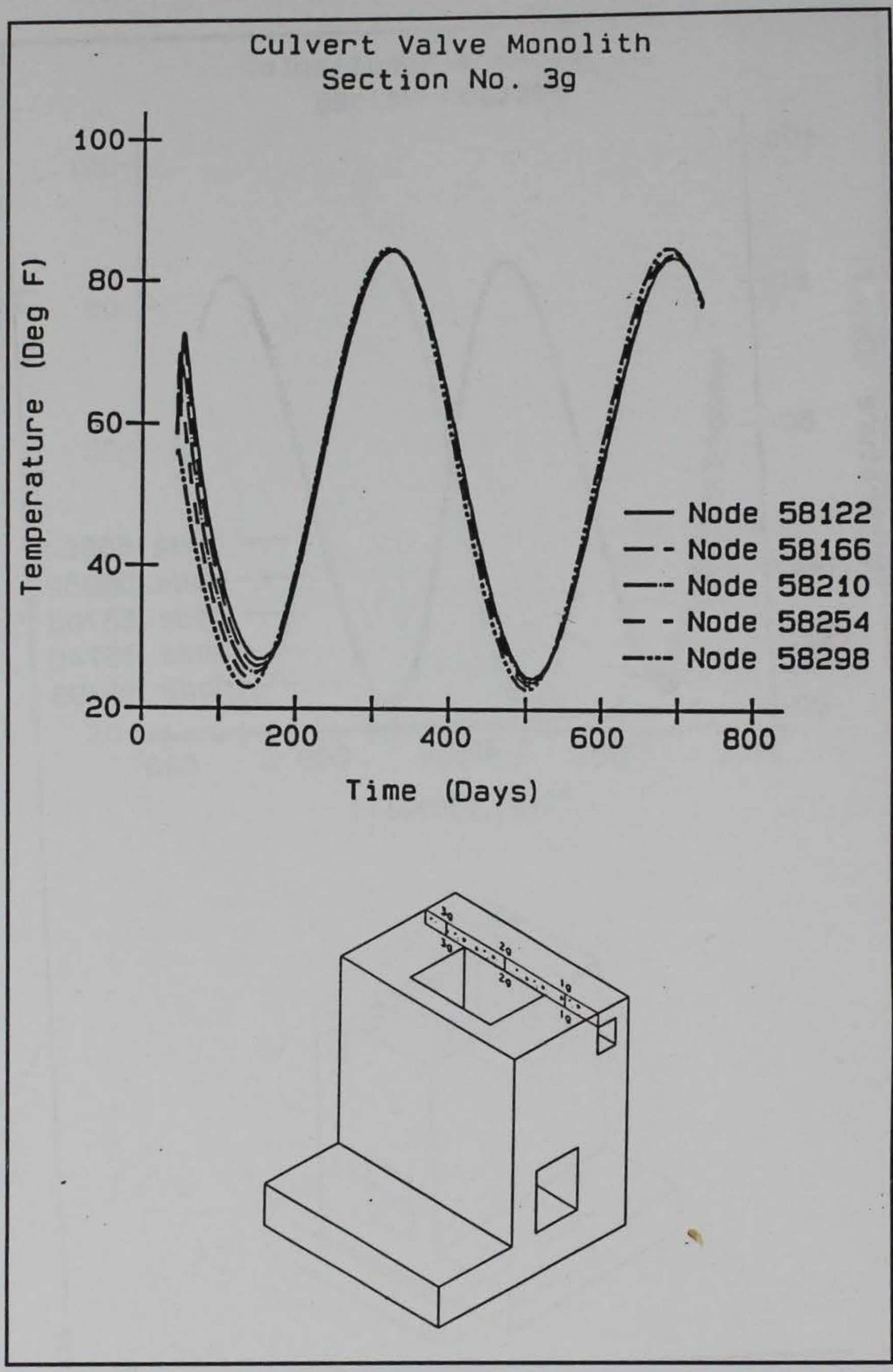

Figure 92. Temperature time-history in section 3g

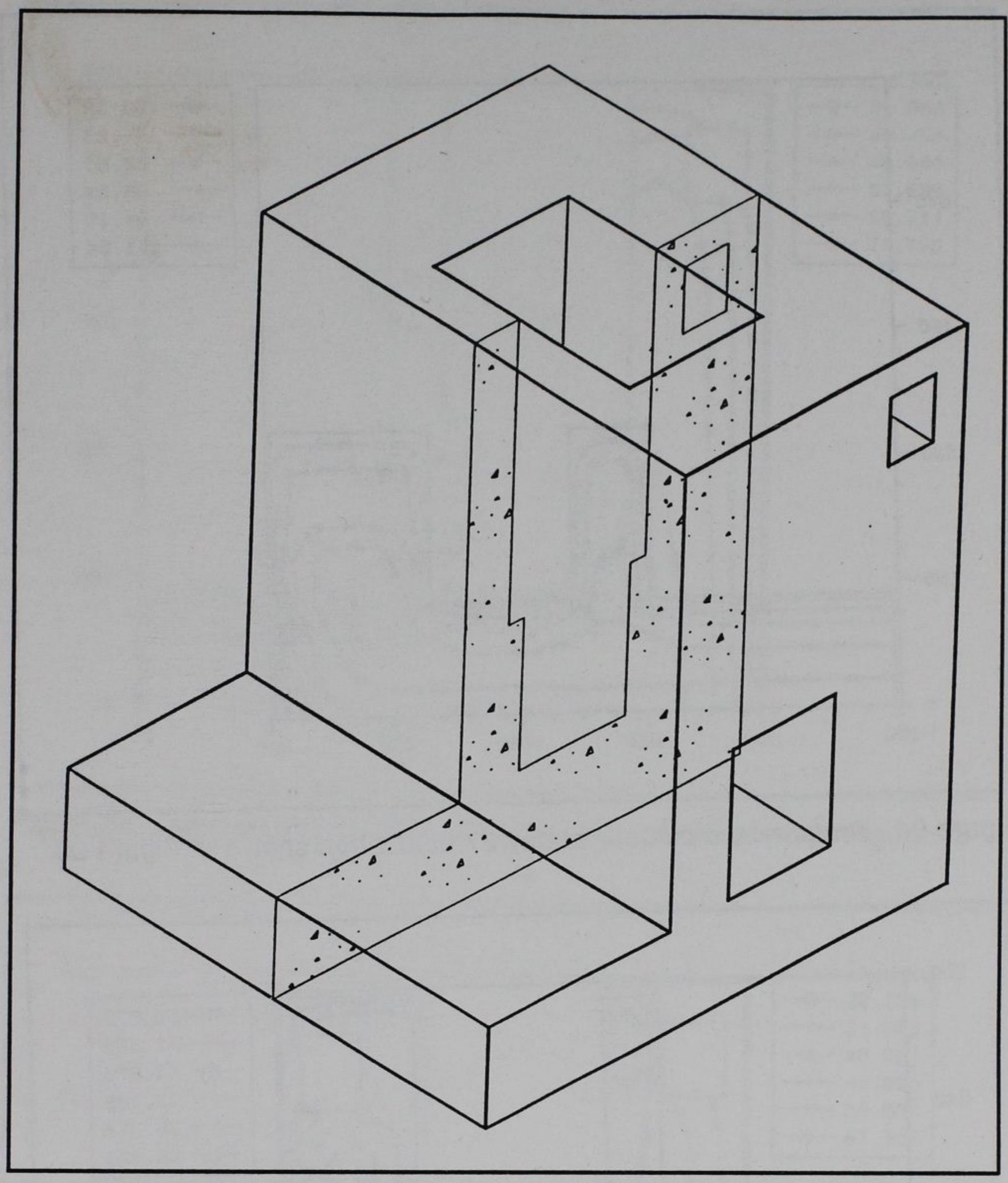

Figure 93. Transverse section locator through culvert valve pit for Figures 94 through 103

directly into the edges of the wall. This is due to the fact that the temperatures of the air and the water are different as described in Chapter 4.

Figure 104 shows the location of the section taken for the contours shown in Figures 105 through 114. For the plots shown at days 27, 52, 90, and 125 (Figures 105, 106, 107, and 108, respectively) the contours are nearly identical to the contours presented for Analysis 1 in Chapter 3 at the same section. Significant differences can be noticed though when contours for day 250 are compared (Figure 109 for Analysis 2 and Figure 39 for Analysis 1). The differences are due to the fact that in Analysis 2 the covers on the openings were removed at day 180 which accounts for the contour lines being parallel to the openings instead terminating at the openings. Significant differences are also obvious when comparing

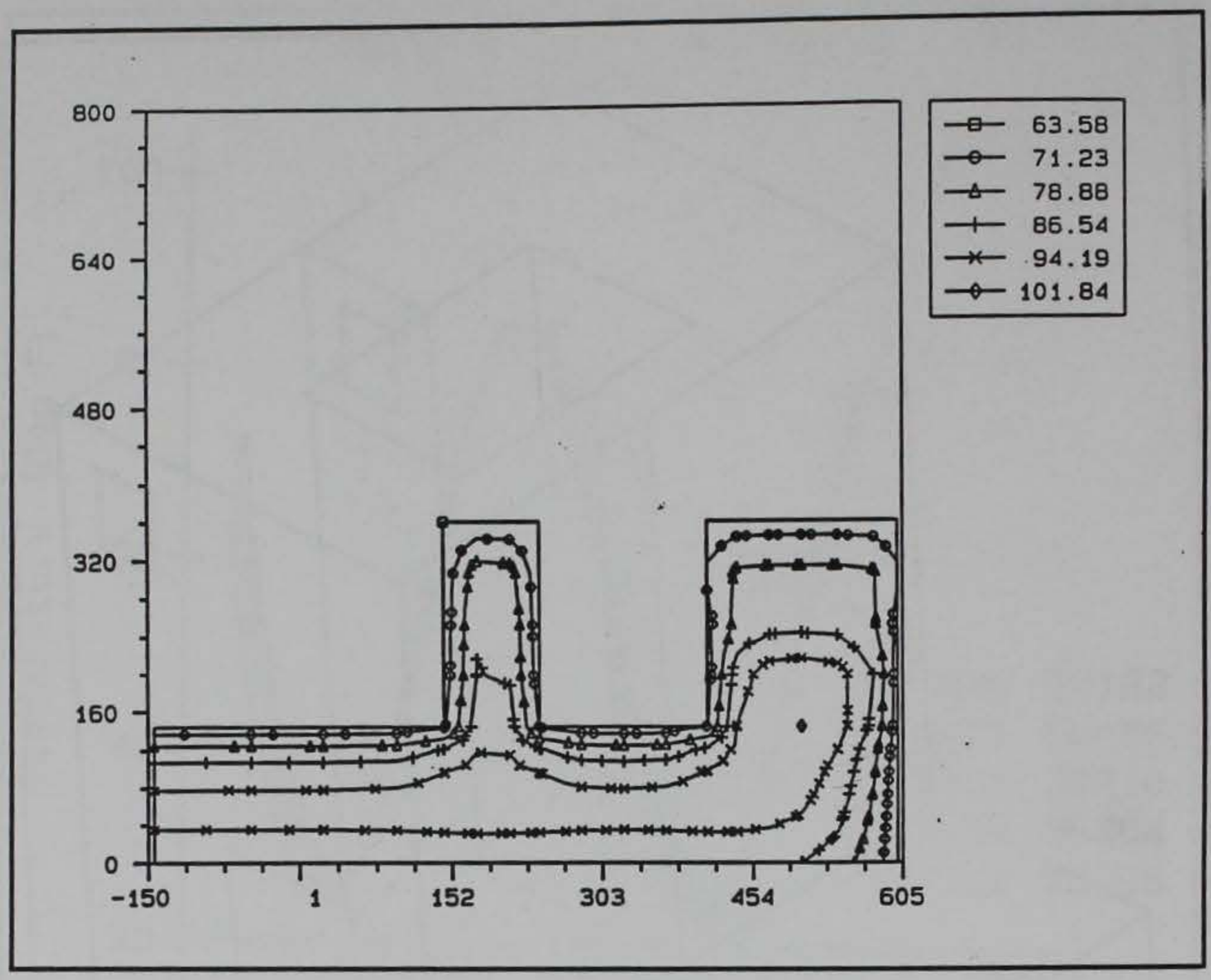

Figure 94. Temperature contour at day 27 at location shown in Figure 93

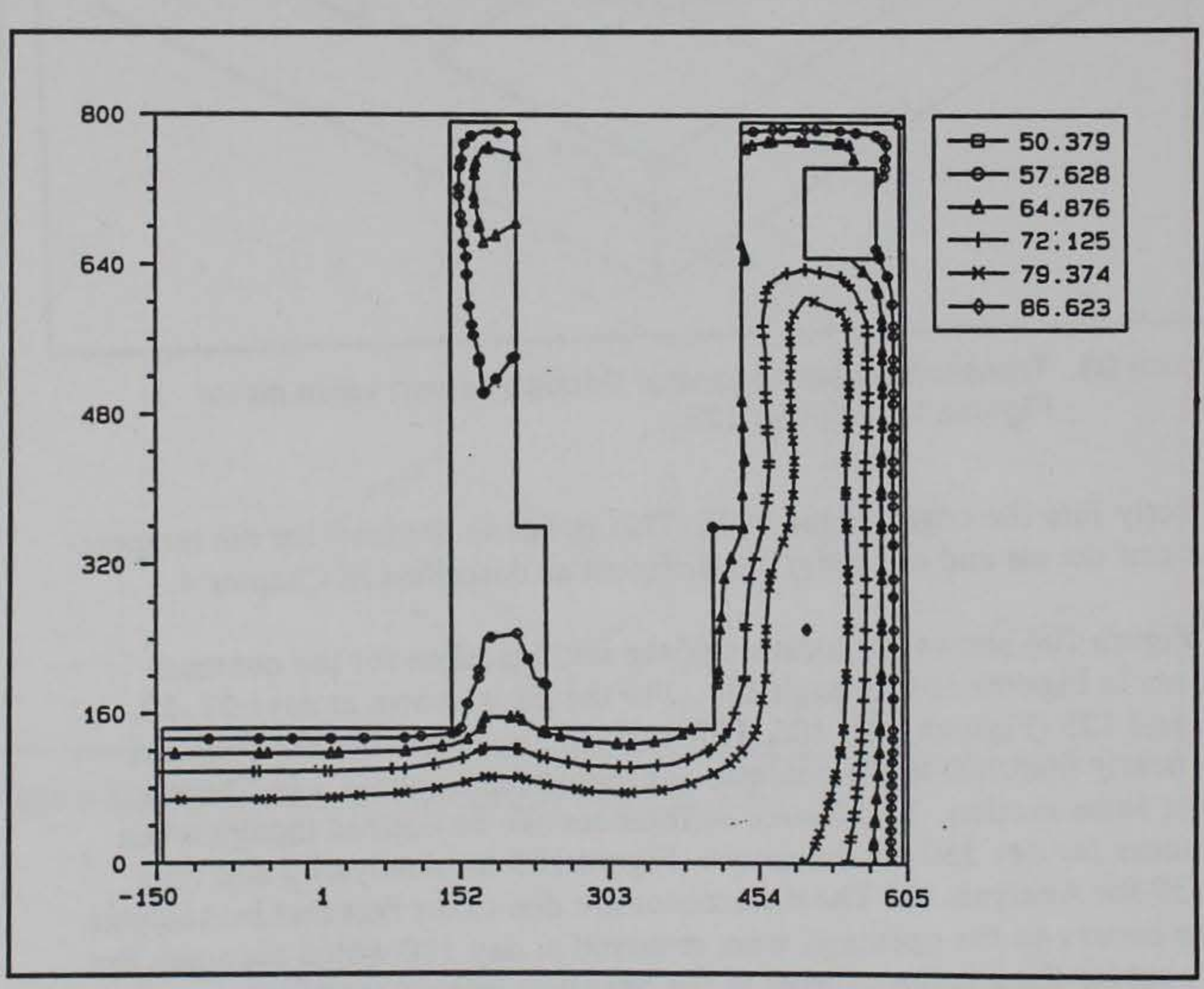

Figure 95. Temperature contour at day 52 at location shown in Figure 93

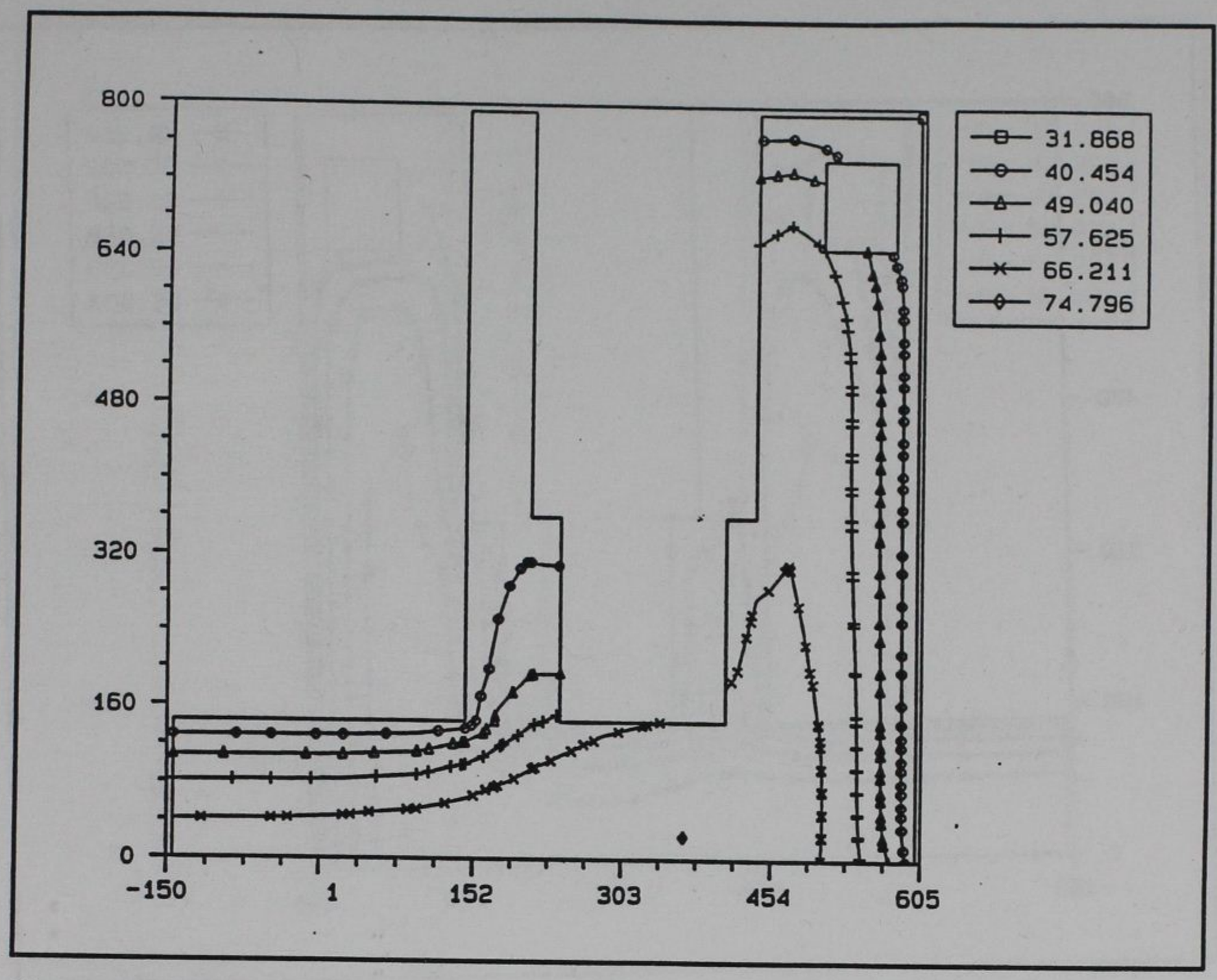

Figure 96. Temperature contour at day 90 at location shown in Figure 93

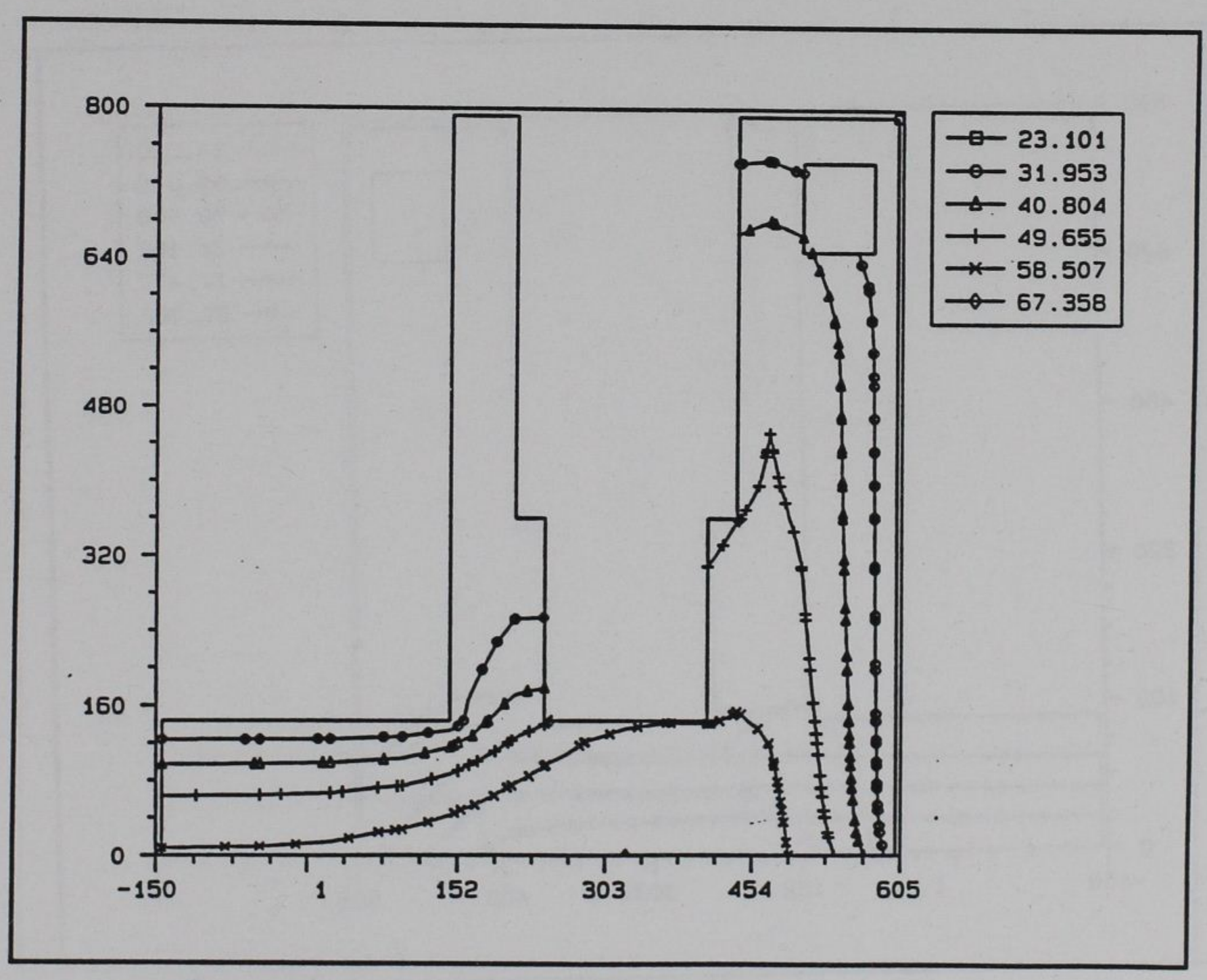

Figure 97. Temperature contour at day 125 at location shown in Figure 93

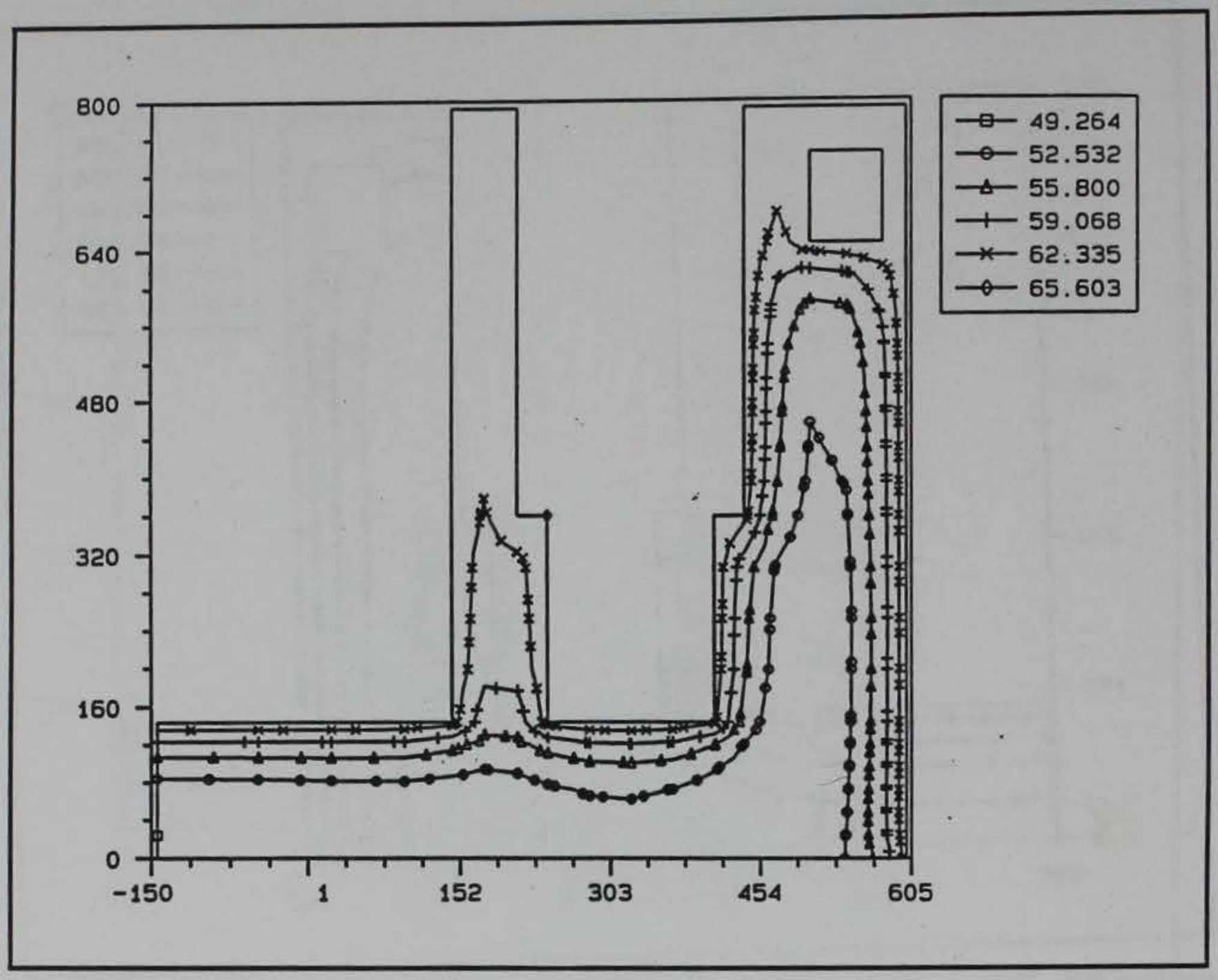

Figure 98. Temperature contour at day 250 at location shown in Figure 93

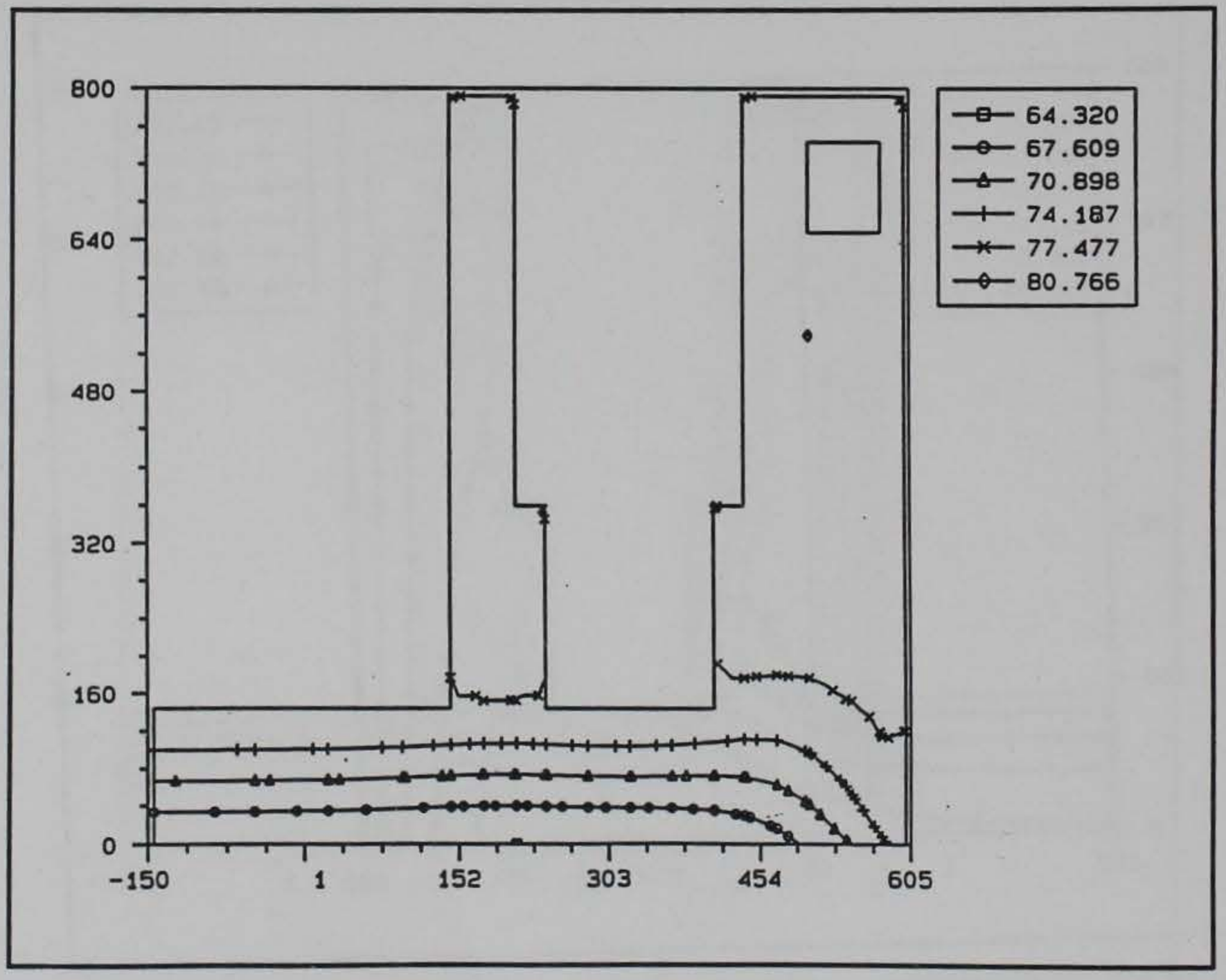

Figure 99. Temperature contour at day 360 at location shown in Figure 93

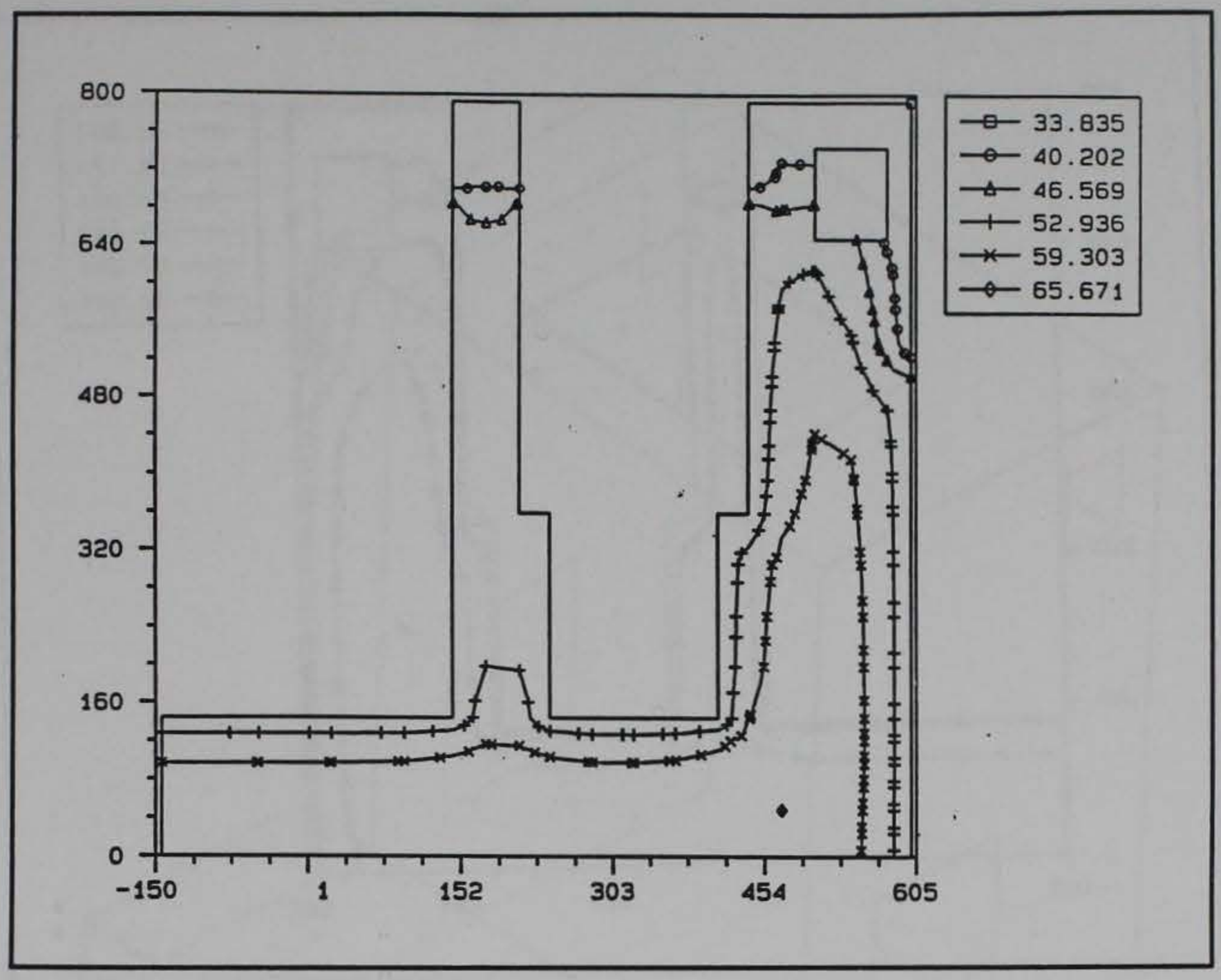

Figure 100. Temperature contour at day 450 at location shown in Figure 93

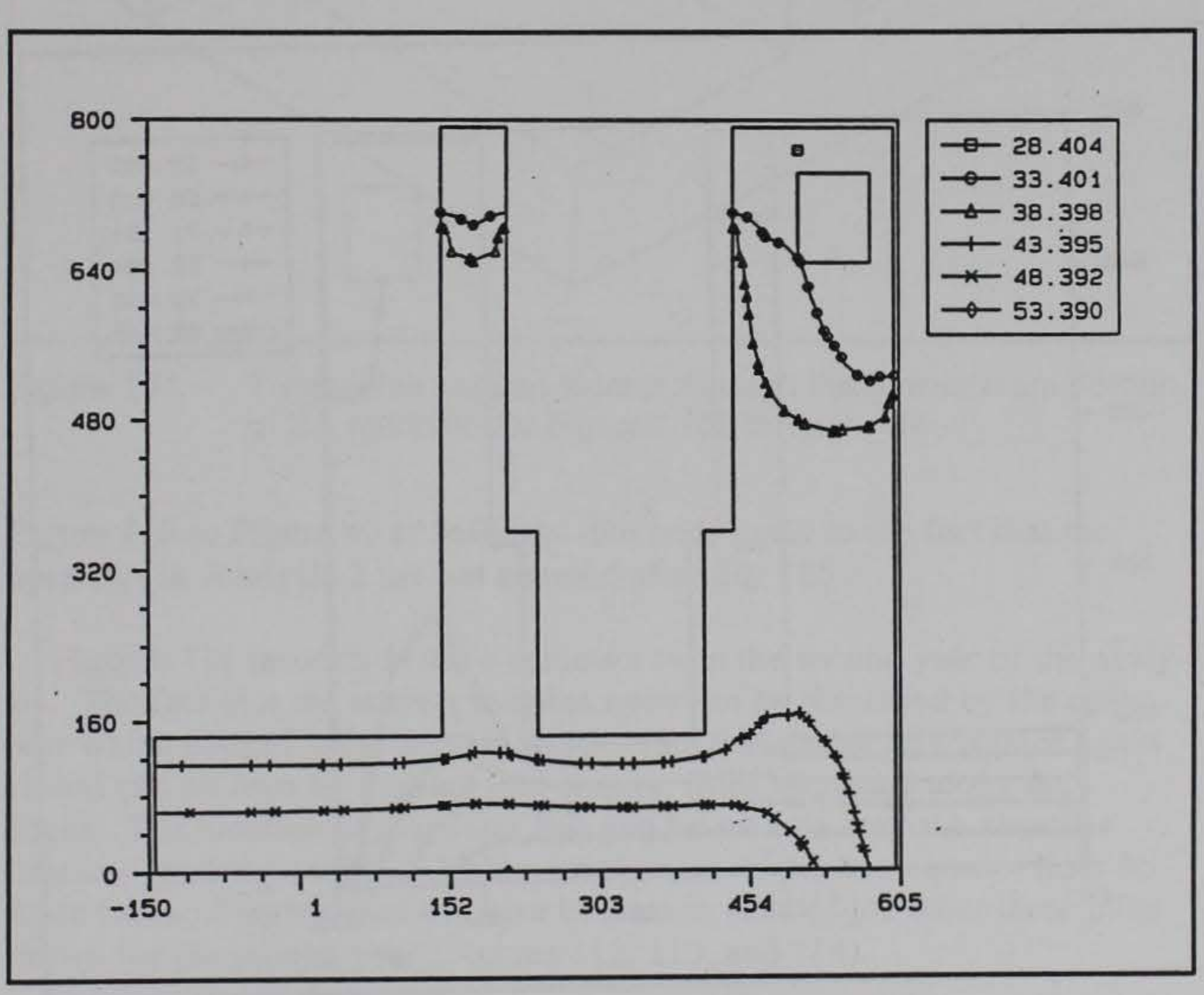

Figure 101. Temperature contour at day 640 at location shown in Figure 93

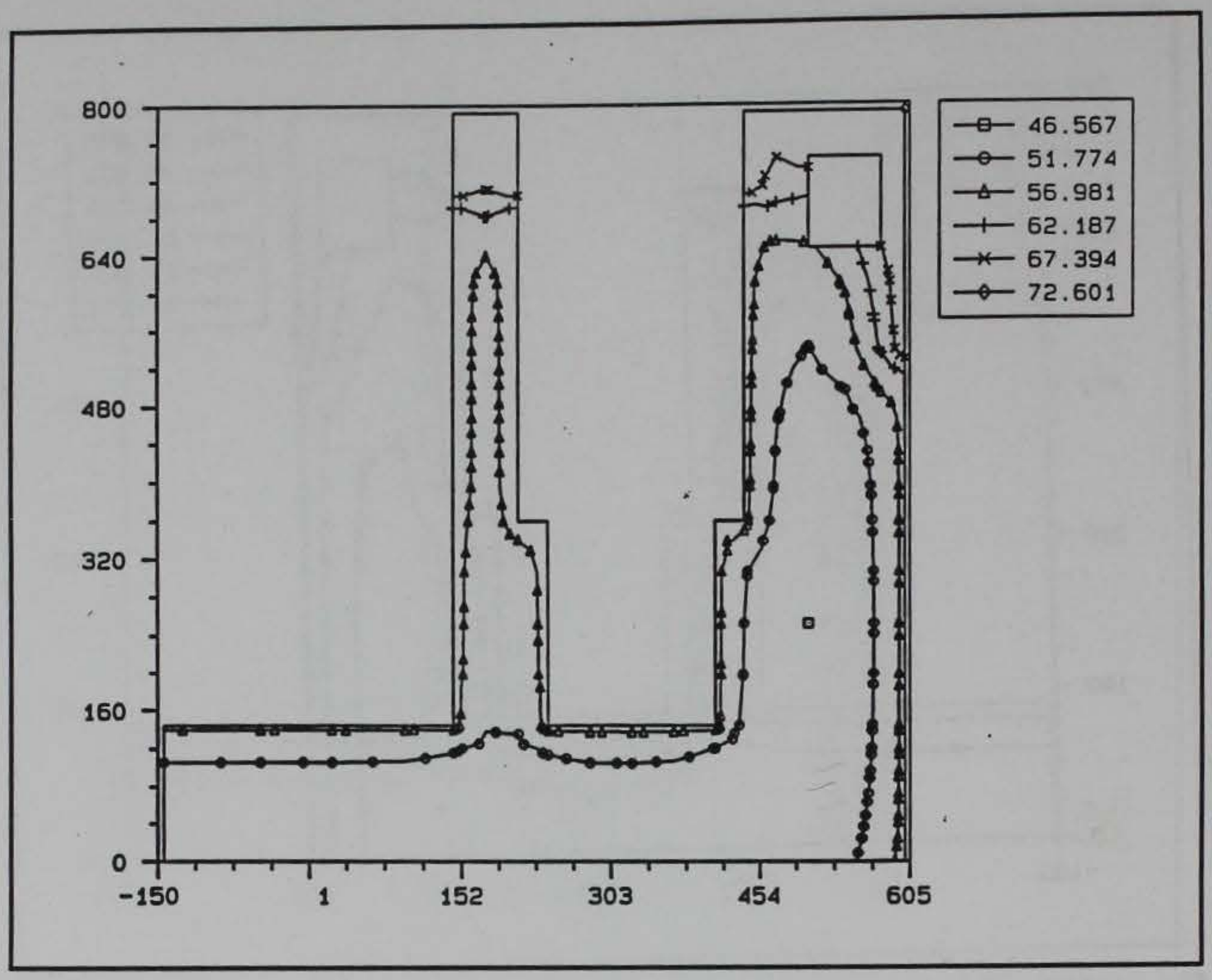

Figure 102. Temperature contour at day 630 at location shown in Figure 93

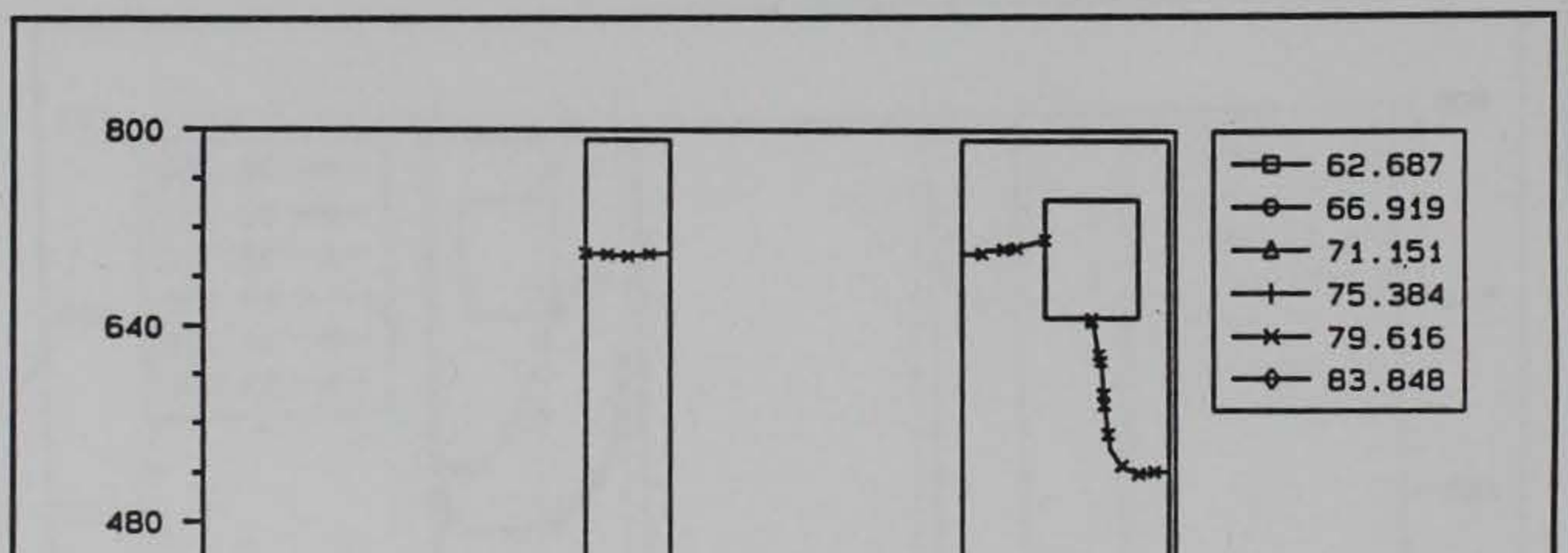

Figure 103. Temperature contour at day 730 at location shown in Figure 93

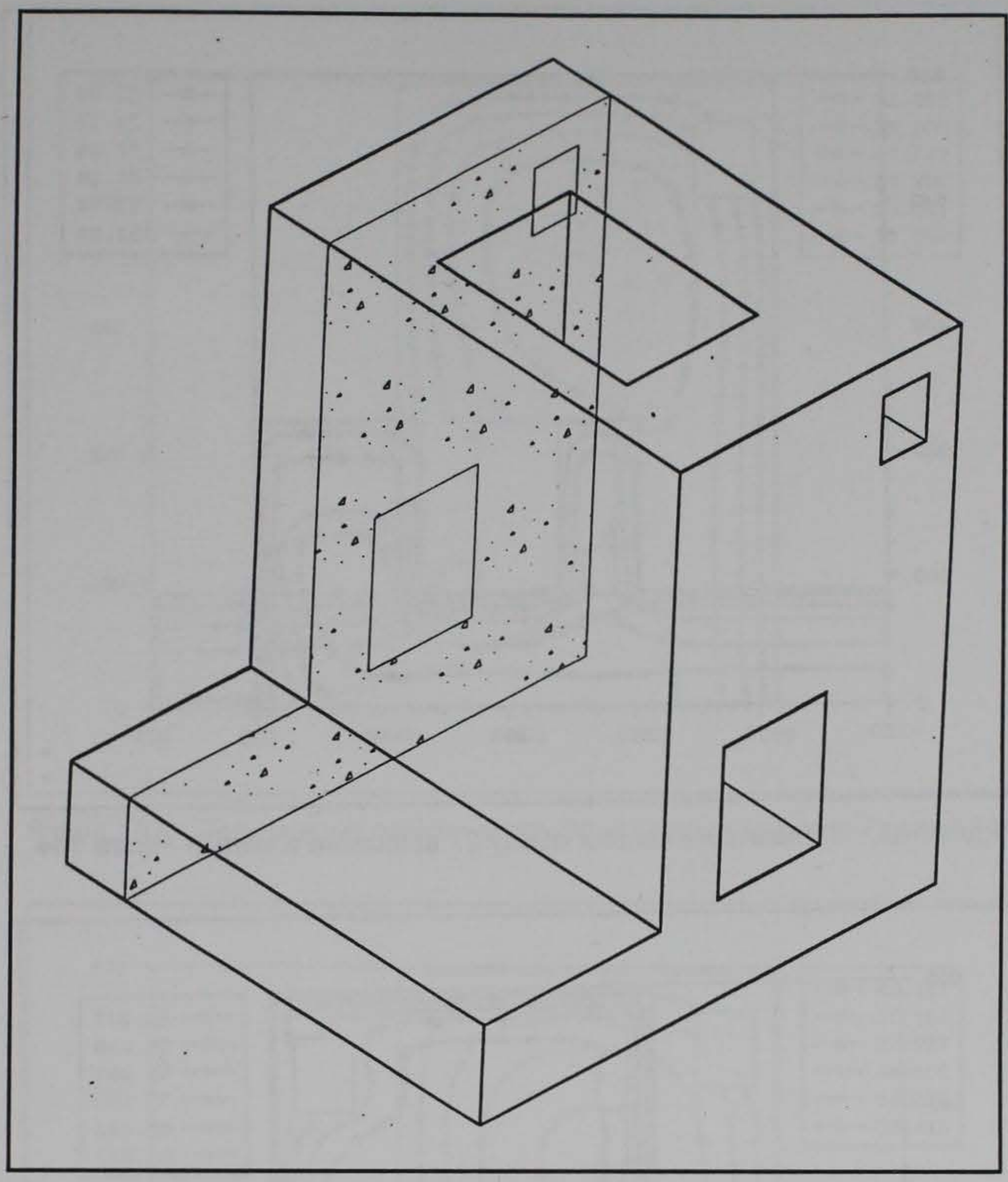

Figure 104. Transverse section locator through the downstream portion of the monolith for Figures 105 through 114

Figure 110 to Figure 40 at 360 days due once again to the fact that the openings in Analysis 2 are not covered after day 180.

Figures 111 through 114 are contours from the second year of the analysis. The fact that the culvert remains open can be identified by the contour which encircles the culvert and the fact that the gallery is once again closed can be seen by the fact that contour lines terminate along the edges. The location of the water line can be seen on both the chamber face and the land wall face by the termination of the two contour lines on those faces. The location can also be seen in each of the other three plots shown for the second year (Figures 112, 113, and 114).

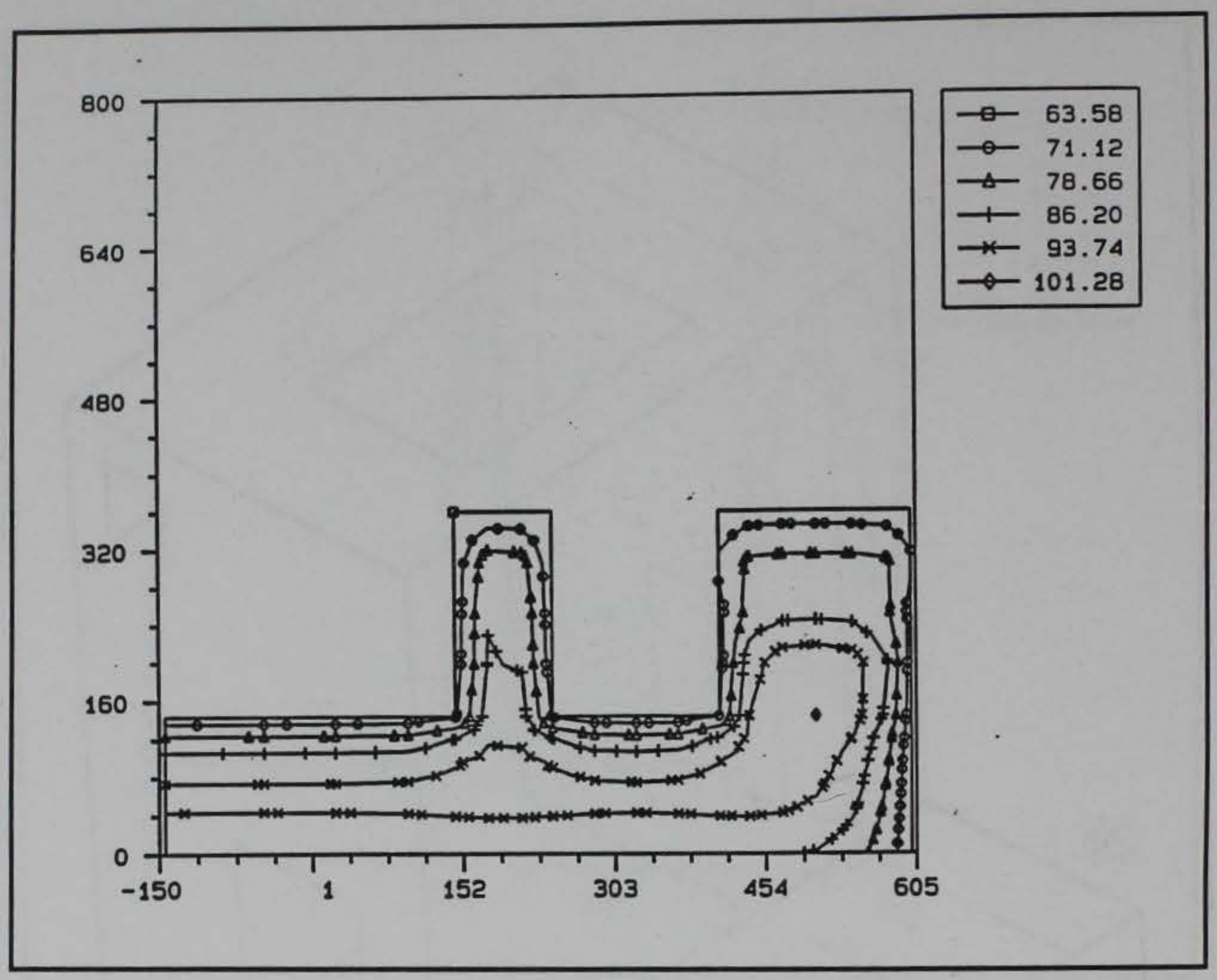

Figure 105. Temperature contour at day 27 at location shown in Figure 104

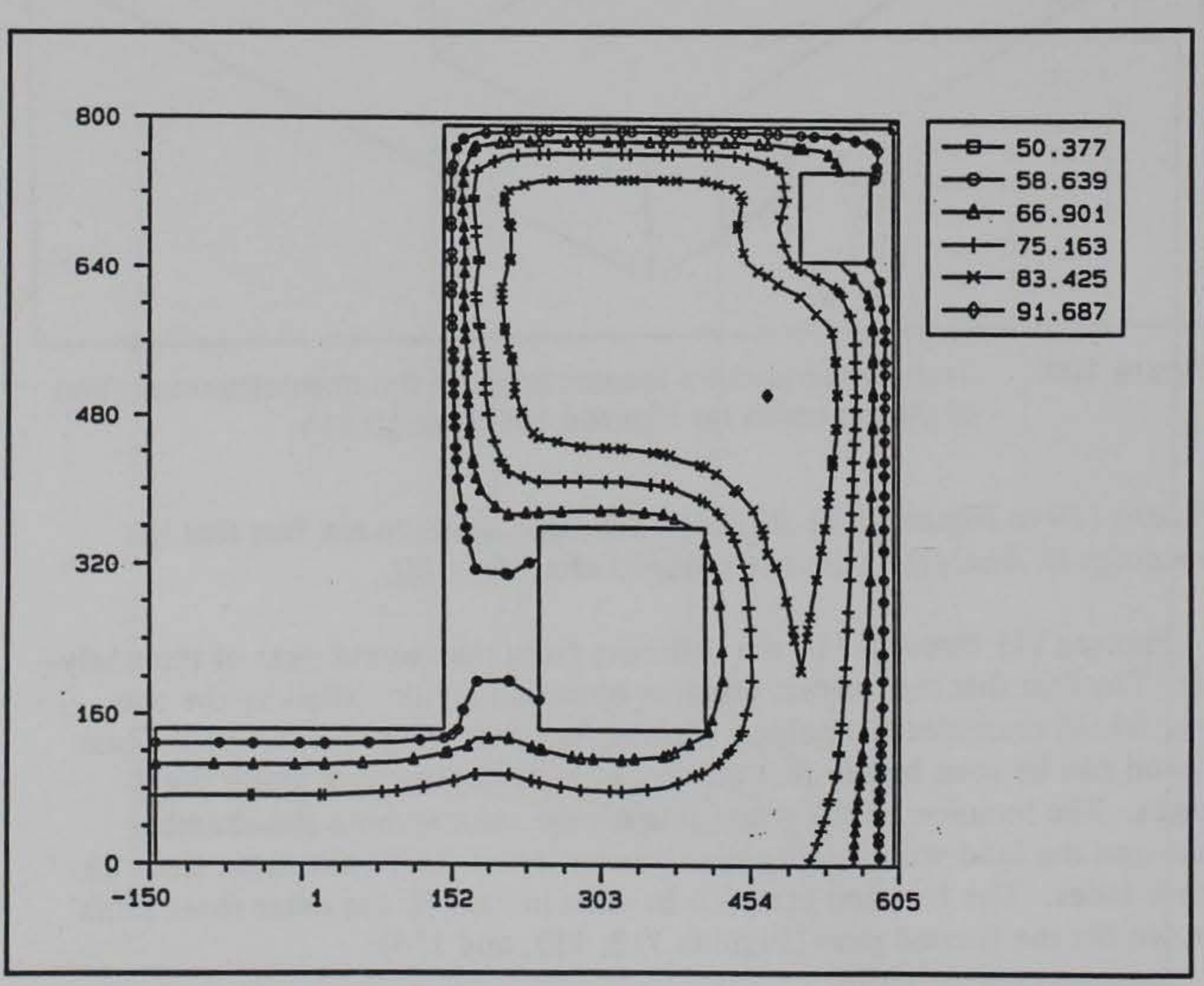

Figure 106. Temperature contour at day 52 at location shown in Figure 104

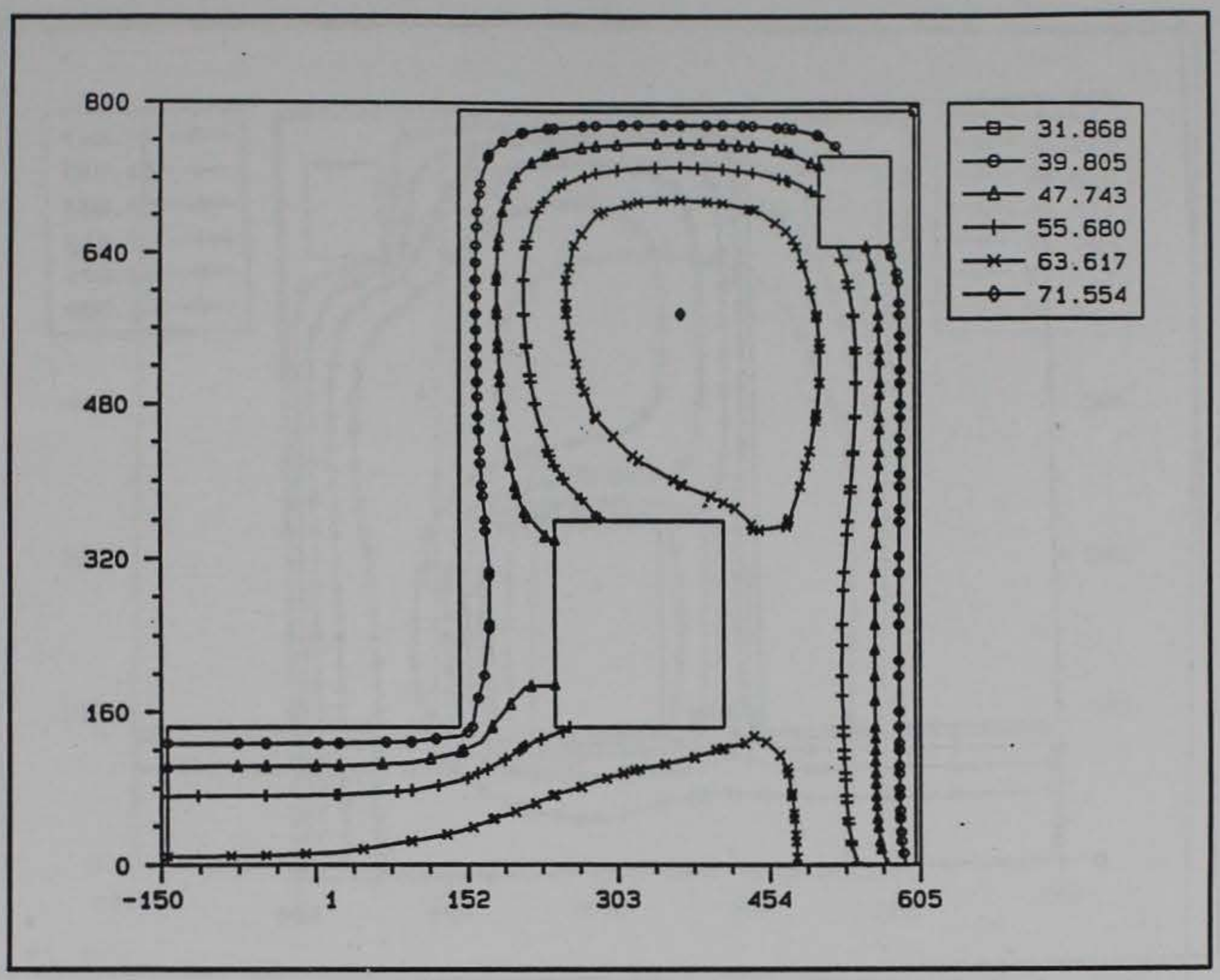

Figure 107. Temperature contour at day 90 at location shown in Figure 104

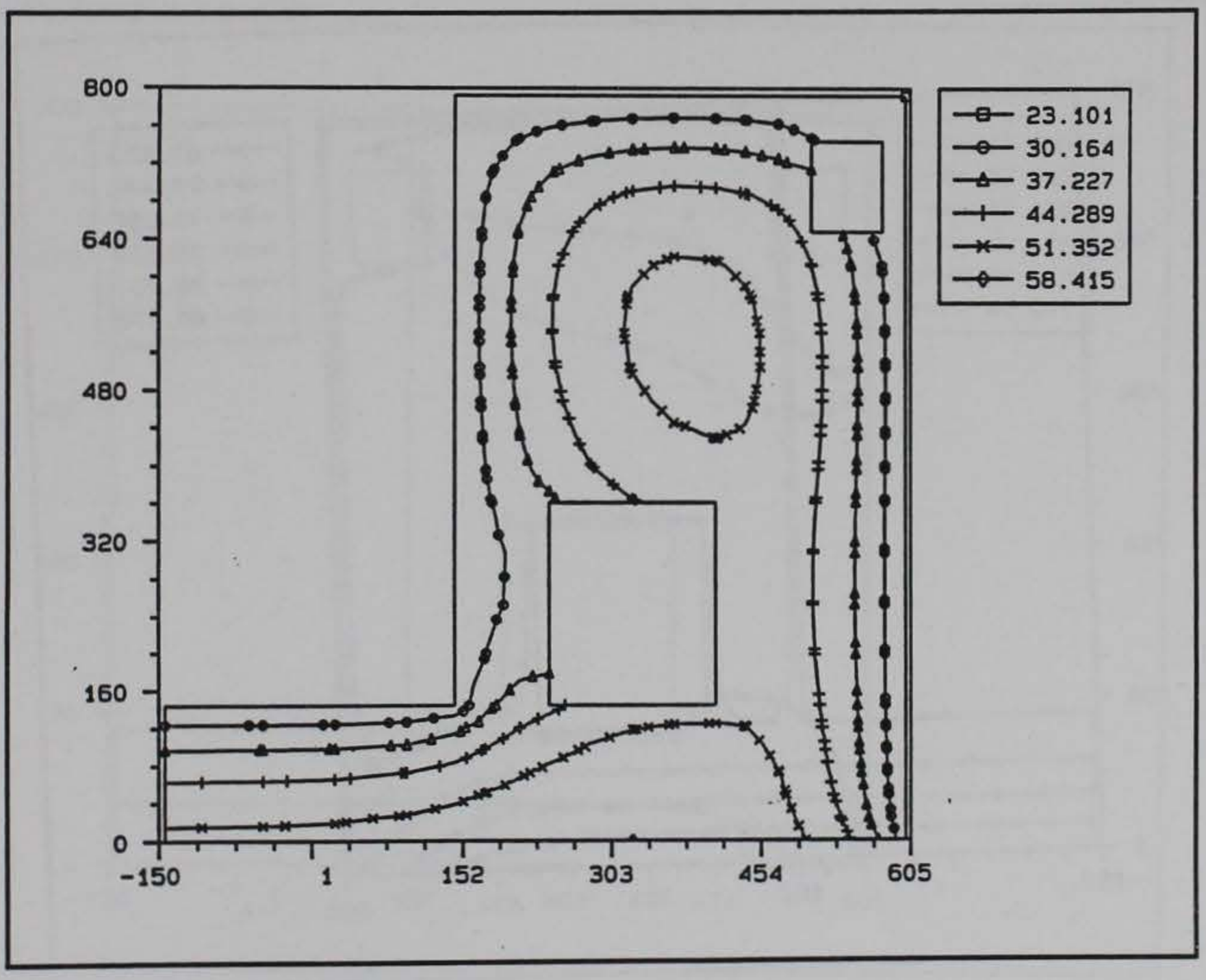

Figure 108. Temperature contour at day 125 at location shown in Figure 104

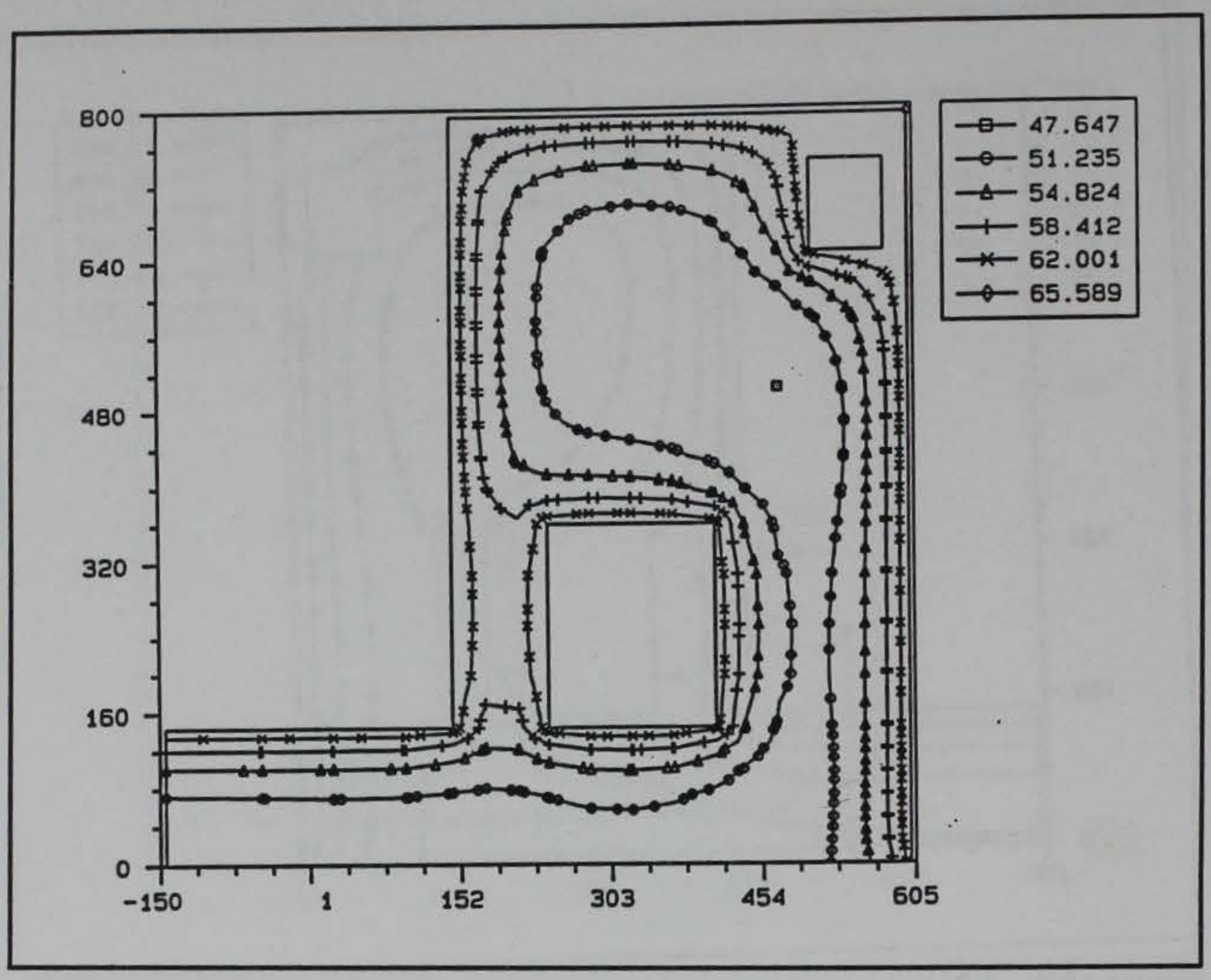

Figure 109. Temperature contour at day 250 at location shown in Figure 104

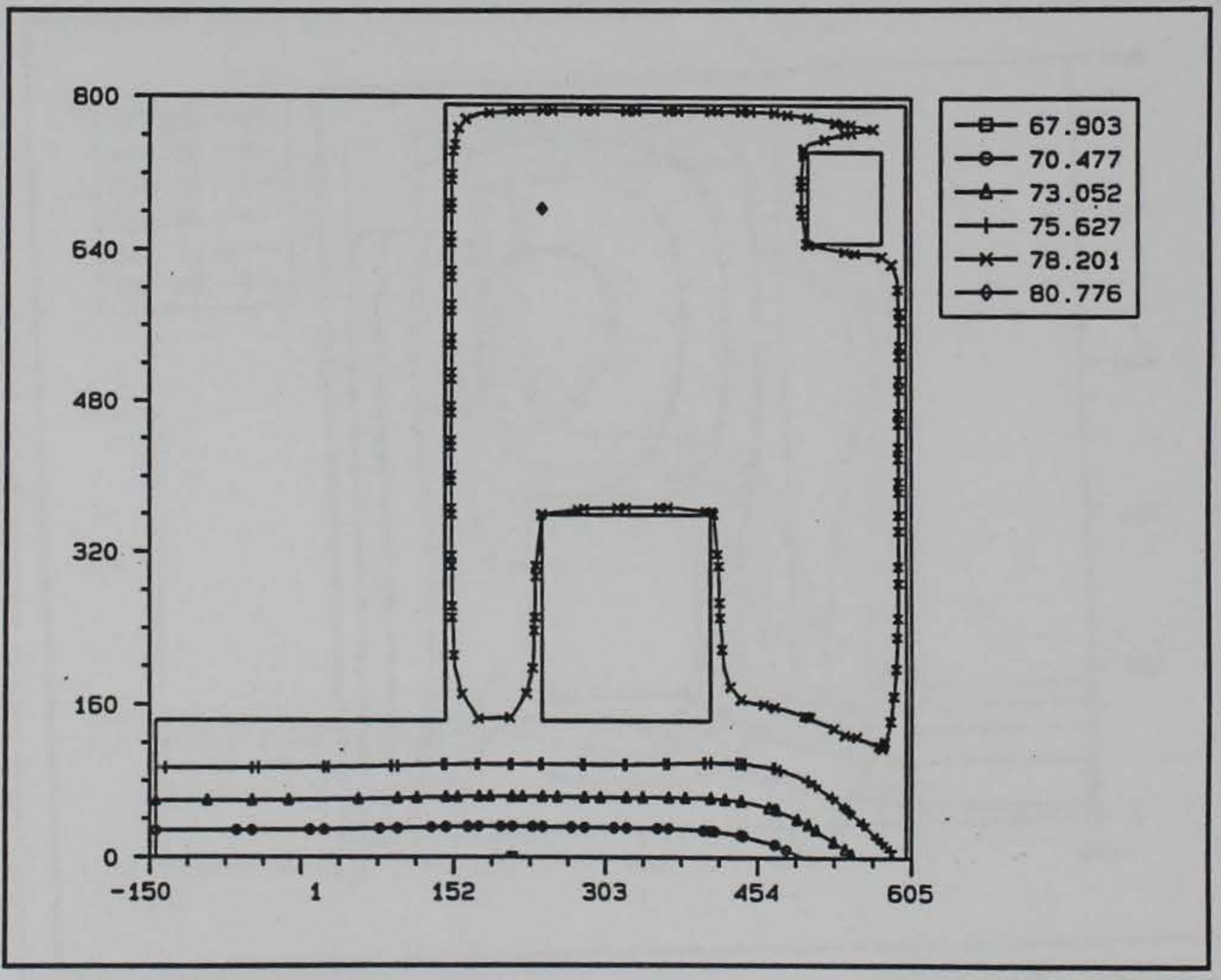

Figure 110. Temperature contour at day 360 at location shown in Figure 104

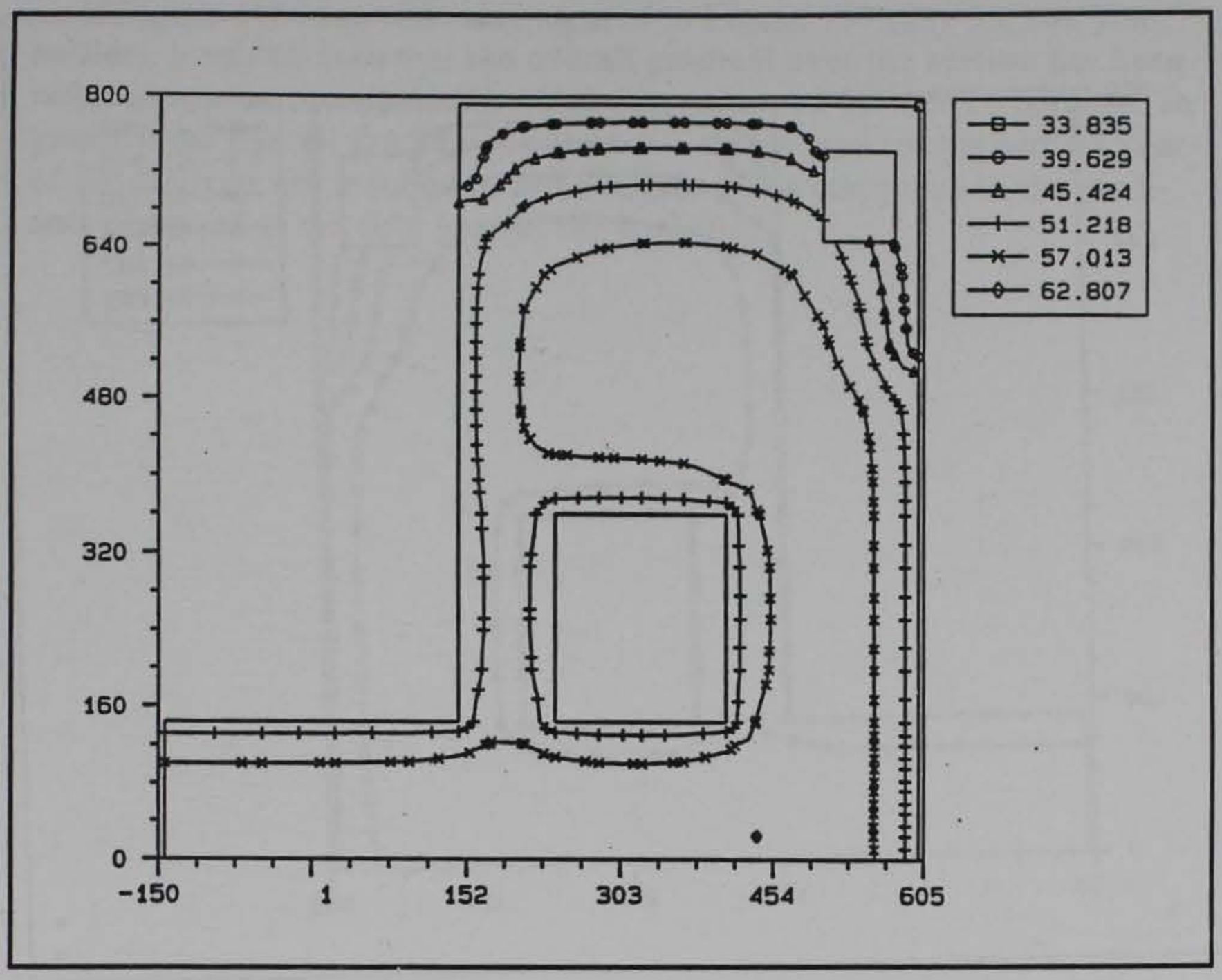

Figure 111. Temperature contour at day 450 at location shown in Figure 104

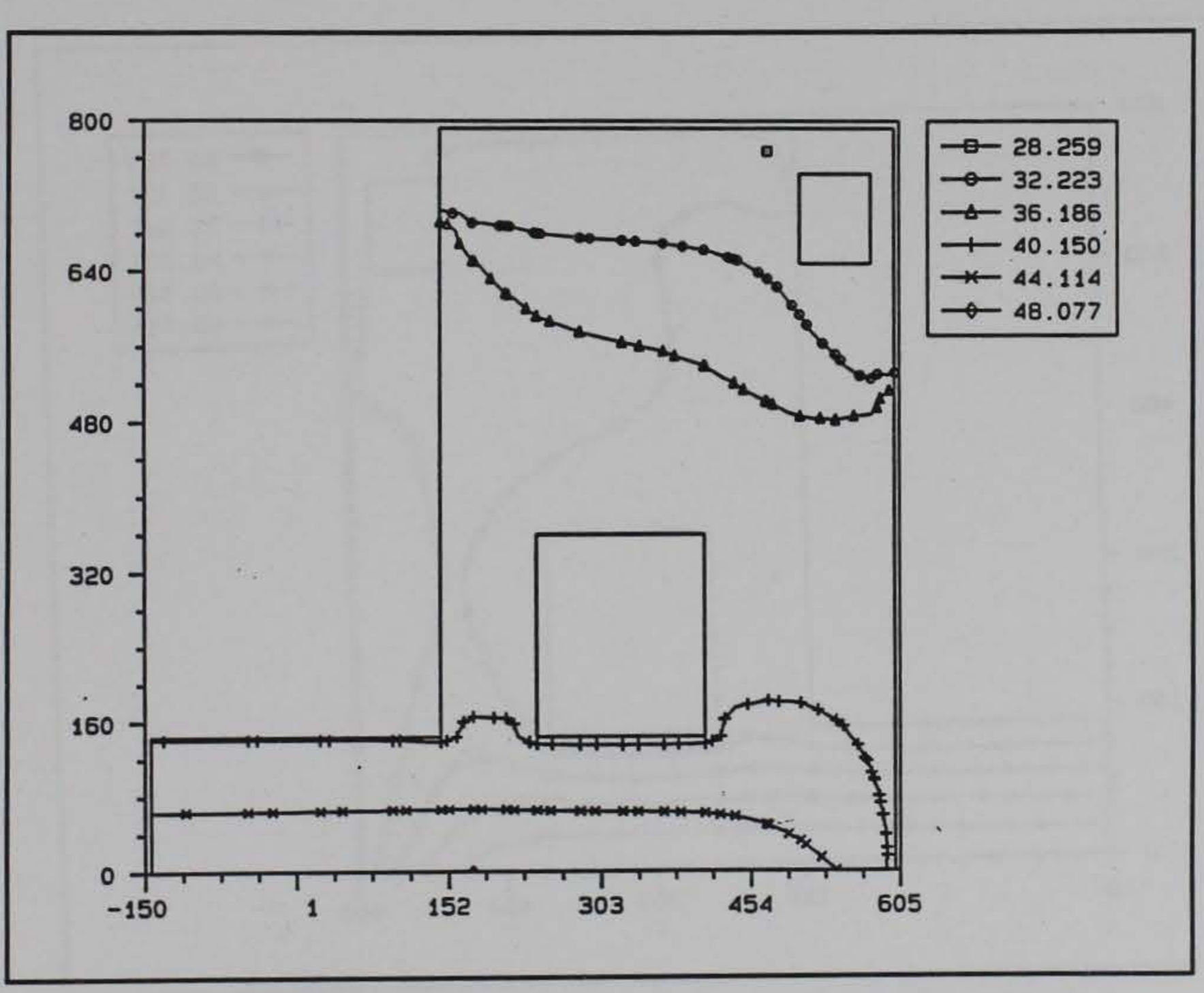

Figure 112. Temperature contour at day 540 at location shown in Figure 104

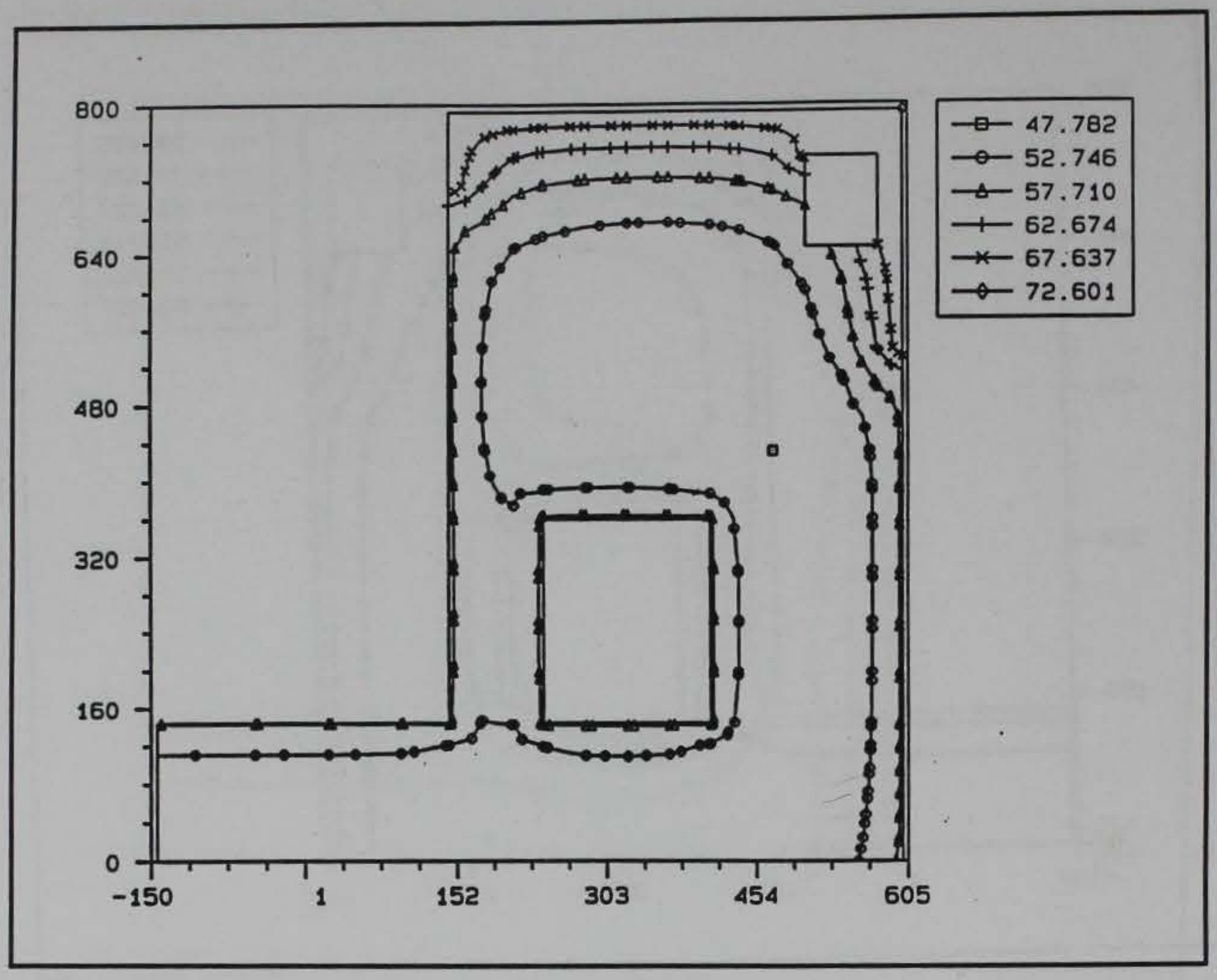

Figure 113. Temperature contour at day 630 at location shown in Figure 104

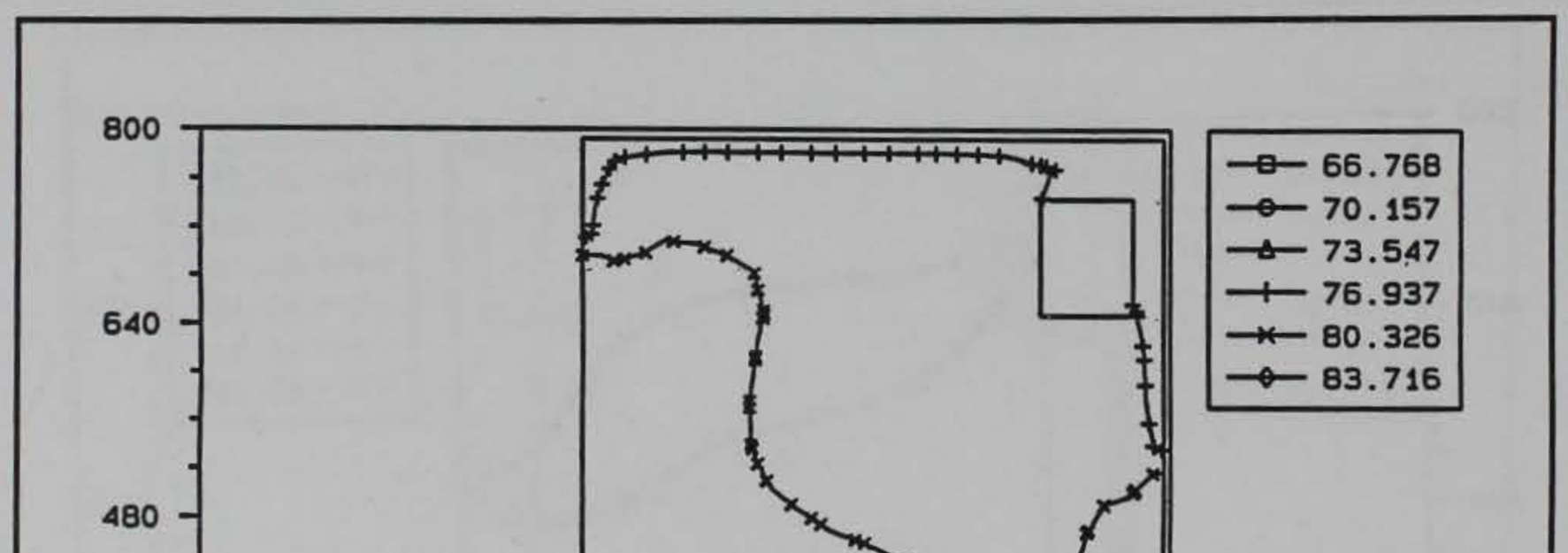

Figure 114. Temperature contour at day 730 at location shown in Figure 104

If Figure 111 (day 450) is compared to Figure 107 (day 90, one year earlier), it can be seen that the overall gradient over the section has been reduced approximately 11 °F, which is a reduction of over 25 percent. In general, the overall gradients observed in the section for the second year of the analysis are reduced to some degree when compared to the gradients observed in the first year of the analysis.

7 Stress Analysis - Analysis 2

Introduction

As in Analysis 1, the stress analysis was performed upon completion of the heat transfer analysis of Analysis 2. In the first year of Analysis 2, the only two loads applied to the structure were the temperatures and the dead weight of the concrete. After 360 days, the service loads as described in Chapter 2 were applied as a static load for the duration of the second year of the analysis.

The results of the stress analysis will include plots of the cracks which formed during the course of the analysis, contour plots of the potential for cracking, contours of maximum principal stress, and time-history plots of stress in the orthogonal directions. In addition, refer to the discussion in Chapter 4 on the smeared crack model used in the analysis.

Crack Location Plots

Crack plots for Analysis 2 are presented in Figures 115 through 120. The changes made for Analysis 2 resulted in the elimination of the large crack above the gallery. A total of three integration points cracked during the course of the analysis. Isometric views of the wall portion of the monolith are shown in Figures 115, 116, and 117 at times which are shortly after the integration points have cracked. The first point to crack was at the downstream, outside corner of the culvert valve pit and occurred on day 62. Figure 115 is shown at day 65. Figures 116 and 117 are taken at days 69 and 73, respectively, and coincide with the time in the analysis when the points at the top, outside corners of the culverts cracked. Presented in Figures 118, 119, and 120 are the front elevation, side elevation, and plan view, respectively, of the monolith wall to provide a better understanding of the crack directions and crack locations. In Figure 118 it can be seen that the crack is extending somewhat at a diagonal

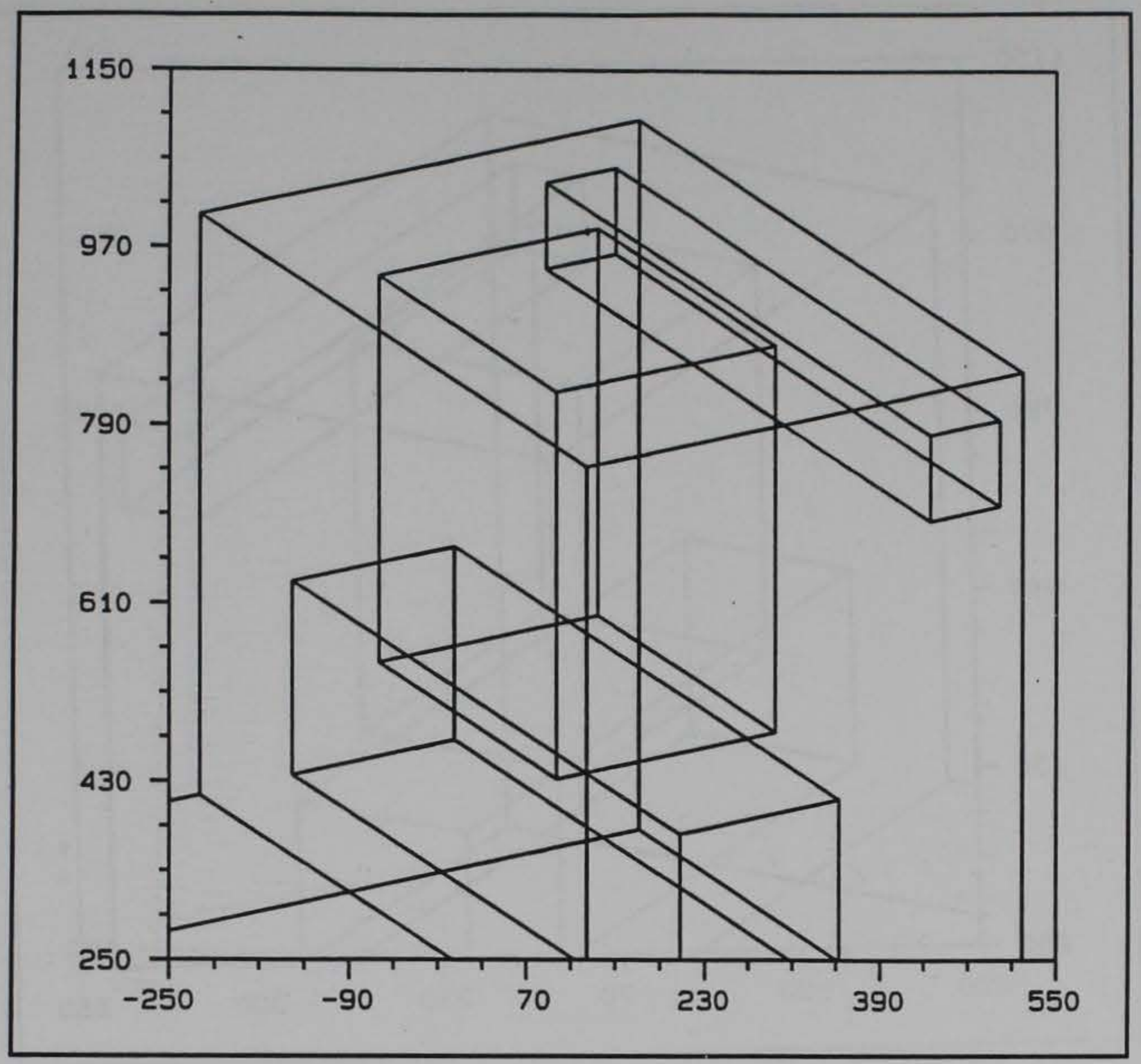

Figure 115. Crack plot, partial isometric view at day 65

away from the corner of the culvert. Likewise, in Figure 120 the crack at the corner of the culvert valve pit angles away from the corner as well.

The integration points which cracked do not appear to be a design problem for the monolith since the three points which cracked were at three different locations. In addition, all three of the points which cracked and opened in tension eventually closed and began carrying compression again. The crack at the corner of the culvert valve pit closed on day 145, and the cracks at the culvert corners closed and day 170. Once the cracks closed, they never reopened again for the remainder of the analysis.

Cracking Potential Contours

Contours of the cracking potentials for Analysis 2 are shown in Figures 121 through 139. Since very little cracking occurred in Analysis 2, the cracking potentials become more important in evaluating the behavior and performance of the structure. In general, the potentials presented in

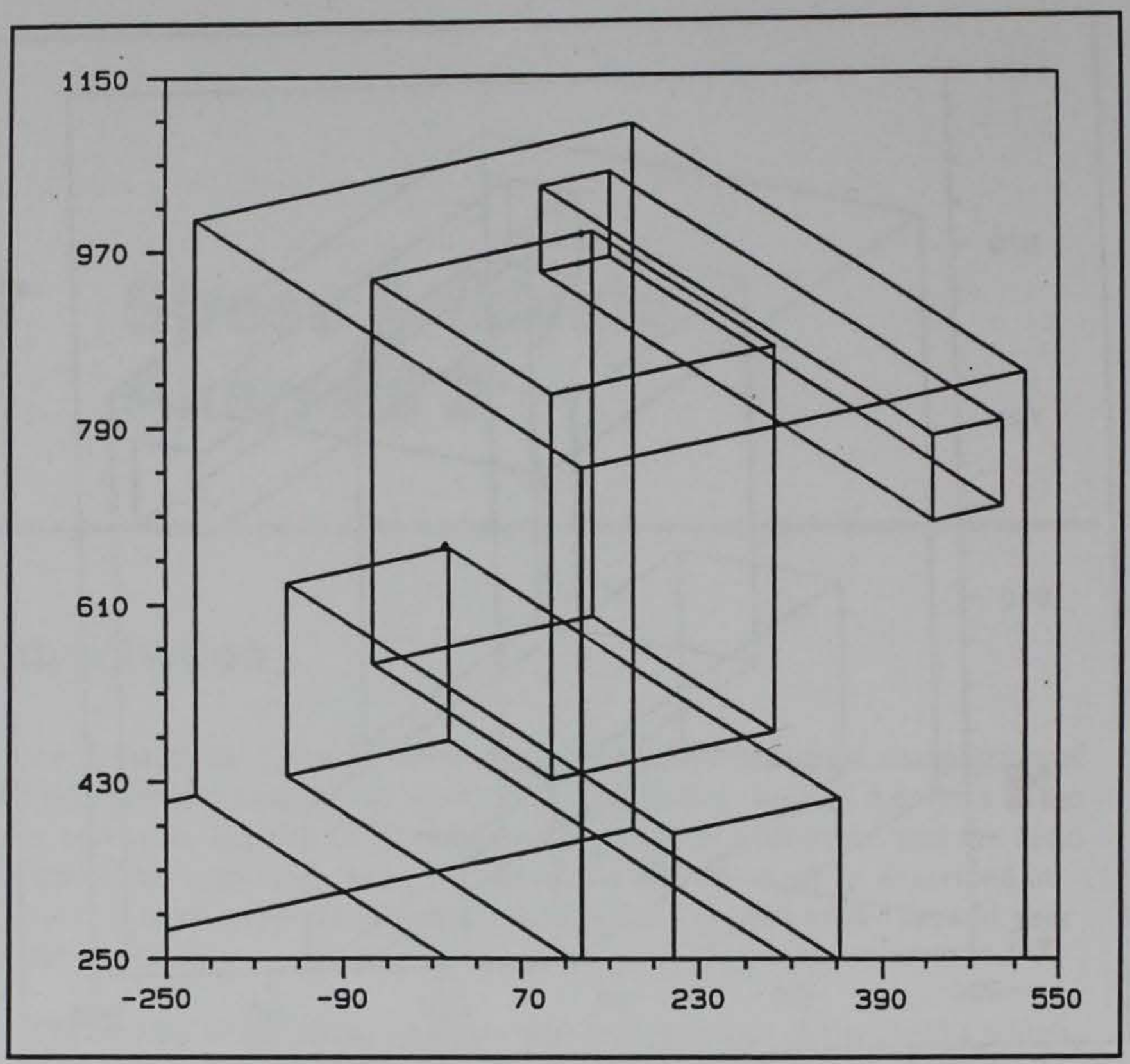

Figure 116. Crack plot, partial isometric view at day 69

this chapter are the same as the potentials presented in Chapter 4 so that comparisons between Analysis 1 and Analysis 2 can be made. In addition, some crack potential contours are also shown in this chapter for the second year of Analysis 2.

Figures 121 through 126 are the cracking potentials at a plane of the monolith which is midlength along the culvert valve pit. This section is shown in Figure 7. Figures 121 and 122 of Analysis 2 correspond to Figures 56 and 57, respectively, of Analysis 1 and as can be seen by comparing these plots there is very little difference in the response of the structure between the two analyses. The similarities between the two analyses are less obvious when Figure 123 is compared to Figure 58. The primary difference is the fact that the potential at the corner of the gallery is much higher in Analysis 1 (Figure 58) than in Analysis 2 (Figure 123). This same difference occurs when comparing Figure 124 at day 209 to Figure 59. It may appear that differences exist in other portions of the structure as well, but this is primarily due to the fact that in Analysis 1 (Figure 59) the contours collect around the corner of the gallery, whereas in Analysis 2 (Figure 124) the contours are distributed more evenly. If the contour values are compared though, it can be seen that the contours are

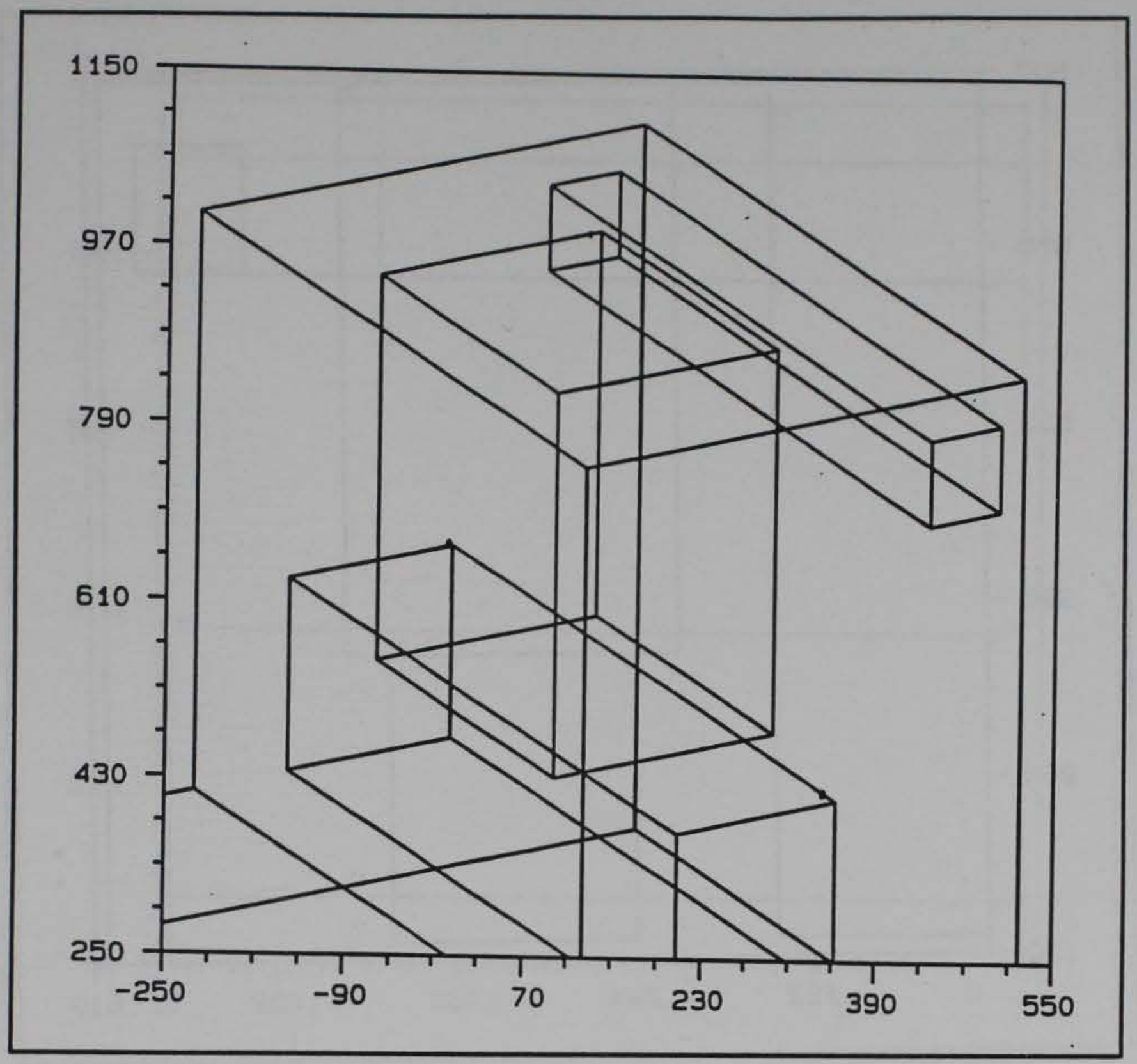

Figure 117. Crack plot, partial isometric view at day 73

nearly identical. These statements are also true when comparing Figure 125 to Figure 60 and Figure 126 to Figure 61.

The next set of plots are for a section taken at the downstream edge of the culvert valve pit and are shown in Figures 127 through 136. Comparison of Figure 127 to Figure 62 indicates that the behavior between the two analyses is generally the same but the potentials near the corners of the culvert valve pit are significantly higher for Analysis 2. This is also true when comparing Figure 128 to Figure 63. Figure 128 is at 65 days and is presented at the same time the crack formed at the corner of the culvert valve pit. It can be seen that the crack has formed by the fact that the location of the maximum crack potential is no longer at the top of the monolith but is a few inches below the top of the monolith. Statements made regarding the comparisons of the two analyses in the previous paragraph can be applied when comparing Figure 129 to Figure 64, Figure 130 to Figure 65, and Figure 131 to Figure 66. It should also be noted in Figures 129 through 131 that at no time does the crack potential get above 52 percent.

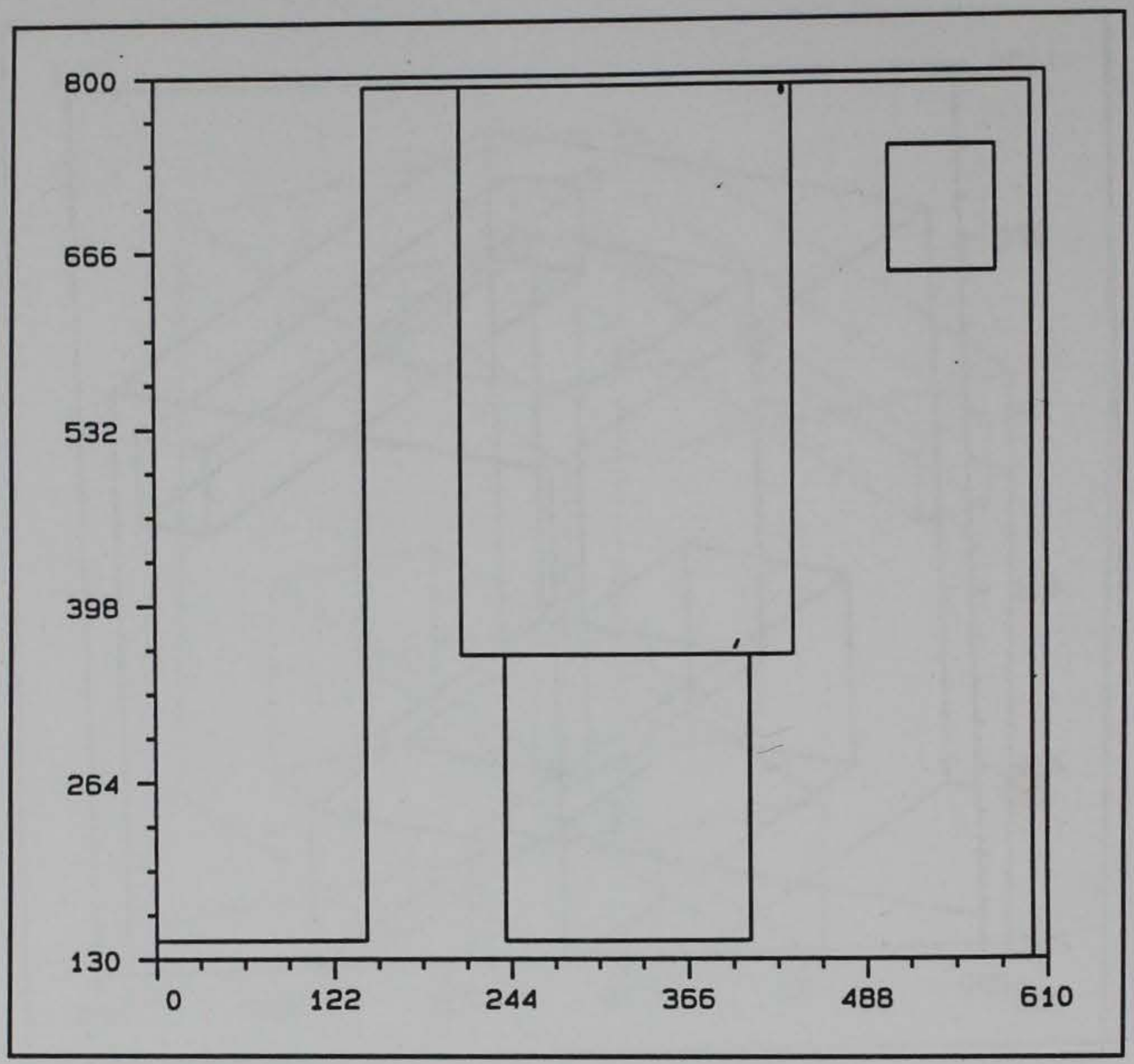

Figure 118. Crack plot, front elevation at day 73

Figures 132 through 136 are plots from the second year of Analysis 2. Once again, none of the potentials reached extremely high values with the maximum occurring at day 639 at a value of 72 percent. Behavior in the second year of the analysis is very similar to the first year of the analysis. This can be seen by comparing Figures 130 and 134 which are plots nearly 1 year apart. The general shape of the contours are very close as well as the magnitudes. Likewise, Figures 131 and 135 can be compared. Again, the general shapes of the contours are very similar, but in this the cracking potential in the second year of the analysis is higher than it was in the first year. This is due to the fact at the points in time observed in these two plots, the gallery has no covers on the openings in the first year but does in the second. This created a 20 percent increase in the cracking potential.

The last two crack potential contour plots (Figures 137 and 138) are taken at the upstream edge of the culvert valve pit. As in Analysis 1, the sections at the upstream and downstream ends of the culvert valve pit are very similar as can be seen by comparing Figures 130 and 137 of Analysis 2. The contour shapes are very much alike, and the magnitudes are also very close. Comparison of Figures 137 and 138 show that the general

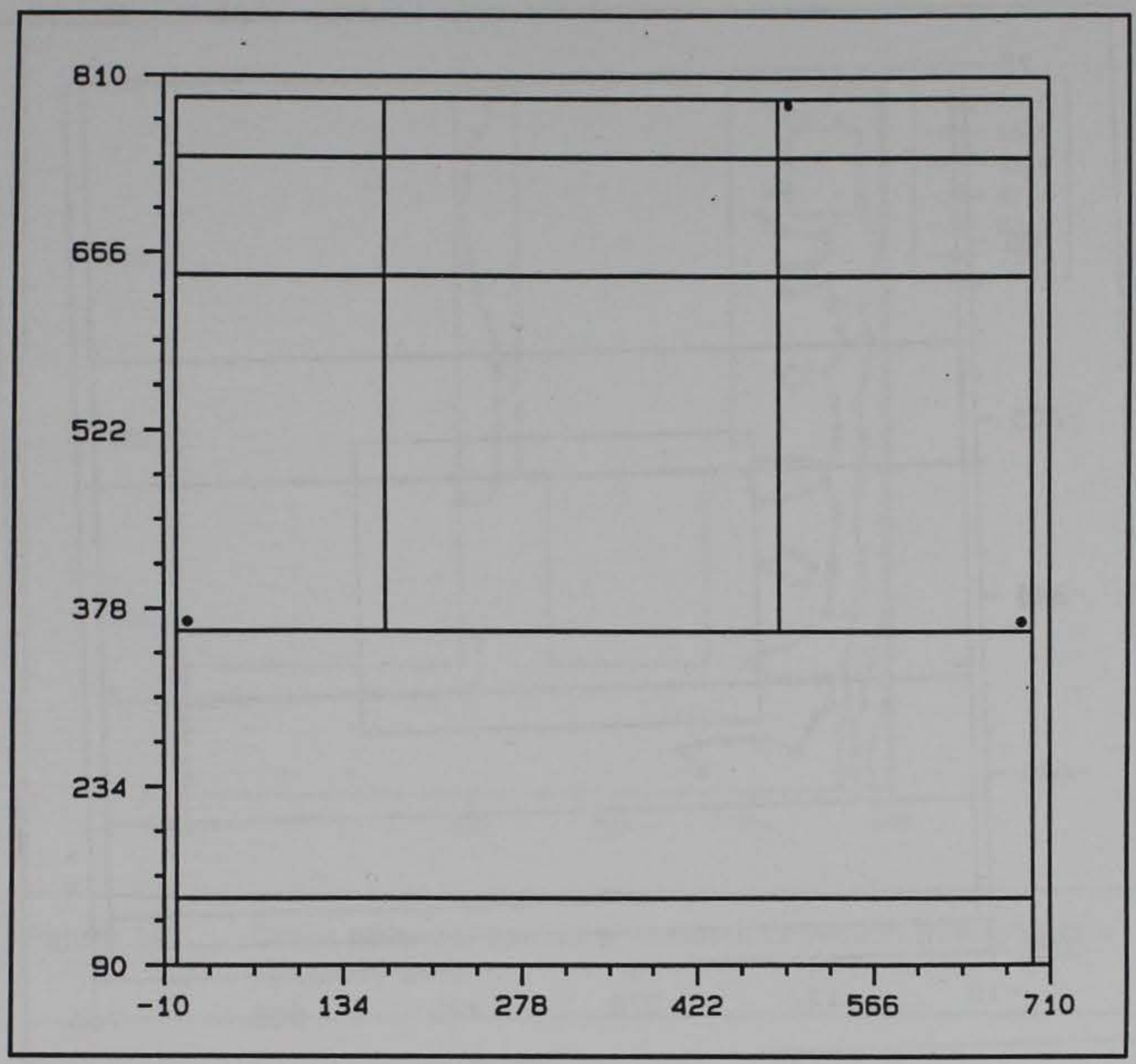

Figure 119. Crack plot, side elevation at day 73

behavior at this section after a years cycle is very similar as was seen in the downstream section.

Maximum Principal Stress Contours

Principal stress contours are not presented for Analysis 2, since comments made when comparing the stress contours to the crack potential contours in Chapter 4 would be generally the same. Some principal stress contours are provided in Appendix B for a transverse section half way between the downstream end of the monolith and the culvert valve pit.

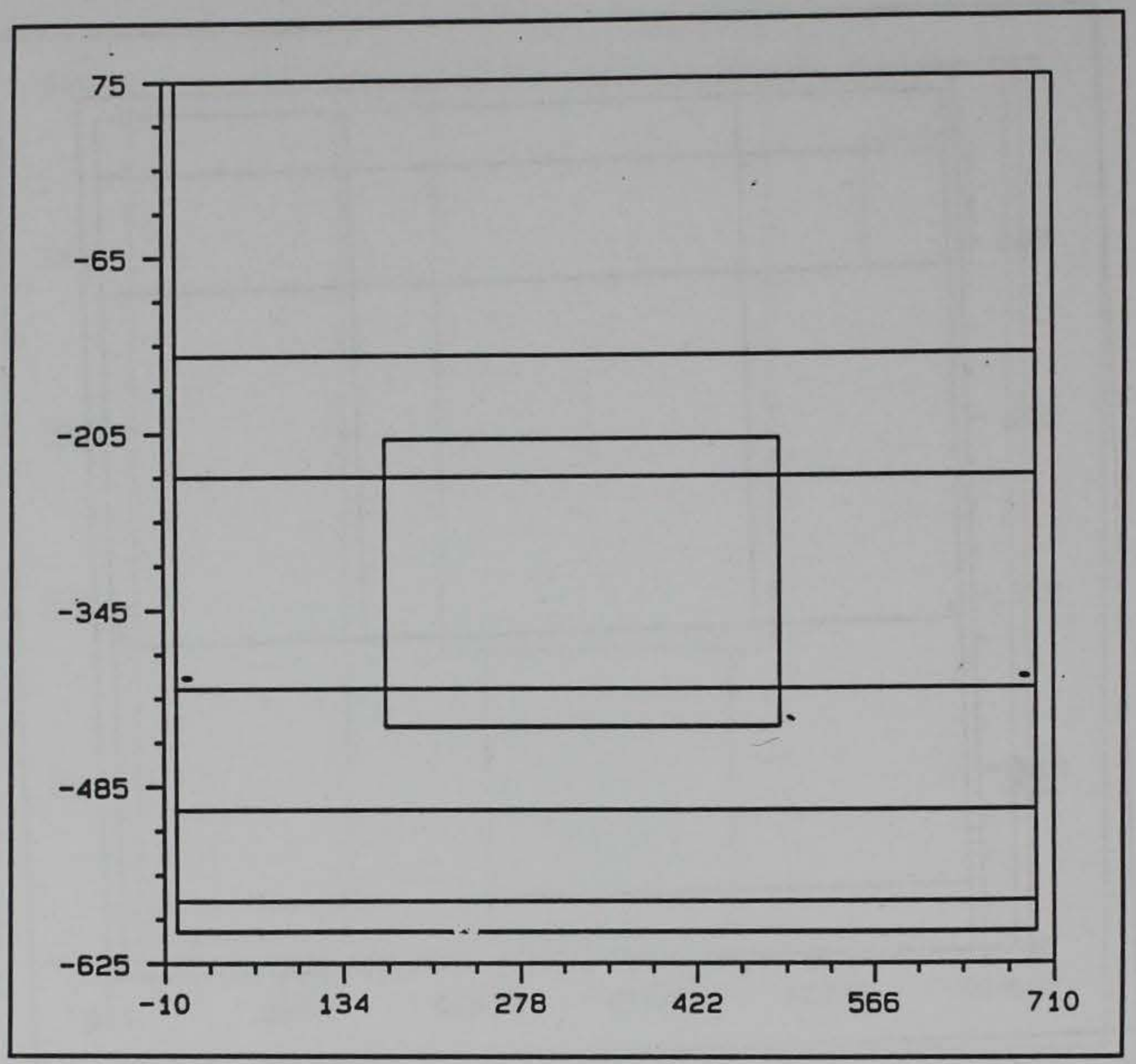

Figure 120. Crack plot, plan view at day 73

Time-History Plots

Figures 139, 140, and 141 are time-history plots of stress at the same locations presented in Chapter 4 for Analysis 1. Figure 139 is a plot of the transverse stress at the corner of the gallery where the cracking occurred in Analysis 1. Since no cracking occurred in Analysis 2, the curves in Figure 139 have no sudden drops like the curves shown in Figure 80 for Analysis 1. The effect of the removing the covers at 180 days can be seen in Figure 139 by the change in the slope of the line for element 3801, integration point 2. This change demonstrates the benefit of removing the covers on the openings in the spring. It should also be noted that element 3801, integration point 2, goes into more compression initially than the same point in Analysis 1 did. This can be attributed to the change in the lift sequence. In Analysis 1 the integration point in Figure 80 was directly adjacent to a lift interface, but in Analysis 2 the lift interface has been moved. Figure 140 is at the same location as Figure 139 but is a plot of the vertical stress. The behavior seen in Figure 139 is also exhibited in Figure 140 except that the initial compression is much larger and the removal of the covers from the openings is much more apparent.

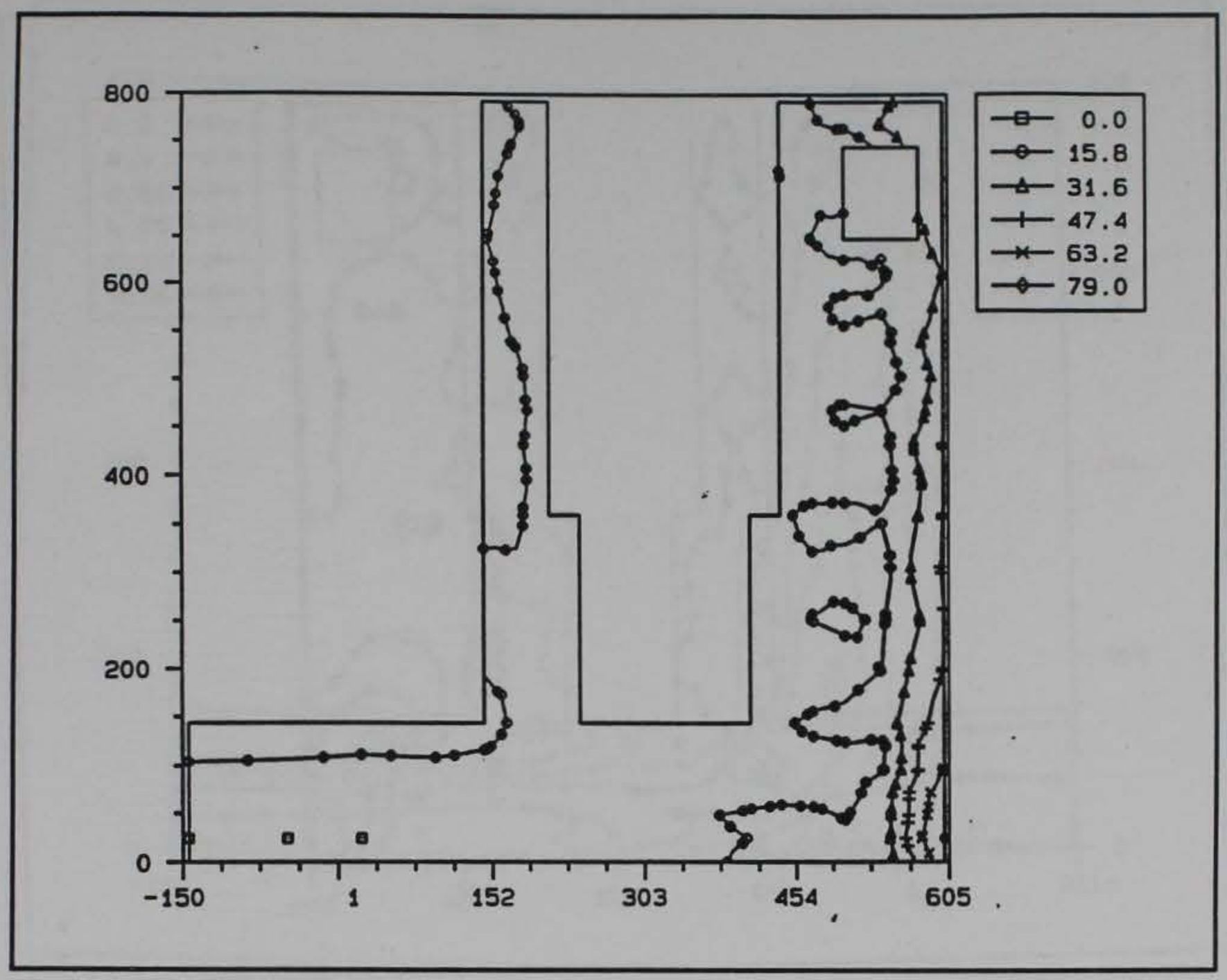

Figure 121. Crack potential contours, transverse section through valve pit at day 64.5

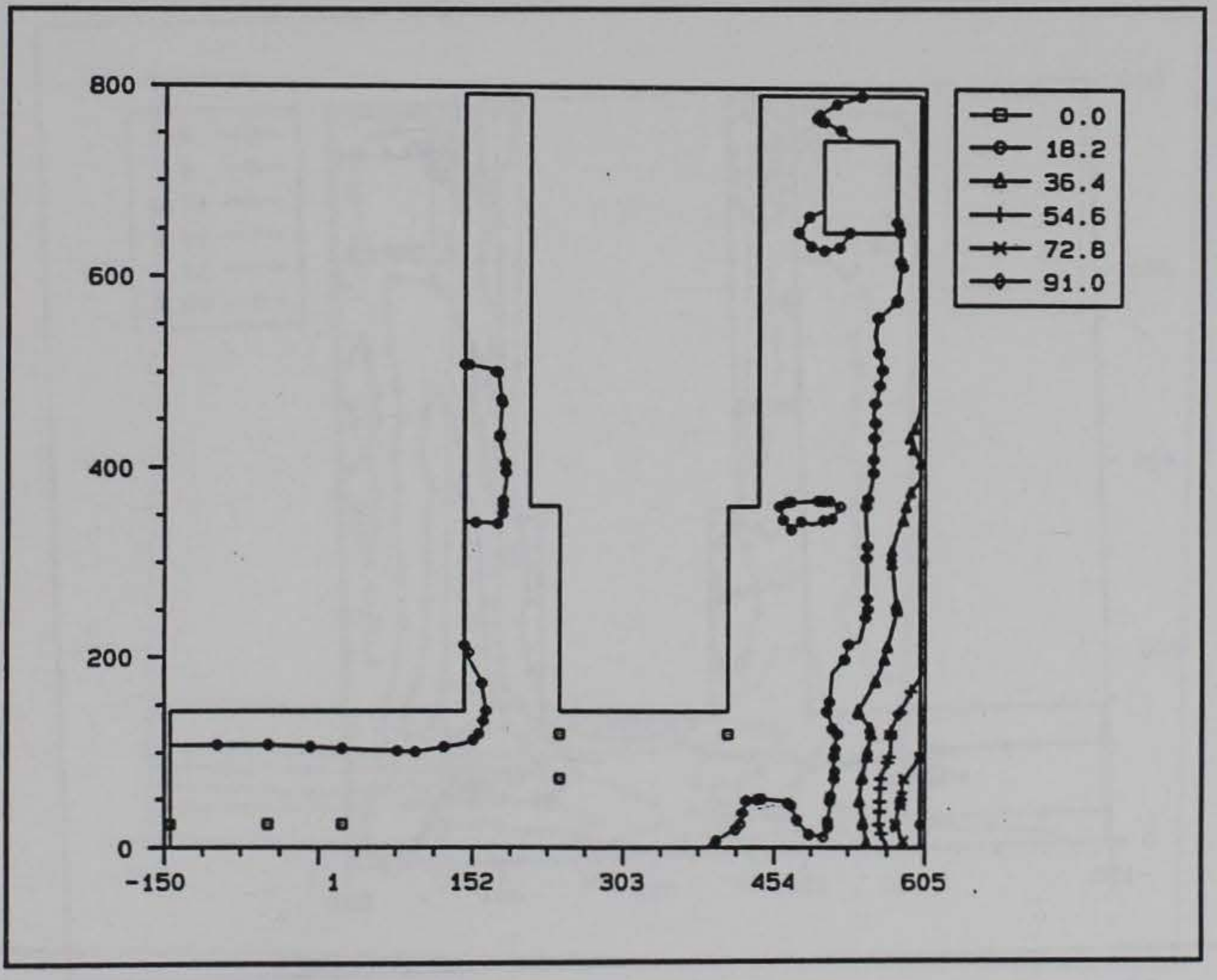

Figure 122. Crack potential contours, transverse section through valve pit at day 100

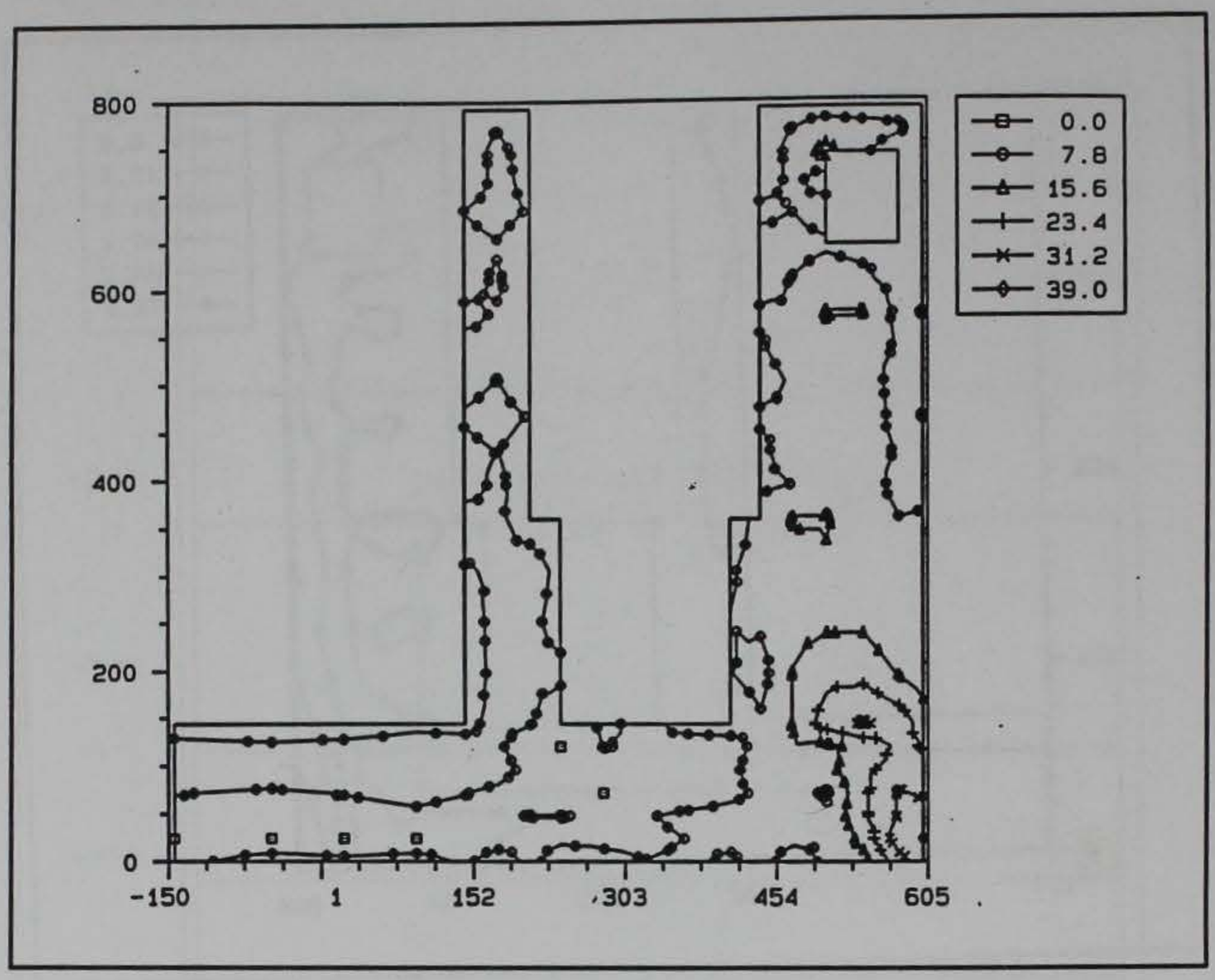

Figure 123. Crack potential contours, transverse section through valve pit at day 169

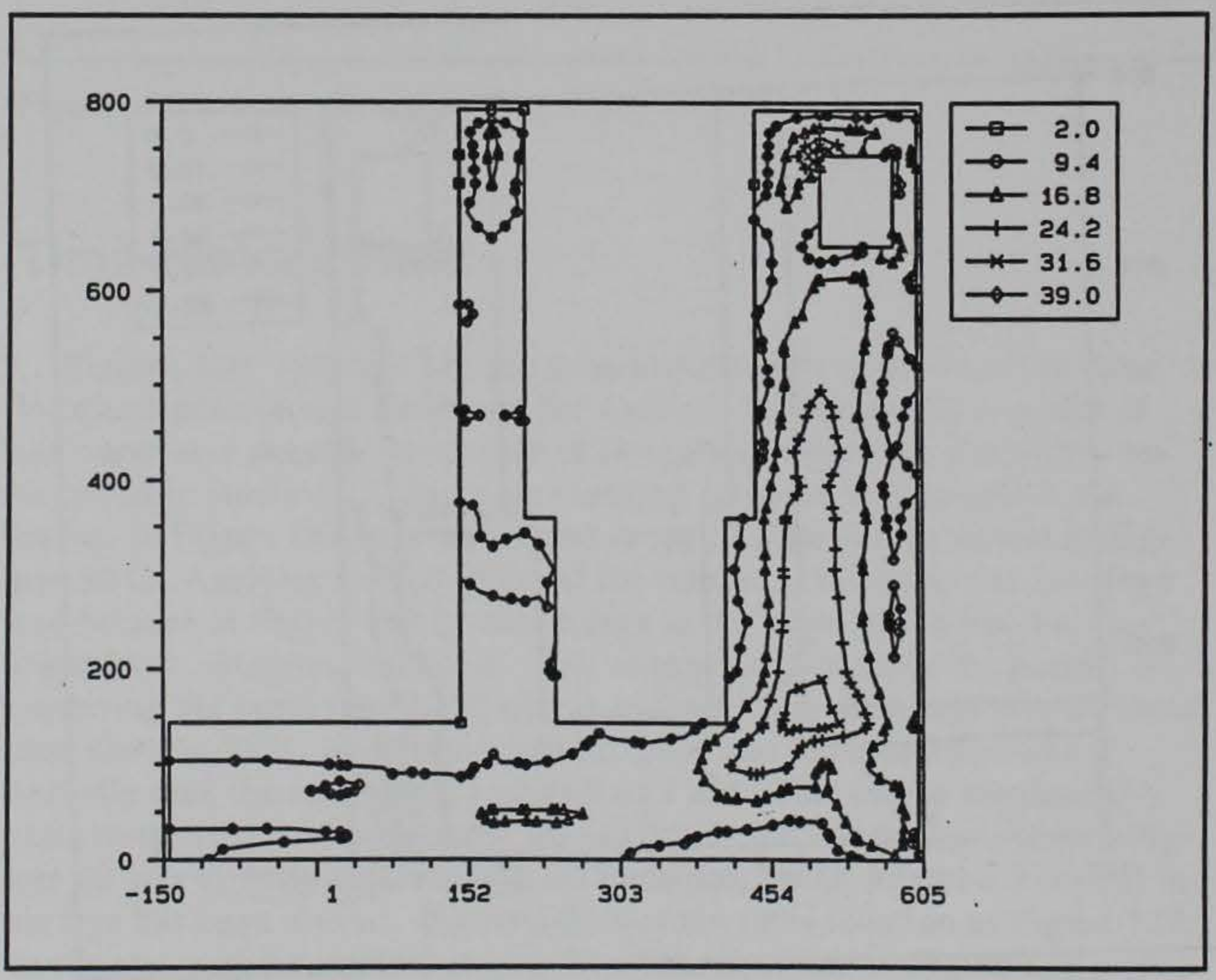

Figure 124. Crack potential contours, transverse section through valve pit at day 209

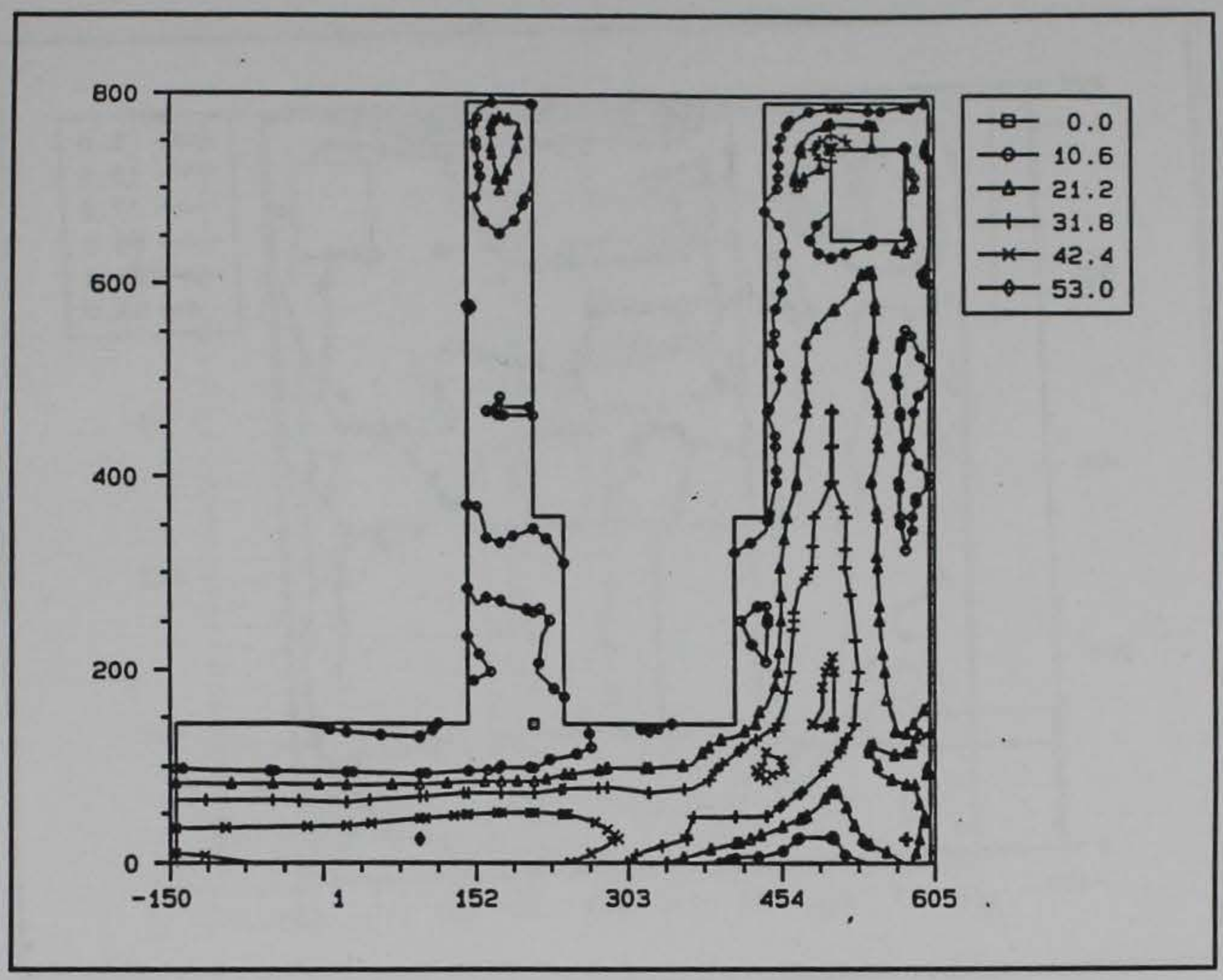

Figure 125. Crack potential contours, transverse section through valve pit at day 269

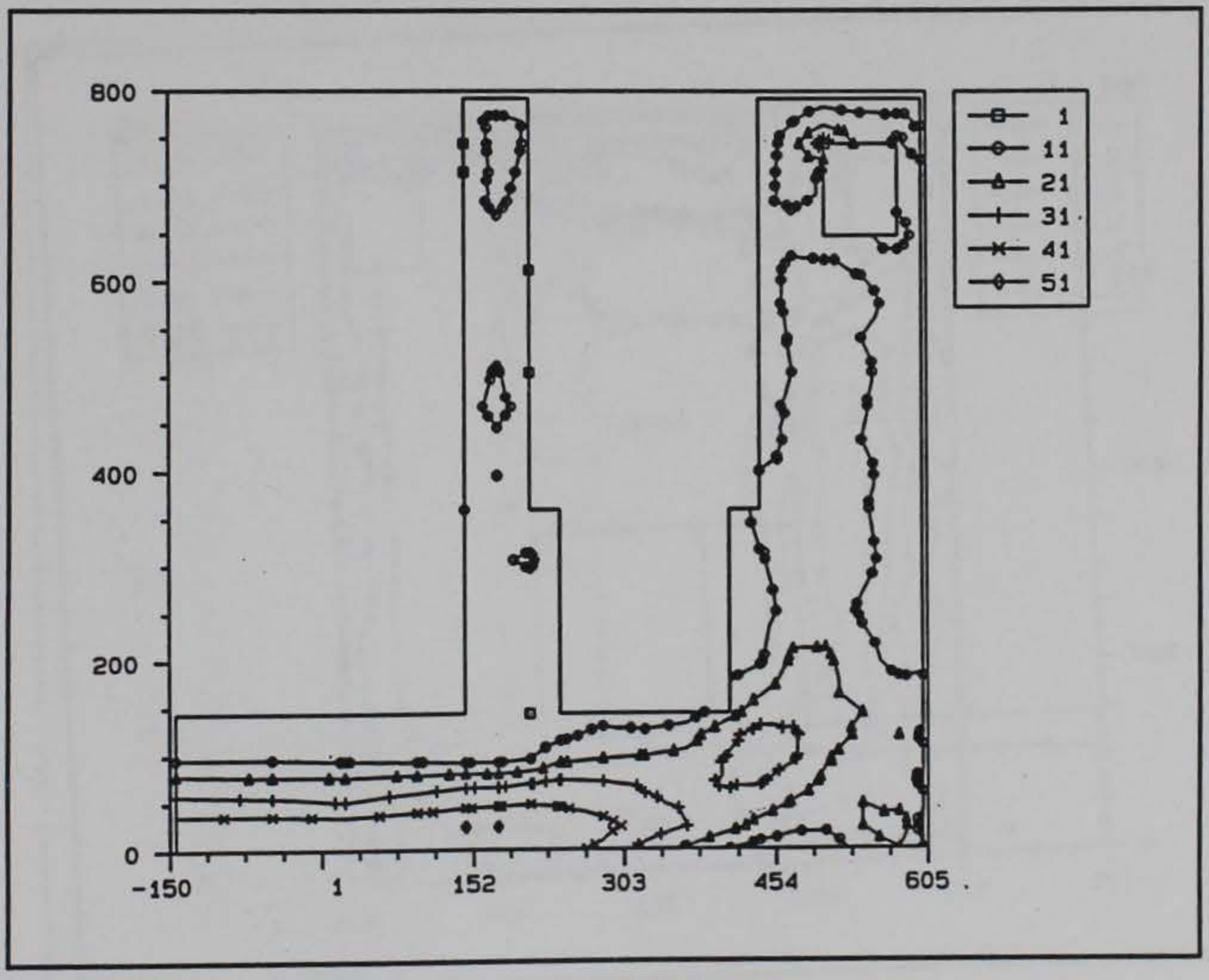

Figure 126. Crack potential contours, transverse section through valve pit at day 359

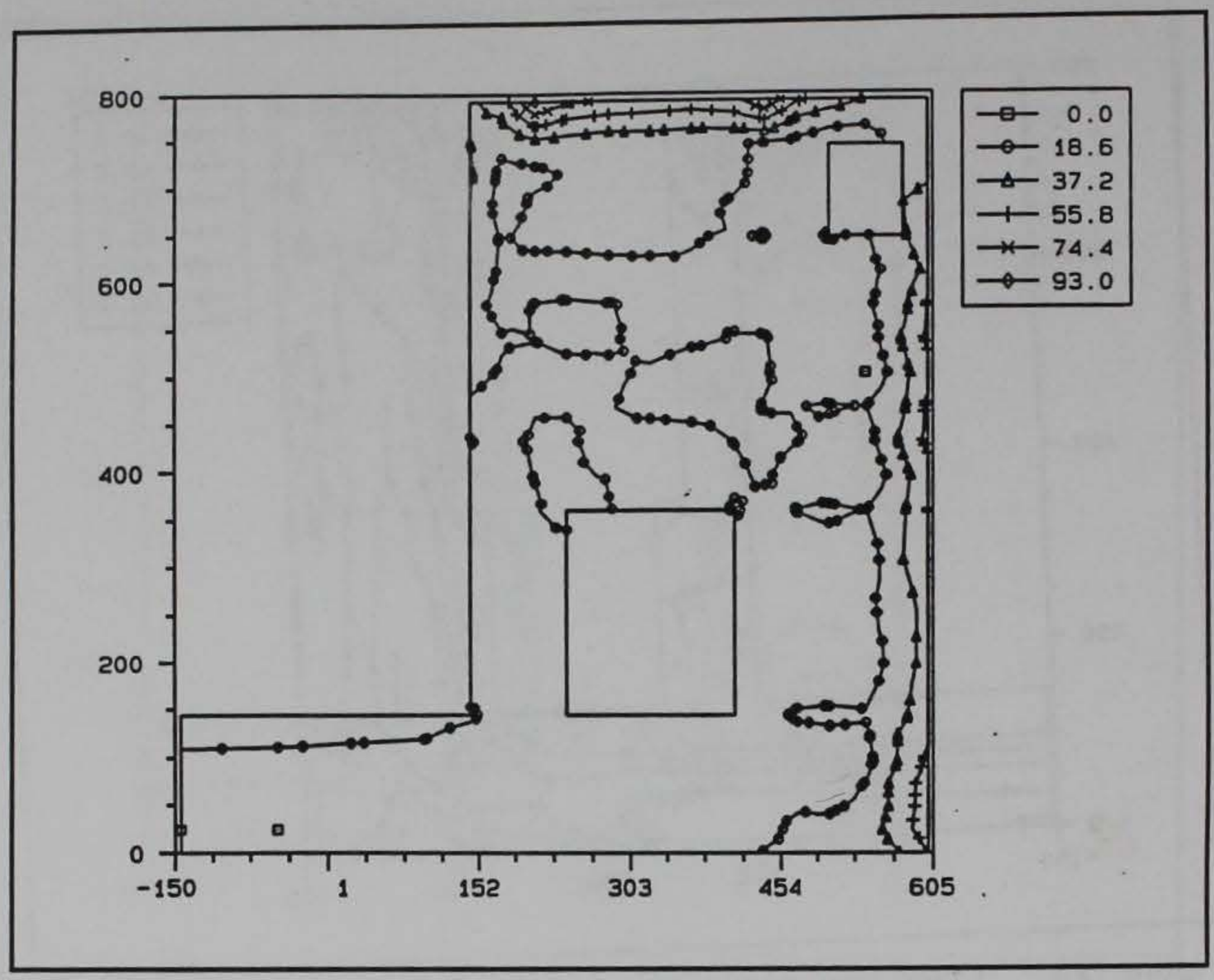

Figure 127. Crack potential contours, transverse section at DS edge of valve pit at day 54

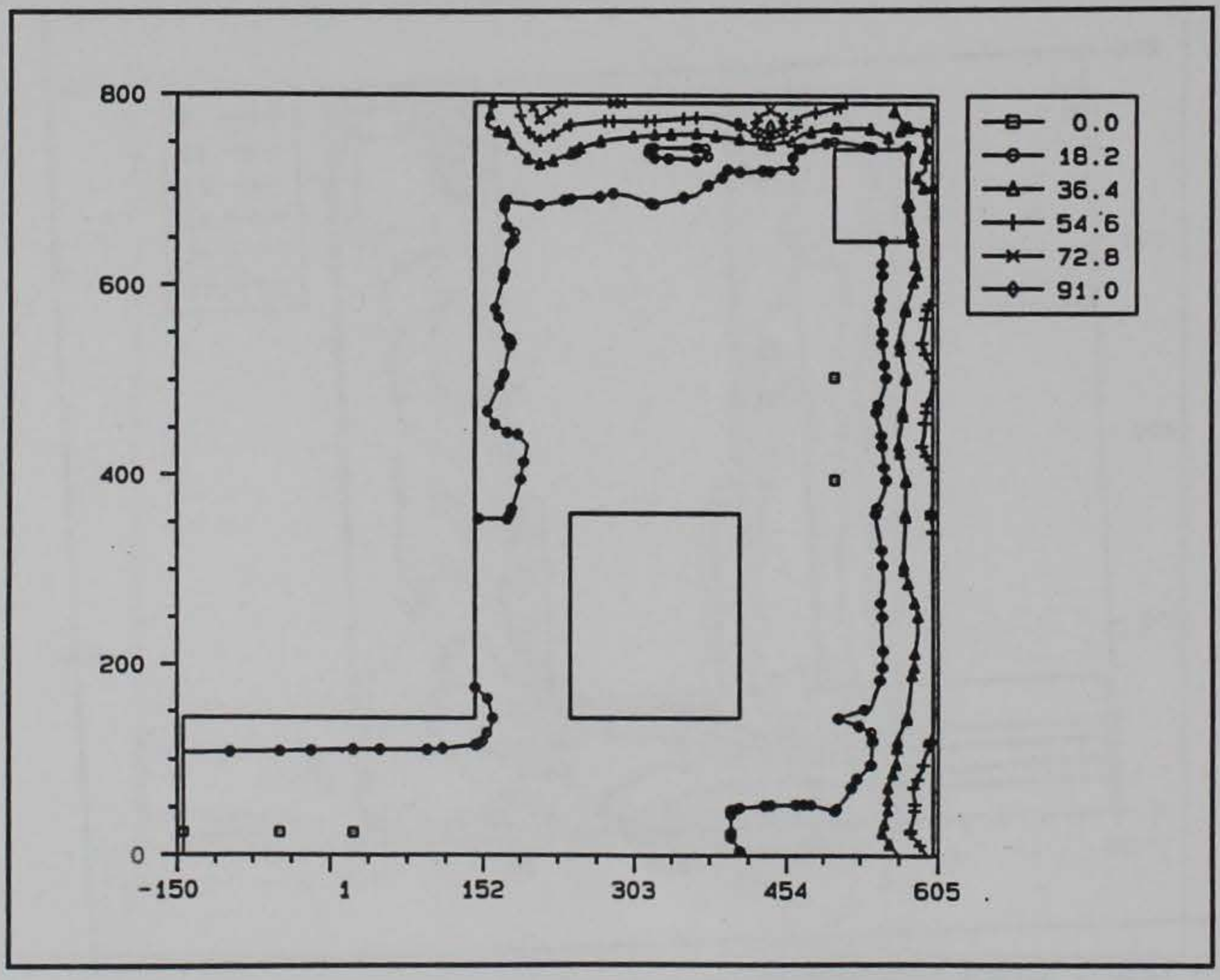

Figure 128. Crack potential contours, transverse section at DS edge of valve pit at day 64.5

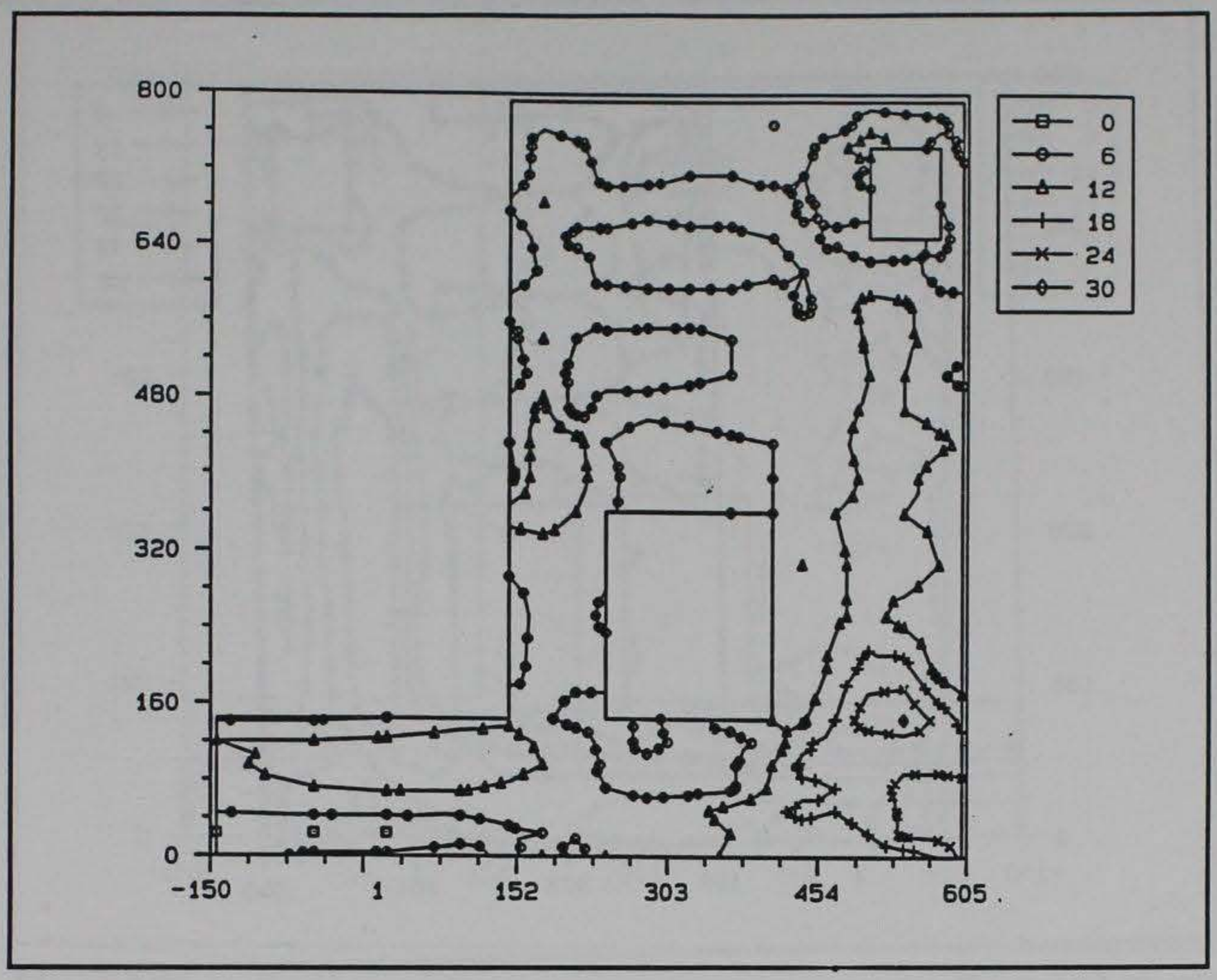

Figure 129. Crack potential contours, transverse section at DS edge of valve pit at day 169

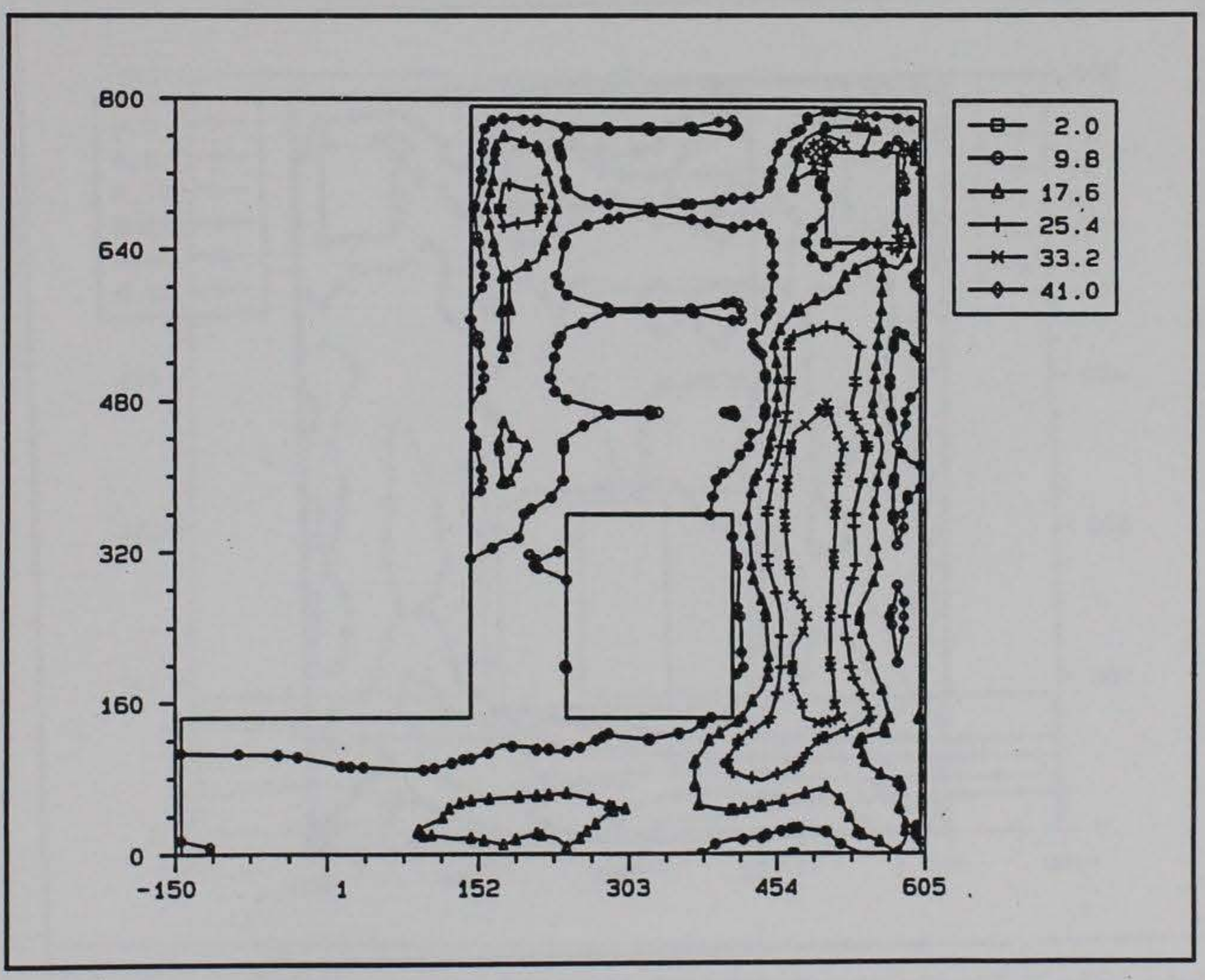

Figure 130. Crack potential contours, transverse section at DS edge of valve pit at day 209

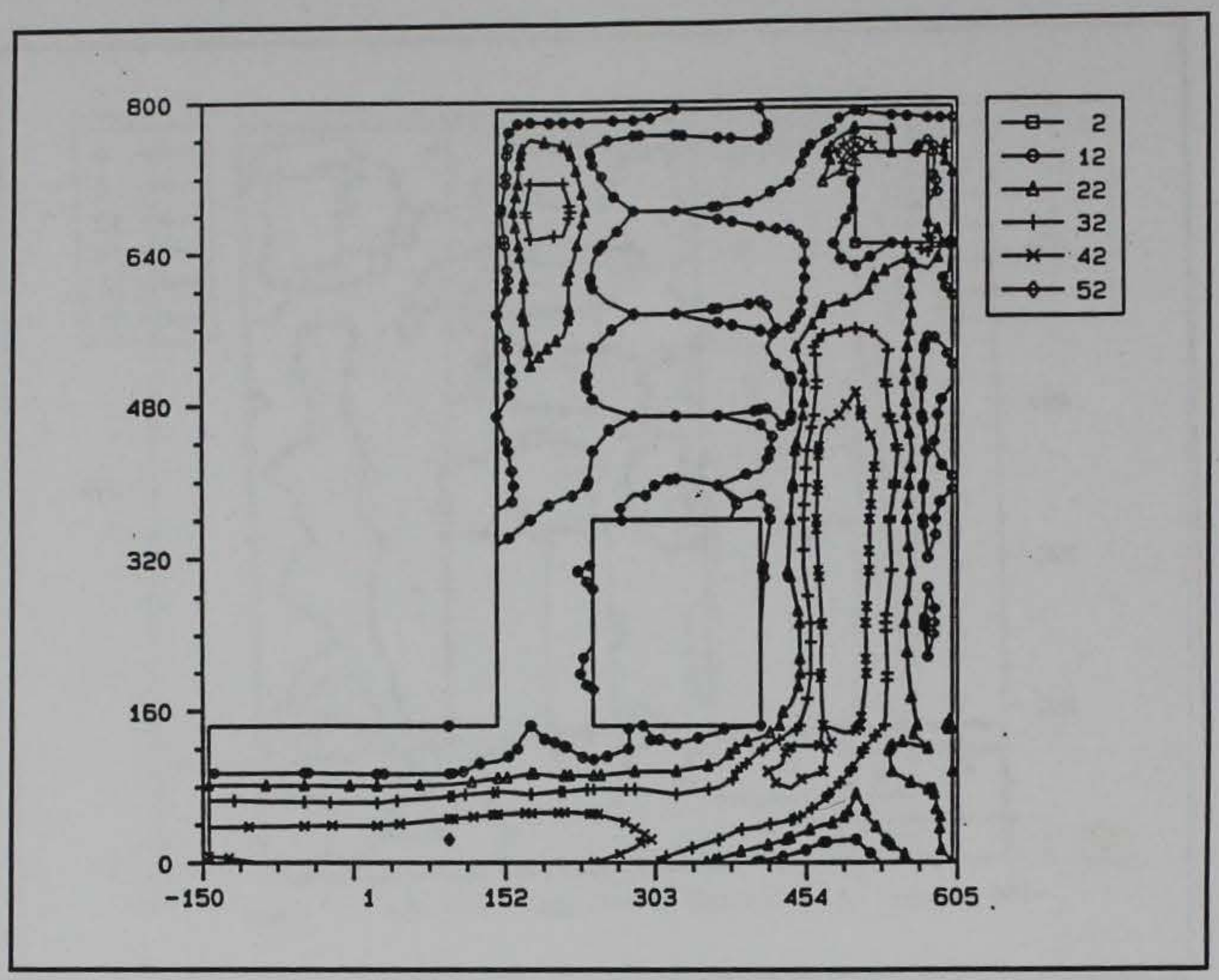

Figure 131. Crack potential contours, transverse section at DS edge of valve pit at day 269

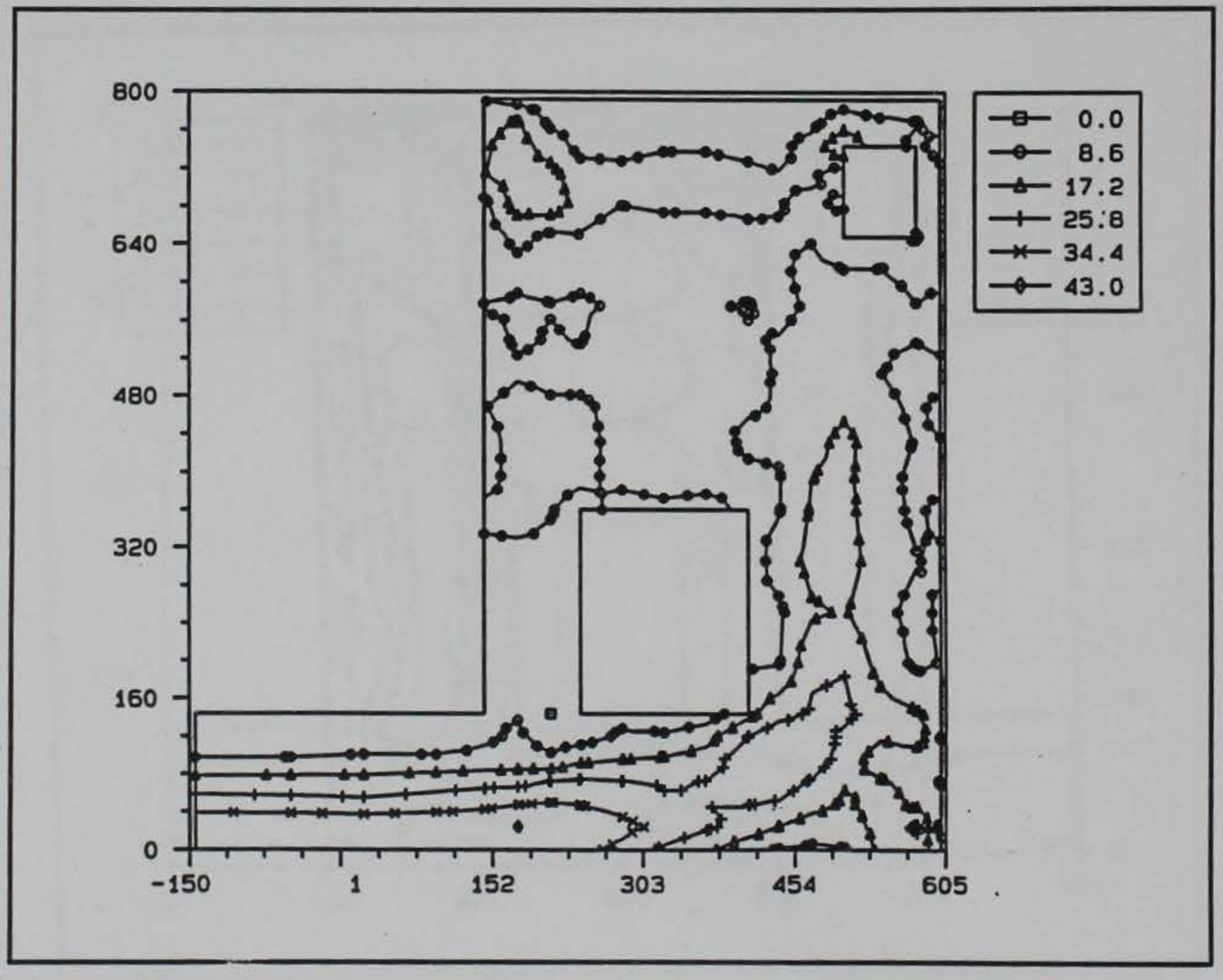

Figure 132. Crack potential contours, transverse section at DS edge of valve pit at day 379

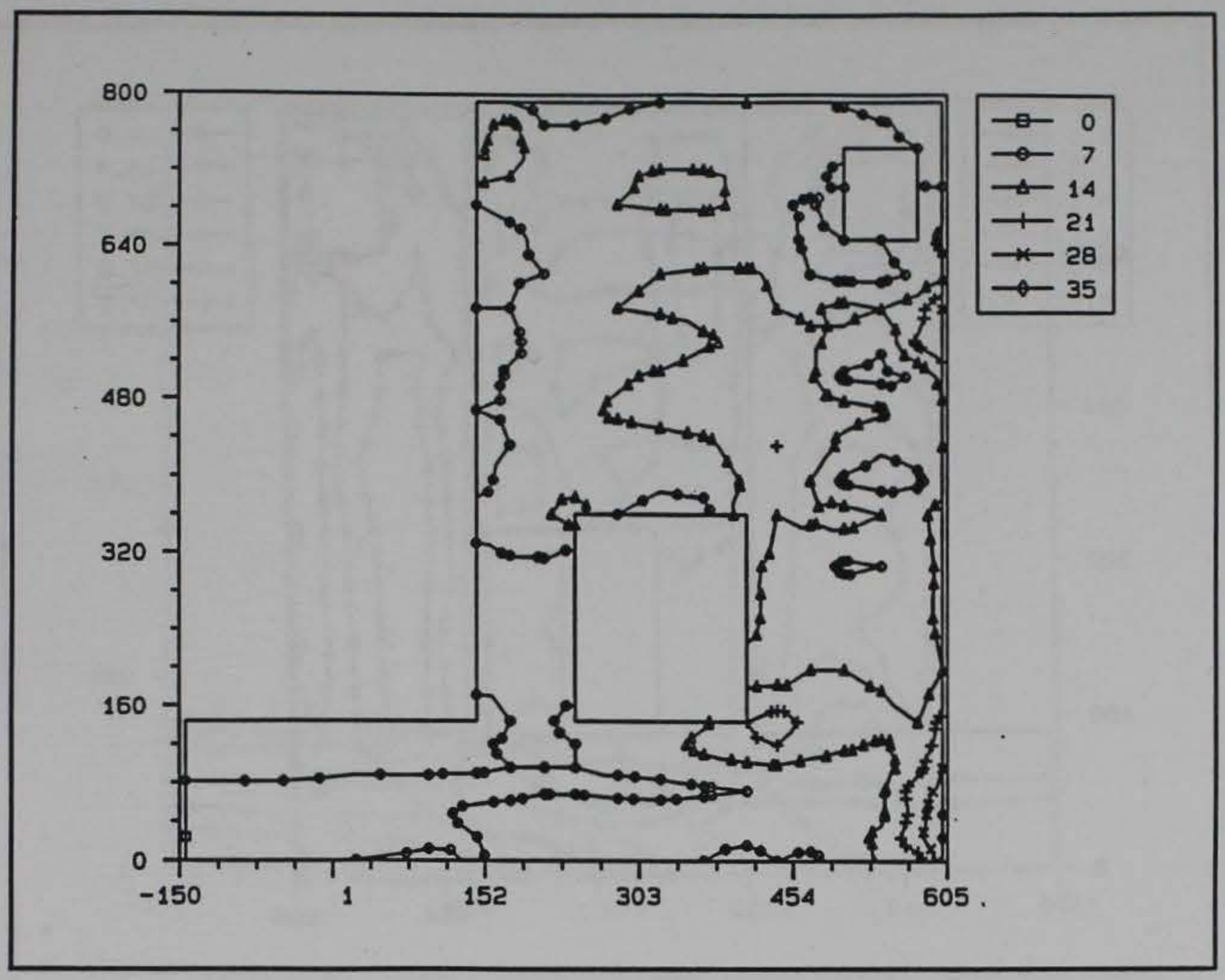

Figure 133. Crack potential contours, transverse section at DS edge of valve pit at day 459

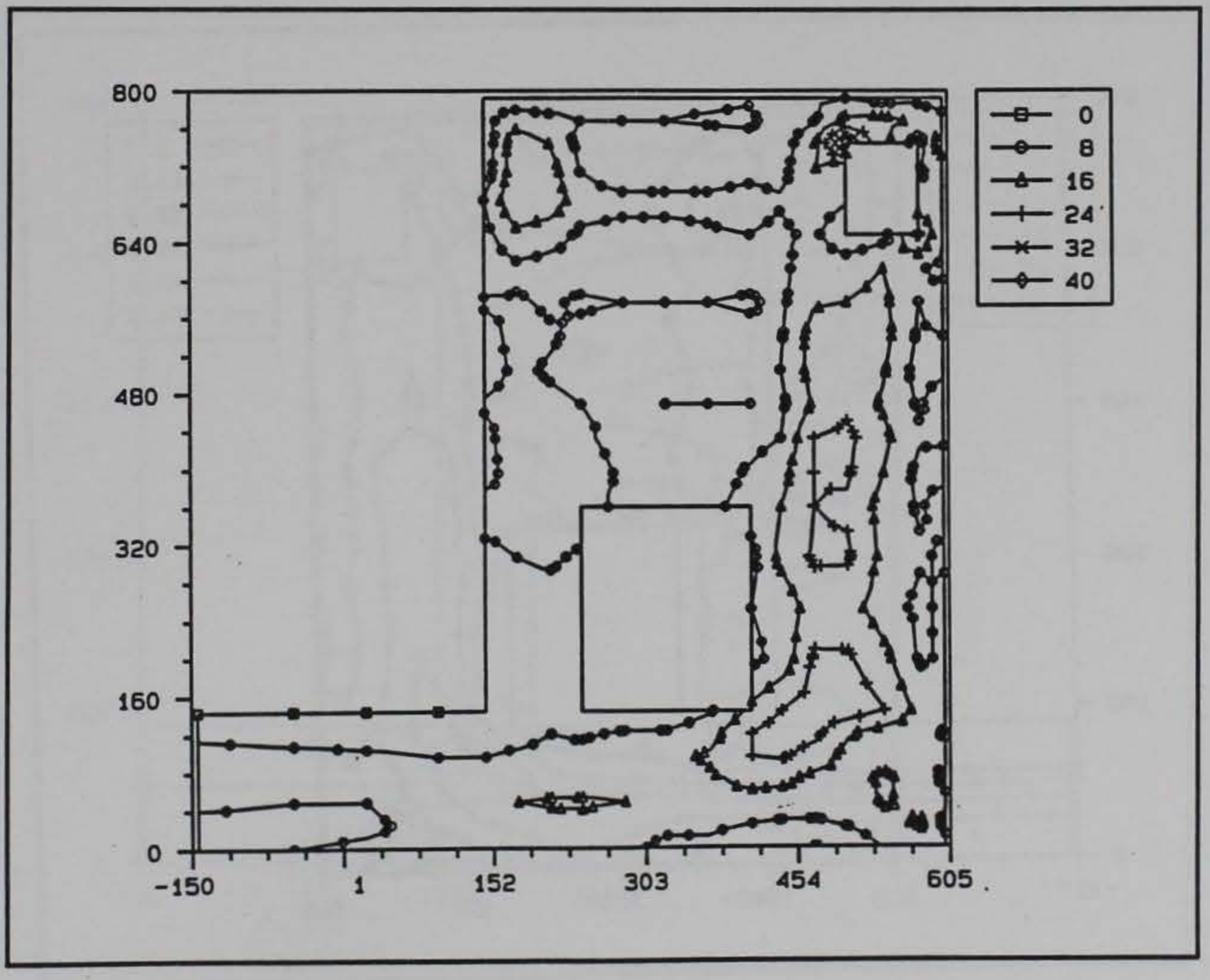

Figure 134. Crack potential contours, transverse section at DS edge of valve pit at day 559

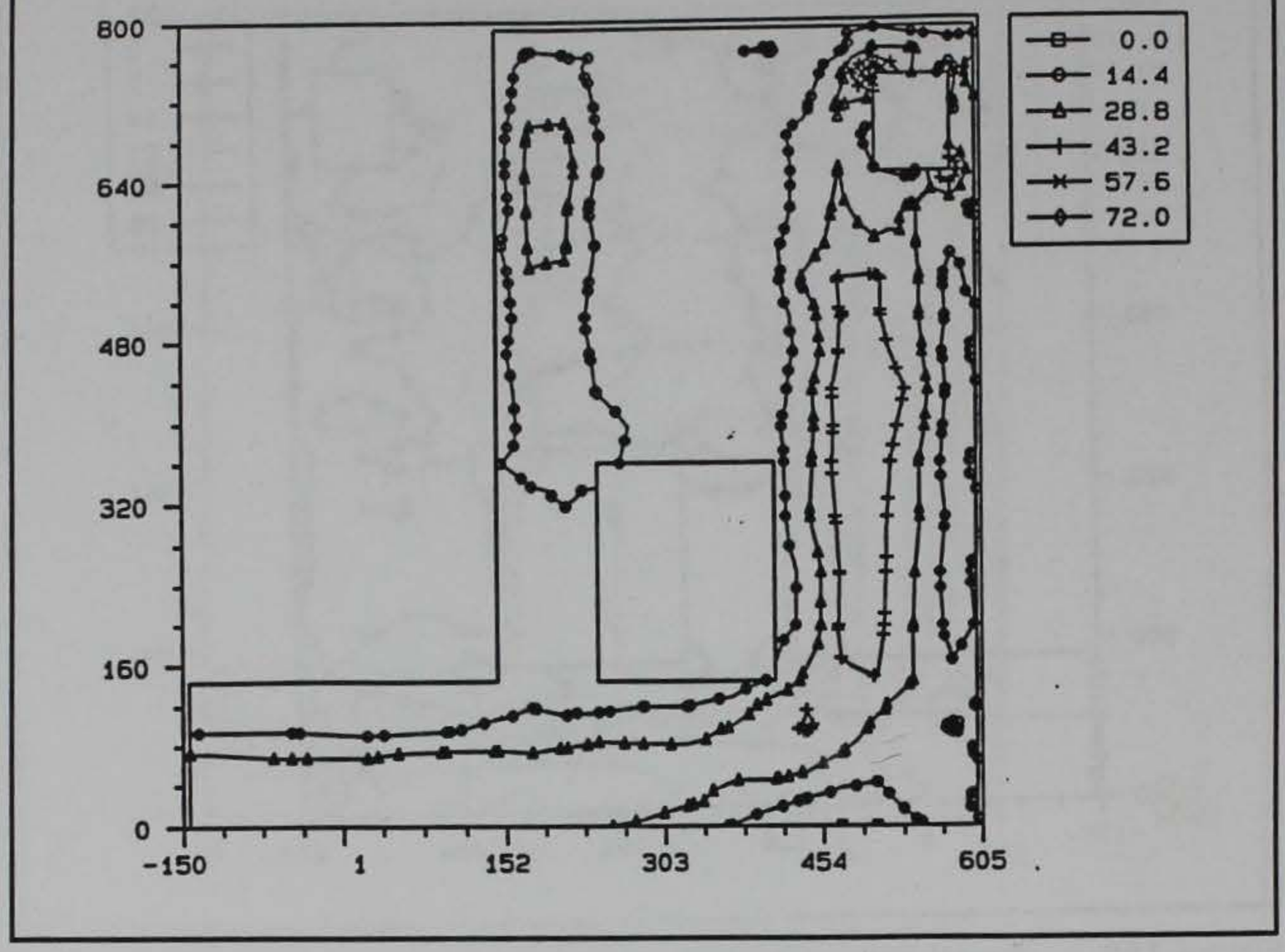

Figure 135. Crack potential contours, transverse section at DS edge of valve pit at day 639

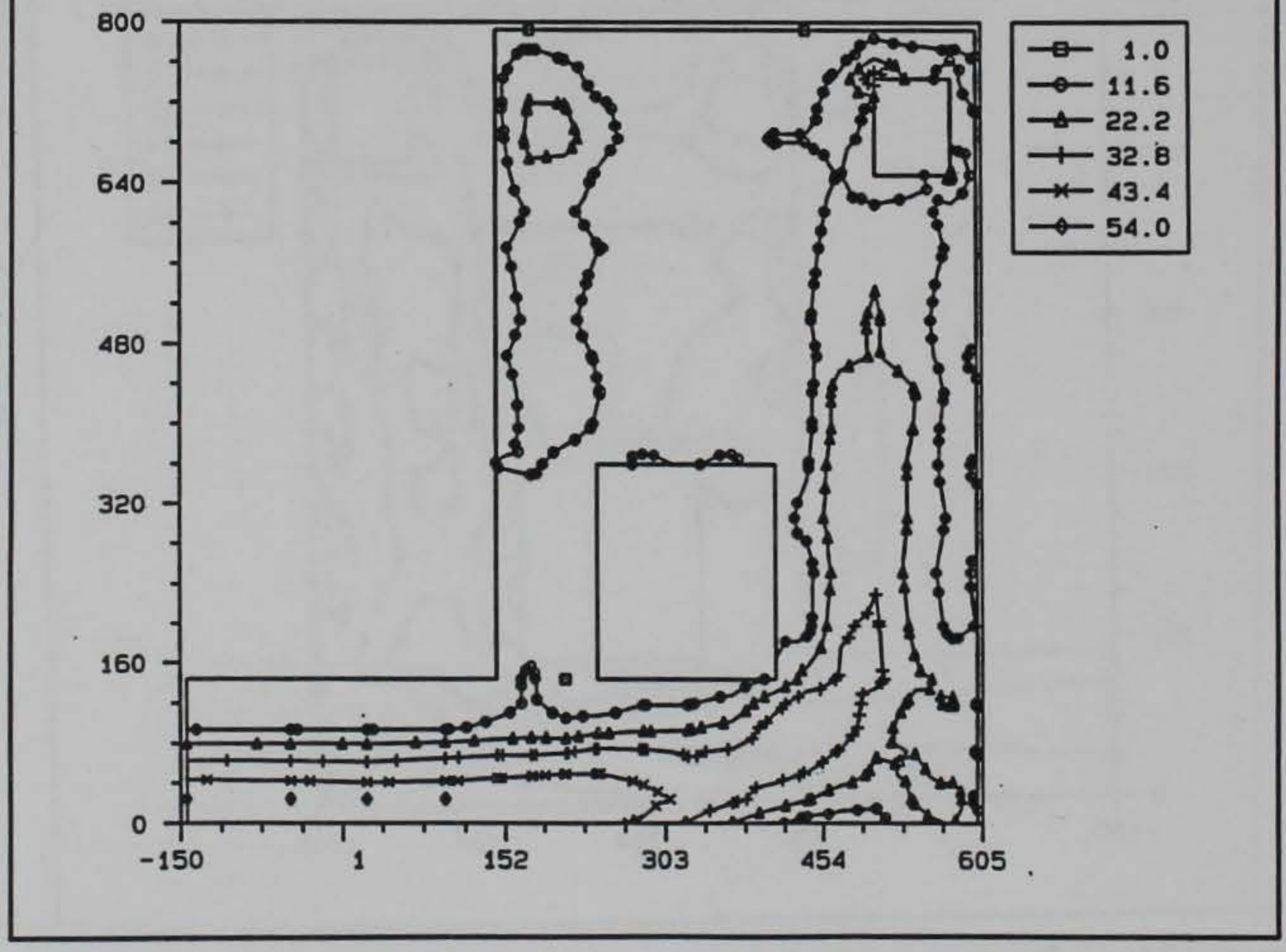

Figure 136. Crack potential contours, transverse section at DS edge of valve pit at day 719

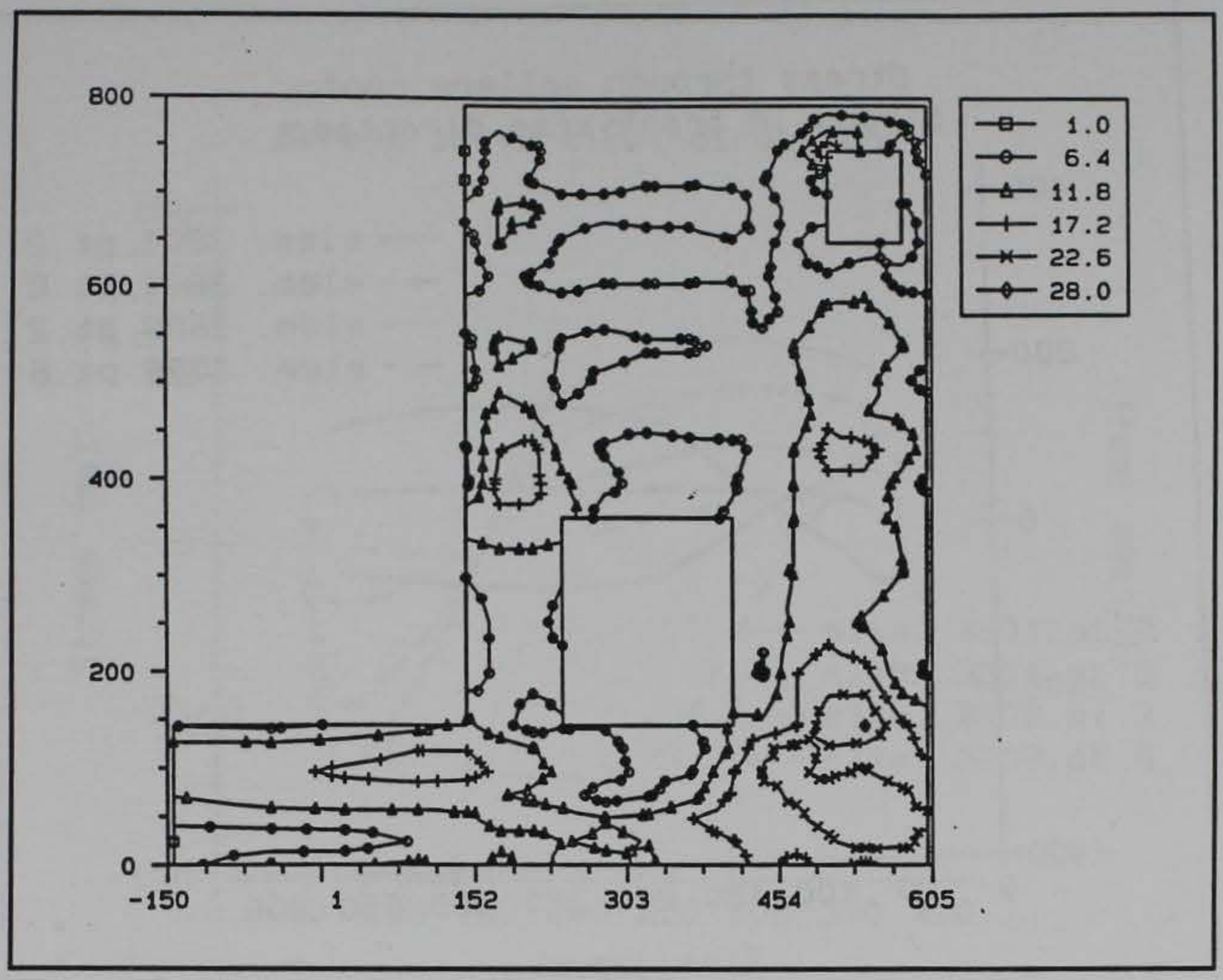

Figure 137. Crack potential contours, transverse section at US edge of valve pit at day 169

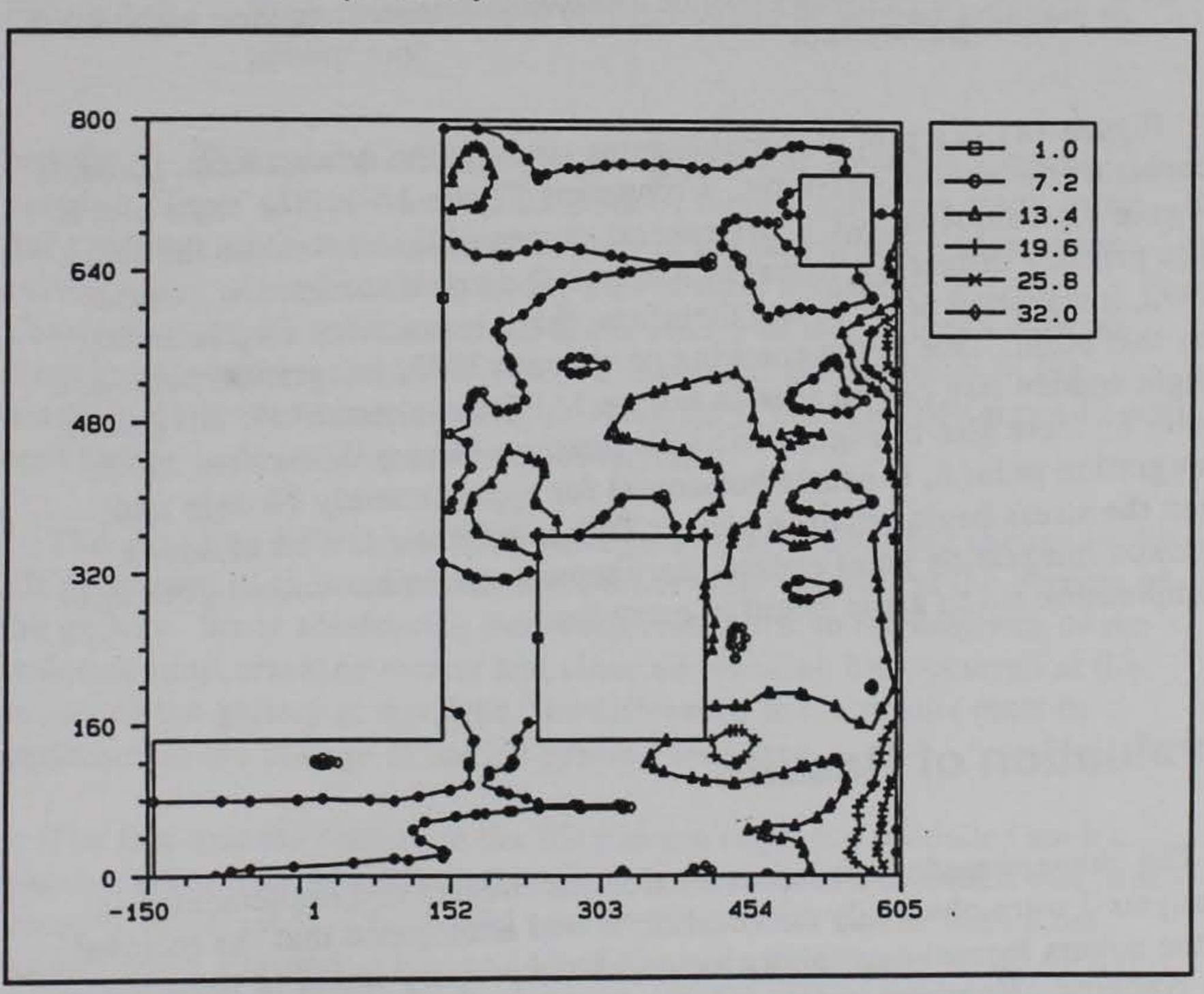

Figure 138. Crack potential contours, transverse section at US edge of valve pit at day 459

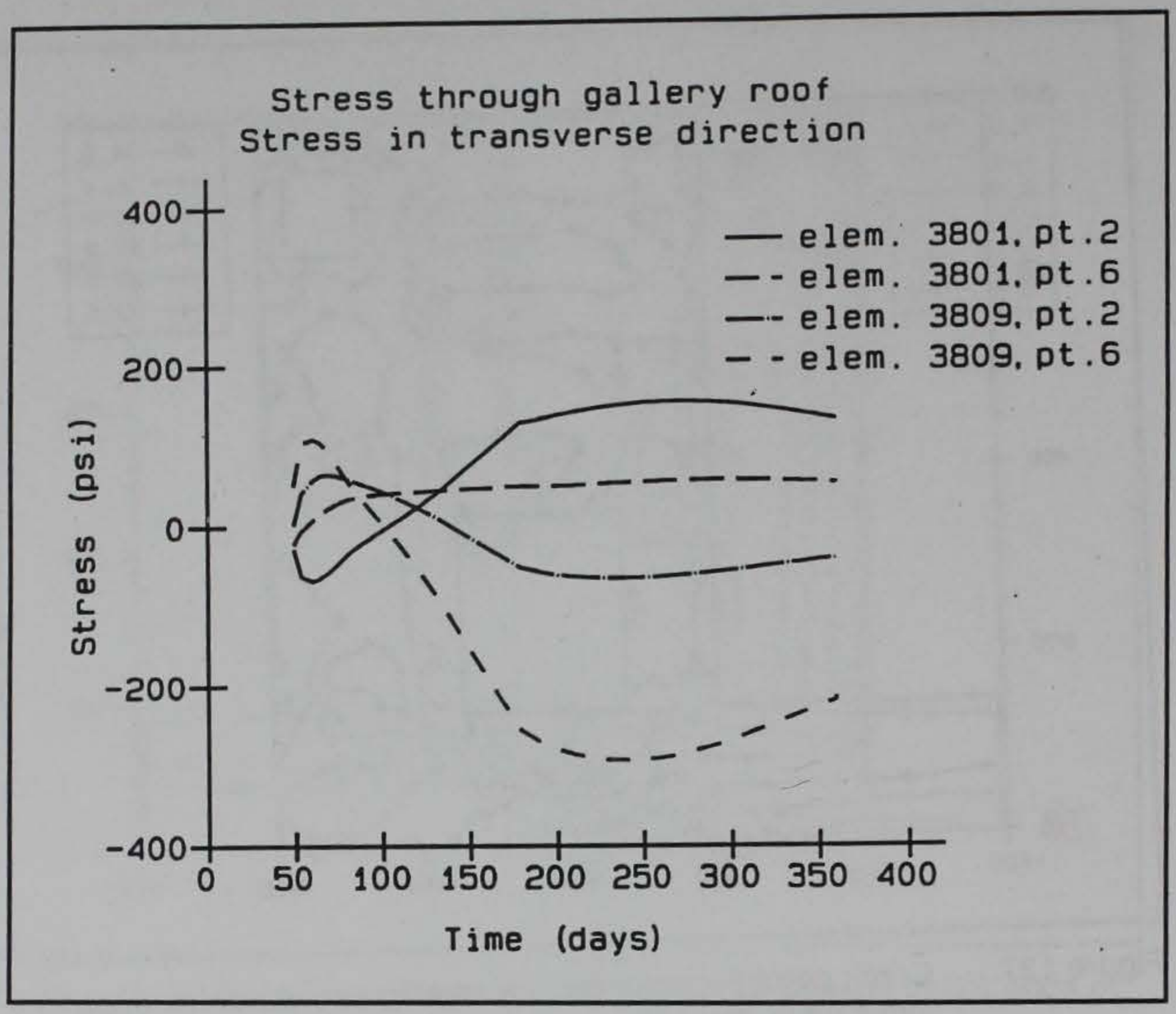

Figure 139. Time-history plot of transverse stress at section adjacent to gallery roof

Figure 141 is a plot of the transverse stress at the downstream, landside corner of the culvert valve pit. Comparing Figure 141 to the same plot in Figure 82 from Analysis 1, the general shapes of the curves are the same. The primary difference is that in Analysis 2 a crack occurred at element 3993, integration point 6, and therefore, there is a sudden drop in stress for that point. Due to the cracking of element 3993, integration point 6, a slight sudden rise can be seen in Figure 141 for element 3993, integration point 8. Note also in Figure 141 how the time-history of element 3993, integration point 6, is nearly horizontal for approximately 70 days and then the stress begins to drop again. This is a demonstration of how a cracked integration point cannot carry tensile stress, but once it goes into compression it can again begin to carry load.

Evaluation of Results

The changes made in the construction parameters and implemented in Analysis 2 were obviously successful. It was anticipated that the removal of the covers from the openings would be the primary factor in reducing the cracking. However, review of the results in this chapter indicates that moving the lift joint away from the top of the culvert was extremely

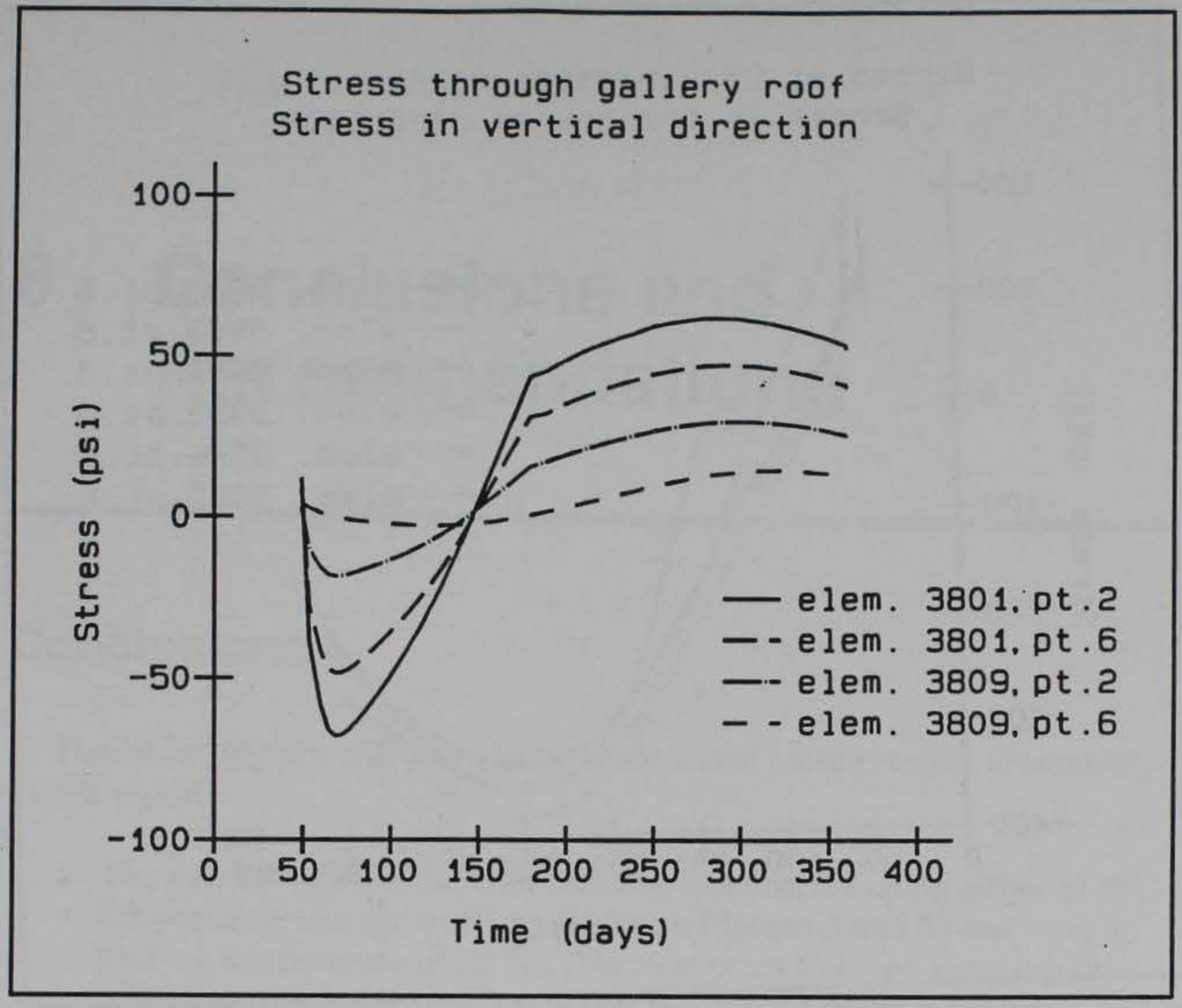

Figure 140. Time-history plot of vertical stress at section adjacent to gallery roof

beneficial. This can be readily seen if Figure 64 of Analysis 1 is compared to Figure 129 of Analysis 2. Both of these figures are crack potential contours taken at transverse sections at the downstream edge of the culvert valve pit and are both at day 169 of their respective analyses. Comparison of the crack potential at the corner of the gallery where the cracking occurred in Analysis 1 shows that the crack potential in Figure 64 is 43 percent at this corner in Analysis 1, but it is only about 12 percent in Figure 129 at this corner in Analysis 2.

The only two differences in the analyses at day 169 is the change in the lift placement sequence and the addition of diagonal bars at the corners of the gallery. Since reinforcing bars contribute little to the behavior of the structure until cracking occurs and since no cracking has occurred at the corner of the gallery at this time, the difference in the results must be attributed to the change in the lift placing sequence.

The fact that the change in the lift placing sequence produced such a positive effect can be attributed to the initial compression which was introduced in Analysis 2. This initial compression effect can be seen most readily when comparing Figure 140 of Analysis 2 to Figure 81 of Analysis 1. The difference can be attributed to the fact that the changes occurring in Analysis 2 in the vicinity of this corner are all occurring to one

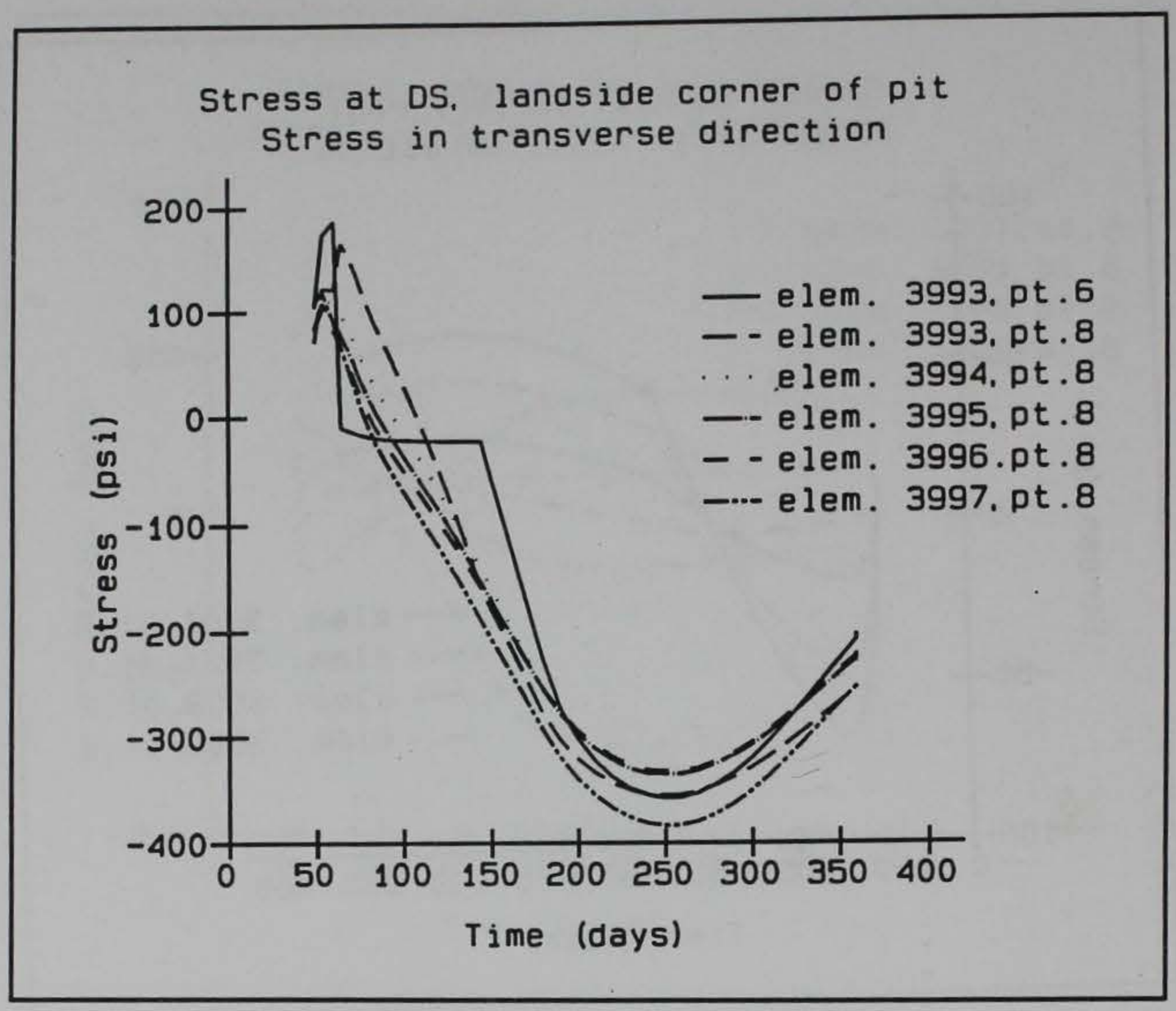

Figure 141. Time-history plot of transverse stress at the downstream, landside corner of the valve pit

material. In Analysis 2, lift 10 is 5 days old when lift 11 is placed and provides an additional discontinuity in the structure. In addition, portions of lift 10 have reached their maximum temperature prior to the placement of lift 11 and are beginning to contract which reduces the magnitude into which lift 11 can go into compression.

8 Conclusions and Recommendations

Conclusions

The following conclusions can be made based on the results presented in this report:

a. The culvert valve monoliths could be constructed using either of the lift sequences in the walls as shown in Figures 3 and 83 and with a placing temperature of 75 °F. There appears to be no cracking or other behavior which indicates that the culvert valve monolith cannot be constructed using the conditions presented in Chapters 2 and 5.

b. The cracking which occurs above the gallery in Analysis 1 does not affect the structural integrity of the structure but could become a maintenance problem during the life of the project if measures were not taken to reduce or eliminate this crack.

c. The crack in the gallery roof is a result of the combination of the lift joint being coincidental with the top of the gallery and of the openings in the culvert remaining covered for the duration of the construction cycle. Changing the lift placing sequence to the sequence shown in Figure 83 and removing the covers in early March eliminated the cracking problem.

d. Three-dimensional analyses of culvert valve monoliths in the performance of a NISA appears to be necessary as witnessed by the formation of the crack at the corner of the culvert valve pit. It is not likely that there is a combination of two-dimensional analyses which could have predicted this cracking.

Recommendations

The following recommendations are made based on the conclusions stated above and on the results presented in this report:

a. The culvert valve monoliths should be constructed using a maximum placing temperature of 75 °F and a lift sequence in the wall as shown in Figure 83. The lift sequence should be adjusted accordingly for the center walls of the culvert valve monoliths. Consideration should also be given to a lift arrangement in the area of the gallery in other monoliths as well.

b. Covers should be placed over all openings at the completion of construction of a monolith, kept in place through the first winter season, and then should be removed no later than March 15. This criteria for covering of openings should provide sufficient protection through the structure's first winter season.

c. Diagonal reinforcing should be placed at the corners of all openings in the monolith.

d. Chamfers should be placed at the corners of the top of the gallery.

References

ANATECH Research Corp. (1992). *ANACAP-U, ANATECH concrete analysis package, version 92-2.2, theory manual,* La Jolla, CA.

Fehl, B. D., Garner, S., James, R., Dunham, R., and Zhang, L. "Nonlinear, incremental structural analysis for the lower miter gate monolith at Olmsted Locks and Dam" (technical report in preparation), U.S. Army Engineer Waterways Experiment Station, Vicksburg, MS.

Fehl, B. D., and Merrill, C. A. "Use of reinforcement in a nonlinear, incremental structural analysis" (technical report in preparation), U.S. Army Engineer Waterways Experiment Station, Vicksburg, MS.

Garner, S., Bombich, A. A., Norman, C. D., Merrill, C. A., Fehl, B. D., and Jones, H. W. (1992). "Nonlinear, incremental structural analysis of Olmsted Locks and Dams - volume I, main text," Technical Report SL-92-28, U.S. Army Engineer Waterways Experiment Station, Vicksburg, MS.

Garner, S., and Hammons, M. (1991). "The development and use of a time-dependent cracking model for concrete," Technical Report SL-91-7, U.S. Army Engineer Waterways Experiment Station, Vicksburg, MS.

Hammons, M., Neeley, B., Alexander, M., Bombich, A., and Garner, S. (1991). "Concrete mixture selection and characterization study, Olmsted Locks and Dam, Ohio River," Technical Report SL-91-9, U.S. Army Engineer Waterways Experiment Station, Vicksburg, MS.

Headquarters, Department of the Army. (1990). "Special design provision for massive concrete structures," Engineering Technical Letter 1110-2-324, Washington, DC.

Hibbitt, Karlsson, and Sorensen. (1989). *ABAQUS user's manual, version 4.8*, Providence, RI.

Merrill, C. A., Fehl, B. D., and Garner, S. "Nonlinear, incremental structural analysis of Olmsted Locks and Dam: phase III" (technical report in preparation), U.S. Army Engineer Waterways Experiment Station, Vicksburg, MS.

Ozisik, M. N. (1985). *Heat transfer, a basic approach*, McGraw-Hill, New York, NY.

Truman, K. Z., Petruska, D., and Ferhi, A. (1992). "Evaluation of thermal and incremental construction effects for monoliths AL-3 and AL-5 of the Melvin Price Locks and Dams," Contract Report ITL-92-3, U.S. Army Engineer Waterways Experiment Station, Vicksburg, MS.

Appendix A
Additional Temperature Results

Temperature contour and temperature time-history plots are provided in this appendix in addition to the contour and time-history plots presented in Chapters 3 and 6 in the main body of the report. The initial set of plots are contour plots from Analysis 1 at a section taken longitudinally through the monolith and a section taken horizontally through the wall of the monolith. From Analysis 2, additional time-history plots are included and finally contour plots are shown at a section through the slab in the chamber portion of the model, at longitudinal and horizontal sections through the monolith wall. A location of the section being shown is given prior to each set of contour plots.

The total time which has elapsed during the course of the analysis for the contour plots can be determined by the AMP designation at the top of each plot.

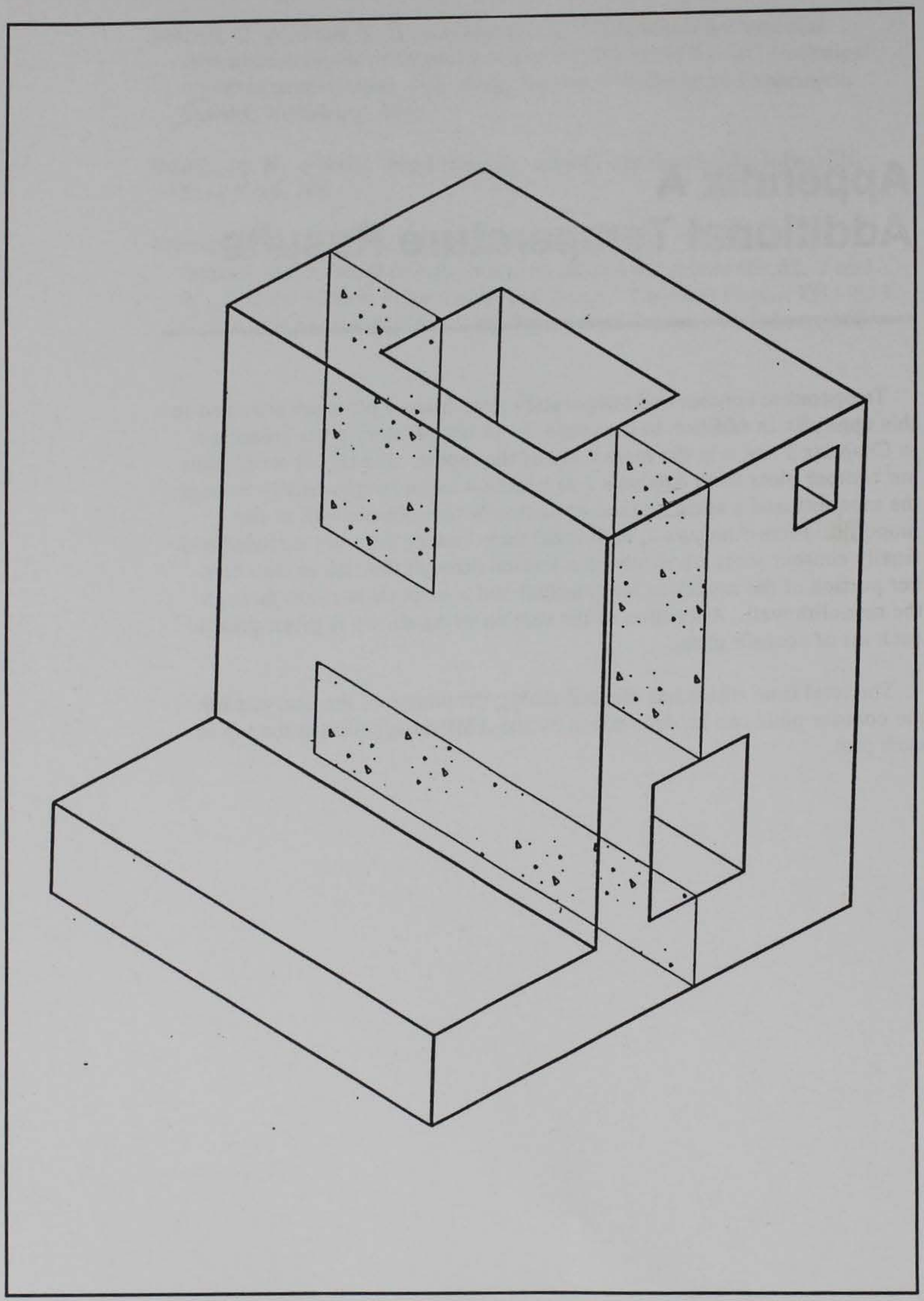

Longitudinal section through culvert valve pit

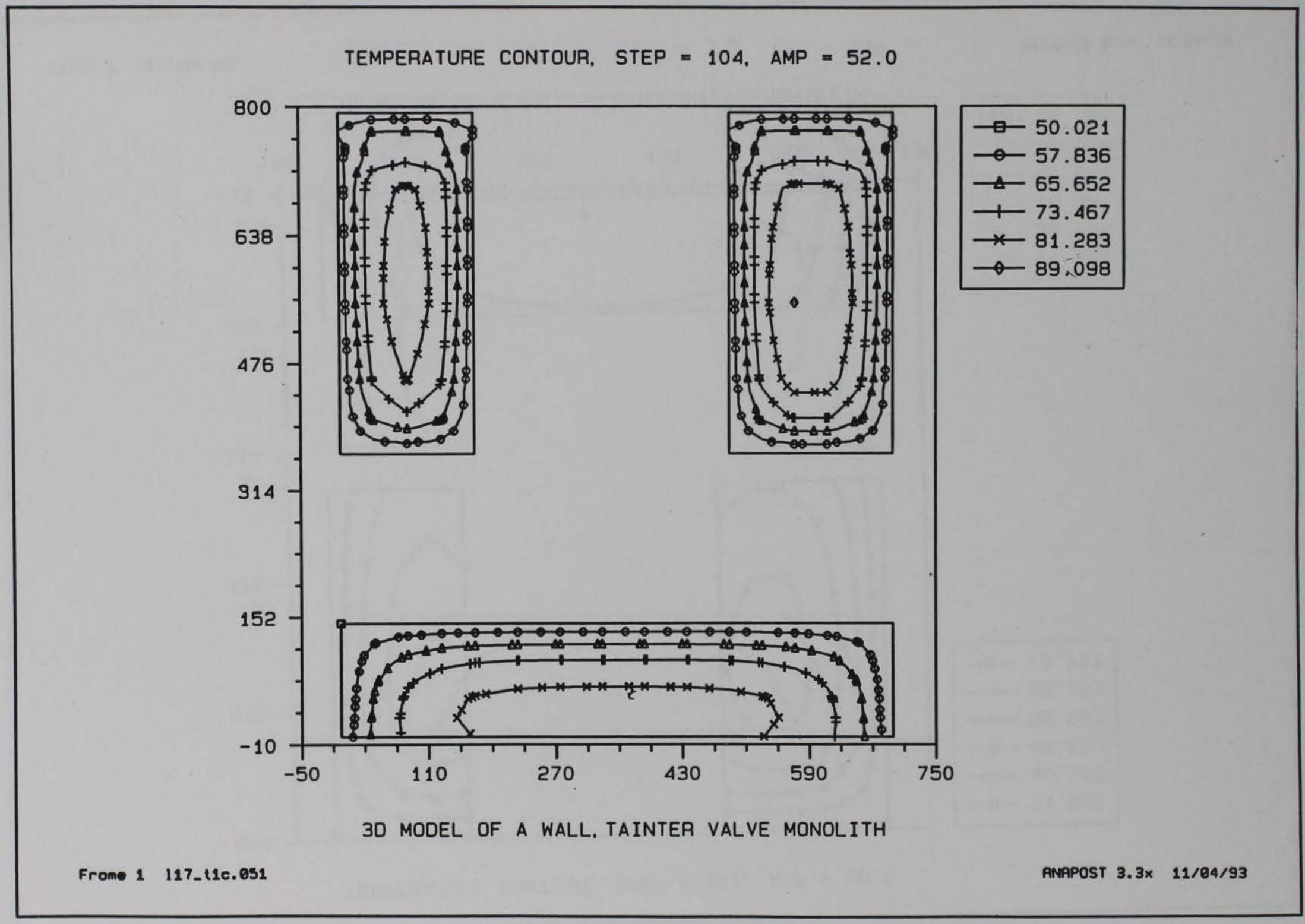
TEMPERATURE CONTOUR, STEP = 104, AMP = 52.0
800
638
476
314
152
-10
-50
110
270
430
590
750
50.021
57.836
65.652
73.467
81.283
89.098
3D MODEL OF A WALL, TAINTER VALVE MONOLITH
Frame 1 117_t1c.051
ANAPOST 3.3x 11/04/93

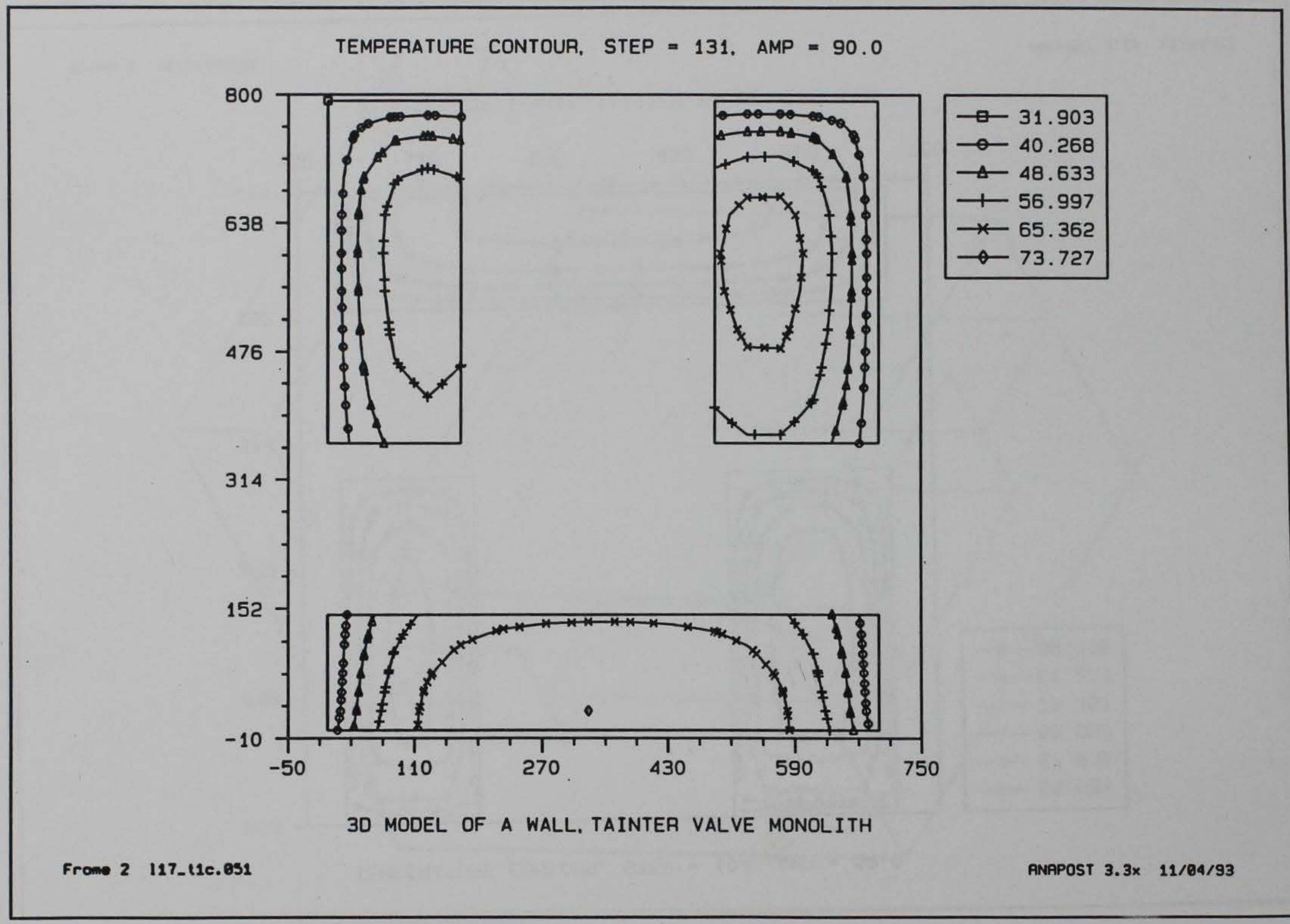
TEMPERATURE CONTOUR, STEP = 131, AMP = 90.0
800
638
476
314
152
-10
-50
110
270
430
590
750
31.903
40.268
48.633
56.997
65.362
73.727
3D MODEL OF A WALL, TAINTER VALVE MONOLITH
Frame 2 117_tic.051
ANAPOST 3.3x 11/04/93

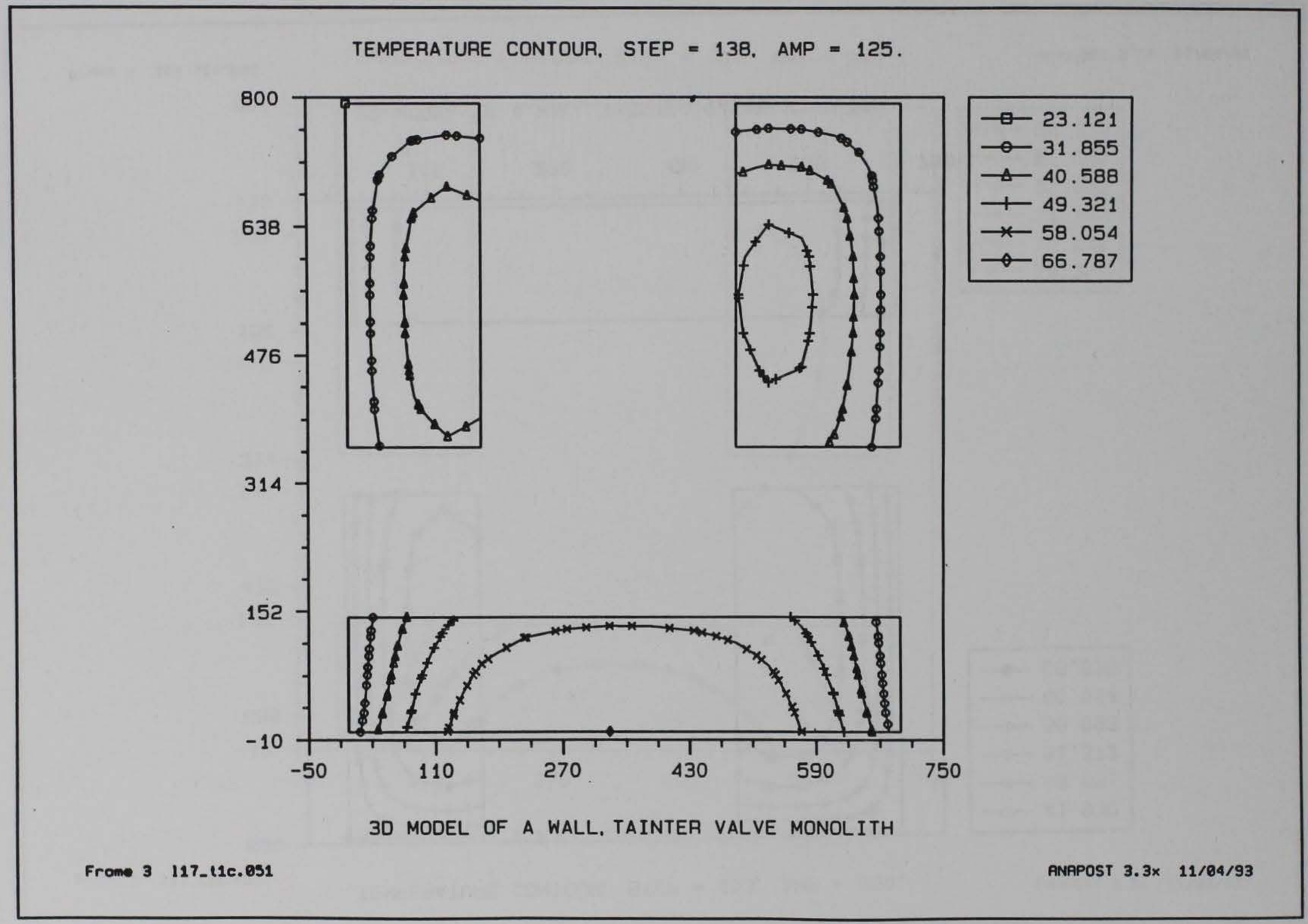
TEMPERATURE CONTOUR, STEP = 138, AMP = 125.
800
638
476
314
152
-10
-50
110
270
430
590
750
23.121
31.855
40.588
49.321
58.054
66.787
3D MODEL OF A WALL, TAINTER VALVE MONOLITH
Frame 3 117_t1c.051
ANAPOST 3.3x 11/04/93

TEMPERATURE CONTOUR, STEP = 153, AMP = 250.

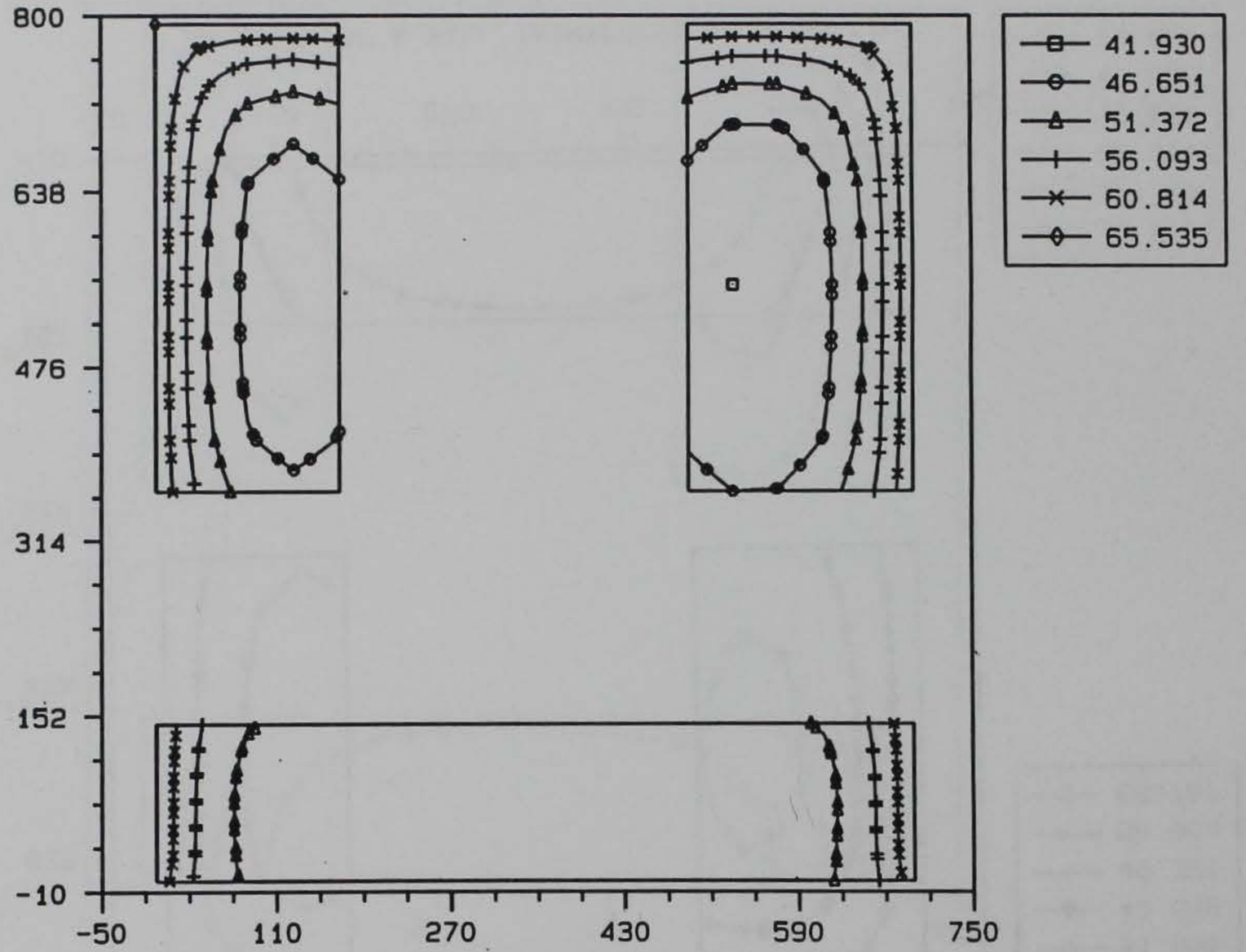

3D MODEL OF A WALL, TAINTER VALVE MONOLITH

Frame 4 117_tic.051

ANAPOST 3.3x 11/04/93

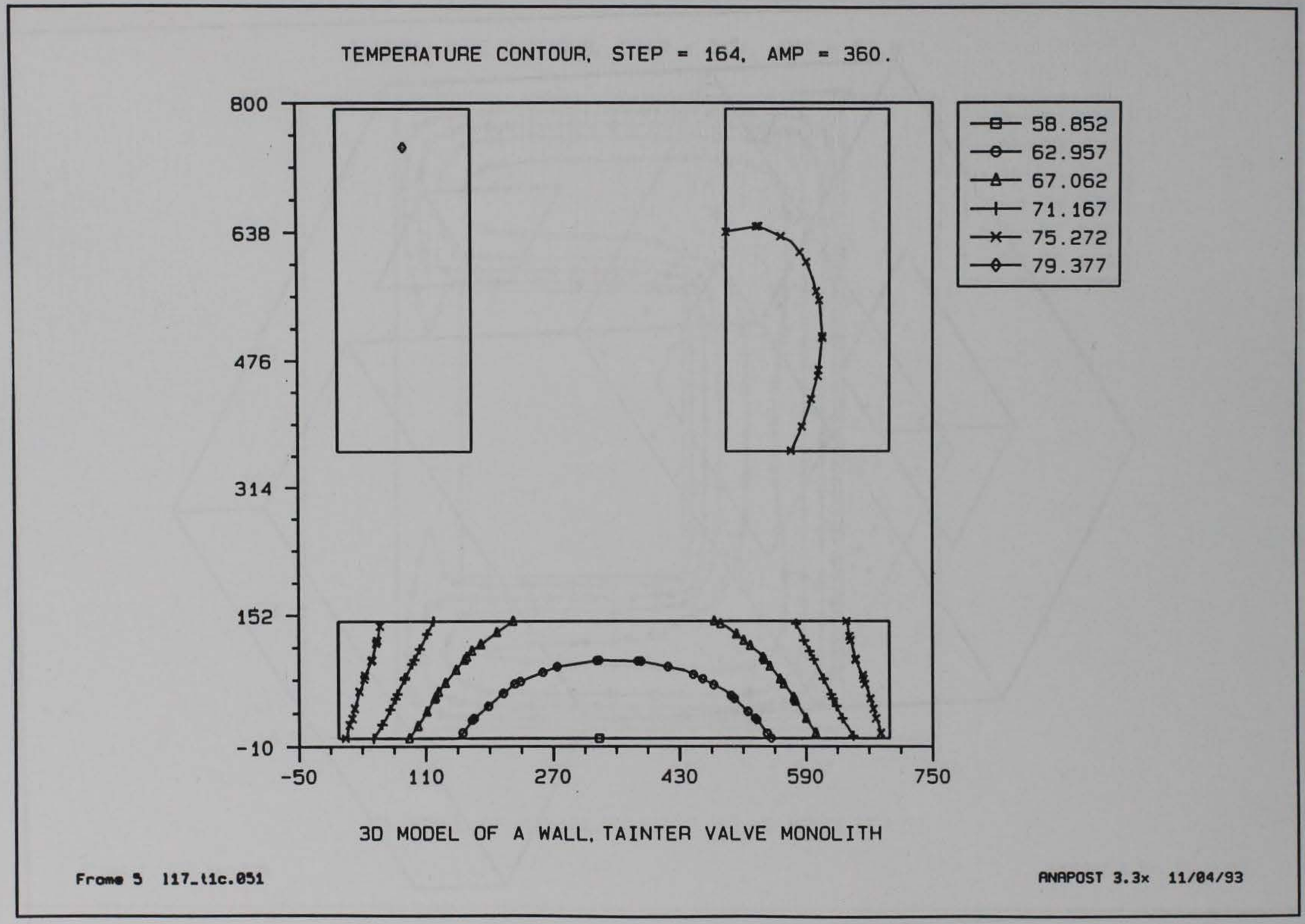
TEMPERATURE CONTOUR, STEP = 164, AMP = 360.
800
638
476
314
152
-10
-50
110
270
430
590
750
58.852
62.957
67.062
71.167
75.272
79.377
3D MODEL OF A WALL, TAINTER VALVE MONOLITH
Frame 5 117_t1c.051
ANAPOST 3.3x 11/04/93

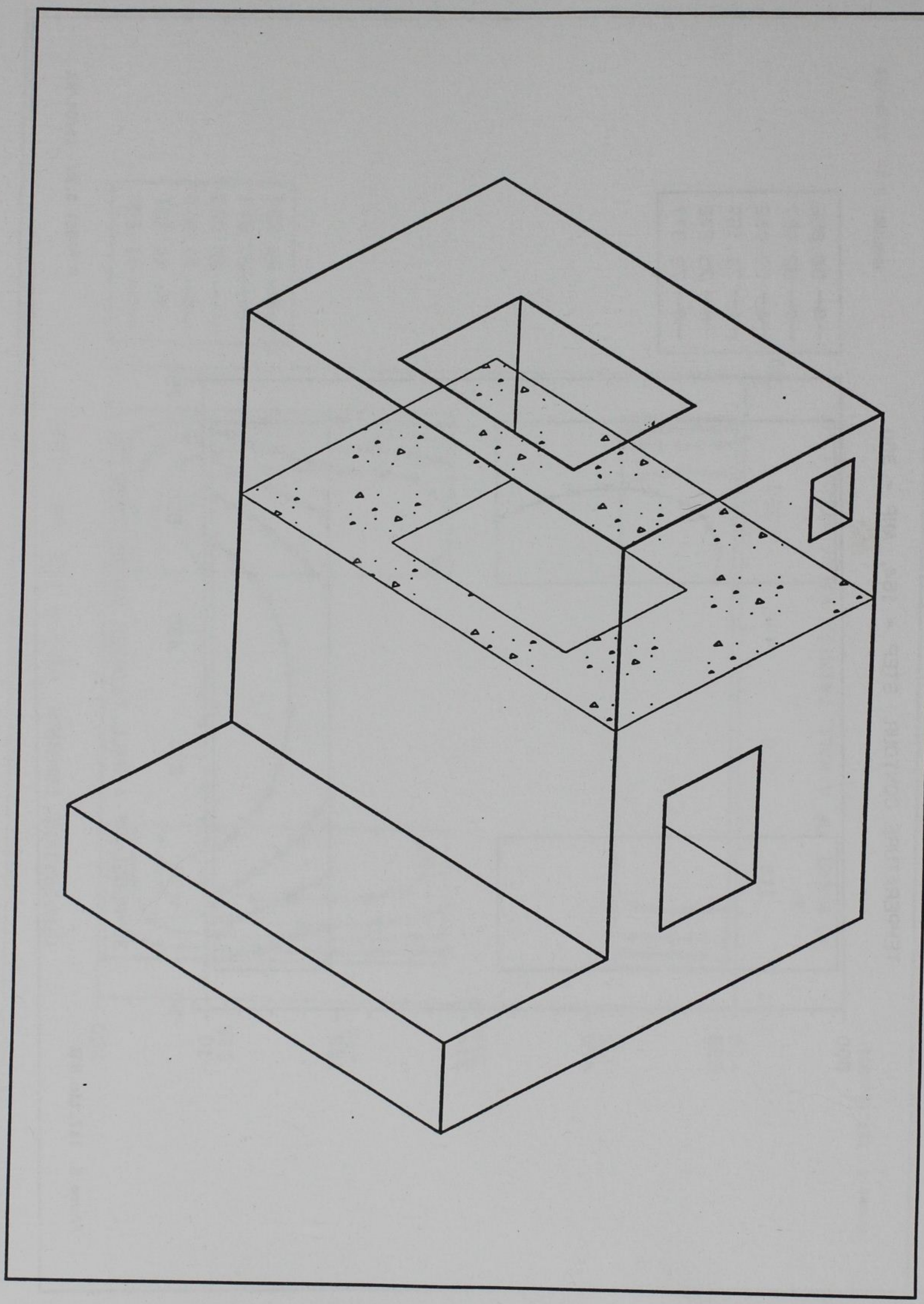

Horizontal section at approximately midheight of the culvert valve pit

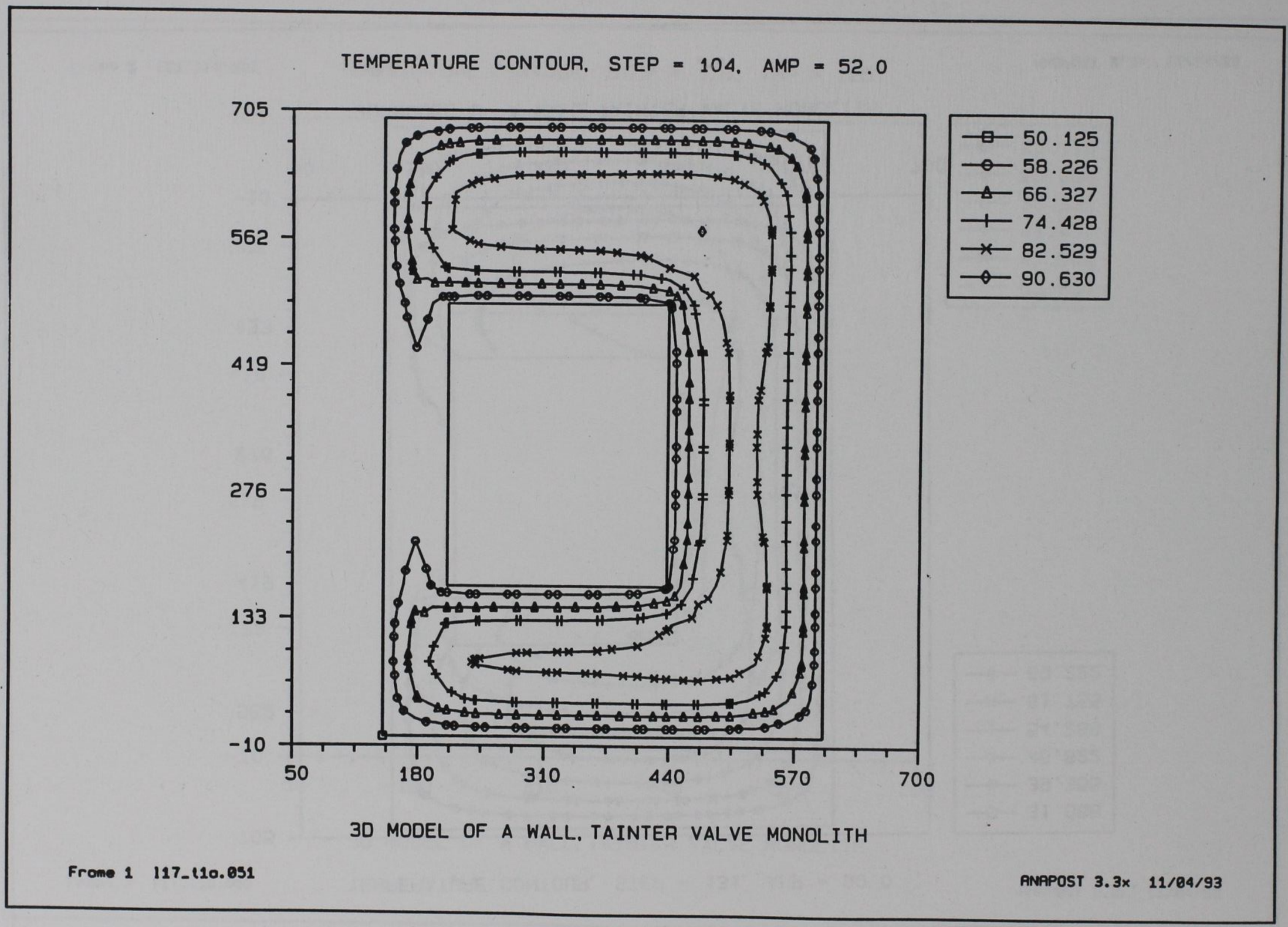
TEMPERATURE CONTOUR, STEP = 104, AMP = 52.0
705
562
419
276
133
-10
50
180
310
440
570
700
50.125
58.226
66.327
74.428
82.529
90.630
3D MODEL OF A WALL, TAINTER VALVE MONOLITH
Frome 1 117_t1o.051
ANAPOST 3.3x 11/04/93

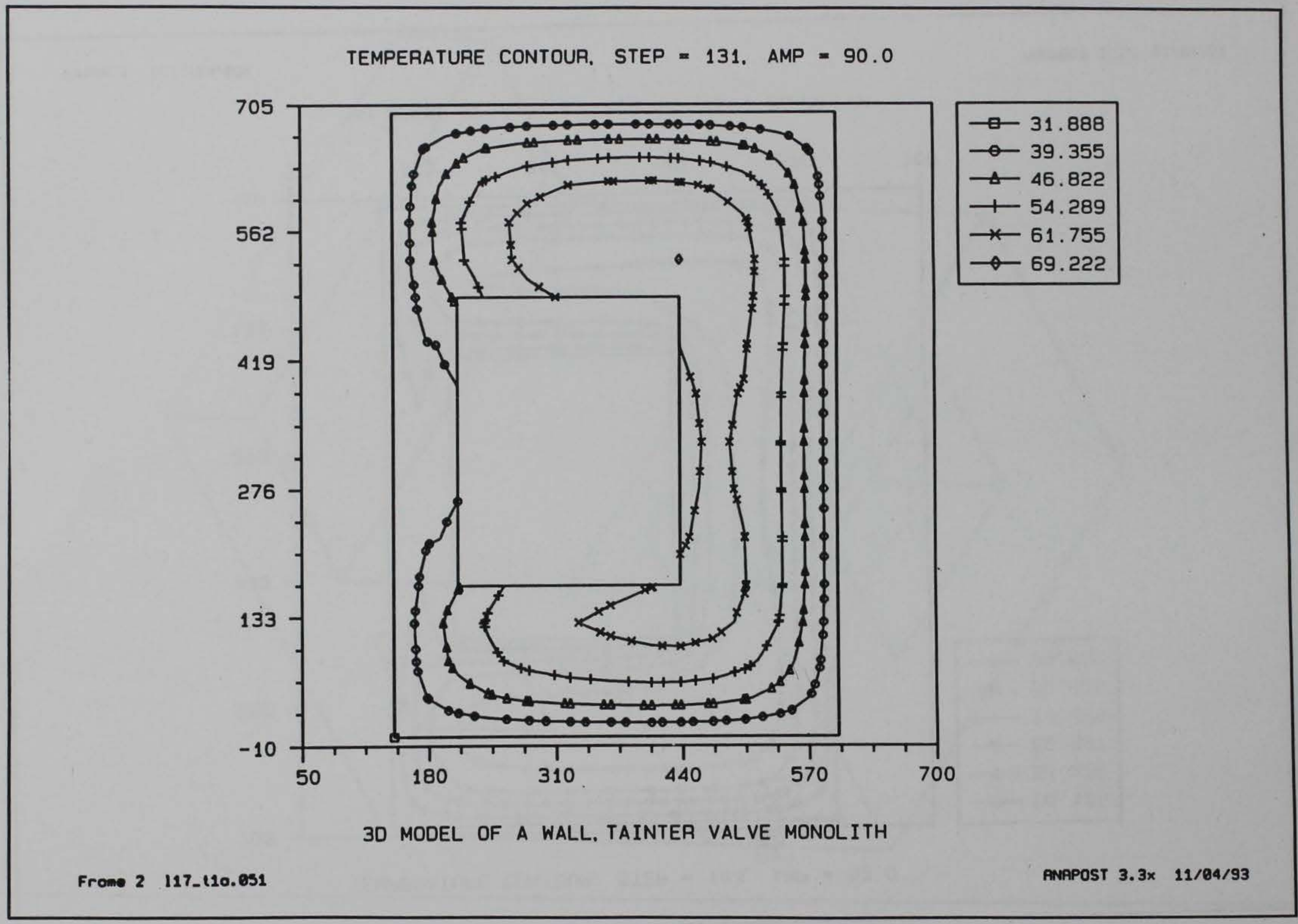
TEMPERATURE CONTOUR, STEP = 131, AMP = 90.0
705
562
419
276
133
-10
50
180
310
440
570
700
31.888
39.355
46.822
54.289
61.755
69.222
3D MODEL OF A WALL, TAINTER VALVE MONOLITH
Frame 2 117_t1a.051
ANAPOST 3.3x 11/04/93

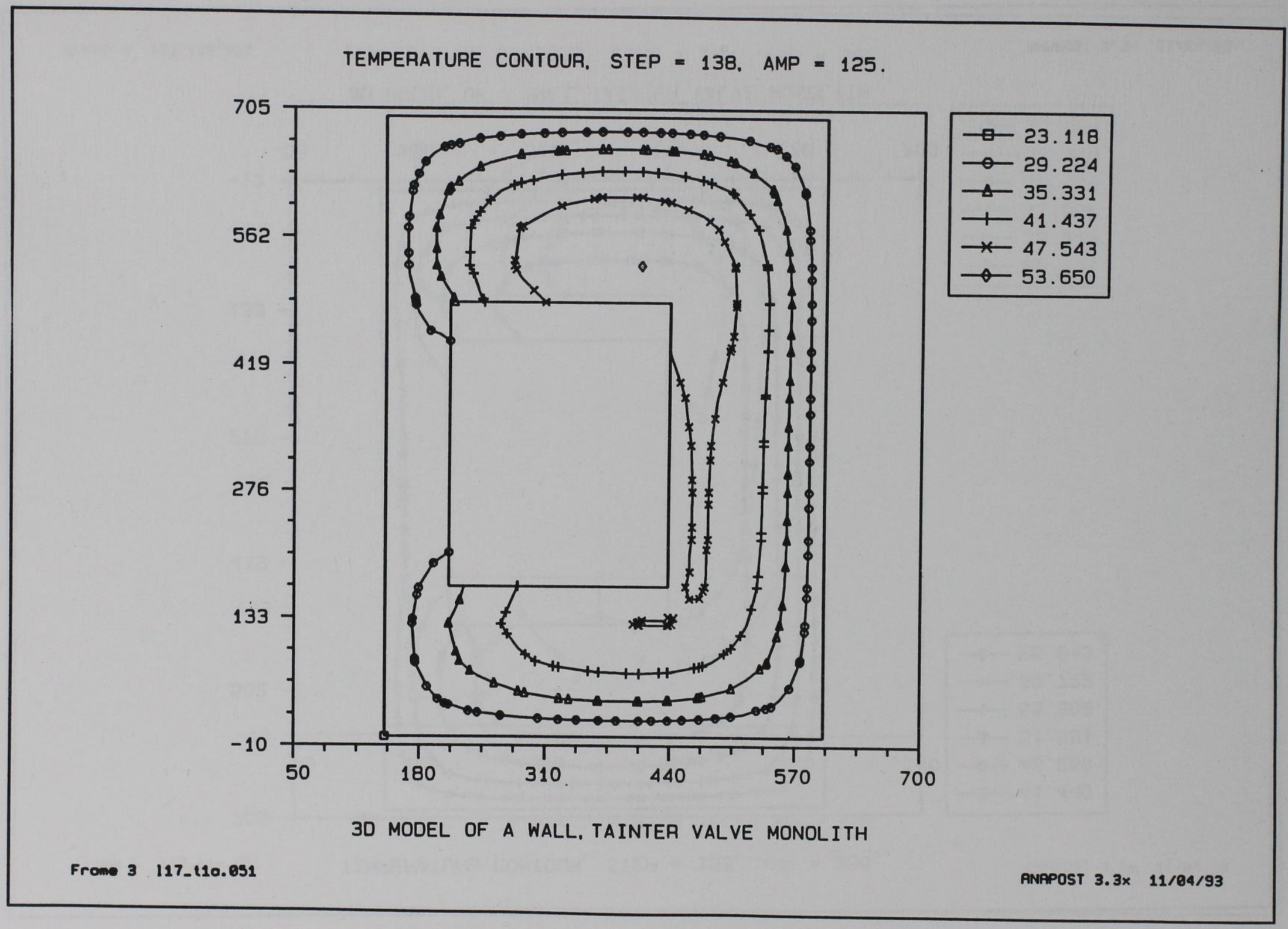
TEMPERATURE CONTOUR, STEP = 138, AMP = 125.
705
562
419
276
133
-10
50
180
310
440
570
700
23.118
29.224
35.331
41.437
47.543
53.650
3D MODEL OF A WALL, TAINTER VALVE MONOLITH
Frome 3 117_t1o.051
ANAPOST 3.3x 11/04/93

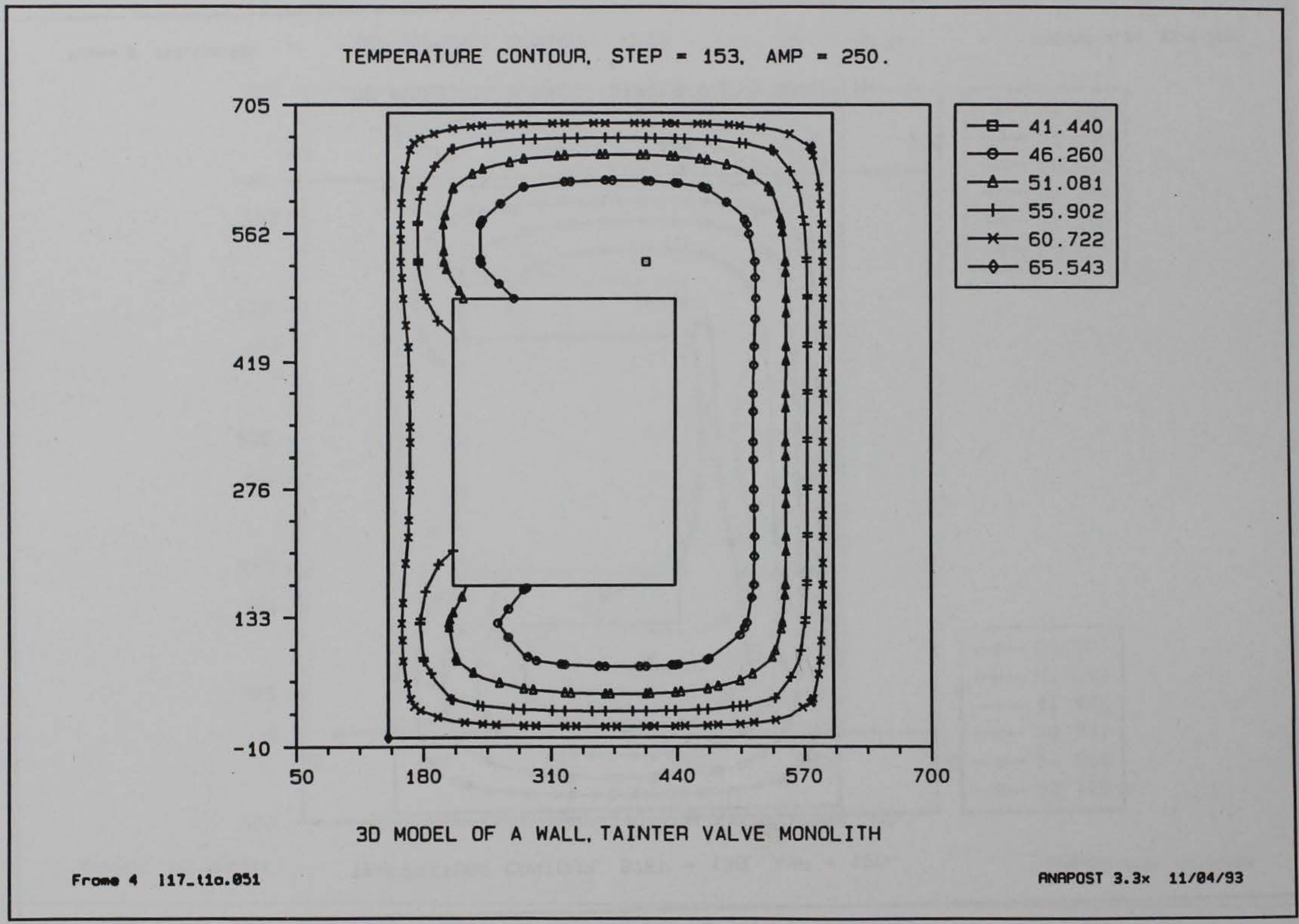
TEMPERATURE CONTOUR, STEP = 153, AMP = 250.
705
562
419
276
133
-10
50
180
310
440
570
700
41.440
46.260
51.081
55.902
60.722
65.543
3D MODEL OF A WALL, TAINTER VALVE MONOLITH
Frame 4 117_t1a.051
ANAPOST 3.3x 11/04/93

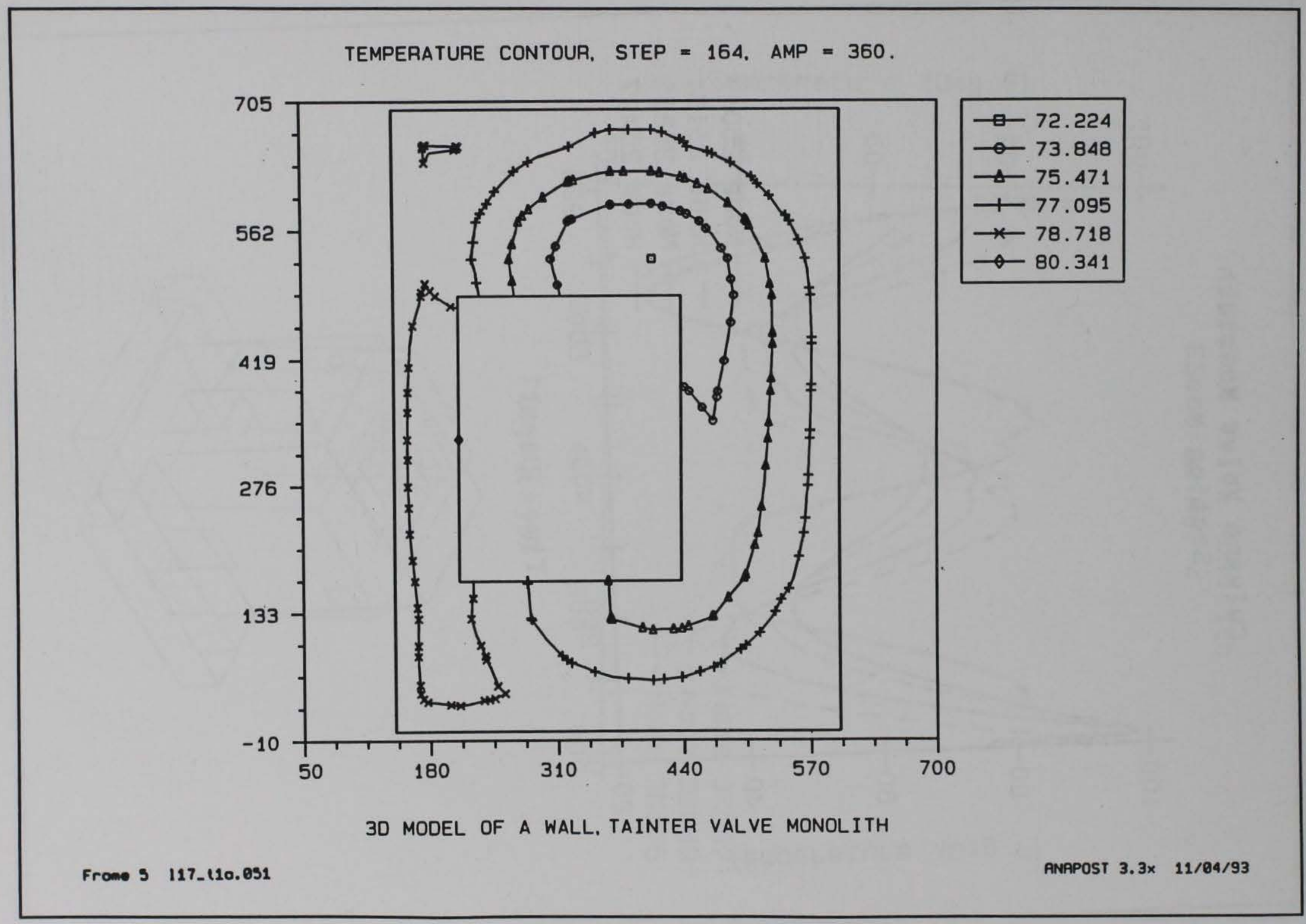
TEMPERATURE CONTOUR, STEP = 164, AMP = 360.
705
562
419
276
133
-10
50
180
310
440
570
700
72.224
73.848
75.471
77.095
78.718
80.341
3D MODEL OF A WALL, TAINTER VALVE MONOLITH
Frame 5 117_tio.051
ANAPOST 3.3x 11/04/93

Culvert Valve Monolith
Section No. 3

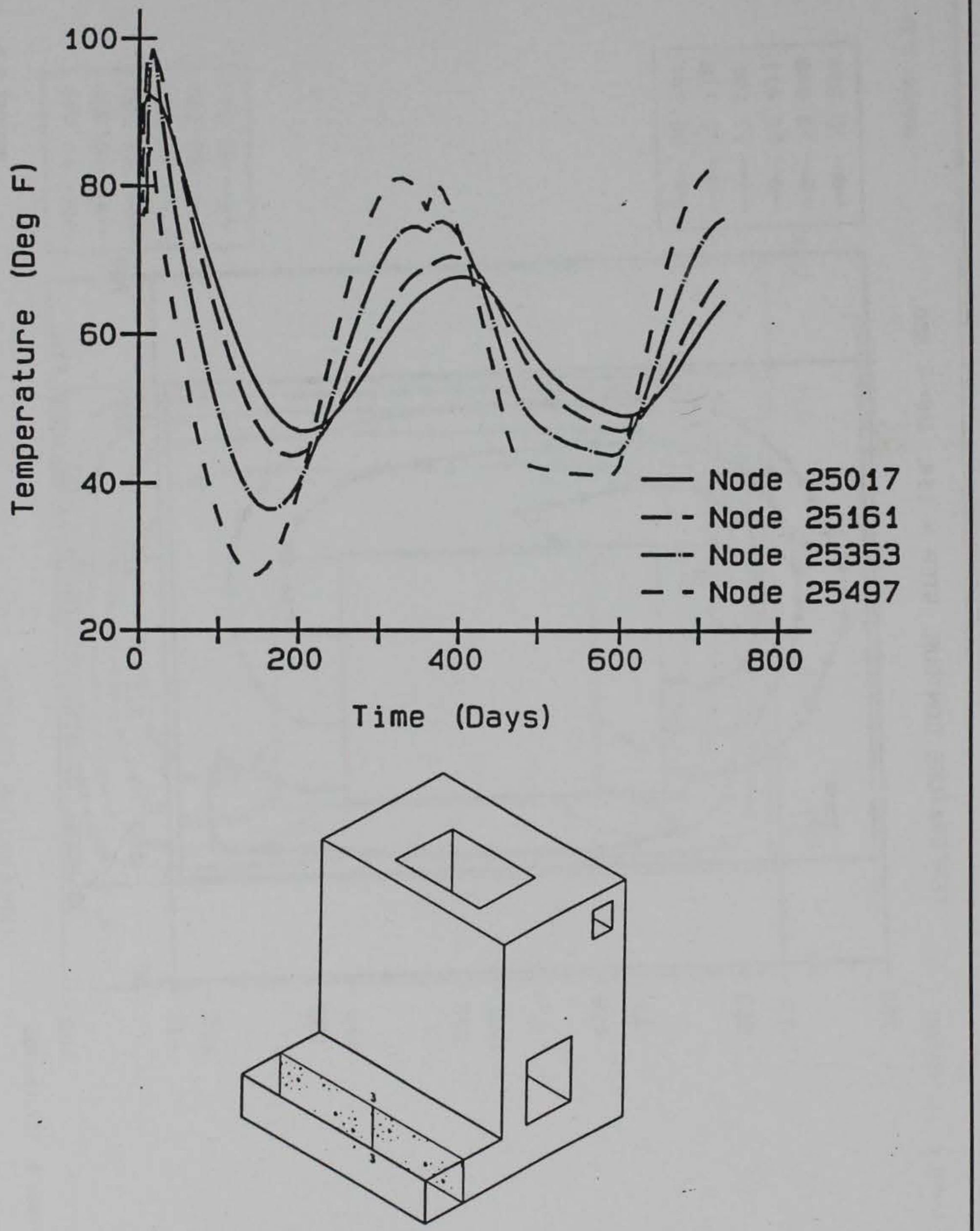

Culvert Valve Monolith
Section No. 4

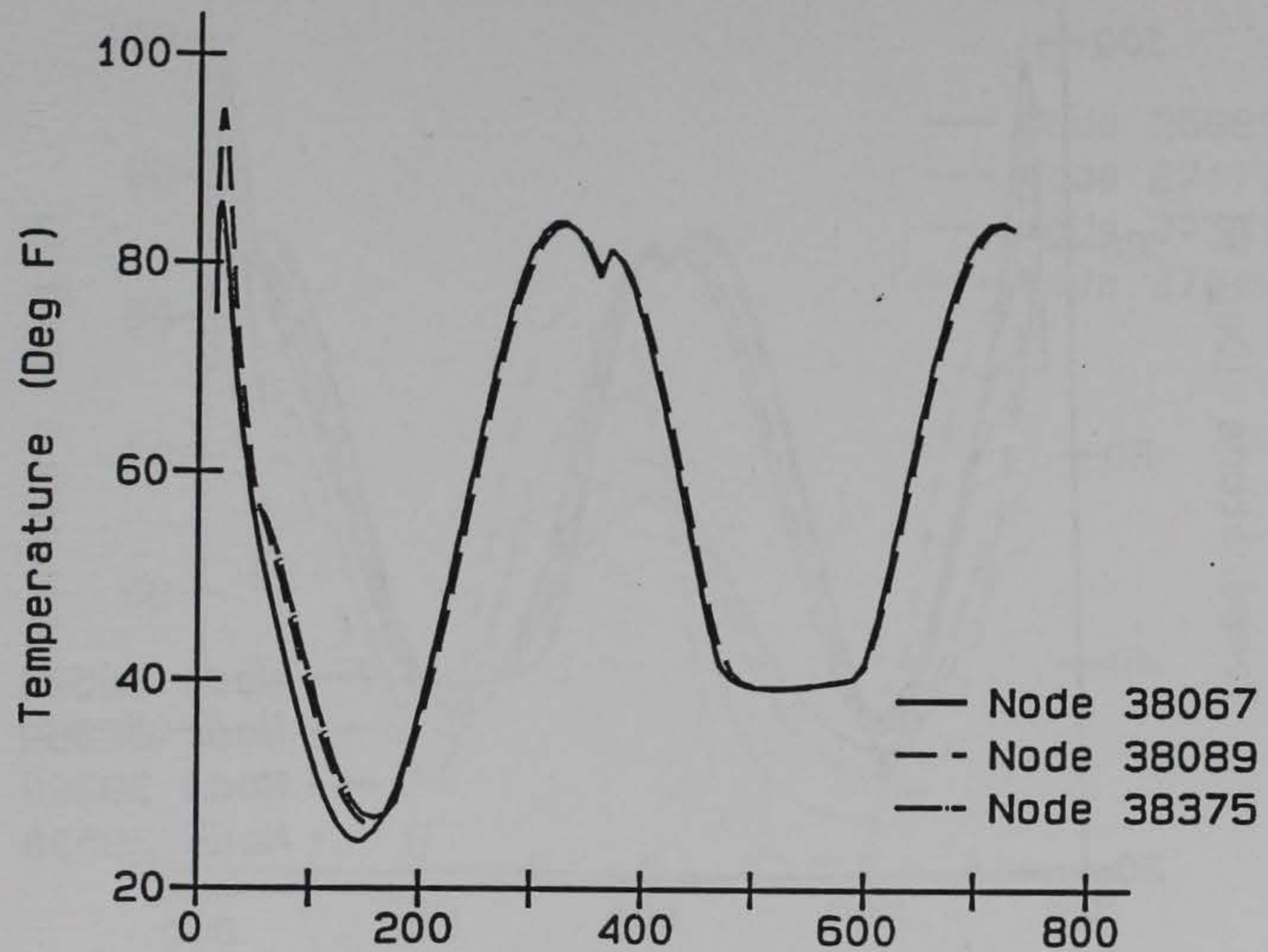

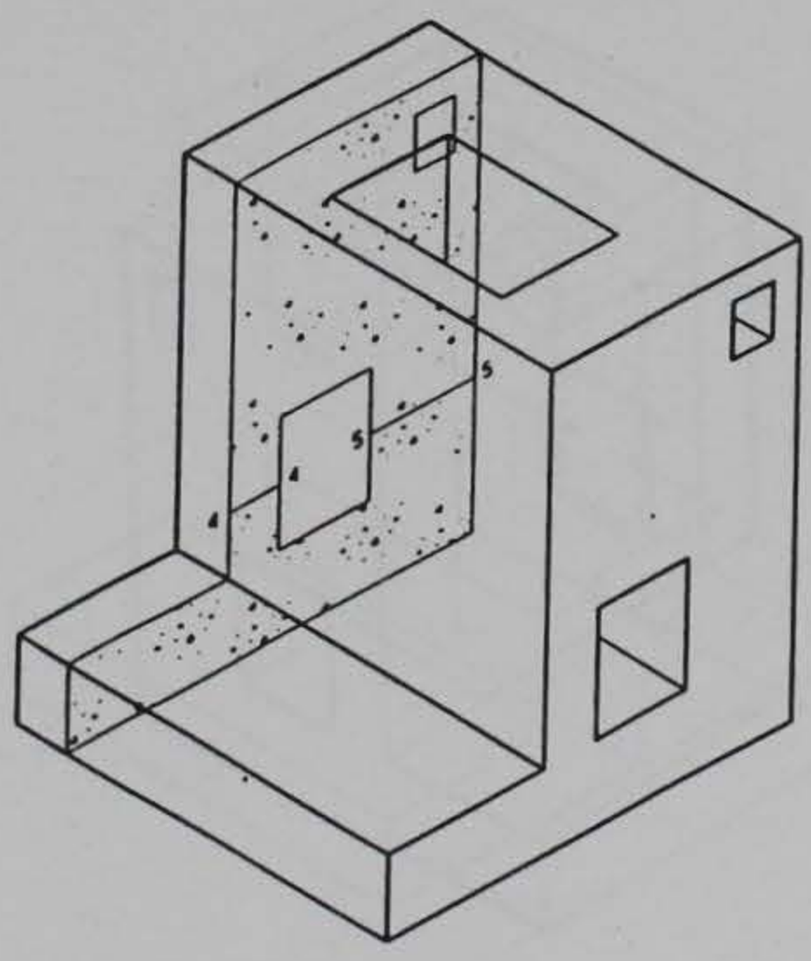

Culvert Valve Monolith
Section No. 5

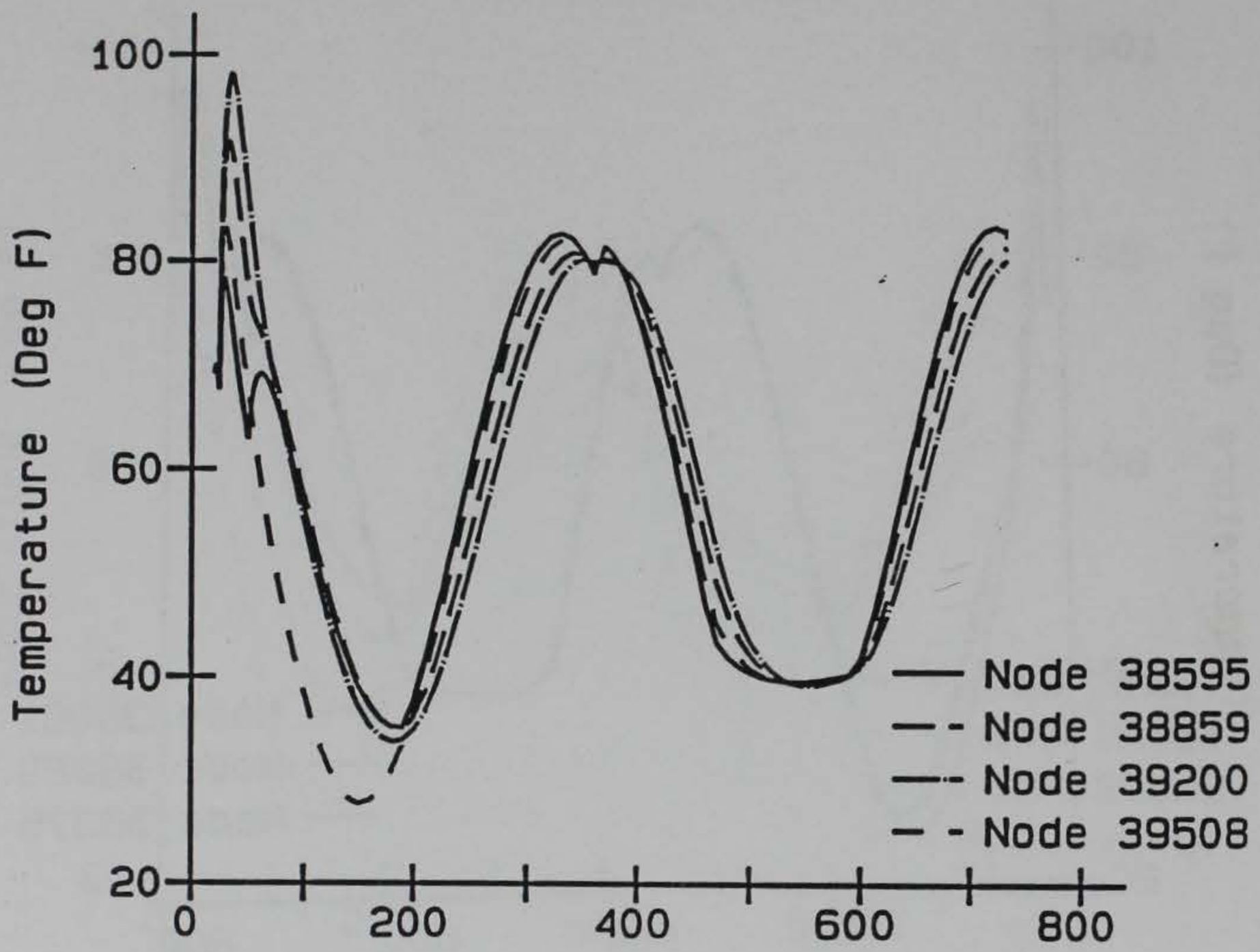

Time (Days)

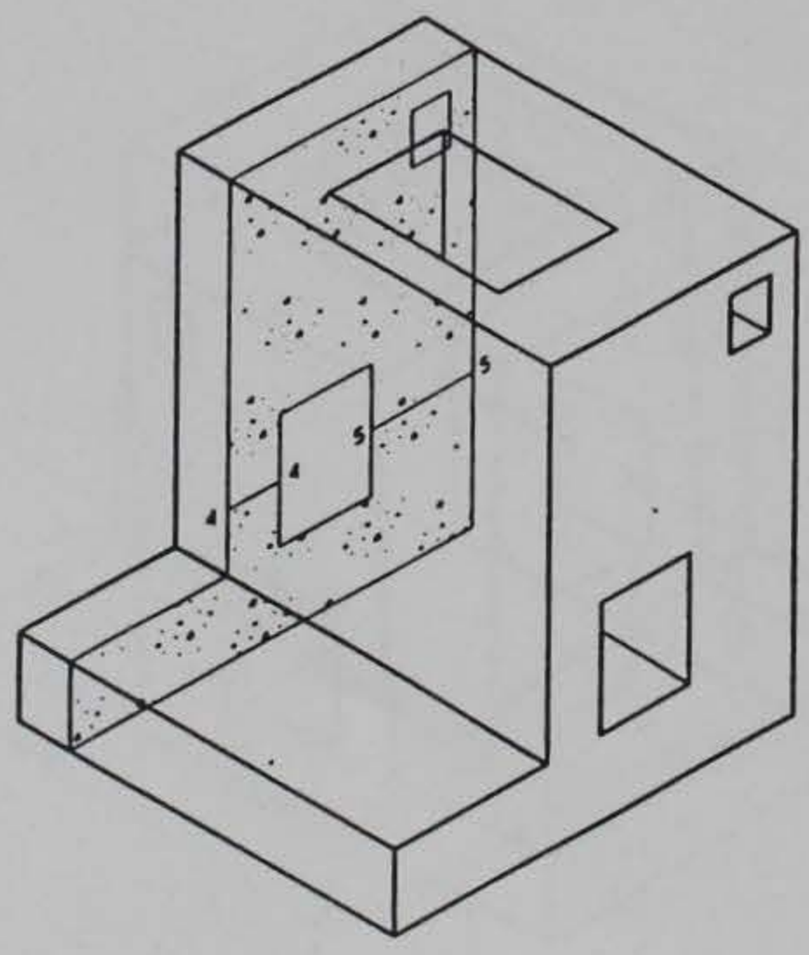

Culvert Valve Monolith
Section No. 6

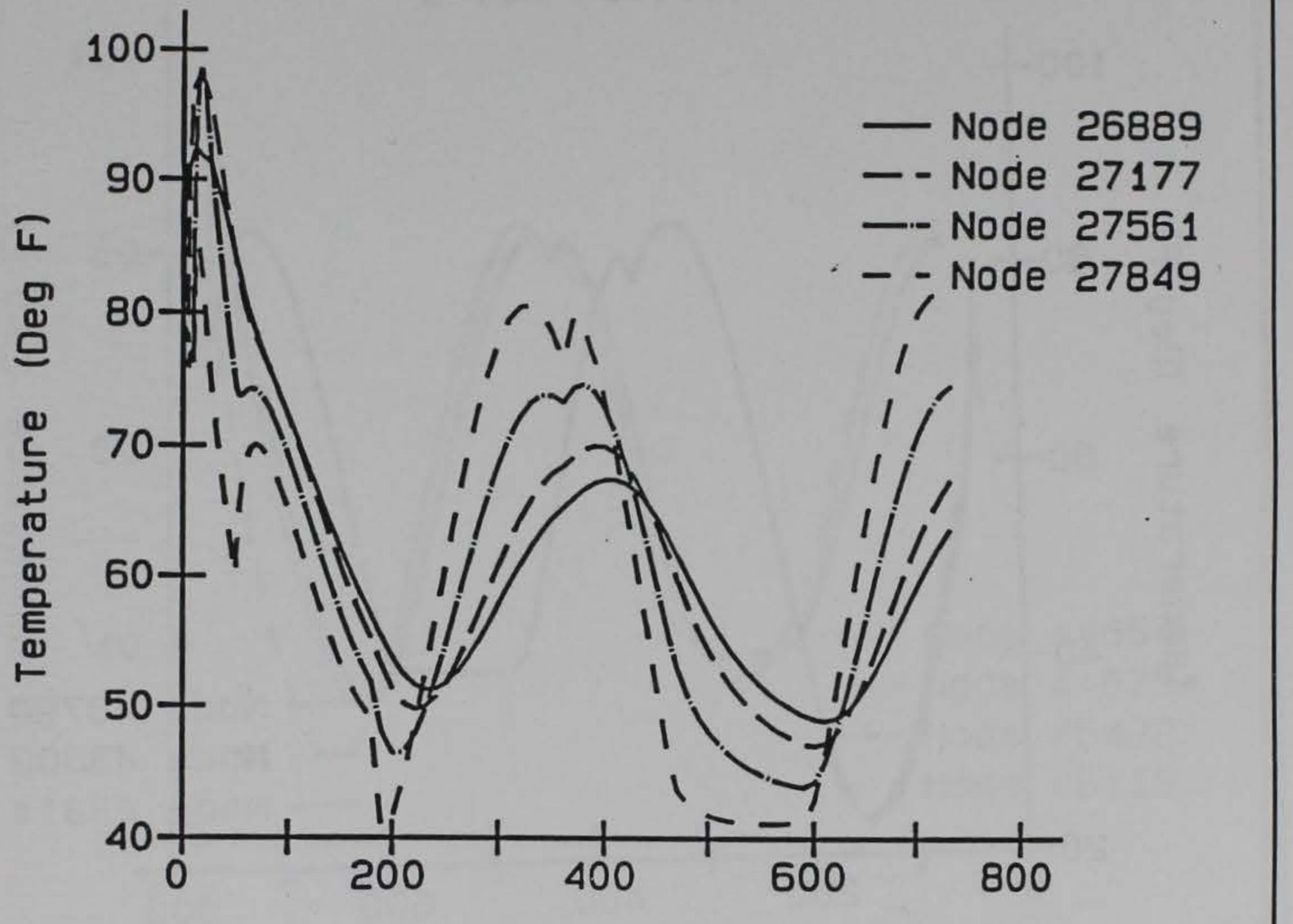

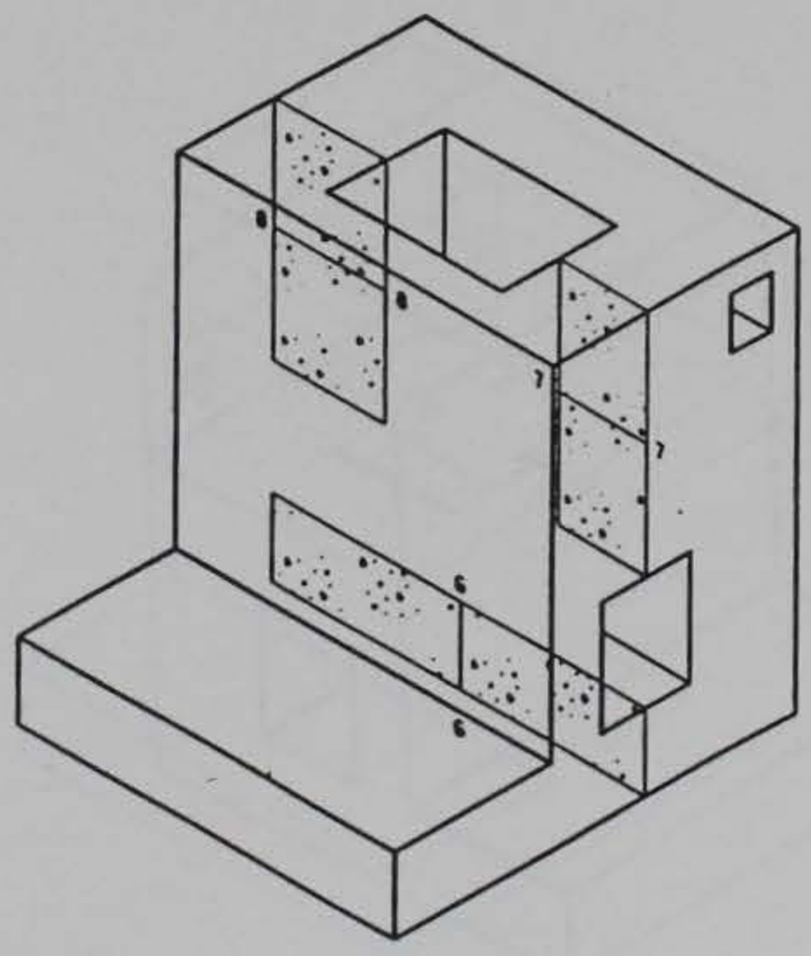

Culvert Valve Monolith
Section No. 9

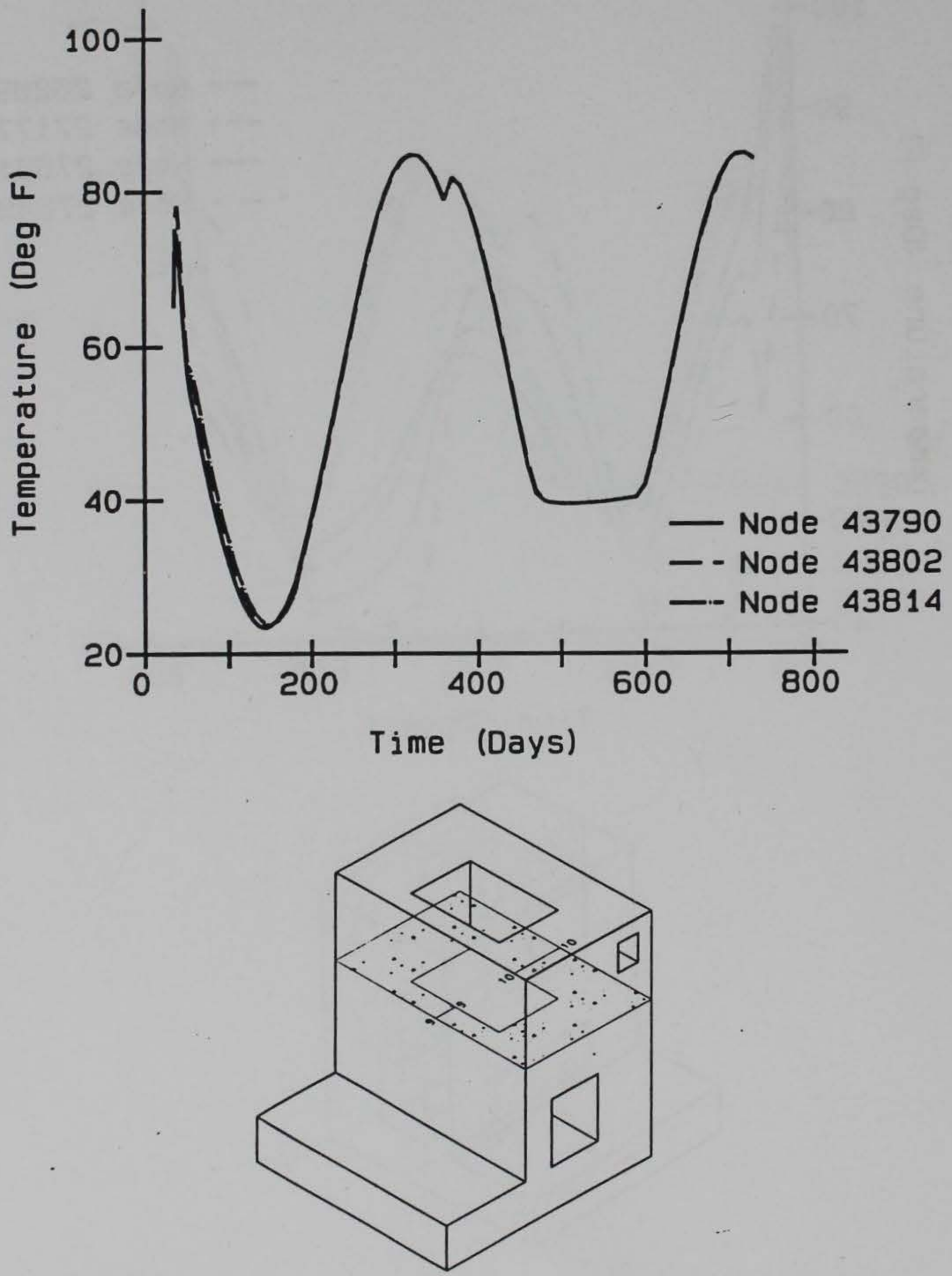

Culvert Valve Monolith
Section No. 10

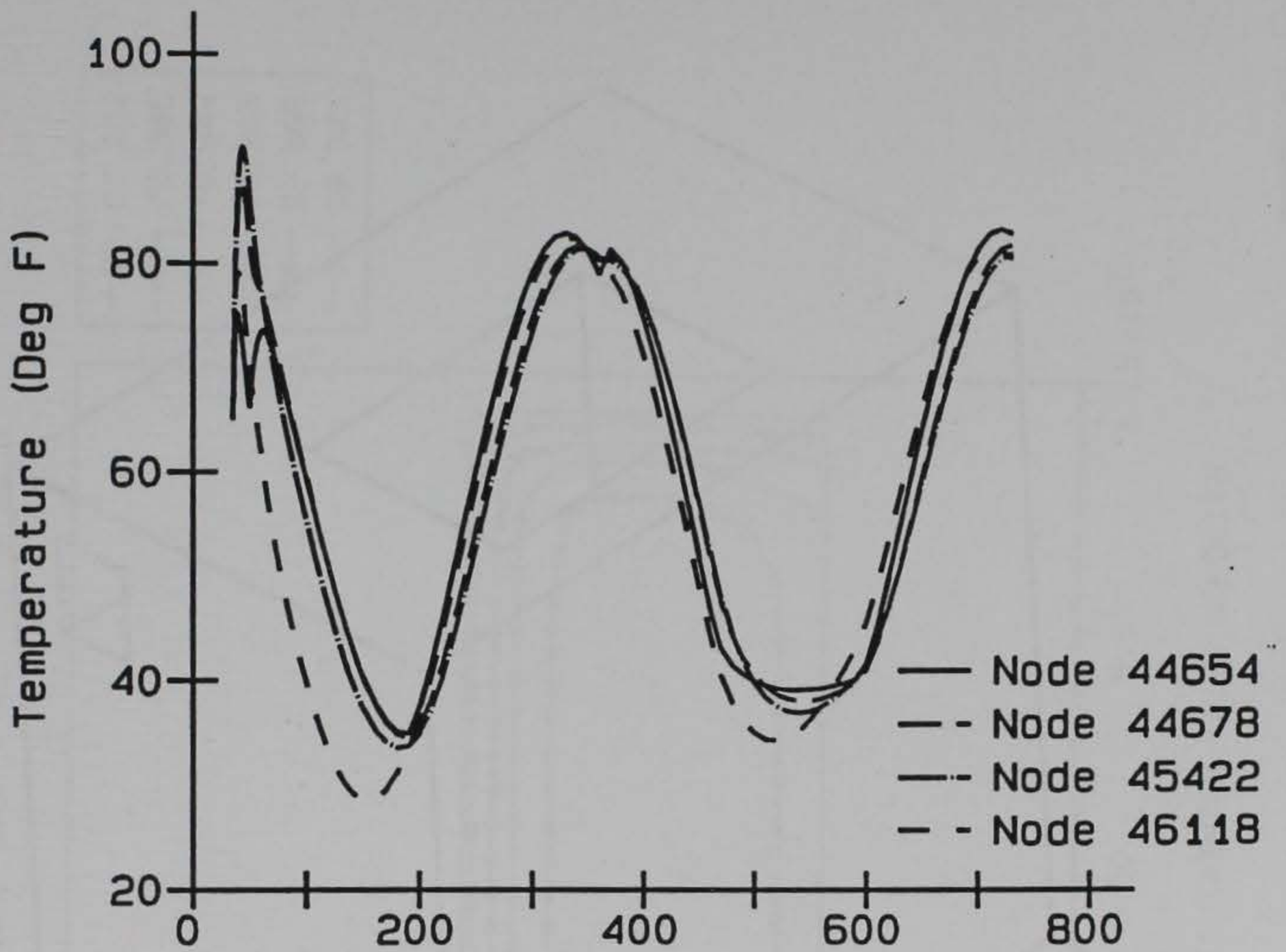

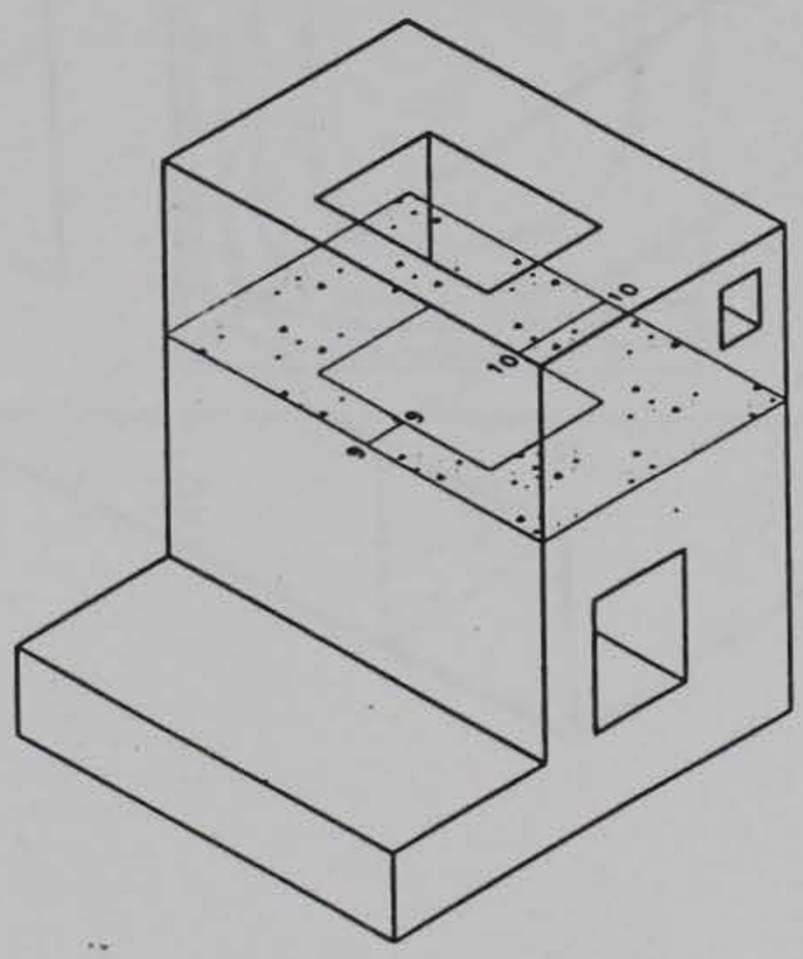

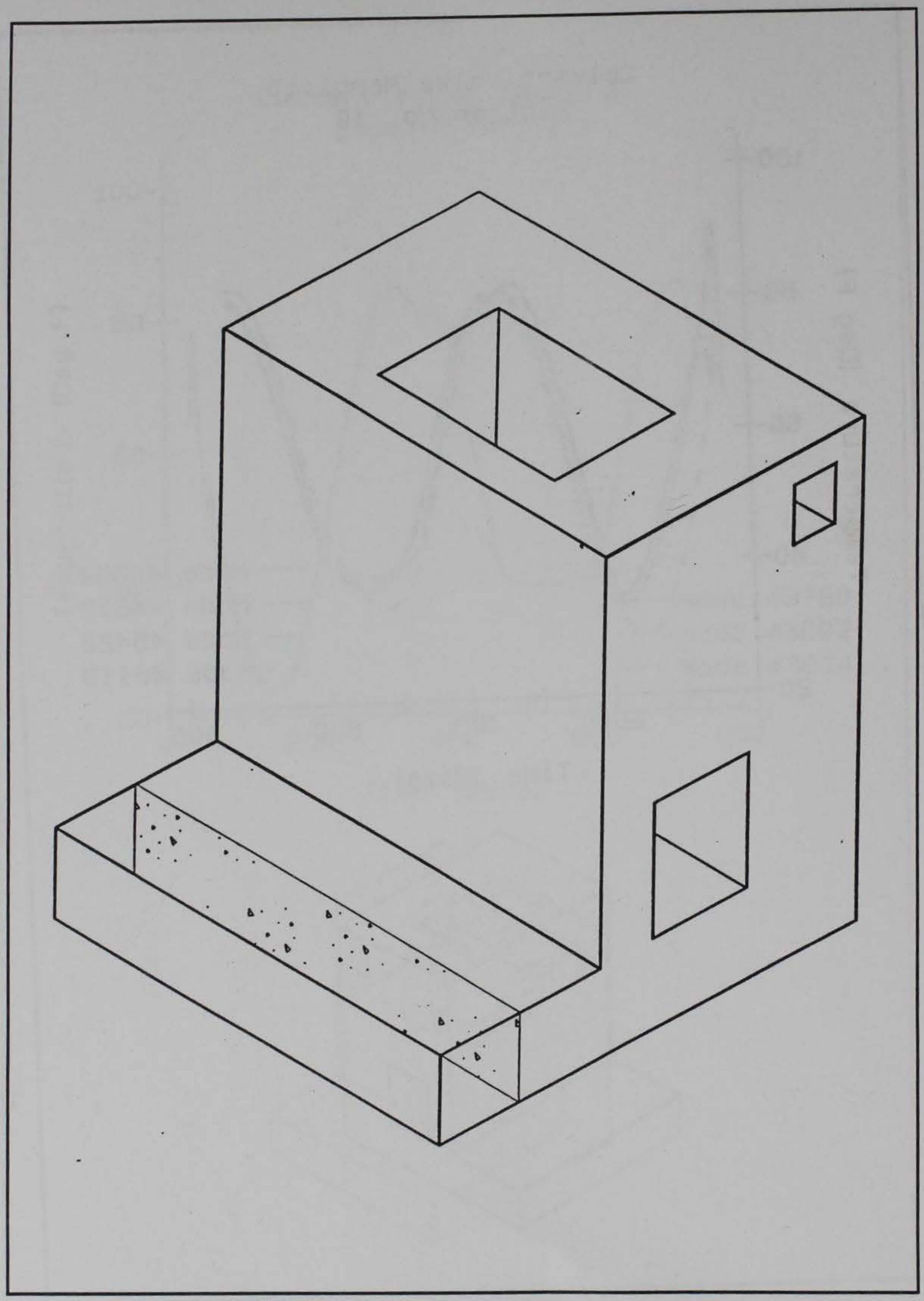

Longitudinal section through slab of monolith

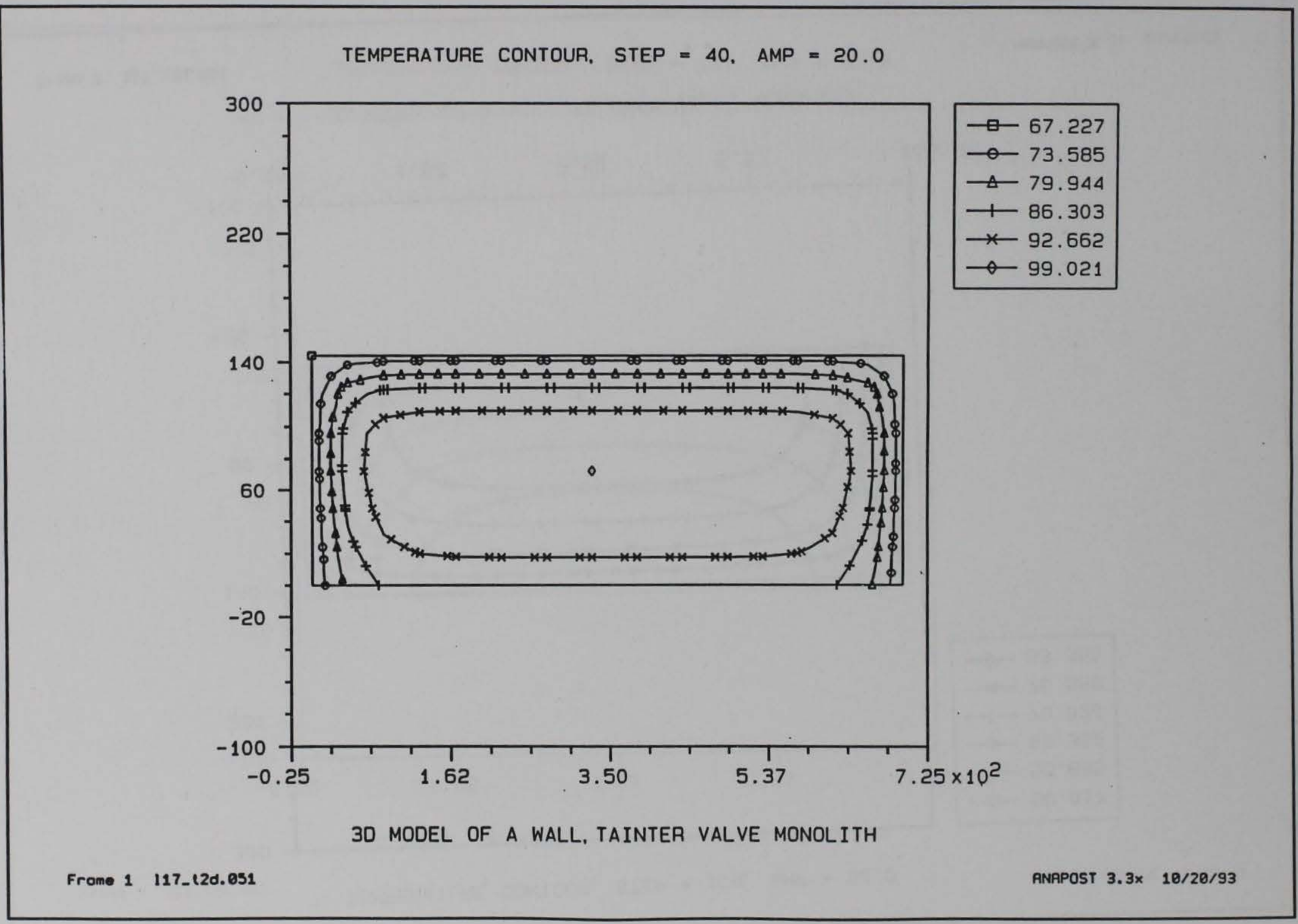
TEMPERATURE CONTOUR, STEP = 40, AMP = 20.0
300
220
140
60
-20
-100
-0.25
1.62
3.50
5.37
7.25 x10^2
67.227
73.585
79.944
86.303
92.662
99.021
3D MODEL OF A WALL, TAINTER VALVE MONOLITH
Frame 1 117_t2d.051
ANAPOST 3.3x 10/20/93

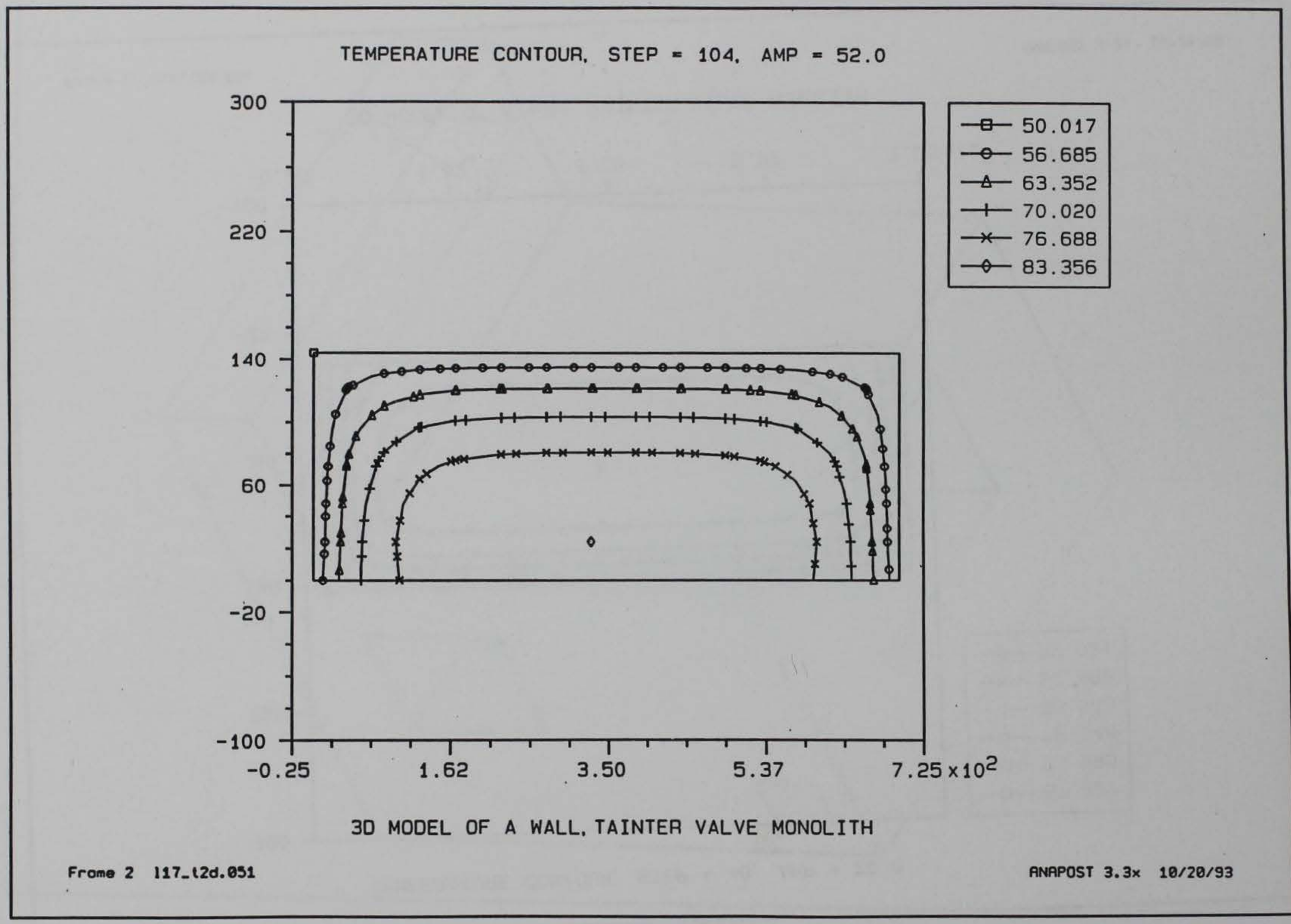
TEMPERATURE CONTOUR, STEP = 104, AMP = 52.0
300
220
140
60
-20
-100
-0.25
1.62
3.50
5.37
7.25 x10^2
50.017
56.685
63.352
70.020
76.688
83.356
3D MODEL OF A WALL, TAINTER VALVE MONOLITH
Frome 2 117_t2d.051
ANAPOST 3.3x 10/20/93

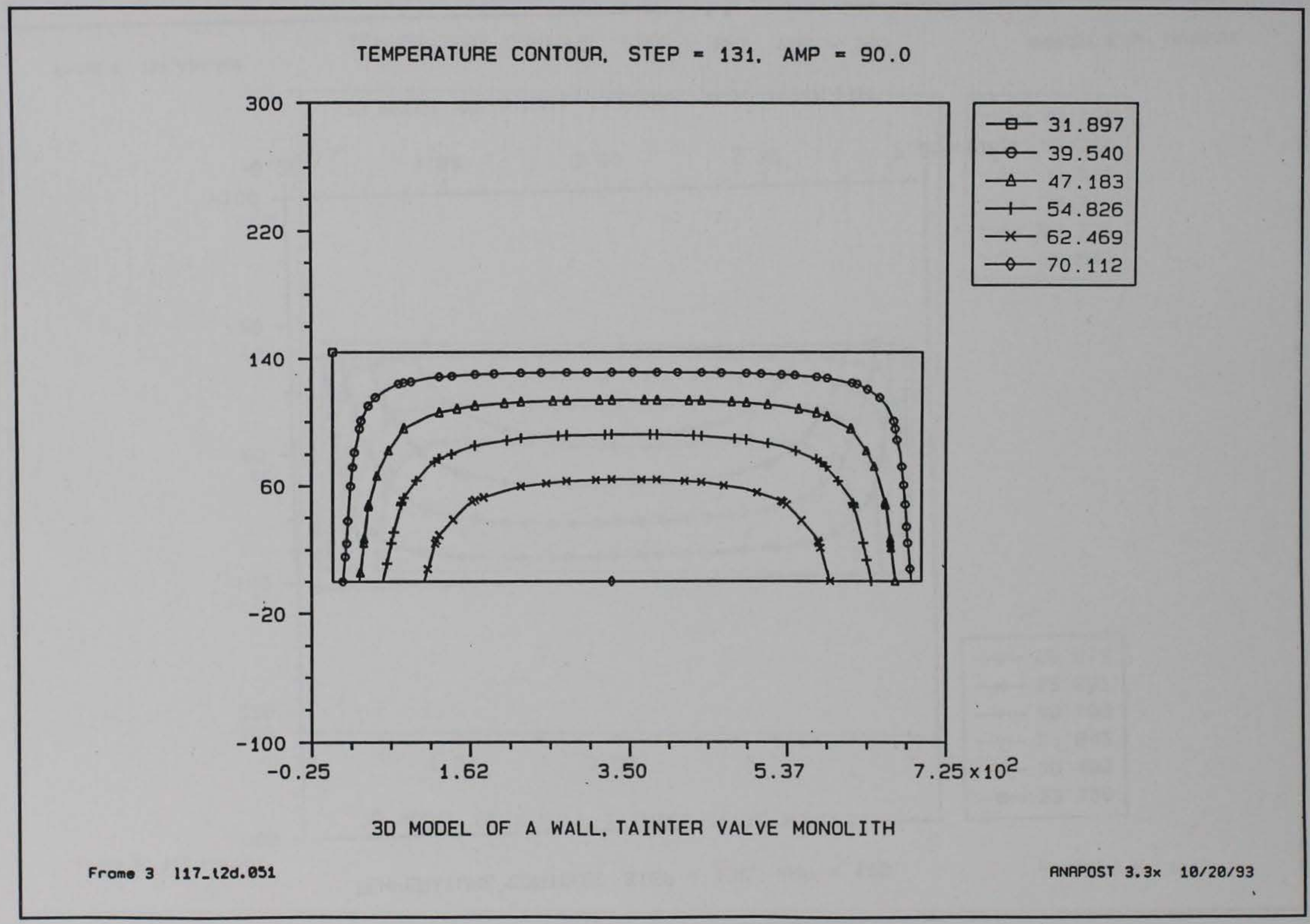
TEMPERATURE CONTOUR, STEP = 131, AMP = 90.0
300
220
140
60
-20
-100
-0.25
1.62
3.50
5.37
7.25 x10^2
31.897
39.540
47.183
54.826
62.469
70.112
3D MODEL OF A WALL, TAINTER VALVE MONOLITH
Frame 3 117_t2d.051
ANAPOST 3.3x 10/20/93

TEMPERATURE CONTOUR, STEP = 138, AMP = 125.

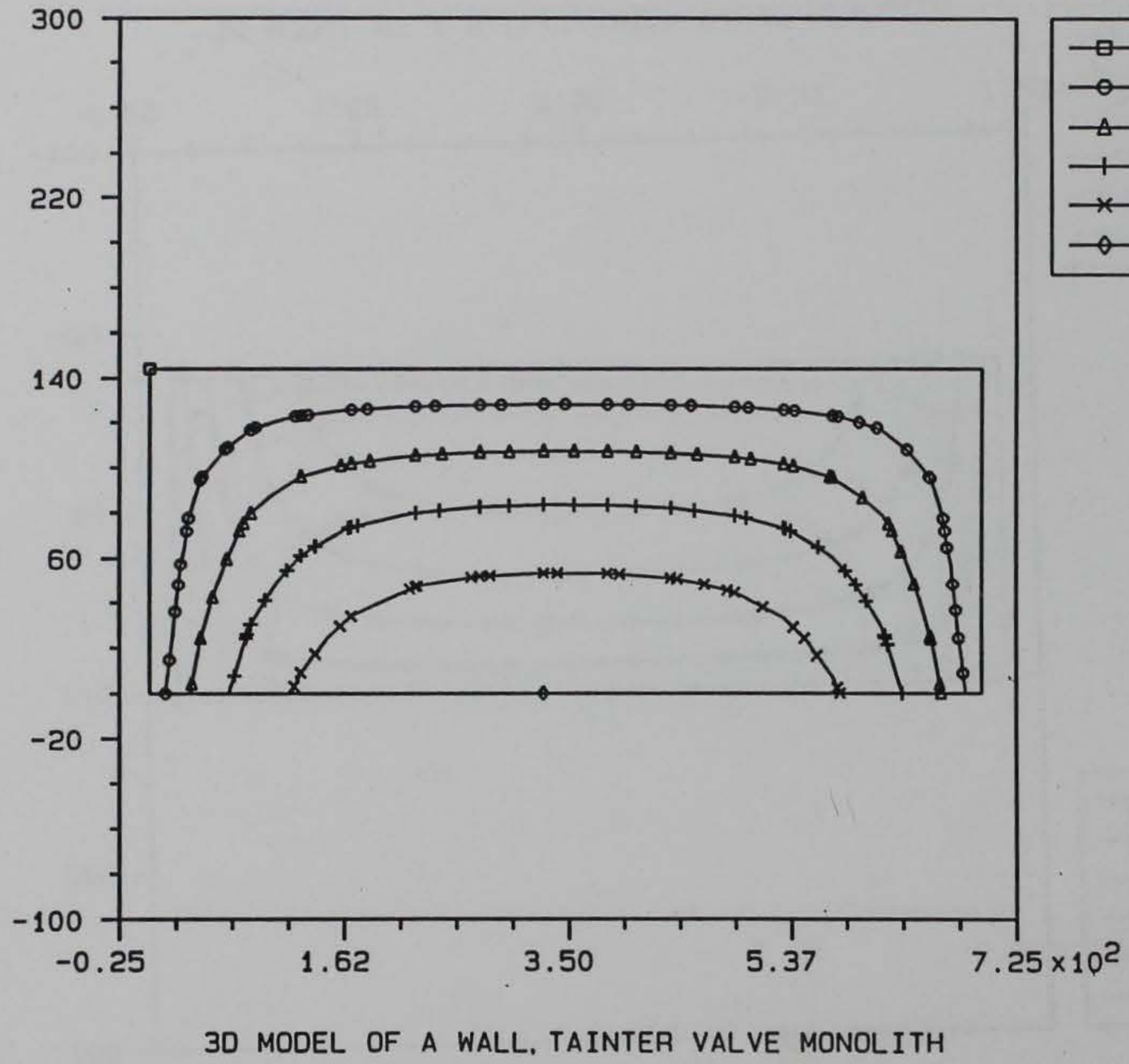

3D MODEL OF A WALL, TAINTER VALVE MONOLITH

Frame 4 117_t2d.051

ANAPOST 3.3x 10/20/93

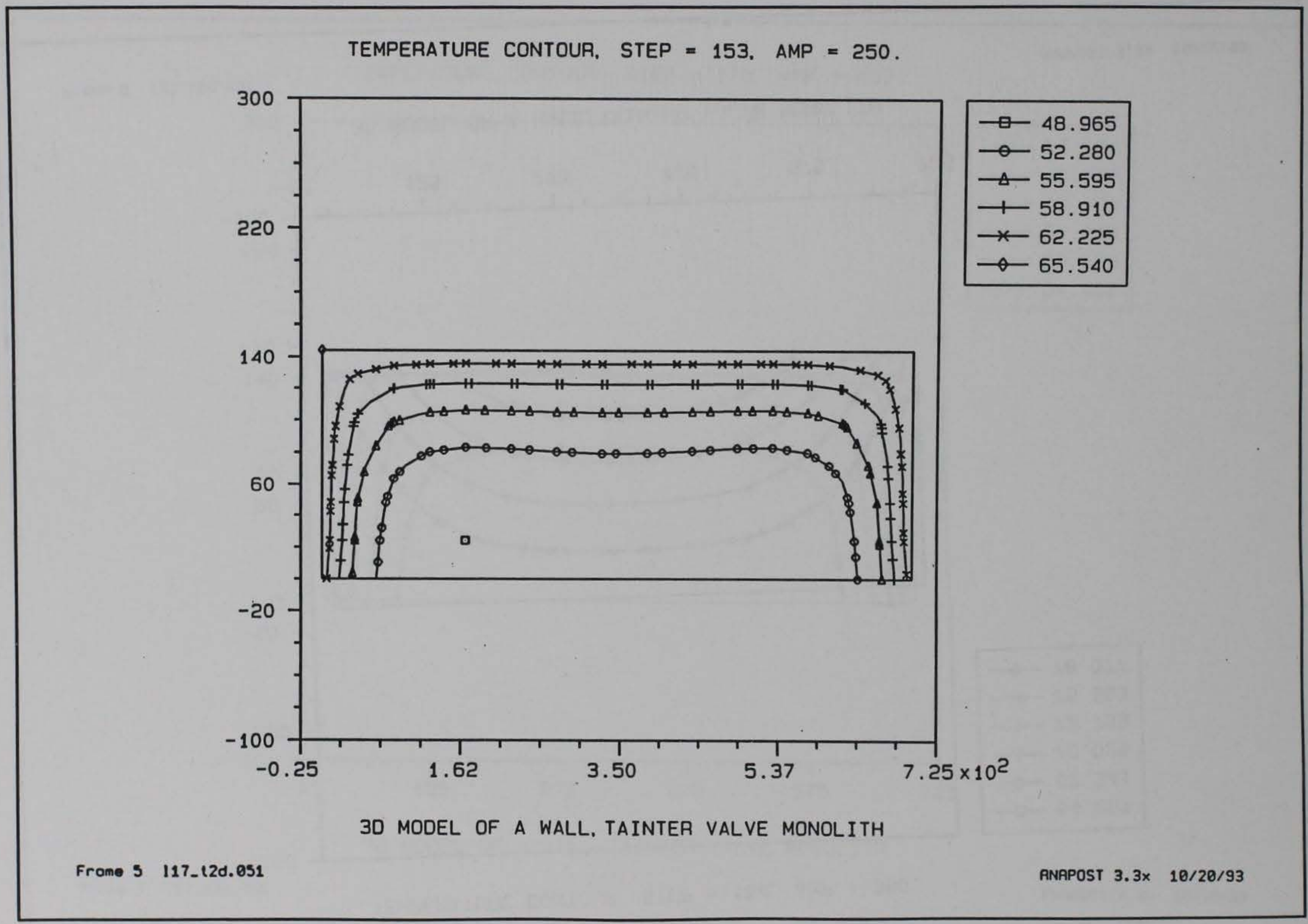
TEMPERATURE CONTOUR, STEP = 153, AMP = 250.
300
220
140
60
-20
-100
-0.25
1.62
3.50
5.37
7.25 x10^2
48.965
52.280
55.595
58.910
62.225
65.540
3D MODEL OF A WALL, TAINTER VALVE MONOLITH
Frome 5 117_t2d.051
ANAPOST 3.3x 10/20/93

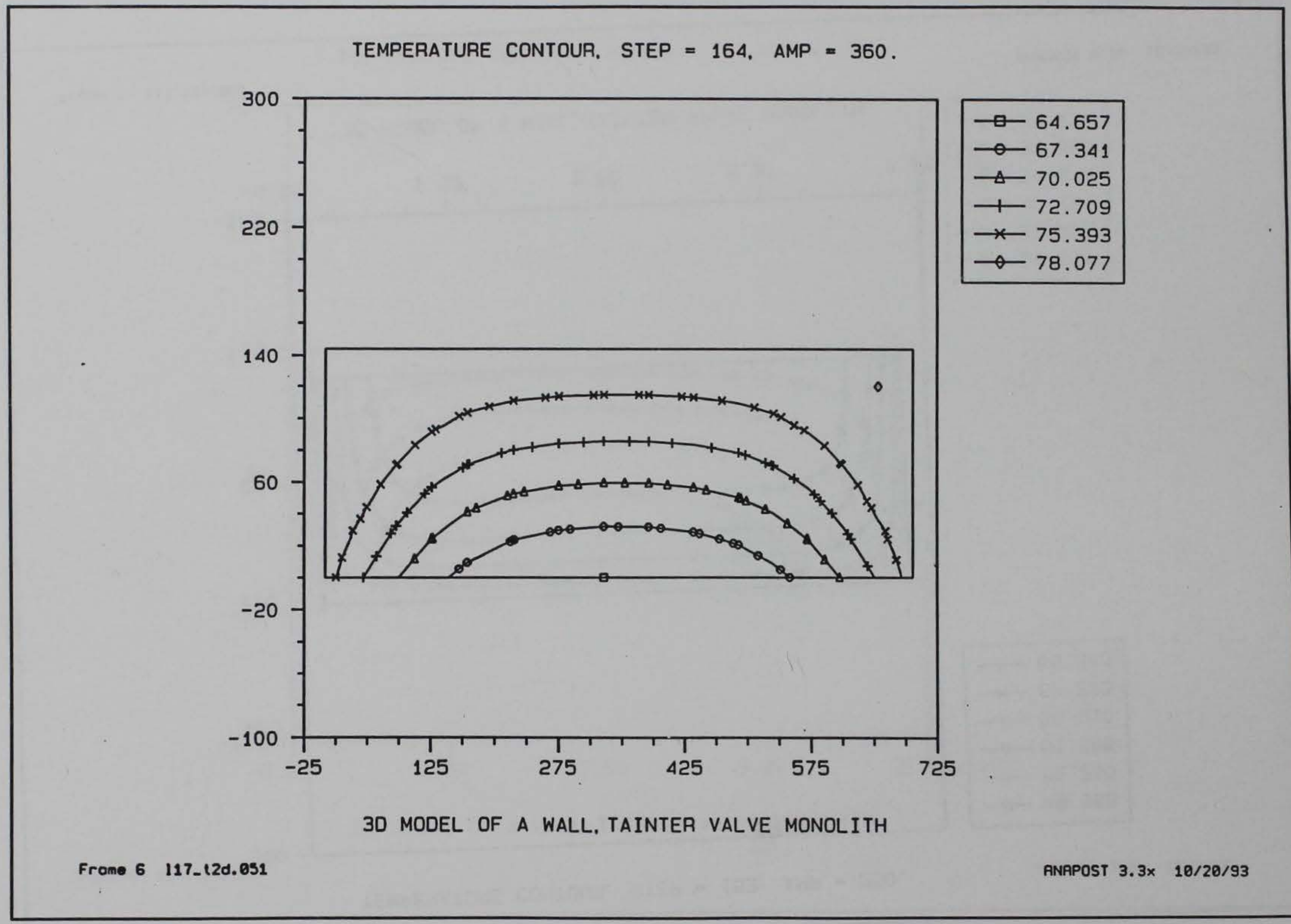
TEMPERATURE CONTOUR, STEP = 164, AMP = 360.
300
220
140
60
-20
-100
-25
125
275
425
575
725
64.657
67.341
70.025
72.709
75.393
78.077
3D MODEL OF A WALL, TAINTER VALVE MONOLITH
Frame 6 117_t2d.051
ANAPOST 3.3x 10/20/93

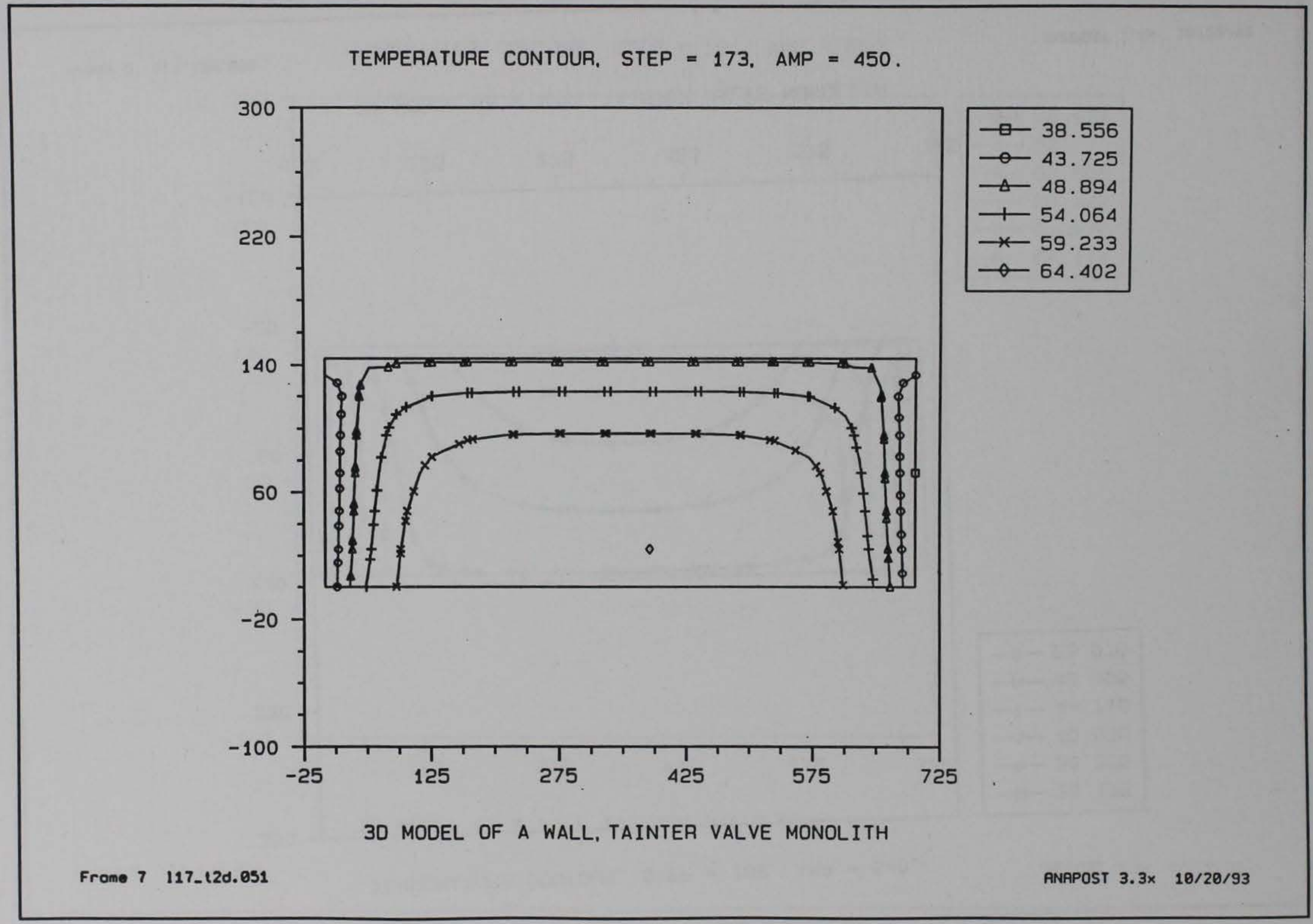
TEMPERATURE CONTOUR, STEP = 173, AMP = 450.
300
220
140
60
-20
-100
-25
125
275
425
575
725
38.556
43.725
48.894
54.064
59.233
64.402
3D MODEL OF A WALL, TAINTER VALVE MONOLITH
Frame 7 117_t2d.051
ANAPOST 3.3x 10/20/93

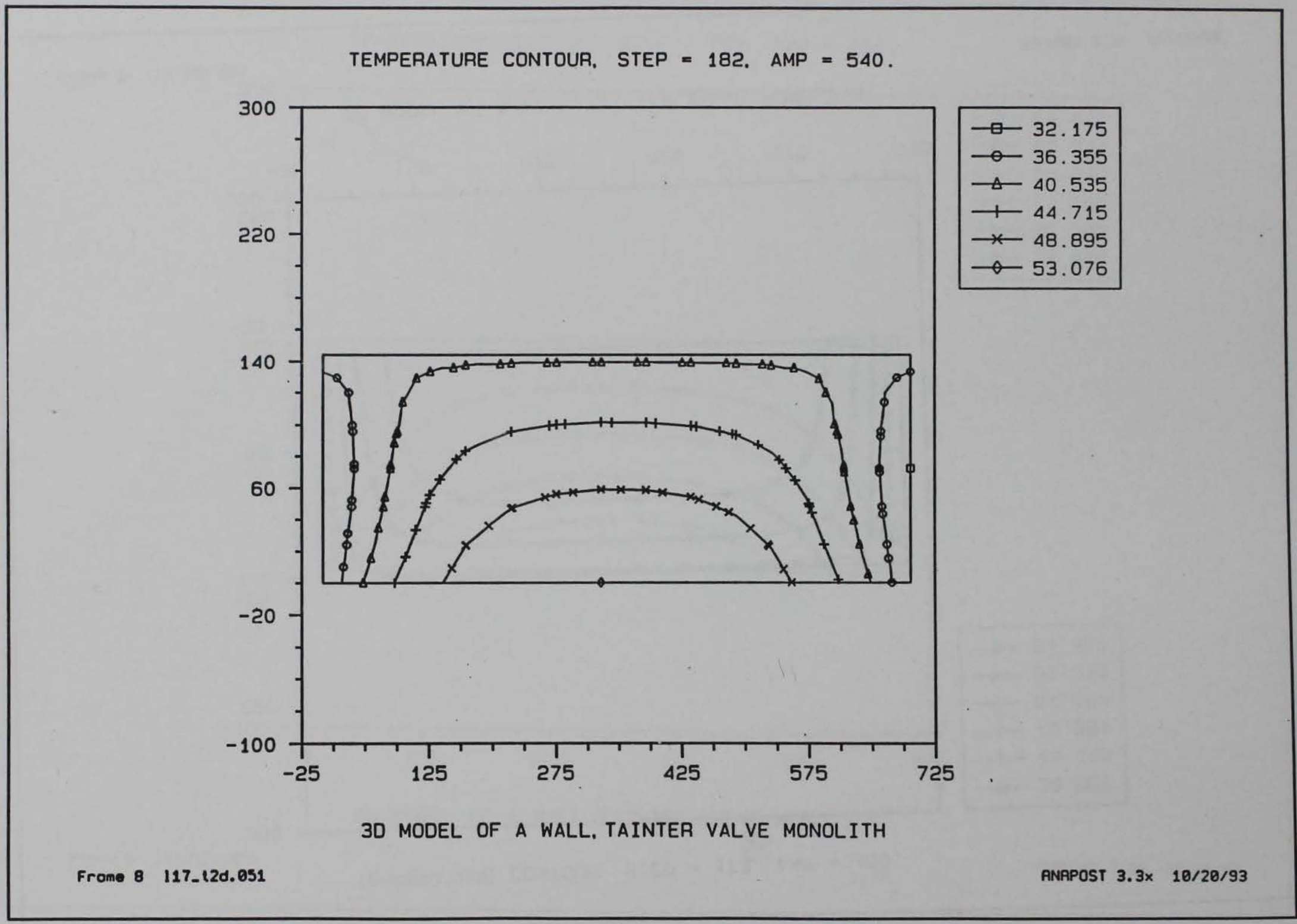
TEMPERATURE CONTOUR, STEP = 182, AMP = 540.
300
220
140
60
-20
-100
-25
125
275
425
575
725
32.175
36.355
40.535
44.715
48.895
53.076
3D MODEL OF A WALL, TAINTER VALVE MONOLITH
Frame 8 117_t2d.051
ANAPOST 3.3x 10/20/93

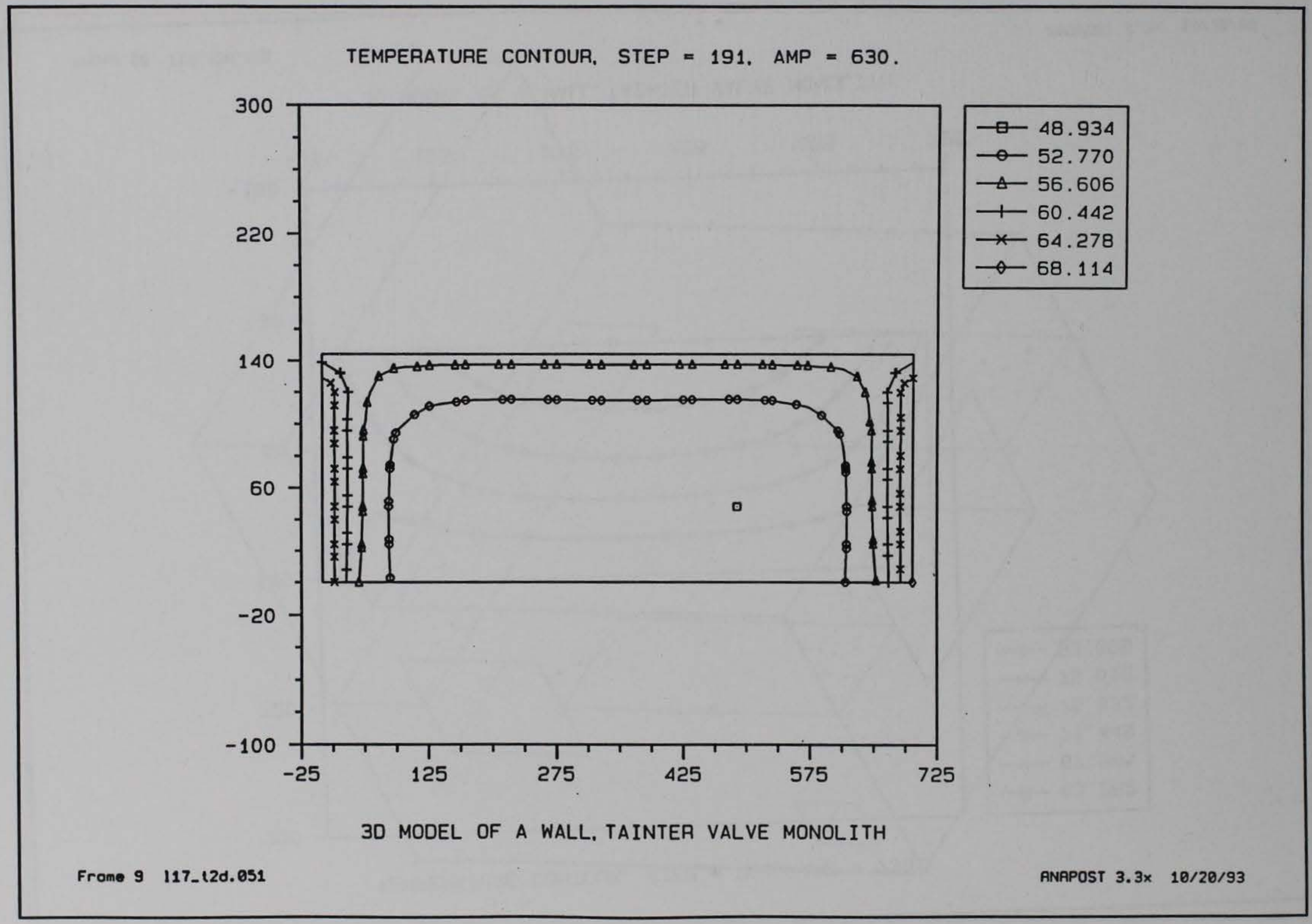
TEMPERATURE CONTOUR, STEP = 191, AMP = 630.
300
220
140
60
-20
-100
-25
125
275
425
575
725
48.934
52.770
56.606
60.442
64.278
68.114
3D MODEL OF A WALL, TAINTER VALVE MONOLITH
Frame 9 117_t2d.051
ANAPOST 3.3x 10/20/93

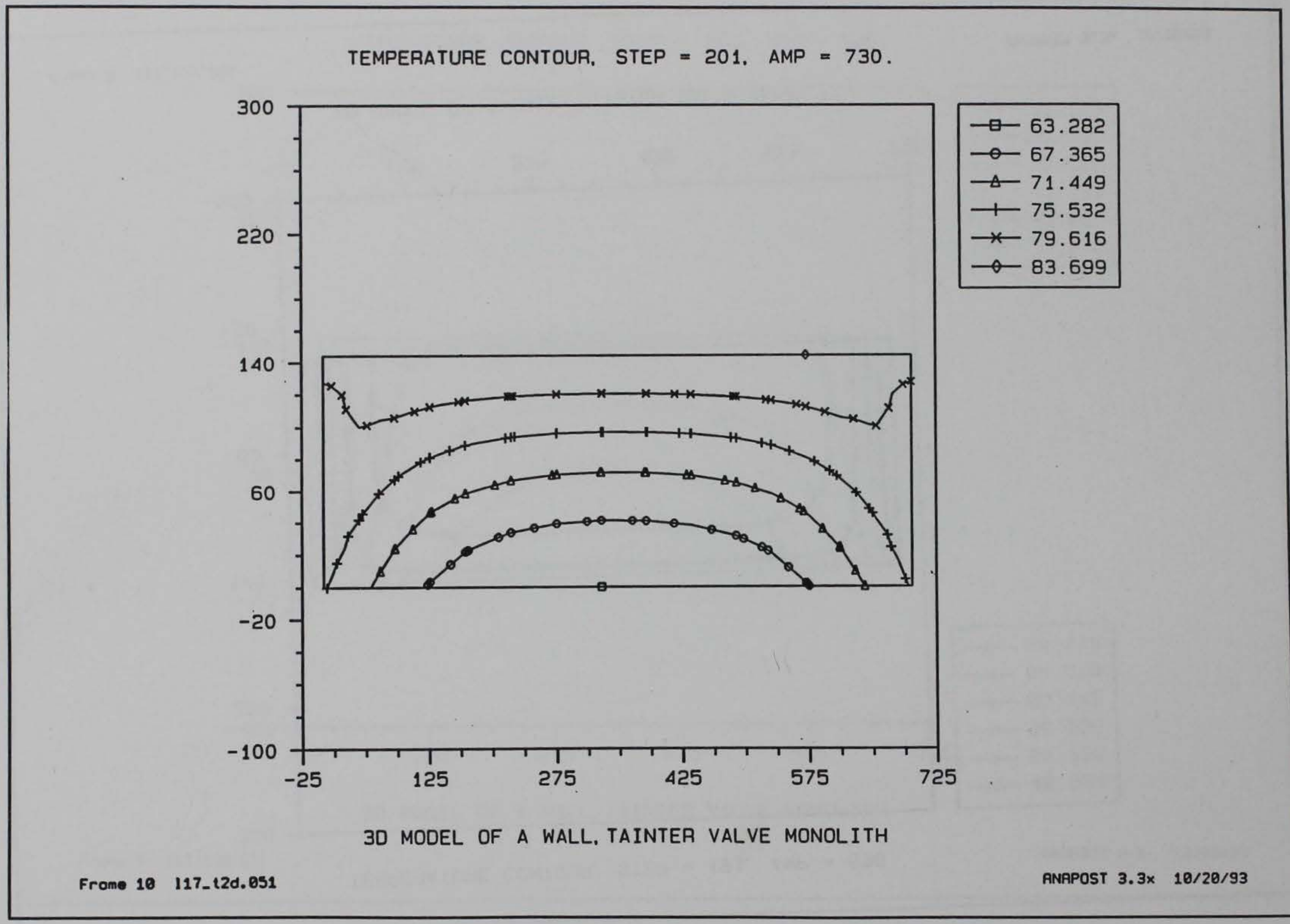
TEMPERATURE CONTOUR, STEP = 201, AMP = 730.
300
220
140
60
-20
-100
-25
125
275
425
575
725
63.282
67.365
71.449
75.532
79.616
83.699
3D MODEL OF A WALL, TAINTER VALVE MONOLITH
Frame 10 117_t2d.051
ANAPOST 3.3x 10/20/93

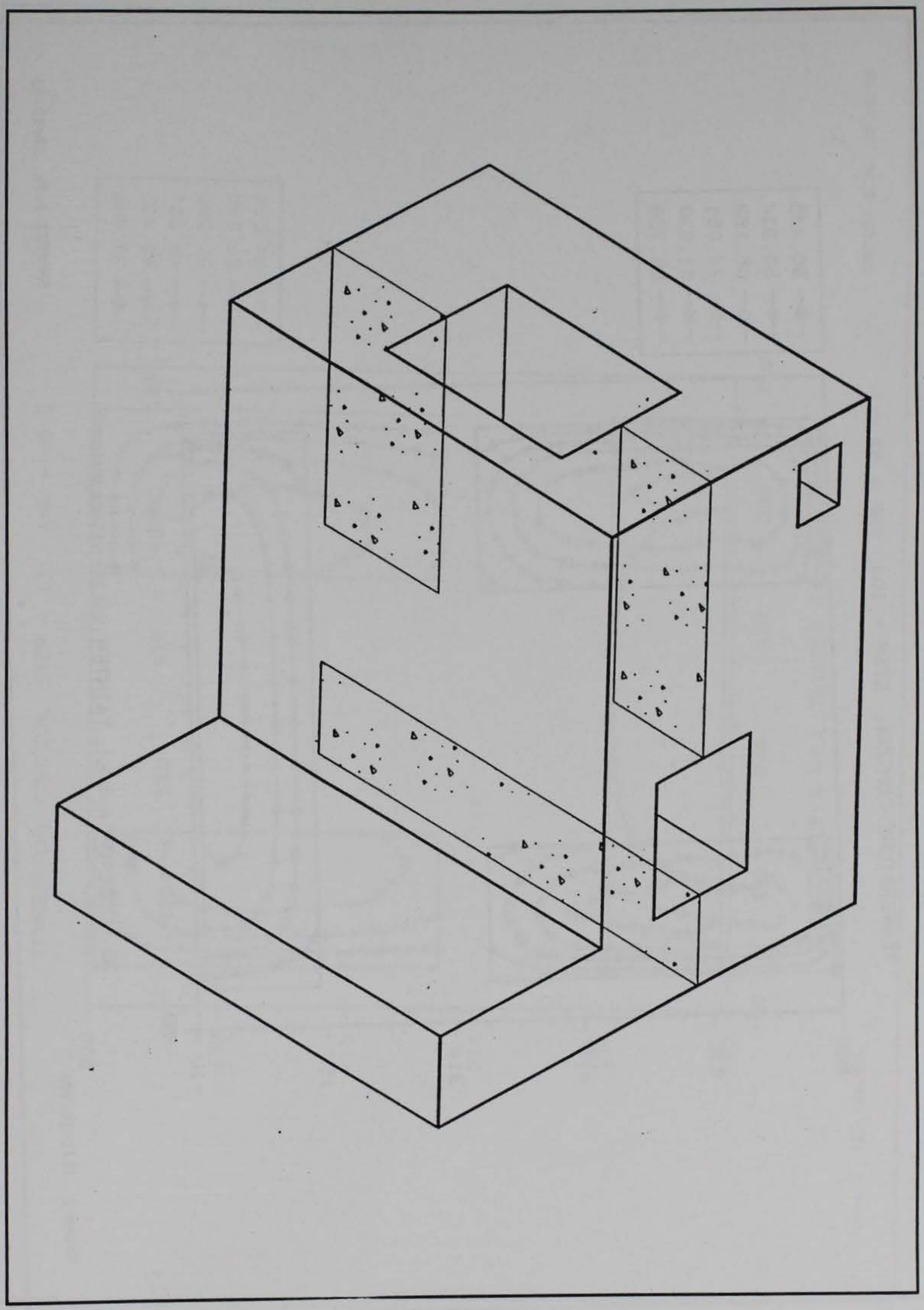

Longitudinal section through culvert valve pit

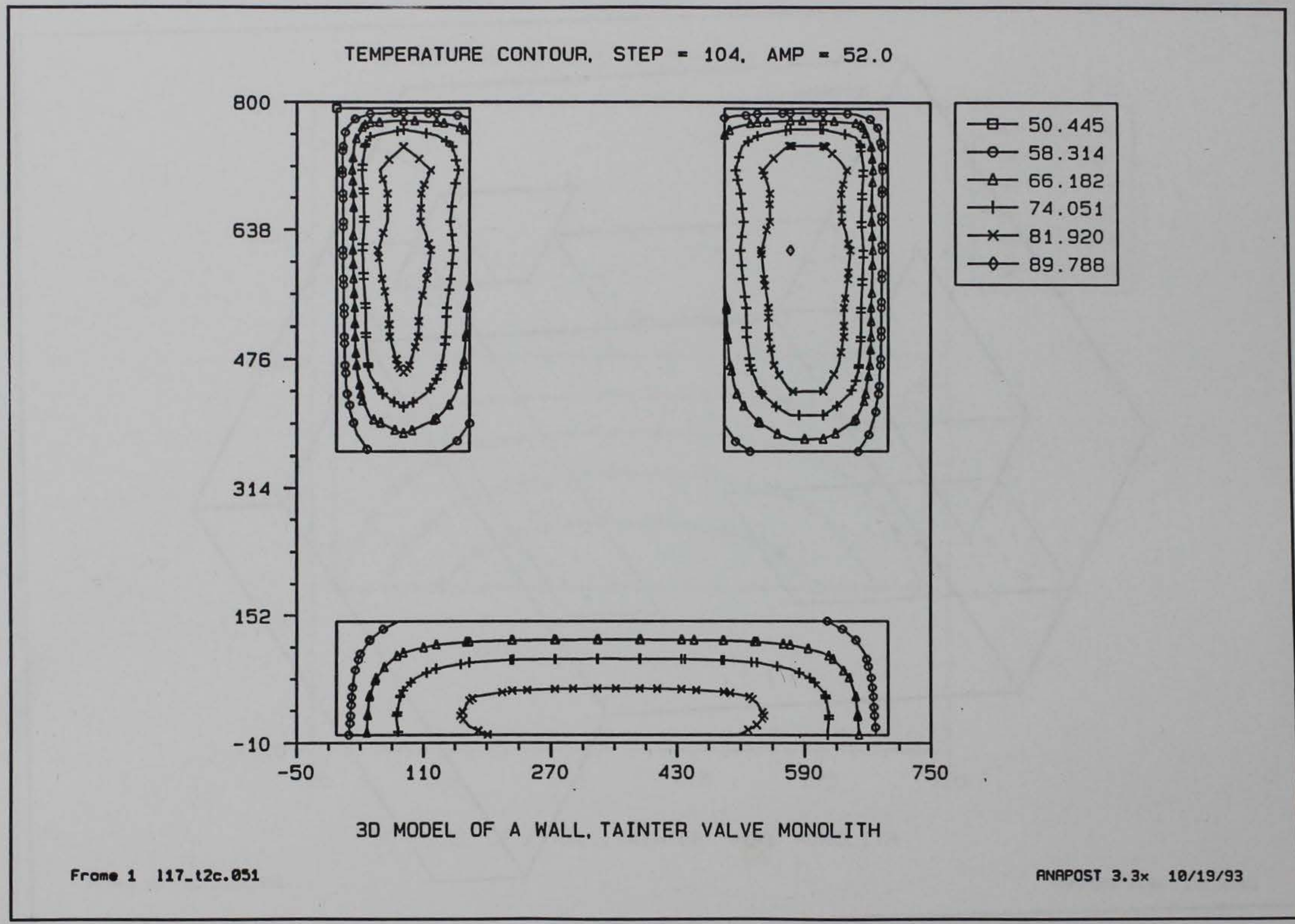
TEMPERATURE CONTOUR, STEP = 104, AMP = 52.0
800
638
476
314
152
-10
-50
110
270
430
590
750
50.445
58.314
66.182
74.051
81.920
89.788
3D MODEL OF A WALL, TAINTER VALVE MONOLITH
Frame 1 117_t2c.051
ANAPOST 3.3x 10/19/93

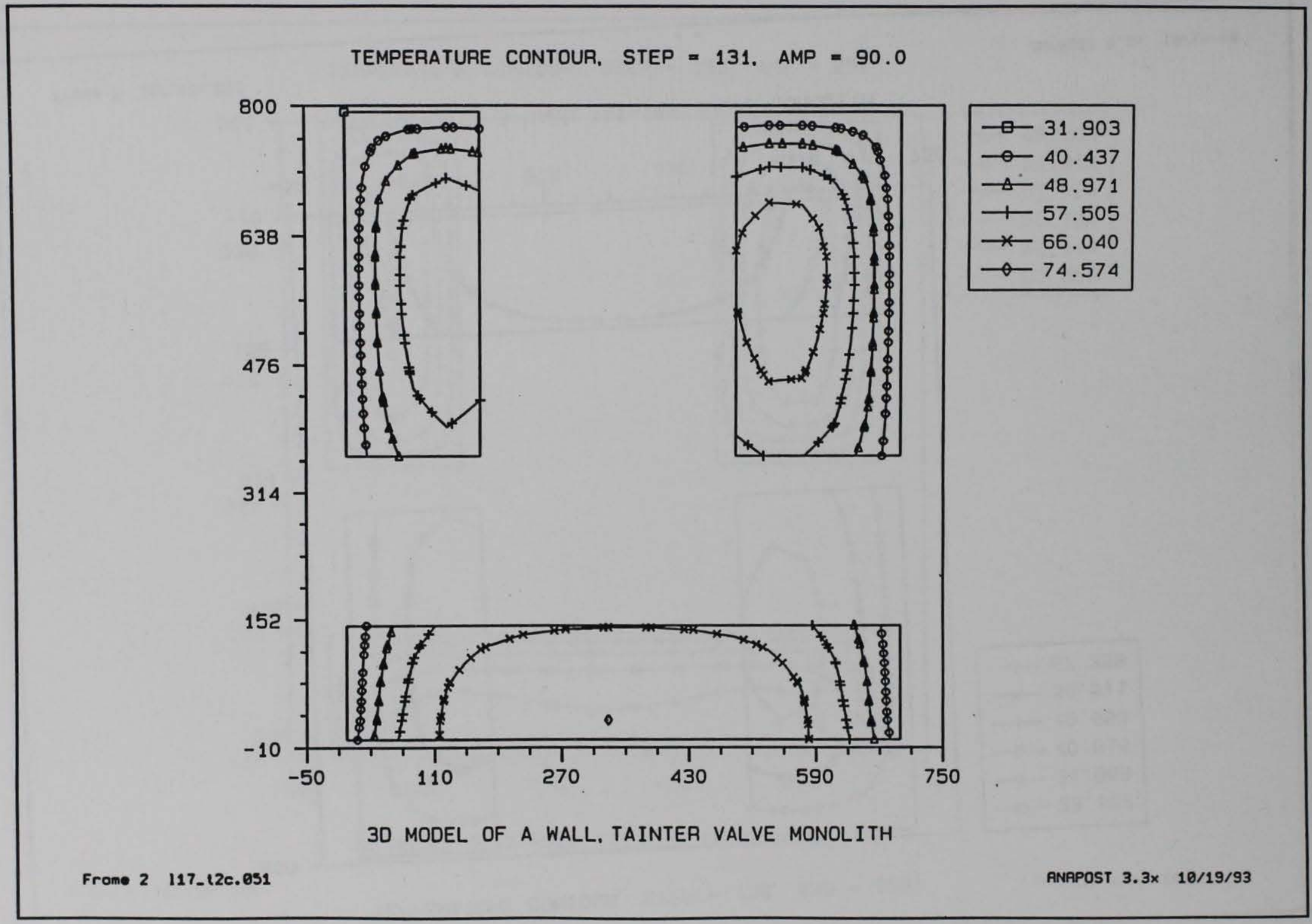
TEMPERATURE CONTOUR, STEP = 131, AMP = 90.0
800
638
476
314
152
-10
-50
110
270
430
590
750
31.903
40.437
48.971
57.505
66.040
74.574
3D MODEL OF A WALL, TAINTER VALVE MONOLITH
Frame 2 117_t2c.051
ANAPOST 3.3x 10/19/93

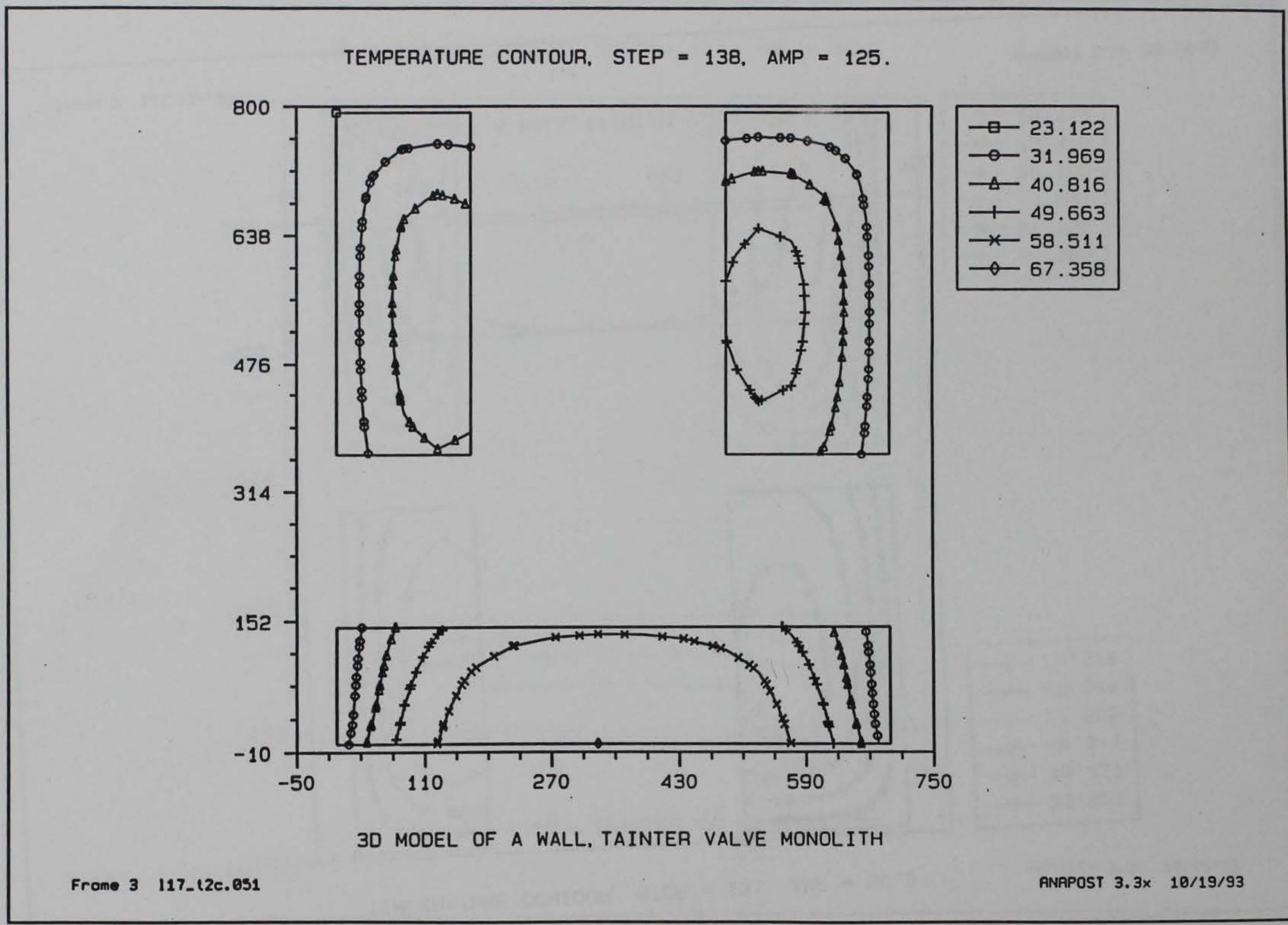
TEMPERATURE CONTOUR, STEP = 138, AMP = 125.
800
638
476
314
152
-10
-50
110
270
430
590
750
23.122
31.969
40.816
49.663
58.511
67.358
3D MODEL OF A WALL, TAINTER VALVE MONOLITH
Frome 3 117_t2c.051
ANAPOST 3.3x 10/19/93

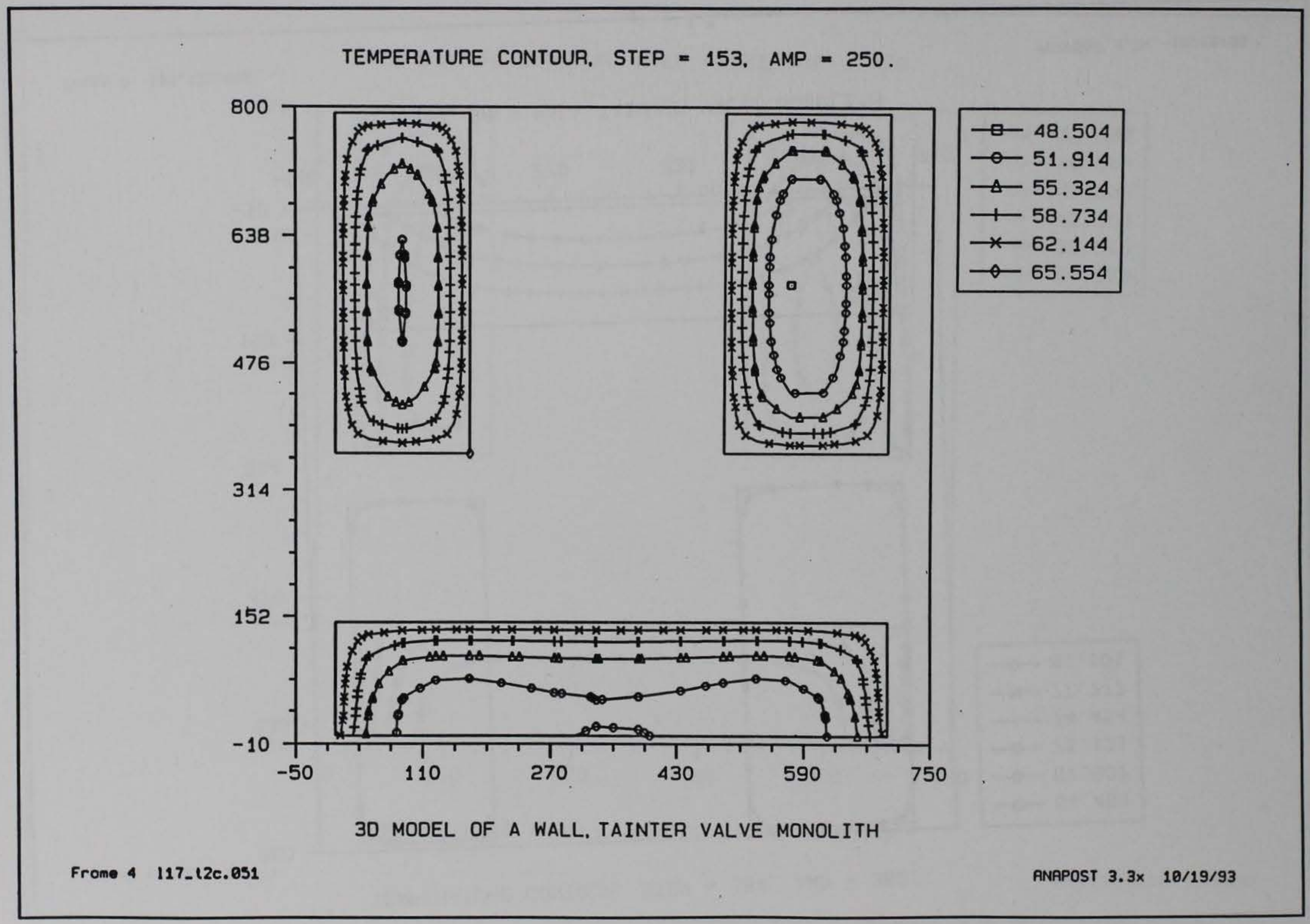
TEMPERATURE CONTOUR, STEP = 153, AMP = 250.
800
638
476
314
152
-10
-50
110
270
430
590
750
48.504
51.914
55.324
58.734
62.144
65.554
3D MODEL OF A WALL, TAINTER VALVE MONOLITH
Frome 4 117_t2c.051
ANAPOST 3.3x 10/19/93

TEMPERATURE CONTOUR, STEP = 164, AMP = 360.

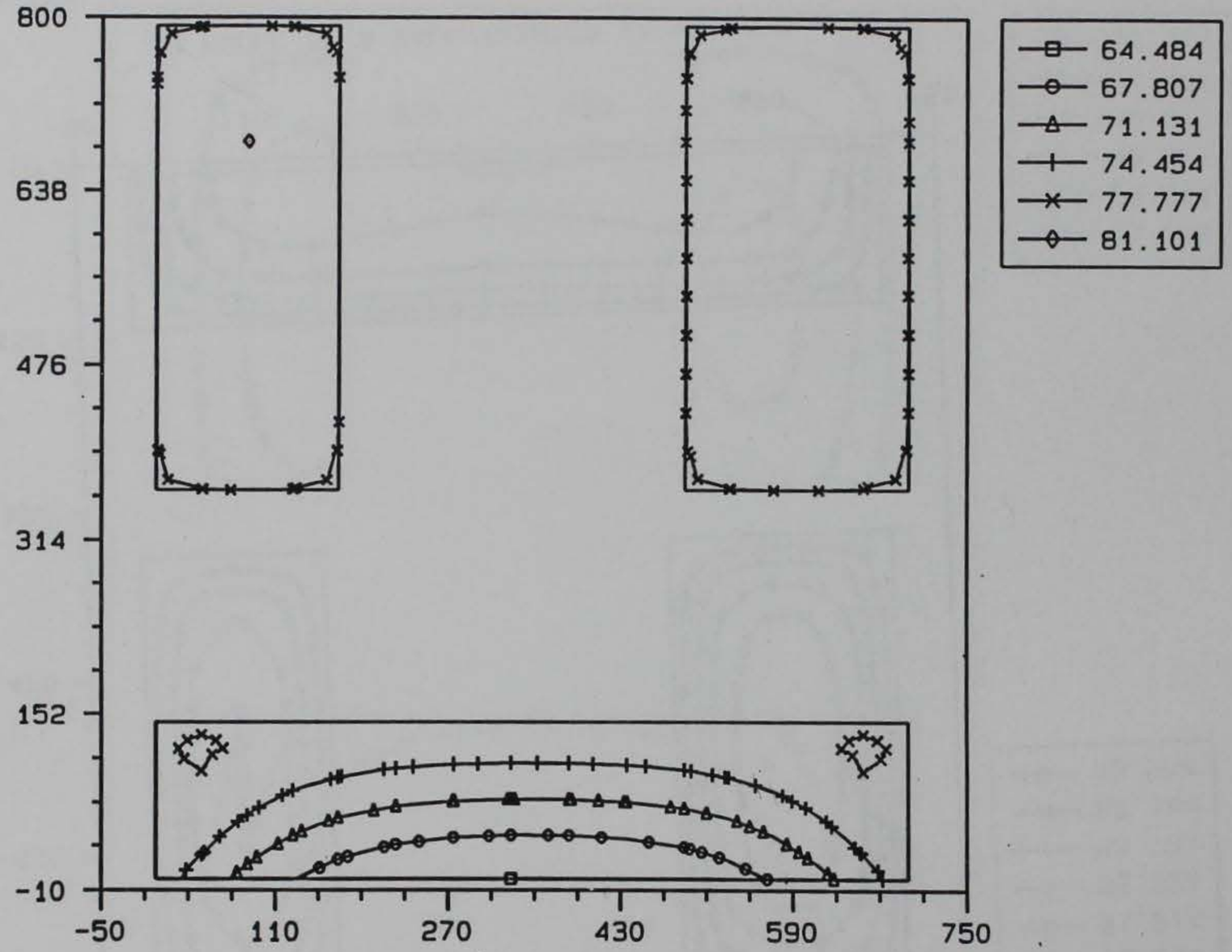

3D MODEL OF A WALL, TAINTER VALVE MONOLITH

Frame 5 117_t2c.051

ANAPOST 3.3x 10/19/93

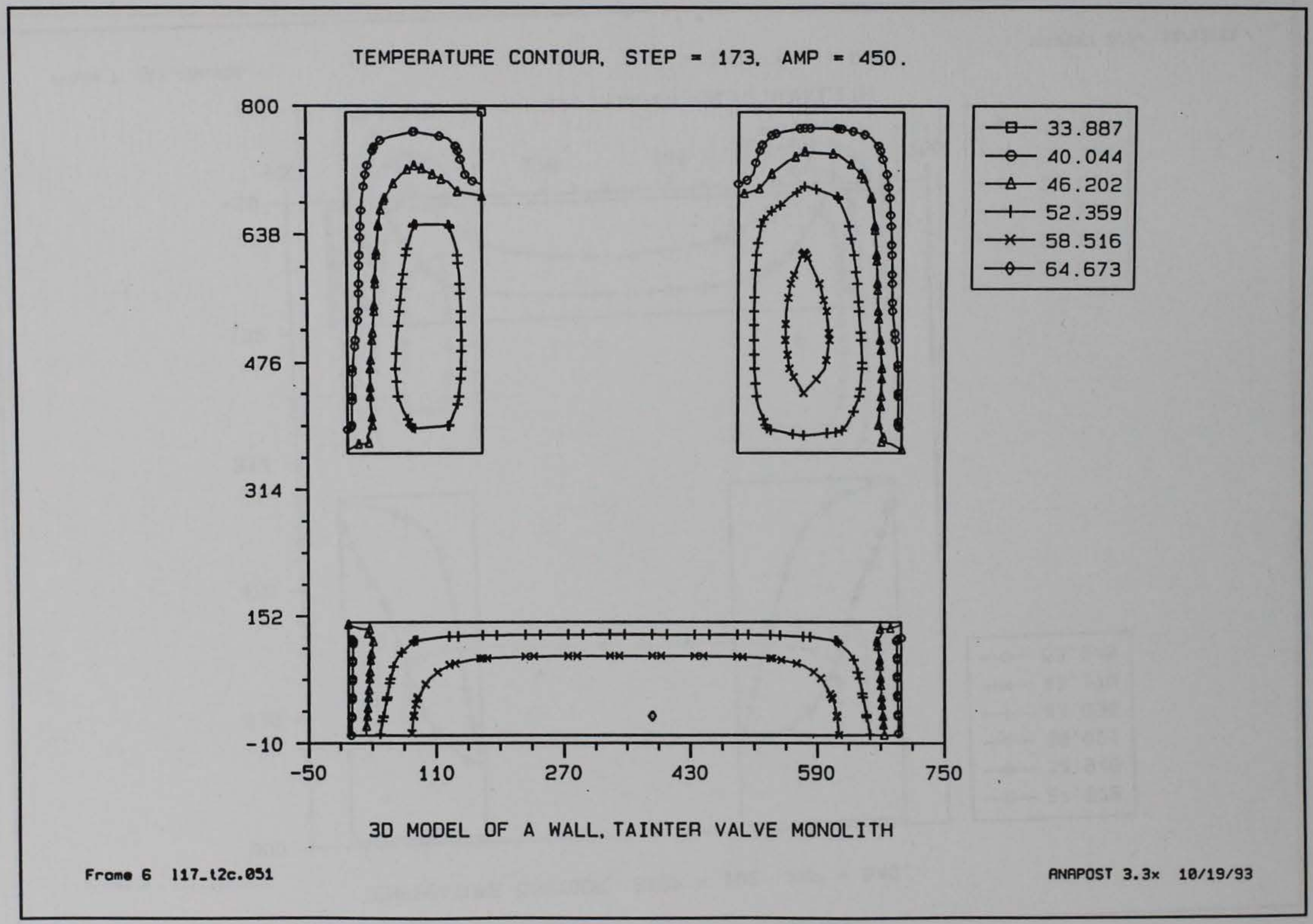
TEMPERATURE CONTOUR, STEP = 173, AMP = 450.
800
638
476
314
152
-10
-50
110
270
430
590
750
33.887
40.044
46.202
52.359
58.516
64.673
3D MODEL OF A WALL, TAINTER VALVE MONOLITH
Frame 6 117_t2c.051
ANAPOST 3.3x 10/19/93

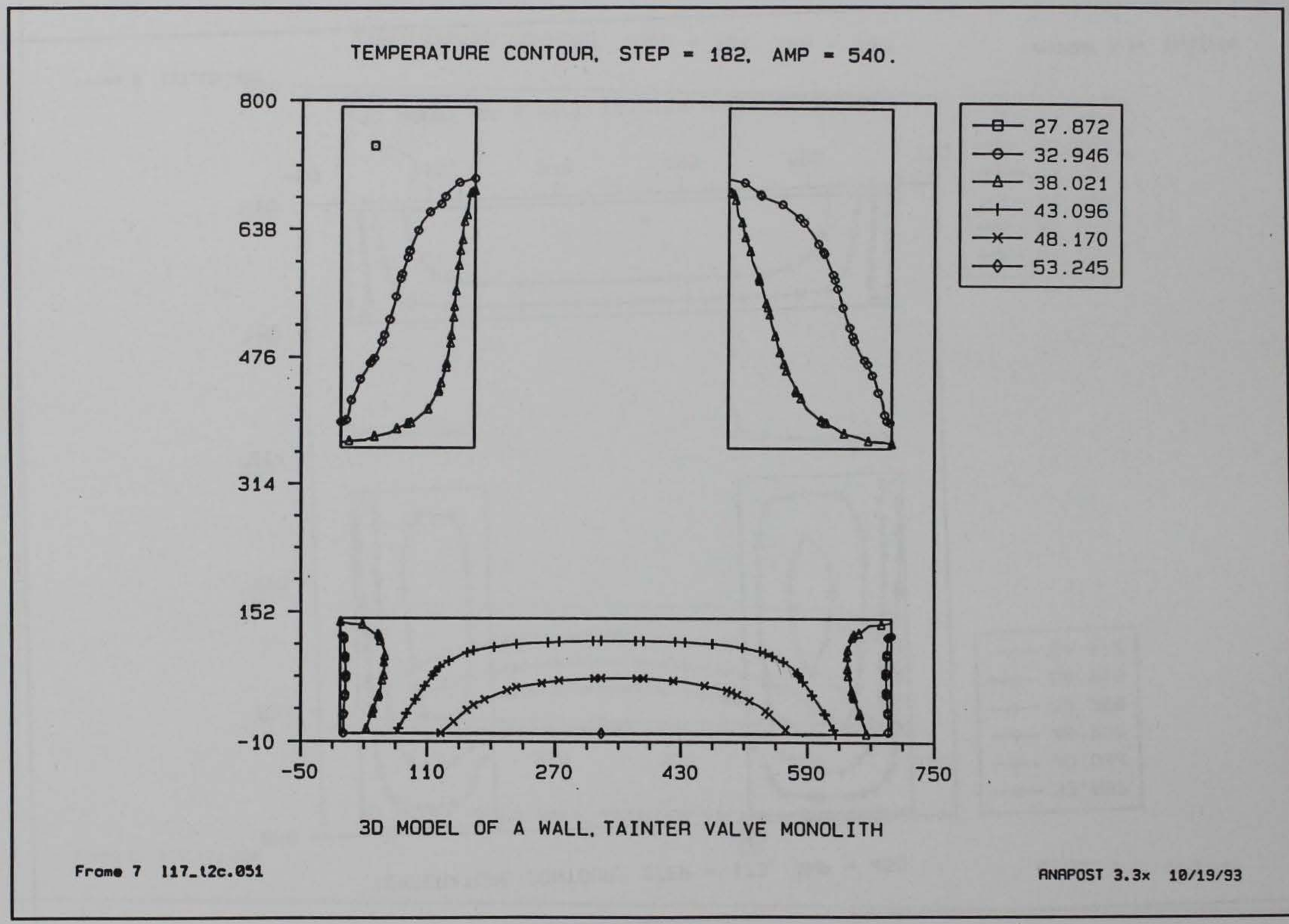
TEMPERATURE CONTOUR, STEP = 182, AMP = 540.
800
638
476
314
152
-10
-50
110
270
430
590
750
27.872
32.946
38.021
43.096
48.170
53.245
3D MODEL OF A WALL, TAINTER VALVE MONOLITH
Frome 7 117_t2c.051
ANAPOST 3.3x 10/19/93

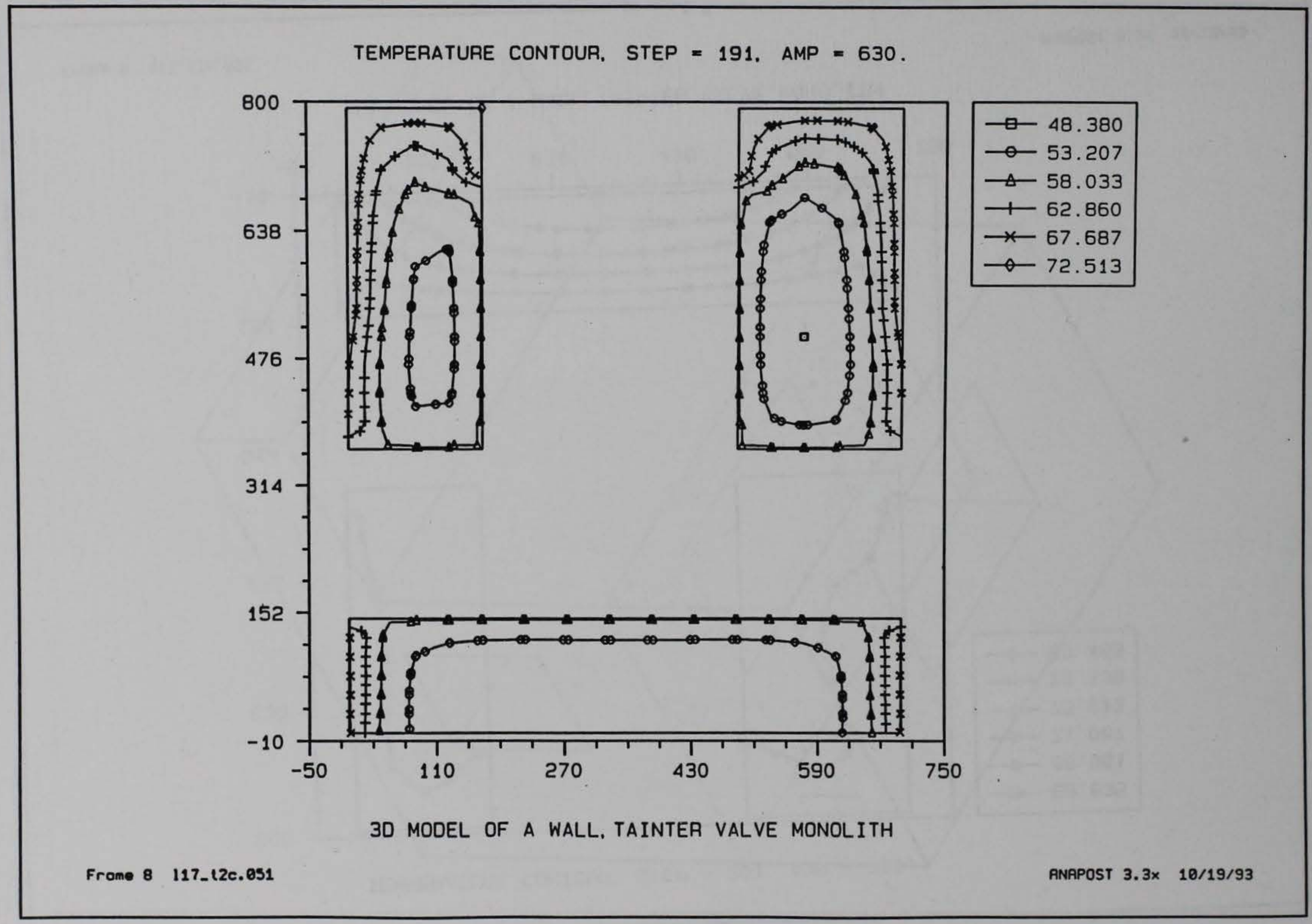
TEMPERATURE CONTOUR, STEP = 191, AMP = 630.
800
638
476
314
152
-10
-50
110
270
430
590
750
48.380
53.207
58.033
62.860
67.687
72.513
3D MODEL OF A WALL, TAINTER VALVE MONOLITH
Frame 8 117_t2c.051
ANAPOST 3.3x 10/19/93

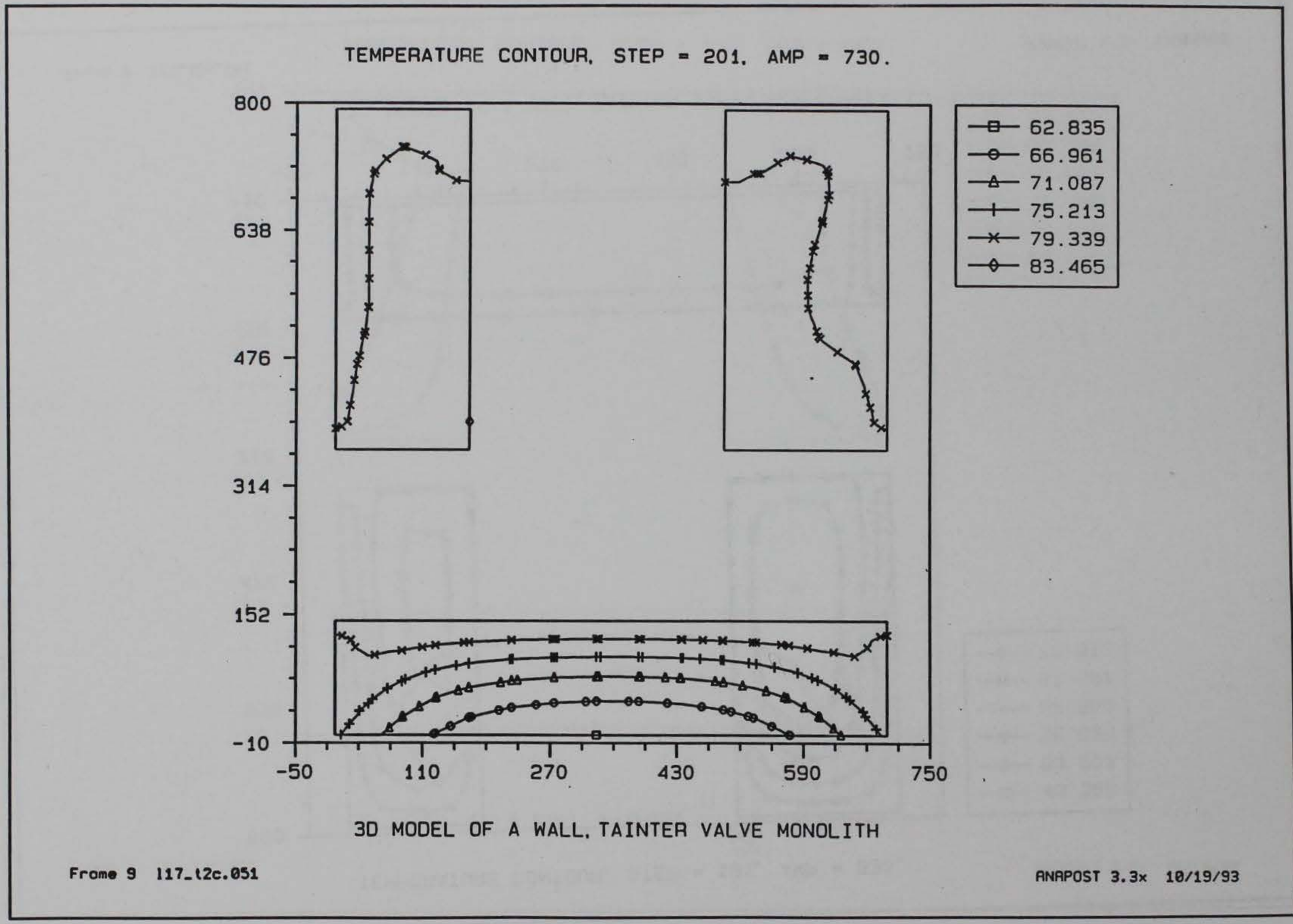
TEMPERATURE CONTOUR, STEP = 201, AMP = 730.
800
638
476
314
152
-10
-50
110
270
430
590
750
62.835
66.961
71.087
75.213
79.339
83.465
3D MODEL OF A WALL, TAINTER VALVE MONOLITH
Frome 9 117_t2c.051
ANAPOST 3.3x 10/19/93

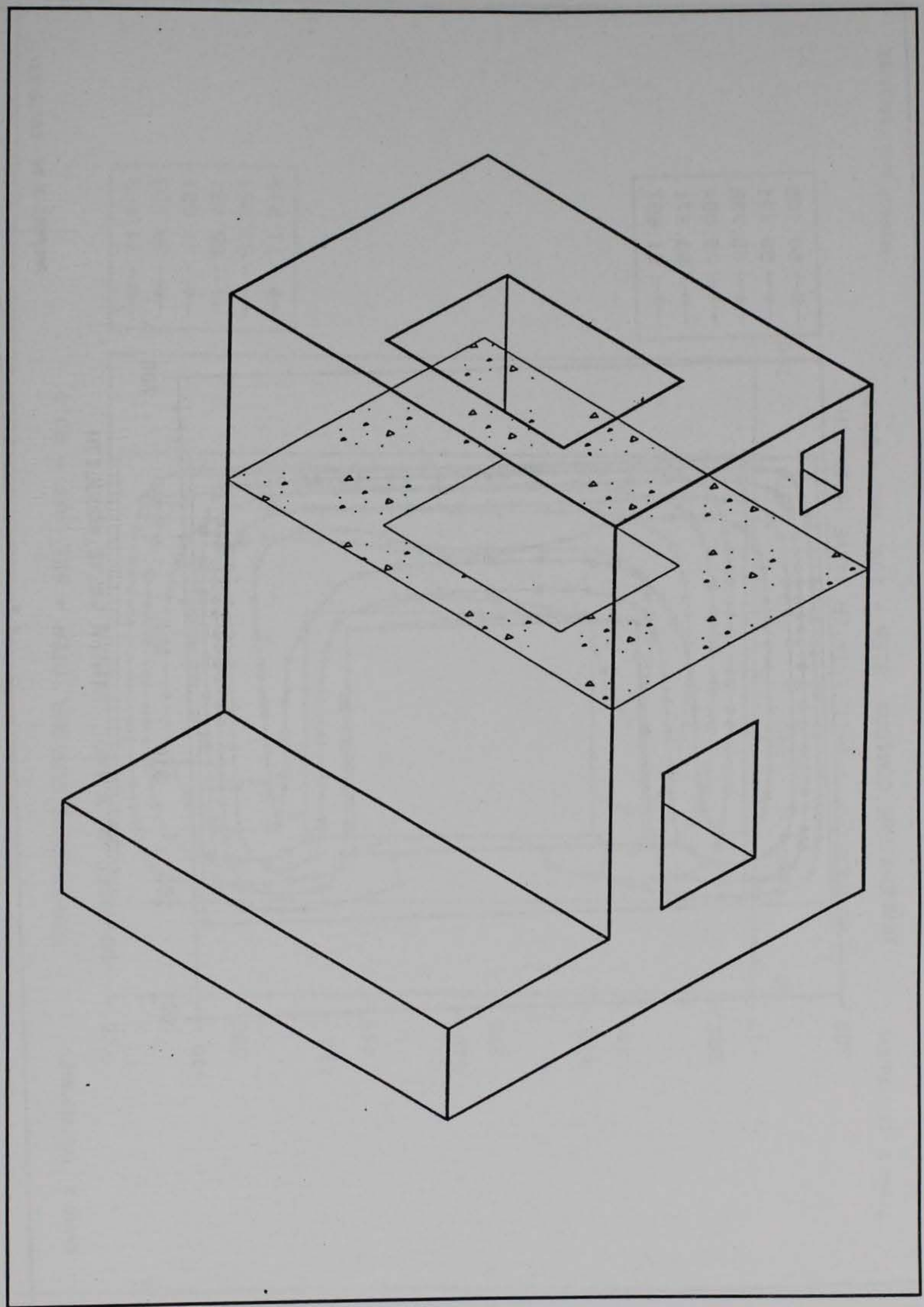

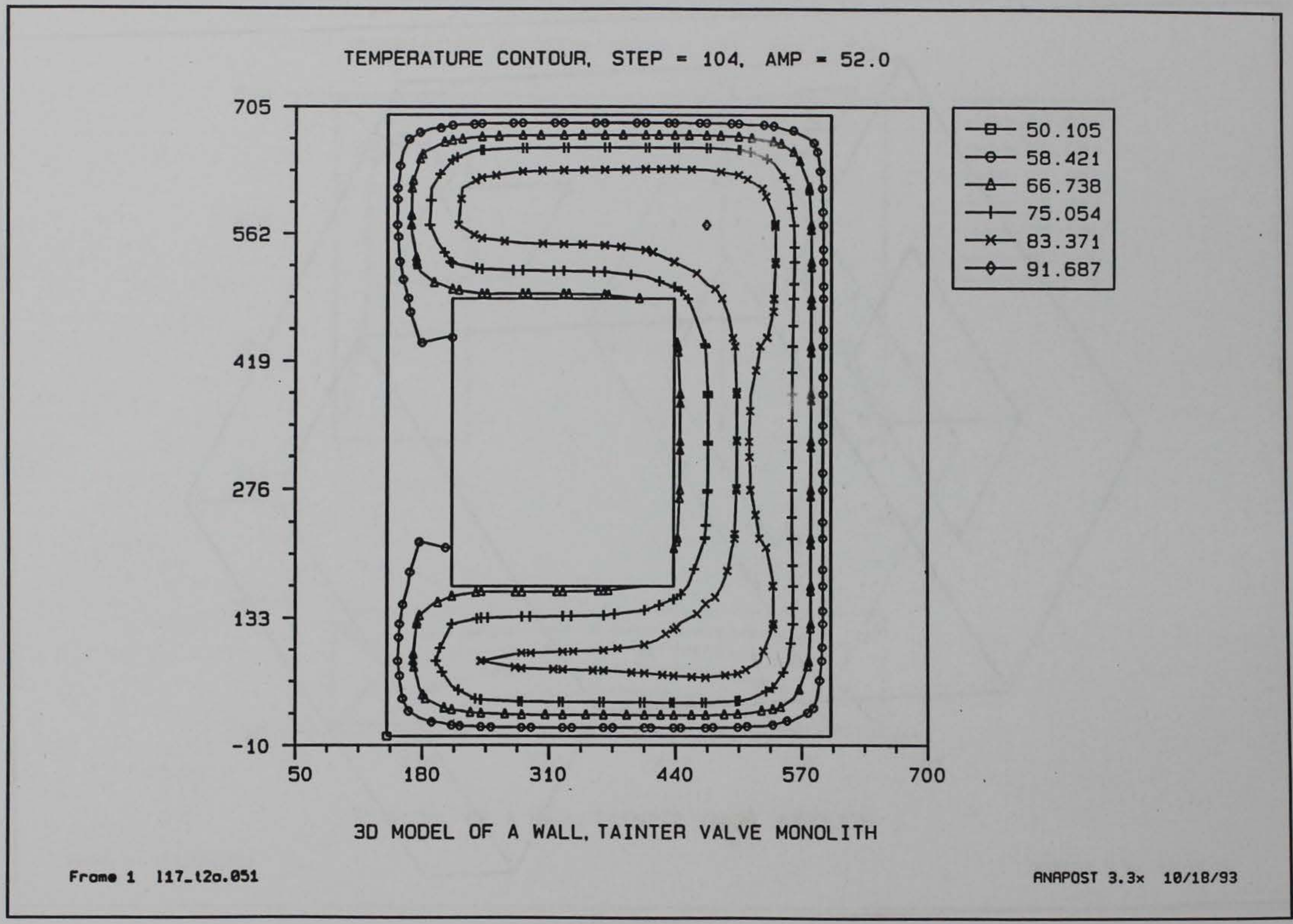
TEMPERATURE CONTOUR, STEP = 104, AMP = 52.0
705
562
419
276
133
-10
50
180
310
440
570
700
50.105
58.421
66.738
75.054
83.371
91.687
3D MODEL OF A WALL, TAINTER VALVE MONOLITH
Frame 1 117_t2a.051
ANAPOST 3.3x 10/18/93

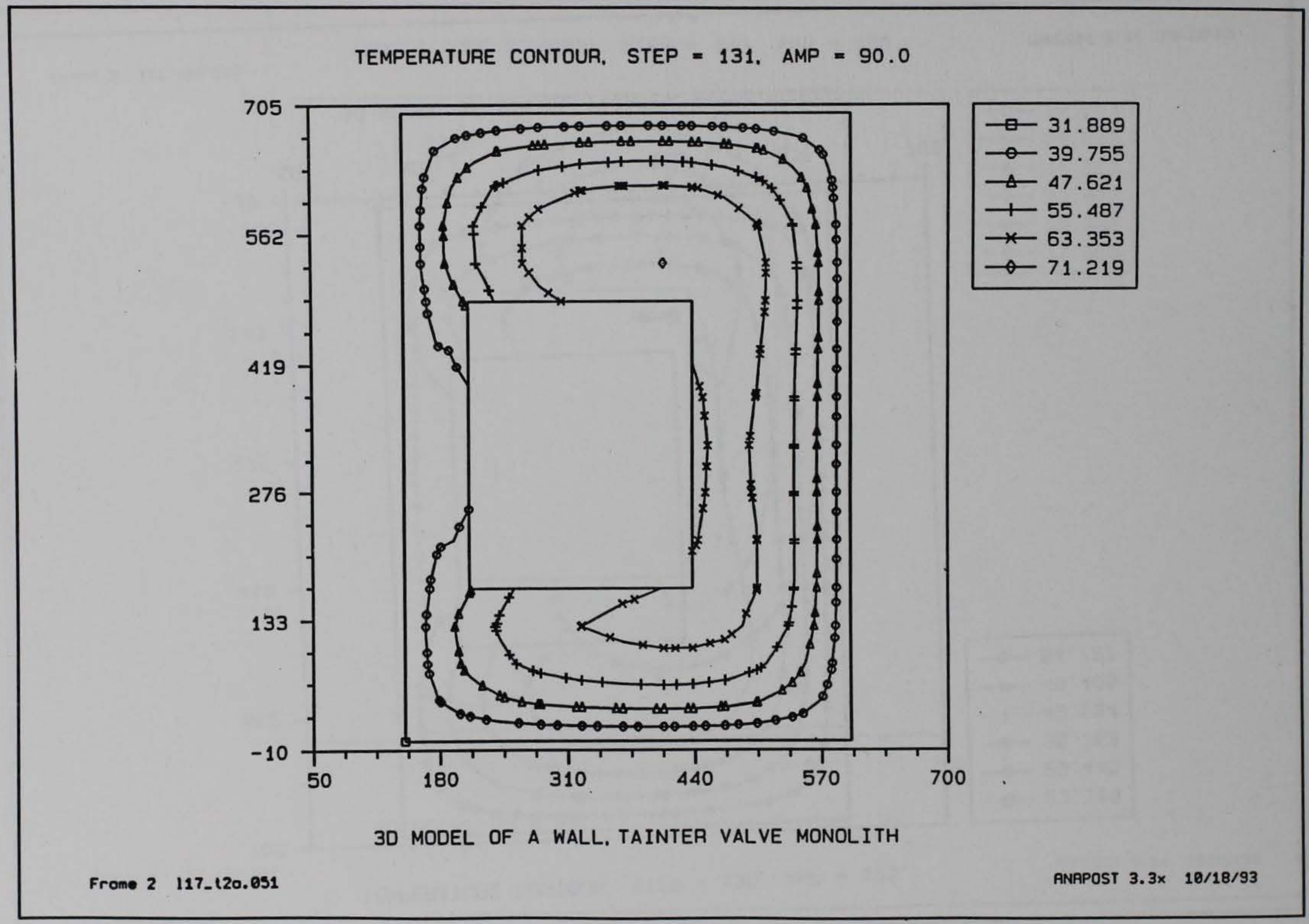
TEMPERATURE CONTOUR, STEP = 131, AMP = 90.0
705
562
419
276
133
-10
50
180
310
440
570
700
31.889
39.755
47.621
55.487
63.353
71.219
3D MODEL OF A WALL, TAINTER VALVE MONOLITH
Frame 2 117_t2o.051
ANAPOST 3.3x 10/18/93

TEMPERATURE CONTOUR, STEP = 138, AMP = 125.

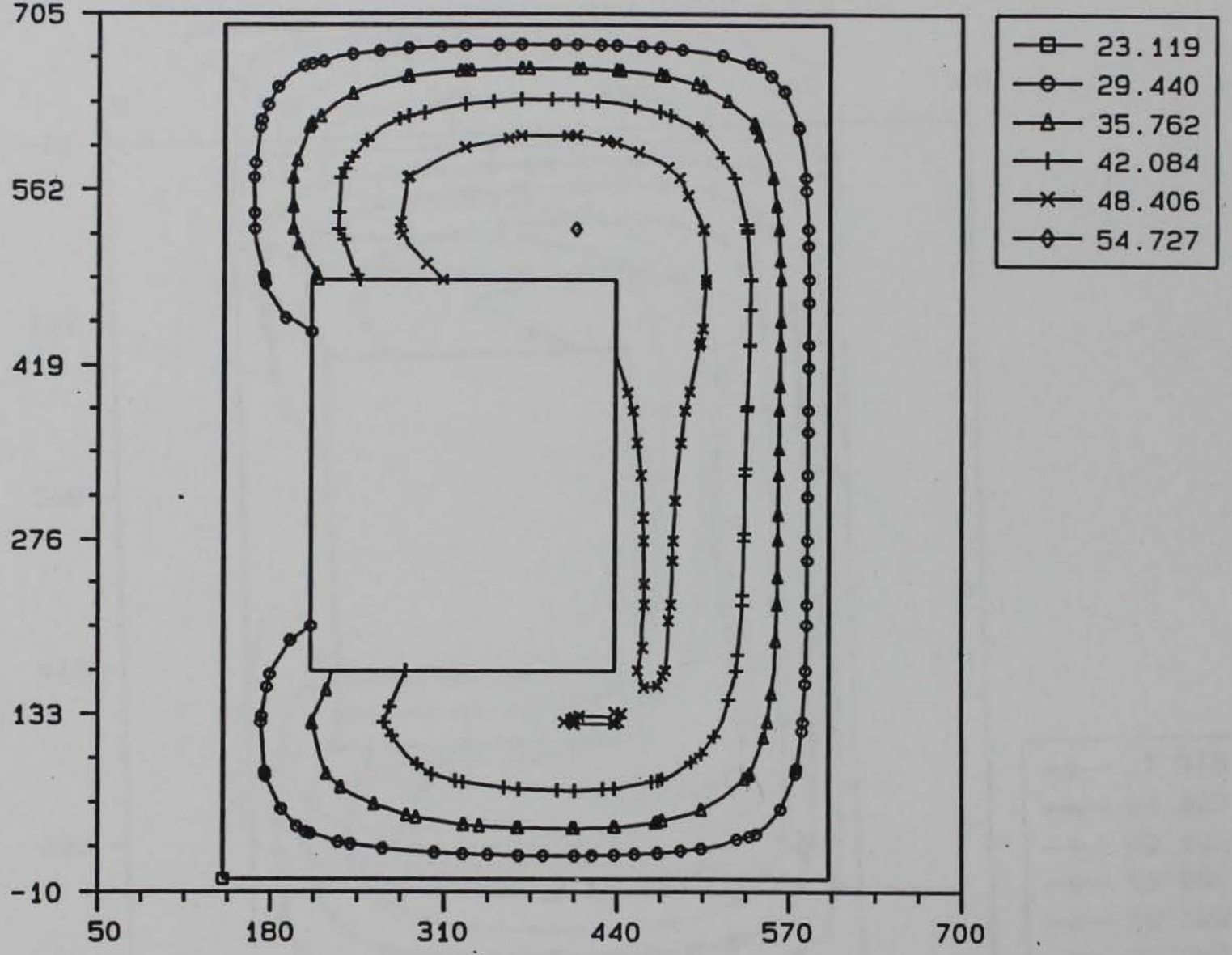

3D MODEL OF A WALL, TAINTER VALVE MONOLITH

Frame 3 117_t2o.051

ANAPOST 3.3x 10/18/93

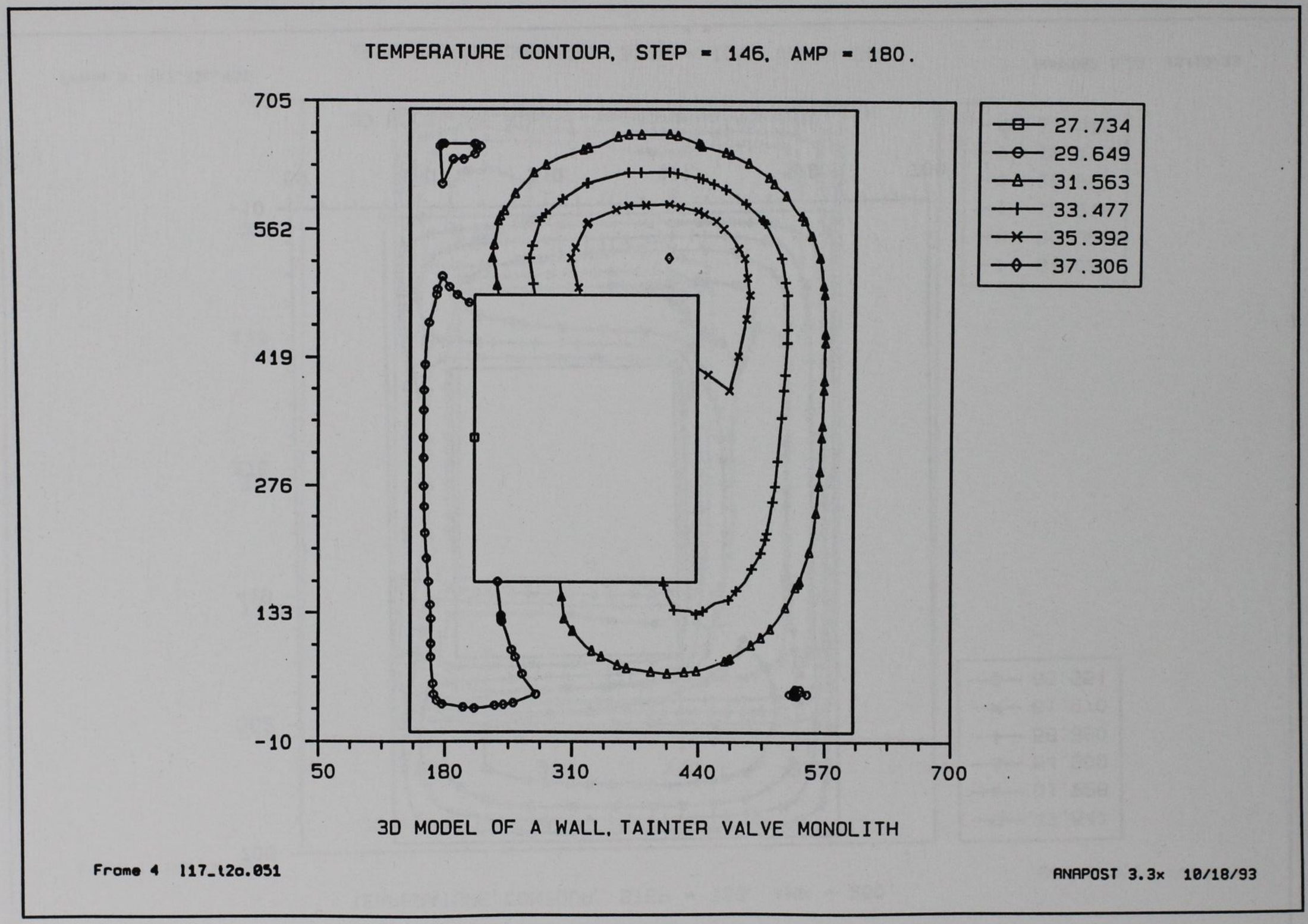
TEMPERATURE CONTOUR, STEP = 146, AMP = 180.
705
562
419
276
133
-10
50
180
310
440
570
700
27.734
29.649
31.563
33.477
35.392
37.306
3D MODEL OF A WALL, TAINTER VALVE MONOLITH
Frame 4 117_t2o.051
ANAPOST 3.3x 10/18/93

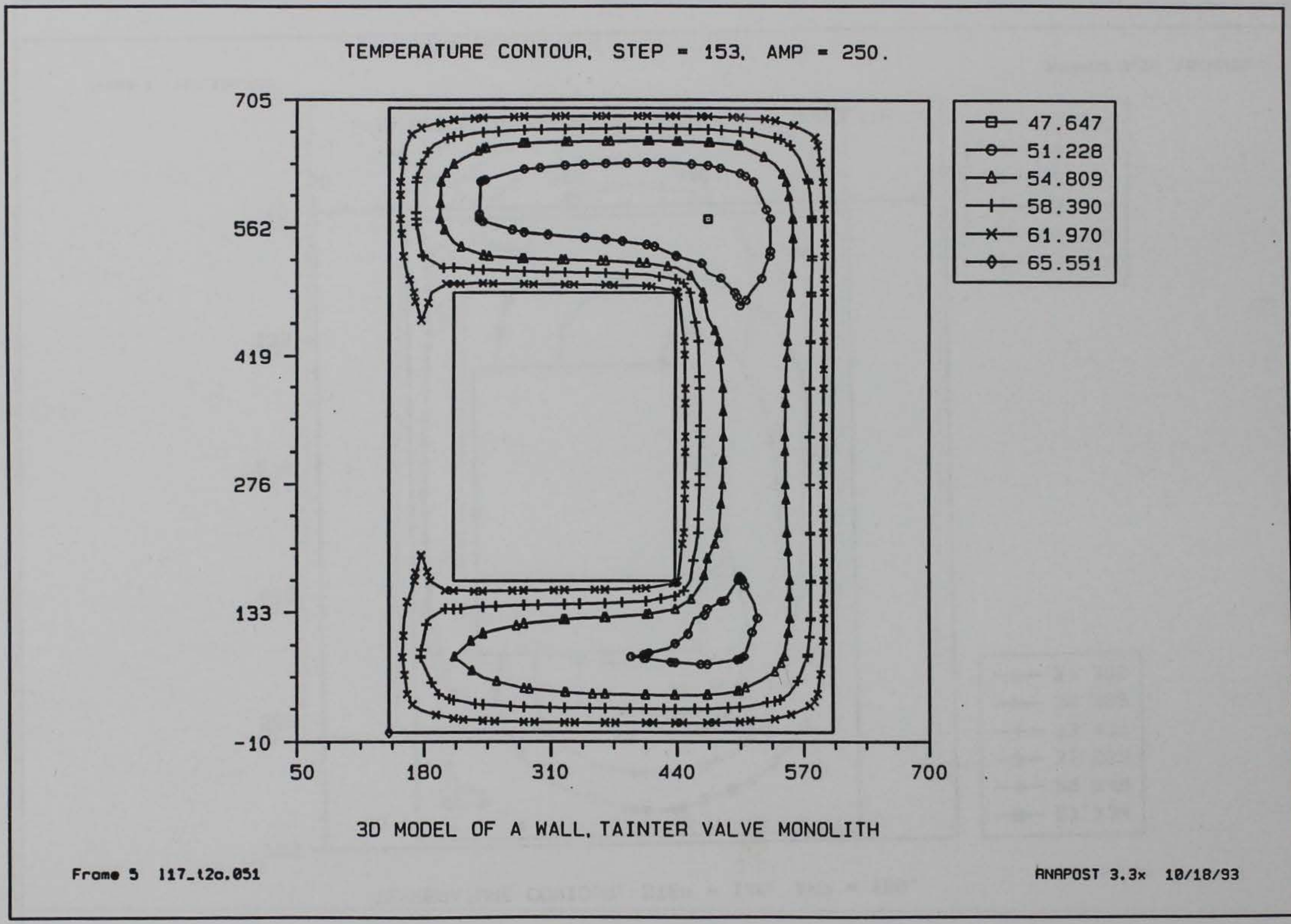
TEMPERATURE CONTOUR, STEP = 153, AMP = 250.
705
562
419
276
133
-10
50
180
310
440
570
700
47.647
51.228
54.809
58.390
61.970
65.551
3D MODEL OF A WALL, TAINTER VALVE MONOLITH
Frame 5 117_t2a.051
ANAPOST 3.3x 10/18/93

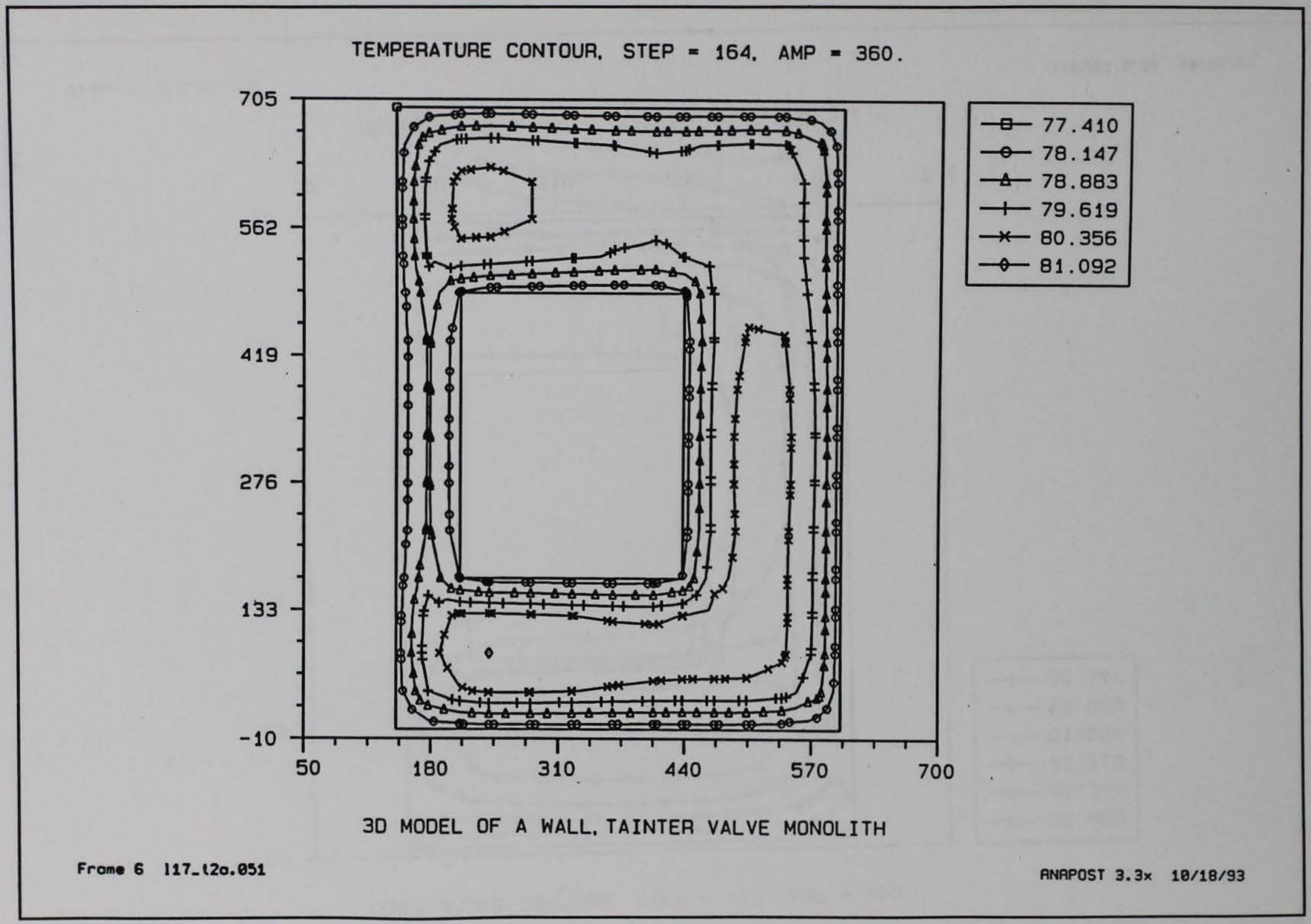
TEMPERATURE CONTOUR, STEP = 164, AMP = 360.
705
562
419
276
133
-10
50
180
310
440
570
700
77.410
78.147
78.883
79.619
80.356
81.092
3D MODEL OF A WALL, TAINTER VALVE MONOLITH
Frame 6 117_t2a.051
ANAPOST 3.3x 10/18/93

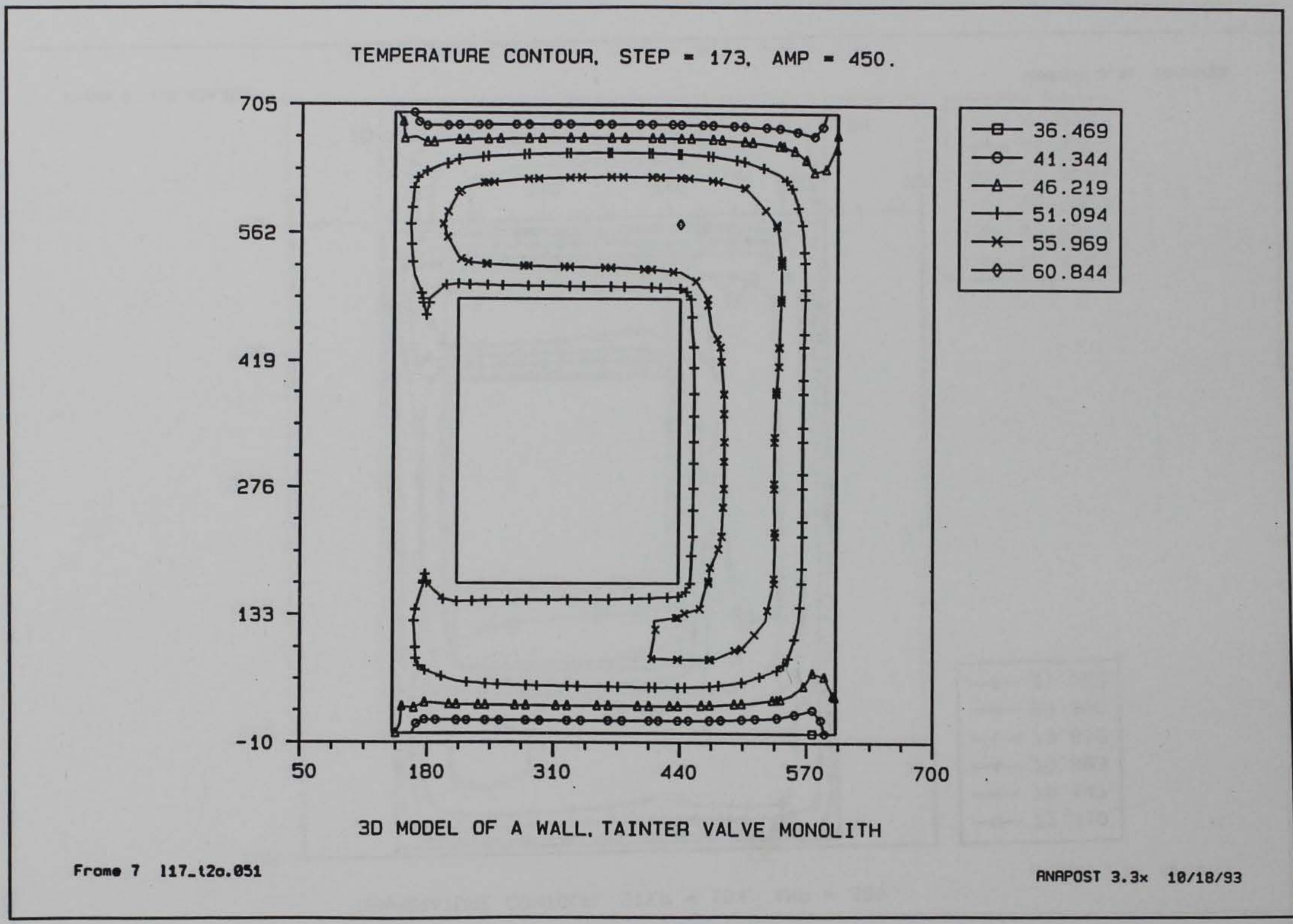
TEMPERATURE CONTOUR, STEP = 173, AMP = 450.
705
562
419
276
133
-10
50
180
310
440
570
700
36.469
41.344
46.219
51.094
55.969
60.844
3D MODEL OF A WALL, TAINTER VALVE MONOLITH
Frame 7 117_t2o.051
ANAPOST 3.3x 10/18/93

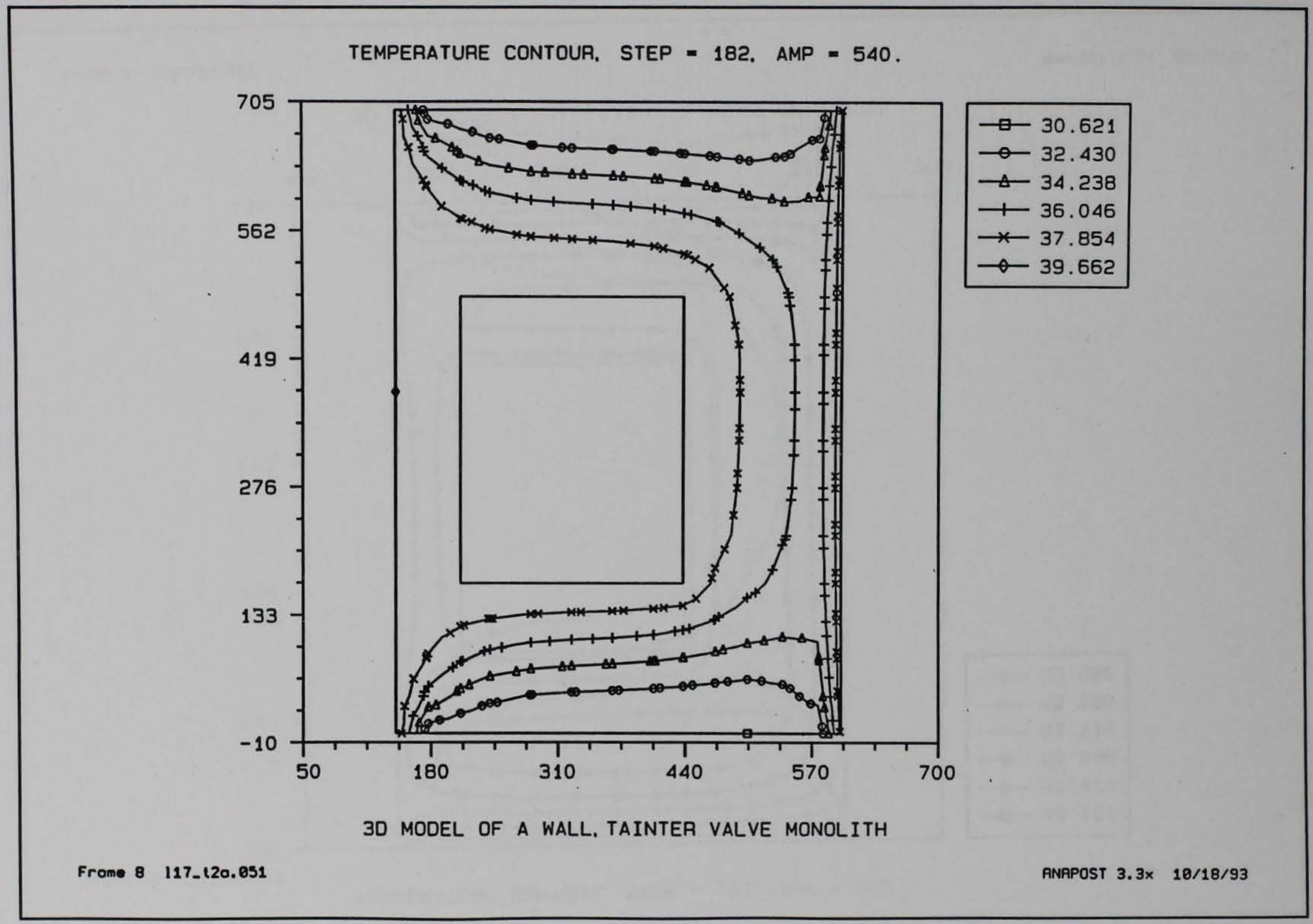
TEMPERATURE CONTOUR, STEP = 182, AMP = 540.
705
562
419
276
133
-10
50
180
310
440
570
700
30.621
32.430
34.238
36.046
37.854
39.662
3D MODEL OF A WALL, TAINTER VALVE MONOLITH
Frame 8 117_t2a.051
ANAPOST 3.3x 10/18/93

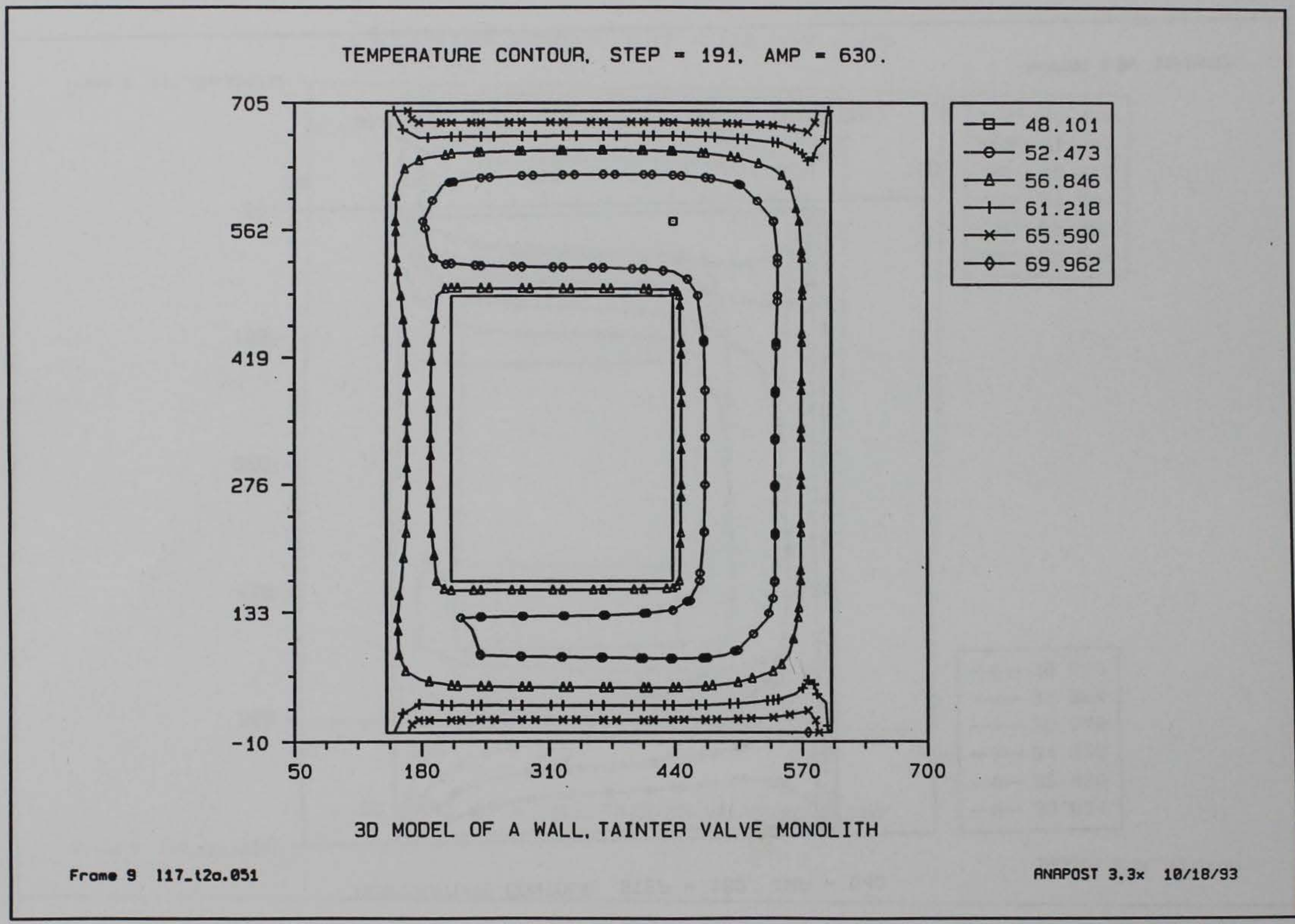
TEMPERATURE CONTOUR, STEP = 191, AMP = 630.
705
562
419
276
133
-10
50
180
310
440
570
700
48.101
52.473
56.846
61.218
65.590
69.962
3D MODEL OF A WALL, TAINTER VALVE MONOLITH
Frame 9 117_t2o.051
ANAPOST 3.3x 10/18/93

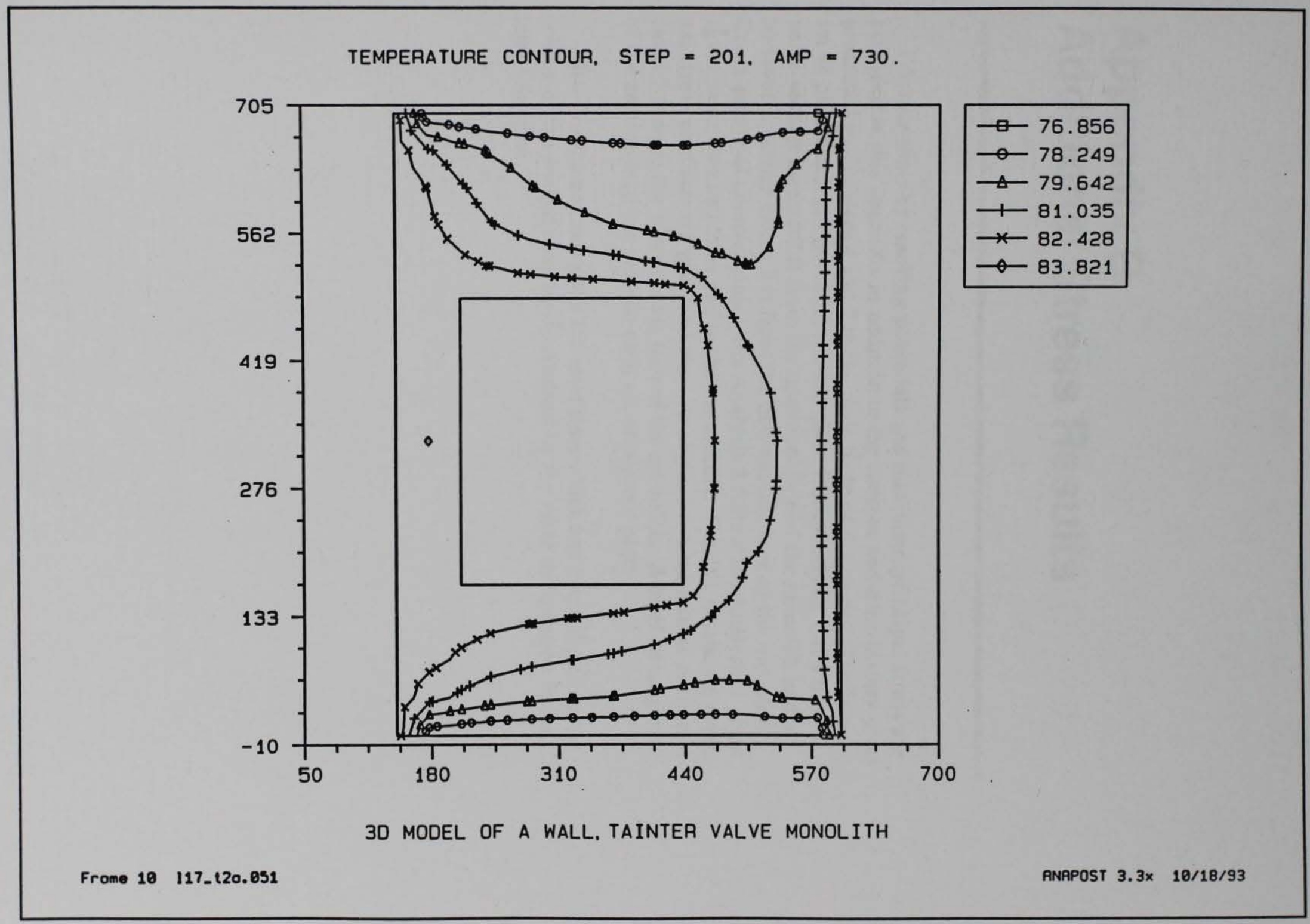
TEMPERATURE CONTOUR, STEP = 201, AMP = 730.
705
562
419
276
133
-10
50
180
310
440
570
700
76.856
78.249
79.642
81.035
82.428
83.821
3D MODEL OF A WALL, TAINTER VALVE MONOLITH
Frame 10 117_t2a.051
ANAPOST 3.3x 10/18/93

Appendix B
Additional Stress Results

Contour plots of cracking potentials and maximum principal stress are provided in this appendix in addition to the contour and time-history plots presented in Chapters 4 and 7 in the main body of the report. The initial set of plots are crack potential contour plots from Analysis 1 at a transverse section located 7 ft from the upstream face of the monolith and a transverse section taken 7 ft from the downstream face of the monolith. Crack potential contour plots from Analysis 2 follow the Analysis 1 plots at the same two locations and in the same order. Finally, maximum principal stress contours are provided from Analysis 2 at a transverse section located 7 ft from the downstream face of the monolith. A brief description of the section is given prior to each set of contour plots.

Also, for the contour plots the total time which has elapsed during the course of the analysis can be determined by the AMP designation at the top of the plot.

Transverse Section Located 7 ft from the Upstream Face of the Monolith

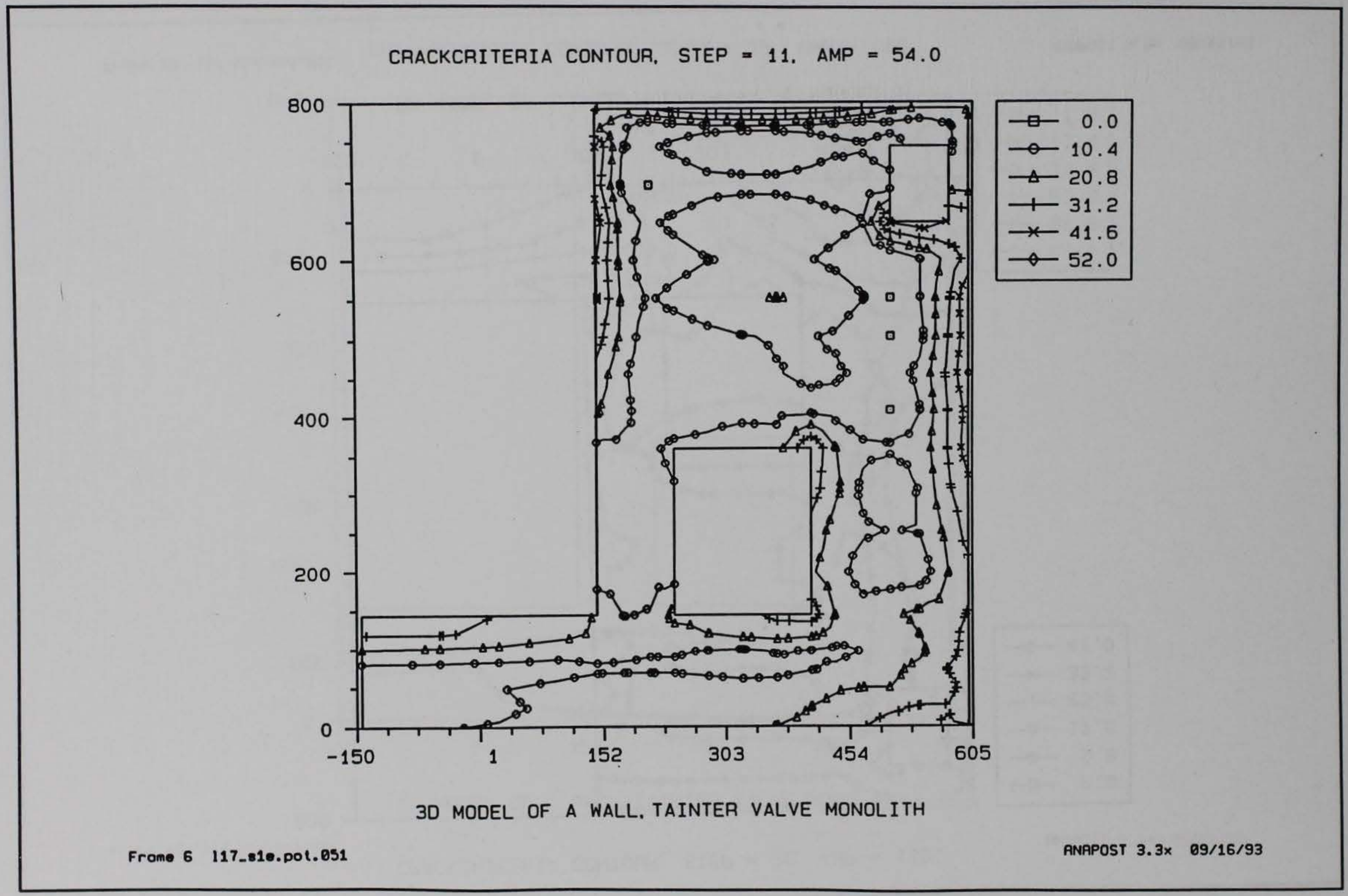
CRACKCRITERIA CONTOUR, STEP = 11, AMP = 54.0
800
600
400
200
0
-150
1
152
303
454
605
0.0
10.4
20.8
31.2
41.6
52.0
3D MODEL OF A WALL, TAINTER VALVE MONOLITH
Frame 6 117_s1e.pot.051
ANAPOST 3.3x 09/16/93

CRACKCRITERIA CONTOUR, STEP = 25, AMP = 119.

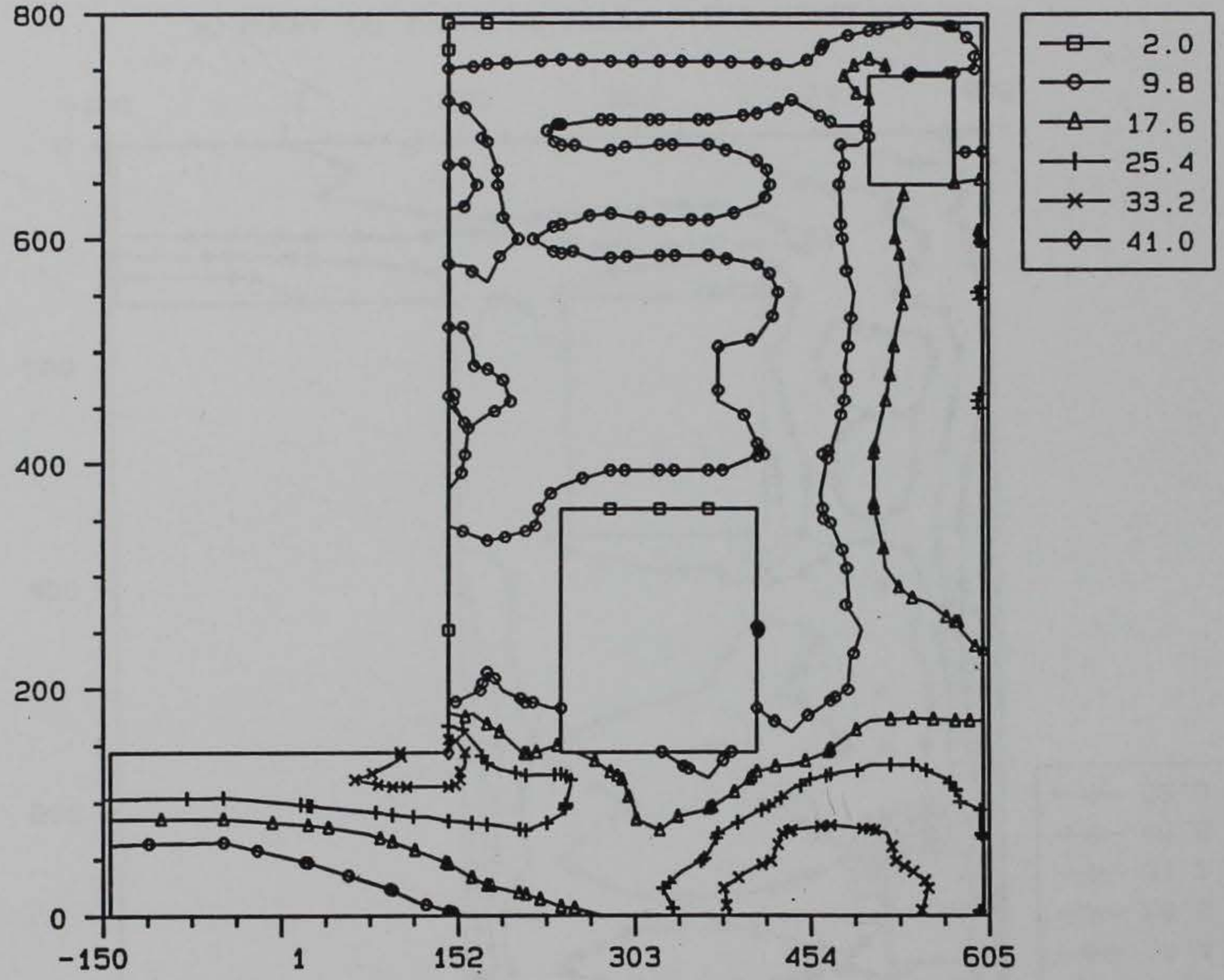

3D MODEL OF A WALL, TAINTER VALVE MONOLITH

Frame 13 117_s1e.pot.051

ANAPOST 3.3x 09/16/93

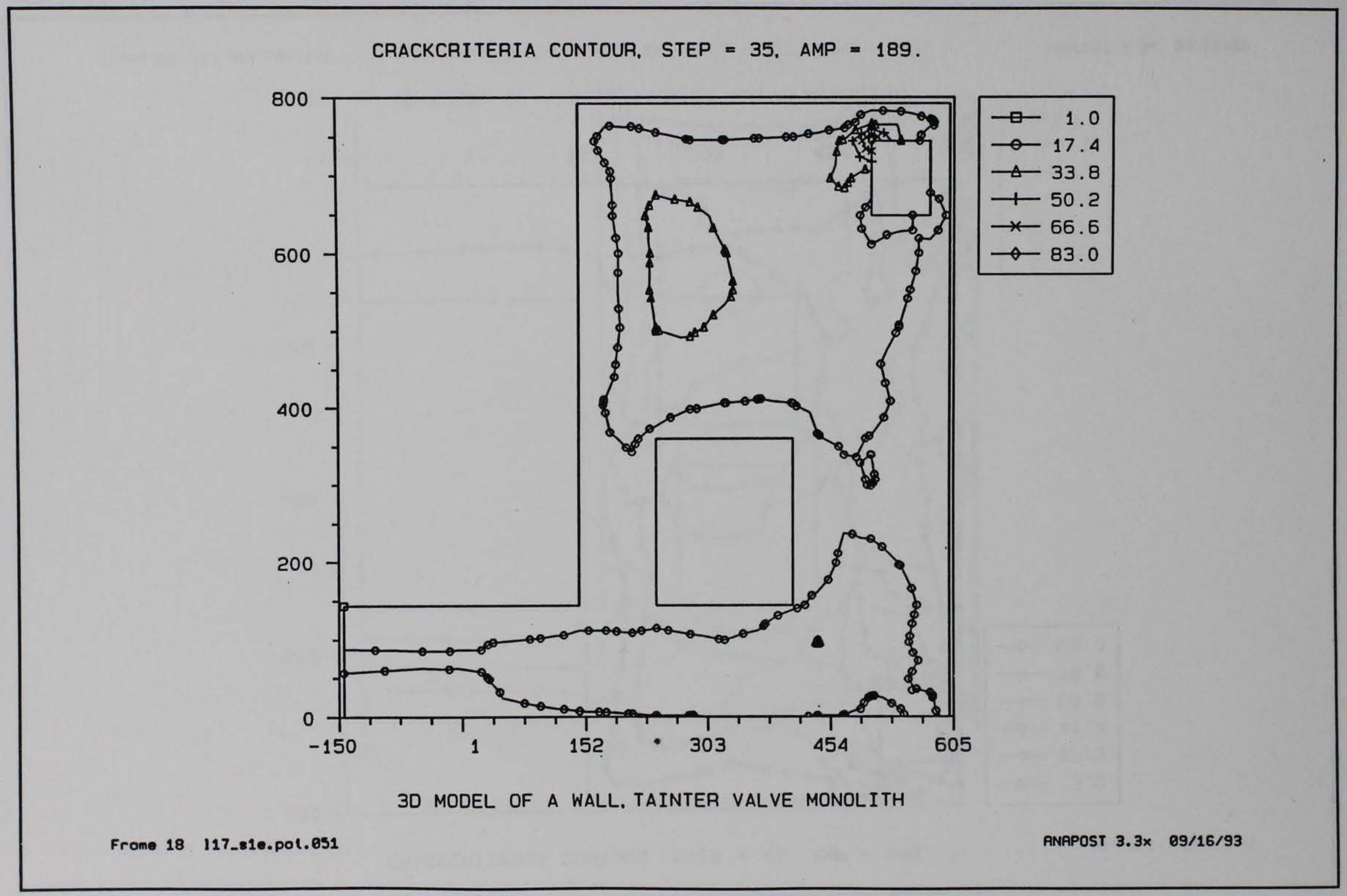
CRACKCRITERIA CONTOUR, STEP = 35, AMP = 189.
800
600
400
200
0
-150
1
152
303
454
605
1.0
17.4
33.8
50.2
66.6
83.0
3D MODEL OF A WALL, TAINTER VALVE MONOLITH
Frome 18 117_s1e.pot.051
ANAPOST 3.3x 09/16/93

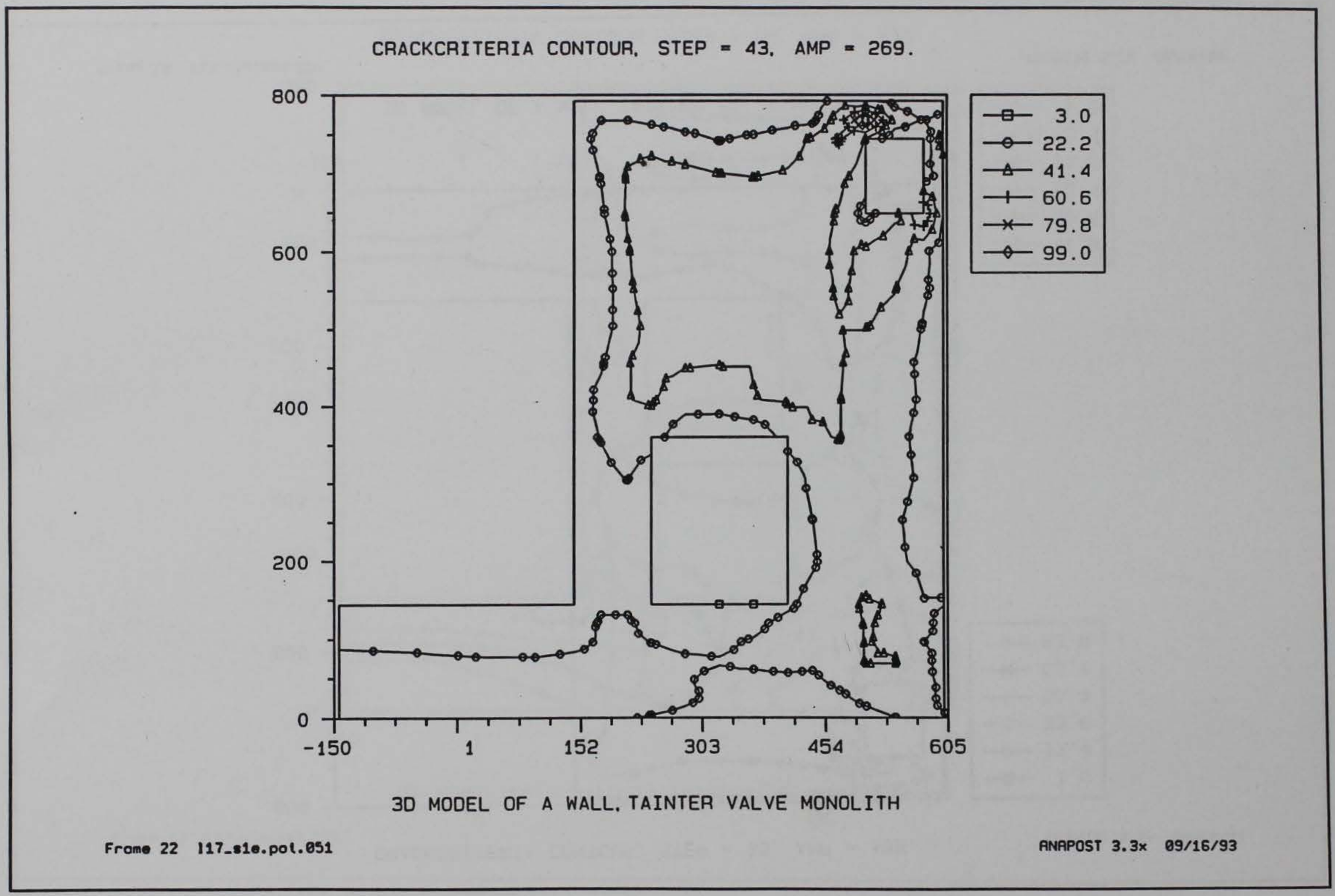
CRACKCRITERIA CONTOUR, STEP = 43, AMP = 269.
800
600
400
200
0
-150
1
152
303
454
605
3.0
22.2
41.4
60.6
79.8
99.0
3D MODEL OF A WALL, TAINTER VALVE MONOLITH
Frame 22 117_s1e.pot.051
ANAPOST 3.3x 09/16/93

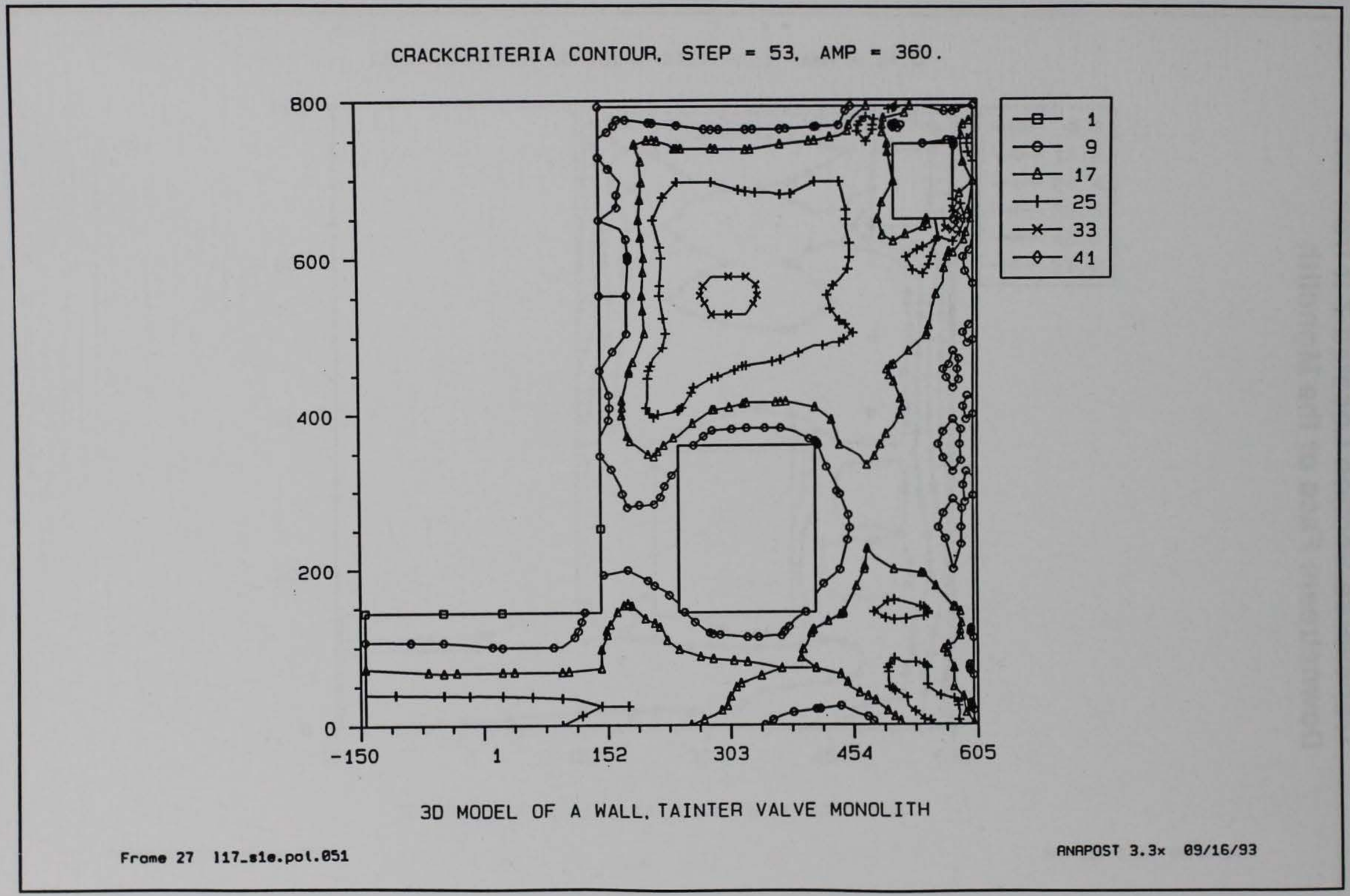
CRACKCRITERIA CONTOUR, STEP = 53, AMP = 360.
800
600
400
200
0
-150
1
152
303
454
605
1
9
17
25
33
41
3D MODEL OF A WALL, TAINTER VALVE MONOLITH
Frame 27 117_s1e.pol.051
ANAPOST 3.3x 09/16/93

Transverse Section Located 7 ft from the Downstream Face of the Monolith

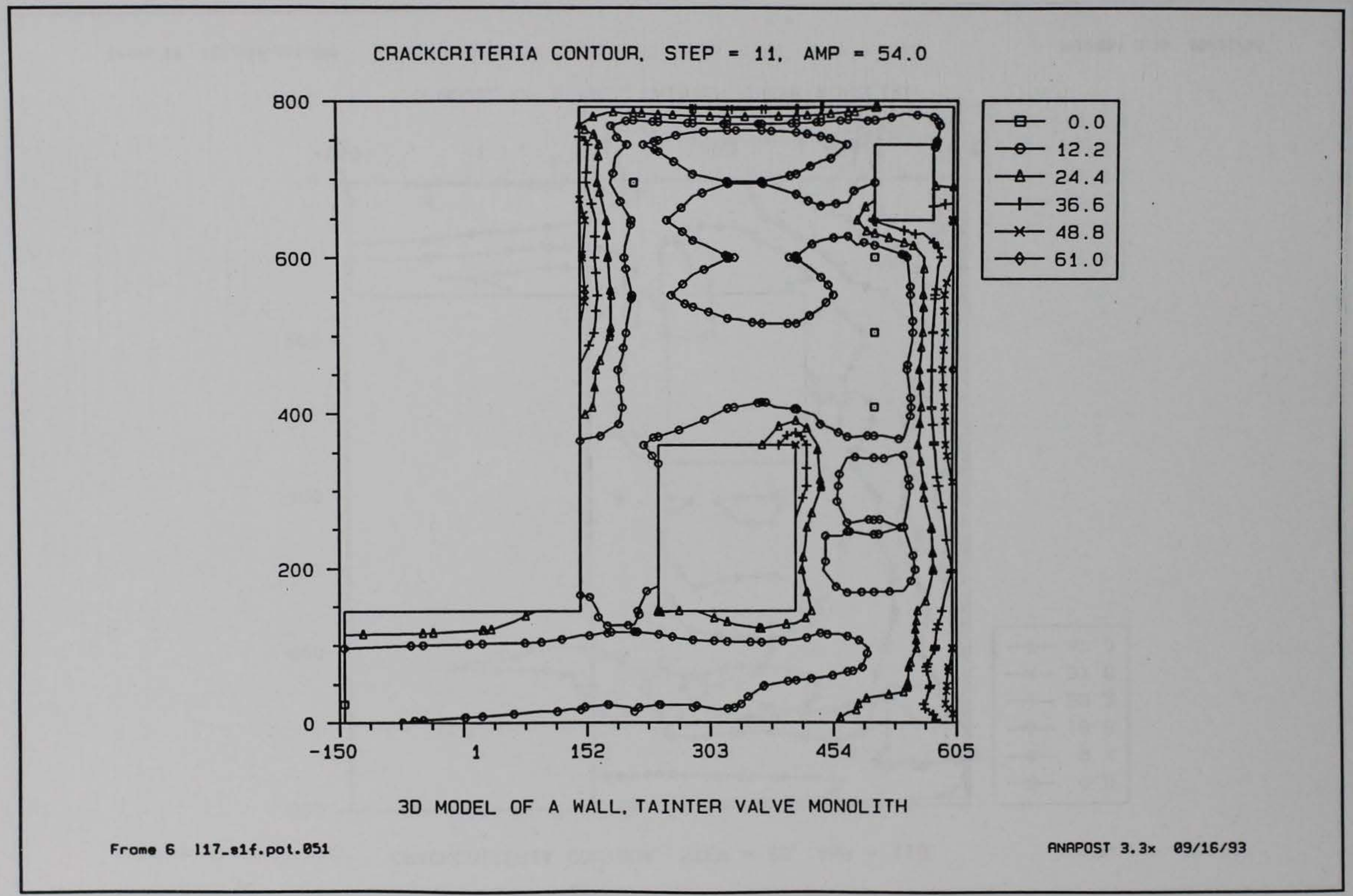
CRACKCRITERIA CONTOUR, STEP = 11, AMP = 54.0
800
600
400
200
0
-150
1
152
303
454
605
0.0
12.2
24.4
36.6
48.8
61.0
3D MODEL OF A WALL, TAINTER VALVE MONOLITH
Frome 6 117_s1f.pot.051
ANAPOST 3.3x 09/16/93

CRACKCRITERIA CONTOUR, STEP = 25, AMP = 119.

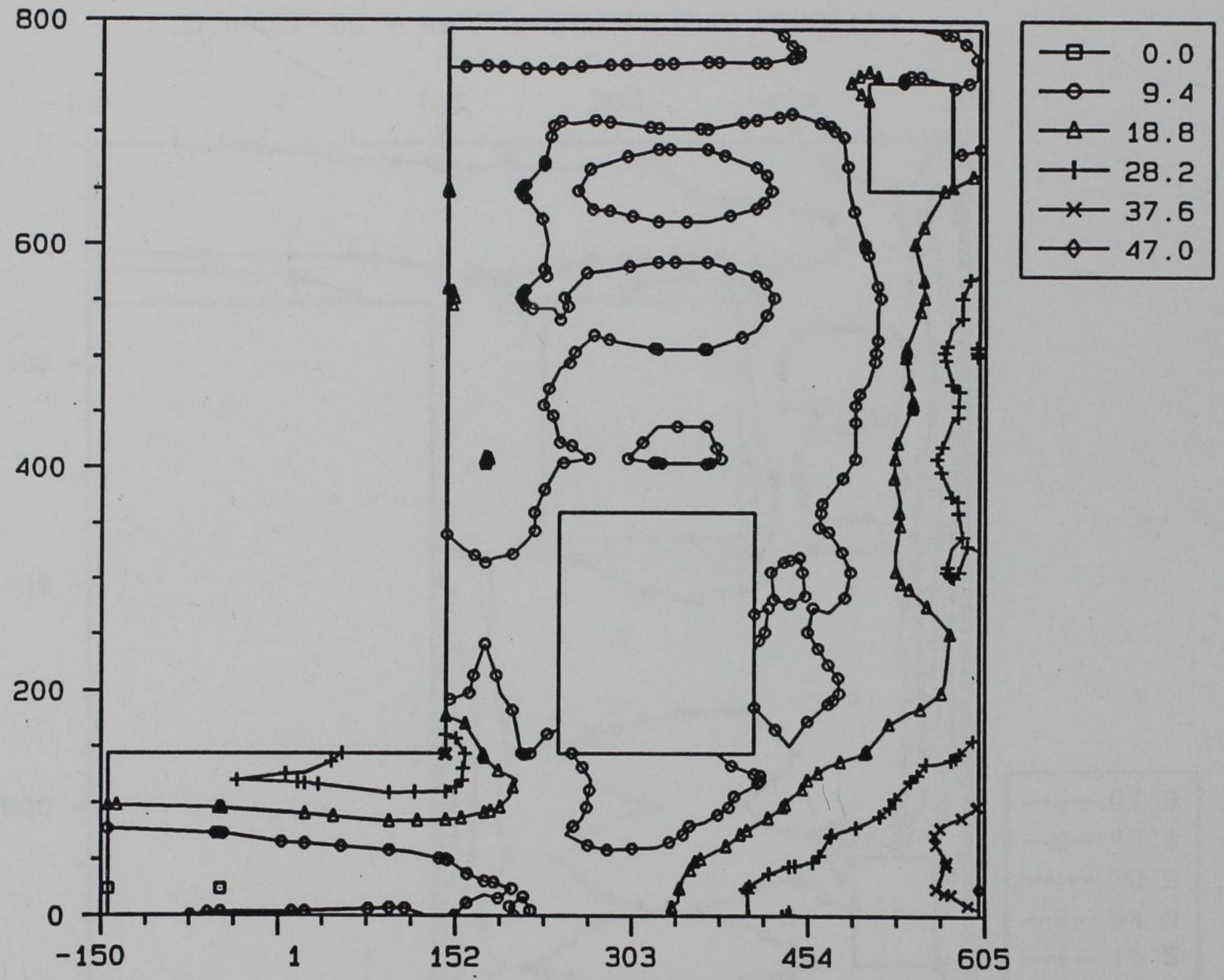

3D MODEL OF A WALL, TAINTER VALVE MONOLITH

Frome 13 117_s1f.pot.051

ANAPOST 3.3x 09/16/93

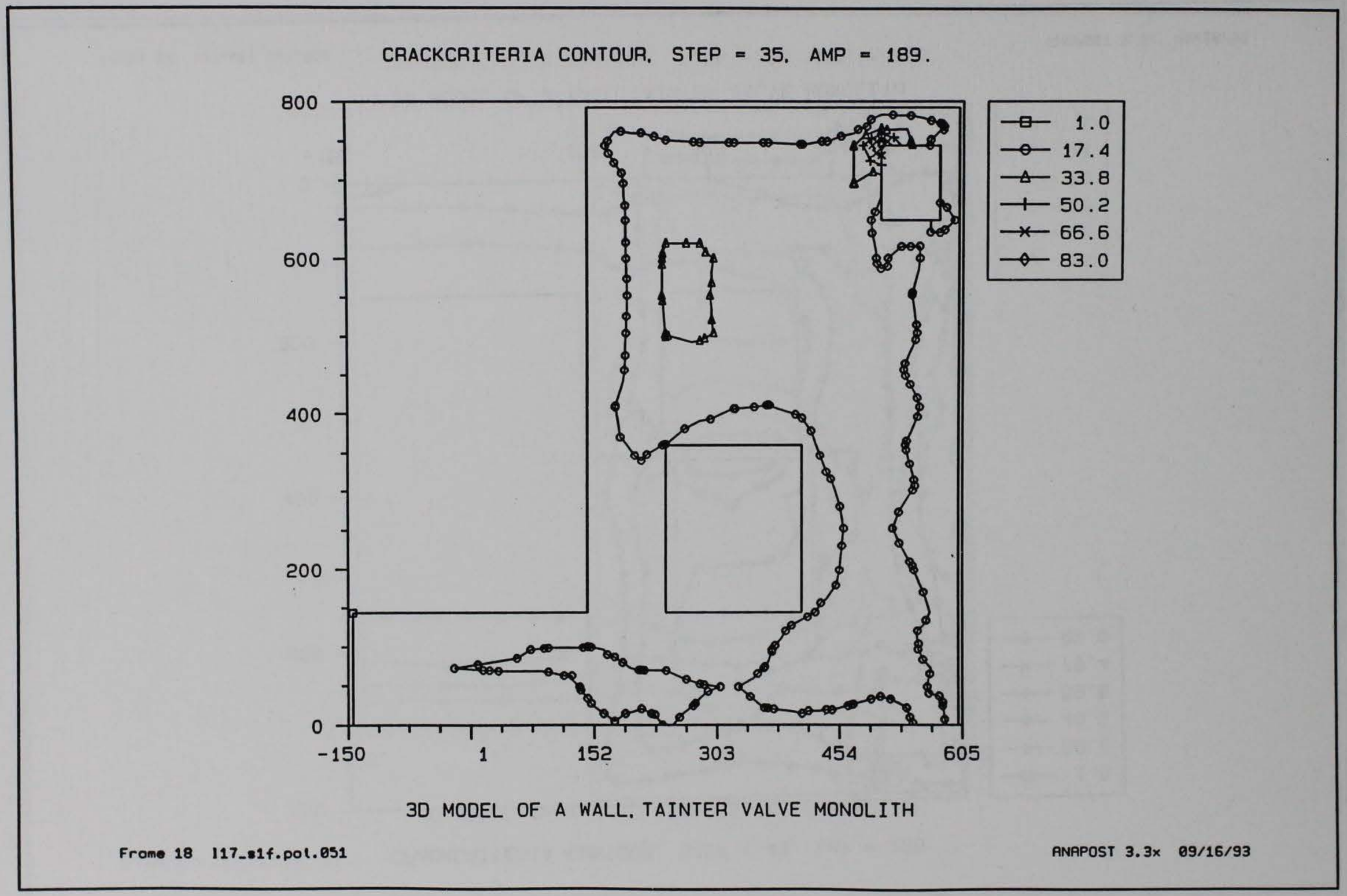
CRACKCRITERIA CONTOUR, STEP = 35, AMP = 189.
800
600
400
200
0
-150
1
152
303
454
605
1.0
17.4
33.8
50.2
66.6
83.0
3D MODEL OF A WALL, TAINTER VALVE MONOLITH
Frame 18 117_s1f.pol.051
ANAPOST 3.3x 09/16/93

CRACKCRITERIA CONTOUR, STEP = 43, AMP = 269.

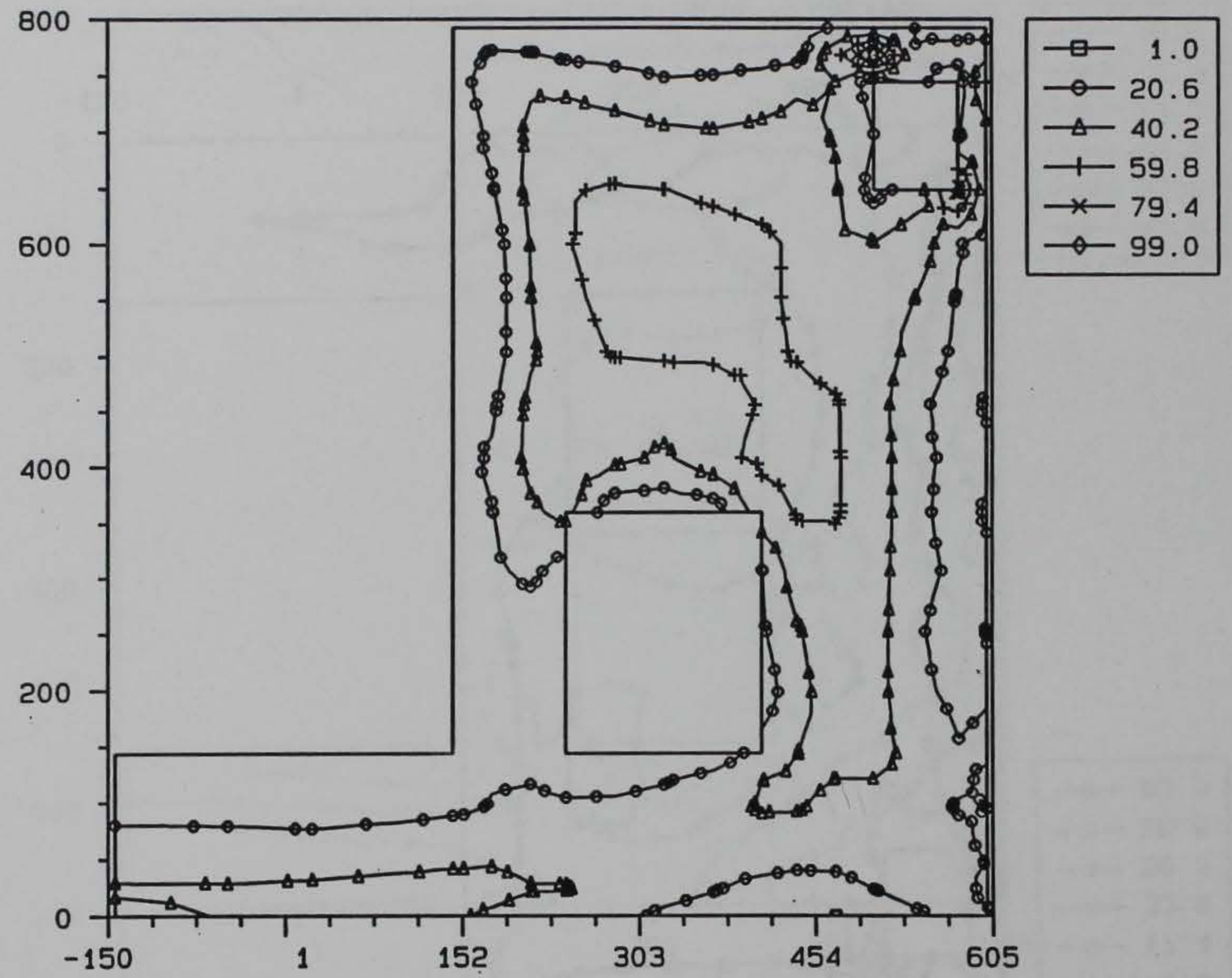

3D MODEL OF A WALL, TAINTER VALVE MONOLITH

Frame 22 117_s1f.pol.051

ANAPOST 3.3x 09/16/93

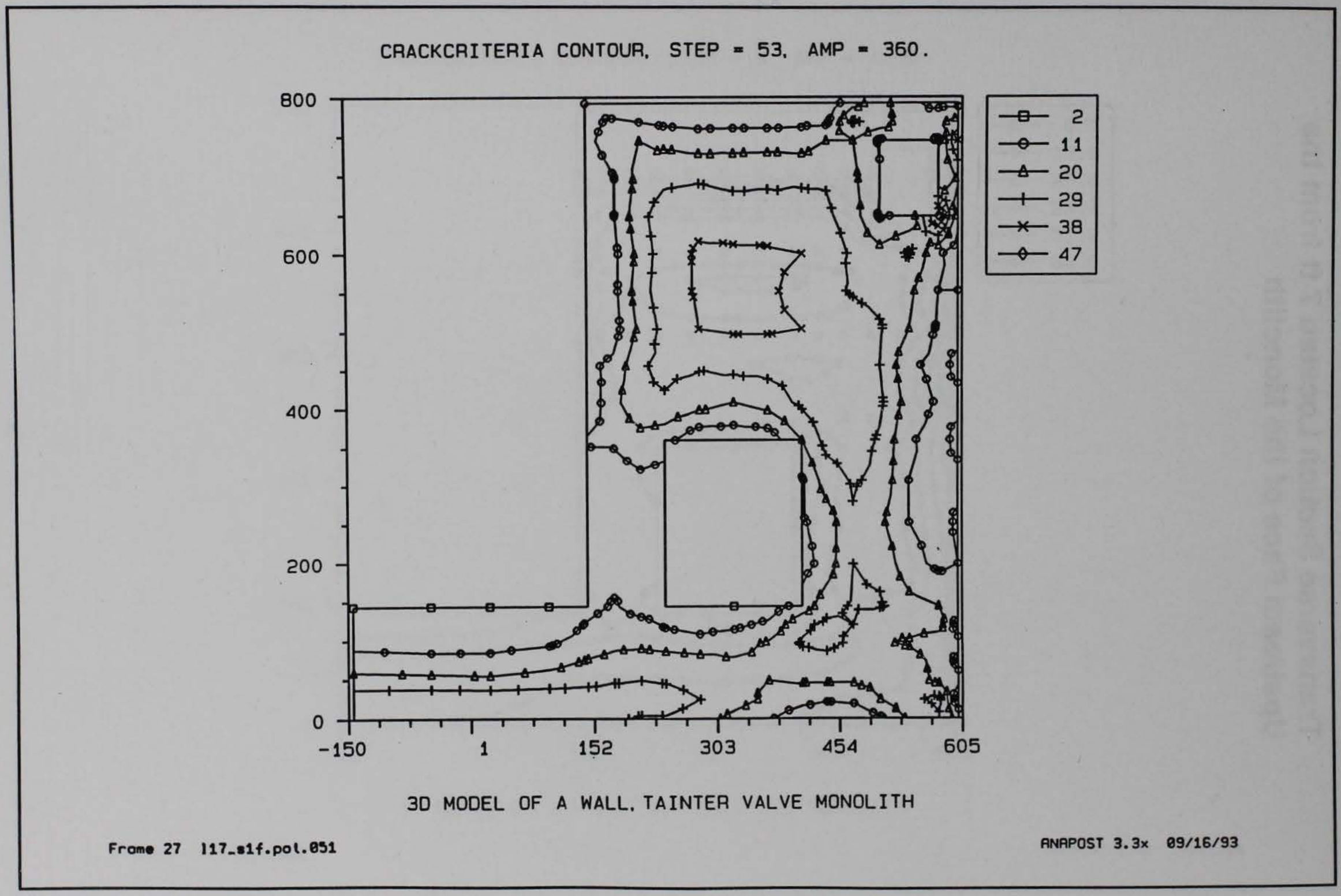
CRACKCRITERIA CONTOUR, STEP = 53, AMP = 360.
800
600
400
200
0
-150
1
152
303
454
605
2
11
20
29
38
47
3D MODEL OF A WALL, TAINTER VALVE MONOLITH
Frame 27 117_s1f.pol.051
ANAPOST 3.3x 09/16/93

Transverse Section Located 7 ft from the Upstream Face of the Monolith

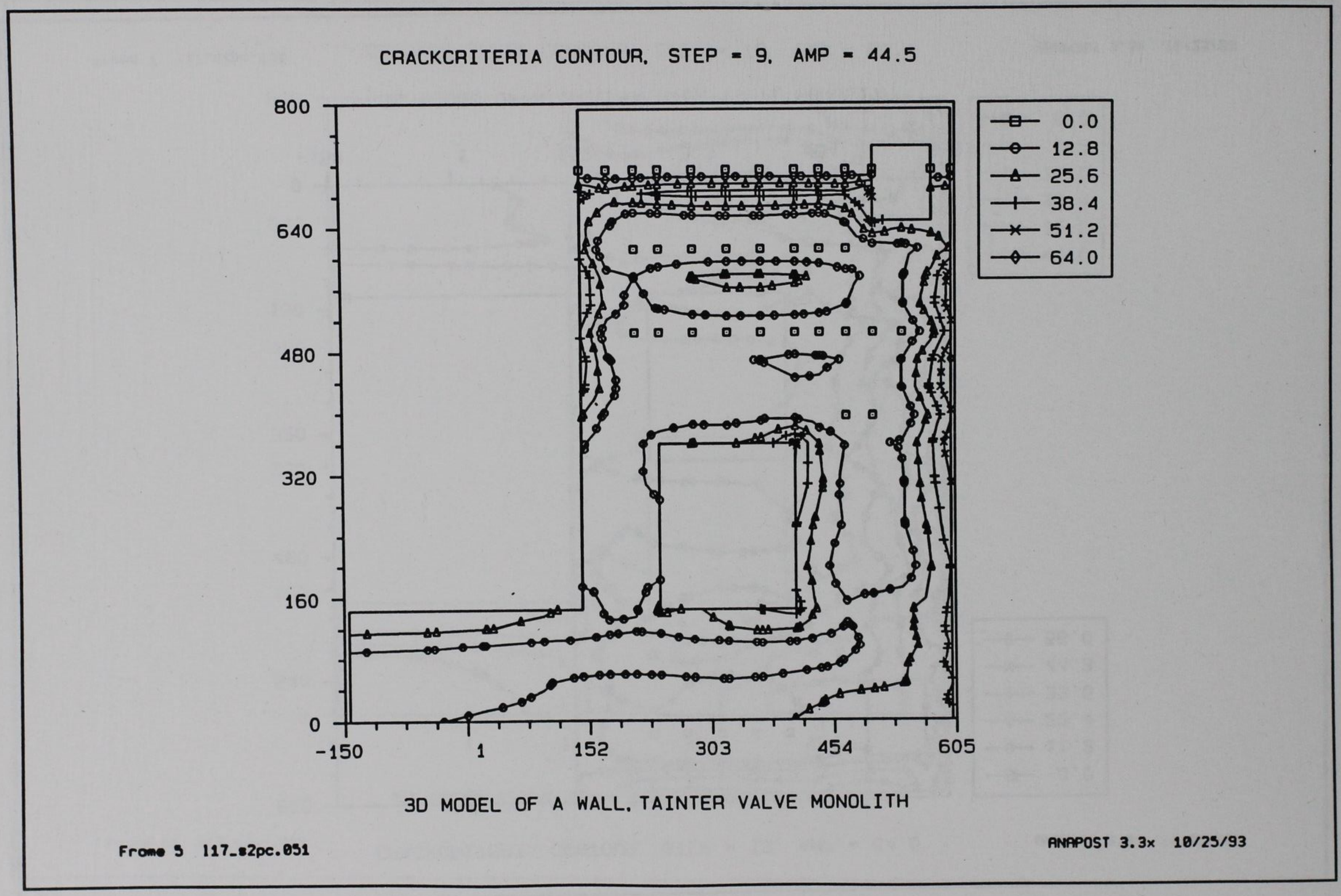
CRACKCRITERIA CONTOUR, STEP = 9, AMP = 44.5
800
640
480
320
160
0
-150
1
152
303
454
605
0.0
12.8
25.6
38.4
51.2
64.0
3D MODEL OF A WALL, TAINTER VALVE MONOLITH
Frome 5 117_s2pc.051
ANAPOST 3.3x 10/25/93

CRACKCRITERIA CONTOUR, STEP = 13, AMP = 64.5

3D MODEL OF A WALL, TAINTER VALVE MONOLITH

Frame 7 117_s2pc.051

ANAPOST 3.3x 10/25/93

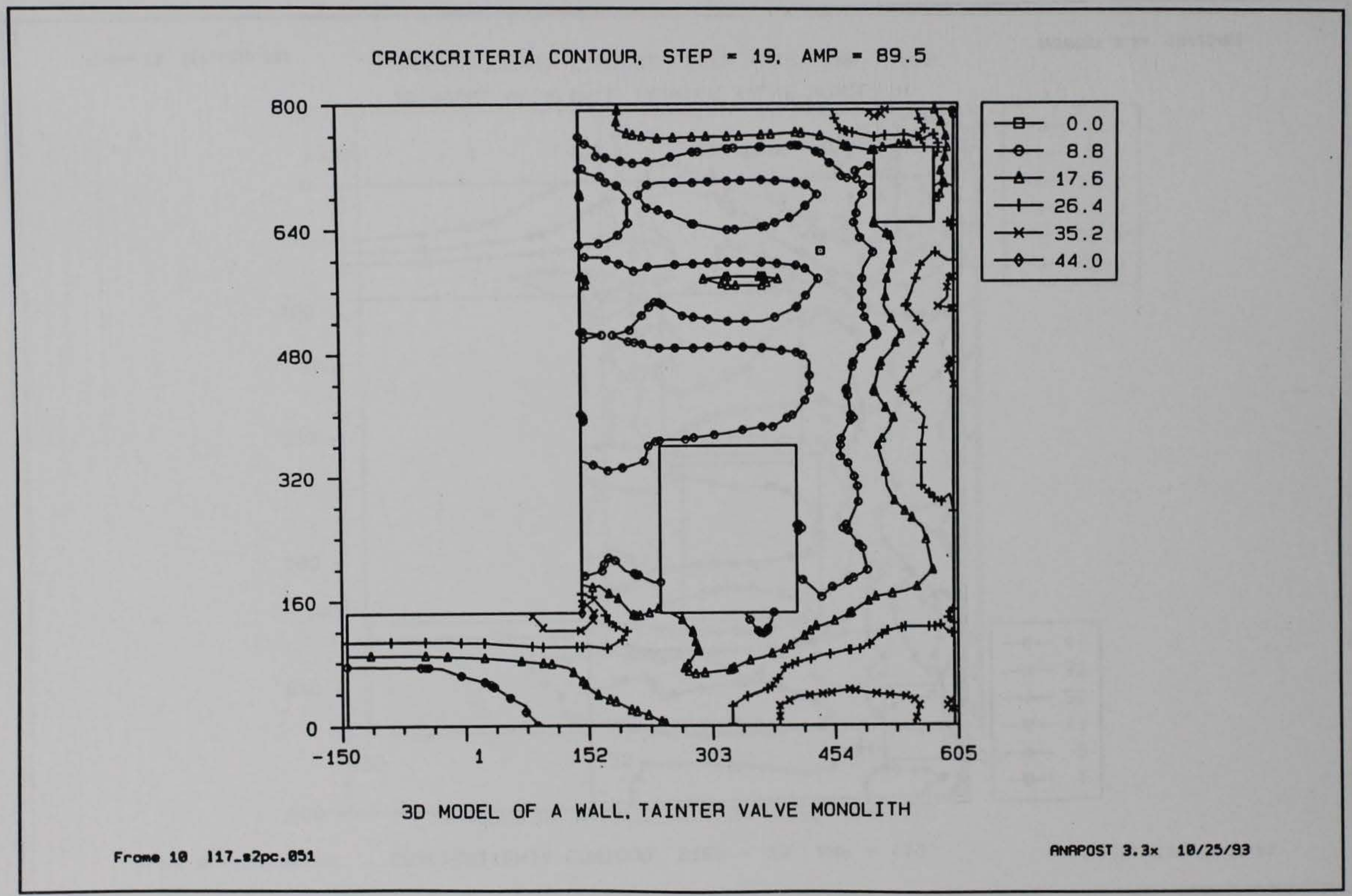
CRACKCRITERIA CONTOUR, STEP = 19, AMP = 89.5
800
640
480
320
160
0
-150
1
152
303
454
605
0.0
8.8
17.6
26.4
35.2
44.0
3D MODEL OF A WALL, TAINTER VALVE MONOLITH
Frame 10 117_s2pc.051
ANAPOST 3.3x 10/25/93

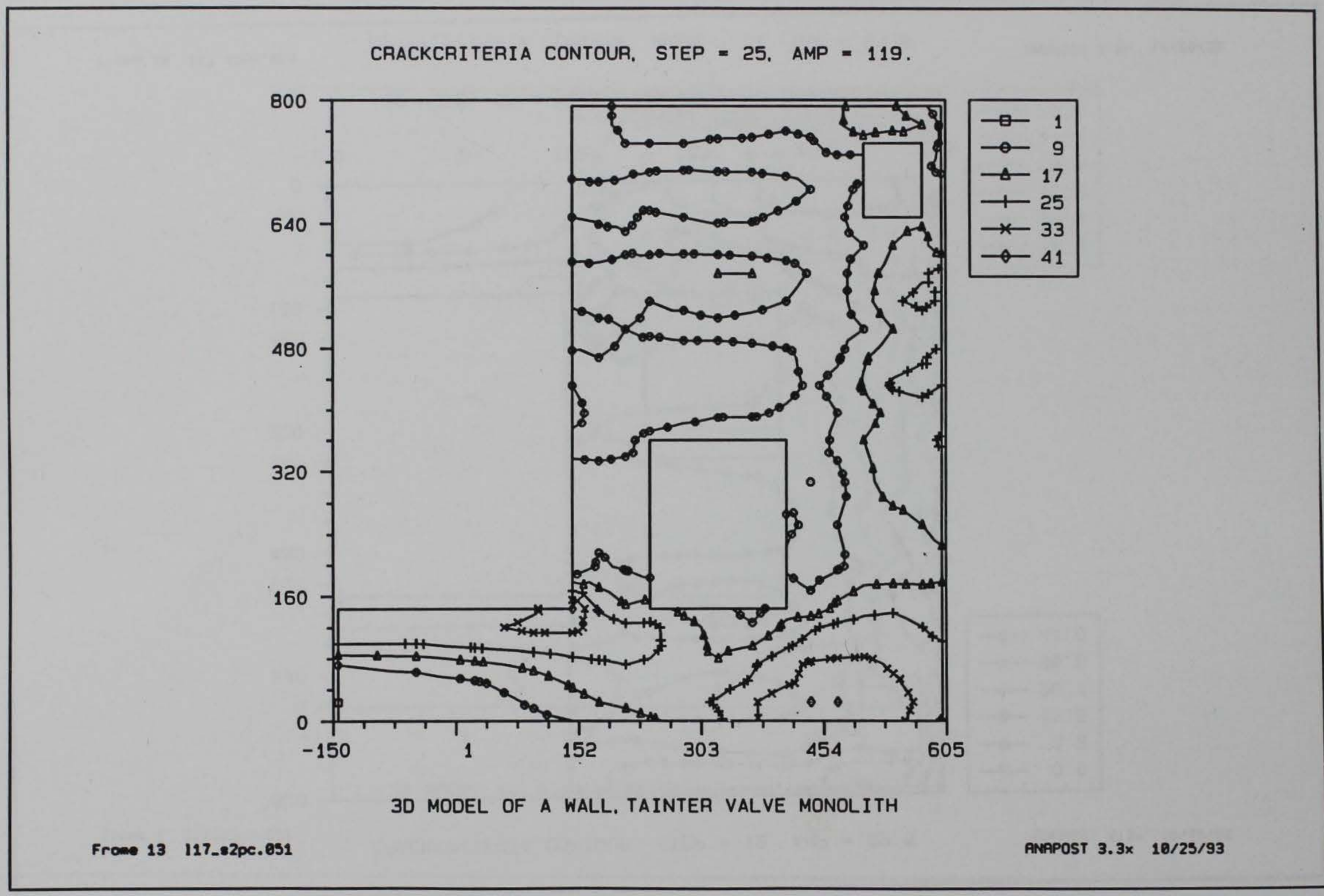
CRACKCRITERIA CONTOUR, STEP = 25, AMP = 119.
800
640
480
320
160
0
-150
1
152
303
454
605
1
9
17
25
33
41
3D MODEL OF A WALL, TAINTER VALVE MONOLITH
Frame 13 117_s2pc.051
ANAPOST 3.3x 10/25/93

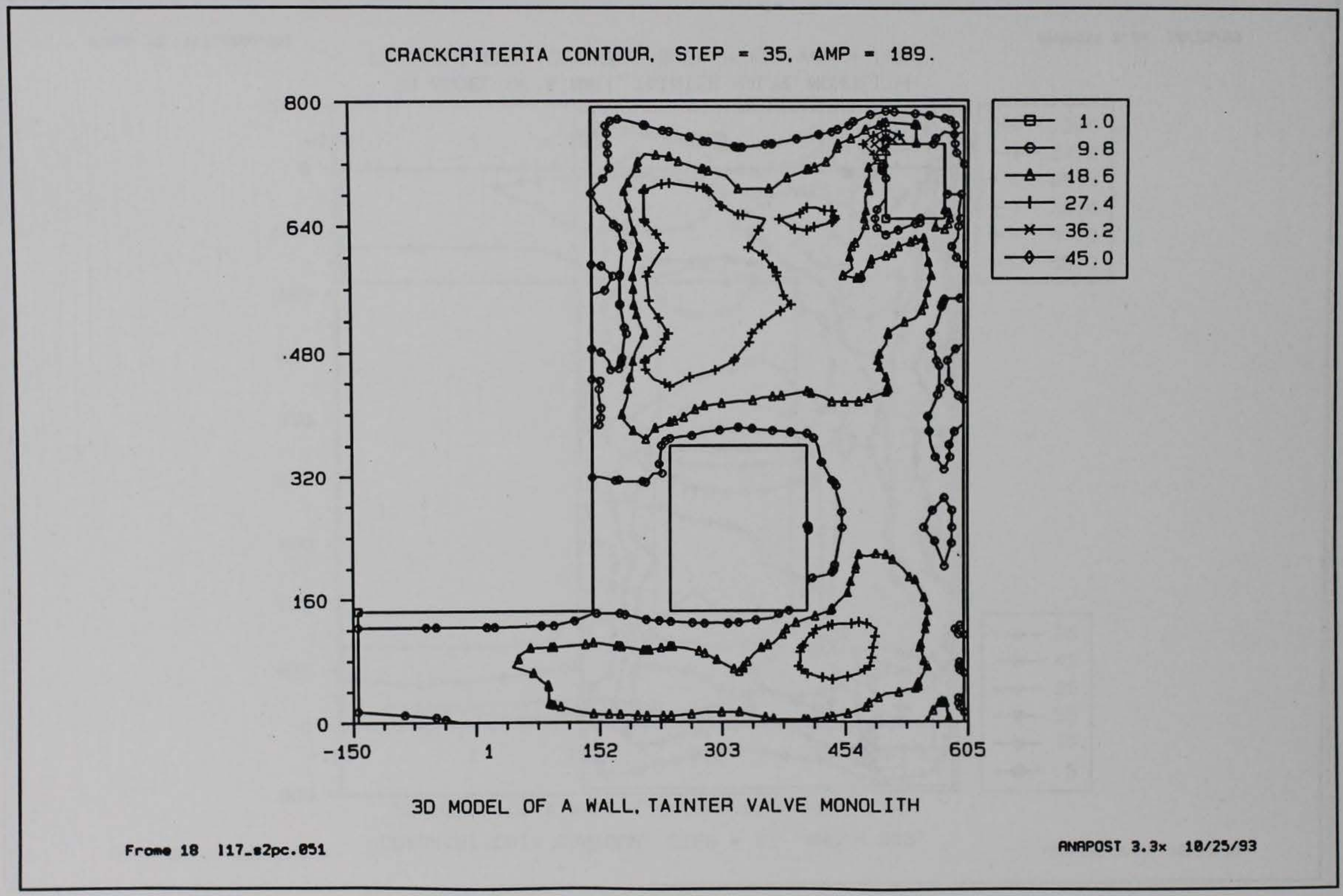
CRACKCRITERIA CONTOUR, STEP = 35, AMP = 189.
800
640
480
320
160
0
-150
1
152
303
454
605
1.0
9.8
18.6
27.4
36.2
45.0
3D MODEL OF A WALL, TAINTER VALVE MONOLITH
Frame 18 117_s2pc.051
ANAPOST 3.3x 10/25/93

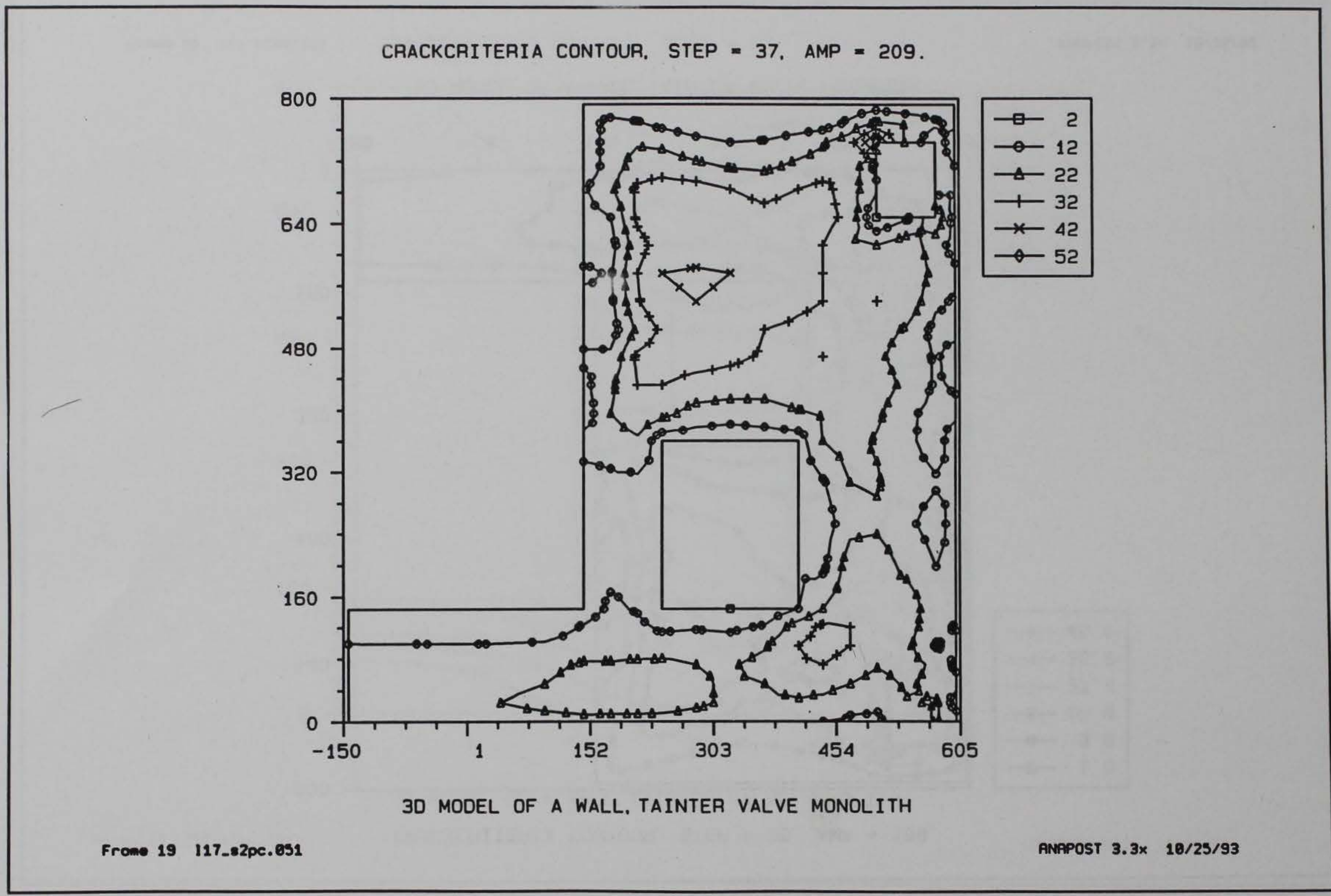
CRACKCRITERIA CONTOUR, STEP = 37, AMP = 209.
800
640
480
320
160
0
-150
1
152
303
454
605
2
12
22
32
42
52
3D MODEL OF A WALL, TAINTER VALVE MONOLITH
Frome 19 117_s2pc.051
ANAPOST 3.3x 10/25/93

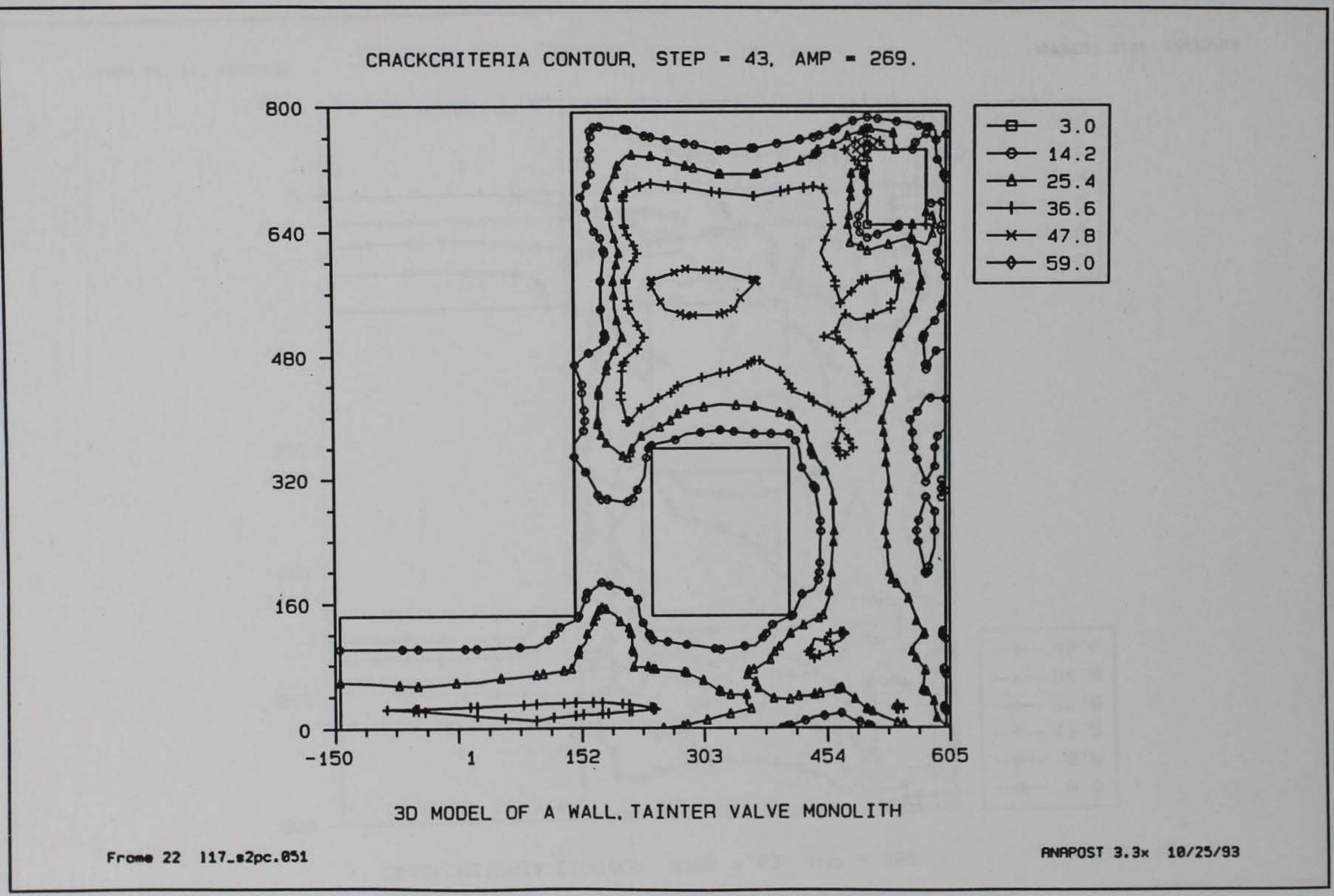
CRACKCRITERIA CONTOUR, STEP = 43, AMP = 269.
800
640
480
320
160
0
-150
1
152
303
454
605
3.0
14.2
25.4
36.6
47.8
59.0
3D MODEL OF A WALL, TAINTER VALVE MONOLITH
Frame 22 117_s2pc.051
ANAPOST 3.3x 10/25/93

CRACKCRITERIA CONTOUR, STEP = 53, AMP = 359.

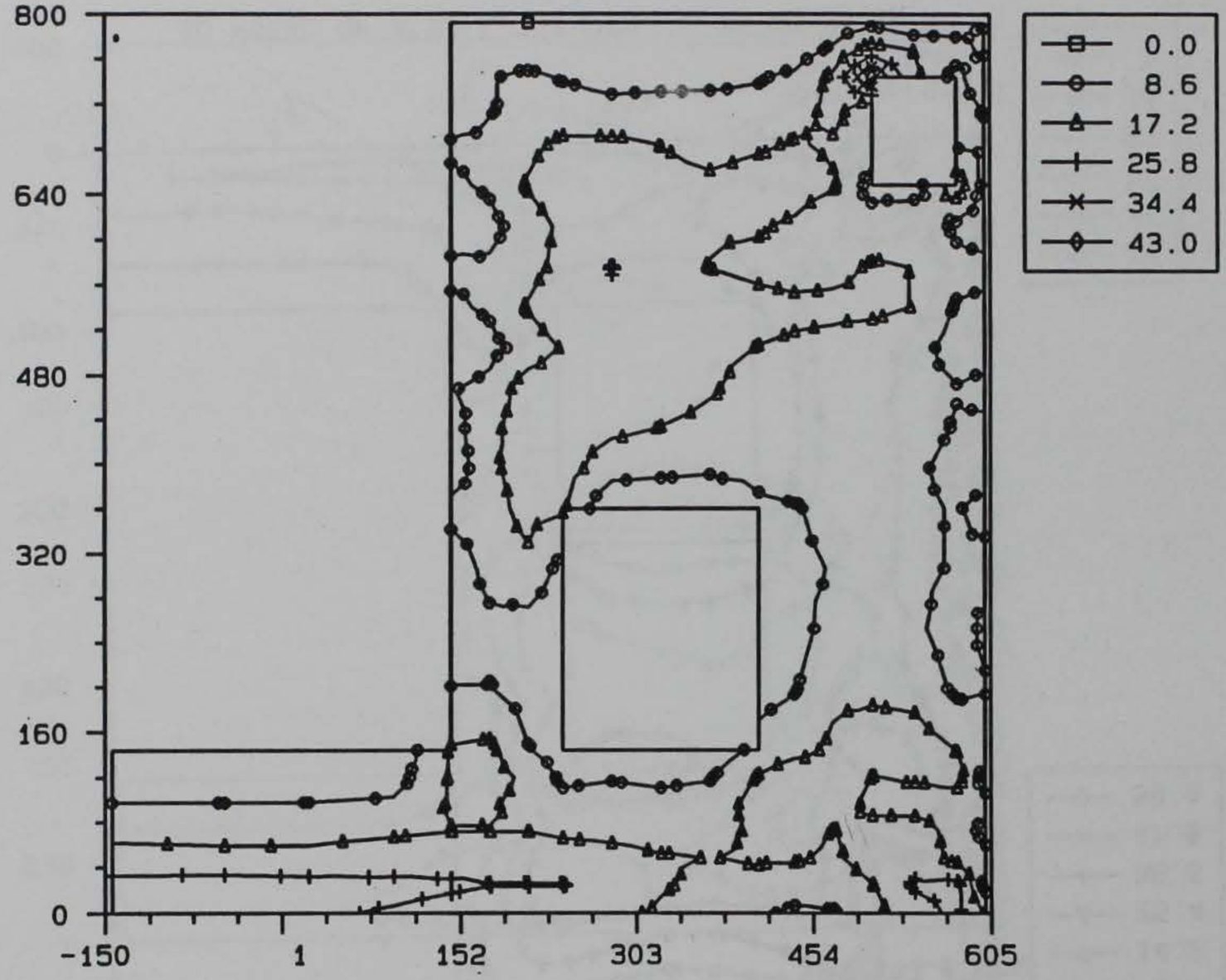

3D MODEL OF A WALL, TAINTER VALVE MONOLITH

Frome 27 117_s2pc.051

ANAPOST 3.3x 10/25/93

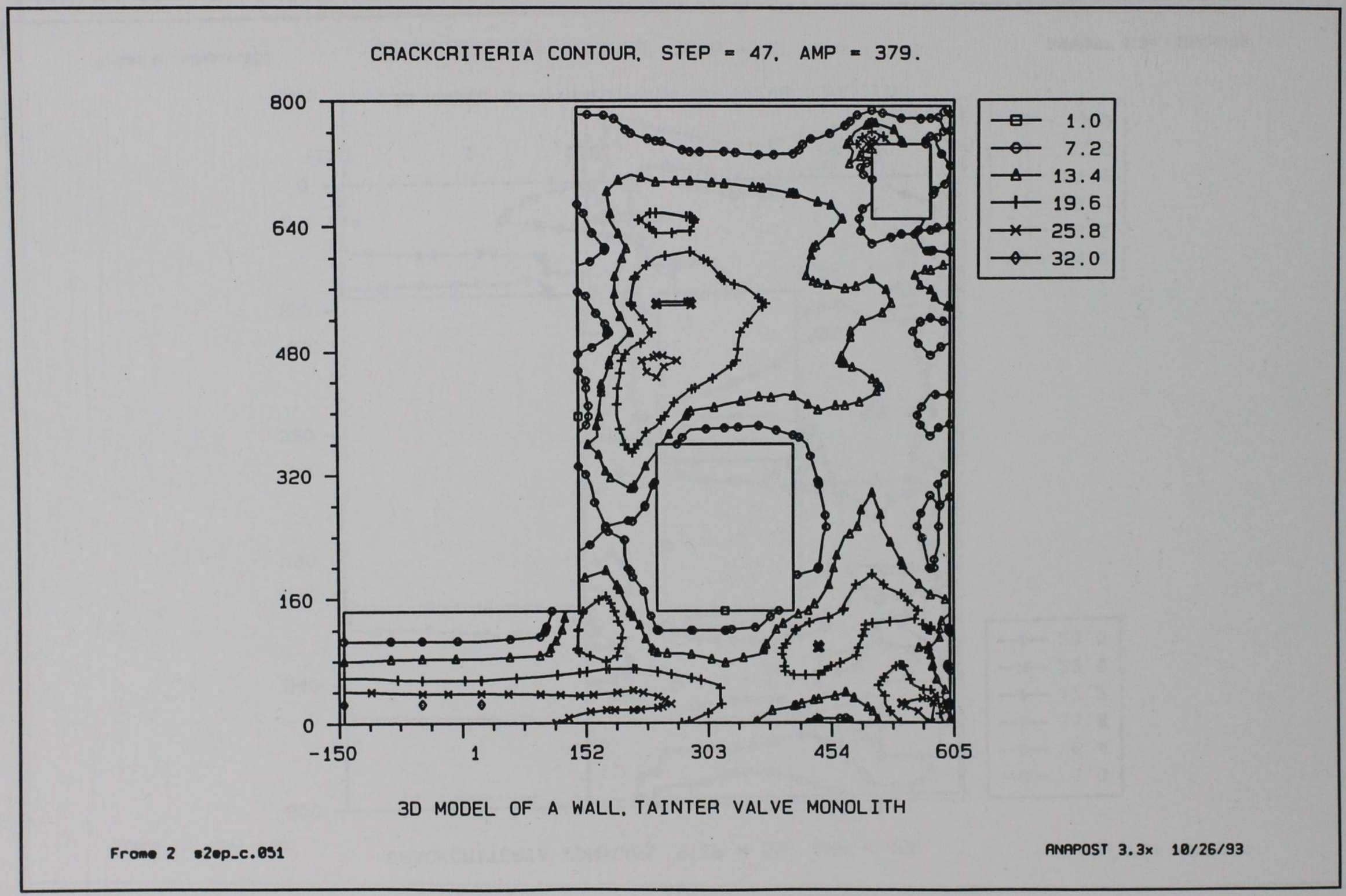
CRACKCRITERIA CONTOUR, STEP = 47, AMP = 379.
800
640
480
320
160
0
-150
1
152
303
454
605
1.0
7.2
13.4
19.6
25.8
32.0
3D MODEL OF A WALL, TAINTER VALVE MONOLITH
Frame 2 s2ep_c.051
ANAPOST 3.3x 10/26/93

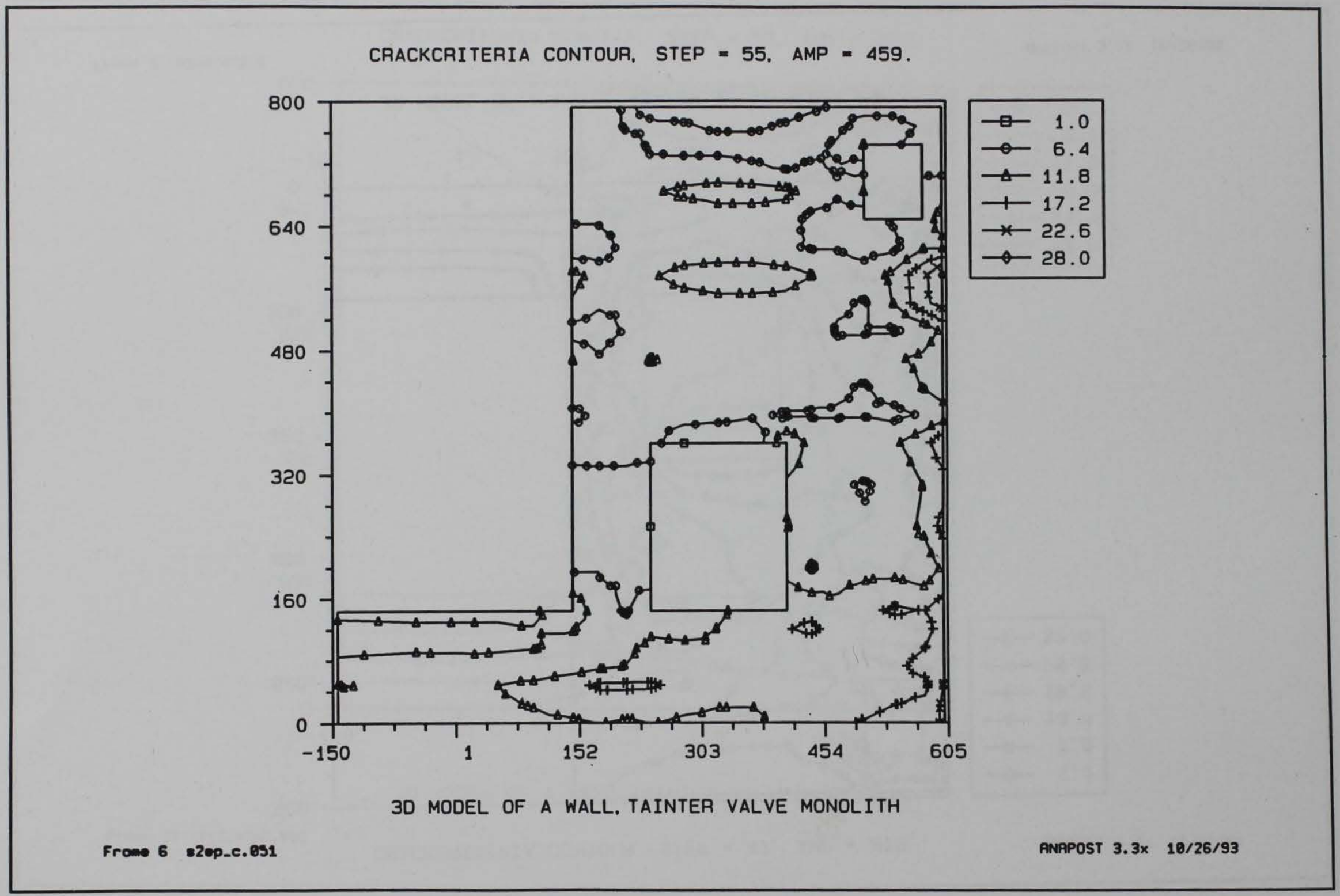
CRACKCRITERIA CONTOUR, STEP = 55, AMP = 459.
800
640
480
320
160
0
-150
1
152
303
454
605
1.0
6.4
11.8
17.2
22.6
28.0
3D MODEL OF A WALL, TAINTER VALVE MONOLITH
Frame 6 s2ep_c.051
ANAPOST 3.3x 10/26/93

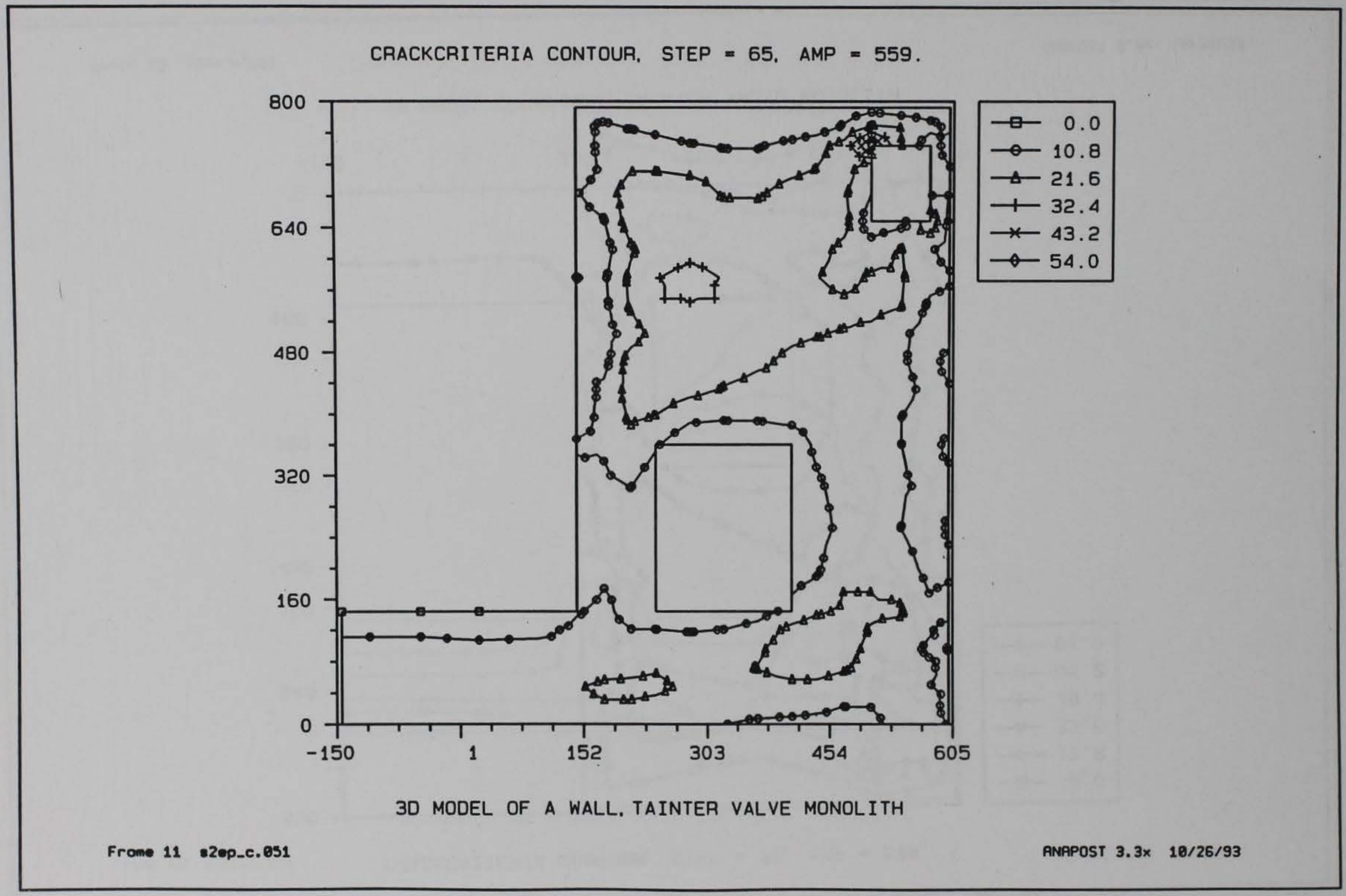
CRACKCRITERIA CONTOUR, STEP = 65, AMP = 559.
800
640
480
320
160
0
-150
1
152
303
454
605
0.0
10.8
21.6
32.4
43.2
54.0
3D MODEL OF A WALL, TAINTER VALVE MONOLITH
Frame 11 s2ep_c.051
ANAPOST 3.3x 10/26/93

CRACKCRITERIA CONTOUR, STEP = 73, AMP = 639.

3D MODEL OF A WALL, TAINTER VALVE MONOLITH

Frame 15 s2ep_c.051

ANAPOST 3.3x 10/26/93

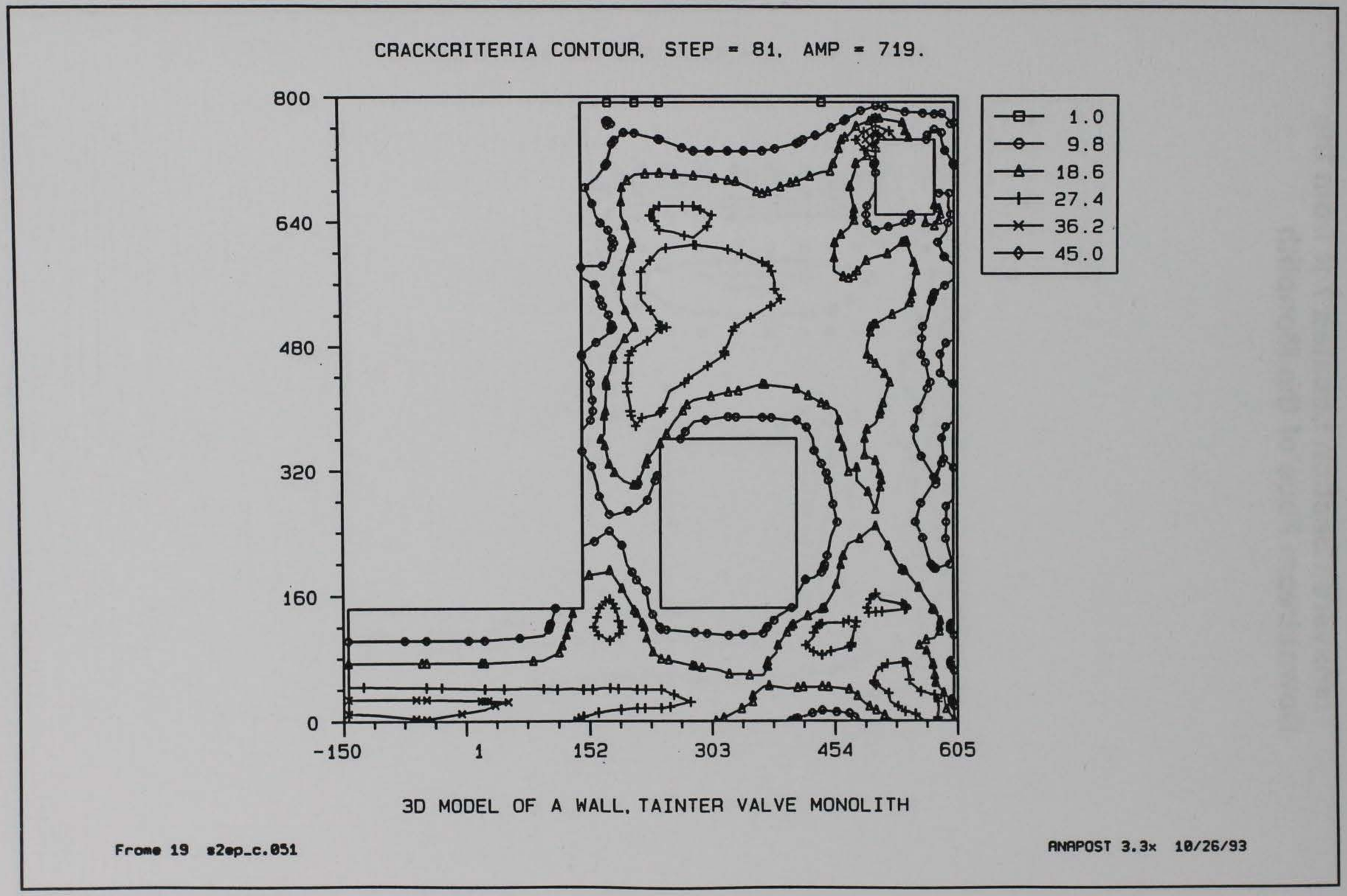
CRACKCRITERIA CONTOUR, STEP = 81, AMP = 719.
800
640
480
320
160
0
-150
1
152
303
454
605
1.0
9.8
18.6
27.4
36.2
45.0
3D MODEL OF A WALL, TAINTER VALVE MONOLITH
Frame 19 s2ep_c.051
ANAPOST 3.3x 10/26/93

Transverse Section Located 7 ft from the Downstream Face of the Monolith

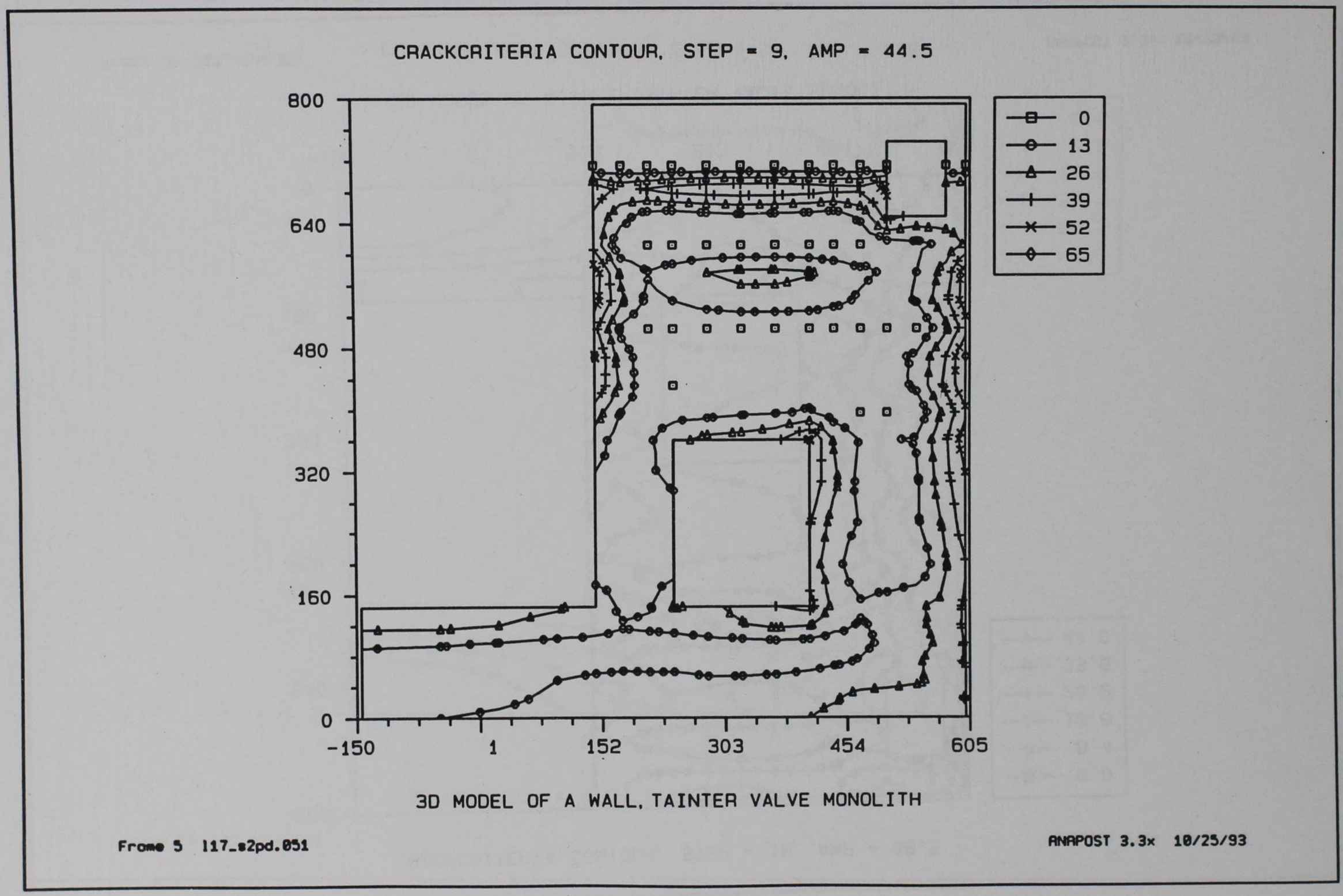
CRACKCRITERIA CONTOUR, STEP = 9, AMP = 44.5
800
640
480
320
160
0
-150
1
152
303
454
605
0
13
26
39
52
65
3D MODEL OF A WALL, TAINTER VALVE MONOLITH
Frome 5 117_s2pd.051
ANAPOST 3.3x 10/25/93

CRACKCRITERIA CONTOUR, STEP = 19, AMP = 89.5

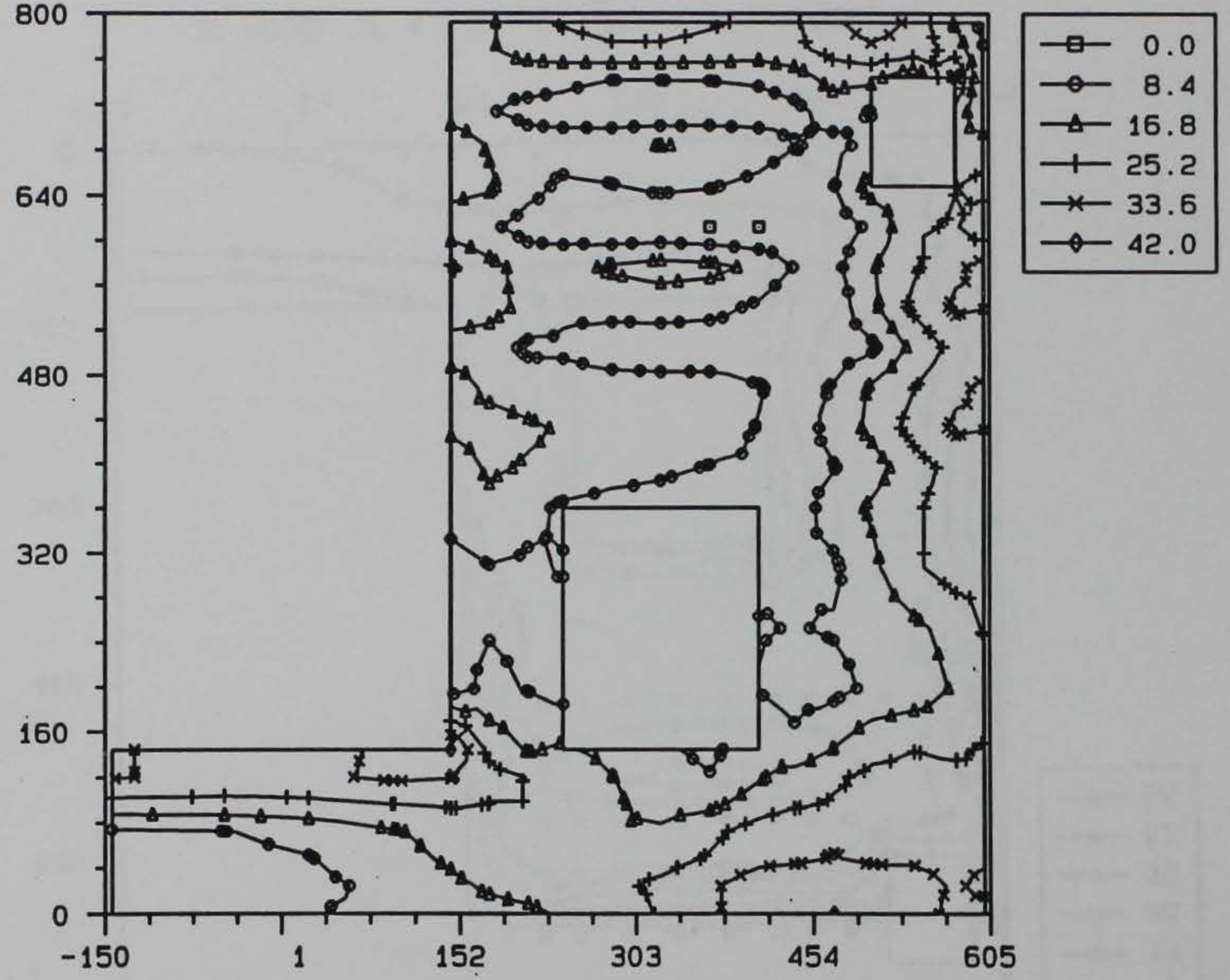

3D MODEL OF A WALL, TAINTER VALVE MONOLITH

Frame 10 117_s2pd.051

ANAPOST 3.3x 10/25/93

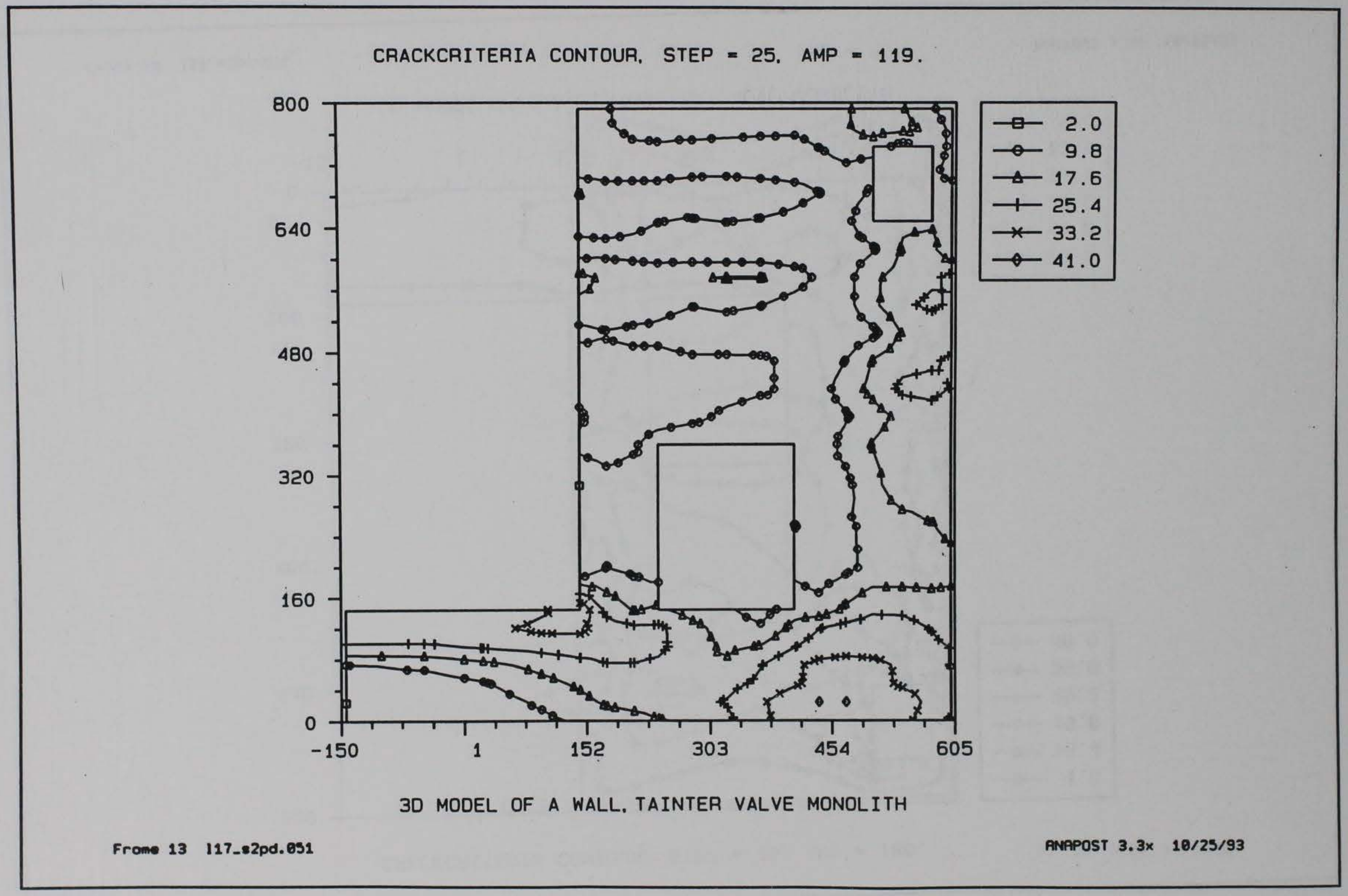
CRACKCRITERIA CONTOUR, STEP = 25, AMP = 119.
800
640
480
320
160
0
-150
1
152
303
454
605
2.0
9.8
17.6
25.4
33.2
41.0
3D MODEL OF A WALL, TAINTER VALVE MONOLITH
Frame 13 117_s2pd.051
ANAPOST 3.3x 10/25/93

CRACKCRITERIA CONTOUR. STEP = 35. AMP = 189.

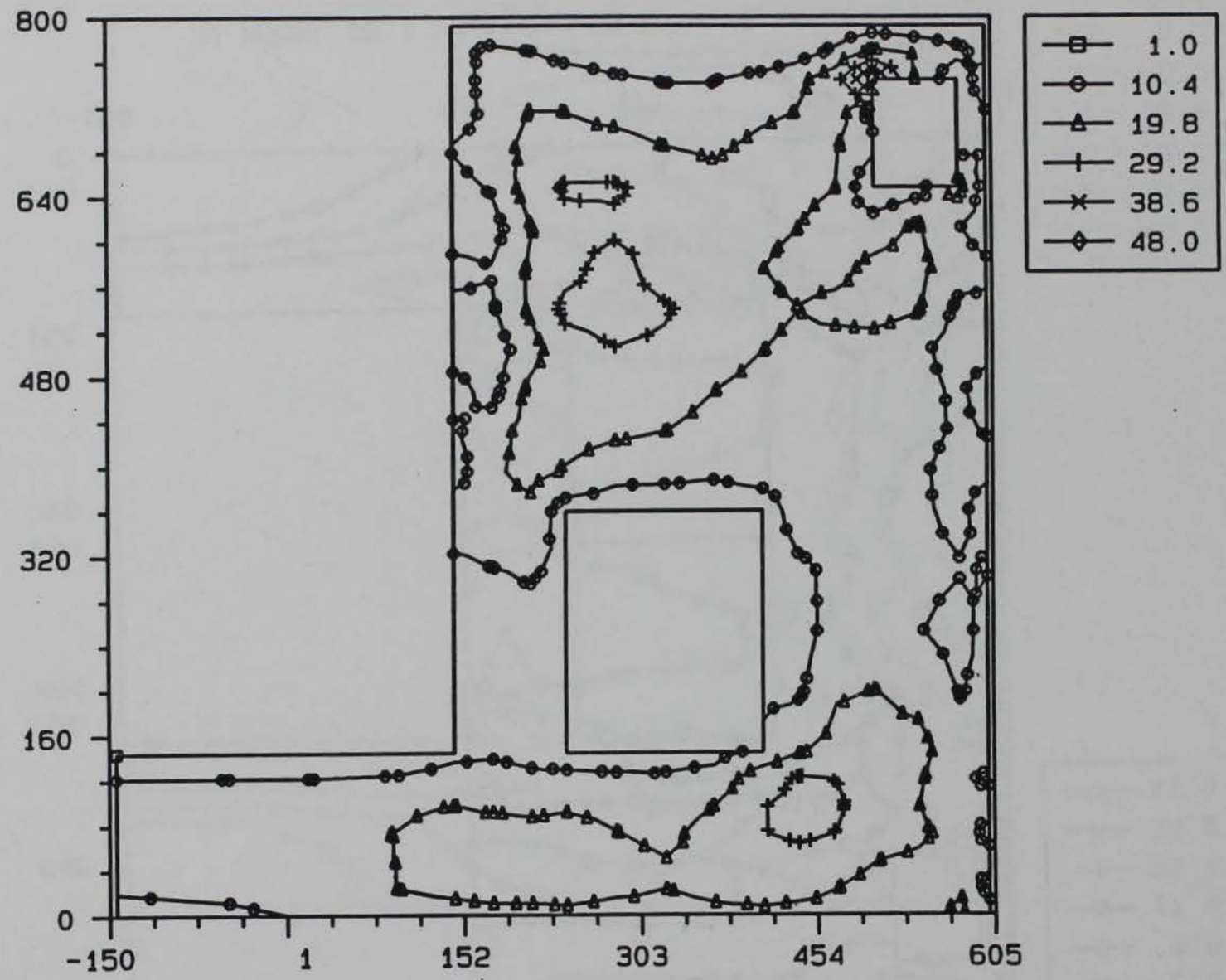

3D MODEL OF A WALL. TAINTER VALVE MONOLITH

Frome 18 117_e2pd.051

ANAPOST 3.3× 10/25/93

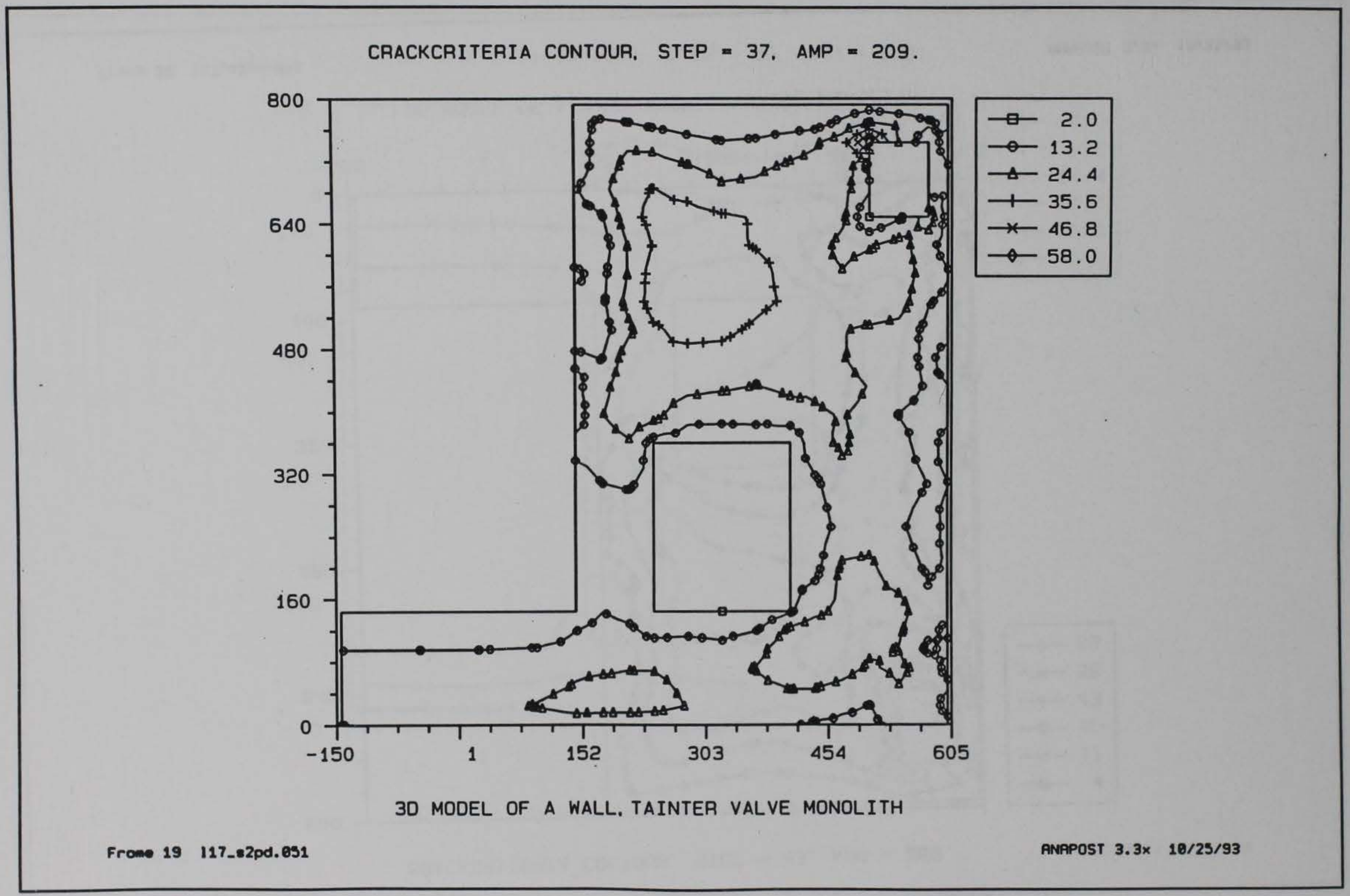
CRACKCRITERIA CONTOUR, STEP = 37, AMP = 209.
800
640
480
320
160
0
-150
1
152
303
454
605
2.0
13.2
24.4
35.6
46.8
58.0
3D MODEL OF A WALL, TAINTER VALVE MONOLITH
Frome 19 117_s2pd.051
ANAPOST 3.3x 10/25/93

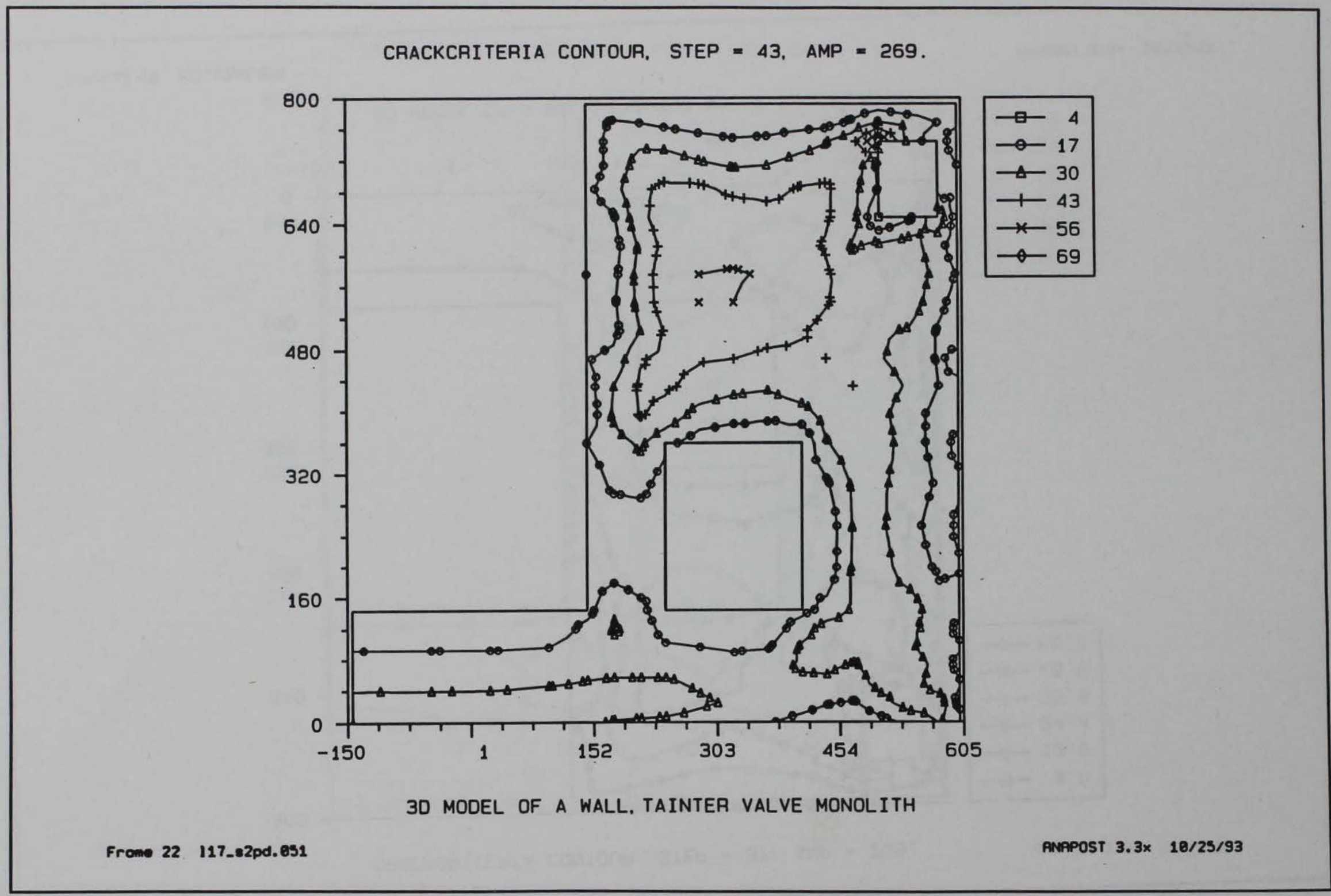
CRACKCRITERIA CONTOUR, STEP = 43, AMP = 269.
800
640
480
320
160
0
-150
1
152
303
454
605
4
17
30
43
56
69
3D MODEL OF A WALL, TAINTER VALVE MONOLITH
Frame 22 117_s2pd.051
ANAPOST 3.3x 10/25/93

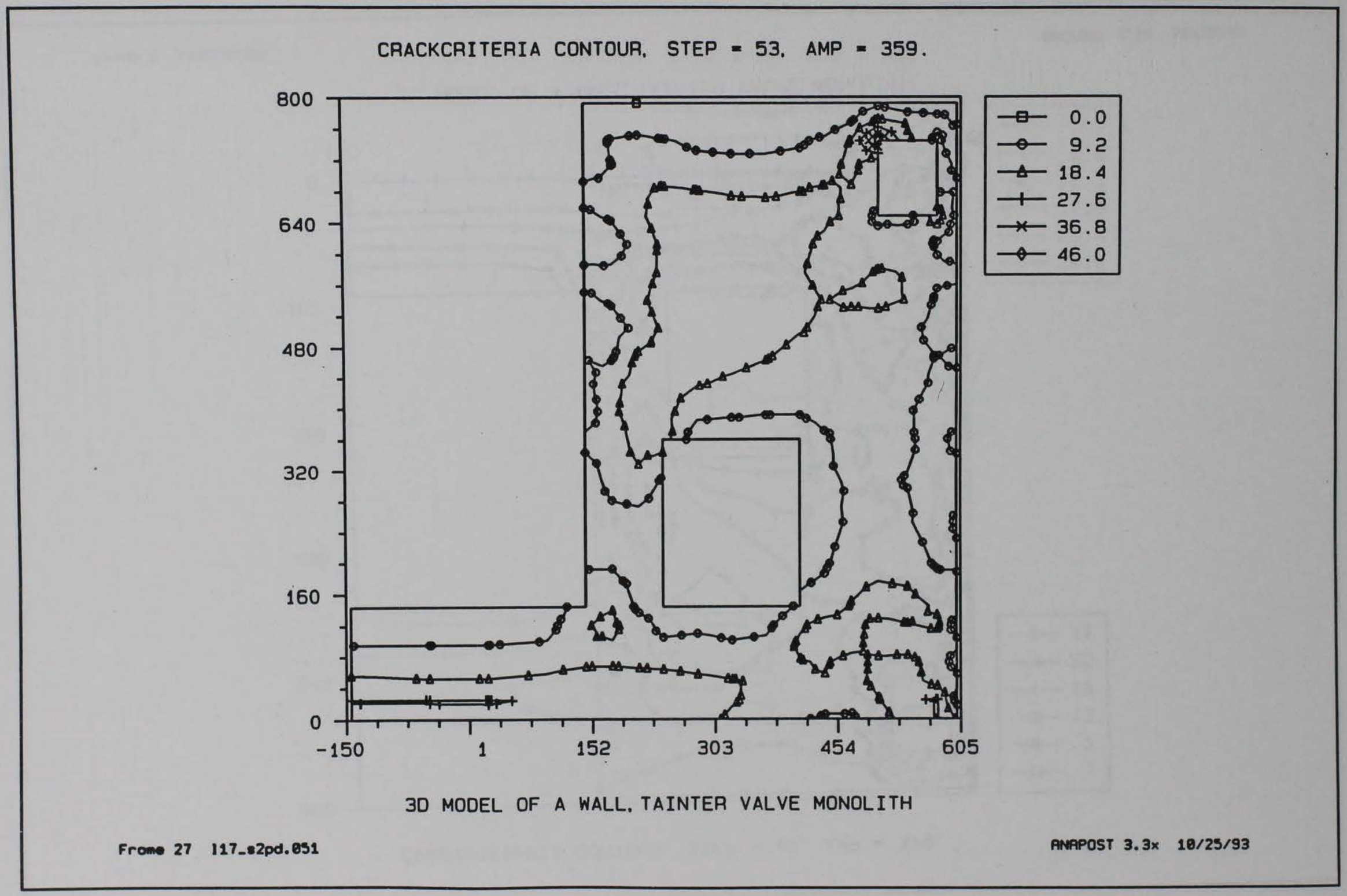
CRACKCRITERIA CONTOUR, STEP = 53, AMP = 359.
800
640
480
320
160
0
-150
1
152
303
454
605
0.0
9.2
18.4
27.6
36.8
46.0
3D MODEL OF A WALL, TAINTER VALVE MONOLITH
Frome 27 117_s2pd.051
ANAPOST 3.3x 10/25/93

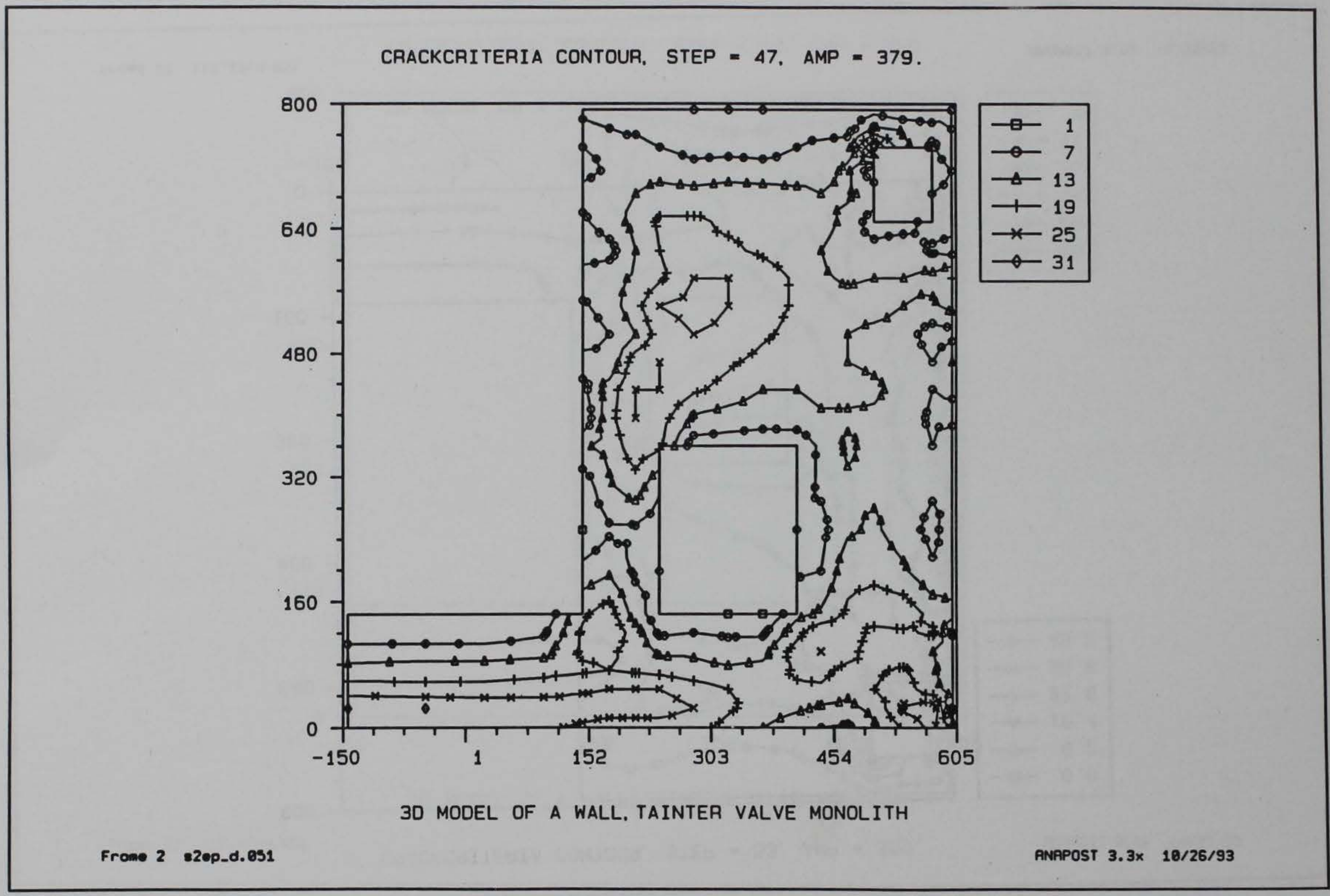
CRACKCRITERIA CONTOUR, STEP = 47, AMP = 379.
800
640
480
320
160
0
-150
1
152
303
454
605
1
7
13
19
25
31
3D MODEL OF A WALL, TAINTER VALVE MONOLITH
Frame 2 s2ep_d.051
ANAPOST 3.3x 10/26/93

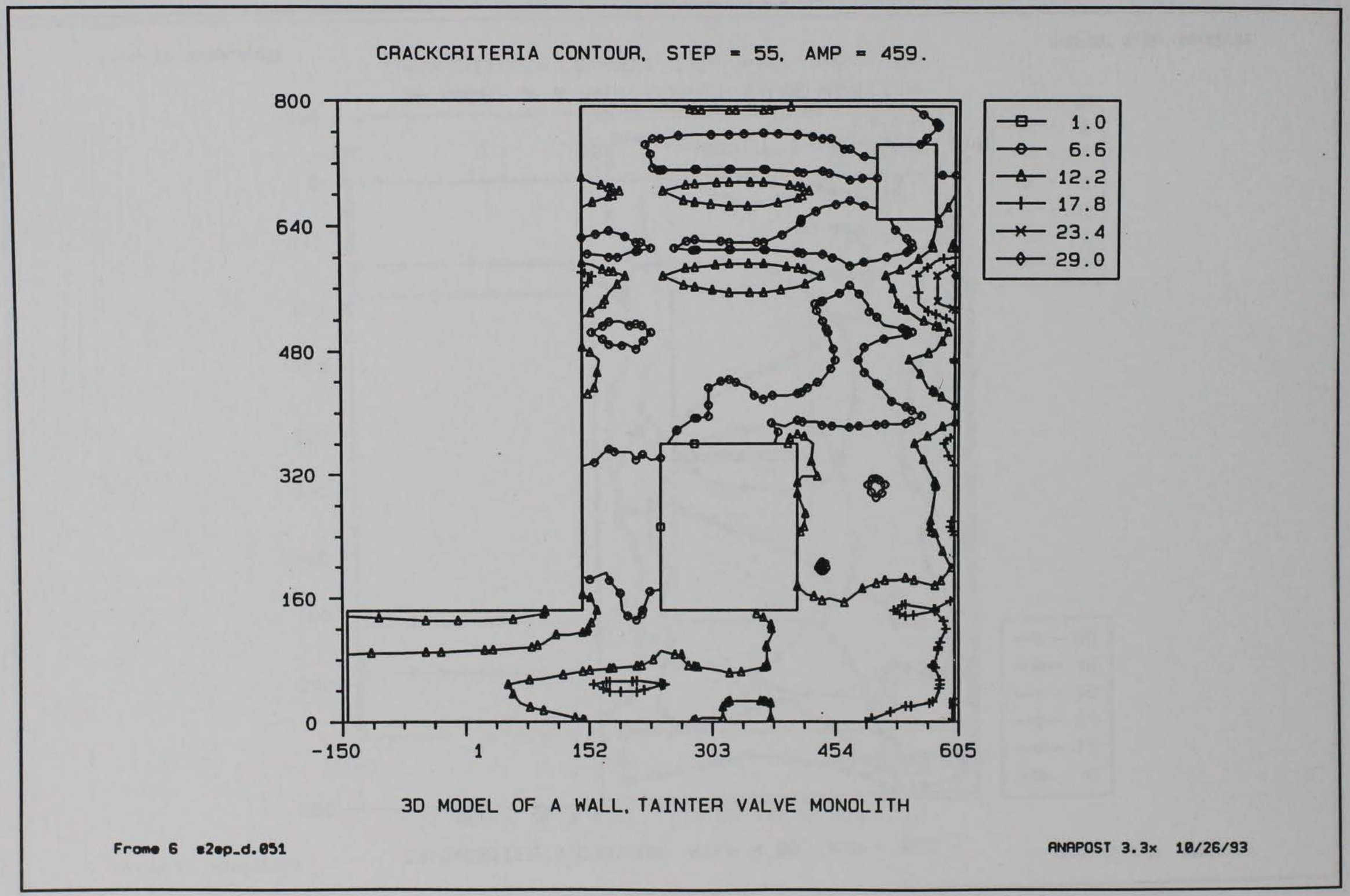
CRACKCRITERIA CONTOUR, STEP = 55, AMP = 459.
800
640
480
320
160
0
-150
1
152
303
454
605
1.0
6.6
12.2
17.8
23.4
29.0
3D MODEL OF A WALL, TAINTER VALVE MONOLITH
Frame 6 s2ep_d.051
ANAPOST 3.3x 10/26/93

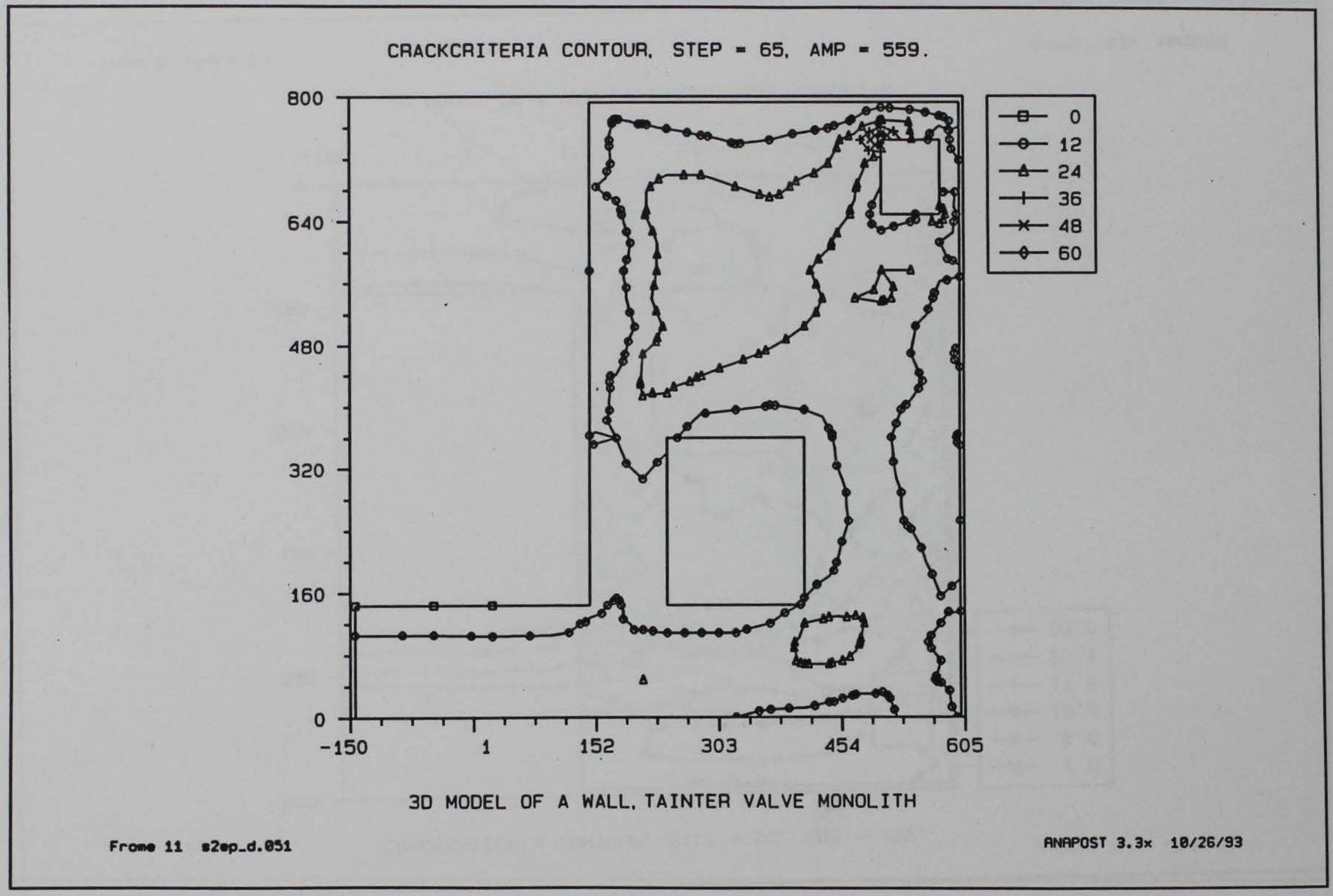
CRACKCRITERIA CONTOUR, STEP = 65, AMP = 559.
800
640
480
320
160
0
-150
1
152
303
454
605
0
12
24
36
48
60
3D MODEL OF A WALL, TAINTER VALVE MONOLITH
Frame 11 s2ep_d.051
ANAPOST 3.3x 10/26/93

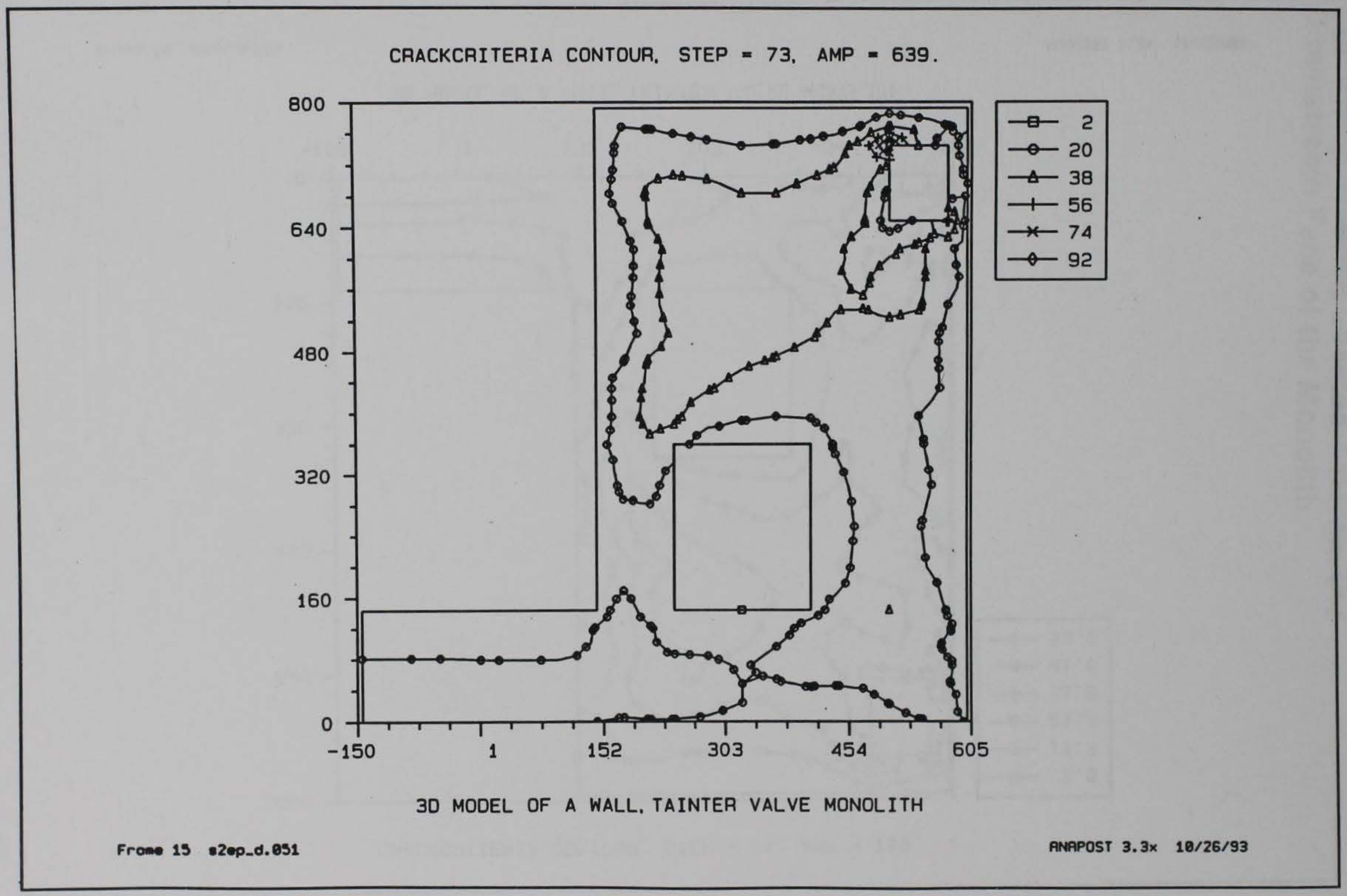
CRACKCRITERIA CONTOUR, STEP = 73, AMP = 639.
800
640
480
320
160
0
-150
1
152
303
454
605
2
20
38
56
74
92
3D MODEL OF A WALL, TAINTER VALVE MONOLITH
Frame 15 s2ep_d.051
ANAPOST 3.3x 10/26/93

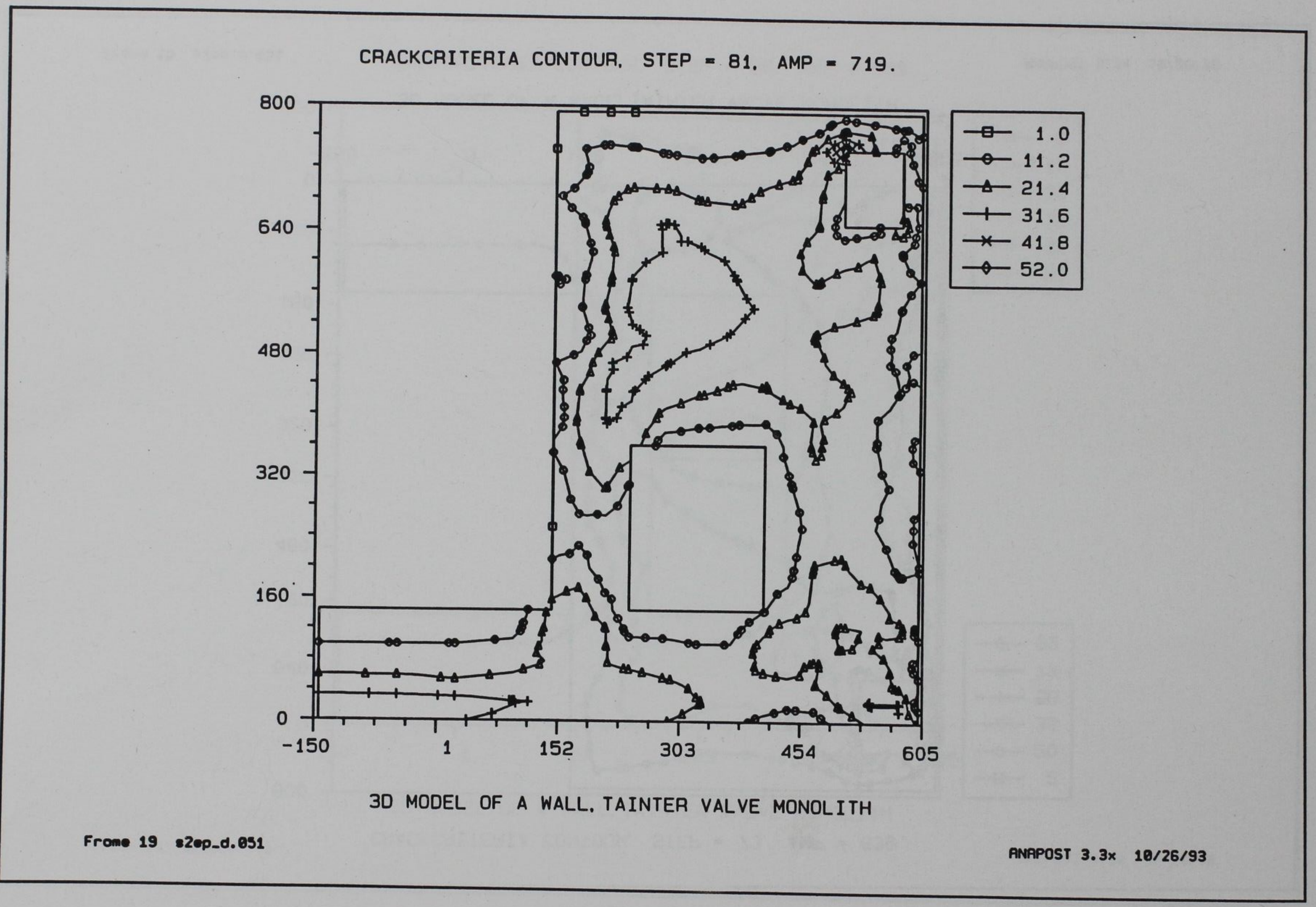
CRACKCRITERIA CONTOUR. STEP = 81. AMP = 719.
800
640
480
320
160
0
-150
1
152
303
454
605
1.0
11.2
21.4
31.6
41.8
52.0
3D MODEL OF A WALL. TAINTER VALVE MONOLITH
Frome 19 s2ep_d.051
ANAPOST 3.3x 10/26/93

Transverse Section Located 7 ft from the Downstream Face of the Monolith

STRESS-SIG1 CONTOUR, STEP = 9, AMP = 44.5

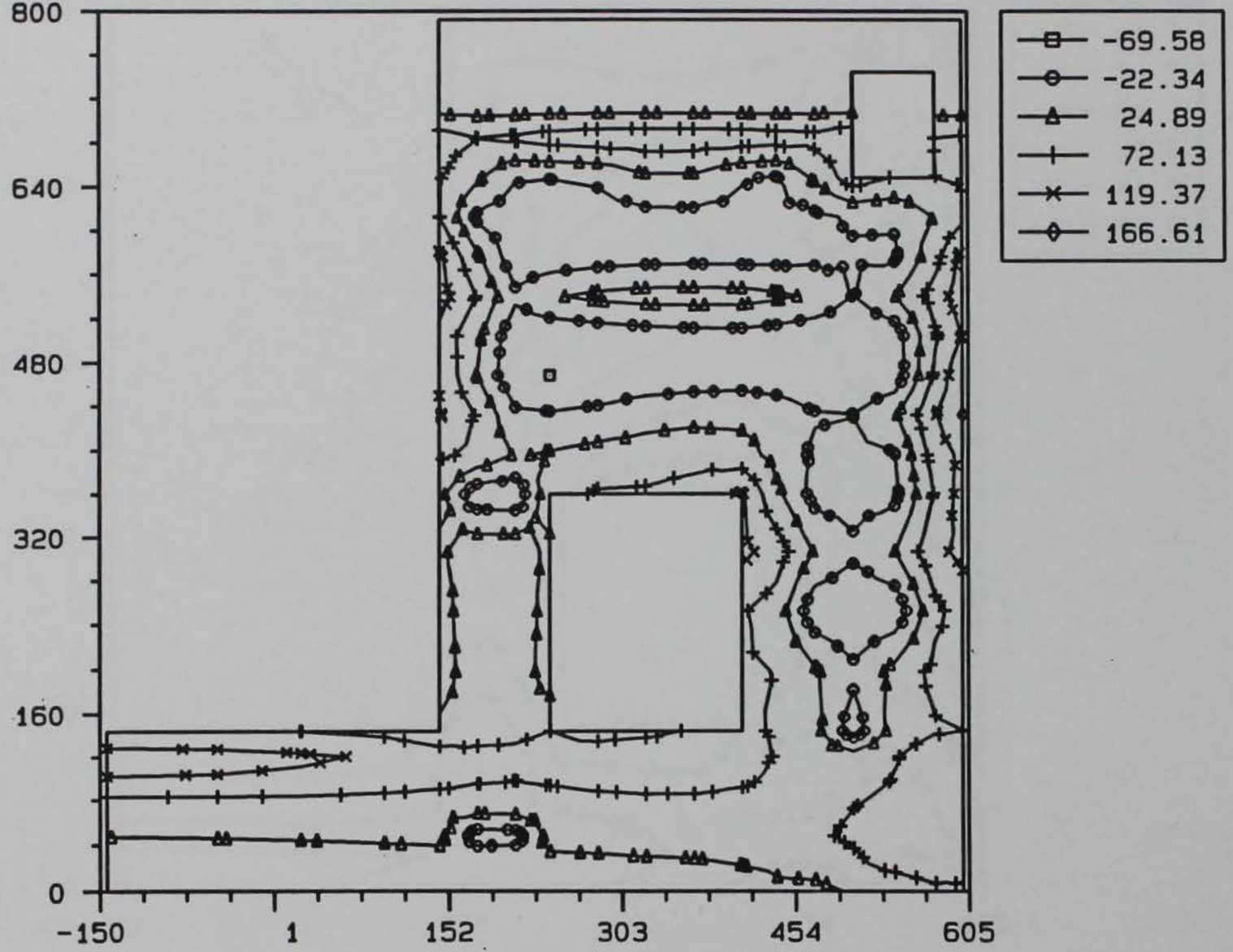

3D MODEL OF A WALL, TAINTER VALVE MONOLITH

Frome 5 117_s2s.051

ANAPOST 3.3x 10/25/93

STRESS-SIG1 CONTOUR, STEP = 19, AMP = 89.5

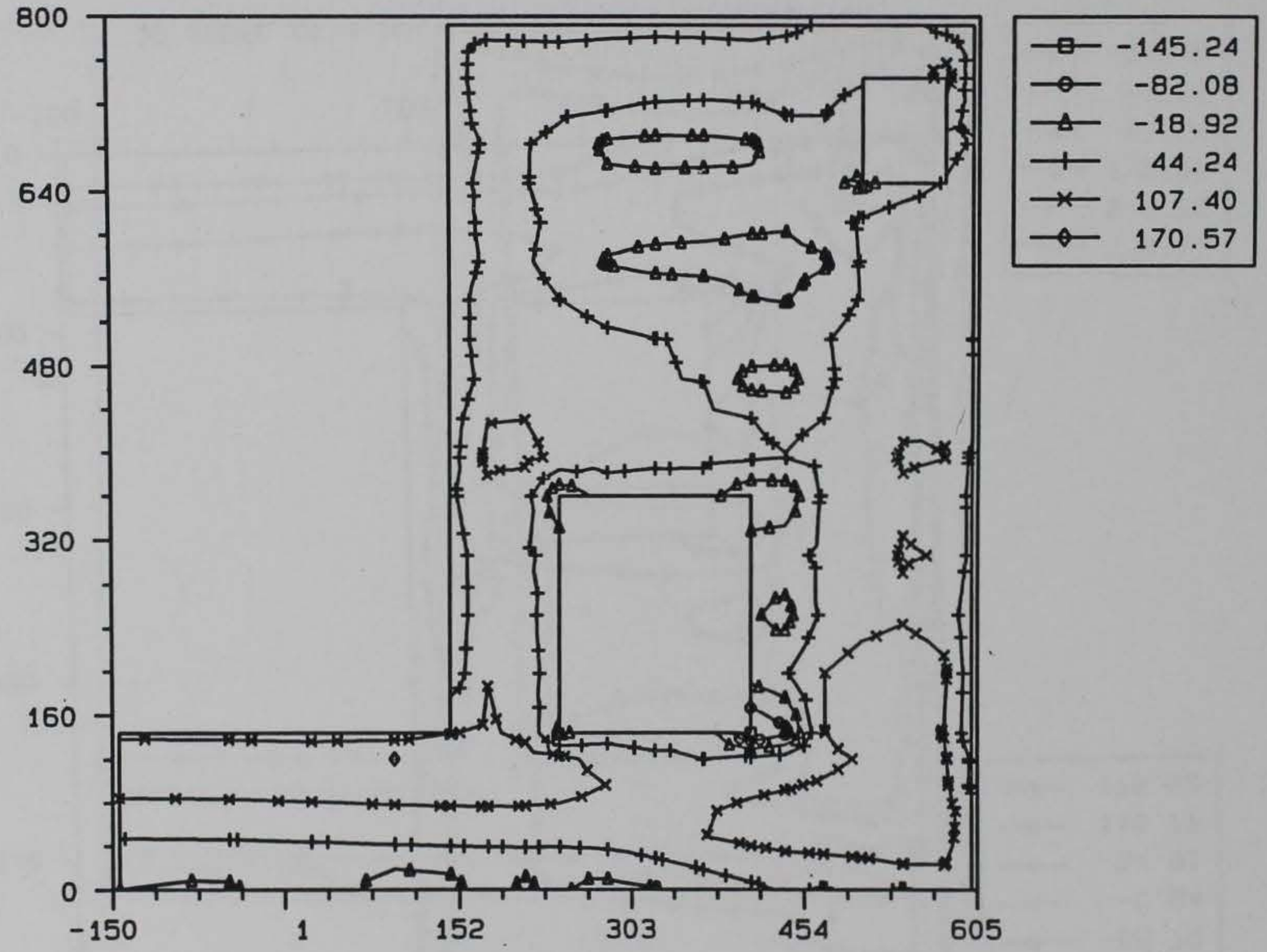

3D MODEL OF A WALL, TAINTER VALVE MONOLITH

Frome 10 117_s2s.051

ANAPOST 3.3x 10/25/93

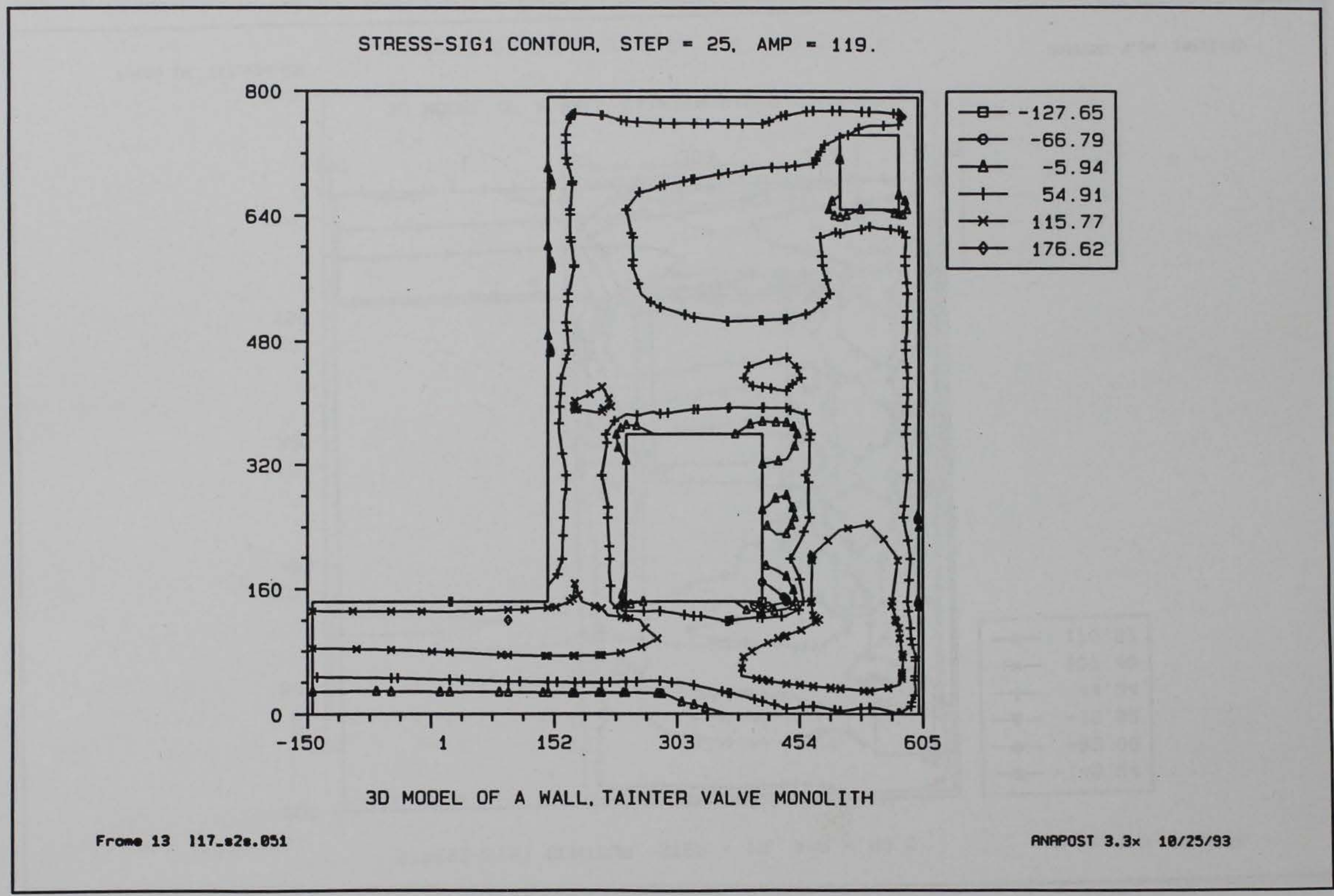
STRESS-SIG1 CONTOUR, STEP = 25, AMP = 119.
800
640
480
320
160
0
-150
1
152
303
454
605
-127.65
-66.79
-5.94
54.91
115.77
176.62
3D MODEL OF A WALL, TAINTER VALVE MONOLITH
Frame 13 117_s2s.051
ANAPOST 3.3x 10/25/93

STRESS-SIG1 CONTOUR, STEP = 35, AMP = 189.

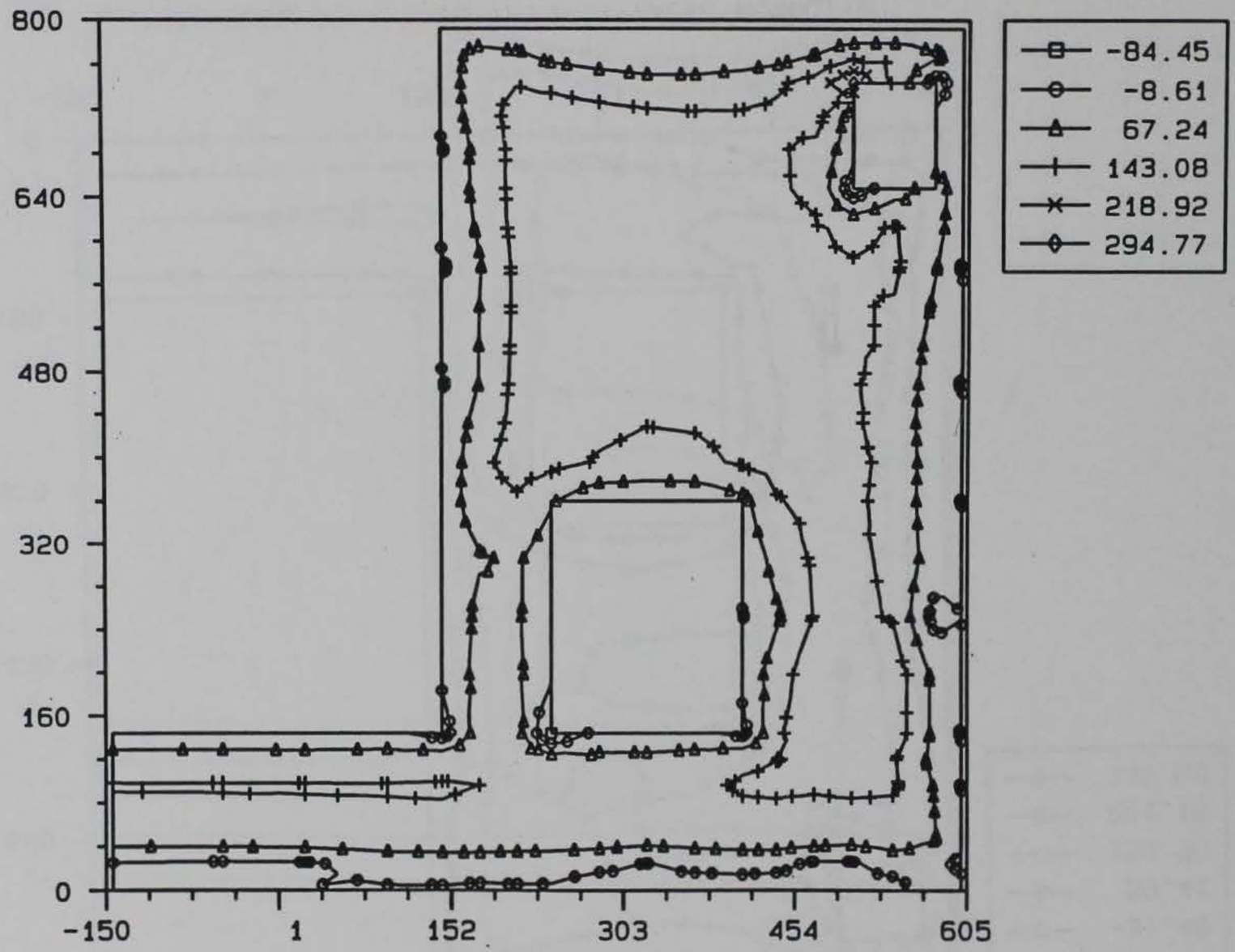

3D MODEL OF A WALL, TAINTER VALVE MONOLITH

Frame 18 117_s2s.051

ANAPOST 3.3x 10/25/93

STRESS-SIG1 CONTOUR, STEP = 37, AMP = 209.

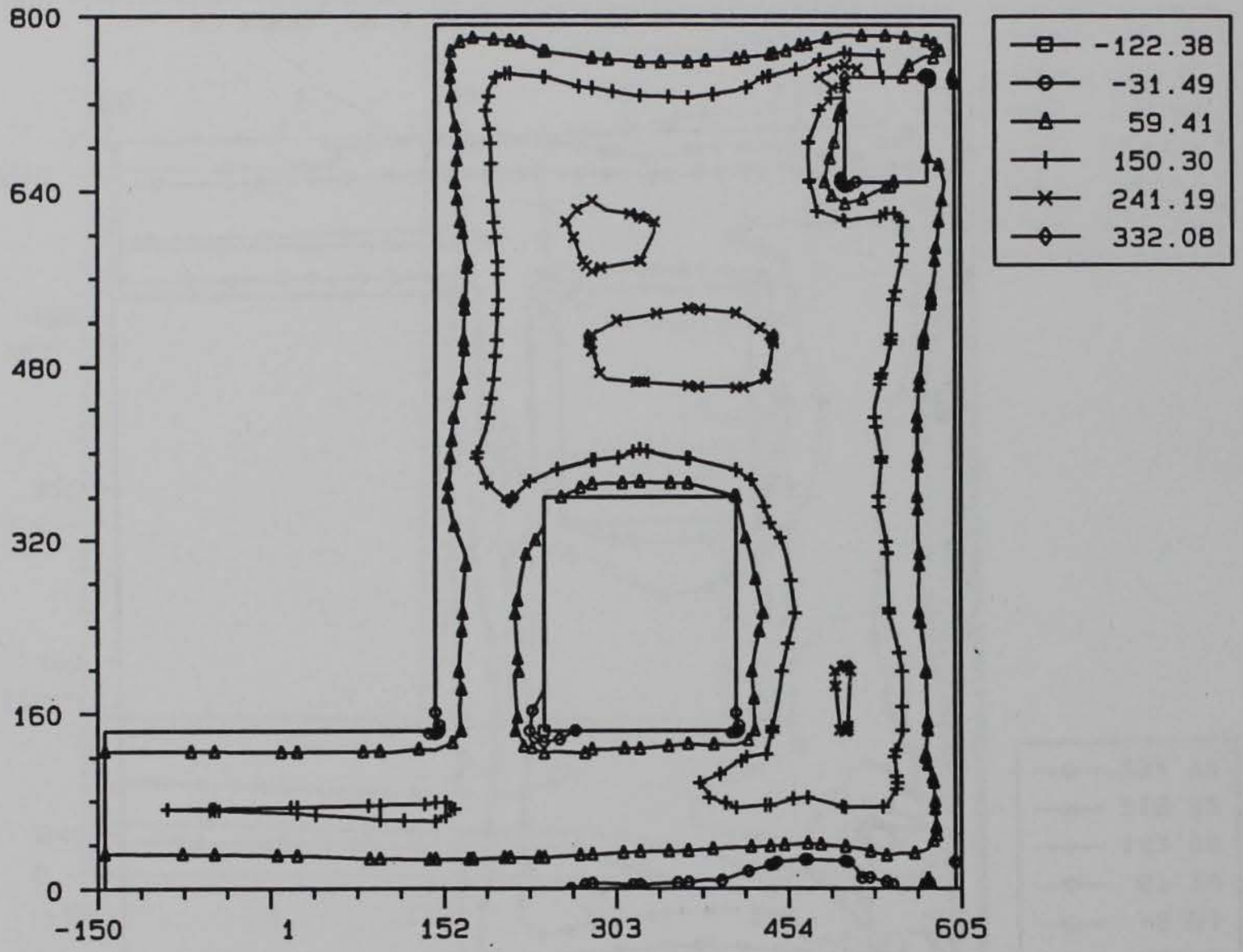

3D MODEL OF A WALL, TAINTER VALVE MONOLITH

Frome 19 117_e2s.051

ANAPOST 3.3x 10/25/93

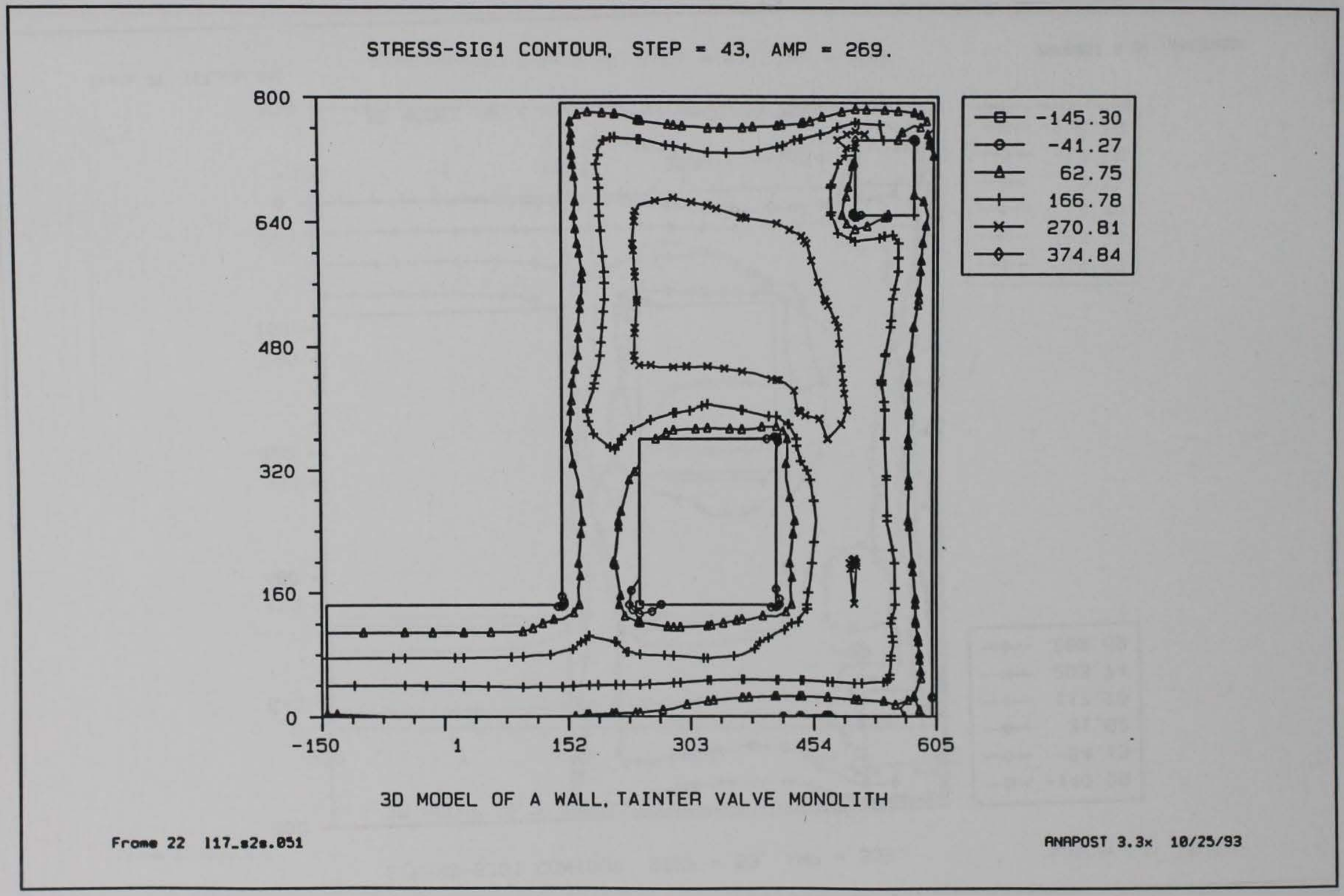
STRESS-SIG1 CONTOUR, STEP = 43, AMP = 269.
800
640
480
320
160
0
-150
1
152
303
454
605
-145.30
-41.27
62.75
166.78
270.81
374.84
3D MODEL OF A WALL, TAINTER VALVE MONOLITH
Frame 22 117_s2s.051
ANAPOST 3.3x 10/25/93

STRESS-SIG1 CONTOUR, STEP = 53, AMP = 359.

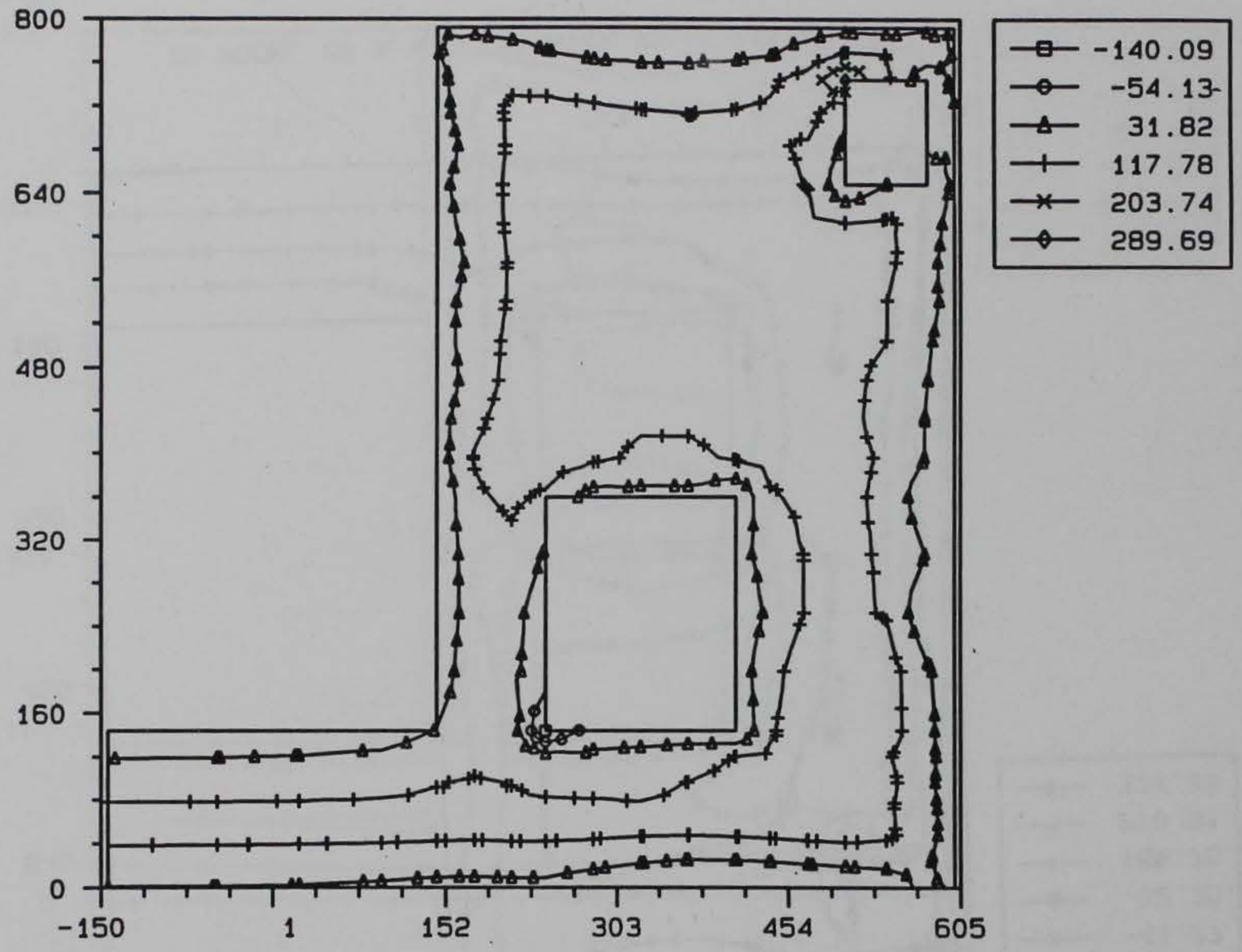

3D MODEL OF A WALL, TAINTER VALVE MONOLITH

Frame 27 117_s2s.051

ANAPOST 3.3x 10/25/93

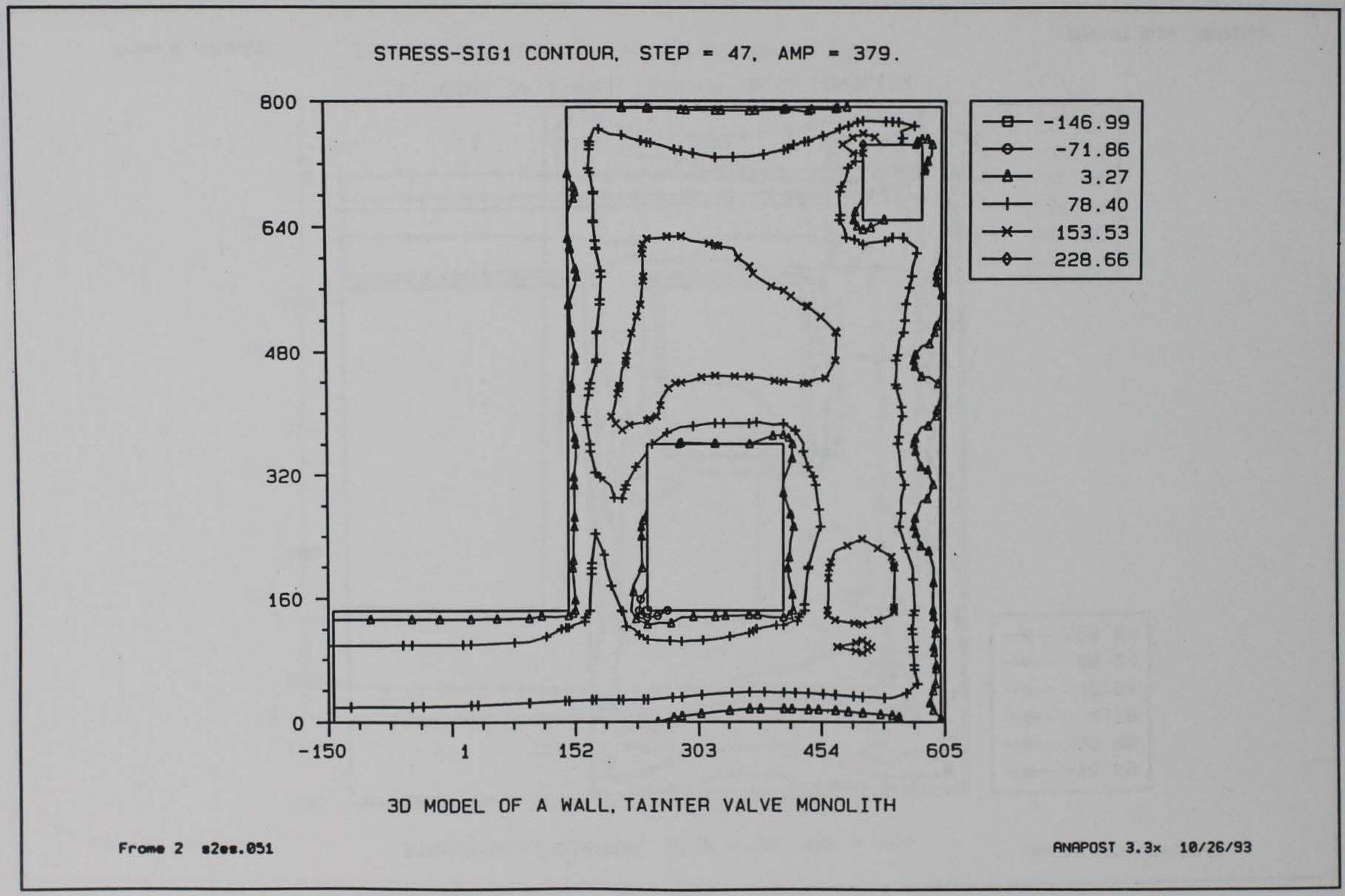
STRESS-SIG1 CONTOUR, STEP = 47, AMP = 379.
800
640
480
320
160
0
-150
1
152
303
454
605
-146.99
-71.86
3.27
78.40
153.53
228.66
3D MODEL OF A WALL, TAINTER VALVE MONOLITH
Frame 2 s2es.051
ANAPOST 3.3x 10/26/93

STRESS-SIG1 CONTOUR, STEP = 55, AMP = 459.

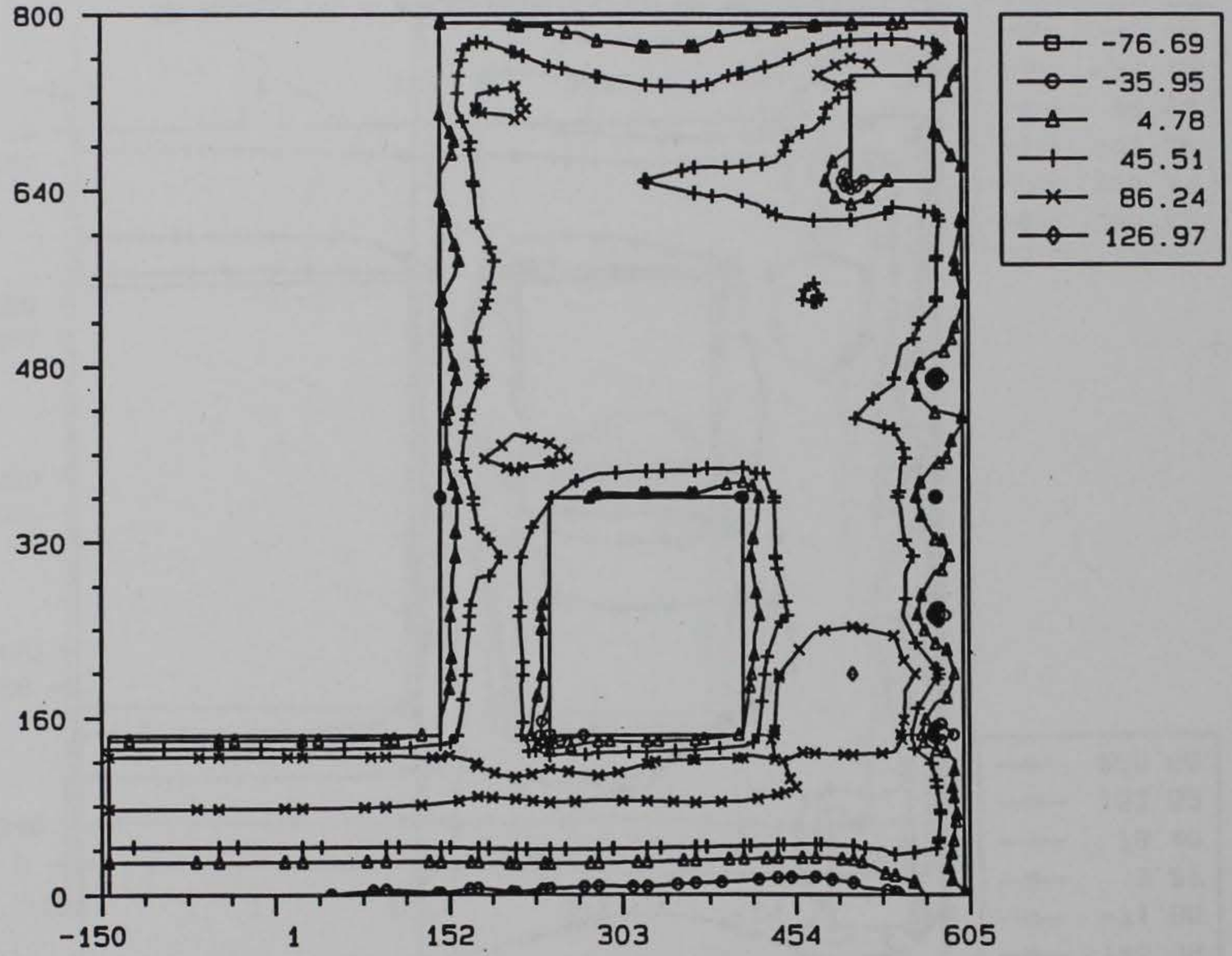

3D MODEL OF A WALL, TAINTER VALVE MONOLITH

Frame 6 s2es.051

ANAPOST 3.3x 10/26/93

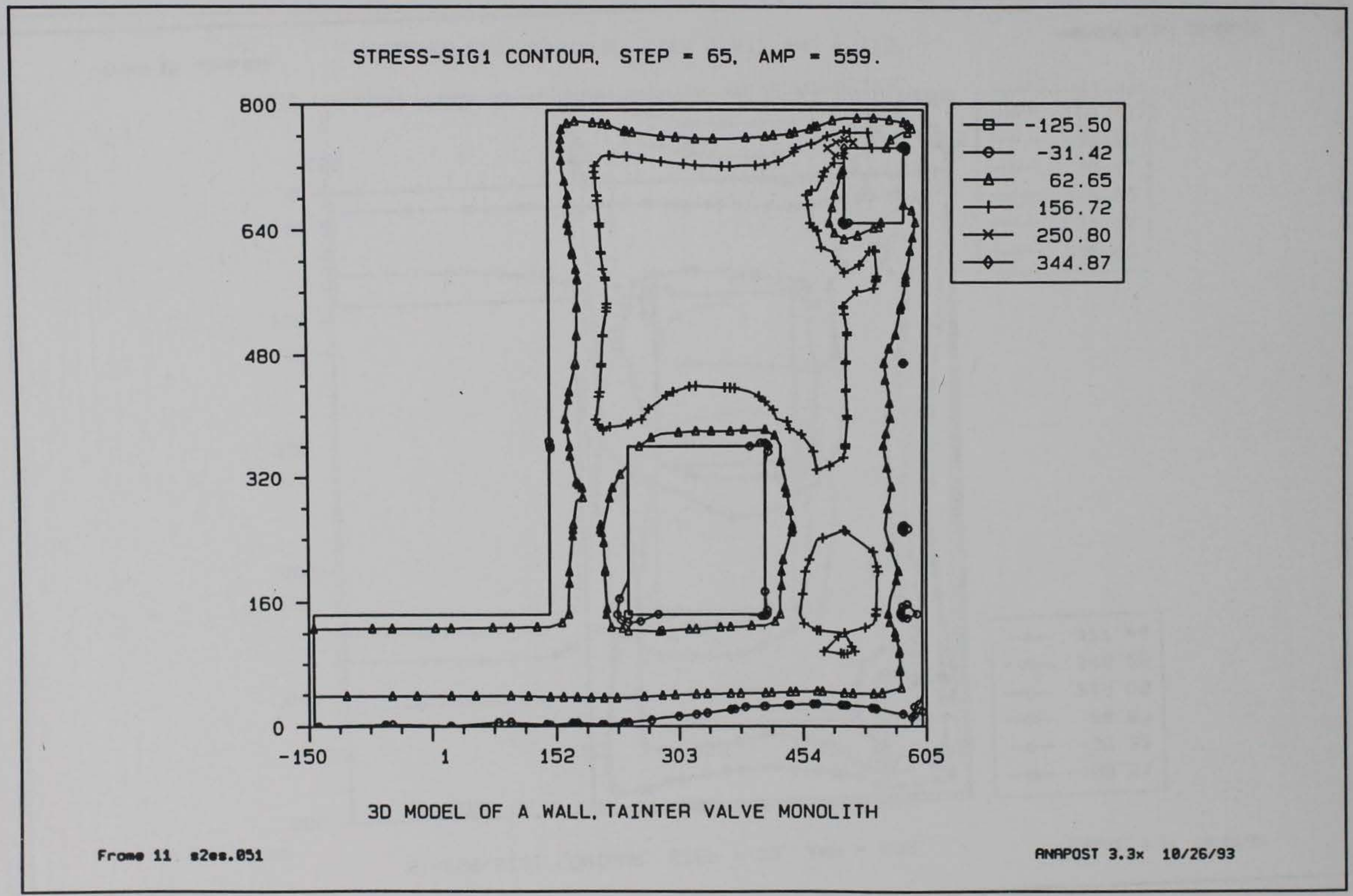
STRESS-SIG1 CONTOUR, STEP = 65, AMP = 559.
800
640
480
320
160
0
-150
1
152
303
454
605
-125.50
-31.42
62.65
156.72
250.80
344.87
3D MODEL OF A WALL, TAINTER VALVE MONOLITH
Frame 11 s2es.051
ANAPOST 3.3x 10/26/93

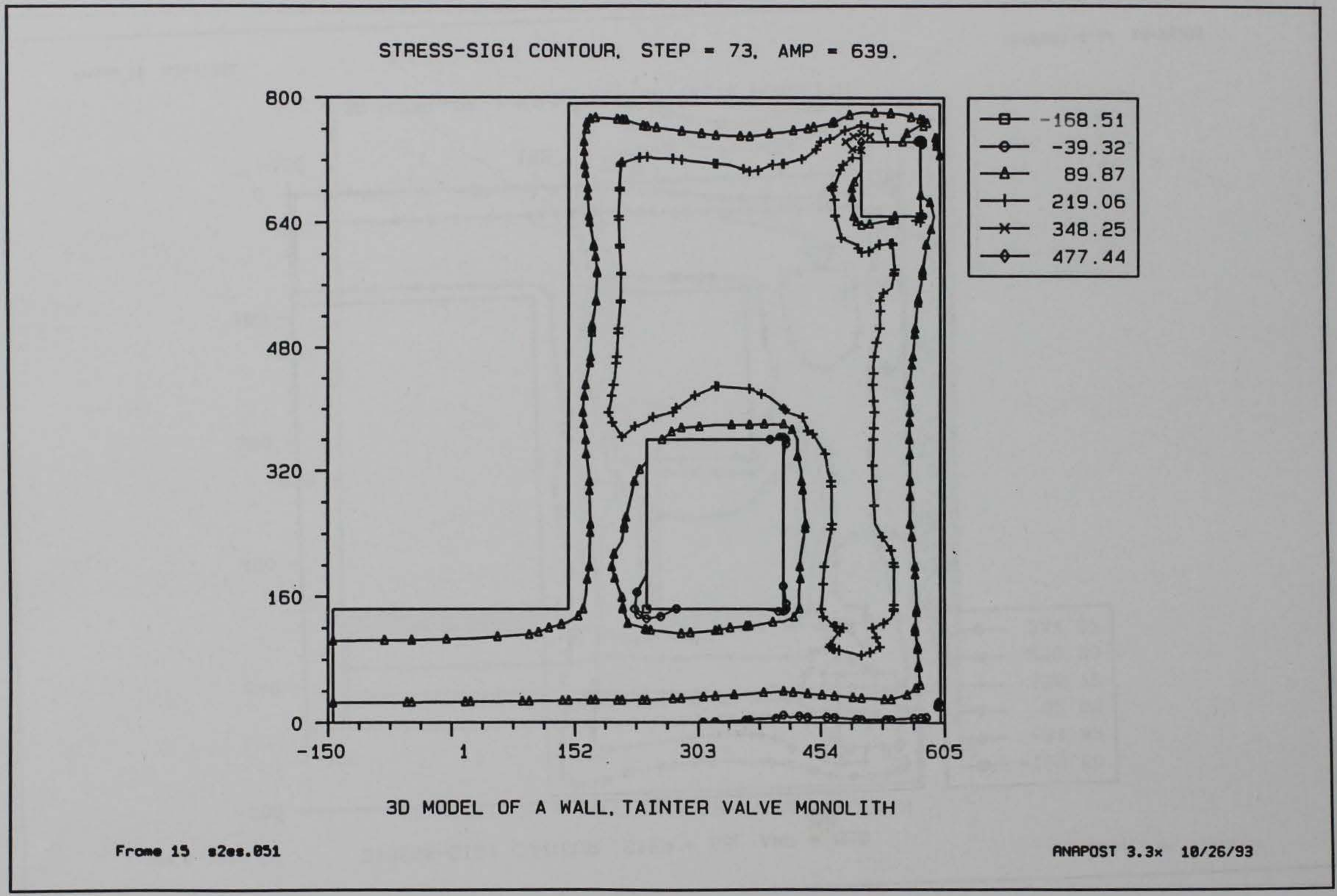
STRESS-SIG1 CONTOUR, STEP = 73, AMP = 639.
800
640
480
320
160
0
-150
1
152
303
454
605
-168.51
-39.32
89.87
219.06
348.25
477.44
3D MODEL OF A WALL, TAINTER VALVE MONOLITH
Frame 15 s2es.051
ANAPOST 3.3x 10/26/93

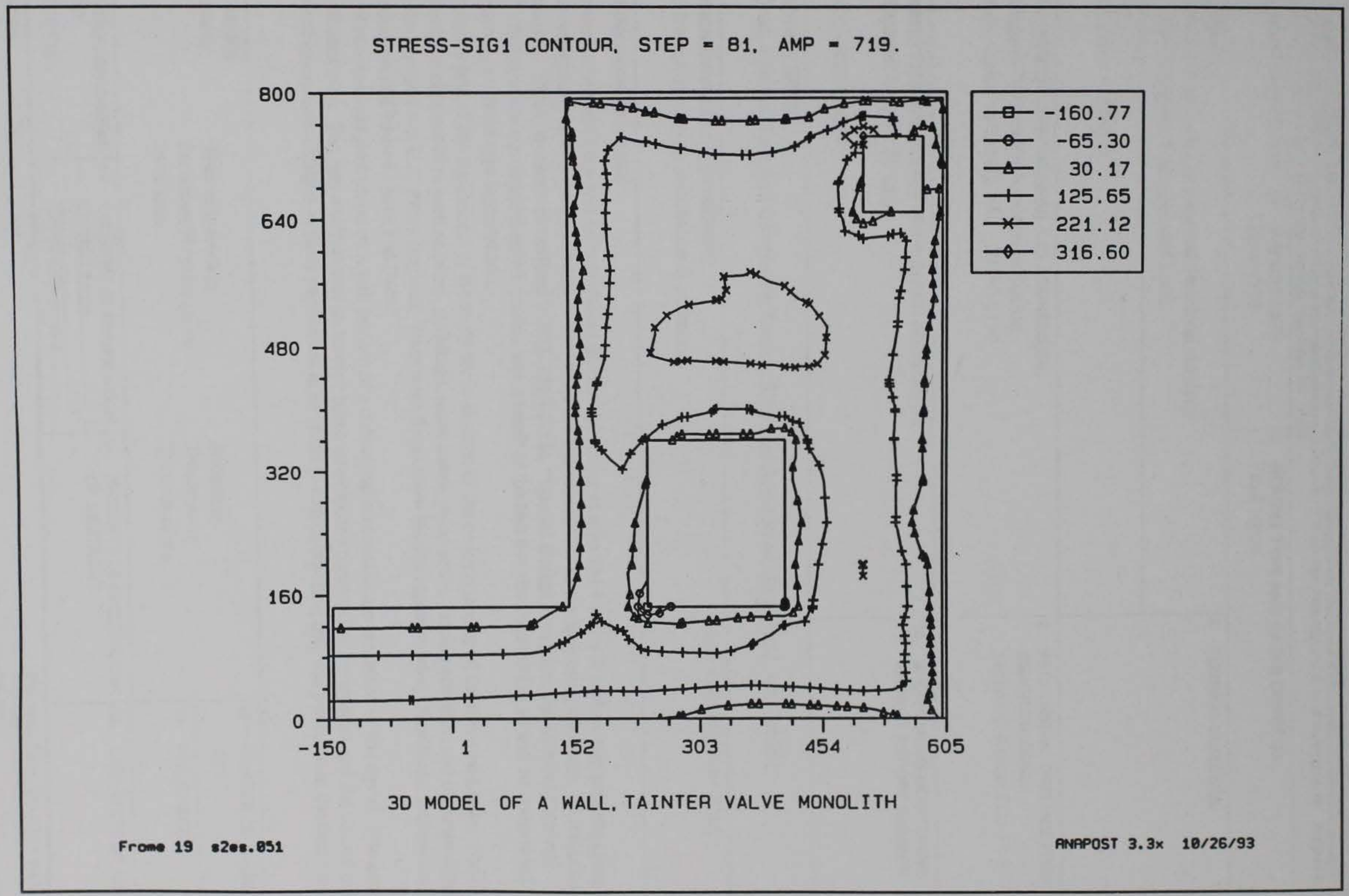
STRESS-SIG1 CONTOUR, STEP = 81, AMP = 719.
800
640
480
320
160
0
-150
1
152
303
454
605
-160.77
-65.30
30.17
125.65
221.12
316.60
3D MODEL OF A WALL, TAINTER VALVE MONOLITH
Frome 19 s2es.051
ANAPOST 3.3x 10/26/93

REPORT DOCUMENTATION PAGE

Form Approved
OMB No. 0704-0188

1. AGENCY USE ONLY *(Leave blank)*

2. REPORT DATE
June 1995

3. REPORT TYPE AND DATES COVERED
Final report

4. TITLE AND SUBTITLE
Three-Dimensional, Nonlinear, Incremental Structural Analysis of a Culvert Valve Monolith Wall, Olmsted Locks

5. FUNDING NUMBERS

6. AUTHOR(S)
Barry D. Fehl, Chris A. Merrill

7. PERFORMING ORGANIZATION NAME(S) AND ADDRESS(ES)
U.S. Army Engineer Waterways Experiment Station
3909 Halls Ferry Road, Vicksburg, MS 39180-6199

8. PERFORMING ORGANIZATION REPORT NUMBER
Technical Report ITL-95-3

9. SPONSORING/MONITORING AGENCY NAME(S) AND ADDRESS(ES)
U.S. Army Engineer District, St. Louis
P.O. Box 59
Louisville, KY 40201-0059

10. SPONSORING/MONITORING AGENCY REPORT NUMBER

11. SUPPLEMENTARY NOTES
Available from National Technical Information Service, 5285 Port Royal Road, Springfield, VA 22161.

12a. DISTRIBUTION/AVAILABILITY STATEMENT
Approved for public release; distribution is unlimited.

12b. DISTRIBUTION CODE

13. ABSTRACT *(Maximum 200 words)*

The Olmsted Locks and Dam will be constructed on the Ohio River at mile 964.4 and will replace two existing locks. Extensive investigations have been undertaken to determine the constructability of the lock using nonlinear, incremental structural analysis (NISA) methods as outlined in ETL 1110-2-324, "Special Design Provisions for Massive Concrete Structures." The need for the comprehensive studies was a result of the fact that the Olmsted Locks will be constructed using the unprecedented w-frame type construction.

This report is a part of the third phase of the study for evaluation of the constructability of the Olmsted Locks. The first two phases evaluated parameters such as creep, shrinkage, plane stress, plane strain, placing schemes, and concrete mixtures, and results are reported in a U.S. Army Engineer Waterways Experiment Station report entitled "Nonlinear, Incremental Structural Analysis of Olmsted Locks and Dam."

Results of two analyses performed on a wall portion of a culvert valve monolith are presented in this report. The analyses were three dimensional. The first analysis was performed based on proposed construction parameters and the second analysis was performed to evaluate changes to those parameters in an effort to reduce cracking that was predicted in the first analysis.

14. SUBJECT TERMS

Aging modulus	Heat of hydration	Shrinkage
Cracking	Incremental construction	Temperature
Creep	Nonlinear	Thermal stress

15. NUMBER OF PAGES
237

16. PRICE CODE

17. SECURITY CLASSIFICATION OF REPORT	18. SECURITY CLASSIFICATION OF THIS PAGE	19. SECURITY CLASSIFICATION OF ABSTRACT	20. LIMITATION OF ABSTRACT
UNCLASSIFIED	UNCLASSIFIED		